

**The Strength of Biaxially Loaded  
Beam-Columns in Flexibly Connected  
Steel Frames.**

**Volume I**

by

**Craig Gibbons.**

First volume of a thesis submitted to the Department of Civil  
and Structural Engineering in partial fulfilment of the  
requirements for the Degree of:

**Doctor of Philosophy**

University of Sheffield

December 1990

**The Strength of Biaxially Loaded Beam-Columns  
in Flexibly Connected Steel Frames.**

**Volume I**

Please note that due to the physical restriction on the maximum thickness of 'soft bound' theses, the appendices to this volume have been temporarily located at the back of Volume II. Upon completion of the assessment of this work, and the inclusion of any modifications or revisions which may be deemed necessary, all copies of both Volumes I and II will be converted to 'hard bound' binding. The increased volume thickness permitted using this technique will enable these appendices to be located in their correct and proper position - at the back of Volume I. Apologies for any confusion this may have caused.

Craig Gibbons 27/1/91

**To Janet  
with all my love.**

# Contents

List of tables. . . . .	x
List of figures. . . . .	xiii
Acknowledgements. . . . .	xxx
Declaration. . . . .	xxxi
Summary. . . . .	xxxii
Notation. . . . .	xxxiii
<b>1 Introduction and Background Work.</b>	<b>1.1</b>
1.1 Introduction. . . . .	1.1
1.2 Historical background. . . . .	1.3
1.2.1 The pinned-end column. . . . .	1.4
1.2.2 End-restrained columns. . . . .	1.6
1.2.3 Frame tests . . . . .	1.9
References. . . . .	1.12
<b>2 The subassemblage tests.</b>	<b>2.1</b>
2.1 Introduction. . . . .	2.1
2.2 Conceptual design of the subassemblage tests specimens . . . . .	2.2
2.2.1 Selection of subassemblage members. . . . .	2.2

2.2.2	Column base fixity. . . . .	2.3
2.2.3	The influence of column length . . . . .	2.5
2.2.4	The influence of beam length. . . . .	2.6
2.2.5	The influence of the 'column loading stub'. . . . .	2.8
2.3	The series of experimental subassemblage tests. . . . .	2.9
2.3.1	Fabrication of the subassemblage specimens. . . . .	2.10
2.3.2	Construction of the subassemblage testing rig. . . . .	2.12
2.3.3	Initial column deformations. . . . .	2.13
2.3.4	Subassemblage erection. . . . .	2.16
2.3.5	Experimental test set-up. . . . .	2.18
2.3.6	Subassemblage test procedure. . . . .	2.19
2.4	Subassemblage test observations and results. . . . .	2.20
2.4.1	Subassemblage test S1 . . . . .	2.20
2.4.2	Subassemblage tests S2. . . . .	2.22
2.4.3	Subassemblage test S3. . . . .	2.23
2.4.4	Subassemblage test S4. . . . .	2.24
2.4.5	Subassemblage test S5. . . . .	2.25
2.4.6	Subassemblage test S6. . . . .	2.26
2.4.7	Subassemblage test S7. . . . .	2.27
2.4.8	Subassemblage test S8. . . . .	2.28
2.4.9	Subassemblage test S9. . . . .	2.29
2.4.10	Subassemblage test S10. . . . .	2.30
2.5	Discussion of results from the experimental subassemblage tests. . . . .	2.31
2.5.1	Mode of failure. . . . .	2.31

2.5.2	Distribution of moments around the subassemblage. . . . .	2.32
2.5.3	Connection behaviour. . . . .	2.34
2.5.4	Ultimate column capacity. . . . .	2.34
2.5.5	Spread of yield across the column section. . . . .	2.36
	References. . . . .	2.36
<b>3</b>	<b>Subassemblage Instrumentation.</b>	<b>3.1</b>
3.1	Introduction . . . . .	3.1
3.2	Displacement measurement. . . . .	3.2
3.2.1	An overview of displacement measurement techniques. . . . .	3.2
3.2.2	Principles of three-dimensional measurement. . . . .	3.5
3.2.3	Construction and testing of a prototype measurement device. . . . .	3.11
3.2.4	Development of the prototype for use in the subassemblage tests. . . . .	3.13
3.2.5	Deflection components measured in the subassemblage tests. . . . .	3.14
3.3	Force measurement. . . . .	3.15
3.3.1	Measurement of longitudinal strains. . . . .	3.15
3.3.2	Summation of the individual strain components. . . . .	3.16
3.3.3	Derivation of the elastic-plastic stress distribution. . . . .	3.18
3.3.4	Derivation of the force components. . . . .	3.20
3.3.5	Overall subassemblage force instrumentation. . . . .	3.22
3.4	Data acquisition. . . . .	3.22
	References. . . . .	3.23
<b>4</b>	<b>Comparisons of Experimental and Analytically Predicted Subassemblage Behaviour</b>	<b>4.1</b>
4.1	Introduction . . . . .	4.1

4.2	The finite element analysis program. . . . .	4.2
4.2.1	Brief overview of computer program analysis techniques. . . . .	4.3
4.3	Modelling of the experimental parameters. . . . .	4.5
4.3.1	Yield and residual stress. . . . .	4.5
4.3.2	Initial deformations and geometric properties. . . . .	4.6
4.3.3	In-plane connection moment-rotation characteristics. . . . .	4.6
4.3.4	Out-of-plane and torsional moment-rotation responses. . . . .	4.7
4.3.5	Beam to column connection position. . . . .	4.8
4.3.6	Column end conditions. . . . .	4.11
4.4	Comparisons of experimental and analytical behaviour. . . . .	4.11
4.4.1	Subassemblage test S1. . . . .	4.12
4.4.2	Subassemblage test S2. . . . .	4.12
4.4.3	Subassemblage test S3. . . . .	4.13
4.4.4	Subassemblage test S4. . . . .	4.14
4.4.5	Subassemblage test S5. . . . .	4.14
4.4.6	Subassemblage test S6. . . . .	4.15
4.4.7	Subassemblage test S7. . . . .	4.16
4.4.8	Subassemblage test S8. . . . .	4.17
4.4.9	Subassemblage test S9 and S10. . . . .	4.17
4.4.10	Investigation of the sensitivity of the predicted behaviour. . . . .	4.18
4.5	Conclusions on the comparisons of observed and predicted behaviour. . .	4.19
	References. . . . .	4.20
<b>5</b>	<b>The full-scale frame tests.</b>	<b>5.1</b>
5.1	Introduction. . . . .	5.1

5.2	General arrangement of the full-scale test frames. . . . .	5.2
5.2.1	Frame members and connection type. . . . .	5.4
5.2.2	Frame construction details . . . . .	5.5
5.2.3	Prevention of column sway. . . . .	5.5
5.3	Measurement of section properties. . . . .	5.6
5.4	Method of load application. . . . .	5.7
5.5	Test frame instrumentation. . . . .	5.8
5.5.1	Deformation measurement. . . . .	5.8
5.5.2	Force measurement. . . . .	5.9
5.5.3	Data logging and experimental control. . . . .	5.9
5.5.4	Processing of recorded data. . . . .	5.10
5.6	Test frame F1 - test parameters and experimental observations. . . . .	5.11
5.6.1	Selection of the loading configuration. . . . .	5.11
5.6.2	Measurement of initial frame deformations. . . . .	5.12
5.6.3	Experimental test procedure and observations. . . . .	5.12
5.7	Frame test F1 - Presentation and discussion of results. . . . .	5.14
5.7.1	The beam loading phase. . . . .	5.15
5.7.2	Loading of column C5. . . . .	5.16
5.7.3	Loading of column C6. . . . .	5.18
5.8	Test frame F2 - test parameters and experimental observations. . . . .	5.21
5.8.1	Selection of the loading configuration. . . . .	5.22
5.8.2	Measurement of initial column deformations. . . . .	5.22
5.8.3	Experimental test procedure and observations. . . . .	5.23
5.9	Test Frame F2 - Presentation and discussion of results. . . . .	5.24



5.9.1	The beam loading phase. . . . .	5.25
5.9.2	The loading of column C8. . . . .	5.26
5.9.3	The loading of column C7. . . . .	5.27
5.10	Summary of the observed column failure loads. . . . .	5.29
5.11	Concluding comments on the full-scale frame tests. . . . .	5.31
	References. . . . .	5.32
<b>6</b>	<b>Connection Moment-rotation Behaviour.</b>	<b>6.1</b>
6.1	Introduction . . . . .	6.1
6.2	The 'isolated' connection tests. . . . .	6.2
6.3	The subassemblage tests. . . . .	6.4
6.4	Frame test F1. . . . .	6.6
6.5	The behaviour of semi-rigid connections in frames. . . . .	6.8
6.5.1	The influence of column web panel flexibility. . . . .	6.9
6.5.2	The influence of beam continuity. . . . .	6.10
6.5.3	The validity of isolated connection tests. . . . .	6.12
6.5.4	A semi-empirical approach for determining $M - \phi$ response. . . . .	6.14
6.6	A summary of observations on connection $M - \phi$ response. . . . .	6.18
	References. . . . .	6.19
<b>7</b>	<b>A Parametric Study of Subassemblage Behaviour.</b>	<b>7.1</b>
7.1	Introduction . . . . .	7.1
7.2	Formation of the study. . . . .	7.2
7.3	Subassemblage configurations. . . . .	7.3
7.4	Loading sequence. . . . .	7.4

7.5	Parameters investigated in the initial phase of the study. . . . .	7.5
7.5.1	Discussion of the result from the first phase of the study. . . . .	7.6
7.5.2	Conclusions from the first phase of the study. . . . .	7.9
7.6	Parameters investigated in the second phase of the study. . . . .	7.10
7.6.1	Discussion of the results from the second phase of the study. . . . .	7.12
7.6.2	Conclusions from the second phase of the study. . . . .	7.16
7.7	Parameters investigated in the third phase of the study. . . . .	7.17
7.7.1	Discussion of the results from the third phase of the study. . . . .	7.18
7.7.2	Conclusions from the third phase of the study. . . . .	7.19
7.8	Concluding remarks on the parametric study. . . . .	7.20
	References. . . . .	7.21
<b>8</b>	<b>The Design of Non-sway Frames with Semi-Rigid Connections.</b>	<b>8.1</b>
8.1	Introduction . . . . .	8.1
8.2	The deformation of semi-rigid frames under serviceability loads. . . . .	8.2
8.2.1	Development of the deflection equations. . . . .	8.3
8.2.2	Linear simplification of the connection moment-rotation response. . . . .	8.7
8.2.3	Validation of the semi-rigid frame deflection equations. . . . .	8.8
8.2.4	Summary of the serviceability design technique. . . . .	8.12
8.2.5	The potential benefits of predicting reduced deflections. . . . .	8.13
8.3	The ultimate design strength of beam-columns. . . . .	8.14
8.3.1	The beam-column problem. . . . .	8.15
8.3.2	The development of interaction equations. . . . .	8.17
8.3.3	The interaction equations in BS 5950: Part 1. . . . .	8.20

8.3.4	The application of interaction equations to steel frame design in BS 5950: Part 1. . . . .	8.21
8.3.5	Beam-column design allowing for semi-rigid connection response. .	8.23
8.3.6	The 'variable stiffness' method. . . . .	8.30
8.3.7	Observations on the application of the BS 5950 simple design method.	8.33
8.3.8	The assessment of effective lengths in simple frame design. . . . .	8.34
8.3.9	The treatment of column disturbing moments in simple frame design.	8.37
8.4	Conclusions. . . . .	8.42
	References. . . . .	8.43
<b>9</b>	<b>Proposals for Future Work.</b>	<b>9.1</b>
9.1	Introduction . . . . .	9.1
9.2	Connection moment-rotation. . . . .	9.1
9.3	The parametric study. . . . .	9.2
9.4	The full-scale frame tests. . . . .	9.3
9.5	The design of semi-rigid frames. . . . .	9.4
9.6	Future experimental studies of semi-rigid frame behaviour. . . . .	9.5
9.7	The strengthening of existing steel stanchions. . . . .	9.5
9.8	The use of tension control bolts. . . . .	9.6
	References. . . . .	9.7
<b>10</b>	<b>Conclusions.</b>	<b>10.1</b>
10.1	Experimentation techniques. . . . .	10.2
10.2	Connection behaviour. . . . .	10.4
10.3	Frame and subassemblage response. . . . .	10.5
10.4	Frame design. . . . .	10.7

**Appendix A - Subassemblage fabrication drawings. . . . . A.1**  
**Appendix B - Frame fabrication drawings. . . . . B.1**  
**Appendix C - Semi-rigid frame design calculations. . . . . C.1**



## **List of tables.**

**Table 2.1: Predicted ultimate loads and mid-column deflections for different connection types and column lengths.**

**Table 2.2: Predicted ultimate loads for different connection types and beam lengths.**

**Table 2.3: Connection type, subassemblage type and column orientation for each of the ten subassemblage test.**

**Table 2.4: Initial column deformations and column head load eccentricities.**

**Table 2.5: Nominal applied beam loads and beam load locations.**

**Table 2.6: Measurements of column base movement during a re-test of subassemblage S1.**

**Table 2.7: A summary of ultimate column capacities and squash loads.**

**Table 4.1: Offsets from the column face to the effective centre of beam support assumed for each model of the subassemblage tests.**

**Table 4.2: Comparison of the experimentally observed and analytically predicted ultimate column capacities.**

**Table 4.3: Analytically predicted ultimate capacities and minor axis moments for supplementary models S2A to S2E.**

**Table 5.1: Total loads applied to the beams in test F1.**

**Table 5.2: Total loads applied to the beams in test F2.**

**Table 5.3: Summary of the column bending moments at the end of the beam loading phase and the ultimate capacities measured in frame tests F1 and F2.**

**Table 6.1: Summary of the 'cantilever' connection test series.**

- Table 7.1: Assumed dead load components for the two types of floor construction.
- Table 7.2: Failure loads ( $\alpha_{pin}$ ) of the models in the initial study.
- Table 7.3: Failure loads ( $\alpha_{res}$ ) of the models in the initial study.
- Table 7.4: Failure loads ( $\alpha_{pin}$ ) of the subassemblages when loaded at the column head only.
- Table 7.5: Plastic moment capacities of the sections used in the second phase of the study.
- Table 7.6: Stiffness ratios for the different beam and column combinations.
- Table 7.7: Nominal column squash loads and ultimate capacities determined from the finite element program.
- Table 7.8a: Values of  $\alpha_{pin}$  for column *C1* with different beam sizes.
- Table 7.8b: Values of  $\alpha_{pin}$  for column *C2* with different beam sizes.
- Table 7.8c: Values of  $\alpha_{pin}$  for column *C3* with different beam sizes.
- Table 7.9: Web cleat performance indicator ( $\beta_{pin}$ ) for different beam and column combinations.
- Table 7.10: Effect of the different loading intensities  $w1$ ,  $w2$  and  $w3$  on the beams *B1*, *B2* and *B3* over a simple 5.5m span.
- Table 7.11a: Failure loads ( $\alpha_{pin}$ ) of column *C1* employing web cleat connections.
- Table 7.11b: Failure loads ( $\alpha_{pin}$ ) of column *C2* employing web cleat connections.
- Table 7.11c: Failure loads ( $\alpha_{pin}$ ) of column *C3* employing web cleat connections.
- Table 8.1: Summary of the rigid connection moments and actual the actual test frame moments.
- Table 8.2: Linear stiffnesses determined from the actual experimental connection moment-rotation data.

- Table 8.3: Summary of the calculated semi-rigid moments and  $\mu$  factors for different linear connection stiffnesses.
- Table 8.4: Average  $\mu$  factors for the four primary beams.
- Table 8.5: Comparison of the pinned, rigid, actual and predicted mid-beam deflections.
- Table 8.6: Comparison of predicted deflections with actual.
- Table 8.7: Comparison of predicted deflections with those of a simple beam span.
- Table 8.8: Predicted ultimate loads of the subassemblage tests using the 'simple' design method.
- Table 8.9: Predicted ultimate loads of subassemblages in the parametric study using the 'simple' design method.
- Table 8.10: Predicted ultimate loads of column segments in frame test F1 using the 'simple' design method.
- Table 8.11: Proposed modification to the standard effective length factors in BS 5950.
-

## List of figures

Figure 1.1: Moment-rotation response for a range of 'simple' connection types.

Figure 1.2: Influence of different 'simple' connection types on the strength of columns of different slenderness.

Figure 2.1: Basic analytical model used in the preliminary studies.

Figure 2.2: Plot of column base stiffness against predicted percentage increase in failure load.

Figure 2.3: Subassemblage from within a more extensive structure.

Figure 2.4: Predicted failure loads for analytical models employing different boundary conditions.

Figure 2.5: The 'edge' and 'corner' column subassemblage configurations considered in the experimental study.

Figure 2.6: General arrangement of the three beam subassemblage.

Figure 2.7: General arrangement of the two beam subassemblage.

Figure 2.8: Column base-plate arrangement used in each of the ten tests.

Figure 2.9: Sliding support bearing used at the end of each beam.

Figure 2.10: General arrangement of the subassemblage testing rig.

Figure 2.11: The subassemblage testing rig with a specimen installed.

Figure 2.12: The subassemblage testing rig with a specimen installed.

Figure 2.13: End view of testing rig base arrangement.

Figure 2.14: Elevation of testing rig base arrangement.

Figure 2.15: Method of inducing the required initial column deformations.

Figure 2.16: Different beam to column connection bolt fixing sequences.



**Figure 2.17: 250kN capacity hydraulic ram used to apply beam loading.**

**Figure 2.18: Summary of the major experimental parameters in test S1.**

**Figure 2.19: Plot of axial load vs. mid-column deflection for test S1.**

**Figure 2.20: Distribution of bending moments at the end of the beam loading phase.**

**Figure 2.21: Distribution of bending moments at the point of maximum applied load.**

**Figure 2.22: Plot of axial load vs. beam support displacements - test S1.**

**Figure 2.23: Plot of axial load vs. beam support displacements - test S2.**

**Figure 2.24: Summary of the major experimental parameters in test S2.**

**Figure 2.25: Plot of axial load vs. mid-column deflection for test S2.**

**Figure 2.26: Distribution of bending moments at the end of the beam loading phase.**

**Figure 2.27: Distribution of bending moments at the point of maximum applied load.**

**Figure 2.28: View along the length of column S2 highlighting the deformation at a post-failure loading level.**

**Figure 2.29: View of column S2 at a post-failure loading level.**

**Figure 2.30: Summary of the major experimental parameters in test S3.**

**Figure 2.31: Plot of axial load vs. mid-column deflection for test S3.**

**Figure 2.32: Distribution of bending moments at the end of the beam loading phase.**

**Figure 2.33: Distribution of bending moments at the point of maximum applied load.**

**Figure 2.34: The head of column S4 showing the two intersecting beams.**

**Figure 2.35: Summary of the major experimental parameters in test S4.**

**Figure 2.36: Plot of axial load vs. mid-column deflection for test S4.**

**Figure 2.37: Distribution of bending moments at the end of the beam loading phase.**

**Figure 2.38: Distribution of bending moments at the point of maximum applied load.**

**Figure 2.39: A local deformation in the flange of column S5 prior to testing.**

**Figure 2.40: Summary of the major experimental parameters in test S5.**

**Figure 2.41: Plot of axial load vs. mid-column deflection for test S5.**

**Figure 2.42: Distribution of bending moments at the end of the beam loading phase.**

**Figure 2.43: Distribution of bending moments at the point of maximum applied load.**

**Figure 2.44: Column S5 at a post-failure level of load illustrating the reverse curve deflected shape of the column.**

**Figure 2.45: Diagrammatic view of column S5 showing the regions where plasticity of the steel caused the shedding of paint from the member surface.**

**Figure 2.46: Summary of the major experimental parameters in test S6.**

**Figure 2.47: Plot of axial load vs. mid-column deflection for test S6.**

**Figure 2.48: Plot of axial load vs. mid-column twist - test S6.**

**Figure 2.49: Distribution of bending moments at the end of the beam loading phase.**

**Figure 2.50: Distribution of bending moments at the point of maximum applied load.**

**Figure 2.51: Summary of the major experimental parameters in test S7.**

**Figure 2.52: Plot of axial load vs. mid-column deflection for test S7.**

**Figure 2.53: Distribution of bending moments at the end of the beam loading phase.**

**Figure 2.54: Distribution of bending moments at the point of maximum applied load.**

**Figure 2.55: Summary of the major experimental parameters in test S8.**

**Figure 2.56: Plot of axial load vs. mid-column deflection for test S8.**

**Figure 2.57: Distribution of bending moments at the end of the beam loading phase.**

**Figure 2.58: Distribution of bending moments at the point of maximum applied load.**

**Figure 2.59: Summary of the major experimental parameters in test S9.**

**Figure 2.60: Plot of axial load vs. mid-column deflection for test S9.**

**Figure 2.61: Distribution of bending moments at the end of the beam loading phase.**

**Figure 2.62: Distribution of bending moments at the point of maximum applied load.**

**Figure 2.63: Summary of the major experimental parameters in test S10.**

**Figure 2.64: Plot of axial load vs. mid-column deflection for test S10.**

**Figure 2.65: Distribution of bending moments at the end of the beam loading phase.**

**Figure 2.66: Distribution of bending moments at the point of maximum applied load.**

**Figure 2.67: Column S10 under a post-failure level of loading.**

**Figure 2.68: Direction of connection rotations at key stages in the subassemblage loading sequence.**

**Figure 2.69: The spread of yield across the column section for test numbers S6 and S7.**

**Figure 3.1: Two dimensional measurement device using three L.V.D.T.'s.**

- Figure 3.2: The effect of out-of-plane movement on the measurement of in-plane displacement.
- Figure 3.3: Three-dimensional co-ordinates of reference points  $P1$ ,  $P2$  and  $P3$  from general point  $A$ .
- Figure 3.4: Location of the three connection points around the specimen.
- Figure 3.5: Co-ordinates of the rotation bar connecting reference points  $A$  and  $B$ .
- Figure 3.6: Arrangement of the three-dimensional measurement system.
- Figure 3.7: Experimental set-up used for testing a prototype of the 3-dimensional measurement system.
- Figure 3.8: Plot of actual vs. measured major axis rotation.
- Figure 3.9: Plot of actual vs. measured minor axis rotation.
- Figure 3.10: Plot of actual vs. measured twist rotation.
- Figure 3.11: Plot of actual vs. measured 'x' displacement.
- Figure 3.12: Plot of actual vs. measured 'y' displacement.
- Figure 3.13: Plot of actual vs. measured 'z' displacement.
- Figure 3.14: Measurement system used at the base of the column.
- Figure 3.15: View along the column illustrating the measurement device at the column centre.
- Figure 3.16: Schematic diagram of the six L.V.D.T. device used at the column centre.
- Figure 3.17: Schematic diagram of the five L.V.D.T. device used at the column head.
- Figure 3.18: Location of three-dimensional measurement devices.
- Figure 3.19: Deformation components measured in the subassemblage tests.
- Figure 3.20: Member actions resulting from longitudinal strains.
- Figure 3.21: Arrangement of 10 strain gauges used at the column centre.

Figure 3.22: Derivation of the 3-D stress distribution from the measured strains.

Figure 3.23: Typical output from the processing program showing the extent of material yield.

Figure 3.24: Plot of applied axial load against axial load measured from the strain gauges.

Figure 3.25: Plot of axial load vs. mid-column minor axis bending moment - test S5.

Figure 3.26: Plot of axial load vs. measured microstrain indicating the degree of correction made to different gauges.

Figure 3.27: Arrangement of four strain gauges used to derive the elastic beam forces.

Figure 3.28: Force components measured in the subassemblage tests.

Figure 4.1: Multi-linear approximation to the  $M - \phi$  response of a web cleat connected to the minor column axis.

Figure 4.2: Multi-linear approximation to the  $M - \phi$  response of a web and seat cleat connected to the major column axis.

Figure 4.3: Components of out-of-plane connection rotation.

Figure 4.4: The effect of beam torsional stiffness on column head restraint.

Figure 4.5: Comparison of the experimentally observed column head minor axis rotation and beam twist for a web cleat connection.

Figure 4.6: Comparison of the experimentally observed column head minor axis rotation and beam twist for a web and seat cleat connection.

Figure 4.7: Offset required in the analytical model to simulate column depth.

Figure 4.8: Typical connection showing the effect of 'strut action'.

Figure 4.9: Two similar structures illustrating the effect of permitting support displacement.

Figure 4.10: Possible shift in the effective centre of beam support for an 'opening' and a 'closing' connection.

Figure 4.11: Experimental and analytical mid-column deflections, S1.

Figure 4.12: Experimental and analytical mid-column twist rotations, S1.

Figure 4.13: Experimental and analytical bending moments at the column head, S1.

Figure 4.14: Experimental and analytical bending moments at the column centre, S1.

Figure 4.15: Experimental and analytical bending moments at the column base, S1.

Figure 4.16: Experimental and analytical mid-column deflections, S2.

Figure 4.17: Experimental and analytical mid-column twist rotations, S2.

Figure 4.18: Experimental and analytical bending moments at the column head, S2.

Figure 4.19: Experimental and analytical bending moments at the column centre, S2.

Figure 4.20: Experimental and analytical bending moments at the column base, S2.

Figure 4.21: Experimental and analytical major axis moments for beam 3, S2.

Figure 4.22: Experimental and analytical mid-column deflections, S3.

Figure 4.23: Experimental and analytical mid-column twist rotations, S3.

Figure 4.24: Experimental and analytical bending moments at the column head, S3.

Figure 4.25: Experimental and analytical bending moments at the column centre, S3.

Figure 4.26: Experimental and analytical bending moments at the column base, S3.

Figure 4.27: Experimental and analytical major axis moments for beam 1, S3.

Figure 4.28: Typically  $M - \phi$  response for a 'closing - closing' connection and a 'closing - opening' connection.

Figure 4.29: Experimental and analytical mid-column deflections, S4.

Figure 4.30: Experimental and analytical mid-column twist rotations, S4.

Figure 4.31: Experimental and analytical bending moments at the column head, S4.

Figure 4.32: Experimental and analytical bending moments at the column centre, S4.

Figure 4.33: Experimental and analytical bending moments at the column base, S4.  
Figure 4.34: Experimental and analytical mid-column deflections, S5.  
Figure 4.35: Experimental and analytical mid-column twist rotations, S5.  
Figure 4.36: Experimental and analytical bending moments at the column head, S5.  
Figure 4.37: Experimental and analytical bending moments at the column centre, S5.  
Figure 4.38: Experimental and analytical bending moments at the column base, S5.  
Figure 4.39: Experimental and analytical mid-column deflections, S6.  
Figure 4.40: Experimental and analytical mid-column twist rotations, S6.  
Figure 4.41: Experimental and analytical bending moments at the column head, S6.  
Figure 4.42: Experimental and analytical bending moments at the column centre, S6.  
Figure 4.43: Experimental and analytical bending moments at the column base, S6.  
Figure 4.44: Experimental and analytical mid-column deflections, S7.  
Figure 4.45: Experimental and analytical mid-column twist rotations, S7.  
Figure 4.46: Experimental and analytical bending moments at the column head, S7.  
Figure 4.47: Experimental and analytical bending moments at the column centre, S7.  
Figure 4.48: Experimental and analytical bending moments at the column base, S7.  
Figure 4.49: Experimental and analytical mid-column deflections, S8.  
Figure 4.50: Experimental and analytical mid-column twist rotations, S8.  
Figure 4.51: Experimental and analytical bending moments at the column head, S8.  
Figure 4.52: Experimental and analytical bending moments at the column centre, S8.  
Figure 4.53: Experimental and analytical bending moments at the column base, S8.  
Figure 4.54: Experimental and analytical mid-column deflections, S9.  
Figure 4.55: Experimental and analytical mid-column twist rotations, S9.

- Figure 4.56: Experimental and analytical bending moments at the column head, S9.
- Figure 4.57: Experimental and analytical bending moments at the column centre, S9.
- Figure 4.58: Experimental and analytical bending moments at the column base, S9.
- Figure 4.59: Experimental and analytical major axis moments for beam 1, S9.
- Figure 4.60: Experimental and analytical mid-column deflections, S10.
- Figure 4.61: Experimental and analytical mid-column twist rotations, S10.
- Figure 4.62: Experimental and analytical bending moments at the column head, S10.
- Figure 4.63: Experimental and analytical bending moments at the column centre, S10.
- Figure 4.64: Experimental and analytical bending moments at the column base, S10.
- Figure 4.65: Experimental and analytical major axis moments for beam 3, S10.
- Figure 4.66: Adjustment to the  $M - \phi$  response of the connection characteristics in model 2DE.
- 
- Figure 5.1: Isometric view indicating the 'active' and 'static' parts of the test frame.
- Figure 5.2: General arrangement of test frame F1, (F2 similar).
- Figure 5.3: Plan views indicating the different column orientations adopted for frame test F1 and F2.
- Figure 5.4: Photograph of test frame F1 prior to testing (active frame at rear).
- Figure 5.5: Photograph of test frame F1 prior to testing.
- Figure 5.6: Typical plan view of frame indicating the position of restraint bars.
- Figure 5.7: Typical 'tie bar' used to prevent column sway.
- Figure 5.8: Elevation and section through the frame illustrating the location of the beam loading points.



- Figure 5.9 :** View of the hydraulic loading rams housed in the basement beneath the test area.
- Figure 5.10:** Arrangement used to apply load at the column head.
- Figure 5.11:** Summary of the various force and deformation components which were measured.
- Figure 5.12:** System used to monitor beam deflection.
- Figure 5.13:** Three-dimensional measurement device used to monitor the deformations at the column centre.
- Figure 5.14:** The 'hanging dumb-bell' rotation measurement device.
- Figure 5.15:** Location of strain gauges on the column members.
- Figure 5.16:** Location of strain gauges on the beam members.
- Figure 5.17:** Schematic diagram showing the experimental set-up.
- Figure 5.18:** A plot of measured rotation against time for one of the 'hanging dumb-bell' rotation devices.
- Figure 5.19:** Elevation and section through test frame F1 indicating the member nomenclature.
- Figure 5.20:** Distribution of rigid frame bending moments resulting from a 'chequer-board' floor load distribution.
- Figure 5.21:** Initial column deformations for test F1.
- Figure 5.22:** Computer generated frame bending moments at the end of the beam loading phase - test frame F1.
- Figure 5.23:** Computer generated frame bending moments at the point of maximum load on column C5.
- Figure 5.24:** Axial load vs. mid-column moments for C5/0-1 and C5/1-2.
- Figure 5.25:** Applied column head load vs. mid-column moments for C5/0-1 and C5/1-2.
- Figure 5.26:** Axial load vs. mid-column deflections for C5/0-1 and C5/1-2.
- Figure 5.27:** Axial load vs. mid-column twist rotation for C5/0-1 and C5/1-2.

- Figure 5.28: Axial load vs. minor axis moment at the top, mid-point and bottom of C5/1-2.
- Figure 5.29: Axial load vs. major axis moment at the top, mid-point and bottom of C5/1-2.
- Figure 5.30: Axial load vs. minor axis moment at the top, mid-point and bottom of C5/0-1.
- Figure 5.31: Axial load vs. major axis moment at the top, mid-point and bottom of C5/0-1.
- Figure 5.32: Axial load vs. moment at the connection of beam SB2 to column C5/1-2.
- Figure 5.33: Axial load vs. moment at the connection of beams PB5 and PB6 to column C5/1-2.
- Figure 5.34: Axial load vs. moment at the connection of beams PB7 and PB8 to column C5/0-1.
- Figure 5.35: Computer generated frame bending moments at the point of maximum load on column C6.
- Figure 5.36: Axial load vs. mid-column moments for columns C6/0-1 and C6/1-2.
- Figure 5.37: Axial load vs. mid-column deflections for columns C6/0-1 and C6/1-2.
- Figure 5.38: Axial load vs. mid-column twist rotation for columns C6/0-1 and C6/1-2.
- Figure 5.39: Axial load vs. minor axis moment at the top, mid-point and bottom of column C6/1-2.
- Figure 5.40: Axial load vs. major axis moment at the top, mid-point and bottom of C6/1-2.
- Figure 5.41: Axial load vs. minor axis moment at the top, mid-point and bottom of column C6/0-1.
- Figure 5.42: Axial load vs. major axis moment at the top, mid-point and bottom of column C6/0-1.
- Figure 5.43: Axial load vs. moment at the connection of beams SB3 and SB6 to column C6/1-2.
- Figure 5.44: Axial load vs. moment at the connection of beams PB6 and PB8 to column C6/1-2.

Figure 5.45: Elevation and section through test frame F2 indicating the member nomenclature.

Figure 5.46: Initial column deformations for test F2.

Figure 5.47: Observed deformed shape of the minor axis of column C8.

Figure 5.48: Observed deformed shape of the minor axis of column C7.

Figure 5.49: Computer generated frame bending moments at the end of the beam loading phase - test frame F2.

Figure 5.50: Computer generated frame bending moments at the point of maximum load on column C8.

Figure 5.51: Axial load vs. mid-column moments for C8/0-1 and C8/1-2.

Figure 5.52: Axial load vs. mid-column deflections for C8/0-1 and C8/1-2.

Figure 5.53: Applied load vs. mid-column deflections for C8/0-1 and C8/1-2.

Figure 5.54: Axial load vs. mid-column twist rotation for C8/0-1 and C8/1-2.

Figure 5.55: Axial load vs. minor axis moment at the top, mid-point and bottom of C8/1-2.

Figure 5.56: Axial load vs. major axis moment at the top, mid-point and bottom of C8/1-2.

Figure 5.57: Axial load vs. minor axis moment at the top, mid-point and bottom of C8/0-1.

Figure 5.58: Axial load vs. major axis moment at the top, mid-point and bottom of C8/0-1.

Figure 5.59: Axial load vs. moment at the connection of beams SB8 and SB11 to column C8/1-2.

Figure 5.60: Axial load vs. moment at the connection of beams PB11 and PB12 to column C8/1-2.

Figure 5.61: Computer generated frame bending moments on column C7 at the penultimate increment before the ultimate load was achieved.

Figure 5.62: Axial load vs. mid-column moments for columns C7/0-1 and C7/1-2.

Figure 5.63: Axial load vs. mid-column deflections for columns C7/0-1 and C7/1-2.

Figure 5.64: Axial load vs. mid-column twist rotation for columns C7/0-1 and C7/1-2.

Figure 5.65: Axial load vs. minor axis moment at the top, mid-point and bottom of column C7/1-2.

Figure 5.66: Axial load vs. major axis moment at the top, mid-point and bottom of column C7/1-2.

Figure 5.67: Axial load vs. minor axis moment at the top, mid-point and bottom of column C7/0-1.

Figure 5.68: Axial load vs. major axis moment at the top, mid-point and bottom of column C7/0-1.

Figure 6.1: Fabrication details of the connections used in the study.

Figure 6.2: Experimental set-up of the 'cantilever' connection test.

Figure 6.3: Experimental set-up of the 'cruciform' connection test.

Figure 6.4: Moment-rotation response of web cleat connections to the column flange.

Figure 6.5: Moment-rotation response of flange cleat connections to the column web.

Figure 6.6: Moment-rotation response of flange cleat connections to the column flange.

Figure 6.7: Moment-rotation response of web and seat cleat connections to the column flange.

Figure 6.8: Moment-rotation response of web and seat cleat connections to the column web.

Figure 6.9: Moment-rotation response of different connections to the column web illustrating the 'loading-unloading' response.

Figure 6.10 Moment-rotation response of flush end plate connections to the column flange.

Figure 6.11 Moment-rotation response of flush end plate connections to the web of a 'corner' column.

- Figure 6.12** Moment-rotation response ('loading-unloading') of flush end plate connections to the web of the 'internal' column.
- Figure 6.13** Moment-rotation response ('loading-loading') of flush end plate connections to the web of the 'internal' column.
- Figure 6.14** Idealised connection moment-rotation response.
- Figure 6.15** Frame test moment-rotation response illustrating the reduced unloading connection stiffness.
- Figure 6.16** Deformation of a connection to the web of a 'corner' column.
- Figure 6.17** Deformation of a connection to the web of an 'internal' column.
- Figure 6.18:** Small beams connected to a flexible web panel via stiff connections.
- Figure 6.19:** Column supporting a pair of beams using the connection shown in figure 6.18.
- Figure 6.20:** Moment-rotation plots from 'isolated' tests of the connection shown in figure 6.18.
- Figure 6.21:** Comparison of the unloading stiffness of a frame connection to the 'internal' column resulting from column deformation, and that from a 'corner' column connection when the loading is removed.
- Figure 6.22:** Internal column with a non-symmetrical arrangement of beams and connection types.
- Figure 6.23:** Possible connection test arrangement which would permit connection rotations resulting from column deformation.
- Figure 6.24:** The individual stiffness components of a beam connection on one side of a column.
- Figure 6.25:** The individual stiffness components of connections to both sides of a column.
- 
- Figure 7.1:** Arrangement of the subframe and subframe model used in the study.
- Figure 7.2:** Assumed pattern of column residual stresses.

- Figure 7.3: Moment-rotation characteristics assumed for the nominal web cleat connection.
- Figure 7.4: Assumed distribution of beam loading for one-way and two-way spanning types of floor construction.
- Figure 7.5: Arrangement of floor loading for load cases 1 to 9.
- Figure 7.6: Load vs. mid-column deflection plot for the four beam subassemblage when loaded at the column head only.
- Figure 7.7: Load vs. mid-column minor axis deflection for load cases 1,2,3 and 6 and loading arrangement A1.
- Figure 7.8: Plot of the top and mid-column minor axis bending moments for load case 6A with beam B1 and a rigid connection.
- Figure 7.9: Minor axis bending moments at the point of failure for load case 6A with beam B1 and a rigid connection.
- Figure 7.10: Plot of load vs. minor column axis displacement for a pinned end column illustrating the adverse effect of the P- $\delta$  effect on initial disturbing moments.
- Figure 7.11: Plot of failure load ( $\alpha_{pin}$ ) vs. beam stiffness for load intensity w1.
- Figure 7.12: Plot of failure load ( $\alpha_{pin}$ ) vs. beam stiffness for load intensity w2.
- Figure 7.13: Plot of failure load ( $\alpha_{pin}$ ) vs. beam load intensity for a type B3 beam.
- Figure 7.14: Plot of failure load ( $\alpha_{pin}$ ) vs. beam load intensity for a type B2 beam.
- 
- Figure 8.1: Comparison of the mid-span deflections for a beams with simple supports and fully rigid supports.
- Figure 8.2: General equation for the rotation at the supports of beam flexibly connected beam.
- Figure 8.3: Beam and column subframe with semi-rigid beam to column connections.
- Figure 8.4: Plot of equation 8.4, the frame line, and a typical non-linear connection moment- rotation response.

- Figure 8.5: Plot illustrating the overestimation of the semi-rigid moment for a given rotation when using the linear initial tangent stiffness.
- Figure 8.6: Plot showing the 'frame line', non-linear connection moment-rotation response and the initial tangent stiffness approximation.
- Figure 8.7: The different forms of linear secant stiffness considered in the study.
- Figure 8.8 : Derivation of the modified initial tangent stiffness,  $C_{k_0}$ .
- Figure 8.9 : Arrangement of test frame F1 illustrating the serviceability loadings.
- Figure 8.10: Plot of permissible beam spans against applied load illustrating the zones where deflection considerations dominate the design.
- Figure 8.11: The three cases for the design of open section beam-columns.
- Figure 8.12: Three-dimensional interaction diagram.
- Figure 8.13: The amplification of the maximum moment due to the deformation of slender columns.
- Figure 8.14: Comparison of equation 8.20 with numerical studies.
- Figure 8.15: Buckled shape of an internal column showing the direction of connection rotation.
- Figure 8.16: Buckled shape of an external column showing the direction of connection rotation.
- Figure 8.17: Moment-rotation response of the two connections at the same level but on either side of an internal column.
- Figure 8.18: Comparison of column moments assumed in simple design and those at the point of collapse.
- Figure 8.19: Effect of column head moment reversal on the maximum span moments of an end bay beam.
- Figure 8.20: Deformed shape of an edge column when the column head moment reverses to zero.

**Figure 9.1: Possible method of increasing the restraint to the head of an existing column.**

**Figure 9.2: Installation of a tension control bolt (T.C.B.).**

**Figure A.1: Subassemblage fabrication drawing 70688/20.**

**Figure A.2: Subassemblage fabrication drawing 70688/22.**

**Figure A.3: Fabrication of pulley mechanisms used in the subassemblage tests.**

**Figure A.4: Fabrication of beam supports used in the subassemblage tests.**

**Figure B.1: Test frame fabrication drawing 70688/F1**

**Figure B.2: Test frame fabrication drawing 70688/F2**

**Figure B.3: Test frame fabrication drawing 70688/F3A**

**Figure B.4: Test frame fabrication drawing 70688/F4A**

**Figure B.5: Test frame fabrication drawing 70688/F6A**

**Figure B.6: Test frame fabrication drawing 70688/F7B**

**Figure B.7: Test frame fabrication drawing 70688/F8A**



## Acknowledgements

The work described in this volume was part of an experimental study into the behaviour of semi-rigid steel frames with semi-rigid connections. The work was principally conducted in the Civil and Structural Engineering Department at the University of Sheffield over the period October 1987 to December 1990.

The success of the project is a measure of the high calibre, commitment and enthusiasm of those who monitored and assisted me in the execution of the work. I would like to thank my supervisors, Prof. David Nethercot and Dr. Pat Kirby, for their guidance and support throughout the project, and also the technical staff in the Department for their practical advice and assistance. Of particular note is my appreciation to Mr. John Surr who was employed as the project technician. The large scale experimental tests were performed at the Building Research Establishment (B.R.E.), near Watford. I would like to thank the staff at B.R.E., notably Dr. David Moore, Mr. David White and Mr. Derick Jenkins, for their co-operation and technical expertise.

Financial support of the project was provided by the Science and Engineering Research Council (S.E.R.C.) and the Building Research Establishment. All the structural steel sections used in the project were donated by British Steel. I am of course grateful to these bodies, without whom this project would not have been possible.

I would like to thank Dr. Y.C. Wang for the use of a sophisticated finite element computer program which he developed at the University of Sheffield. The predictions of this analytical tool figure prominently in this thesis. I would also like to thank Dr. M. Celikag who conducted a series of isolated connection tests against which the connection responses observed by the author in the subassemblage and frame tests was subsequently compared.

Finally, a special thank you goes to all the staff and students in the Department of Civil

and Structural Engineering whose friendship and support have made my stay at the University a thoroughly enjoyable and rewarding experience. Of particular note is my appreciation to Jeff Peters and Kath Steer for providing my wife and I with a roof over our heads whilst I was preparing the final sections of this thesis.

## Declaration

Except where specific reference has been made to the work of others, this thesis is the result of my own work. No part of this thesis has been submitted to any University or other educational establishment for a Degree, Diploma or other qualification.

Chapter 7 of this thesis reports the findings of a detailed parametric study which was undertaken to investigate the behaviour of steel column subassemblages. Dr. Y.C. Wang, who developed the analytical tool which was used, kindly assisted in the numerical modelling of the various subassemblages which were studied. However, the concept and planning of the study, the selection of the appropriate subassemblage models and the complete appraisal of the results is solely the work of the author. The co-operation of Dr. Wang on this aspect of the work is greatly appreciated.



.....

Craig Gibbons

## Summary

This thesis describes the experimental appraisal of a series of 10 'non-sway' steel column subassemblages, each comprising a 6m long column with up to three 1.5m long beams, together with two full-scale 3 storey, 2 bay, single span, non-sway steel frames (typical overall dimensions 9m x 10m x 3.5m). The subassemblages tests were conducted in the Department of Civil and Structural Engineering at the University of Sheffield whilst the much larger frame tests were carried out at the Building Research Establishment. In all cases, the beam and column elements were connected using 'simple' bolted steelwork connections. The aim was to investigate the effect of the inherent rotational stiffness (semi-rigid characteristics) of such connections on the behaviour of steel frames in which the columns were loaded biaxially and were not restricted to in-plane deformation. The appraisal of the results from these experiments clearly shows that the stiffness of even the most modest connection can have a significant influence on the distribution of bending moments, the ultimate column capacity and deflection of frame members.

The experimental data were subsequently used to validate the predictions of a sophisticated finite-element computer program which was developed specifically to analyse 3-dimensional column subassemblages employing semi-rigid connections. This thesis documents this validation and reports the findings of an extensive parametric study which was then conducted to investigate the influence of semi-rigid connection behaviour on a wide range of subassemblage configurations.

Comparisons with the experimentally observed and analytically predicted ultimate capacities of the subassemblage and frame tests showed that 'commonly used' methods of frame design are unduly conservative. The author has therefore proposed a number of design approaches for both ultimate and serviceability limit state loading conditions which take into account the inherent benefits of semi-rigid joint action.

## Notation.

This section summarises the general notations which have been adopted throughout this thesis. Symbols which have been used once only and which are of a more specific nature have been explained at the appropriate place in the text.

$A$	Cross-sectional area.
$B$	Warping bi-moment.
$C$	Connection stiffness.
$C^*$	Effective connection stiffness.
$C_i$	Initial tangent connection stiffness.
$C_{ko}$	Initial tangent connection stiffness modified according to the ultimate moment capacity of the connection.
$C_M$	Secant stiffness corresponding to the design moment capacity of the connection.
$C_u$	Unloading connection stiffness.
$C_{ult}$	Secant stiffness corresponding to the ultimate moment capacity of the connection.
$C_{10}$	Secant stiffness corresponding with a 0.01 radian rotation of the connection.
$E$	Young's modulus for steel.
$E_r$	Reduced modulus.
$G, G_A,$ $G_B$	Joint bending stiffness ratio (U.S.A. nomenclature).
$G^*$	Effective joint bending stiffness ratio (U.S.A. nomenclature).
$I_b$	Second moment of area of the beam.
$I_c$	Second moment of area of the column.
$I_{xx}, I_{yy}$	Second moment of area about the x-x and y-y section axes.

$J$	Torsion constant.
$k$	Effective length factor.
$K$	Bending stiffness.
$K_b$	Bending stiffness of a beam.
$K_{bc}$	Bending stiffness of a beam including the connection stiffness component.
$K_c$	Bending stiffness of a column.
$K_{tot}$	Total rotational stiffness at a column node.
$L$	Length.
$L_b$	Beam length.
$L_c$	Column length/height.
$L_e$	Effective length ( $L_e = kL$ ).
$M$	Applied bending moment.
$M_p$	Plastic moment.
$M_{sr}$	Bending moment at a semi-rigid connection.
$M_x, M_y$	Bending moments applied with respect to the x-x and y-y section axes.
$P$	Applied axial load.
$P_{crit}$	Critical load.
$P_{cy}, P_{cx}$	Ultimate axial resistance of a section for buckling with respect to the x-x and y-y section axes.
$P_{des}$	Ultimate axial load predicted from design.
$P_E$	Euler buckling load.
$P_{squash}$	Squash load of a section.
$P_{test}$	Ultimate axial load observed specifically in an experimental test.
$p_y$	Yield stress of steel.

$w$	Uniformly distributed load.
$Z_{xx}, Z_{yy}$	Elastic section modulus with respect to the x-x and y-y axes of a section.
$\alpha_{pin}$	Failure load of a column non-dimensionalised with respect to the failure load of the same column with pinned ends.
$\alpha_{res}$	Failure load of a column non-dimensionalised with respect to the failure load of the same column when loaded at the column head only.
$\beta_{pin}$	Connection performance indicator.
$\delta_{pin}$	Deflection at the centre of a simply supported beam.
$\delta_{rigid}$	Deflection at the centre of a beam rigidly connected to the columns.
$\delta_{sr}$	Deflection at the centre of a beam semi-rigidly connected to the columns.
$\delta_{x,y,z}$	Deflections in the direction of the x,y and z Cartesian axes.
$\epsilon$	Strain.
$\theta_{x,y,z}$	Rotations with respect to the x, y and z Cartesian axes.
$\mu$	Ratio of the semi-rigid moments ( $M_{sr}$ ) to the rigid moments ( $M_{rigid}$ ) in a frame.
$\mu_{ave}$	Average of the $\mu$ factors at each end of a beam.
$\sigma$	Direct stress.
$\phi_b$	Rotation at the support of a beam.
$\phi_c$	Rotation of a column at the node point.
$\phi_{pin}$	Rotation at the support of a simply supported beam.

# Chapter 1

## Introduction and Background

### Work.

#### 1.1 Introduction

It is widely appreciated that 'non-sway' steel frames designed with moment resisting connections (i.e. connections which allow the transfer of bending moments between the beams and column) will result in lighter structural frames. However, it is often argued that any savings in the weight of such frames is offset by the increased fabrication cost of potentially complex connection details. For this reason, the most common method of design of 'non-sway' steel framed structures is the so called 'simple construction' design method [1.1]. This method assumes that the beam to column connections behave like simple 'pins', making the fabrication of such connections as simple as possible.

It is perhaps less widely appreciated that typical fabricated connections resulting from a 'simple' frame design (e.g. web cleats, flange cleats and flush end-plates), do in fact possess an inherent degree of rotational stiffness. Such simple connections may therefore be considered as semi-rigid, i.e. they possess a rotational stiffness which is intermediate

between that of a true pinned connection (zero stiffness), and that of a fully fixed connection (infinite stiffness). Therefore, the inclusion of the semi-rigid characteristics of simple connections into steel frame design has the potential of producing lighter, more efficient structures - in which an increase of actual frame stiffness is realised - without necessarily increasing the connection fabrication costs.

The aim of this research project was to address this latter point by performing both experimental and analytical studies, in which the general condition of 'non-sway', three-dimensional behaviour was considered to illustrate, and ultimately quantify, the potential benefits of semi-rigid connection response. Finally, the aim was to collate these observations, together with those of other researchers, and formulate a convenient and coherent method of semi-rigid, 'non-sway' frame design which could be utilised by practising steelwork designers.

The individual chapters in this thesis correspond with the major components of the research project. Chapter 2 presents a detailed report on the testing of a series of 10 full-scale column subassemblage specimens which was performed at the University of Sheffield. In addition to presenting and discussing the results, the findings of an initial parametric study which was carried out to determine the optimum experimental test conditions is also reported. In addition to the subassemblage tests, an experimental investigation was performed on two full-scale, one bay, two span, two/three storey semi-rigid frames. These particular tests were performed in the Large Structures Testing Laboratory at the Building Research Establishment near Watford. A description of the tests, together with a discussion of the results, is presented in Chapter 5.

The three-dimensional nature of the experimental studies, introduced above, presented a number of challenges when selecting appropriate means of instrumentation. Chapter 3 of the thesis is devoted to this problem and traces the development of the three-dimensional force and displacement measurement systems which were devised specially for this project.



One of the specific objectives of the subassemblage tests was to provide the necessary experimental data with which to validate the predictions of a sophisticated finite element computer program [1.2]. Chapter 4 presents a 'one-to-one' comparison of the experimental results and those predicted using this analytical tool. Having verified the ability of the computer program to predict restrained beam-column behaviour, the author then used the program to investigate the influence of a wide range of parameters on a large number of subassemblage models. The description and findings of this parametric study are presented in chapter 7.

As discussed above, one of the principal aims of the study was to develop methods of semi-rigid design which could be used by practising steelwork designers. This topic is addressed in chapter 8 which presents a brief overview of design techniques, past and present, and introduces those methods proposed by the author which appear to achieve a reasonable compromise between accuracy of approach and ease of use.

At all stages in this project, a number of significant observations have been made which warrant further investigation. For the benefit of fellow researchers, these aspects of the work have been collated in chapter 9 as a series of recommendations for future study.

## **1.2 Historical background.**

This section presents a relatively brief historical background to the subject and introduces some of the key developments that have played a significant role in advancing the understanding of column behaviour. For clarity, the historical review has concentrated on the main subject areas of pinned-end columns, end-restrained columns and frame tests. It should be noted that the historical appraisal of certain aspects of the work have been reported in more detail in the appropriate chapters where the specific nature of the review has more relevance (e.g. development of design equations, chapter 8, and instrumentation techniques, chapter 3).

### 1.2.1 The pinned-end column.

The corner-stone of column theory is the Euler column, a mathematically straight, prismatic, pinned-end, perfectly centrally loaded strut which is slender enough to buckle at a stress below the proportional limit of the material. The buckling load (also known as the critical load, bifurcation load or Euler load) is given by:-

$$P_E = \frac{\pi^2 EI}{L^2} \quad (1.1)$$

where  $EI$  is the elastic flexural stiffness and  $L$  is the length of the column. This equation forms the basis of many modern strut theories and design approaches with  $P_E$  being the reference load against which the strength of actual columns is compared.

The pinned-end column also represents the classical reference datum on which many experimental appraisals of columns have been based. Early column strength equations (circa 1840) were of an empirical nature, based on the results of experimental studies on nominally pinned-end columns. However, the limitations of such equations were soon realised and an approach with a more theoretical base was sought.

It was apparent that the behaviour of real steel columns was influenced by geometrical imperfection and the presence of internal stress distributions. As early as 1908, it was proposed that residual stresses resulting from the cooling of hot rolled steel sections was the cause of an observed reduction in the strength of columns with an intermediate slenderness [1.3]. The influence of residual stresses on the buckling strength of both rolled members and welded plates was subsequently noted by others [1.4, 1.5].

Systematic research into the effects of residual stress on column behaviour was initiated in the late 1940's under the guidance of Research Committee A of the Column Research Council (C.R.C.) [1.6, 1.7, 1.8]. The culmination of these efforts resulted in the pub-

lication of Technical Memorandum No. 1 which proposed the basic 'C.R.C. Column Strength Curve'. The formula was derived using the concept of an effective tangent modulus which took into account the effects of residual stress and other material non-linearities, but which ignored the effect of initial deformations. A similar initiative had been orchestrated by the Steel Structures Research Committee with a view to reviewing the then present methods of design and applying 'modern' theory to the design of steel structures. The results of this particular Committees work formed the basis of the British Standard, BS 449 'Specification for the use of structural steel in buildings' [1.9], first published in 1932. The increasing use of higher grade steels prompted the publication of a second edition of the C.R.C. guide (1966) which noted the importance of initial deflections in the design of pinned-end columns.

Further research on the effects of residual stresses and initial deformations was brought about by commercial demand for an ever increasing range of structural section types. Investigations of column imperfections by Bjorhovde and Tall [1.10, 1.11], and in Europe by Beer and Shultz [1.12], led to the computation of 112 different strength curves covering a variety of column shapes and material strengths. Comparisons of the appropriate curve with full scale test data had shown discrepancies, in terms of strength prediction, of less than 5%. For the purposes of design, these 112 curves were categorised, primarily depending on the type of section, into a maximum of five distinct design curves. This concept of 'multiple column curves' is much in evidence in a number of current International steelwork design codes.

A more comprehensive historical review of the research into pinned-end columns can be found in references 1.13 and 1.14, whilst a summary of the many pinned- end column tests which have been performed is presented in reference 1.15.

### 1.2.2 End-restrained columns.

A review of experimental pinned-end column tests performed between 1880 and 1925 by the Special Committee on Steel Column Research of the American Society of Civil Engineers, indicated that the columns had behaved almost as if their remote ends had been fixed [1.16]. This was attributed to the frictional restraint present in the inadequate spherical supports at the remote ends of the columns. Although unintentional, this experimental error did alert researchers of the time to the beneficial effect of end-restraint.

The obvious disparity in the behaviour of columns with pinned and rigidly fixed support conditions was addressed in the early C.R.C. and BS 449 design formulae, introduced in section 1.2.1, by considering the concept of effective length. Here, the column is designed as a pinned-end column of length  $KL$ , which has the same strength as the restrained member of length  $L$ . For combinations of the extreme end conditions of pinned and rigidly fixed, the values of the effective length factor,  $K$ , were well known.

Whilst the above simple method for assessing the effective length of columns is widely used, and features in most of the present codes of practice for steelwork design, it does have a number of accepted limitations. For a column with end conditions which fall between the extremes of pinned and fully fixed, which applies to all columns in 'real' frames, the selection of an appropriate effective length is usually left to the intuition of the designer. However, it was realised that, in the case of rigid frames, the restraint conditions at the end of the columns were directly related to the stiffness of the inter-connecting beams. This led to the publication of design nomographs, also known as alignment charts, which enabled a more accurate prediction of the critical load, and hence effective length, of columns in rigid frames.

In the early 1960's, Lay and Galambos [1.17] carried out experimental studies on a series of seven column subassemblages in which the beams were rigidly connected to the column (welded joints). The purpose of this study was to provide experimental verification of

restrained column theories proposed for use in the plastic design of multi-storey steel frames [1.18]. Tests with similar objectives were recently performed on biaxially loaded continuous columns by Cuk et al [1.19].

Arguably the most significant study of restrained columns with rigid connections was that performed by Gent and Milner [1.20]. Using machined scale models of column subassemblages under biaxial loading conditions, they demonstrated the phenomenon of column moment reversal (moment shedding). Here, the beams which initially applied the disturbing moments, restrained the rotation at the column ends as failure was induced. The results of the study had shown that columns with large initial disturbing moments failed at a higher load than the same column with pinned-end supports. The inference was that the effect of disturbing moments on columns in rigid frames was less than that implied by the design methods of the time.

It had long been realised that the benefits, in terms of enhanced column restraint and advantageous distributions of beam bending moments, which had been observed for rigidly connected frames could be applied to frames with semi-rigid connections. It is evident that strictly speaking all connections fall into this category as no real connection can achieve the idealised performance of the extremes of pinned and fully rigid. To stimulate research in the design and analysis of semi-rigid frames, the Structural Stability Research Council produced a comprehensive bibliography [1.21]. This document referenced all the experimental connection tests that had been performed since the first recorded test by Wilson and Moore on riveted connections in 1917 [1.22]. Other compilations of experimental connection data have been produced by Nethercot [1.23] and Goverdhan [1.24].

The principal measure of connection response is the moment-rotation relationship, also known as the  $M-\phi$  curve. Figure 1.1 shows the typical  $M-\phi$  curve for a range of simple connections. It is evident that the relationship is non-linear, with the tangent to the curve representing the connection stiffness at that loading level. The smaller slope of

the web-cleat curve compared to that of the extended end-plate therefore represents the lower stiffness of this particular connection.

The increased interest into semi-rigid research prompted further experimental studies on isolated connection response [1.25, 1.26, 1.27]. These included assessments of the out-of-plane and torsional behaviour [1.28] and the possible detrimental effects of a 'lack of fit' of connection components [1.29]. The recent advances in computer technology, combined with the demand for large amounts of connection data, prompted a number of researchers to formulate finite element analytical models to predict connection  $M-\phi$  behaviour [1.30, 1.31, 1.32]. However, the complexity of modelling the precise interaction between connection components has meant that such analytical models are inaccurate, and at best of limited application. Therefore, at present, experimental testing remains the most accurate and reliable means of assessing the behaviour of connections.

One of the first experimental investigations of the effect of 'simple' semi-rigid connections on column behaviour was performed by Bergquist [1.33]. He conducted tests on a series of five 'I' shaped, two-dimensional, column subassemblages in which the beams were connected to the column by web cleat connections. Whilst the results from these tests clearly showed the potential benefits of semi-rigid joint action, the particular 'self-contained' turnbuckle arrangement which was used to load the beams resulted in an unrealistic pattern of loads. This deficiency was subsequently addressed by Davison [1.34] who performed a series of tests on full scale, 2-dimensional, non-sway column subassemblages and frames using a range of connection types and 'realistic' loading arrangements.

In recent years, researchers have developed sophisticated finite element analysis techniques to investigate the behaviour of columns restrained by semi-rigid connections, notably Chen [1.35], Jones et al. [1.36], Razzaq and Chang [1.37] and Rifai et al. [1.38]. These analytical tools, which were restricted to in-plane response, enabled researchers to perform parametric studies to examine the effects of column imperfections, slender-

ness and connection type. Figure 1.2, extracted from reference 1.34, shows the influence of different 'simple' semi-rigid connections on columns of different slendernesses. It is evident that the most marked increase in strength occurs where the columns have a moderate to high slenderness.

A finite element computer program was recently developed by Wang [1.2] which was capable of analysing 3-dimensional column subassemblages with semi-rigid connections. This represented a significant advance in the appraisal of restrained columns. At the time the program was developed (1989), experimental data on the behaviour of 3-dimensional column subassemblages incorporating flexible joints, with which to verify the program, was not available. However, the program had successfully predicted the behaviour of the rigidly connected, biaxially loaded column subassemblages [1.39] investigated by Gent and Milner [1.20]. One of the aims of the research project reported in this thesis was to generate the necessary experimental data and to carry out a thorough verification of this particular program.

### 1.2.3 Frame tests

One of the major aspects of this research study was the testing of two full scale, three dimensional, non-sway frames. This section presents a brief review of some of the most significant experimental studies of frame behaviour which have been conducted in the past.

The first appraisals of steel frame behaviour were performed on existing buildings in the United States in the 1920's. Specifically, measurements were made of the strains in the columns of the Equitable Building, Des Moines, Iowa [1.40], and the American Insurance Union Building, Columbus, Ohio [1.41]. The results of these investigations had shown that the forces in the columns were considerably higher than expected. However, these

findings have since been questioned due to the manner in which the steel strains were measured [1.42].

In Britain, members of the Steel Structures Research Committee were conscious of the fact that the Code of Practice which they had drafted [1.9], did not reflect the true behaviour of real framed structures. Shortly after the draft had been published (1931), they initiated the investigation of a series of existing 'real' steel structures and purpose made large scale frames. The existing structure was the Geological Museum, South Kensington, London [1.43]. The building was five storeys high and incorporated nominal riveted beam to column connections. Strains, and hence forces, were measured with considerable difficulty by monitoring the 'gap' between reference points over a 12 inch gauge length at 54 different locations around the frame. The large scale model study was conducted at the Building Research Station and comprised a three storey, two bay, one span frame constructed throughout using 8" x 4" steel joists [1.44]. The connections in this instance comprised a top and bottom angle cleat with bolt fasteners. Although in both cases the connections were considered 'light', both the frames behaved almost as if they were rigidly connected.

The advent of improved strain measurement techniques meant that 'real' steel frames could be appraised during the construction stage with the minimum of disruption. Studies were therefore extended to investigate the Cumberland Hotel at Marble Arch [1.45] - a conservatively designed structure with heavy beam to column connections, the Euston Offices [1.46] - a more orthodox structure, and a block of London flats of very light construction [1.47]. In each case, the frames were shown to behave almost as if the connections were fully rigid. This was at variance with the assumptions underlying the BS 449 method of design.

In 1964, a Joint Committee of the Institute of Welding and the Institution of Structural Engineers reported a simplified design method for fully rigid multi-storey welded steel frames [1.48]. To verify the method, a full scale, three storey, two bay, one span rigid



frame was tested at the Building Research Station. The results of this test are presented in reference 1.49. A further development of the design method permitted the use of higher grade steels and accordingly a second more extensive test was performed [1.50]. A series of 19 tests on rigidly jointed, 3-dimensional, three storey scale model frames were also performed at the Building Research Station by Taylor [1.51]. The aim of these tests was to verify a simplified collapse criterion for continuous columns.

In the United States a series of four, two-dimensional, two storey, two bay rigidly connected braced frames was investigated by Yura and Lu [1.52]. The results of the tests had shown that in each case the failure loads were greater than those predicted from plastic theory with a discrepancy of less than 4%. One significant observation was that it appeared that the sequence of plastic hinge formation had little or no effect on the ultimate load. A comprehensive list of rigid frame tests which have been performed in the United States between the 1940's and 1960's can be found in reference 1.53.

Experimental tests on the behaviour of semi-rigid steel frames are much less common and have invariably been conducted in the recent past. Of note are tests by Stelmack et al [1.54] in which the performance of two storey, one bay and one storey, two bay frames was investigated. The frame connections comprised a flange and seat cleat and in each case sway was permitted. The aim of the study was to investigate serviceability behaviour, in which the frames remained totally elastic, and to determine whether frames 'shake down' under repeated cyclic load. The other notable experimental study is that by Davison [1.34] in which the behaviour of two full-scale, three storey, two bay frames was investigated. These particular frames were non-sway and incorporated 'simple' cleated beam to column connections.

## References.

- 1.1 British Standard: BS 5950 *'The structural use of steelwork in buildings, Part 1, Code of practice for design in simple continuous construction : Hot Rolled Sections'*, British Standards Institution, London, 1990.
- 1.2 Wang, Y.C., *'Ultimate strength analysis of three-dimensional structures with flexible restraints'*, Ph.D. Thesis, Department of Civil and Structural Engineering, University of Sheffield, U.K., June 1988.
- 1.3 Howard, J.E., *'Some results of the tests of steel columns in progress at the Watertown Arsenal'*, Proc. Am. Soc. Test. Mater., Vol.8, 1908, p. 336.
- 1.4 Salmon, E.H., *'Columns'*, Oxford Technical Publishers, London, 1921.
- 1.5 Madsen, I., *'Report of crane girder tests'*, Iron Steel Eng., Vol. 18, No. 11, 1941, p. 47.
- 1.6 Osgood, W.R., *'The effect of residual stress on column strength'*, Proc. 1st U.S. Natl. Cong. Appl. Mech., June 1951, p. 415.
- 1.7 Yang, H., Beedle, L.S. and Johnston, B.G., *'Residual stress and the yield strength of steel beams'*, Weld J., Res. Suppl., Vol. 31, 1952, pp. 224-225.
- 1.8 Beedle, L.S., and Tall, L., *'Basic column strength'*, Am. Soc. Civil Engrs., Journ. Struct. Div., Vol. 86, No. ST7, 1960, pp. 139-173.
- 1.9 British Standard BS 449 , *'The use of structural steel in buildings'*, The British Standards Institution, London, 1932.
- 1.10 Bjorhovde, R., *'Deterministic and probabilistic approaches to the strength of steel columns'*, Ph.D. Dissertation, Lehigh University, Bethlehem, Pa., May 1972.
- 1.11 Bjorhovde, R. and Tall, L., *'Maximum column strength and the multiple column curve concept'*, Rep. No. 337.29, Lehigh University, Fritz Eng. Lab., Bethlehem, Pa., October 1971.
- 1.12 Beer, H. and Schultz, G., *'Theoretical basis for the european column curves'*, Constr. Met., No. 3, 1970, p. 58.
- 1.13 Ballio, G. and Mazzolani, F.M., *'Theory and design of steel structures'*, Chapman and Hall, London, 1983, pp. 371-378.
- 1.14 *'Guide to stability design criteria for metal structures'*, 4th Edition, Ed. T.V. Galambos, Wiley-Interscience, 1988.

- 1.15 Fukumoto, Y., Nethercot, D.A. and Galambos, T.V., '*Experimental data for the buckling of steel structures - NDSS stability of metal structures*', 3rd. Int. Colloq. S.S.R.C., Toronto, May 1983, pp. 609-630.
- 1.16 Progress Report of the Special Committee on Steel Column Research, Trans., Am. Soc. Civil Engrs., Vol. 89, 1926, pp. 1526-1536.
- 1.17 Lay, M.G. and Galambos, T.V., '*The Experimental behaviour of restrained columns*', Welding Research Council, Bulletin No. 110, November 1965, pp. 17-38.
- 1.18 Ojalvo, M. and Levi, V., '*Columns in planar continuous structures*', Proc., Am. Soc. Civil Engrs., Journ. Struct. Div., 89, STI, Feb. 1963.
- 1.19 Cuk, P.E., Rogers, D.F. and Trahair, N.S., '*Inelastic buckling of continuous steel beam-columns*', Journ. Construct. Steel Research, Vol. 6, No.1, 1986, pp. 21-50.
- 1.20 Gent, A.R. and Milner, H.R., '*The ultimate load capacity of elastically restrained H-Columns under biaxial bending*', Proc. Inst. Civil Engrs., No. 41, 1968, pp. 685-704.
- 1.21 Structural Stability Research Council, '*Connections bibliography*', Task Group 25, Third Draft, March 1987.
- 1.22 Wilson, W.M. and Moore, H.F., '*Tests to determine the rigidity of riveted joints in steel structures*', University of Illinois, Engineering Experimental Station, Bulletin No. 104, Urbana, USA, 1917.
- 1.23 Nethercot, D.A., '*Steel beam to column connections - A review of test data and their applicability to the evaluation of the joint behaviour of the performance of steel frames*', C.I.R.I.A. Project Record, RP 338, 1985.
- 1.24 Goverdhan, A.V., '*A collection of experimental moment-rotation curves and evaluation of prediction equations for semi-rigid connections*', Masters Thesis, University of Vanderbilt, Nashville, Tennessee, December 1983.
- 1.25 Davison, J.B., Kirby, P.A. and Nethercot, D.A., '*Rotational stiffness characteristics of steel beam-to-column connections*', Journ. Construct. Steel Research, No.8, 1987, pp. 17-54.
- 1.26 Aggarwal, A.K. and Coates, R.C., '*Moment-rotation characteristics of bolted beam-to-column connections*', Journ. Construct. Steel Research, Vol.6, No. 4, 1986, pp. 303-318.

- 1.27 Moore, D.B. and Sims, P.A.C., '*Preliminary investigation into the behaviour of extended end-plate steel connections with backing plates*', Journ. Construct. Steel Research, No. 6, 1986, pp. 95-122.
- 1.28 Celikag, M., '*Moment-rotation behaviour of steel beam-to-column connections.*', Ph.D. Thesis, Department of Civil and Structural Engineering, University of Sheffield, U.K., February 1990.
- 1.29 Davison, J.B., Kirby, P.A. and Nethercot, D.A., '*Effect of lack of fit on connection restraint*', Journ. Construct. Steel Research, Vol. 8, 1987, pp. 55-69.
- 1.30 Frye, M.J. and Morris, G.A., '*Analysis of flexibly connected steel frames*', Canadian Journal of Civil Engineers, September 1975, 2, No. 3, pp. 280-291.
- 1.31 Lipson, S.L. and Hague, M.I., '*Elastic-plastic analysis of single-angle bolted-welded connections using the finite element method*', Composites and Structures, December 1978, No. 6, pp. 533-545.
- 1.32 Krishnamurthy, N., Huang, H., Jeffrey, P.K. and Avery, L.K., '*Analytical  $M - \phi$  Curves for end-plate connections*', Am. Soc. Civil Engrs., January 1979, p. 133.
- 1.33 Bergquist, D.J., '*Tests on columns restrained by beams with simple connections*', Report No. 1, American Iron and Steel Institute Project No. 189, Department of Civil Engineering, The University of Texas, Austin, Texas, January 1977.
- 1.34 Davison, J.B., '*Strength of beam-columns in flexibly connected steel frames*', Ph.D. Thesis, Department of Civil and Structural Engineering, University of Sheffield, U.K., June 1987.
- 1.35 Chen, W.F., '*End restraint and column stability*', Am. Soc. Civil Engrs., Journ. Struct. Div., Vol. 106, No. ST11, November 1980, pp. 2279-2295.
- 1.36 Jones, S.W., Kirby, P.A. and Nethercot, D.A., '*Effect of semi-rigid connections on steel column strength*', Journ. Construct. Steel Research, Vol. 1, No. 1, 1980, pp. 38-46.
- 1.37 Razzaq, Z. and Chang, J.G., '*Partially restrained imperfect columns*', additional papers, Conference on Joints in Structural Steelwork, Teesside, April 1981, Pentech Press Ltd., pp. 6.57-6.80.
- 1.38 Rifai, A.M., '*Behaviour of columns in sub-frames with semi-rigid joints*', Ph.D. Thesis, Department of Civil and Structural Engineering, University of Sheffield, U.K., June 1990.

- 1.39 Wang, Y.C. and Nethercot, D.A., '*Ultimate strength analysis of three-dimensional column subassemblages with flexible connections*', Journ. Construct. Steel Research, Vol. 9, No. 4, 1988, pp. 235-264.
- 1.40 Fuller, A.H., '*Measurements of stresses in four steel columns of the Equitable Building, Des Moines, Iowa*', Iowa State College of Agriculture and Mechanic Arts, Engineering Experiment Station, Bulletin No. 72, Ames (Iowa), 1924.
- 1.41 Morris, C.T., '*Dead load stresses in the columns of a tall building*', Ohio State University, Engineering Experimental Station, Bulletin No. 40, Columbus, 1928.
- 1.42 Baker, J.F., '*Early steelwork research*', Journ. Construct. Steel Research, Vol.1, No.1, September 1980, pp. 3-9.
- 1.43 Faber, O., '*Report on observed stresses in a steel frame structure at the Museum of Practical Geology, South Kensington*', Second Report of the Steel Structures Research Committee, H.M.S.O., London 1934, p. 44-60.
- 1.44 Baker, J.F., '*An investigation of the stress distribution in a number of three-storey building frames*', Second report of the Steel Structures Research Committee, H.M.S.O., London, 1934, pp. 241-318.
- 1.45 Baker, J.F., '*An investigation of the stress distribution in the steel framework of a modern hotel building*', Final report of the Steel Structures Research Committee, H.M.S.O., London, 1936, pp. 8-139.
- 1.46 Baker, J.F., '*An investigation of the stress distribution in the steel framework of a modern office building*', Final report of the Steel Structures Research Committee, H.M.S.O., London, 1936, pp. 140-227.
- 1.47 Baker, J.F., '*An investigation of the stress distribution in the steel framework of a modern residential flats building*', Final report of the Steel Structures Research Committee, H.M.S.O., London, 1936, pp. 228-249.
- 1.48 Joint Committee Report on fully rigid, multi-storey, welded steel frames. The Inst. Struct. Engrs., December 1964.
- 1.49 Wood, R.H., Needham, F.H. and Smith, R.F., '*Tests on a multi-storey rigid steel frame*', The Structural Engineer, Vol. 46, No. 4, April 1968, pp. 107-120.
- 1.50 Smith, R.F. and Roberts, E.H., '*Test of a full-scale rigid-jointed multi-storey frame in high-yield steel (BS 4360, Grade 50)*', B.I.S.R.A. Open Report, Report No. EG/A/17/71.

- 1.51 Taylor, D.A., '*An experimental study of continuous columns*', Proc. Inst. of Civil Engrs., Vol. 53, 1972, pp. 1-17.
- 1.52 Yura, J.A. and Lu, L.W., '*Ultimate load tests on braced multi-storey frames*', Am. Soc. Civil Engrs., Journ. Struct. Div., Vol. 95, No. ST10, October 1969, pp. 2243-2264.
- 1.53 Yarimci, E., Yura, J.A. and Lu, L.W., '*Techniques for testing structures permitted to sway*', Experimental Mechanics, August 1967, pp. 321-331.
- 1.54 Stelmack, T.W., Marley, M.J. and Gerstle, K.H., '*Analysis and tests of flexibly connected steel frames*', Journ. of Struct. Enging., Vol.112, No.7, July 1986, pp. 1573-1588.

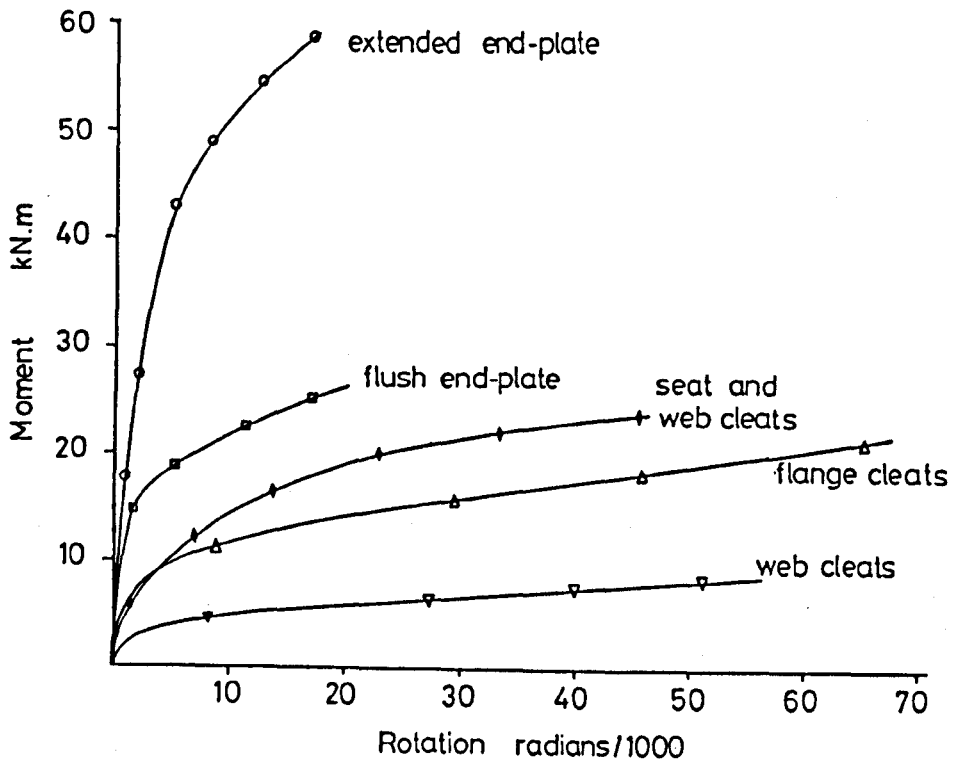


Figure 1.1: Moment-rotation response for a range of 'simple' connection types.

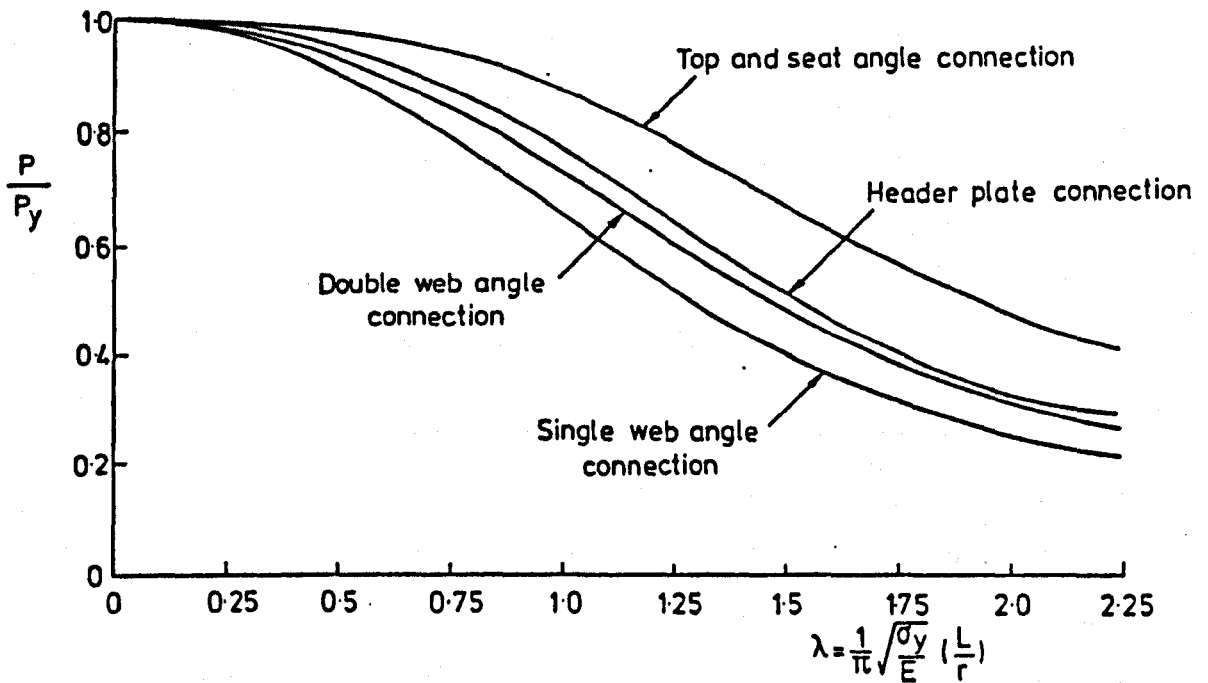


Figure 1.2: Influence of different 'simple' connection types on the strength of columns of different slenderness.

## Chapter 2

# The subassemblage tests.

### 2.1 Introduction

A subassemblage may be considered as a limited isolated frame, or a collection of members taken from a more extensive structure. The analysis of appropriate subassemblages represents a convenient way of simplifying the complex analysis of complete structures whilst maintaining a reasonable approximation to the 'in-frame' behaviour. In terms of experimental studies, the testing of subassemblage specimens has the advantage over individual isolated elements in that it permits the effects of member interaction to be investigated without the expense associated with the full-scale testing of the complete structure. For this reason, subassemblage specimens have been incorporated into many experimental studies of structural frame behaviour [2.1, 2.2, 2.3].

This section of the thesis reports on the experimental investigation of a series of 10 such subassemblage specimens. As well as documenting the experimental observations, the extensive initial parametric studies which were undertaken to assess and minimise potential errors in the complex experimental test set-up are also reported. The final sections of the chapter present an in-depth appraisal of the results obtained and discusses the



most important findings from the tests.

## **2.2 Conceptual design of the subassemblage tests specimens**

In addition to providing a direct comparison against the results from tests on isolated connections (chapter 6) and complete frames (chapter 5), the aim of the subassemblage tests was to validate the predictions of a sophisticated finite element computer program developed specifically for analysing 3- dimensional restrained beam columns [2.4] (chapter 4). The availability of the program at the planning stage provided an opportunity to conduct a parametric study which investigated the predicted behaviour of the proposed subassemblage specimens prior to fabrication. Specifically, the program was used to develop a general subassemblage configuration which failed at manageable loads, which deformed within the limits of the available instrumentation devices and which was relatively insensitive to possible variations in the performance of the experimental boundary conditions.

### **2.2.1 Selection of subassemblage members.**

It had been decided that the section sizes used to fabricate the subassemblages specimens should be similar to those used in other recent studies of flexibly connected steel structures [2.5, 2.6]. This maintained a common theme of study and enabled close comparisons to be made between various aspects of work carried out by independent researchers. A 152 x 152 x 23 UC section was used to fabricate the column and 254 x 102 x 22 UB

sections were used for the beams. The nominal geometric properties of these sections were incorporated into the basic analytical model which was used to carry out the initial parametric studies (figure 2.1). To allow the relative effect of various parameters to be observed, the same beam loading arrangement, initial column out-of-straightness and material properties were incorporated into all the preliminary finite element models.

### 2.2.2 Column base fixity.

Initially, it was presumed that the subassemblage columns would be supported at their base by a 'pin' type connection. Such a support condition would correspond to the base condition assumed by many designers of non-sway steel framed structures.

The behaviour of structural steel columns with 'pinned' support conditions has been investigated by many experimental researchers. A report on the findings from experiments on pinned-end columns performed prior to 1925 [2.7], concluded that the frictional restraint present in the spherical seat supports had a profound effect on column behaviour. In some instances, the rotational restraint at the simple supports caused the columns to behave almost as if they were fully fixed at their ends. Since the time of these early studies experimental researchers have developed support arrangements and test procedures which restrict the potential support restraint to a minimum. Support details which have been used include crossed knife-edge joints [2.8], multiple bearings [2.9] and hydraulically pressurised bearing systems [2.10, 2.11]. These complex, and often expensive, devices reflect the difficulty of producing connections which closely represent the ideal of true zero rotational stiffness. It was hoped that the use of such complex and expensive 'frictionless' base supports could be avoided. A parametric study was therefore carried out specifically to assess the influence on column behaviour of any rotational restraint which may be present in a more modest base connection.

In total, 12 analytical models were studied with linear major and minor axis base stiffnesses ranging from that of a true pin (zero stiffness) to a fully fixed condition (infinite stiffness). In this particular instance, the column length was 6.0m and the characteristics of a web cleat were assumed for the beam to column connections.

Figure 2.2 shows the resulting plot of predicted percentage increase in failure load for different linear base stiffnesses over that for a pinned base column. As expected, the plot shows that small variations in base stiffness have a significant effect on the failure load of columns with relatively flexible base connections. Any small restraint which may be present in the experimental simulation of a true pin connection would, therefore, have a significant effect on the performance of the subassembly. From an experimental point of view, the plateau region of the plot is of greater interest. This represents a region for which the failure load is relatively insensitive to modest variations in the stiffness of the base connection. The lower limit of the plateau corresponds to a base bending stiffness of approximately 3000 kNm/radian. Experimental studies by Picard et al. [2.12, 2.13] have shown that under the influence of axial load, modest base-plate connections possess a comparable degree of rotational restraint. The rotational stiffness of a four bolt base plate connection, connected to a 200mm x 200mm column section, studied by Picard is shown on the plot in figure 2.2 for axial loads of 100 kN and 450 kN. It is evident that the predicted failure load is relatively insensitive to variations in the bending stiffness of such a connection.

On the basis of this parametric study a fixed, or near fixed, base connection was adopted for the base support in the series of subassembly tests. Any deviation in the true, or measured, characteristics of the connection would therefore not be expected to have an appreciable effect on either the subassembly performance or the accuracy of the subsequent detailed analytical modelling of the test.

### 2.2.3 The influence of column length

Obviously, the length of the column would have a profound effect on the ultimate sub-assembly carrying capacity. As it was intended that all the columns in the experimental study would be the same length, initial studies were carried out to determine the most appropriate column length which could be adopted throughout.

The basic analytical model described above was analysed with column lengths of 3.0m, 4.0m and 6.0m. using the moment-rotation characteristics of a range of different connection types. These included the four connection types which were ultimately to be included in the experimental study - web cleat, flange cleat, web and seat cleat and flush end plate - plus the hypothetical extremes of a true pin (zero stiffness) and fully fixed (infinite stiffness). The model used in this particular study had a fully fixed column base condition as recommended from the results of the study described in the previous section. The predicted ultimate loads,  $P_u$ , and the mid-column major axis deflection at failure,  $d_c$ , for the above cases are presented in table 2.1. As predicted from classical strut theory, the ultimate load carrying capacities decrease for increasing column lengths. The range of failure loads for each particular column,  $P_{u(fixed)} - P_{u(pin)}$ , increases as the length of the column is increased. This latter point is significant. Experimental tests could be carried out to identify the influence of each particular connection type on a column 6.0m long, where the range of failure loads is relatively large. However, experimental studies of a 3.0m long column, where the range of failure loads is small, would yield little information on the relative performance of the individual connections types. A similar argument could be extended to the observed deformations at the centre of the column.

This apparent increased connection restraint offered to slender columns, or more appropriately to columns where the  $P_u/P_{squash}$  ratio is significantly less than 1, is fundamental to semi-rigid theory and has been investigated by a number of researchers [2.14, 2.15]. The implications of this phenomenon have been discussed in greater detail in chapter 8

of the thesis which deals with semi-rigid design considerations. However, for the purpose of the initial conceptual design of the subassembly tests, these results suggested that a 6.0m long column should be adopted for the experimental test specimens. At this length, the column slenderness,  $L/r_{yy}$ , would be at the upper end of the range which would be usual in real column design. However, due to the fixed base condition and the rotational restraint from the interconnecting beams, the effective slenderness  $L_E/r_{yy}$  was significantly less, typically in the range 85 to 120 depending on the type of connection employed.

It is interesting to note from the data presented in table 2.1 that the predicted failure of the subassembly employing flush end-plate connections was indistinguishable from that employing fully rigid connections. It would appear therefore that there is a limit on the stiffness/strength of a connection for which a benefit can be observed in terms of column capacity. On the basis of this result, it was decided that the flush end-plate would be the stiffest connection considered in the experimental subassembly study.

#### 2.2.4 The influence of beam length.

The magnitude of the rotational restraint offered to the column by the connecting beams is dependent on the magnitude of both the stiffness of the beam,  $K_{beam}$ , and the stiffness of the beam to column connection,  $K_{con}$ . The total effective rotational stiffness,  $K_{bc}$ , due to the combination of these individual stiffness components, as proposed by Galambos [2.16], can be written in the form:

$$K_{bc} = \frac{K_{beam}K_{con}}{K_{beam} + K_{con}} \quad (2.1)$$

It is evident from the above equation that for a low beam stiffness, the flexibility of the beam dominates. As a result, varying the stiffness of the connection of a relatively flexible beam has little effect on the total rotational restraint. A study was therefore

carried out to ensure that the beam lengths proposed for the subassemblage tests resulted in sufficient variations to enable the effect of the different semi-rigid connection types to be observed experimentally.

Analytical studies were carried out on a range of beam to column connection types in subassemblages with beam lengths of 1.5m, 2.0m, 3.0m and 4.0m. The boundary condition envisaged at the remote end of each of the beams permitted displacement in the direction of the column axis, whilst preventing both in-plane and twist rotations. A beam with such a support condition will possess an in-plane bending stiffness equivalent to that of a beam spanning twice the length. The vertical axis through the support therefore effectively represented the line of symmetry between adjacent subassemblages in a complete, regular, non-sway frame (figure 2.3). The stiffnesses of the beams used in the analytical study were therefore equivalent to beams spanning between columns at 3.0m, 4.0m, 6.0m and 8.0m centres respectively. The predicted failure loads of the analytical models are presented in table 2.2.

Due to the restricted space available in the subassemblage test area, the maximum beam length which could be conveniently accommodated in the experimental study was approximately 1.5m, equivalent to an actual beam span of 3.0m. At that length, the difference in the predicted failure load for a subassemblage with web cleat connections, compared with that employing flush end plate connections, was 40kN. As expected, this difference in failure load decreased as the length of the beam increased. For a beam length of 4.0m, the difference was reduced to 24kN. It was considered that at a beam length of 1.5m, the 40kN range of failure loads was sufficiently large to allow the influence of the different types of connection to be observed experimentally.

### 2.2.5 The influence of the 'column loading stub'.

In the experimental study a 'loading stub' was provided to ensure that the column head load was evenly dispersed across the section at beam connection level. The 'loading stub' effectively comprised of a short 210mm extension of the column above the centreline of the beams. A limited analytical study was carried out to assess the likely effect, if any, of such a stub on subassemblage behaviour.

Figure 2.4 shows the boundary conditions and predicted failure loads for the finite element models *1A*, *1B*, *2A*, *2B*, *3A* and *3B*. In the type *A* models the beam to column connections were modelled on the moment rotation characteristics of a simple web cleat connection. In the type *B* tests, the connection was modelled as a true pin with zero rotational stiffness.

Model type *1* investigated the effect of permitting vertical displacements only at the column head and at the remote end of each of the beams. Comparison of models *1A* and *1B* shows that with such boundary conditions, variations in the rotational stiffness of the beam to column connection had little effect on the column failure load. This was because the rotational restraint at the head of the column was effectively equal to the large bending stiffness of the short, positionally restrained loading stub. Any rotational restraint which was provided by the beam to column connection was effectively insignificant in comparison. Obviously, an experimental investigation using similar boundary conditions would yield very little information on the effects of semi-rigid connections on the behaviour of the subassemblage.

A study was carried out on models which relieved the positional restraint on the loading stub. Firstly, model type *2* in which movement was permitted along the axis of the beams, and secondly, model type *3* in which positional restraint was relieved from the column head. As expected, these models predicted lower failure loads than the corresponding values of model *1*. In models *2* and *3*, the rotational restraint at the column

head was provided solely by the beam to column connections. Unlike model type 1, it is evident from the predicted failure loads of the *A* and *B* type models that varying the moment rotation characteristics of the connection had a significant effect on the behaviour of the subassemblage. Obviously, experimental studies employing support conditions similar to those used in model type 2 or type 3 would provide better information on the relative effects of various semi-rigid connections.

In the experimental testing, it was inevitable that some degree of positional restraint would be provided both at the head of the column by the loading jack, and at the remote ends of the beams by the testing rig. It would therefore have been difficult to truly represent the support conditions of either models 2 or 3. However, results of the analysis show that only very small displacements, typically less than 0.5mm, are necessary to fully relieve the clamping action of the loading stub observed in model 1. The restraint provided by the loading jack, testing rig and the beam to column connections was sufficiently flexible to accommodate such small movement. The column could therefore be expected to behave in a manner intermediate between that predicted by the type 2 and type 3 models. As the two models behaved in a similar fashion, in terms of failure load and deformation, the behaviour of the subassemblage could be predicted with confidence without the need to quantify the actual loading stub restraint provided by either the loading jack or the test rig.

### **2.3 The series of experimental subassemblage tests.**

A total of ten subassemblage tests, designated S1 to S10, have been carried out. Figure 2.5 shows the two types of subassemblage configuration which were considered in the study. The subassemblage containing three beams represents an edge column arrangement from a more extensive structure, whilst that with just two beams represents a corner



column. A summary of the connection type, column orientation and subassemblage type adopted for each test is presented in table 2.3.

At an early stage, it was proposed that the test programme should include an edge column arrangement which incorporated a positional restraint to the minor axis at the column centre. The aim was to create a test specimen in which the effective slenderness of both the major and minor column axes were approximately equal. However, the practical difficulties of constructing a minor axis positional restraint which did not apply an unquantifiable out-of-plane restraint to the major axis was soon realised. It was inevitable that the results from such a test would be unreliable and, as a consequence, it was not incorporated into the final test programme.

### **2.3.1 Fabrication of the subassemblage specimens.**

The general arrangement of the two types of subassemblage considered in the study are shown in figures 2.6 and 2.7. All the subassemblages in the study comprised a 6.24m long 152x152x23UC column section (6.03m base plate to beam centreline plus a 0.21m loading stub) with up to three 254x102x22UB beam sections measuring 1.542m (or 1.459m) between the the column and support centrelines. All the steel used to fabricate the subassemblage members was nominally grade 43A to BS4360 [2.17]. The four connection types used in the study - web cleat, web and seat cleat, flange cleat, flush end plate - were fabricated and detailed in exactly the same way as the connections used in the isolated joint performance study discussed in chapter 6 and those used in other recent experimental studies [2.5,2.6]. As in the joint tests, 16mm diameter grade 8.8 bolts were used throughout complying with BS4320 [2.18] with bright steel form A washers beneath each nut and bolt head. The subassemblage fabrication drawings are presented in Appendix A.

For certain subassembly tests, the members were fabricated from the same steel stock lengths used to fabricate the elements in the isolated joint tests. This maintained a continuity of material properties between the tests and thus permitted close comparison between various aspects of the experimental behaviour. A comprehensive appraisal of the physical and geometric properties of the steel used in the joint, subassembly and frame tests together with details of stock steel locations is presented in a separate volume to this thesis [2.19].

The fixed base condition was achieved by welding a 700 x 700 x 20mm thick steel base-plate to each of the column sections. The plate was bolted to the spreader beams of the testing rig by 28 No. 20mm diameter H.S.F.G. bolts on a 200mm x 100mm grid across the plate. Figure 2.8 shows a photograph of the base-plate from one of the subassembly tests. The base-plate was very large when compared to those which may be encountered in practice. However, such a large unstiffened base-plate was necessary to facilitate the method devised for inducing the prescribed initial column deformations, described in section 2.3.3., and to provide the necessary high base stiffness discussed in section 2.2.2.

As discussed in section 2.2.4, the bending stiffness of the relatively short beams was increased by adopting a support condition at the remote ends which permitted movement in a direction parallel to the column axis, but which prevented in-plane rotation and twisting. The 'sliding' support devices were modified versions of those used in a recent study of 2-dimensional subassembly behaviour [2.5]. The beams were connected to the support via a substantial end-plate, extended both top and bottom, to effect a rotationally stiff connection. Fabrication details of the beam support detail are presented in Appendix A whilst figure 2.9 shows a photograph of the support with a beam installed.

### **2.3.2 Construction of the subassemblage testing rig.**

The rig used to test the subassemblage specimens was constructed from over seven tonnes of 305 x 102 RSC steel sections pre-drilled on a 100mm x 100mm grid, and was bolted together using over 300 No. 20mm diameter High Strength Friction Grip (H.S.F.G.) bolts. At intersections between principal vertical and horizontal members, nine bolts were used in a 3 x 3 grid to effect stiff connections capable of resisting any tendency for the structure to 'rack'. The testing rig was 'self-straining', that is to say that all reactive forces were contained within, and resisted by, the rig. However, as a safety precaution and to maximise overall stiffness, the rig was securely fixed to the floor of the testing hall at regular intervals. Figure 2.10 shows the general arrangement of the test rig on plan and elevation, whilst figures 2.11 to 2.12 show photographs of the rig viewed from various angles with a specimen installed.

Ideally, the subassemblages would have been tested with the axis of the columns vertical, thus simulating the orientation of a column in a 'real' structure. However, the restricted headroom available in the test area, the access requirements and the potential difficulties of constructing a 'vertical test rig' dictated that the subassemblages were tested in the horizontal position. Although in this orientation the disturbing effect of the column self weight would influence the initial deformation of the specimen, the effect was taken into account in the subsequent analytical modelling of the tests.

The initial parametric studies of subassemblage behaviour (section 2.2) had illustrated the benefit of adopting a very stiff column base support condition. In the testing rig a series of vertical and horizontal 305 x 102 RSC spreader beams, fixed to the four main longitudinal tie members, were used to obtain a very stiff column base support (figure 2.13 and 2.14). During one of the subassemblage tests, deflection measurements were taken at locations on the column base to assess the rigidity of the supporting frame. The significance of these results is discussed in section 2.4.1.

### **2.3.3 Initial column deformations.**

Prior to fabrication, the column sections were found to be almost straight with typically only 1.0mm to 1.5mm deformation at the centre of a 6.2m length of column. The testing of such near straight column sections can cause sudden bifurcation type failures which can result in the loss of experimental data at the point of collapse. A preferred approach was adopted in which the columns were tested with a more significant initial out-of-straightness, typically of the order of  $L/1000$ . This has the advantage of:-

1. Producing a much more controllable, progressive collapse allowing the characteristics of the column at the point of maximum load to be accurately monitored.
2. It predetermines the direction of column failure. This is important when maximising the available travel of deflection measurement systems at the centre of the column.
3. It reflects the more onerous lack of straightness limit of practical members.

In the presence of initial deformations the detrimental effect of residual stresses on the column capacity can be increased. That is to say that the initial deformation and residual stress pattern have a synergistic effect in which their combined effect is greater than the sum of the individual parts [2.20]. However, this usually applies to heavy column sections of relatively small slenderness with large residual stresses. In this instance, where light sections have been used and the column is of a moderate to high slenderness, the reverse is true with the effects of residual stresses being reduced [2.21].

Initially it was considered that the columns would have to be bent plastically to attain the required initial deformation. However, this approach was considered unsatisfactory

as the plastic strains induced at the column centre could have had a significant influence on column behaviour. A secondary problem was the difficulty of physically installing the 6.24m long column in the available testing machines to induce plastic flexure. An alternative approach considered was the application of a small lateral load to the centre of the column during the initial stages of the test, thus ensuring a specific direction of failure. This method was adopted in a recent experimental study of two-dimensional subassemblage behaviour [2.5]. However, it was considered that the presence of such a loading device could cause the following problems:-

1. Additional congestion around the mid point of the column resulting in insufficient room to install the displacement measurement devices.
2. Possible variation in lateral loading during the course of a test.
3. Although the presence of a lateral load could be taken into account in the subsequent analytical modelling of the tests, in a three-dimensional situation it would be difficult to quantify the in-plane and out-of-plane column restraint offered by the loading device.

The method for inducing initial deflections which was ultimately used, and which was developed specifically for this series of tests, permits the column to be deformed elastically into the shape of an arc of prescribed amplitude without applying lateral load. The process of operations is best illustrated by considering figure 2.15.

1. The end of the column which was to be welded to the base-plate was cut with a slight chamfer (2mm across the depth of the section). The large base-plate was bolted into position in the test rig. With the column in the position it would occupy when the complete subassemblage was installed, the displacement controlled screw jack was advanced to apply a 'nipping load' to hold the column firmly in position.
2. The column head load was then increased causing the chamfered gap at the column base to close. This effectively changed the angle between the column

centreline and the base-plate thereby deforming the column into an arc.

3. The screw jack was advanced until the required bow was observed at the column centre. With the column held fixed in the required deformed shape, the column was welded to the base-plate thus fixing the base angle.
4. The load was then backed off and the column, complete with base-plate, removed ready to be reinserted during the subassembly erection (section 2.3.4). Because the base angle was now fixed, reinserting the column into the testing rig caused the column to adopt the prescribed deformed shape without the assistance of an applied column load.

Due to the eccentric pressures beneath the chamfered base combined with the relatively high column slenderness, the axial load required to induce the deformed shape in the first instance was relatively small, typically less than 60kN.

As the angle between the column and the base-plate was fixed to a small critical value, it was important that during the final erection stage the base-plate was relocated in exactly the same position it had occupied when the initial column deformations were induced. This was facilitated by using a large base-plate in which the potential for angular variation during re-bolting was reduced. To effect a stiff base-plate connection, it is common practice to provide a series of stiffeners at the base of the column. However, stiffeners were not used as the differential heating effects due to the welding process would have irreversibly changed the induced base angle.

As a direct result of adopting the above procedure, the use of the often erratic 'as delivered' out-of-straightness of rolled column sections was avoided. With the exception of test S6, in which the column minor axis was almost perfectly straight, a similar initial shape of column was used throughout, thus ensuring a high degree of compatibility between tests. By avoiding the use of column sections in which the initial deformations form a reverse or double curve, the subsequent analytical modelling of the tests was much simplified.

#### 2.3.4 Subassemblage erection.

From the results of the first subassemblage test, S1, it was apparent that the precise order in which the subassemblages were to be erected would influence the performance of the support conditions at the remote ends of the beams. In test S1, when the beams were installed, the bolts connecting the web cleats to the beams had been tightened before the bolts which connected the cleat to the column. Because the distance between the two horizontal beam support centrelines was fixed, any minute shortfall in the combined length of the beam and cleat generated axial forces in the beams as the contact surfaces of the column and cleat were bolted together (figure 2.16). Such axial forces caused the beam supports to 'lock' rather than travel freely along their bearings.

This problem was resolved by reversing the sequence of bolt tightening. Contact surfaces which were perpendicular to the beam axis, i.e. cleat to column face, were tightened first followed by those surfaces which were parallel, i.e. cleat to beam. Any shortfall in the length of the beam was then accommodated by the clearance of cleat to beam bolt holes, thus preventing the generation of axial forces in the beams. This revised sequence of bolt tightening was adopted in all subsequent tests and in each case the beams deflected smoothly along their end bearings. It was not possible to use a flush end plate connection, in which all the contact surfaces are perpendicular to the beam axis, for both beams *B1* and beam *B3*. The lack of dimensional tolerance on the overall beam length would have inevitably generated axial forces in the beams as the end plates were bolted to the column. The influence of flush end plate connections was therefore studied by considering a two beam, edge column type subassemblage in which the problem of dimensional tolerance did not arise.

The sequence of subassemblage erection which was adopted in tests S2 to S10 can be

summarised as follows:-

1. The vertical beam *B2* was installed and bolted to the support bearing.
2. The column was then positioned and the base-plate bolted to the testing rig, the process to set the initial angle between the base-plate and the column having previously been carried out.
3. Beams *B1* and *B3* were installed and bolted to their respective support bearings.
4. Beam *B2* was then bolted to the column head to position the column in its correct vertical alignment.
5. The column was then located in the correct horizontal alignment and a small 'nip' load was applied by the screw jack to firmly hold the column in position.
6. The horizontal beams, *B1* and *B3*, were then bolted to the column observing the correct tightening sequence as discussed above.

All the bolts were tightened to the same torque, 160Nm, as those connections in the corresponding joint tests [2.6] and the recent experimental two-dimensional subassembly study [2.5].

Prior to erection, the main elements of the subassembly were painted with a coat of white matt emulsion paint. Although during subassembly tests the flaking of the paint did give an indication of the extent of yielded material, its principal function was to highlight the subassembly members on subsequent photographic records.



### **2.3.5 Experimental test set-up.**

Each beam was loaded by a single 250kN capacity hydraulic ram via a hardened steel ball acting at a distance of between 400mm and 845mm from the column centreline (figure 2.17). In the figure the ram has been backed away from the face of the beam. The retractable steel strip which connects the upper and lower ball seats was a means of preventing the ball bearing from falling off the jack when the beam was unloaded. The jacks were load controlled and, once a required limiting value had been attained, applied a constant beam load to the subassemblage irrespective of the resulting member deformations. Two separate electric pumps were used to energise the hydraulic beam rams. In instances where three beams were loaded, at least two of the beams had to be supplied by the same pump and hence applied the same load. The load was monitored by calibrated pressure transducers situated in the oil supply housing of each ram.

A 500kN capacity screw jack, positioned eccentric to both the major and minor column axes, applied load to the head of the column. This jack was displacement controlled and enabled the subframe to be deformed beyond the ultimate load in a safe and controlled manner. A 500kN capacity load cell, which incorporated a spherical seat, measured the applied column head load.

The three-dimensional nature of both the subassemblage deformations and member forces, combined with the need to accurately monitor the behaviour of the column in the elastic-plastic range, required careful consideration as to the methods adopted for force and displacement measurement. In the early stages of the research programme, much effort was expended in the development of measurement systems which were capable of accurately deciphering the individual components of three-dimensional behaviour. For clarity, the development and appraisal of these measurement systems together with the overall force and displacement instrumentation and the data acquisition techniques has been presented separately in chapter 3 of the thesis.

### **2.3.6 Subassemblage test procedure.**

Prior to carrying out a test, precise measurements were made of the initial column deformations and the beam and column head load eccentricities. These values are summarised in table 2.4. In addition, the initial geometry of the three-dimensional displacement monitoring systems was recorded (see chapter 3).

An initial 'nip load' was present in the subassemblage columns at the start of each test. This load was relatively small, typically less than 10kN, and had been applied to facilitate the subassemblage erection (see section 2.3.4). For the purpose of carrying out the test, the load instrumentation devices were configured to read zero under this nip load. The magnitude of the initial column load was added to the overall loading when the experimental data were processed after completion of the test.

The basic loading sequence, which was used for all the subassemblage tests, was as follows:-

1. The beam loads were applied first in increments up to a prescribed limiting value.
2. With the beam loads held constant, the column head load was increased to fail the column.
3. After failure and the required column deformation had been attained, the beam loading was reduced in increments to zero.
4. With the beam loading reduced to zero, the column head load was reversed back to the initial 'nip load'.

Typically, the beam loads were applied in a minimum of ten equal increments up to their prescribed limiting value, with data being scanned at every increment. The magnitude

and position of the beam loadings are summarised in table 2.5 for each of the subassemblage tests. During the beam loading phase of the test the screw jack, which applied load to the head of the column, was continuously advanced to maintain the initial 'nip loading'.

During the column head loading phase of the test the screw jack was advanced at a constant rate corresponding to an increase in column axial stress of between 5 and 7 N/mm<sup>2</sup> per minute. During this phase of the test, data scans were taken at every 20kN of applied load, but as failure approached the scan increment was reduced to record the deterioration of column stiffness in more detail. The column head screw jack was continually advanced beyond the ultimate column capacity until a significant amplitude of deformation was observed at the column centre.

## **2.4 Subassemblage test observations and results.**

This section explains the progressive development of the loading arrangements and experimental parameters selected for each of the individual subassemblage tests S1 to S10, and reports aspects of the observed experimental behaviour.

### **2.4.1 Subassemblage test S1**

This first subassemblage test employed web cleat connections to connect each of the three beams to the column. To avoid excessive beam deformation, the beam load points were positioned relatively close to the column with an eccentricity of only 400mm from the

column centreline. It had been the intention to apply a 50kN load to each of the beams. However, due to a calibration factor error in the data logging equipment - detected after completion of the test - the load applied to beam 1 was only 5kN. Figure 2.18 shows a schematic summary of the major experimental parameters which were present in this test.

The test was conducted in the manner described in section 2.3.6. The measured ultimate load carrying capacity of the column was 468.1 kN. Figure 2.19 shows a plot of the observed load-deflection response at the centre of the column whilst figures 2.20 and 2.21 show the distribution of bending moments around the subassemblage at the end of the beam loading phase and at the point of maximum load capacity.

Figure 2.22 shows a plot of the support displacements for each of the three beams during the course of the test. The vertical portions of the plot for beam 1 clearly show that the support had locked solid rather than travelled smoothly along the sliding bearings. During the unloading phase of the test, a load bang was heard as the locked beam reverted back to its correct position. This phenomenon was attributed to the precise order in which the specimen had been erected in the testing rig (see section 2.3.4) and also due to the small load inadvertently applied to beam 1. As a comparison, figure 2.23 shows a plot of the travel of the beam support bearings for test S2 in which a revised erection sequence was adopted. It is evident that in this second test, the bearings performed as required travelling smoothly along the bearings. This set a precedent for the erection sequence which was used in all the remaining tests in the series.

The failed specimen S1 was re-tested to check the deflections of the rig at the base of the column and ensure that a stiff base condition was being achieved. The location of the four dial gauges used to monitor the base-plate deformation, together with the recorded deflections, are presented in table 2.6. As expected, the deflections at gauges 1 and 3 were larger than those of 2 and 4 due to the direction of the minor axis bending moment at the column base. The magnitude of the differences between these deflections shows that at

a column load of 450kN, the absolute base rotation was approximately 0.00035 radians. The corresponding minor axis bending moment at the base was 18.0 kNm giving a base stiffness of 51400 kNm/rad. This compares favourably with the minimum base stiffness (3000 kNm/rad) required to closely simulate a fully fixed base condition as discussed in the initial analytical appraisal of section 2.2.2.

It is interesting to note however that the maximum load carrying capacity of the re-tested specimen with the corrected arrangement of beam loads was 450kN, relatively close to the ultimate load capacity observed in test S1. As test S1A was a re-test of a failed specimen, the results obtained are of limited value and as a consequence will not be presented nor discussed further.

#### **2.4.2 Subassemblage tests S2.**

This particular test used flange cleats to connect each of the beams to the column. As a precautionary measure, the beam loads in test S1 were positioned quite close to the column and as a result, very little beam deformation was observed. In an attempt to induce greater beam deformation, the beam point loads in test S2 were positioned further away from the column centreline (beam 1 and beam 3 at 630mm and beam 2 at 700mm). The initial minor axis deflection at the centre of the column was 9mm ( $L/670$ ), larger than had been adopted in test S1. Figure 2.24 shows a schematic summary of the major experimental parameters of this test.

As in test S1A, each beam was loaded with a single load of approximately 50kN. At the end of the beam loading phase, load was applied to the column head until the ultimate column capacity of 503.0 kN was achieved. The screw jack at the column head was allowed to travel beyond the ultimate capacity condition until the minor axis deflection at the centre of the column was in excess of 100mm. Figure 2.25 shows the resulting load-

deflection plot for the column centre whilst figures 2.26 and 2.27 show the distribution of bending moments around the subassemblage at the end of the beam loading phase and at the point of failure. Figures 2.28 and 2.29 highlight the post failure deformation of the subassemblage.

Due to the problem of the friction in the beam support bearings encountered during test S1, their performance was closely monitored during test S2. The bearings behaved as required throughout the full duration of this and all subsequent tests.

It was during this particular test that a slight modification was made to the subassemblage loading sequence. The axial shortening of the column during the beam loading phase had caused the nip load, initially applied to the column head by the screw jack, to reduce to zero. It was considered that such a situation could permit the position of the column head to shift slightly under the influence of applied beam moments and therefore change the measured column head eccentricities. For all subsequent tests, the screw jack was therefore advanced during the beam loading phase to maintain the initial column head load.

### **2.4.3 Subassemblage test S3.**

Web and seat cleats were used to connect each of the three beams to the column. The position and magnitude of the beam loads together with the minor axis bow at the column centre remained the same as those used in test S2. Figure 2.30 shows a summary of the principal experimental parameters present in this test.

Figure 2.31 shows a plot of the deflections at the centre of the column during the test. The maximum applied load was 542.6 kN corresponding with a minor axis central deflection of 33 mm. Figures 2.32 and 2.33 show the distribution of bending moments around

the subassembly at the end of the beam loading phase and at the point of failure. As in the previous tests, the load carrying capacity decreased progressively once the maximum load had been attained. The test was terminated when the minor axis deflection of the column was 89 mm.

#### **2.4.4 Subassembly test S4.**

Section 2.3.4 discussed the importance of adopting a specific method of subassembly erection which prevented the generation of axial erection forces in the beams. The method utilised the clearance in the bolt holes of cleated connections to overcome the zero dimensional tolerance between the end supports of beams 1 and 3. In this particular test, the flush-end plate connection was investigated, a joint type which itself possesses zero longitudinal dimensional tolerance. To overcome this problem, a two beam corner column type subassembly was studied in which beam 1, and hence the overall dimensional restriction, was omitted. Figure 2.34 shows a close up of the intersection of the two beams at the head of the column.

A schematic summary of the major experimental parameters present in this test is shown in figure 2.35. The test was conducted in the manner discussed previously and was terminated when the observed minor axis deflection at the column centre was 96.5 mm. The maximum load applied to the column was 494.7 kN. Figure 2.36 shows a plot of the load-deflection characteristics of the column whilst figures 2.37 and 2.38 show the subassembly bending moment distribution at the end of the beam loading stage and at the point of maximum load.

#### **2.4.5 Subassemblage test S5.**

This test was the first of a series of three which investigated the performance of the subassemblage with the vertical beam, beam 2, connected to the minor axis of the column (see table 2.3). Test S5 used web cleats to connect the beams to the columns and was therefore a companion to test S1.

Only modest beam loads had been applied in tests S1 to S4 and as a result, the maximum induced beam stresses were only 70% of yield. To save time and to introduce an element of material continuity, the beams in tests S1 to S3 were re-used in test S5 to S7. Because the column was now in a different orientation, the re-used beams occupied different positions to those in the first four tests [2.19].

Figure 2.39 shows a photograph of a local deformation which was present in the steel column before the test was carried out. The bow in the flange, which probably occurred as a result of handling during transportation, had an amplitude of 3 mm and was situated on the top face 710mm down from the under- side of beam 1.

The schematic summary of the test parameters presented in figure 2.40 shows that only 30kN was applied to the vertical beam, beam 2. This limited the moment applied to the minor axis of the column in an attempt to generate greater major axis column action. Unequal loads were applied to the horizontal beams, beam 1 and beam 3, to induce a significant disturbing moment about the major axis of the column. This was assisted by the column head screw jack which was positioned eccentric to the major axis but coincident with the minor axis.

As on previous occasions, the beam loads were applied in a fixed ratio in ten equal increments up to their prescribed maximum values followed by the column head load to failure. The load deflection plot at the centre of the column is presented in figure 2.41 whilst figures 2.42 and 2.43 show the distribution of bending moments around the subassemblage at the end of the beam loading phase and at the point of failure. The



maximum applied loading was 479.0 kN. Figure 2.44 is a photograph of the specimen in a post failure condition in which the reverse curvature of the minor axis in the region of the column base can be detected.

During the final stages of the test in which the column was being deformed beyond its ultimate capacity, zones of flaking paint appeared at particular points on the column (figure 2.45). These zones provided an indication of those regions which had been strained beyond the yield point of the material. As expected, there appeared to be no plastic straining around the head of the column. This was because the moment capacity of the restraining web cleat connections was significantly less than the minor axis plastic moment capacity of the column section.

#### 2.4.6 Subassemblage test S6.

In all the previous tests, a significant initial deformation had been induced at the centre of the columns. As discussed in section 2.3.3, this resulted in tests which failed in a progressive and controlled manner. The aim of test S6 was to investigate the behaviour of the subassemblage when such initial deformations were reduced. Ultimately such a test would be used to assess the ability of the finite element models to predict the bifurcation type failure associated with near straight columns. Figure 2.46, which illustrates the experimental parameters present in this particular test, shows that the initial minor axis deflection at the column centre was only 0.5mm whilst that for the major axis was 1.5mm. The arrangement of beam loads was similar to that adopted for the previous test, S5.

Figure 2.47 shows the load-deflection plot for the centre of the column. As expected the 'near-straight' column deflected significantly less than any previous column for a given level of pre-failure load and as a result attained a higher ultimate carrying capacity of

614.0 kN. As failure approached, a sudden bifurcation of equilibrium occurred causing the rapid increase in minor axis deflections at the column centre. This sudden increase in the rate of deflection is illustrated by the increased spacing of the data points on the deflection plot. Up to the point of bifurcation the twist at the column centre had been relatively small. However, figure 2.48 shows that at the point of failure the twist increased dramatically. Figures 2.49 and 2.50 show the bending moment distribution around the frame at the end of the beam loading phase and at the point of maximum load capacity.

In an attempt to record the post-bifurcation behaviour of the column, the manual data trigger which initiated the scanning of the instrumentation devices was repeatedly activated in quick succession. As a result the input buffer of the computer, which housed the experimental logging software, was 'swamped' with data causing the logging systems to 'crash'. The test was therefore terminated when the minor axis deflection observed at the column centre was only 58mm.

#### **2.4.7 Subassemblage test S7.**

The orientation of the column in this test was similar to that adopted in both tests S5 and S6 with the vertical beam connected to the minor axis of the column. Web and seat cleats were used to connect each of the three beams to the column.

One specific aim of this test was to investigate the behaviour of the subassemblage under more onerous conditions of major axis deformation. The schematic representation of the major experimental parameters studied, as presented in figure 2.51, shows that the induced initial major axis deformation was greater than that for the minor axis. To produce larger beam deformations, the loads in the horizontal beams, Beam 1 and Beam 3, were relocated further away from the column centreline ( at 845mm on beam 1 and

at 830mm on beam 3). In addition, the magnitude of the loads was increased to create a relatively large imbalance of applied moment about the major axis of the column.

The test was carried out in a similar manner to previous tests as described in section 2.3.6. The subassemblage was continually deformed beyond the ultimate capacity of 490.0 kN until the observed minor axis deflection at the column centre was 85mm. The resulting load-deflection plot is shown in figure 2.52. As expected, the observed major axis deflections were significantly greater than those which had been observed in either tests S5 or S6. Figure 2.53 shows the distribution of bending moments around the subassemblage at the end of the beam loading phase whilst figure 2.54 shows the distribution of moments at the point of failure.

#### **2.4.8 Subassemblage test S8.**

In tests S5, S6 and S7, the vulnerability of the column to minor axis deformation limited the amount of load which could be applied to the vertical beam, beam 2. In the final tests of the series, S8, S9 and S10, the orientation of the column reverted back to that used initially, in which beams 1 and 3 were connected to the minor axis of the column. This enabled larger total beam loads to be applied to the subassemblage and provided the potential to produce larger major axis column moments. The beams used in the final three tests were fabricated from new lengths of steel unlike tests S5, S6 and S7, in which the beams had been re-used from previous tests

In test S8, web cleats were used to connect the beams to the column. The subassemblage was therefore similar to the first specimen S1. Equal loads were applied to each of the three beams in increments of 10kN until the maximum beam strain was 1200 microstrain (approximately  $250\text{N}/\text{mm}^2$ ), corresponding to a nominal maximum applied beam loading of 85kN. The other principal test parameters present are summarised in figure 2.55.

The maximum column capacity was 482.0 kN. Figure 2.56 shows the load- deflection plot for the column centre. Figure 2.57 shows the resulting distribution of bending moments around the subassemblage at the end of the beam loading phase, whilst figure 2.58 shows the distribution of moments at the point of failure.

#### **2.4.9 Subassemblage test S9.**

Flange cleats were used to connect each of the beams to the column. The test was therefore of a similar arrangement to test S2. Figure 2.59 shows the principal experimental parameters which were present in this particular test. As in test S8, the same load was applied to each of the three beams but in this instance the nominal maximum beam load was higher at 95kN. The test was carried out in the manner described previously and attained a maximum load capacity of 526.0 kN. The test was terminated when the minor axis deflection at the column centre was 58mm. As expected, the increased connection stiffness combined with the increased beam loading produced significantly greater major axis column deformation and bending moments than had been observed in test S8.

The plot of deflections against applied load for the column centre is presented in figure 2.60. Figure 2.61 shows the resulting distribution of bending moments around the sub-assemblage at the end of the beam loading phase whilst figure 2.62 shows the distribution of moments at the point of failure.

#### 2.4.10 Subassemblage test S10.

The final subassemblage test incorporated two different connection types. Web and seat cleats were used on the horizontal beams (beams 1 and 3) and a flush end plate connected the vertical beam (beam 2) to the major axis of the column. Figure 2.63 shows a summary of the principal experimental parameters. The high load applied to beam 2 combined with the relatively stiff flush end plate connection had the potential to transmit a large bending moment to the major axis of the column and thus promote a high degree of major/minor column axis interaction.

The subassemblage was tested using the procedure discussed in section 2.3.6 with the beam loads applied in ten equal increments in a 2:3:2 ratio to beams 1,2 and 3 respectively. The column failed when the total applied load was 520.1 kN. Figure 2.64 shows a plot of the measured deflections at the column centre against the total applied load. The plot shows that the major axis deflections were significantly larger than those for the minor axis during the initial stages of the test and thus illustrates the degree of major/minor axis interaction which had been achieved. This is also apparent from the large major axis column moment shown on the bending moment distribution plots in figures 2.65 and 2.66. One outcome of the increased major/minor axis interaction was the increased twist induced at the centre of the column (see chapter 4). Figure 2.67 shows the column under a post-failure load condition and illustrates the large twist rotation observed.

## 2.5 Discussion of results from the experimental subassemblage tests.

A discussion on the general observations and conclusions from the experimental subassemblage study is reported in this section. It should be noted that a discussion on the detailed aspects of subassemblage behaviour is presented in chapter 4 where the experimental results are compared with those predicted from the finite element computer program [2.4].

### 2.5.1 Mode of failure.

In all ten of the subassemblages studied, the column failed as a result of excessive minor axis deformation. This occurred despite efforts to induce predominately major axis deformation, particularly in the later tests. In test S10 (see section 2.4.10), a loading arrangement was used which, at the end of the beam loading phase, induced a major axis moment at the column head of 23.2kNm (45.0kNm nominal  $M_{px}$ ) and a major axis deflection at the column centre of 14.6mm (11.6mm absolute). The corresponding moment and deformation about the minor axis was 0.5kNm (14.0kNm nominal  $M_{py}$ ) and 6.1mm (15.1mm absolute) respectively. A situation therefore existed which was expected to promote a high degree of major/minor column axis interaction. However, the near vertical nature of the mid-column major axis deflection plot during the second phase of the test, shown in figure 2.64, illustrates the resistance of the column to major axis failure. The difficulties of inducing significant major axis action in the experimental appraisal of pinned-end steel columns <sup>have</sup> ~~has~~ previously been reported by Birnstiel [2.22].

### 2.5.2 Distribution of moments around the subassemblage.

The plots of the bending moment distributions for each of the ten tests are presented under section 2.4. They show the bending moments at both the end of the beam loading phase and on reaching the maximum column load. It should be noted that the plots were generated from the measurement of bending moments at only a limited number of locations and, as a result, they represent only simple 'straight line' approximations to the actual moment distributions. An examination of the plots shows that, in some instances, there is an apparent imbalance of bending moments at the intersection of the beams with the column. This is principally due to the effect of the column head load acting eccentrically to the column centreline and the torsional resistance effects from the beam, or beams, perpendicular to the plane of the moment diagrams.

In tests where an appreciable disturbing moment was applied to the minor axis of the column (i.e. tests numbers S1,S4,S5,S6 and S7) a reversal of the moment occurred at the column head as the failure load was approached. In the remaining tests, in which the column head minor axis moment at the end of the beam loading phase was negligible (i.e. test numbers S2,S3,S8,9 and S10), the moment increased as the column approached failure but without reversing sign. In all cases, the induced minor axis column head moment at the point of ultimate load was of the opposite sign to that induced at the column centre. As a result, the minor axis of all the columns in the study deformed in the shape of a double reverse curve (figure 2.45).

The column head minor axis moment at the point of failure was a direct result of the restraint, both in-plane and torsional, from the intersecting beams. The beams resisted the head rotation of the column as it deformed laterally at the mid-point under the influence of increased compressive load. In instances where a beam framed into each side of the column minor axis, one of the connections continued to 'close' with increasing beam moment (loading- loading), whilst the other beam 'opened' exhibiting moment reduction (loading- unloading). In some instances, the 'closing' connection attained the

full moment capacity of the connection whilst the 'opening' connection experienced a full reversal of the beam moment. This redistribution of moments around the column head at the point of failure is clearly evident from the bending moment plots. Figure 2.68 shows a diagrammatic summary of the direction of connection rotation at key stages in the loading sequence.

Comparing the 'end of beam loading' and the 'point of failure' bending moment diagrams for each of the individual tests, the difference between the major and the minor axis moment distributions is quite apparent. Unlike the minor column axis, there appears to be only a small change in the major axis moments from the end of the beam loading up to the point of failure. As discussed in section 2.5.1, this is verified by the lack of major axis deflection observed after completion of the beam loading phase of the test. Although sometimes small, all test specimens exhibited a reduction of the major axis moment at the column head as the failure load was reached. This phenomenon was similar to the moment reversal discussed above for the minor axis but is evident to a much less extent. Such a moment reduction only occurred when failure was imminent and the column had almost zero stiffness. Only then could the major axis of the column deform appreciably, causing the connection with the major axis beam to 'open' and thus reduce the applied moment.

The concept of moment reversal is a fundamental aspect of restrained beam column behaviour and has been observed in rigidly connected frames, both model and full scale, by a number of experimental researchers [2.23, 2.24]. As far as the author is aware, these subassemblage tests are the first to illustrate moment reversal in a flexibly connected 3-dimensional steel structure using full-scale components.



### 2.5.3 Connection behaviour.

Significantly, there was very little evidence of permanent connection distress in any of the subassemblage tests. Inspection of flange and web cleats following testing revealed negligible deviation from their original 'L' shaped section. This was despite the moment capacity of the connections being attained in a number of instances. This can be explained by the relatively small maximum connection rotations observed - typically in the range 0.012 to 0.025 radians. These are significantly less than the maximum rotations induced during many isolated experimental joint tests [2.25, 2.26] in which the maximum induced rotation often exceeded 0.13 radians resulting in substantial permanent connection deformation.

As discussed in section 2.5.2, it is clearly evident from the distributions of bending moments that connections in the tests exhibited the 'loading-loading' and 'loading-unloading' behaviour characteristic of connections in restrained beam-columns. This is substantiated by the nature of the measured moment- rotation response of the individual connections. For clarity a full appraisal of connection behaviour, together with comparisons of their behaviour when tested in isolation, is presented separately in chapter 6 of the thesis.

### 2.5.4 Ultimate column capacity.

Table 2.7 shows a summary of the ultimate applied loads,  $P_{ult}$  and the non-dimensional load ratio  $P_{ult}/P_{squash}$  for each of the subassemblage tests.  $P_{squash}$  was determined from the stub column tests reported in reference 2.19. Due to variations in the experimental parameters studied, detailed quantitative comparisons between the capacity of different subassemblage specimens is not possible. However, the failure loads do indicate general

trends which can be commented upon:-

As expected those tests (S1, S5 and S8) employing web cleat connections, the least stiff of the connections studied, produced the lowest column capacities; all had a  $P_{ult}/P_{squash}$  ratio of 0.51. With the exception of test S6, in which a bifurcation type failure gave an artificially high ultimate capacity, all those tests with only a single beam connection to the column minor axis (S4, S5 and S7) produced a relatively low  $P_{ult}/P_{squash}$  ratio (less than 0.53), irrespective of the connection type employed.

Tests S2 and S9 both employed flange cleat connection types, had a symmetrical arrangement of beam loading about the minor axis and had a similar initial minor axis deflection at the column centre. It is interesting to note that each test produced the same  $P_{ult}/P_{squash}$  ratio of 0.56 despite the greatly increased major axis moment applied to test S9. A similar effect can be illustrated when comparing the results of tests S9 and S10. The web and seat cleat connections used in test S10 possess a moment-rotation behaviour similar to that of the flange cleat connection used in test S9. Although the major axis moment applied to column S10 was significantly greater, both tests produced the same  $P_{ult}/P_{squash}$  ratio of 0.56. This apparent inability of the major axis moment to significantly reduce the ultimate capacity of the column is the subject of an analytical parametric study presented in chapter 7.

The author has compared the ultimate capacities measured in the experimental study with those predicted using conventional design techniques. For clarity however, this appraisal has been included in chapter 8 of the thesis which deals with semi-rigid frame design.

### 2.5.5 Spread of yield across the column section.

Chapter 3 reports in detail the methods developed for measuring the strain, and hence stress, distribution at the base, mid-point and top of the column. Computer processing of the measured strains enabled the spread of material yield to be traced across the section. Figure 2.69 shows these traces at both the base and centre of the column for each of the test specimens S6 and S7 as the failure load was approached.

The spread of yield shown for the test specimen S7 is typical of that observed in most of the subassemblage tests. Yield was detected at a relatively early stage, in this instance 83% of the ultimate failure load, occurring first at the extremities of the flanges at the mid-point of the column. From the point of first yield up to the failure load the yield spread in a slow and progressive manner. The extent of yield observed on the upper and lower flanges of the section reflected the relative magnitudes of the major and minor axis bending moments acting at that location on the column. The one test in which the spread of yield was significantly different was test S6. This test specimen was initially very straight and failed as a result of a bifurcation of equilibrium. The lack of pre-failure minor axis deformation is evident from the spread of yield plots shown in figure 2.69. Due to the much reduced minor axis deflection and minor axis moments, the first yield was detected at a much higher level of load, 94% of failure load. Once yield had occurred it spread rapidly under the influence of the relatively high axial stress and coincided with the accelerated mid-column minor axis deformation discussed in section 2.4.6.

### References.

- 2.1 Bergquist, D.J., '*Tests on columns restrained by beams with simple connections.*', American Iron and Steel Institute, Project No. 189, Report No.1, Dept. of Civil Eng., University of Texas, 1977.

- 2.2 Lay, M.G. and Galambos, T.V., '*Tests on beam and column subassemblages.*', Fritz Engineering Laboratories, Report No. 278.4 and 278.10.
- 2.3 Kirby, P.A., Davison, J.B. and Nethercot, D.A., '*Large scale tests on column subassemblages and frames.*', published in '*Connections in Steel Structures: Behaviour Strength and Design.*', ed. R. Bjorhovde, J. Brozzetti and A. Colson, Elsevier Applied Science, 1988, pp. 291-299.
- 2.4 Wang, Y.C., '*Ultimate strength analysis of three-dimensional structures with flexible restraints*', Ph.D. Thesis, Department of Civil and Structural Engineering, University of Sheffield, U.K., June 1988.
- 2.5 Davison, J.B., '*Strength of beam-columns in flexibly connected steel frames*', Ph.D. Thesis, Department of Civil and Structural Engineering, University of Sheffield, U.K., June 1987.
- 2.6 Celikag, M., '*Moment-rotation behaviour of steel beam-to-column connections.*', Ph.D. Thesis, Department of Civil and Structural Engineering, University of Sheffield, U.K., February 1990.
- 2.7 Progress Report of the special committee on steel column research, Trans., Am. Soc. Civil Engrs., Vol. 89, 1926, pp. 1526-1536
- 2.8 May, I.M., '*Crossed knife edge joints for testing columns.*', Proc. Inst. Civil Engrs., Part 2, No. 65, Dec. 1978, pp. 917-919.
- 2.9 Estuar, F.R. and Tall, L., '*Testing of pinned end steel columns.*', Test methods for compression members, Am. Soc. Testing Mats., STP 419, 1967, pp. 80-96.
- 2.10 Kato, B., '*Column buckling curves of welded steel tubes.*', Proc., International Colloquium on Column Strength, Paris, 23-24 November 1972, pp. 225-235.
- 2.11 Templin, R.L., '*Hydraulically supported spherically seated compression testing machine platens.*', Proc. Am. Soc. Testing Mats., Vol. 42, 1942, pp. 968-976.
- 2.12 Picard, A. and Beaulieu, D., '*Rotational restraint of a simple column base connection.*', Canadian Journ. Civil Eng., No. 12, 1985, pp. 126-136.
- 2.13 Picard, A. and Beaulieu, D. and Perusse, B., '*Rotational restraint of a simple column base connection.*', Canadian Journ. Civil Eng., No. 14, 1987, pp. 49-57.
- 2.14 Lui, E.M. and Chen, W.F., '*Strength of columns with small end restraint.*', The Structural Engineer, Vol. 61B, No. 1, Part B, 1983, London, pp. 17-26.

- 2.15 Jones, S.W., Kirby, P.A. and Nethercot, D.A., '*Effect of semi-rigid connections on steel column strength*', Journ. Construct. Steel Research, Vol. 1, No. 1, 1980, pp. 38-46.
- 2.16 Galambos, T.V., '*Discussion of small end restraint effects on the strength of H-columns.*', Journ. Struct. Div., Am. Soc. Civil Engrs., Vol 109, ST4, April 1982, pp. 1067-1077.
- 2.17 British Standard BS 4360, '*Specification for weldable structural steels*', The British Standards Institution, London, 1990.
- 2.18 British Standard BS 4190, '*Specification for ISO metric black hexagon bolts, screws and nuts*', The British Standards Institution, 1967.
- 2.19 Gibbons, C., '*The strength of biaxially loaded beam-columns in flexibly connected steel frames - Volume 2: A survey of the mechanical and geometric properties of structural steel sections*', Ph.D. thesis, Department of Civil and Structural Engineering, University of Sheffield, Dec. 1990.
- 2.20 Bjorhovde, R., '*Effect of end restraint on column strength - practical applications.*', Am. Inst. Steel Const., Vol. 21, No. 1, 1984, pp. 1-13.
- 2.21 '*Guide to stability design criteria for metal structures*', 4th Edition, Ed. T.V. Galambos, Wiley-Interscience, 1988.
- 2.22 Birnstiel, C., '*Experiments on H-columns under biaxial bending*', Journ. Struct. Div., Am. Soc. Civil Engrs., Vol. 94, No. ST10, Oct. 1968, pp. 2424-2449.
- 2.23 Gent, A.R. and Milner, H.R., '*The ultimate capacity of elastically restrained H-columns under biaxial bending.*', Proc. Inst. Civil Engrs., Vol. 41, Dec. 1968, pp. 685-704.
- 2.24 Wood, R.H., Needham, F.H. and Smith, R.F., '*Tests on a multi-storey rigid steel frame*', The Structural Engineer, Vol. 46, No. 4, April 1968, pp. 107-120.
- 2.25 Aggarwal, A.K. and Coates, R.C., '*Moment-rotation characteristics of bolted beam to column connections.*', Journ. Construct. Steel Research, Vol. 6, No. 4, 1986, pp. 303-318.
- 2.26 Davison, J.B., Kirby, P.A. and Nethercot, D.A., '*Rotational stiffness characteristics of steel beam to column connections*', Journ. Construct. Steel Research, Vol. 8, 1987, pp. 17-54.

Connection type	3.0m long column		4.0m long column		6.0m long column	
	Pu(kN)	dc(mm)	Pu(kN)	dc(mm)	Pu(kN)	dc(mm)
Pinned	734	1.4	616	1.7	340	2.0
Web cleat	792	2.1	724	2.7	532	4.3
Flange cleat	791	2.6	730	3.9	568	6.3
Web and seat	791	2.3	730	3.5	560	5.6
Flush end	791	2.5	730	3.7	572	6.2
Fixed	791	2.7	730	3.8	572	6.3

Table 2.1: Predicted ultimate loads and mid-column deflections for different connection types and column lengths.

Beam to column connection type	Predicted failure load Pu (kN)			
	1.5m beam	2.0m beam	3.0m beam	4.0m beam
Pinned	340	336	334	332
Web cleat	532	520	512	500
Flange cleat	568	554	532	512
Web and seat	560	550	532	512
Flush end plate	572	560	542	524
Fixed	572	564	544	526

Table 2.2: Predicted ultimate loads for different connection types and beam lengths.

Subframe Test	Beam to Column Connection Type	Edge/Corner Subframe	Column * Orientation
S1	Web cleats	E	A
S2	Flange cleats	E	A
S3	Web and seat cleats	E	A
S4	Flush end plate	C	A
S5	Web cleats	E	B
S6	Flange cleats	E	B
S7	Web and seat cleats	E	B
S8	Web cleats	E	A
S9	Flange cleats	E	A
S10	Web and seat cleats (Beams 1 and 3) Flush end plate (Beam 2)	E	A

\* Column Orientations shown in section

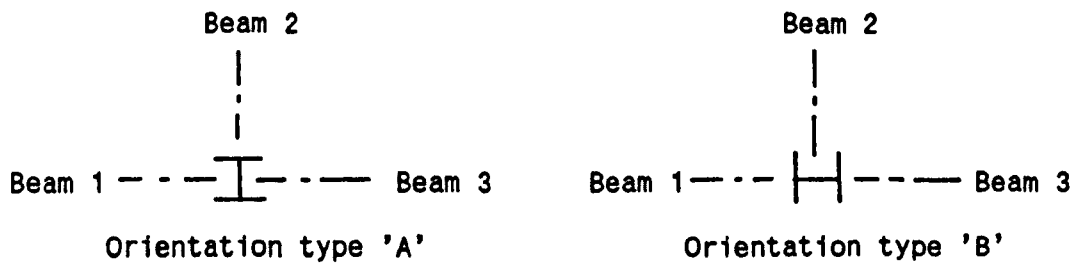


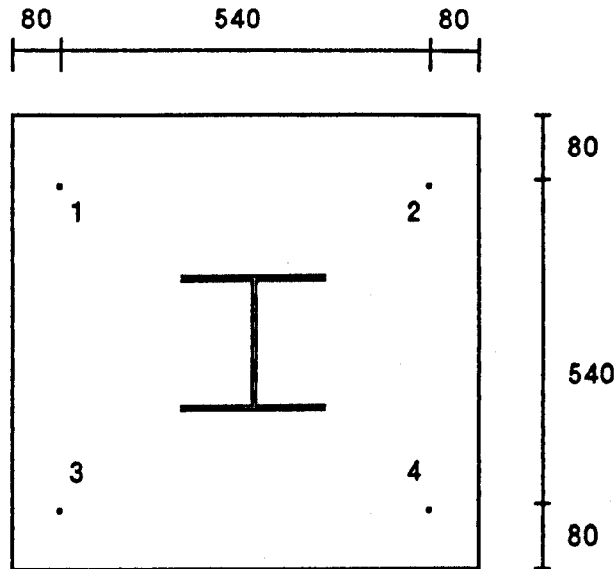
Table 2.3: Connection type, subassemblage type and column orientation for each of the ten subassemblage test.

Subframe Test	Column head load eccentricity (mm)		Initial deformations at mid column (mm)	
	Major	Minor	Major	Minor
S1	+7.0	-7.0	+1.0	+6.0
S2	+6.5	-6.5	-1.5	+9.0
S3	+7.5	-7.5	+3.0	+9.0
S4	+8.0	-9.0	+1.0	+7.5
S5	-10.0	0.0	+4.0	-9.0
S6	-12.0	-2.0	+1.5	-0.5
S7	-6.5	-1.0	+6.5	-5.0
S8	-6.5	-16.0	-3.0	+6.5
S9	-8.5	-13.5	-3.5	+10.0
S10	-4.0	-15.5	+3.0	+7.0

Table 2.4: Initial column deformations and column head load eccentricities.

Subframe Test	Beam load offset (mm)			Nominal Maximum Beam Load (kN)		
	Beam1	Beam2	Beam3	Beam1	Beam2	Beam3
S1	400	400	400	5	50	50
S2	630	700	633	50	50	50
S3	630	700	633	50	50	50
S4	-	695	625	-	50	50
S5	617	708	637	30	30	60
S6	615	713	635	30	30	60
S7	845	709	830	45	45	90
S8	843	700	838	10	85	85
S9	840	697	840	95	95	95
S10	840	698	840	88	132	88

Table 2.5: Nominal applied beam loads and beam load locations.



Column Load (kN)	Displacement at locations on column base (mm)			
	1	2	3	4
250	0.48	0.41	0.38	0.33
290	0.56	0.51	0.48	0.43
330	0.66	0.61	0.61	0.53
380	0.79	0.67	0.75	0.62
450	0.97	0.80	0.95	0.77

Table 2.6: Measurements of column base movement during a re-test of subassemblage S1.



Test	Ultimate column capacity (P <sub>ult</sub> ) kN	Column squash load (P <sub>squash</sub> ) kN	Load ratio P <sub>ult</sub> /P <sub>squash</sub>
S1	468.1	913.1	0.51
S2	503.0	892.0	0.56
S3	542.6	982.1	0.55
S4	494.7	934.7	0.53
S5	479.0	938.5	0.51
S6	614.0	941.5	0.65
S7	490.0	953.6	0.51
S8	482.2	954.8	0.51
S9	526.0	935.1	0.56
S10	520.1	925.1	0.56

Table 2.7: A summary of ultimate column capacities and squash loads.

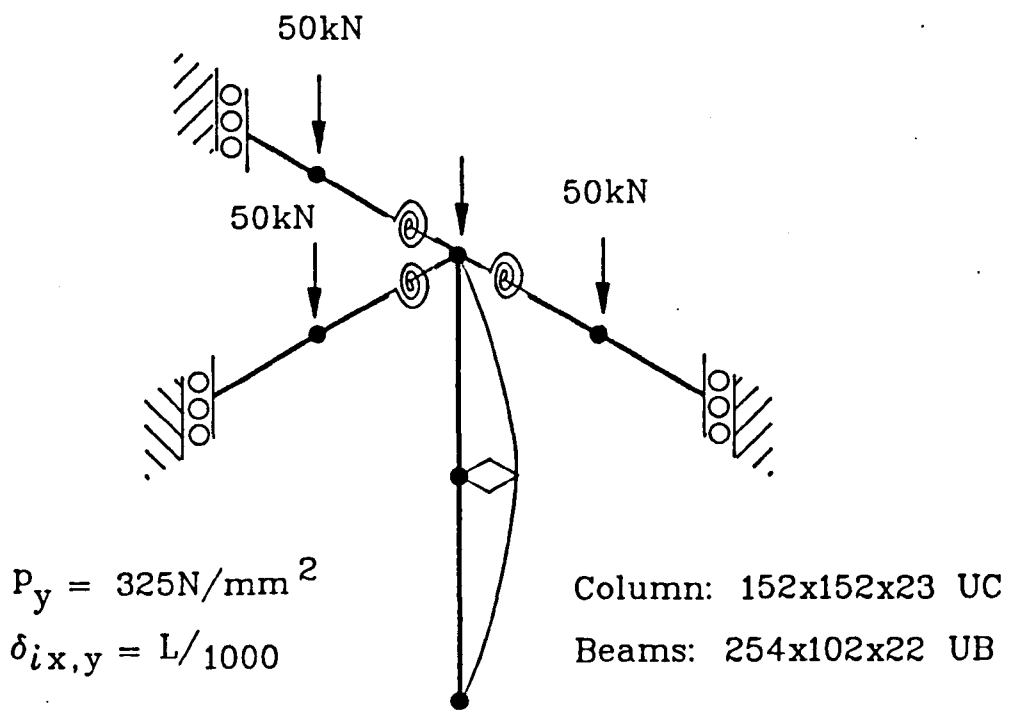


Figure 2.1: Basic analytical model used in the preliminary studies.

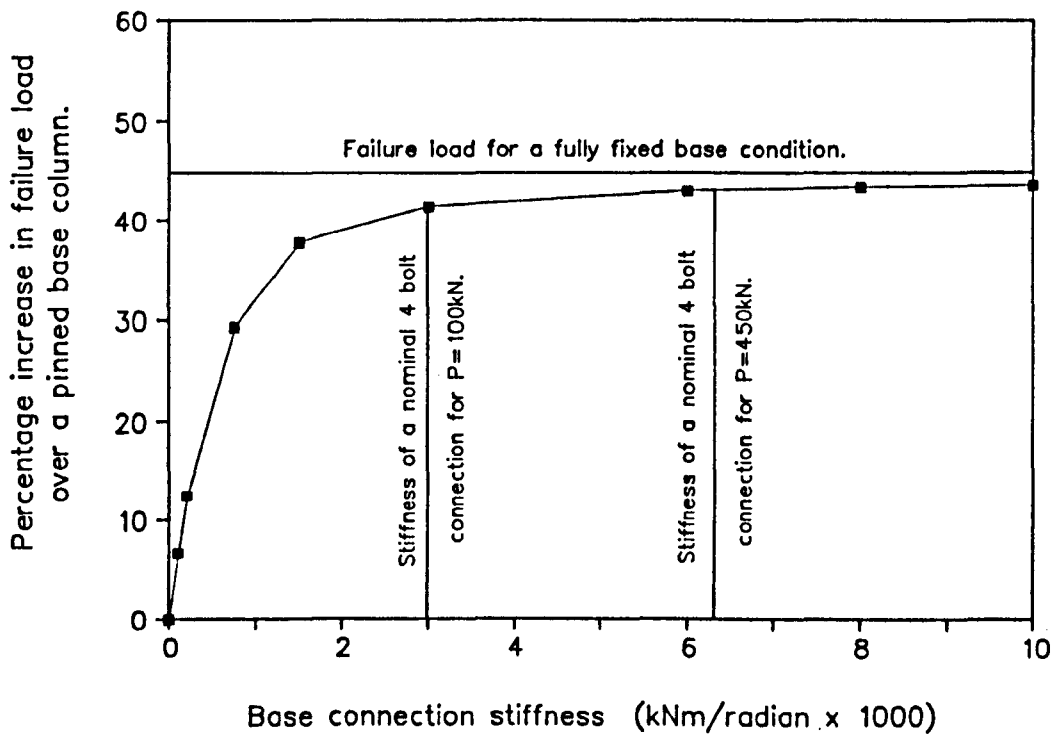


Figure 2.2: Plot of column base stiffness against predicted percentage increase in failure load.

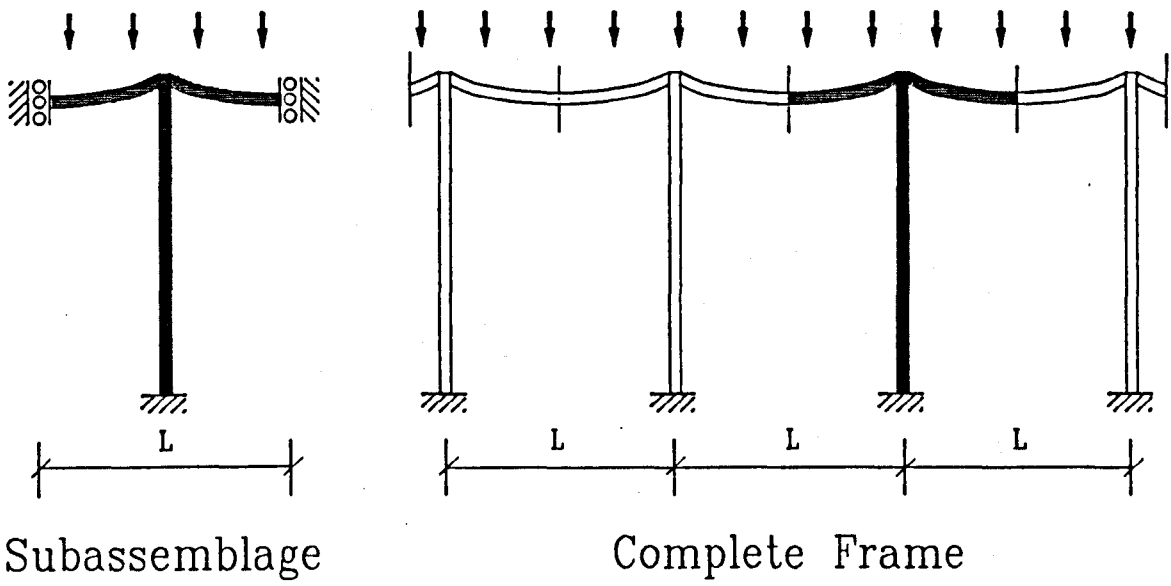


Figure 2.3: Subassemblage from within a more extensive structure.

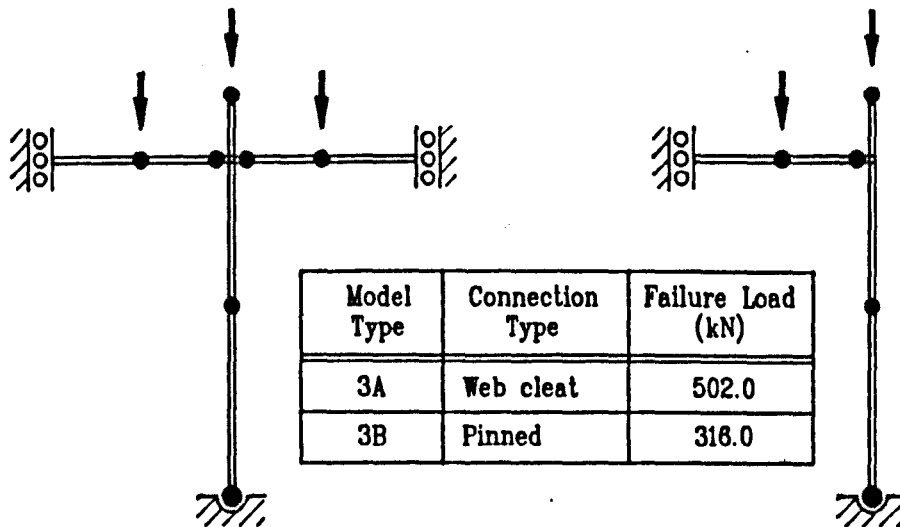
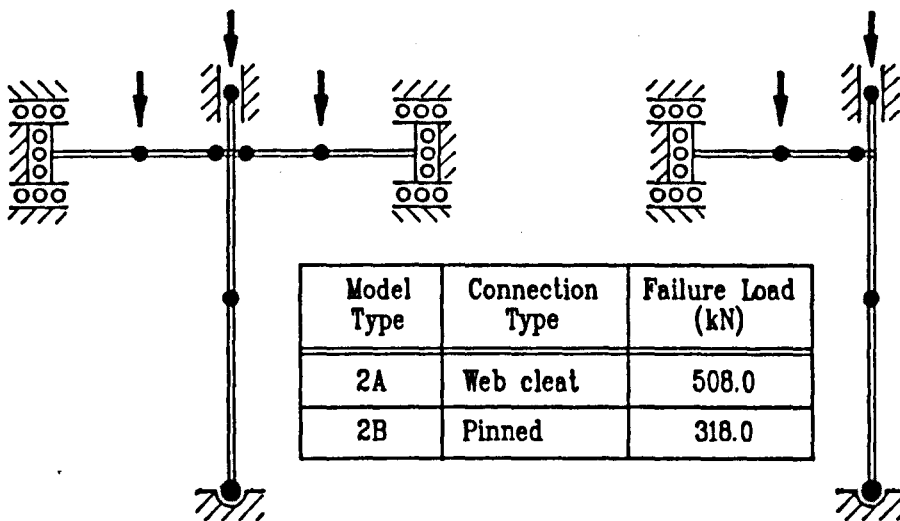
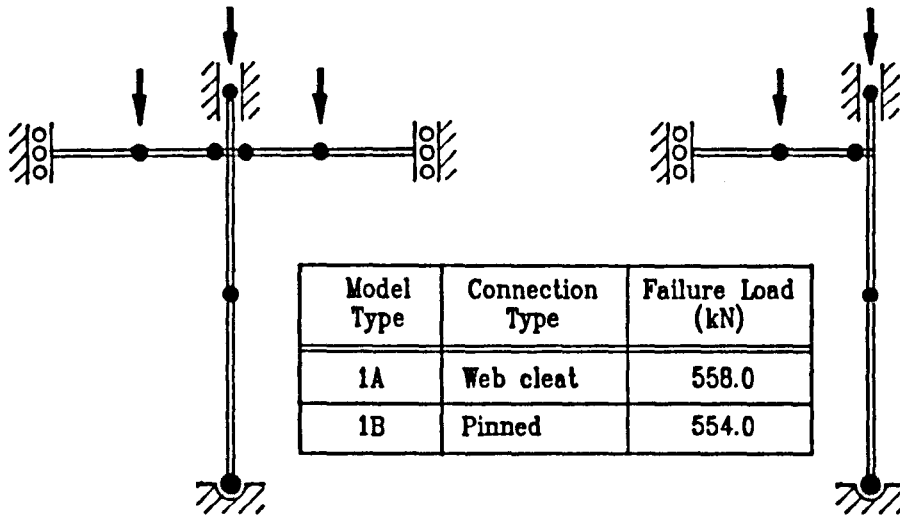


Figure 2.4: Predicted failure loads for analytical models employing different boundary conditions.

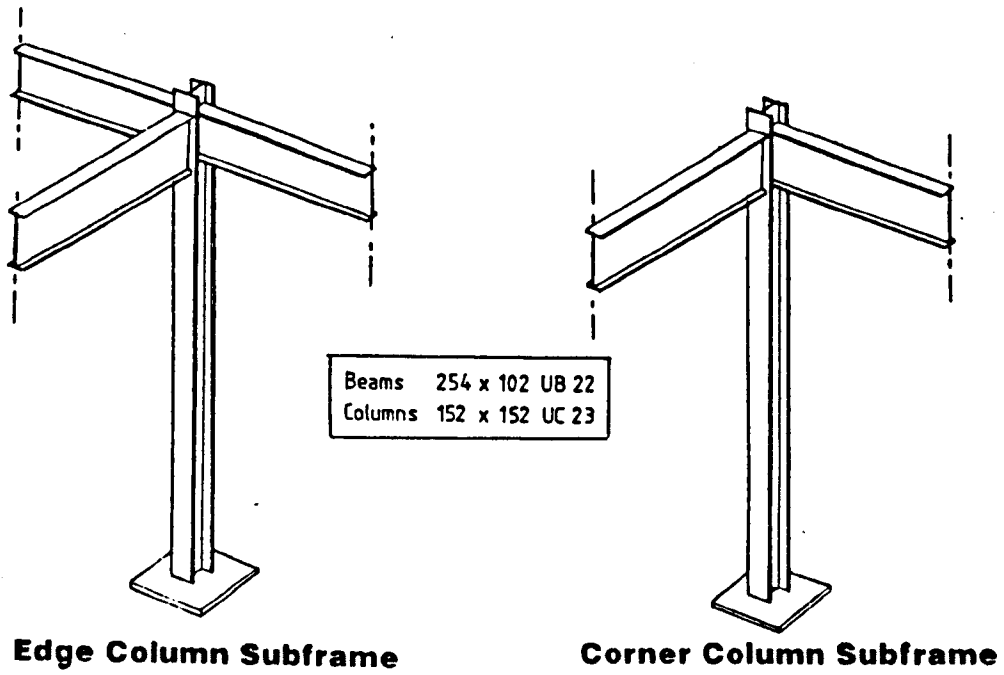


Figure 2.5: The 'edge' and 'corner' column subassemblage configurations considered in the experimental study.

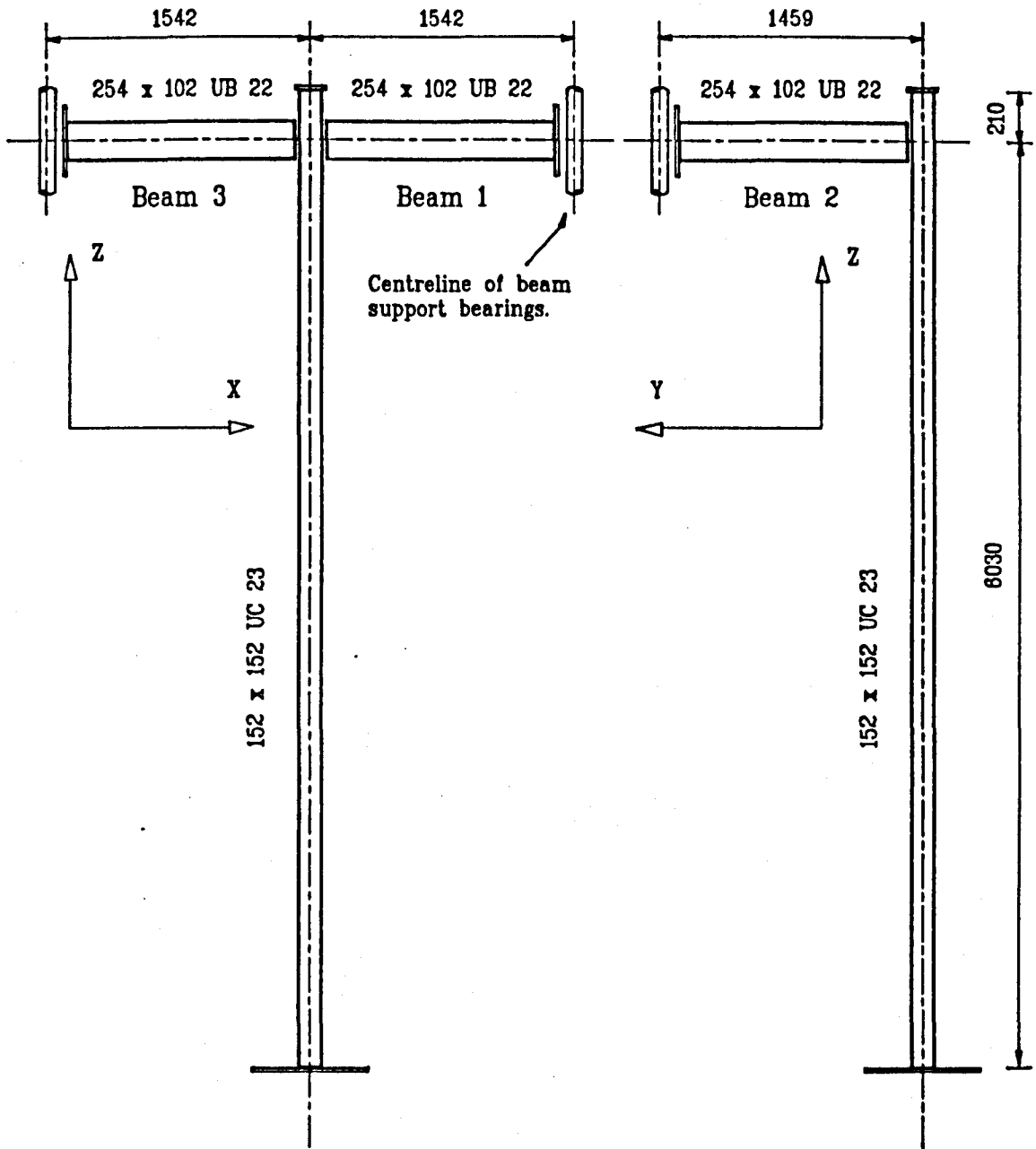


Figure 2.6: General arrangement of the three beam subassemblage.

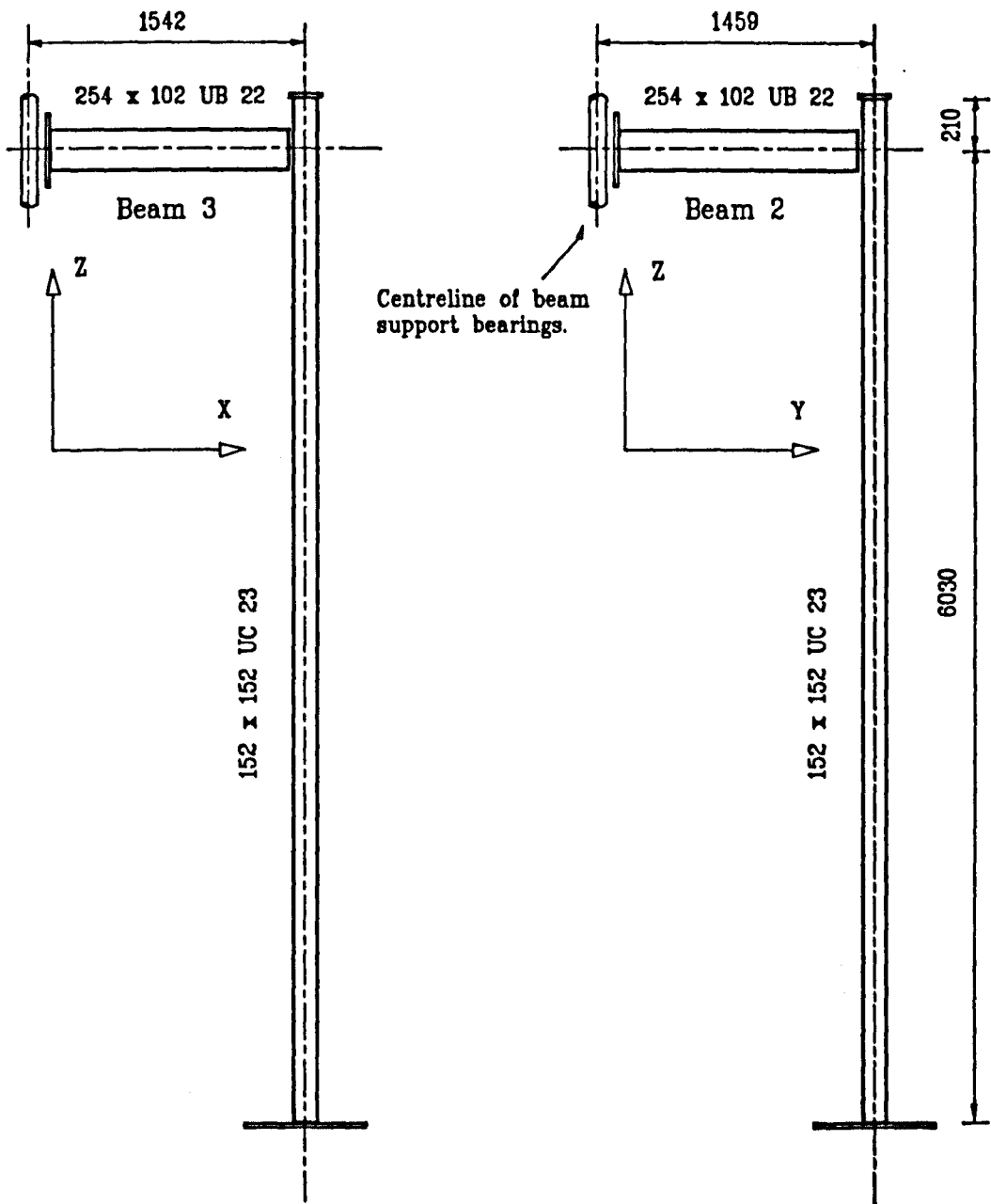


Figure 2.7: General arrangement of the two beam subassemblage.

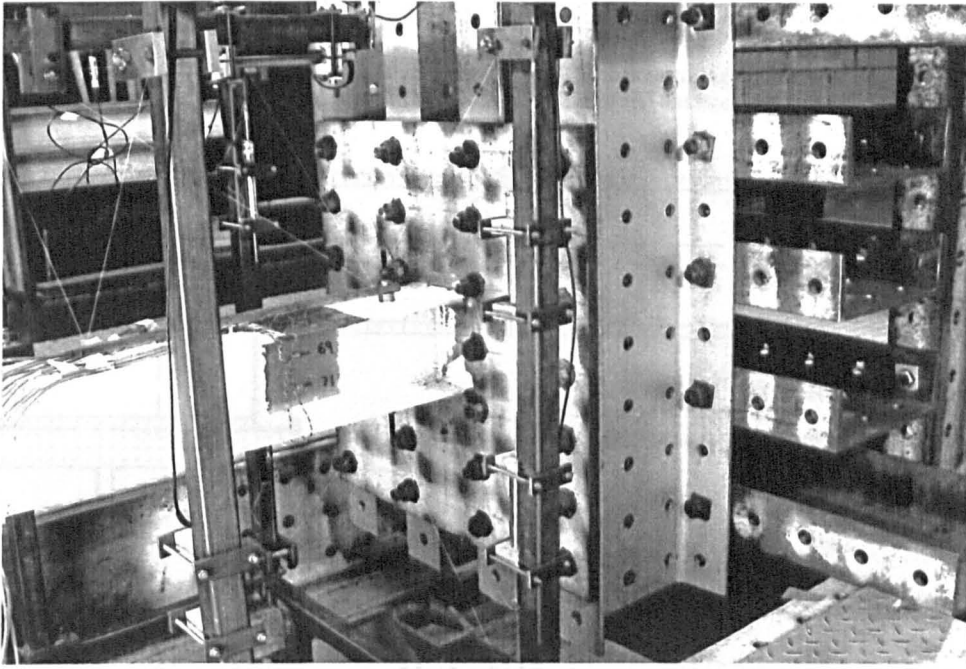


Figure 2.8: Column base-plate arrangement used in each of the ten tests.

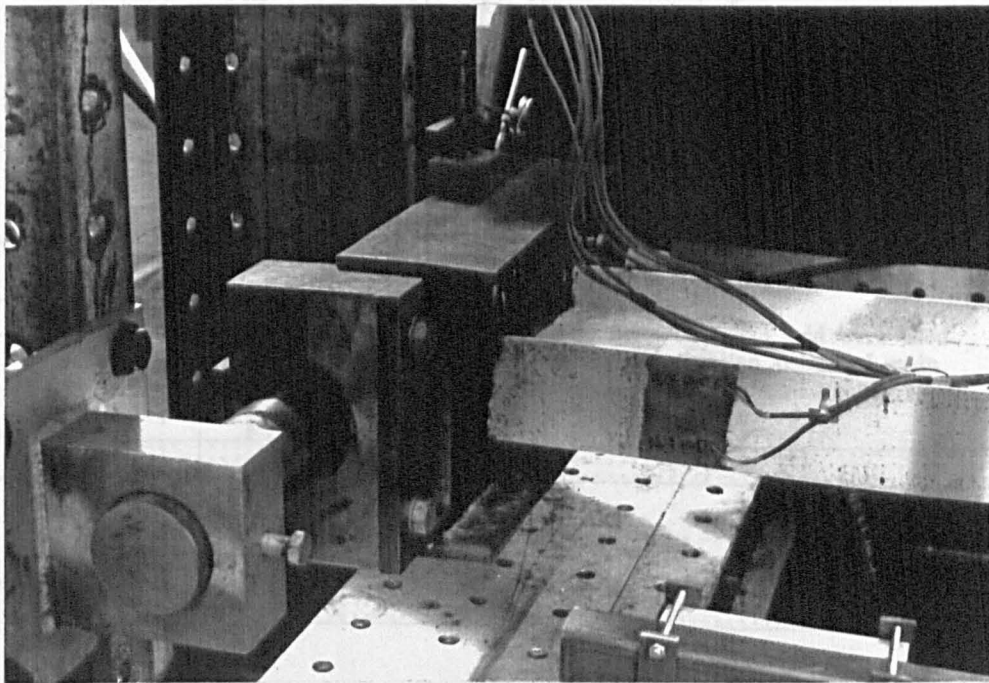
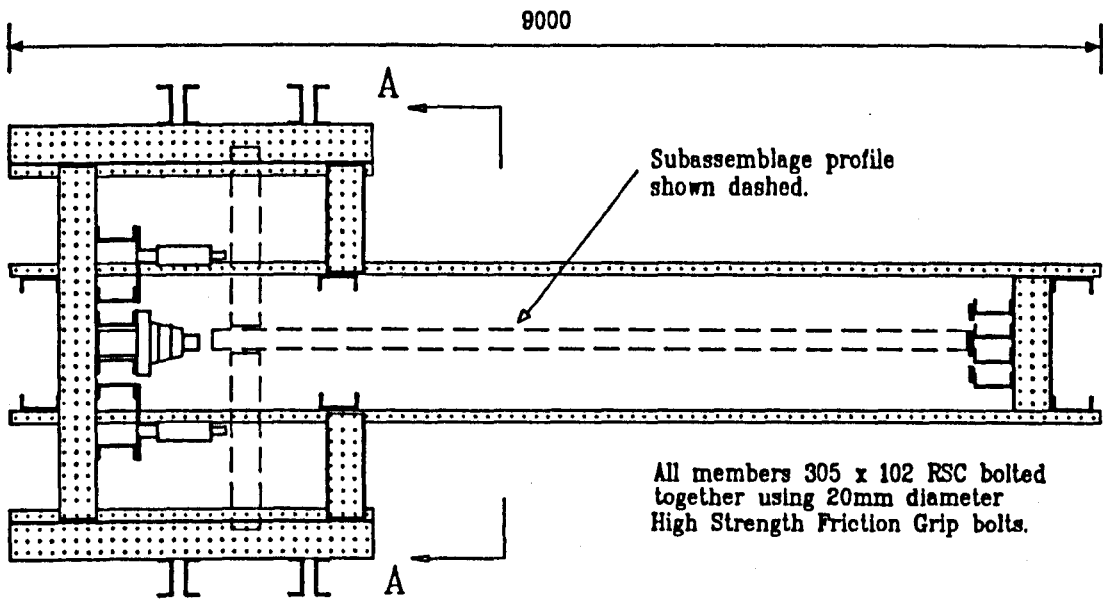


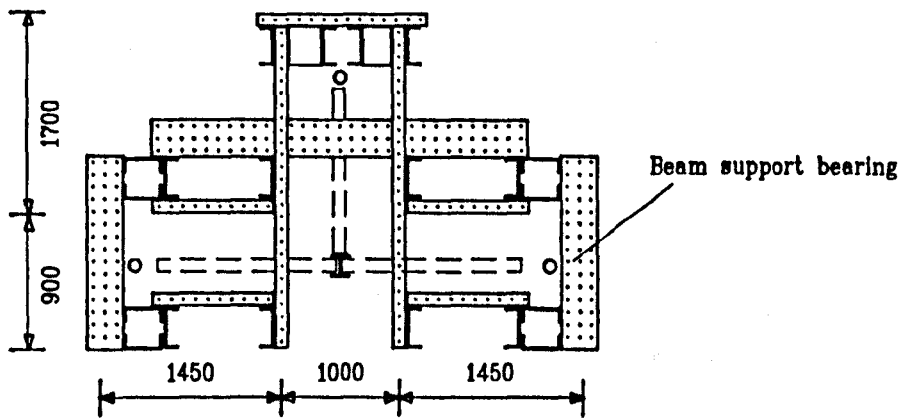
Figure 2.9: Sliding support bearing used at the end of each beam.

Figure 2.10: General arrangement of the experimental testing rig.

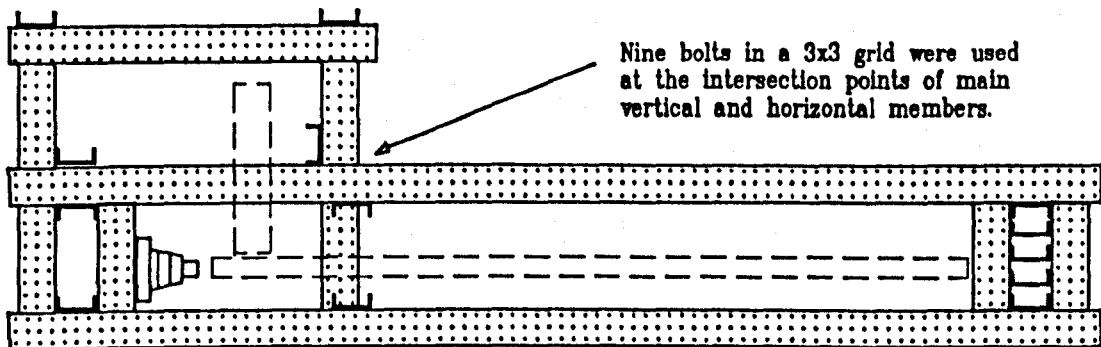




Plan at 900mm level



Section A-A



Longitudinal Elevation

Figure 2.10: General arrangement of the subassembly testing rig.

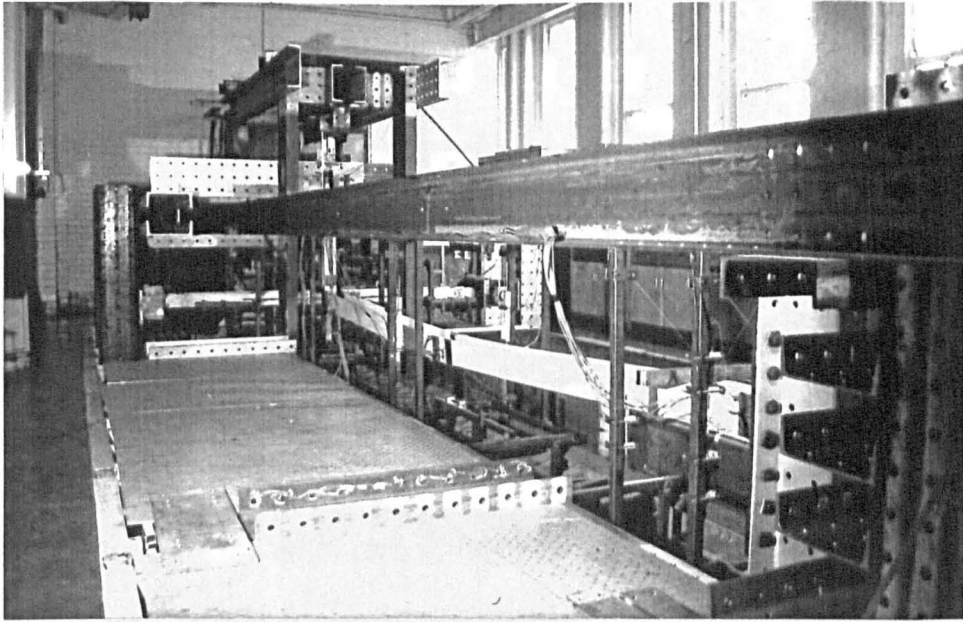


Figure 2.11: The subassembly testing rig with a specimen installed.

Figure 2.13: End view of testing rig base arrangement.

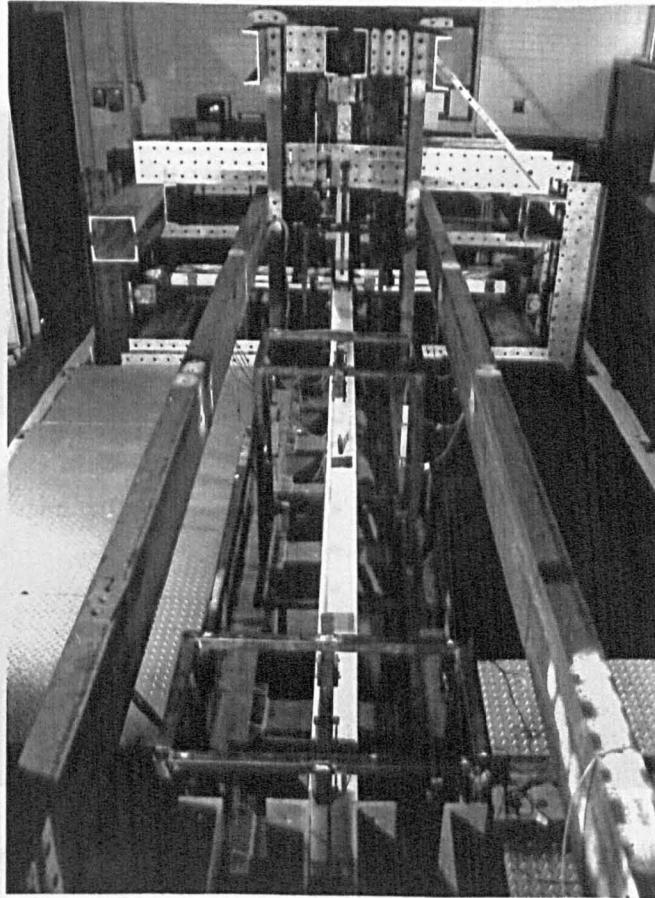


Figure 2.12: The subassembly testing rig with a specimen installed.

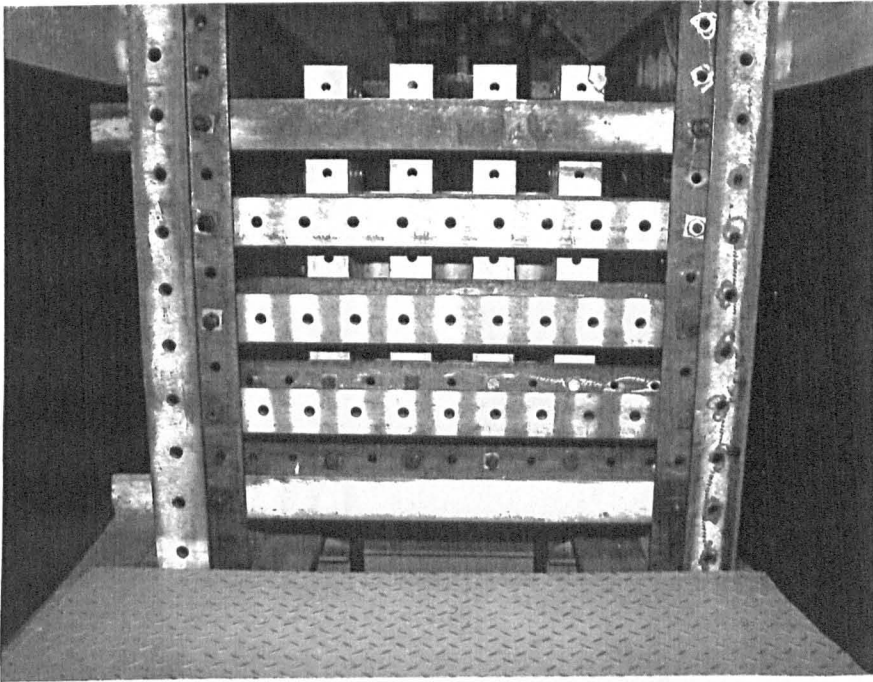


Figure 2.13: End view of testing rig base arrangement.



Figure 2.14: Elevation of testing rig base arrangement.

A small eccentric 'nip' load was applied to hold the column firmly in position.

Column specimen was placed in the test rig with the base-plate bolted in position.

Column section cut with a slight (2mm) chamfer at the base.

Stage 1

Increasing the column head load caused the chamfer at the base to close and deformed the column in the shape of an arc.

Stage 2

When the required bow was observed at the centre, the load was held constant and the column was welded to the base-plate

Stage 3

On removing the specimen from the test rig, the induced base angle is clearly evident.

Stage 4

Figure 2.15: Method of inducing the required initial column deformations.

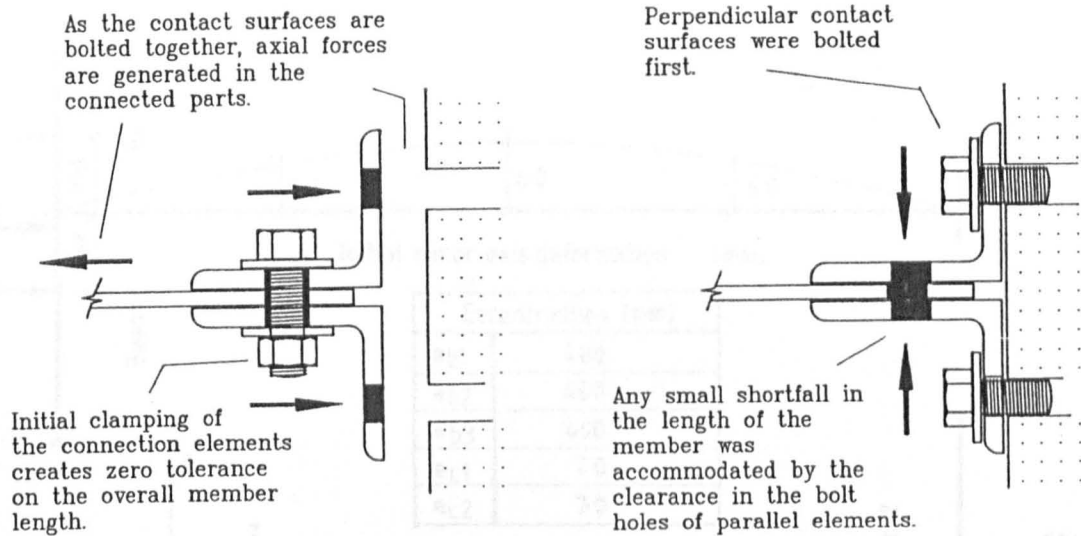


Figure 2.16: Different beam to column connection bolt fixing sequences.

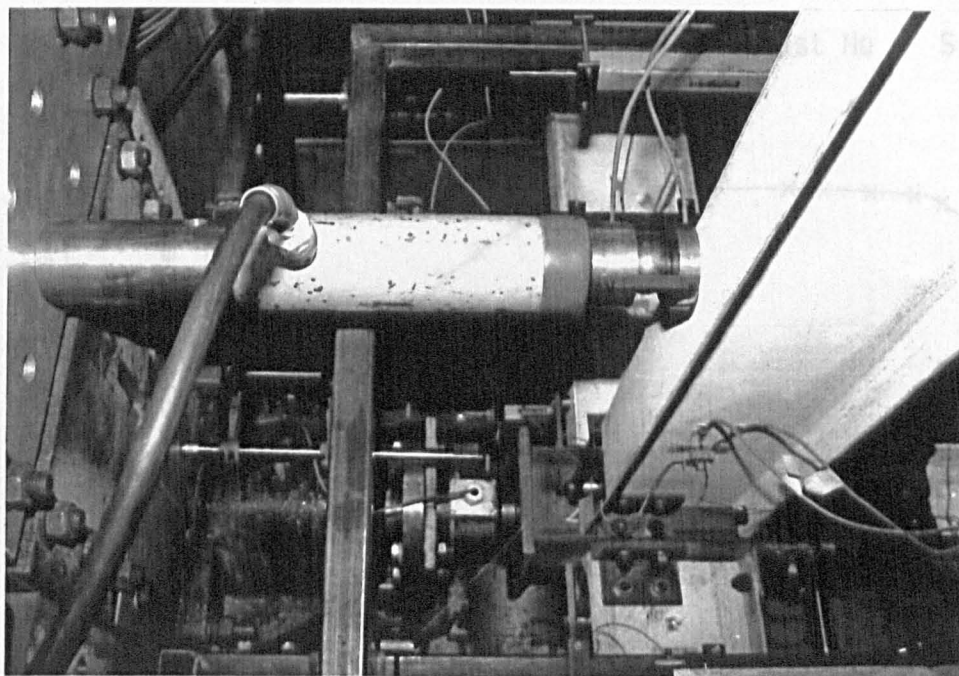


Figure 2.17: 250kN capacity hydraulic ram used to apply beam loading.

# Subassemblage test S1

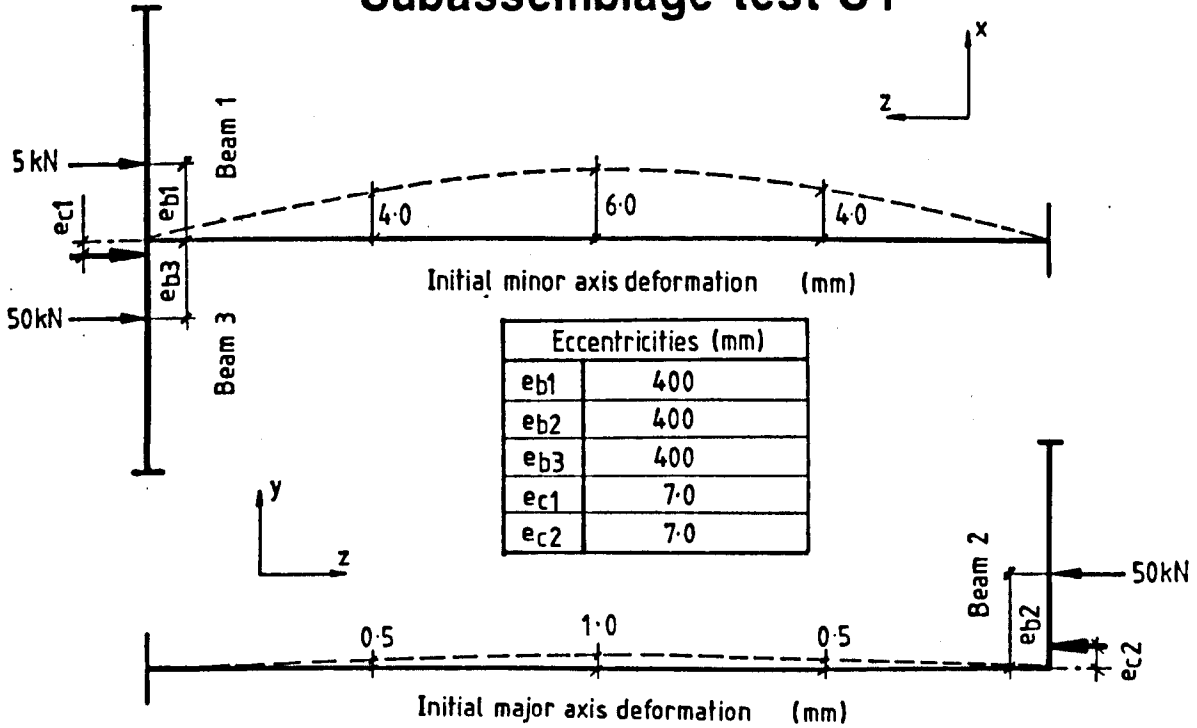


Figure 2.18: Summary of the major experimental parameters in test S1.

Deflection at the column centre

Test No : S1

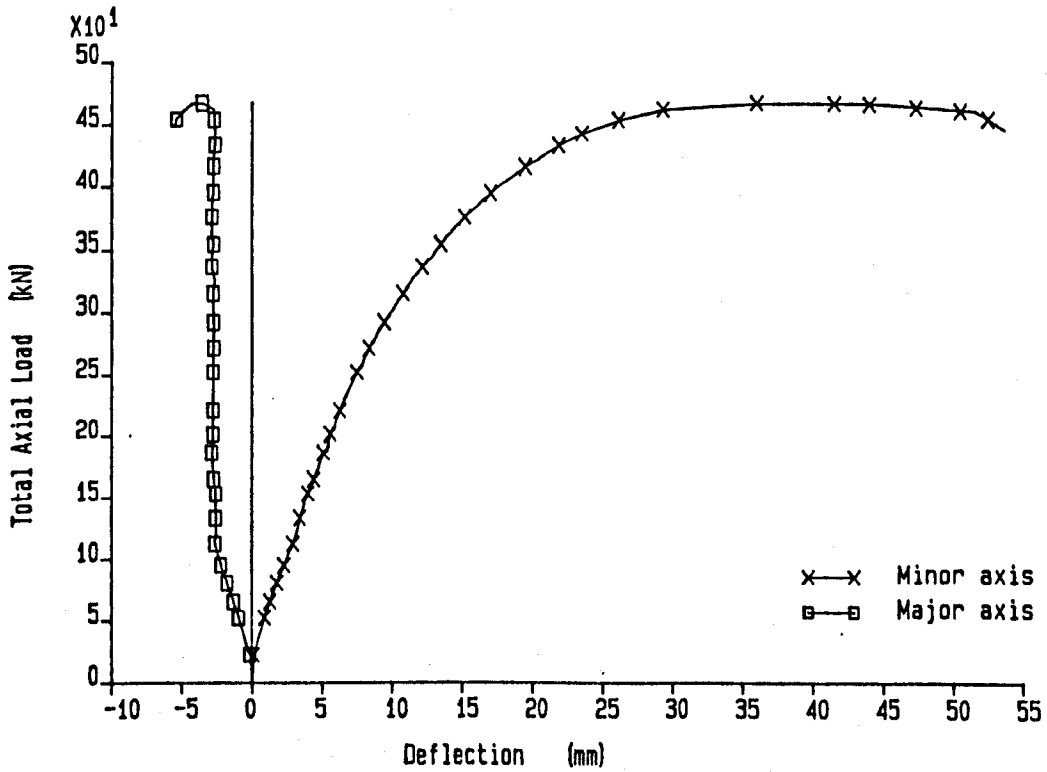


Figure 2.19: Plot of axial load vs. mid-column deflection for test S1.

Bending Moment Diagram - Test No. S1

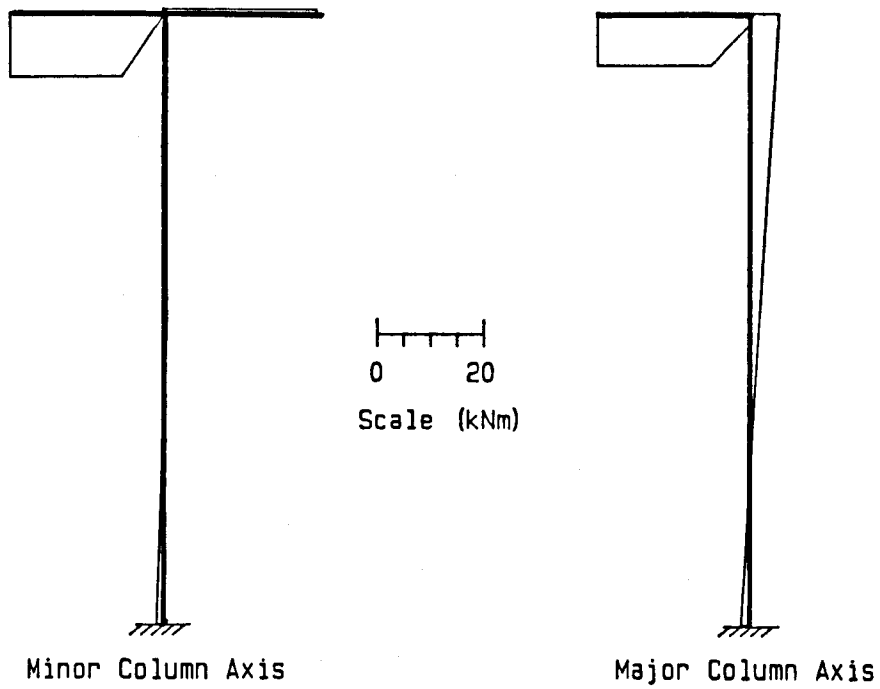


Figure 2.20: Distribution of bending moments at the end of the beam loading phase.

Bending Moment Diagram - Test No. S1

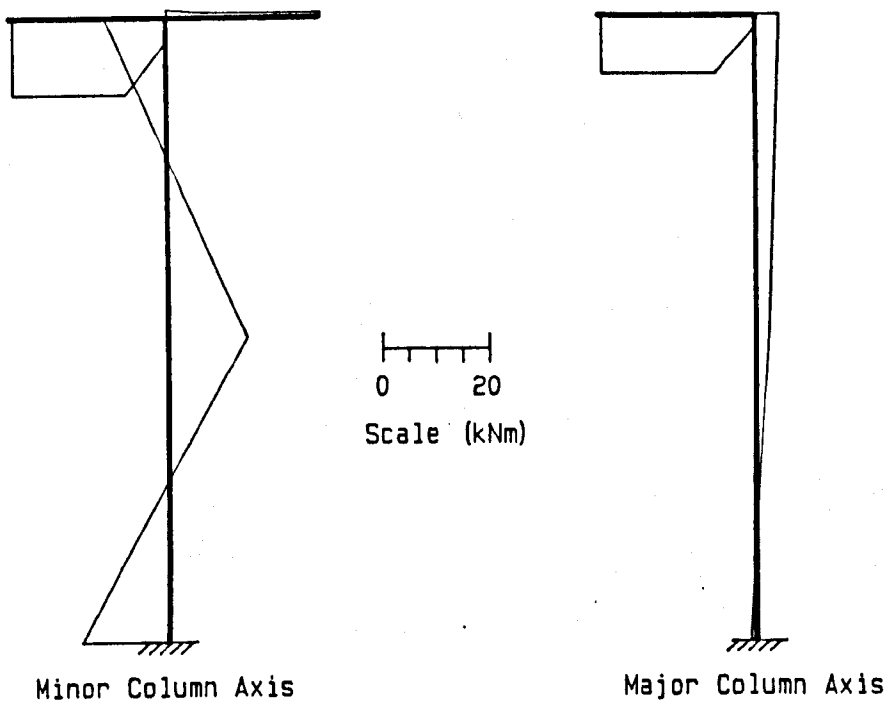


Figure 2.21: Distribution of bending moments at the point of maximum applied load.

Travel of the beam support bearings

Test No : S1

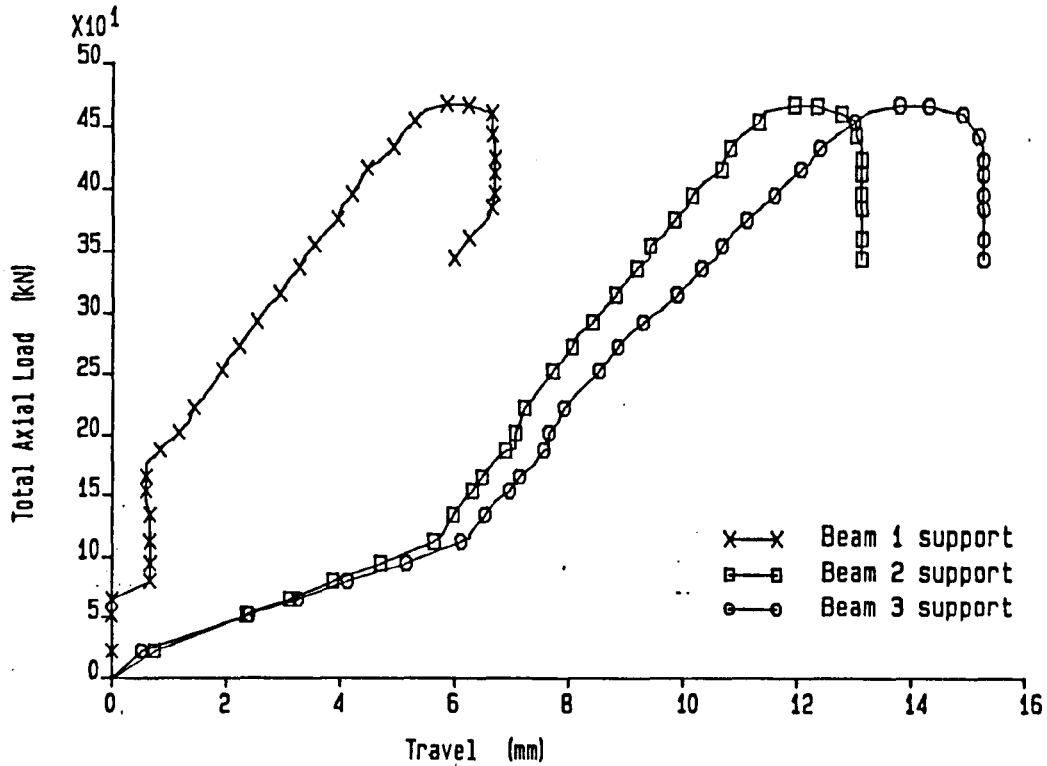


Figure 2.22: Plot of axial load vs. beam support displacements - test S1.

Travel of the beam support bearings

Test No : S2

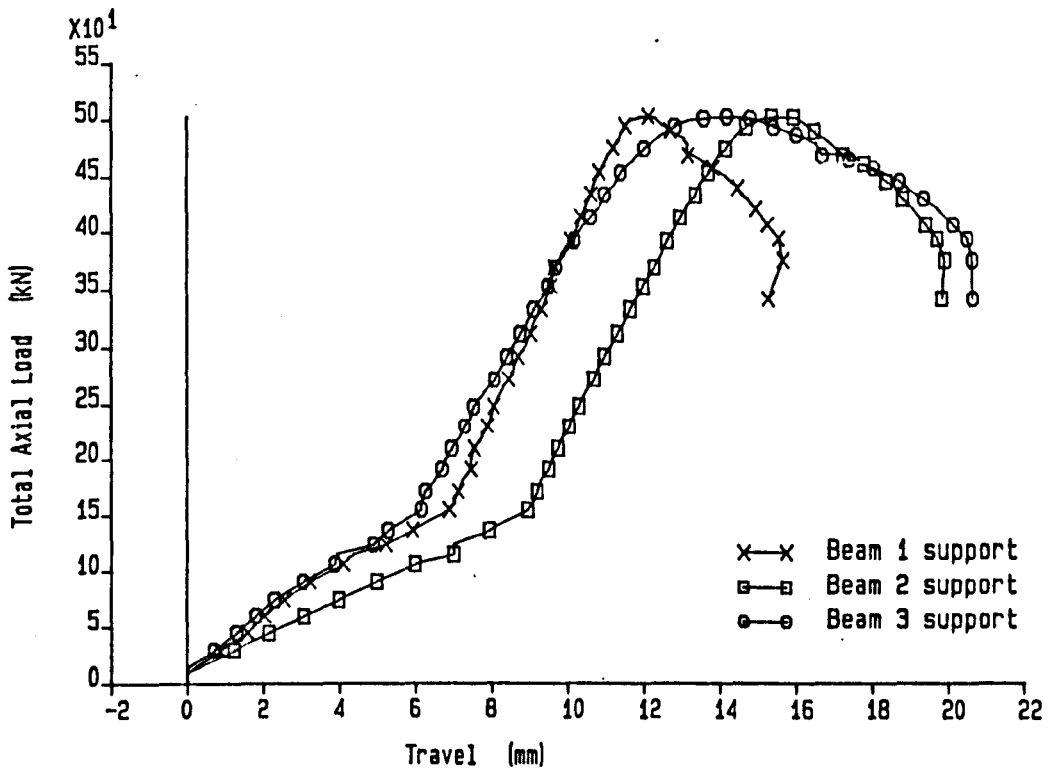


Figure 2.23: Plot of axial load vs. beam support displacements - test S2.



# Subassemblage test S2

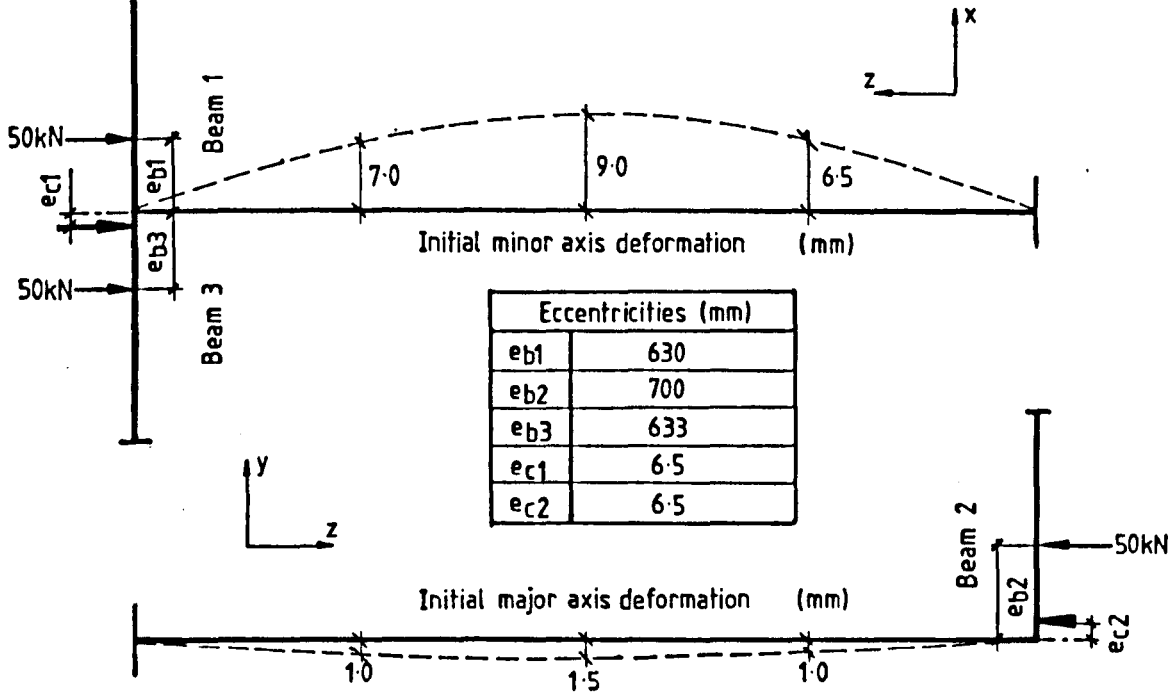


Figure 2.24: Summary of the major experimental parameters in test S2.

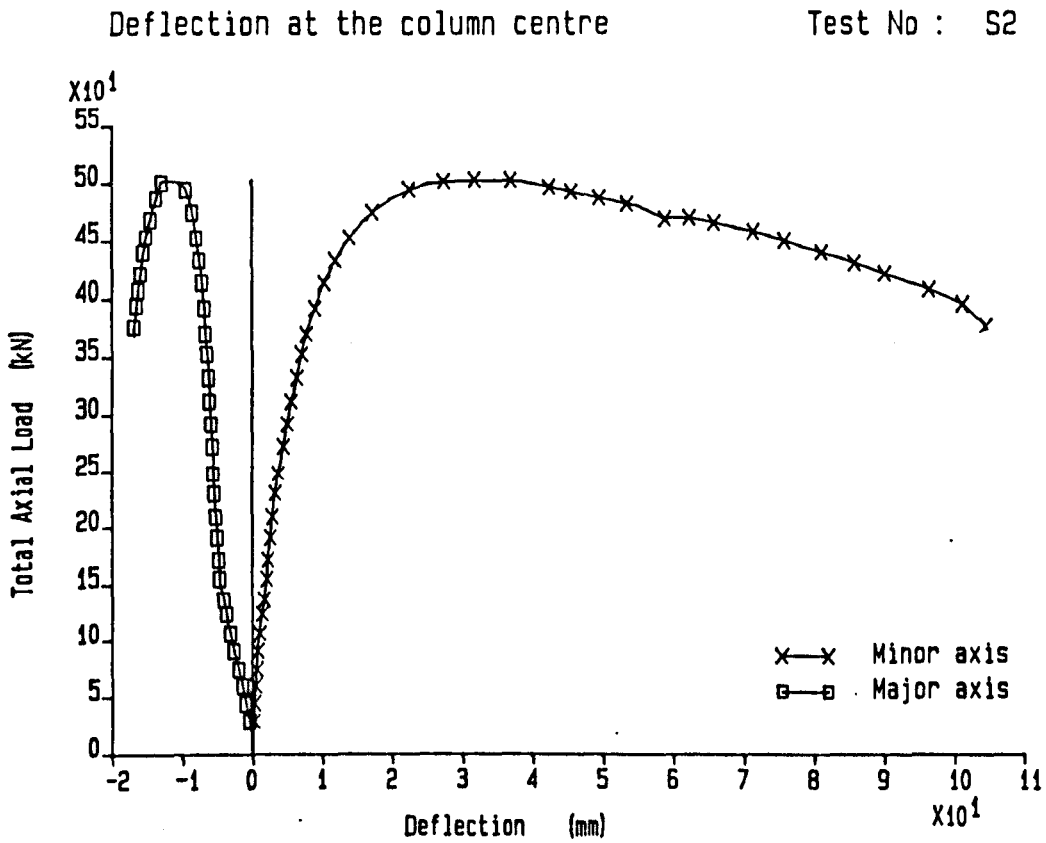
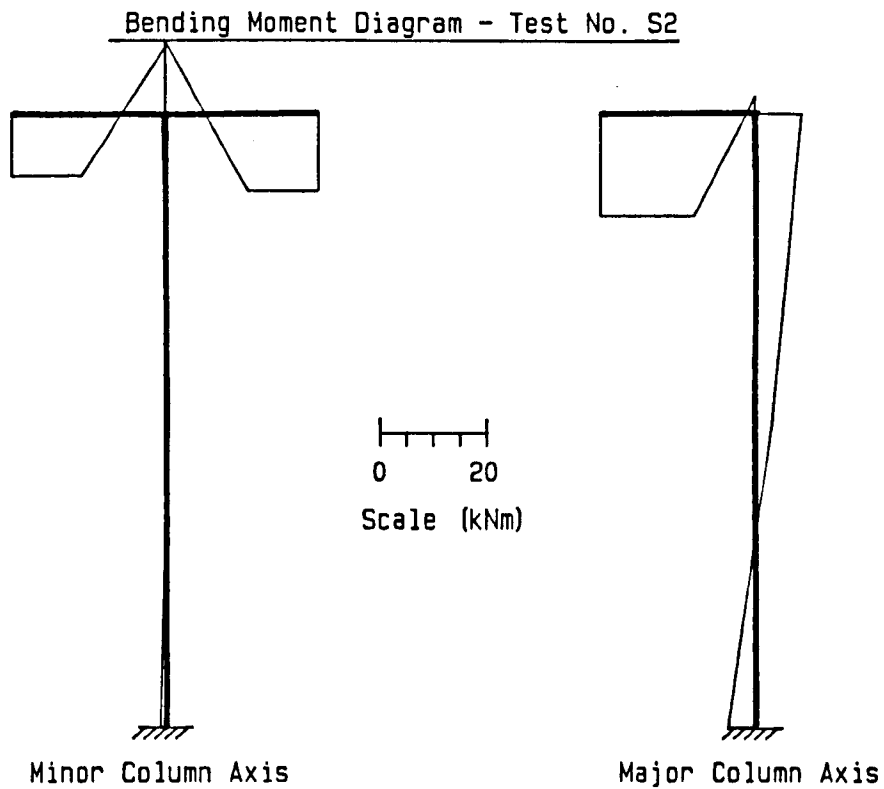
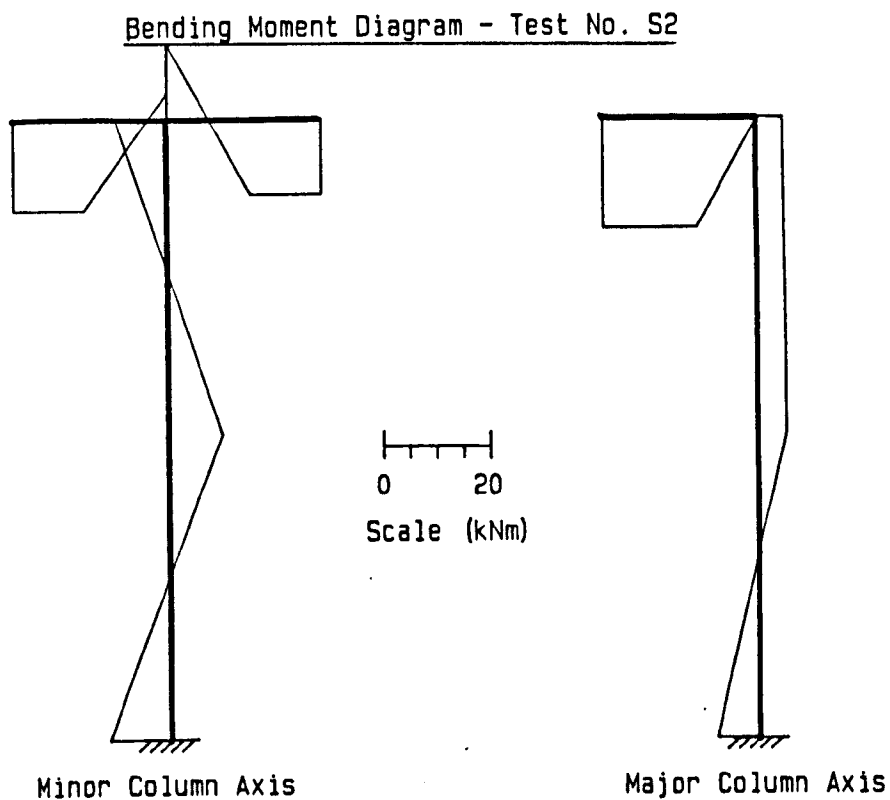


Figure 2.25: Plot of axial load vs. mid-column deflection for test S2.



**Figure 2.26: Distribution of bending moments at the end of the beam loading phase.**



**Figure 2.27: Distribution of bending moments at the point of maximum applied load.**

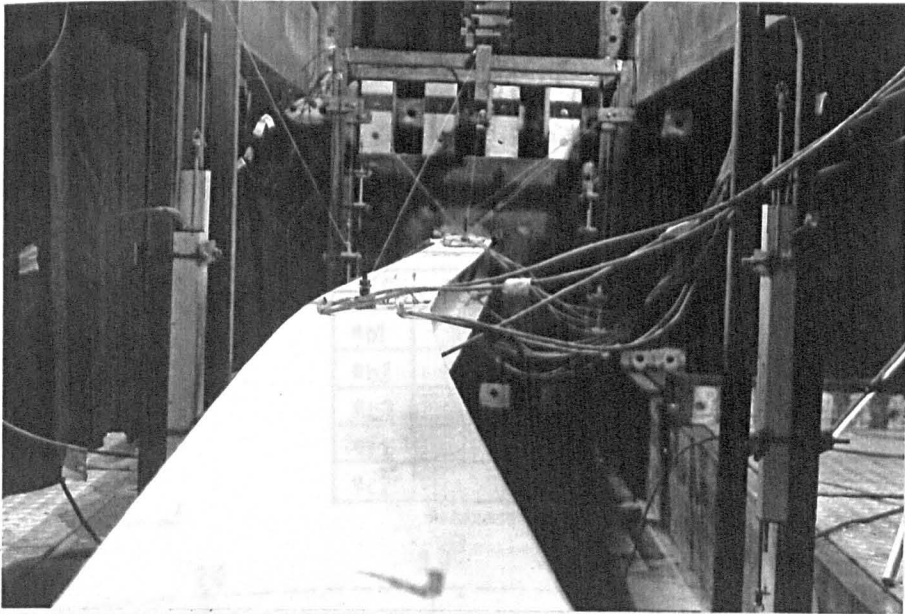


Figure 2.28: View along the length of column S2 highlighting the deformation at a post-failure loading level.

Figure 2.29: Summary of the major experimental parameters in test S3.

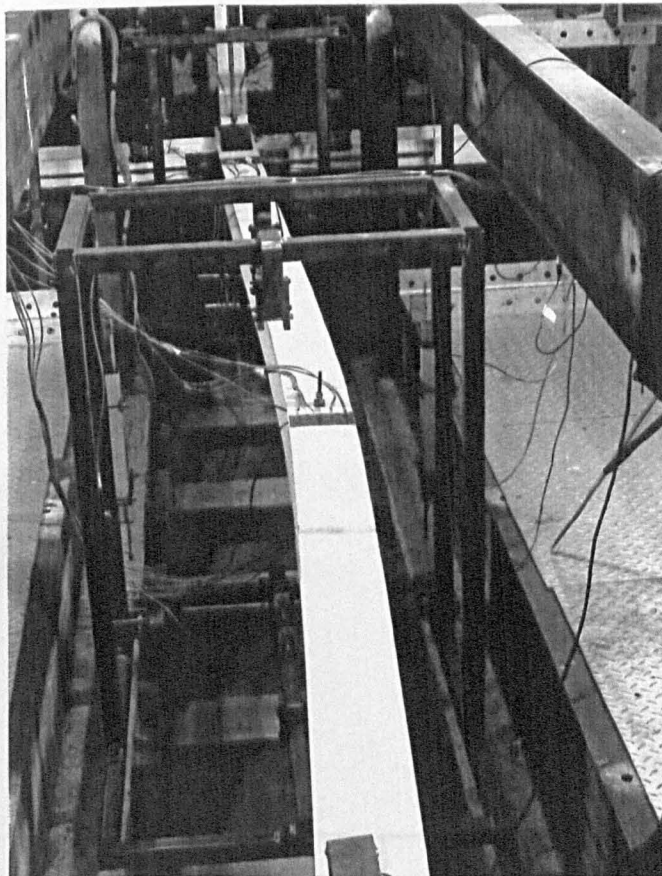


Figure 2.29: View of column S2 at a post-failure loading level.

# Subassemblage test S3

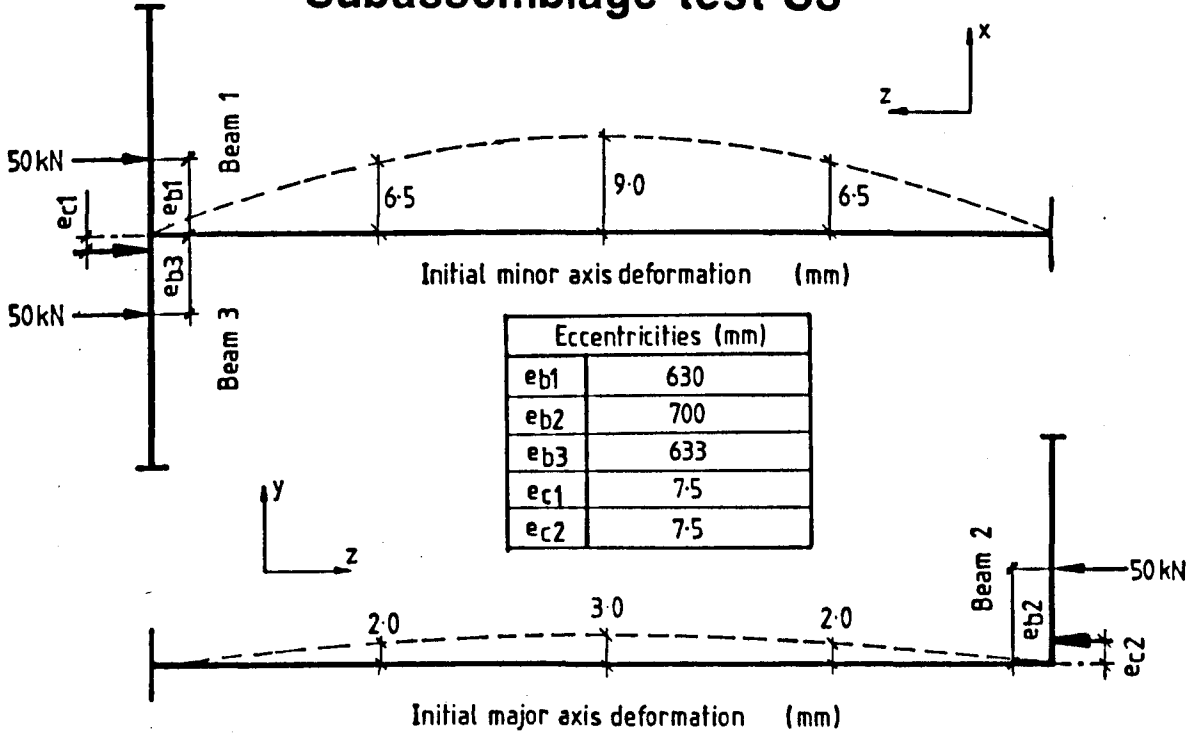


Figure 2.30: Summary of the major experimental parameters in test S3.

Deflection at the column centre

Test No : S3

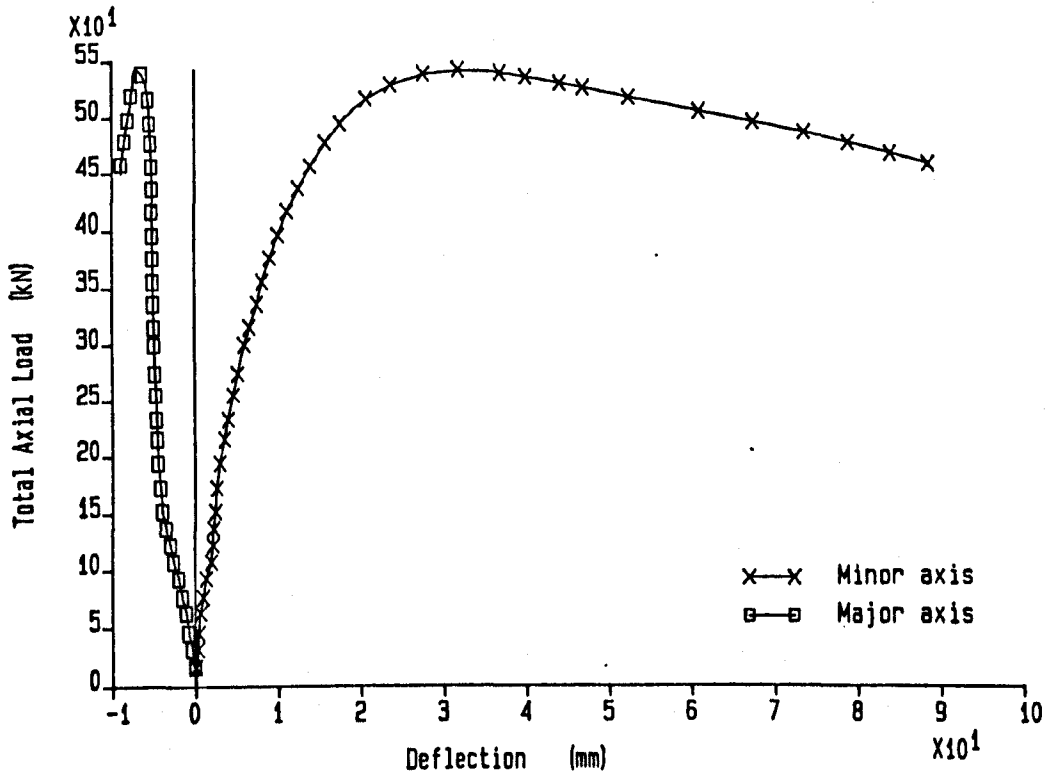


Figure 2.31: Plot of axial load vs. mid-column deflection for test S3.

Bending Moment Diagram - Test No. S3

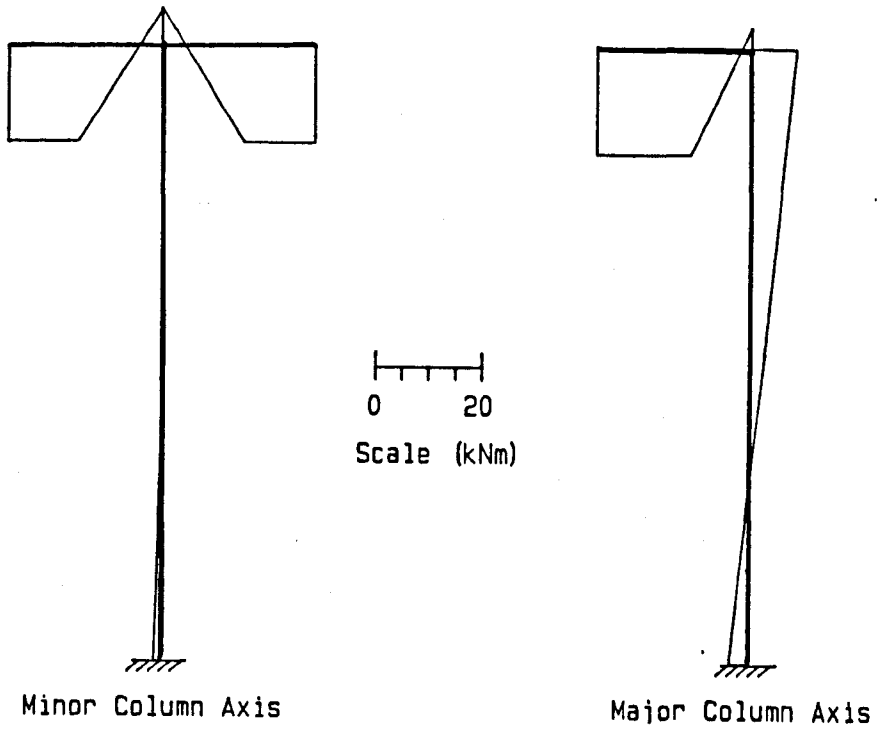


Figure 2.32: Distribution of bending moments at the end of the beam loading phase.

Bending Moment Diagram - Test No. S3

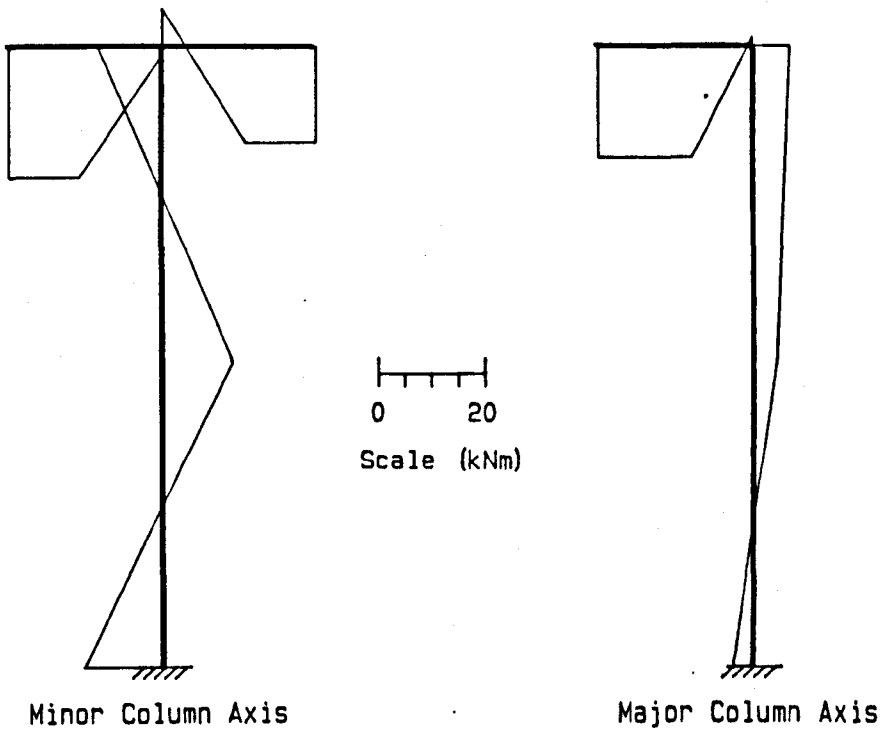


Figure 2.33: Distribution of bending moments at the point of maximum applied load.

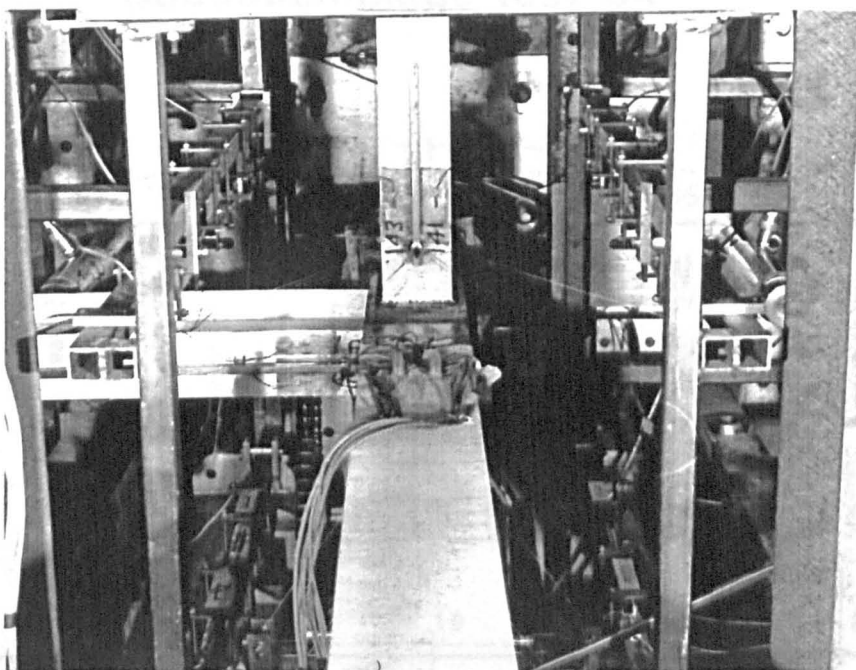


Figure 2.34: The head of column S4 showing the two intersecting beams.

Figure 2.35: Summary of the major experimental parameters in test S4.

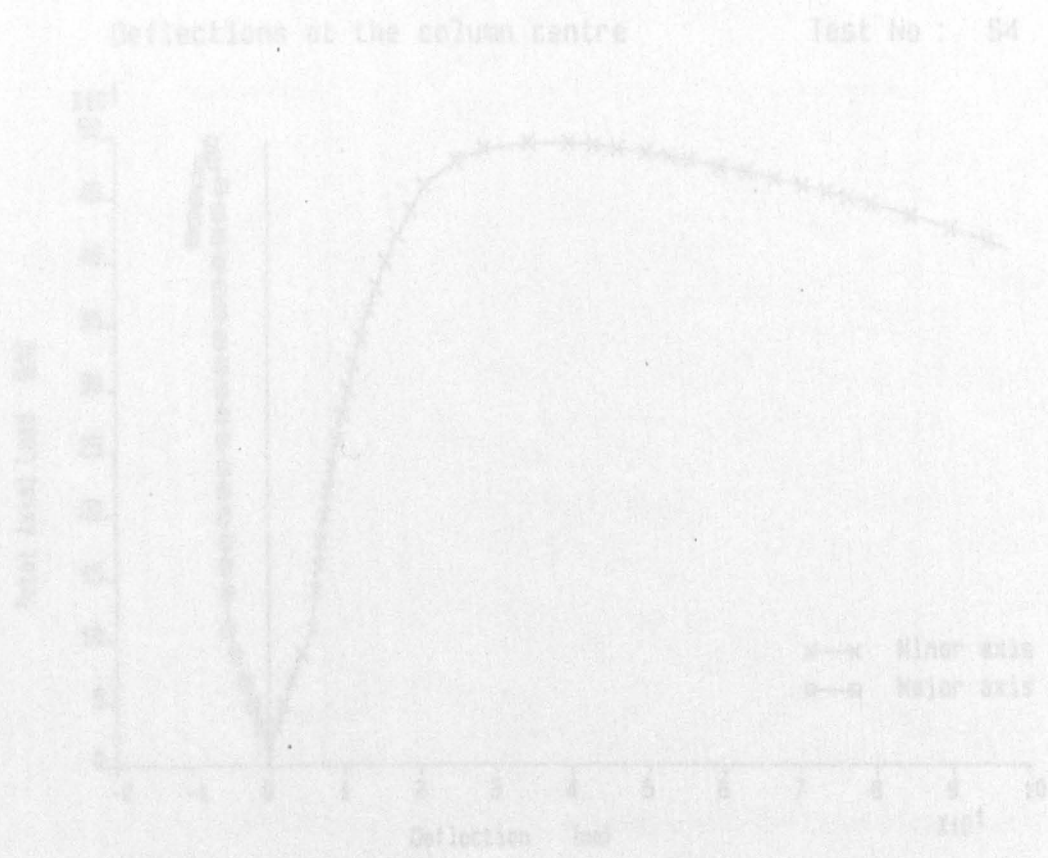


Figure 2.36: Plot of axial load vs. mid-column deflection for test S4.

# Subassemblage test S4

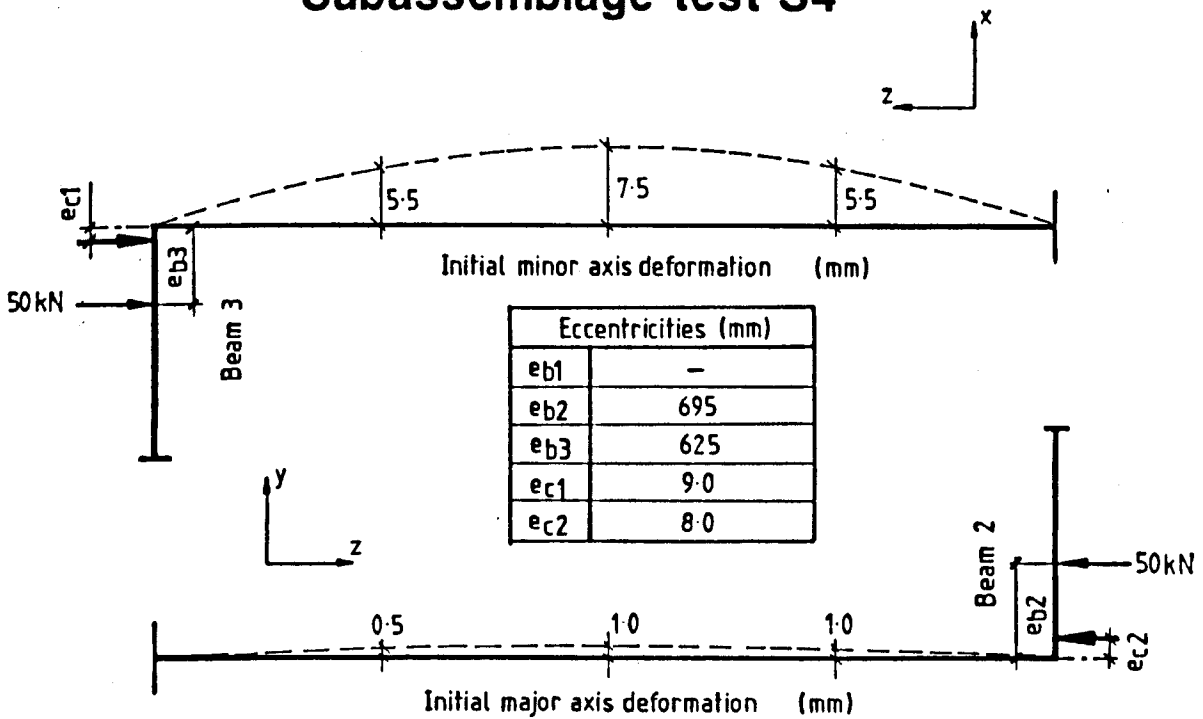


Figure 2.35: Summary of the major experimental parameters in test S4.

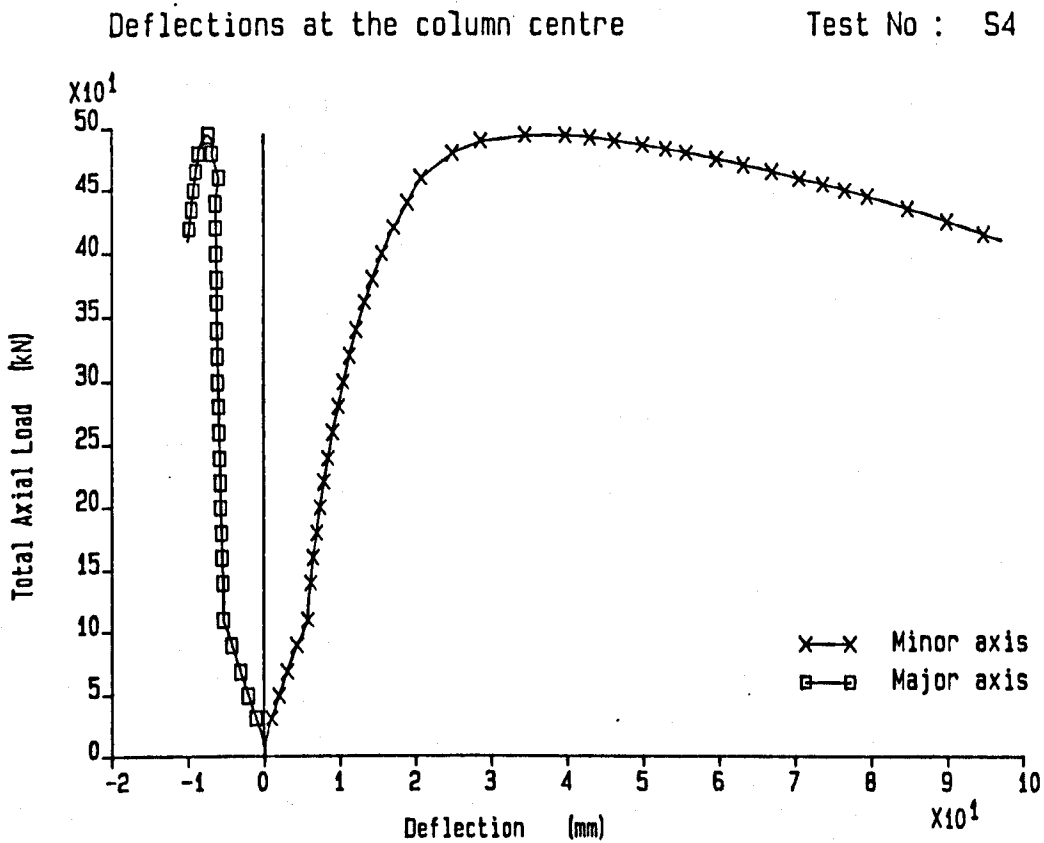


Figure 2.36: Plot of axial load vs. mid-column deflection for test S4.

Bending Moment Diagram - Test No. S4

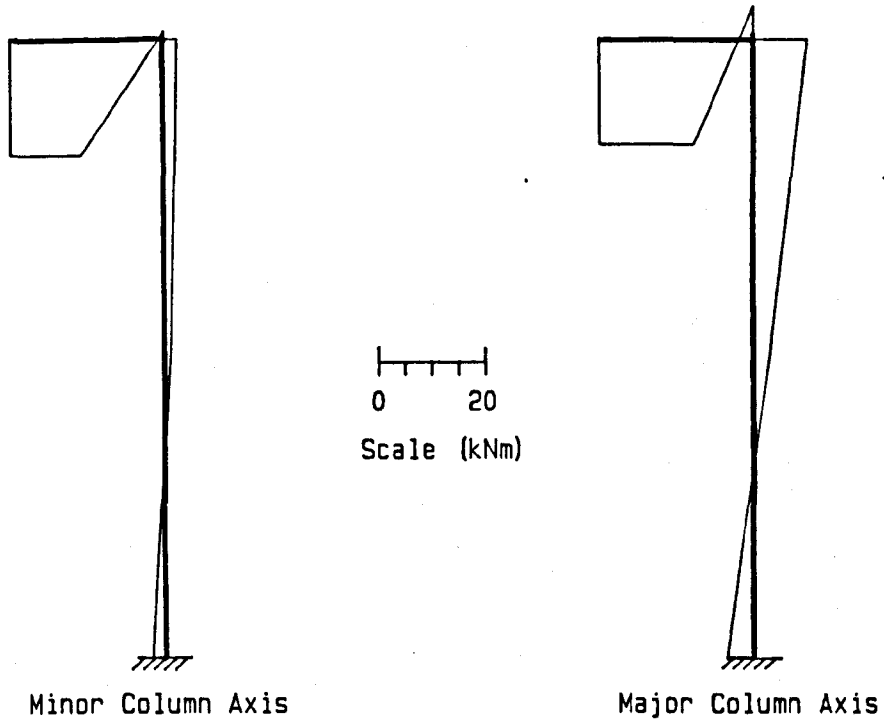


Figure 2.37: Distribution of bending moments at the end of the beam loading phase.

Bending Moment Diagram - Test No. S4

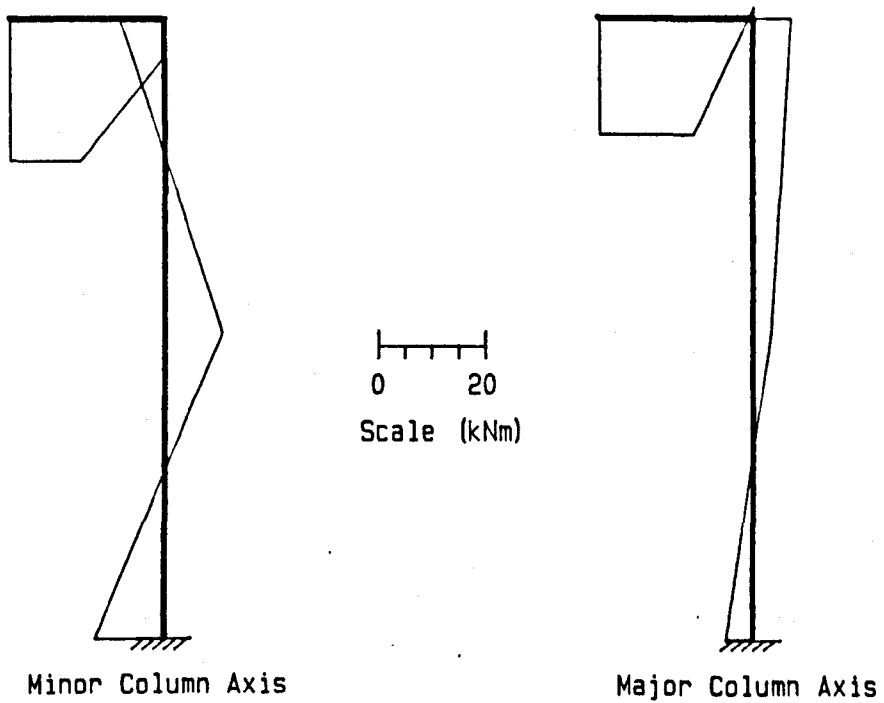


Figure 2.38: Distribution of bending moments at the point of maximum applied load.



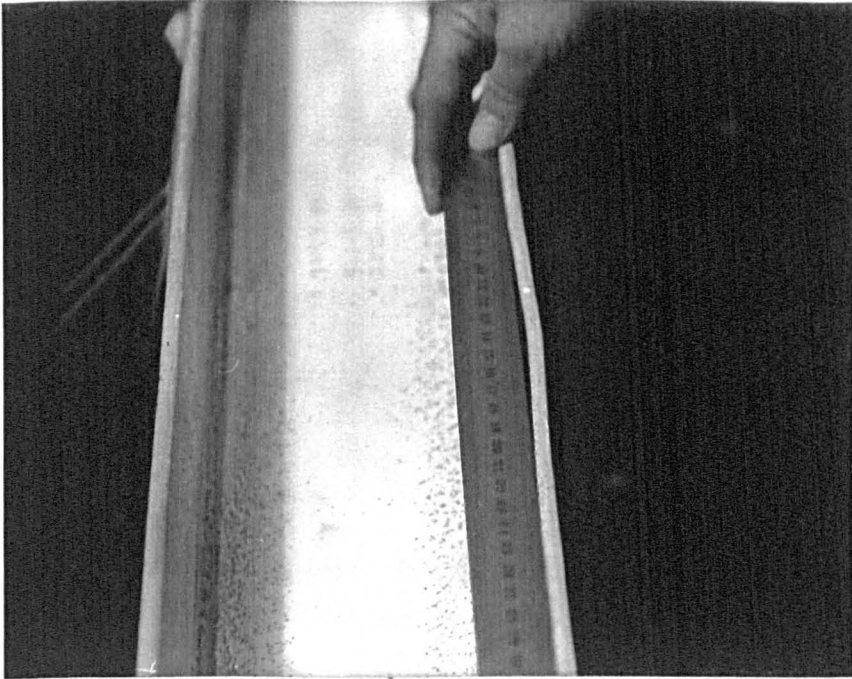


Figure 2.39: A local deformation in the flange of column S5 prior to testing.

# Subassemblage test S5

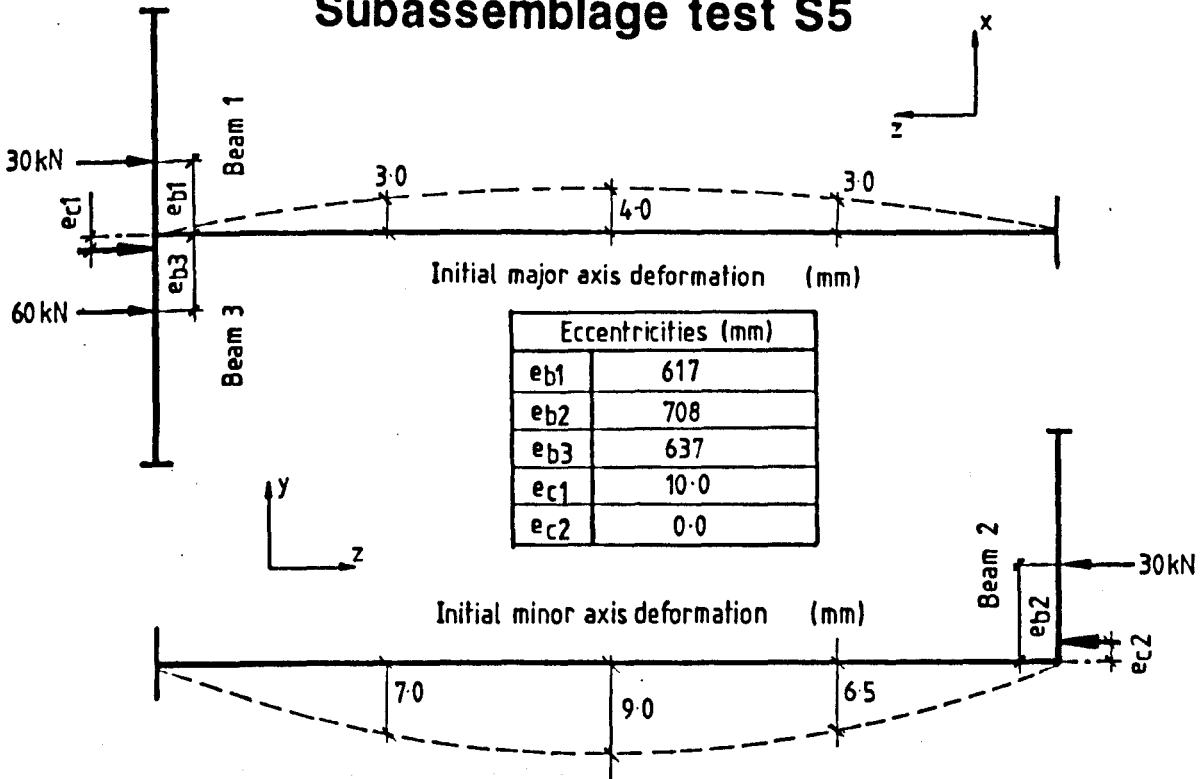


Figure 2.40: Summary of the major experimental parameters in test S5.

Deflection at the column centre

Test No : S5

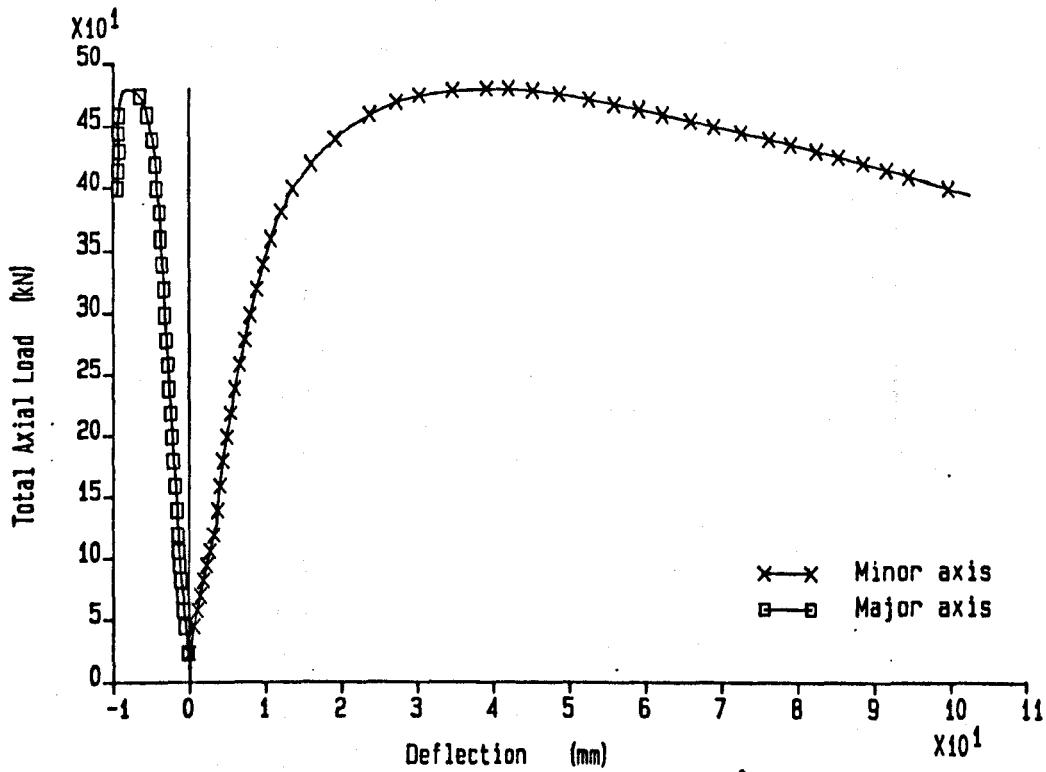
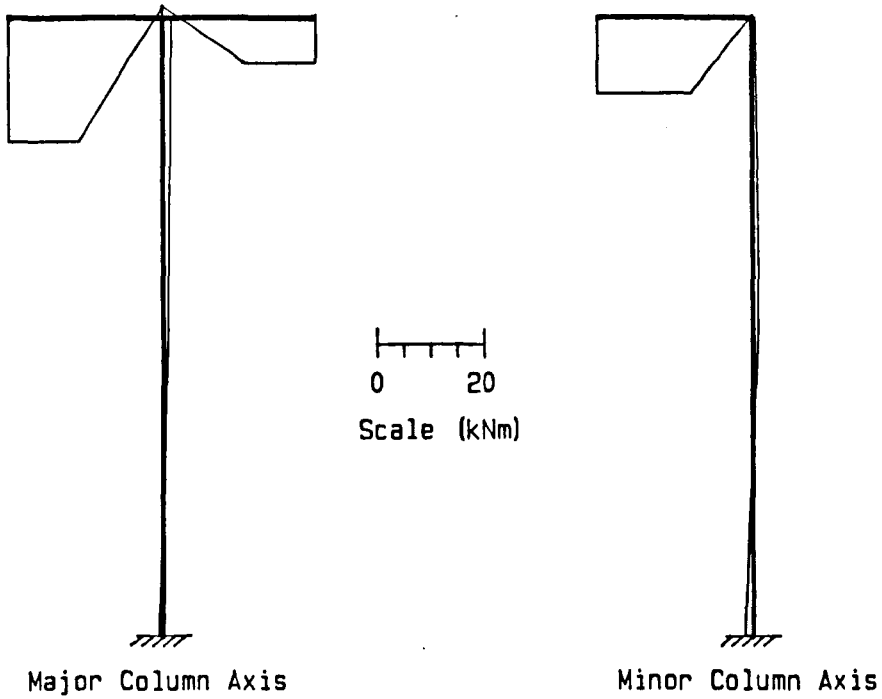


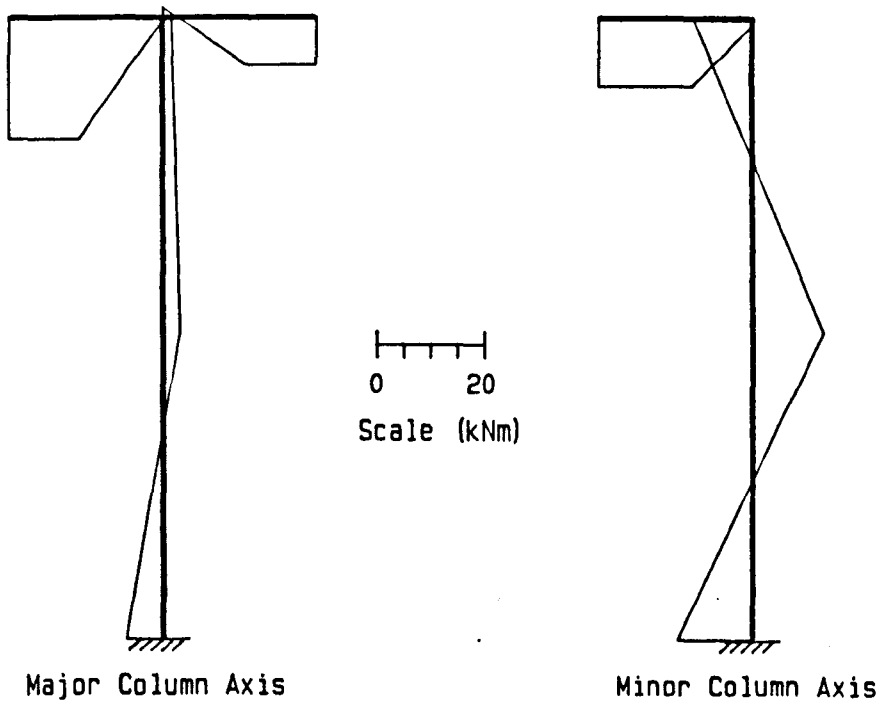
Figure 2.41: Plot of axial load vs. mid-column deflection for test S5.

Bending Moment Diagram - Test No. S5



**Figure 2.42: Distribution of bending moments at the end of the beam loading phase.**

Bending Moment Diagram - Test No. S5



**Figure 2.43: Distribution of bending moments at the point of maximum applied load.**

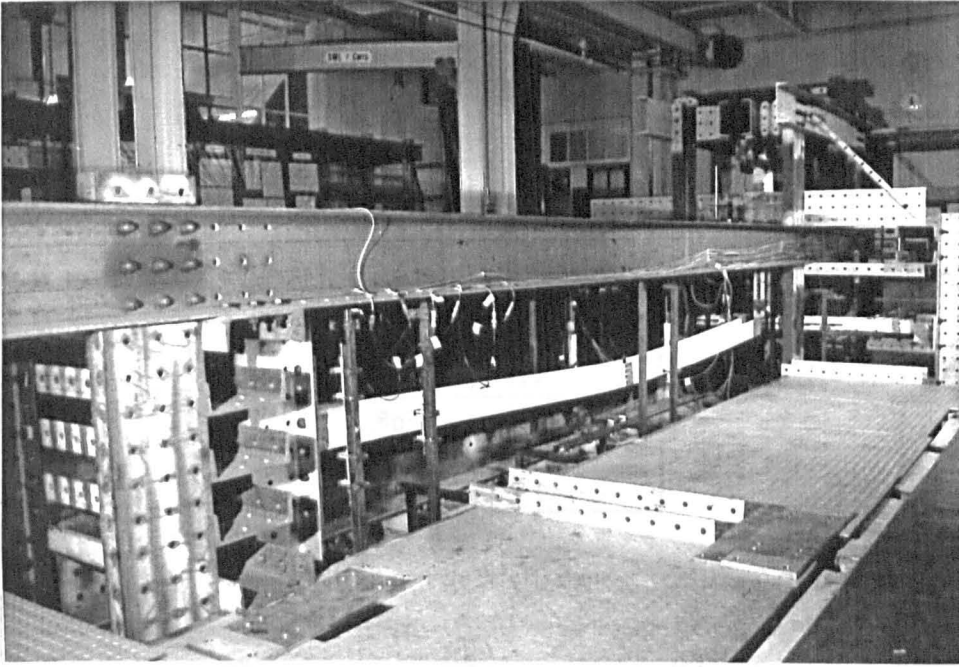


Figure 2.44: Column S5 at a post-failure level of load illustrating the reverse curve deflected shape of the column.

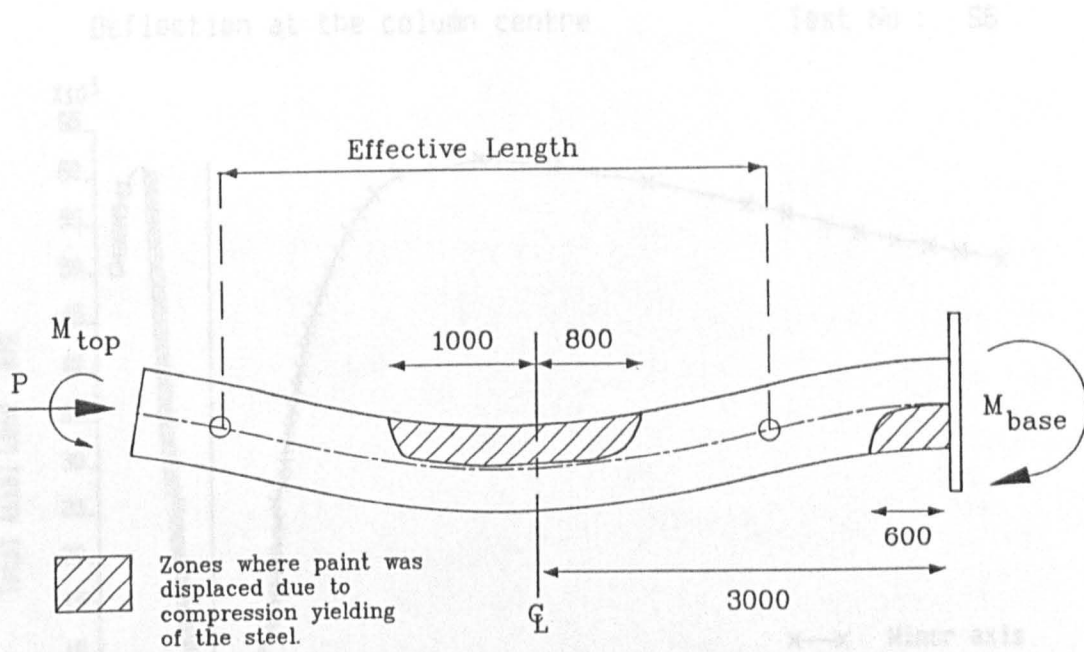


Figure 2.45: Diagrammatic view of column S5 showing the regions where plasticity of the steel caused the shedding of paint from the member surface.

Figure 2.46: Plot of axial load vs. mid-column deflection for test S5.

# Subassemblage test S6

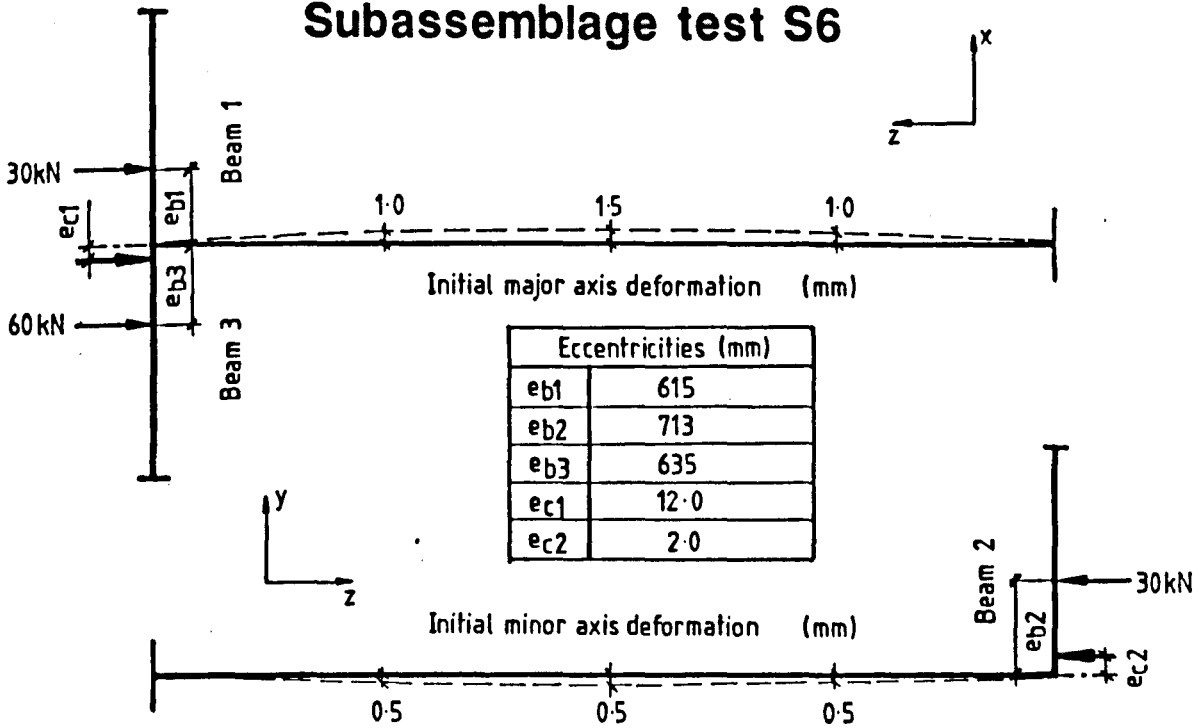


Figure 2.46: Summary of the major experimental parameters in test S6.

Deflection at the column centre

Test No : S6

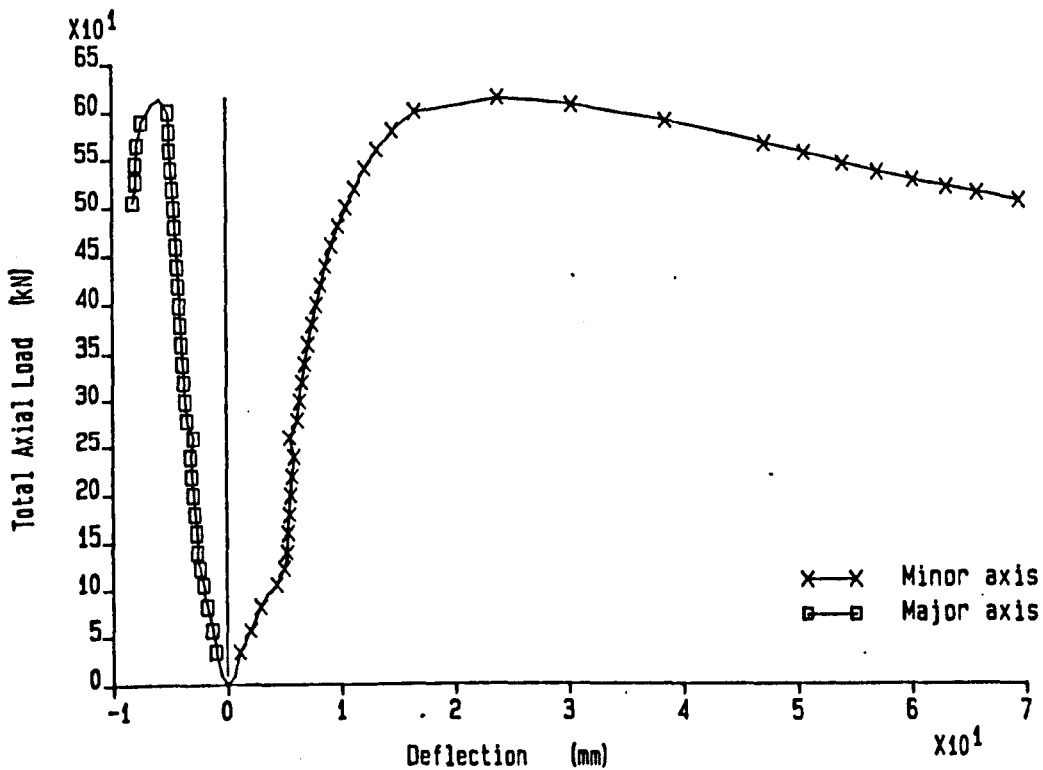


Figure 2.47: Plot of axial load vs. mid-column deflection for test S6.

Twist rotation at the column centre.

Test No : S6

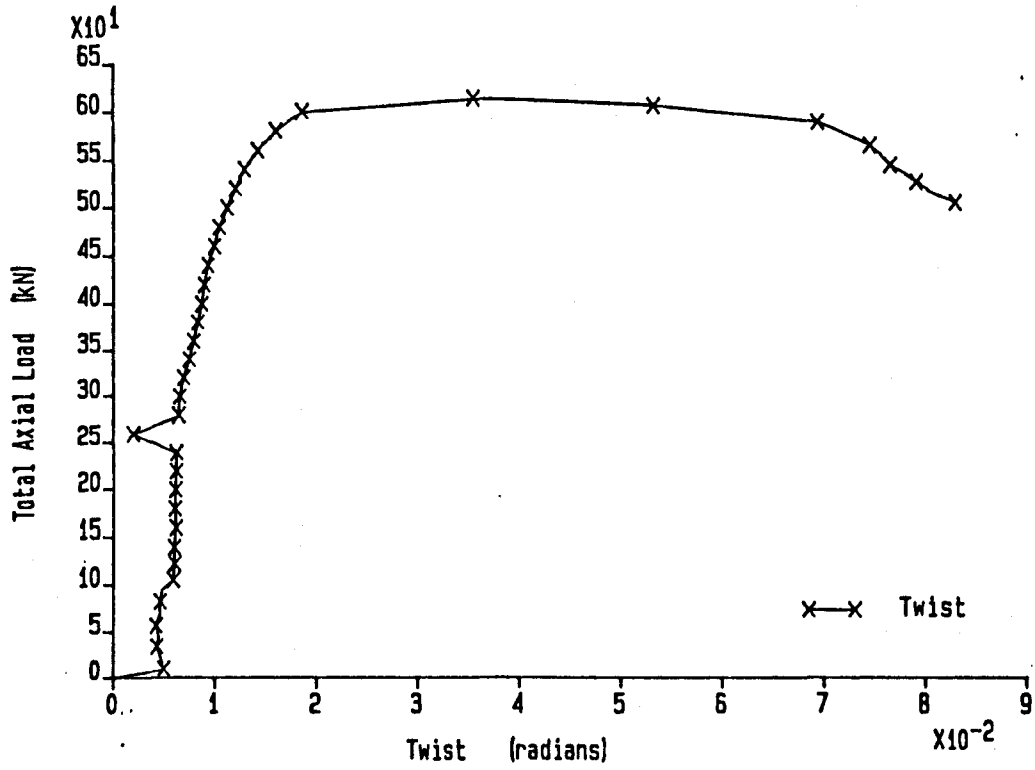


Figure 2.48: Plot of axial load vs. mid-column twist - test S6.

Bending Moment Diagram - Test No. S6

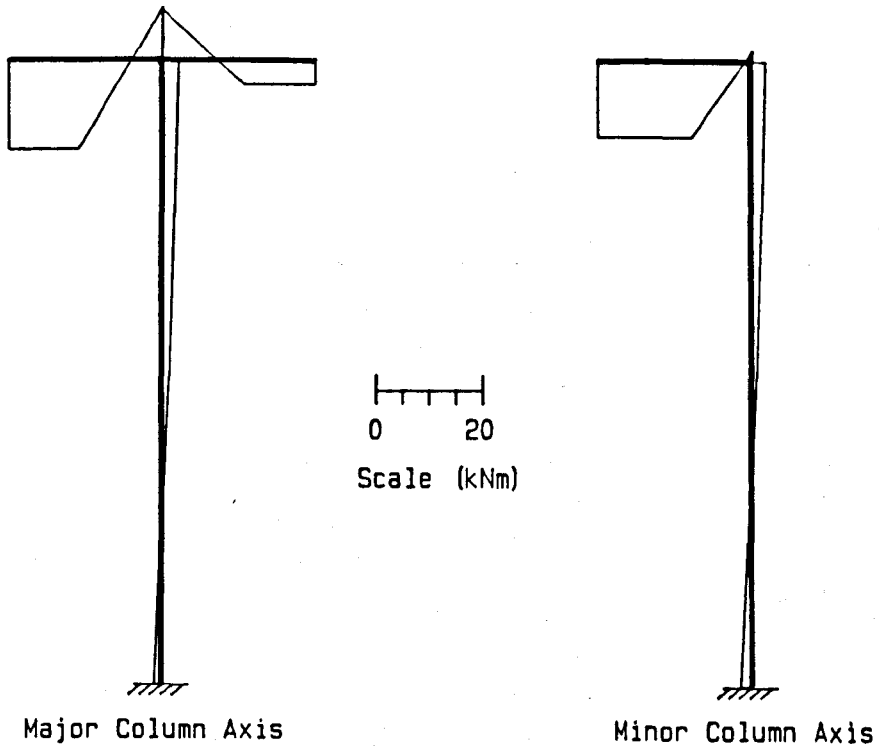


Figure 2.49: Distribution of bending moments at the end of the beam loading phase.

Bending Moment Diagram - Test No. S6

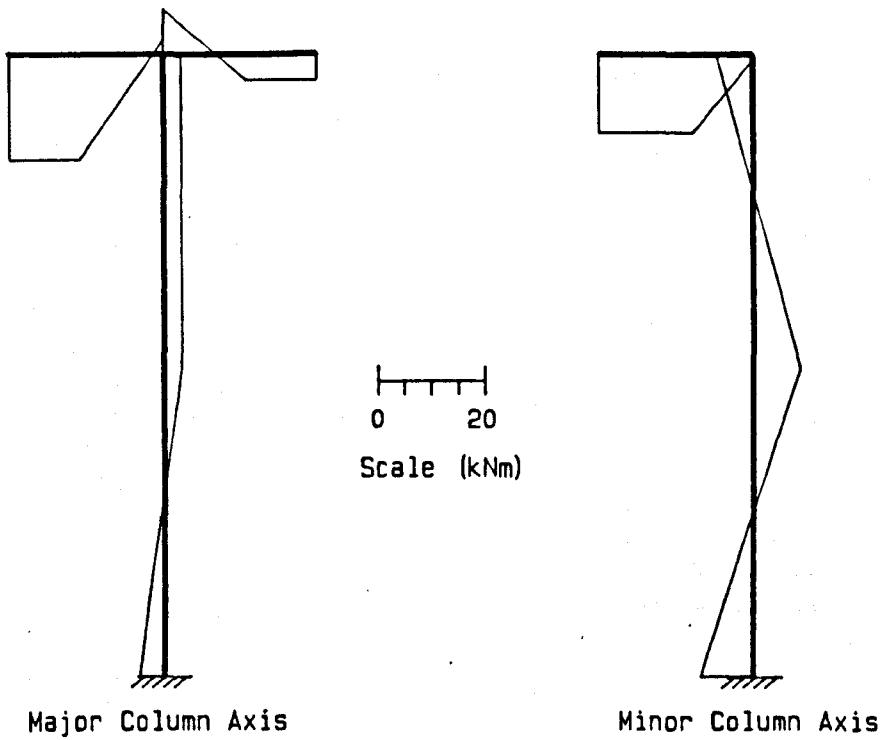


Figure 2.50: Distribution of bending moments at the point of maximum applied load.

# Subassemblage test S7

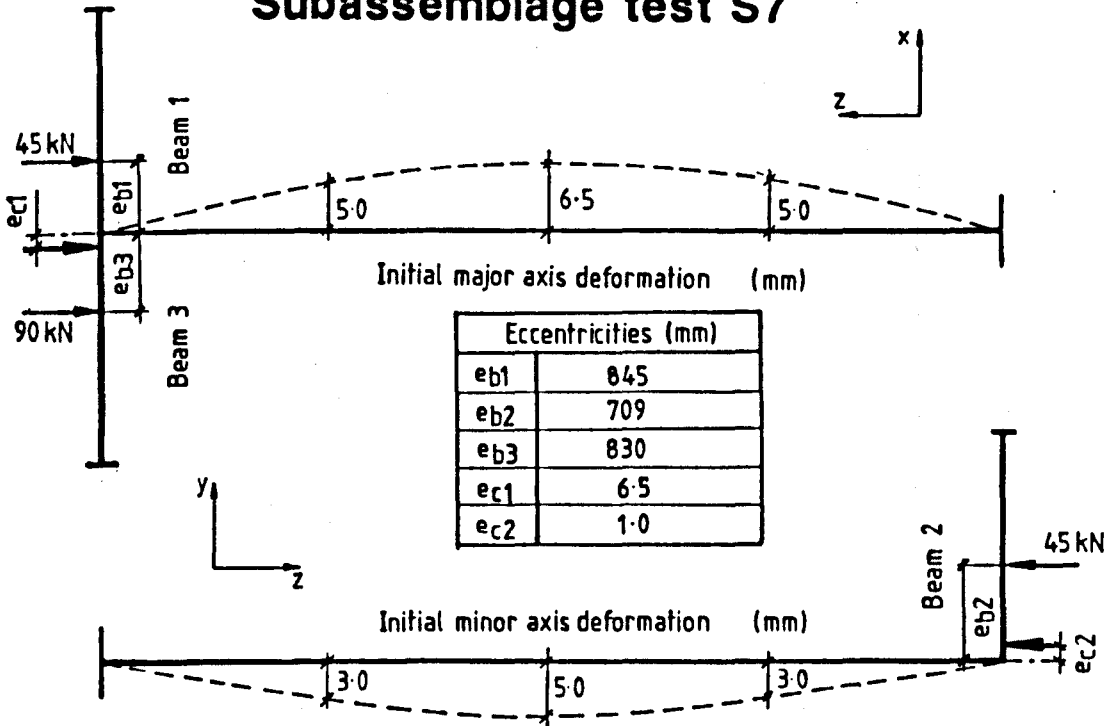


Figure 2.51: Summary of the major experimental parameters in test S7.

Deflections at the column centre

Test No : S7

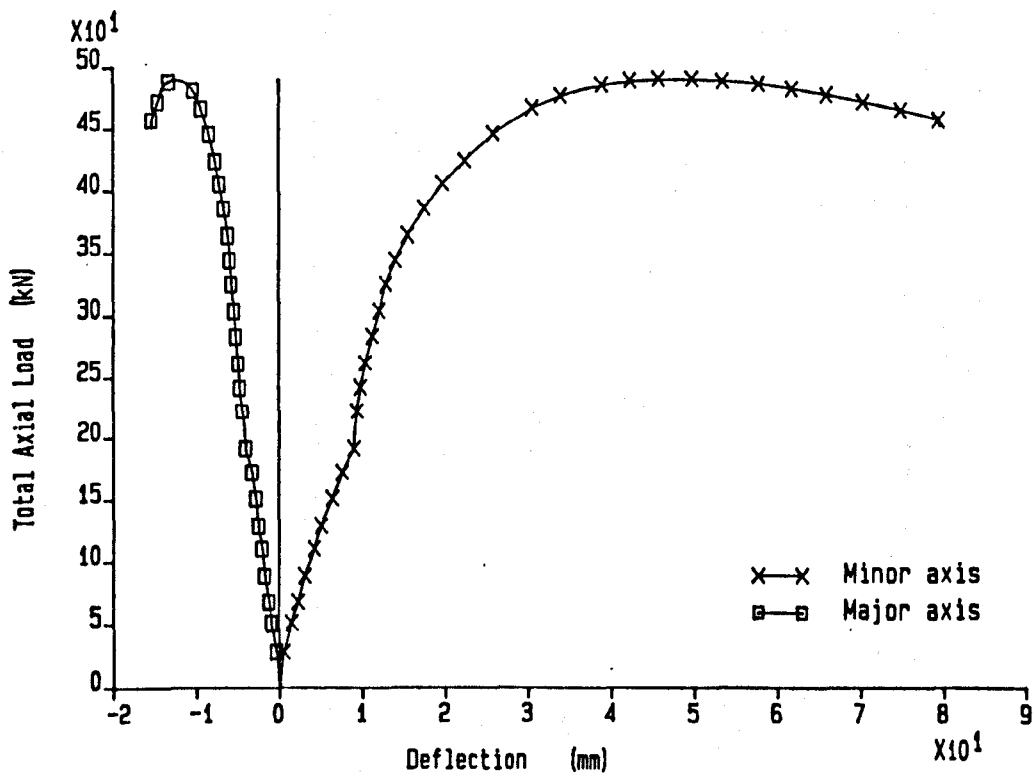


Figure 2.52: Plot of axial load vs. mid-column deflection for test S7.



Bending Moment Diagram - Test No: S7

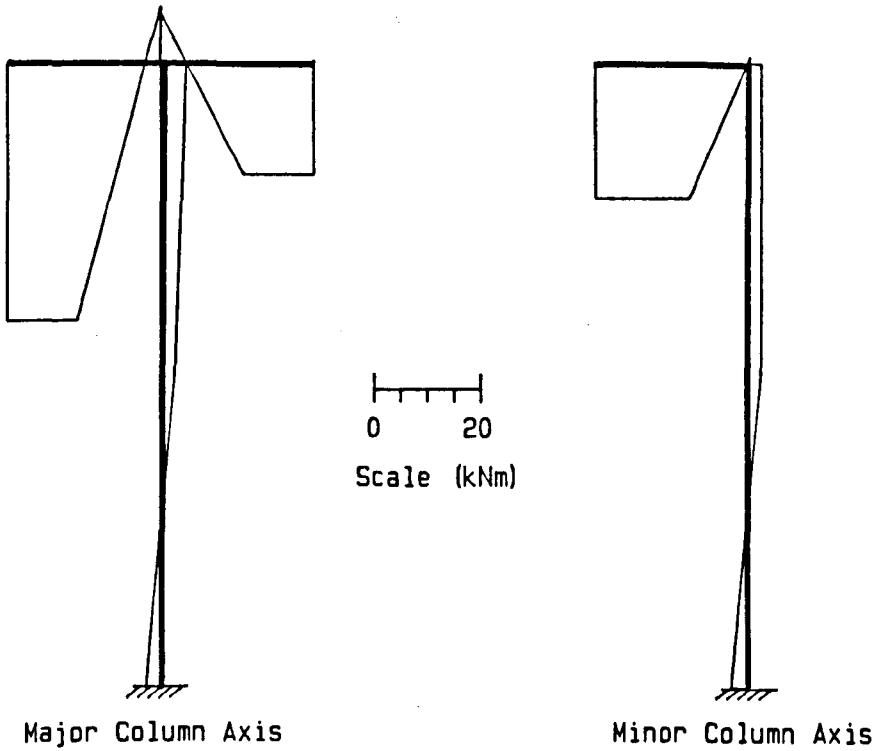


Figure 2.53: Distribution of bending moments at the end of the beam loading phase.

Bending Moment Diagram - Test No. S7

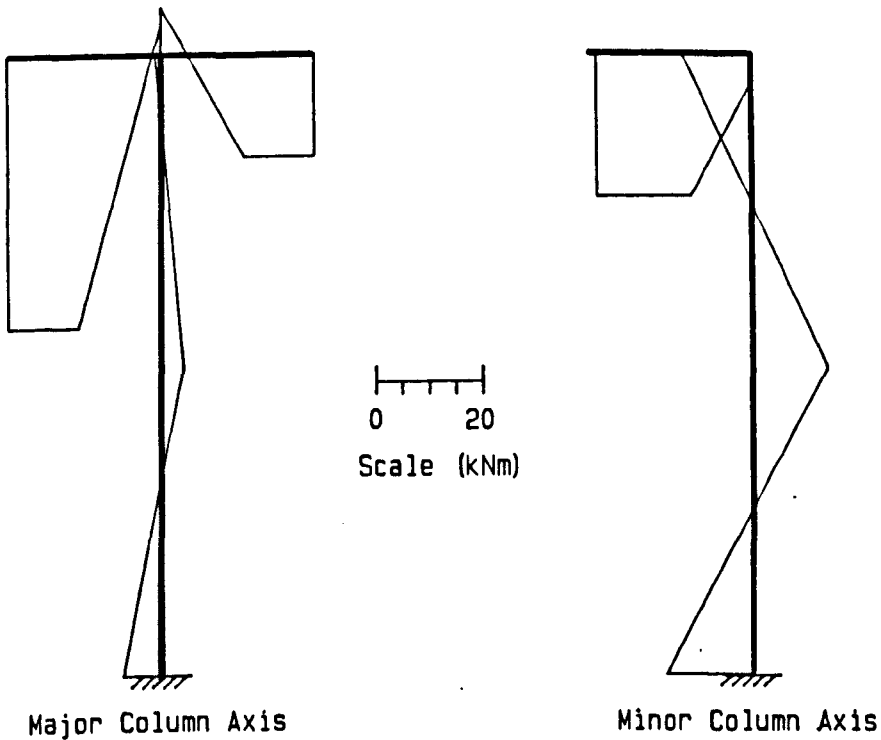


Figure 2.54: Distribution of bending moments at the point of maximum applied load.

# Subassemblage test S8

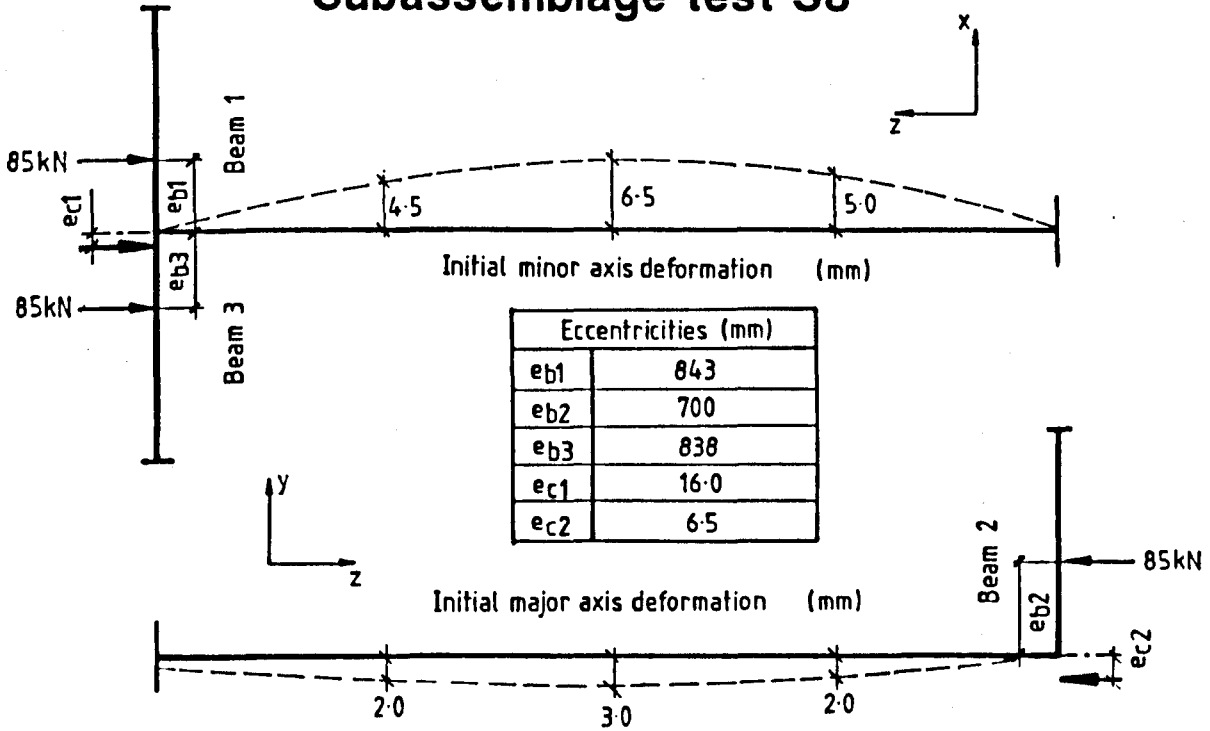


Figure 2.55: Summary of the major experimental parameters in test S8.

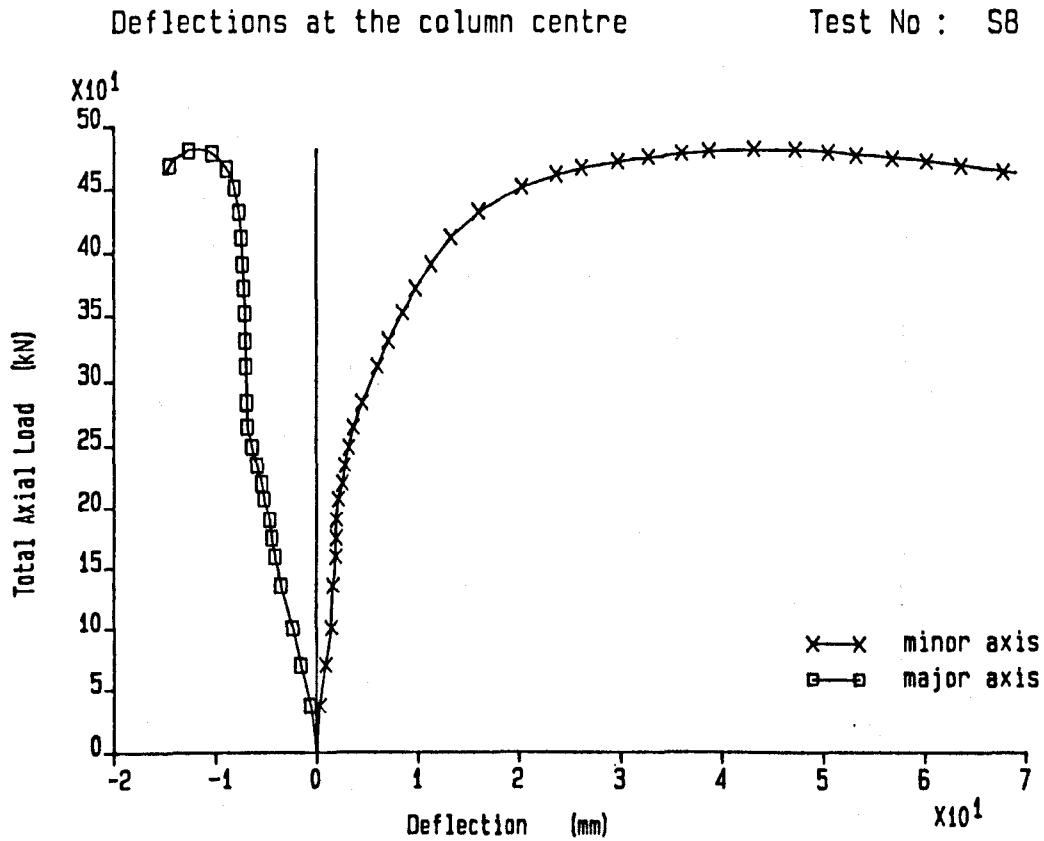


Figure 2.56: Plot of axial load vs. mid-column deflection for test S8.

Bending Moment Diagram - Test No. S8

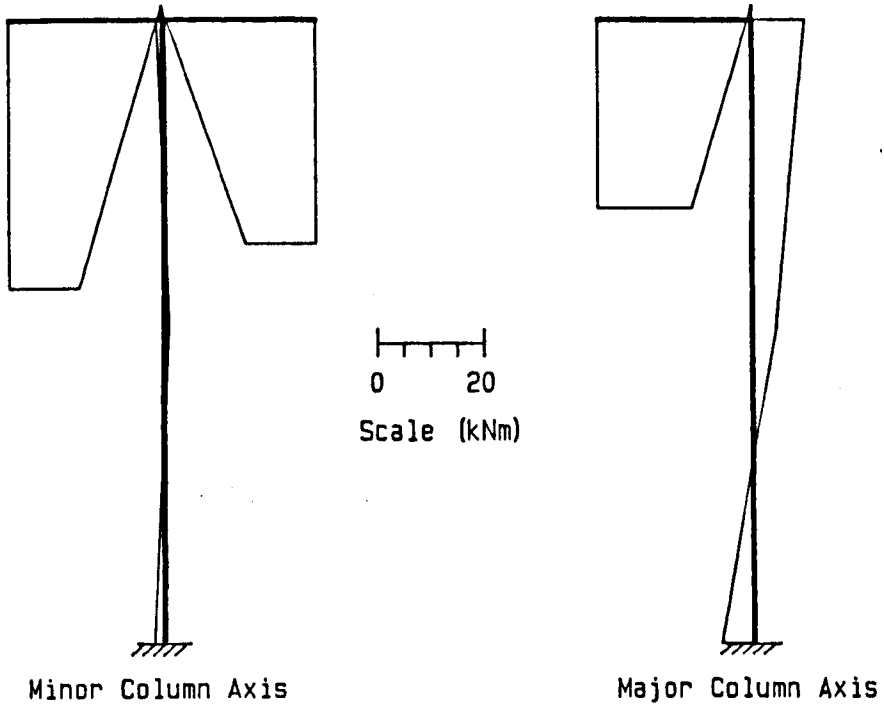


Figure 2.57: Distribution of bending moments at the end of the beam loading phase.

Bending Moment Diagram - Test No. S8

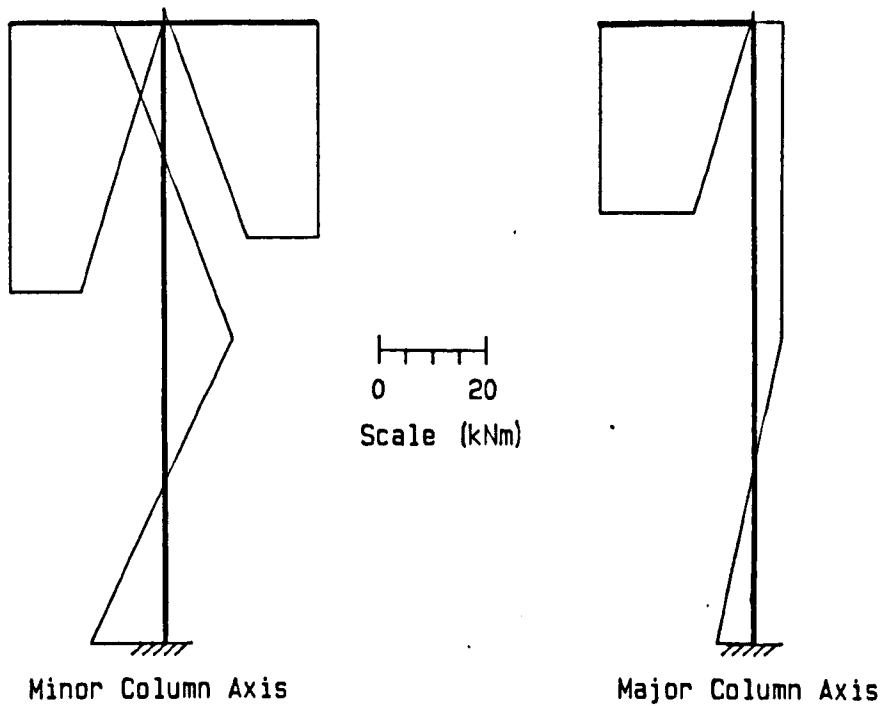


Figure 2.58: Distribution of bending moments at the point of maximum applied load.

# Subassemblage test S9

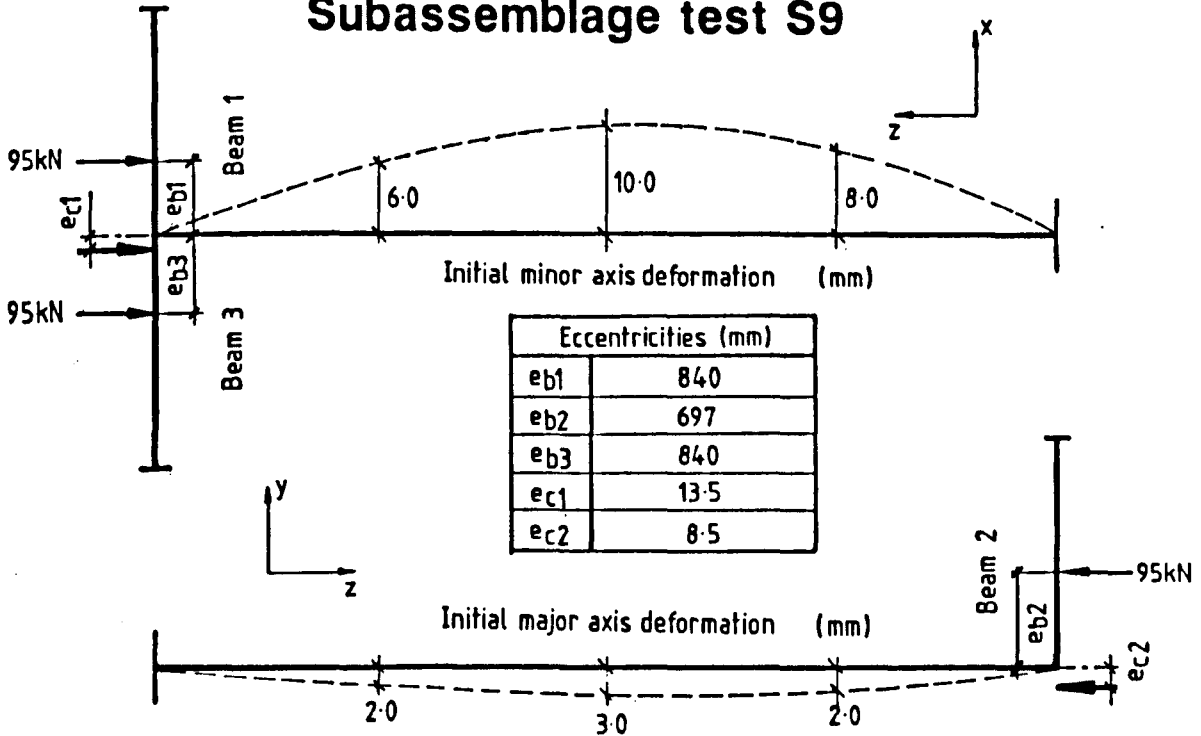


Figure 2.59: Summary of the major experimental parameters in test S9.

Deflections at the column centre

Test No : S9

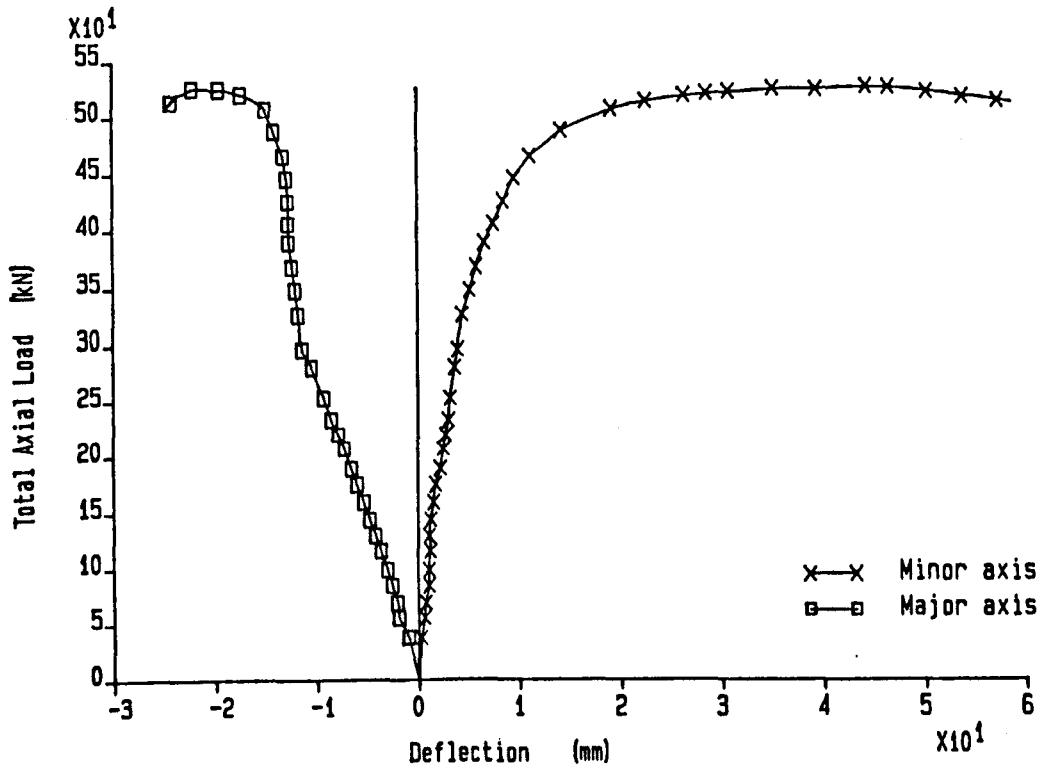


Figure 2.60: Plot of axial load vs. mid-column deflection for test S9.

Bending Moment Diagram - Test No. S9

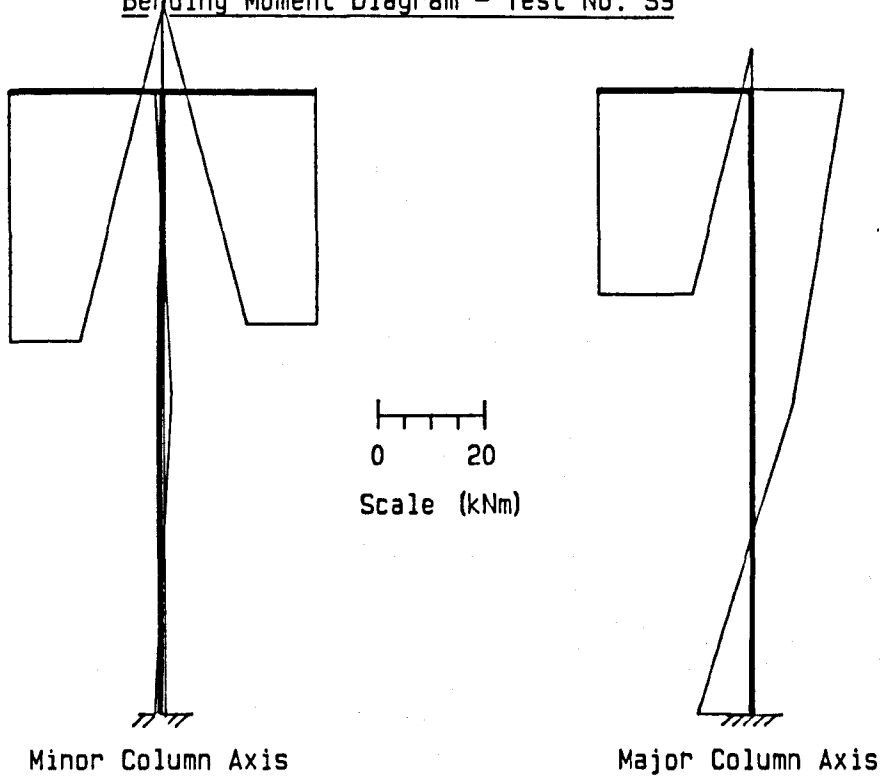


Figure 2.61: Distribution of bending moments at the end of the beam loading phase.

Bending Moment Diagram - Test No. S9

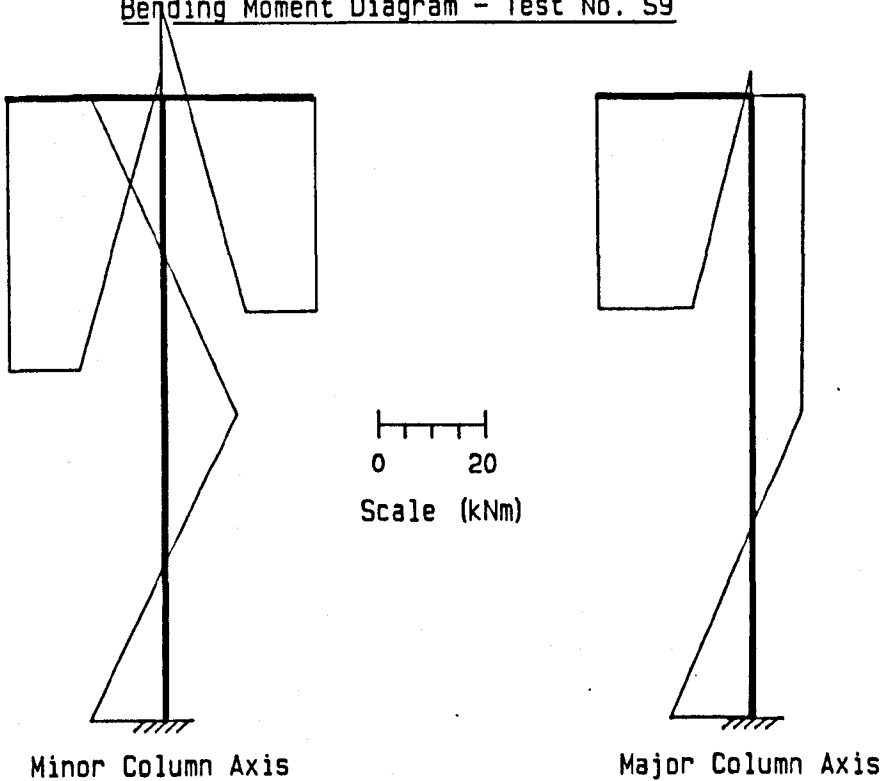


Figure 2.62: Distribution of bending moments at the point of maximum applied load.

# Subassemblage test S10

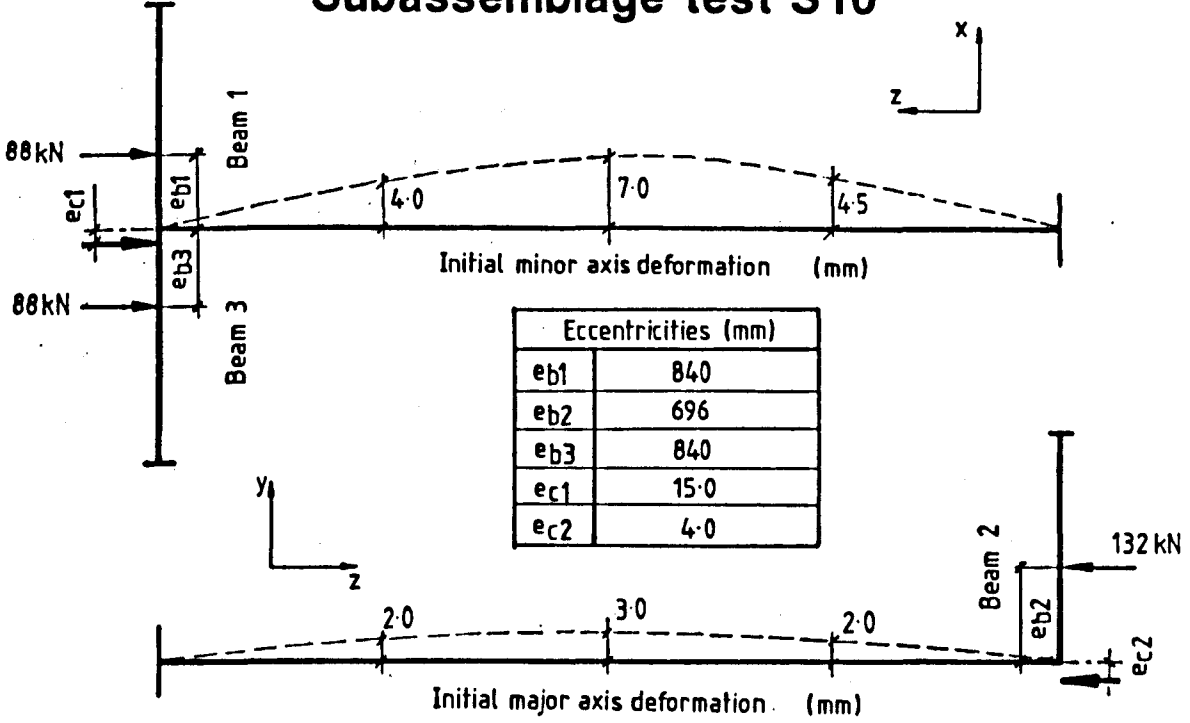


Figure 2.63: Summary of the major experimental parameters in test S10.

Deflections at the column centre

Test No : S10

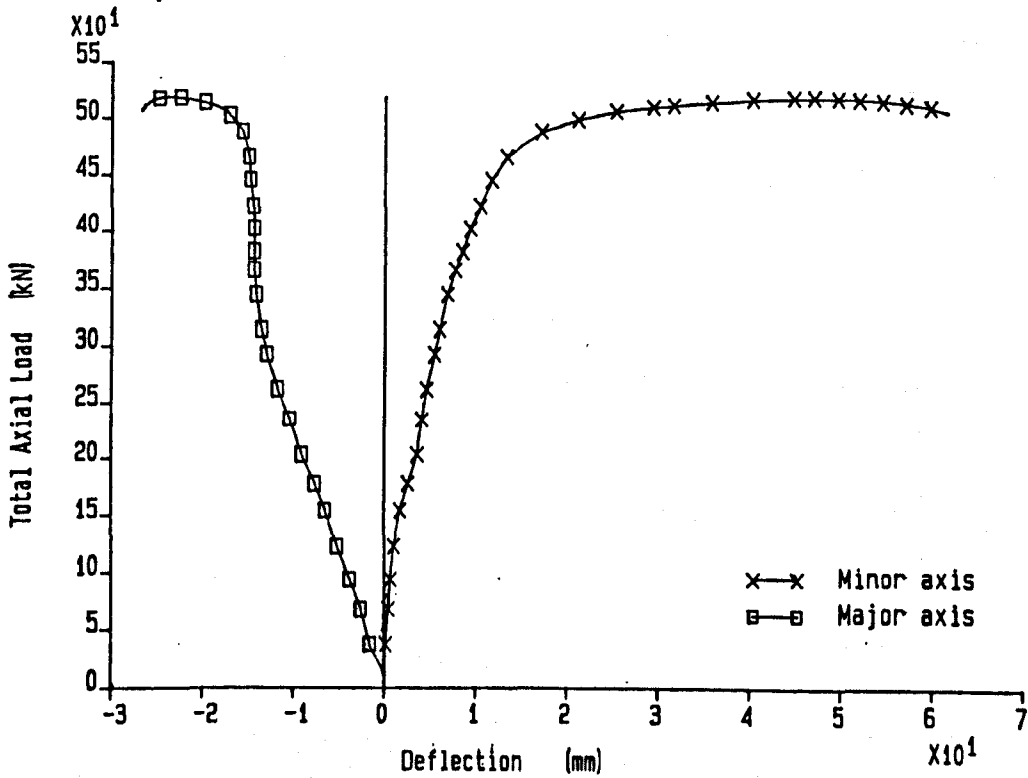


Figure 2.64: Plot of axial load vs. mid-column deflection for test S10.

Bending Moment Diagram - Test No. S10

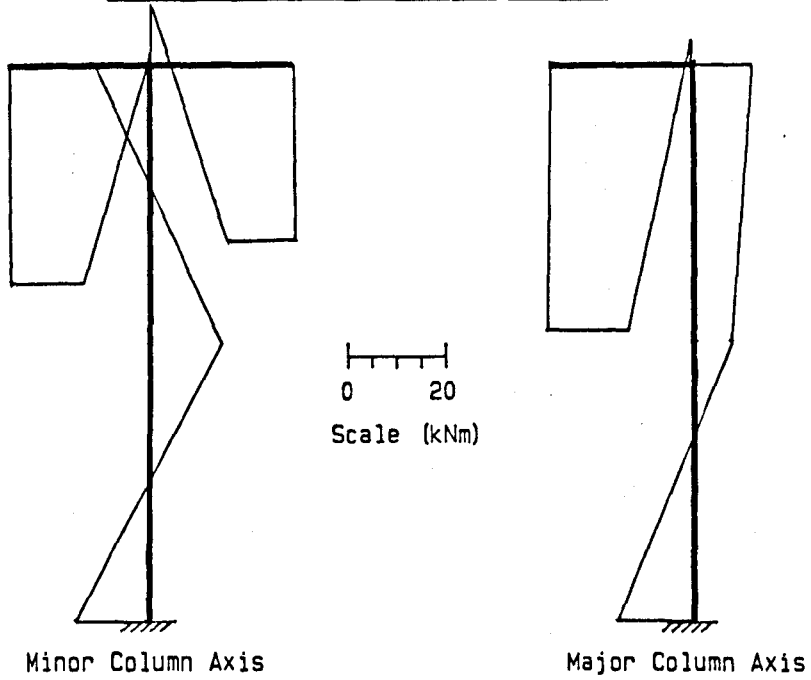


Figure 2.65: Distribution of bending moments at the end of the beam loading phase.

Bending Moment Diagram - Test No. S10

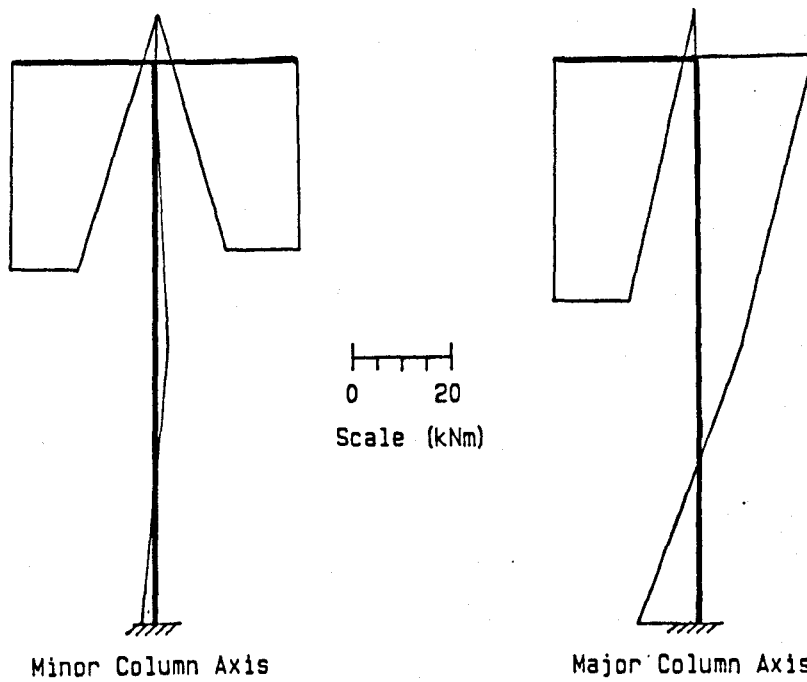


Figure 2.66: Distribution of bending moments at the point of maximum applied load.

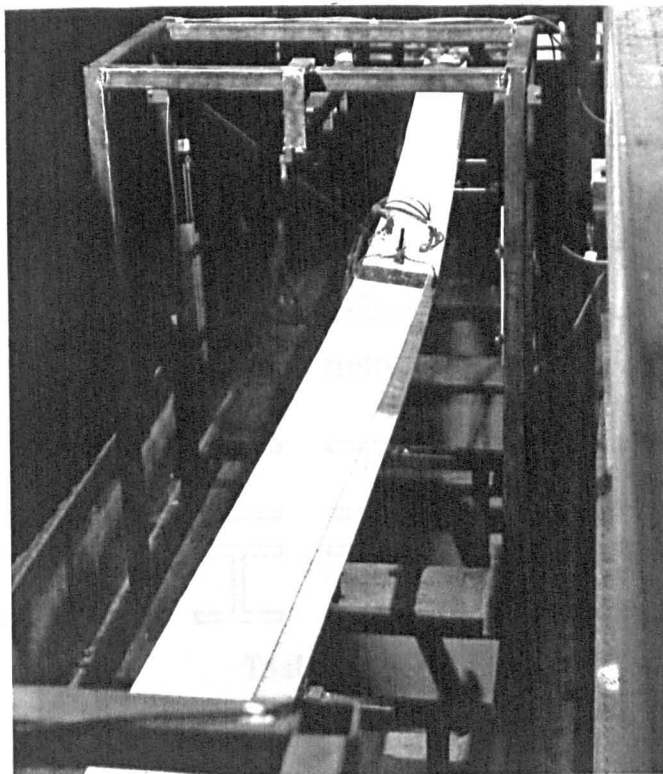


Figure 2.67: Column S10 under a post-failure level of loading.

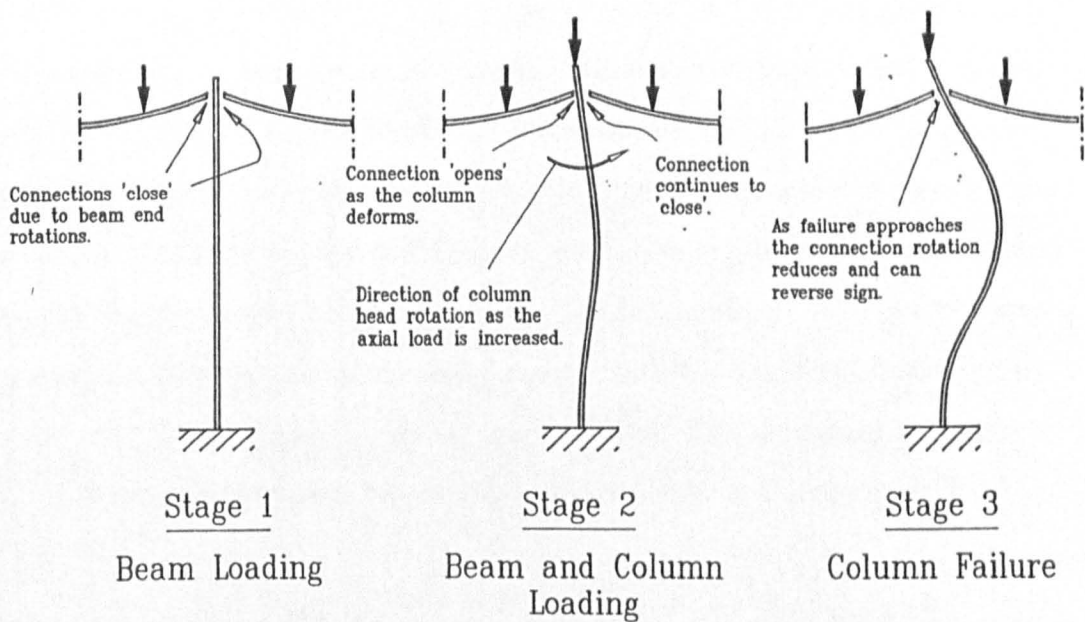


Figure 2.68: Direction of connection rotations at key stages in the subassembly loading sequence.



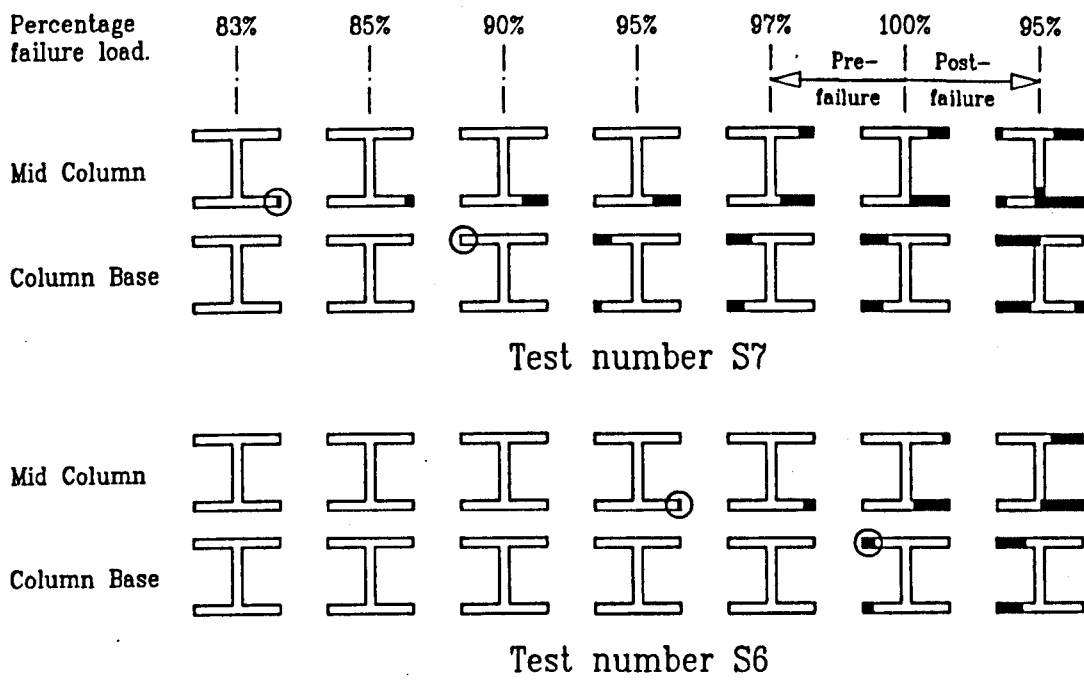


Figure 2.69: The spread of yield across the column section for test numbers S6 and S7.

## Chapter 3

# Subassembly Instrumentation.

### 3.1 Introduction

Accurate measurement of the response of test specimens to controlled actions is fundamental to all experimental study. The majority of the response monitoring used in the subassembly tests was devoted to recording the deformed shape of the subassembly and assessing the forces within individual components. Due to the 3-dimensional nature of the experimental tests, and the relatively high level of accuracy required, careful consideration had to be given to the way in which such responses were monitored. The following sections report the development of the 3-dimensional force and displacement measurement systems used in the study together with the overall subassembly instrumentation and data acquisition techniques employed. The specialised instrumentation devices developed specifically for the study formed the basis of two papers [3.1,3.2].

## 3.2 Displacement measurement.

One of the principal objectives of the experimental study was to verify the predictions of the sophisticated finite element computer program developed specifically to analyse flexibly connected 3-dimensional columns [3.3]. To permit close comparison between the experimentally observed and the analytically predicted data, it was essential that the three-dimensional deformation of the test specimens could be monitored accurately. However, the numerous instrumentation devices and measurement procedures which have been developed over the years are invariably restricted to one or two-dimensional, in-plane, operation. Used on their own, such devices would be of only limited use when monitoring full three-dimensional displacement. Therefore, before commencing any of the subassemblage tests, a measurement system had to be developed which was capable of accurately monitoring all six possible degrees of three-dimensional movement ( $\delta_x, \delta_y, \delta_z, \theta_x, \theta_y, \theta_z$ ), and which also satisfied the operational requirements of low cost, ease of use and relative compactness.

### 3.2.1 An overview of displacement measurement techniques.

It was immediately apparent that in order to satisfy the low cost requirement, the three-dimensional measurement system would have to incorporate readily available instrumentation devices. A thorough study was therefore made of measurement devices and measurement techniques which have been used successfully by experimental researchers in the past.

One of the most fundamental measurement devices used in experimental studies is the dial gauge. This simple, but relatively accurate device has been used by a number of researchers to monitor the mid height deflections of steel columns [3.4]. In experimental

work carried out by Birnstiel on the biaxial behaviour of 'H' columns [3.5], nine dial gauges were used to monitor both the in-plane and out-of-plane displacements of each of the four flange tips at the mid-height of the column. By applying geometric principles the twist rotation could be determined in addition to the overall major and minor axis deflections.

A number of researchers have used surveying techniques to determine the deformation of test specimens. In experimental studies on the moment-rotation characteristics of bolted end-plate connections [3.6], plane mirrors were used in conjunction with surveying theodolites to amplify the observed connection rotations. A similar method was used by Gent and Milner [3.7] to monitor the very small end rotations of a series of model test columns.

Devices which have been used to give a direct measure of rotation include the level gauge. This device is basically a spirit level mounted on an adjustable bracket which is rigidly clamped to the test specimen. After a rotation has occurred, a micrometer screw is adjusted to re-align the 'spirit bubble' back to its level starting position. A measure of the absolute rotation which has occurred can then be read directly from a calibrated scale. This simple but effective device was used in a study of the performance of a series of pinned-end steel columns [3.4].

The one major disadvantage of the above devices is that data had to be recorded manually. The manual collection of large amounts of data is not only labour intensive, but can be prone to human error. The development of micro electronics and computers since the time of these experiments has meant that large amounts of experimental data are now invariably recorded electronically and automatically.

Electolytic level gauges were used by Wood et al [3.8] to measure rotations in an experimental investigation into the behaviour of multi-storey, multi-bay, rigidly jointed steel frames. Using this device, the change in the electrical resistance caused by a bubble of

air travelling through an electrolytic solution could be monitored automatically. The position of the bubble, and hence the measured resistance, were directly related to the magnitude of rotation which had occurred. A complete appraisal of the operating characteristics of the electrolytic level gauge, also known as the 'Electrolevel', are presented in reference 3.9.

Recent studies at the Building Research Establishment on the behaviour of two dimensional steel frames [3.10], used a hanging dumb-bell rotation device. The dumb-bell was connected to the test specimen via a thin strip of spring metal. Rotations were calculated from measurements of the flexural strains in the metal strip as the specimen rotated relative to the dumb-bell. Although accurate, both this device and the electrolytic level gauge each use gravity as a reference datum. Obviously, in a situation where the principal rotations occur in a plane normal to the direction of gravity, such measuring devices are inappropriate.

An interesting displacement measurement system was used in a full-scale study of the in-situ performance of 'Z' purlin roofing systems [3.11]. Remotely controlled video cameras monitored the shifts of two target markers on a transparent armature which was fixed to the face of a 'Z' purlin. The change in position of the markers relative to a fixed reference background enabled the displacements and twist rotations of the purlin to be calculated. This elaborate method of remote monitoring was a safety precaution as the roof tests were potentially dangerous.

In experimental studies of the performance of plate girders [3.12], three L.V.D.T.'s (Linear Voltage Displacement Transducer) were combined to provide a single device capable of measuring displacements  $\delta_x$  and  $\delta_y$ , and rotation  $\theta_x$ . The L.V.D.T.'s which monitored the change in length of three strings,  $L1$ ,  $L2$  and  $L3$ , were connected to two points on a 'rotation bar' which was rigidly fixed to the specimen (figure 3.1). Movements of the specimen caused corresponding movements of the 'rotation bar'. By applying simple 2-dimensional geometric principles to the changes in string lengths, the shifts  $\delta_x$  and  $\delta_y$

could be determined for each of the points *A* and *B*. Although the device was only capable of measuring in one plane, it did have the advantage that unlike many commercially available rotation devices, its operation was totally independent of gravity. In a recent study of the behaviour of continuous beam-columns [3.13], five L.V.D.T.s were used in combination to enable five components of 3-dimensional movement to be monitored. It was considered that these particular methods of measurement using L.V.D.T.'s could be extended to develop a measurement system capable of deciphering all six components of full 3-dimensional deformation.

The L.V.D.T. measurement devices discussed above may be described as 'zero redundant' as the number of L.V.D.T.'s used equalled the number of deformation components which could be determined. A device capable of monitoring all six components of deformation would require a minimum six L.V.D.T.'s. However, the precise number of L.V.D.T.'s and the manner in which they were deployed would not only affect the sensitivity of the device, but would also influence physical access around the specimen. The aim was therefore to determine the optimum L.V.D.T. configuration which best suited the experimental set-up and the required accuracy of measurement.

### **3.2.2 Principles of three-dimensional measurement.**

There are two possible approaches to monitoring the 3-dimensional movements of an object using L.V.D.T.'s. Firstly, measurements can be made of the 2-dimensional, in-plane, movements of an object in a manner which is not sensitive to movements in the third dimension. This can usually be achieved by providing large distances between the specimen and fixed reference points. This is perhaps best illustrated by considering the hypothetical example shown in figure 3.2 in which an L.V.D.T. is monitoring the change in length of a cord of length *L* connecting specimen object *A* to fixed reference point

*B.* If the initial distance between points *A* and *B* is relatively small then for movement  $\delta_x$  and  $\delta_y$  of point *A*, the new cord length,  $L'$ , will be larger than  $L + \delta_x$ . The out of plane movement,  $\delta_y$ , is therefore significant and it is not possible to determine either the  $\delta_x$  or  $\delta_y$  components of movement from this single length measurement. If however, the initial distance between points *A* and *B* is increased, the effect of the out of plane shift,  $\delta_y$ , is reduced. For large values of  $L$ , the out of plane effect becomes insignificant and the revised chord length will be approximately equal to  $L + \delta_x$ . Measurement of the change in length of the chord will therefore provide a close approximation of the shift in the x-direction at point *A*.

Although this principle could be extended to derive all the degrees of movement associated with three-dimensional deformation, the large lengths required between the specimen and reference points would have severely restricted access in and around the test rig. An alternative principle was therefore sought which could determine the 3-dimensional movements of the specimen in a more direct manner.

The general formula for the distance  $L$  between two points,  $A_1$  and  $A_2$ , defined with respect to Cartesian axes  $x, y$  and  $z$ , is given by [3.14]:-

$$L^2 = (x_2 - x_1)^2 + (y_2 - y_1)^2 + (z_2 - z_1)^2 \quad (3.1)$$

It can be shown that if the distance of a general point  $A(x, y, z)$  is known from three different fixed points, then the  $x, y$  and  $z$  co-ordinates of point *A* can be determined. If the distance of the three fixed reference points  $P_1, P_2$  and  $P_3$ , from the general point  $A(x, y, z)$ , are  $L_1, L_2$  and  $L_3$  respectively, then:-

$$L_1^2 = (x - x_1)^2 + (y - y_1)^2 + (z - z_1)^2 \quad (3.2)$$

$$L_2^2 = (x - x_2)^2 + (y - y_2)^2 + (z - z_2)^2 \quad (3.3)$$

$$L_3^2 = (x - x_3)^2 + (y - y_3)^2 + (z - z_3)^2 \quad (3.4)$$

If the points,  $P_1, P_2$  and  $P_3$ , are given the co-ordinates  $(0,0,b)$ ,  $(-a,0,0)$  and  $(a,0,0)$  respectively, as shown in figure 3.3, then the above equations can be simplified to:-

$$L_1^2 = x^2 + y^2 + (z - b)^2 \quad (3.5)$$

$$L_2^2 = (x + a)^2 + y^2 + z^2 \quad (3.6)$$

$$L_3^2 = (x - a)^2 + y^2 + z^2 \quad (3.7)$$

The unknown  $x, y$  and  $z$ , co-ordinates of a point  $A$  can be easily derived by simultaneously solving the above equations.

$$x_a = \frac{L_2^2 - L_3^2}{4a} \quad (3.8)$$

$$z_a = \frac{1}{2b} \left( \frac{L_2^2}{2} - L_1^2 + \frac{L_3^2}{2} - (a^2 - b^2) \right) \quad (3.9)$$

the  $y$  co-ordinates can be determined by back substituting the known  $x$  and  $z$  co-ordinates into eqn. 3.7

$$y_a = \left( L_3^2 - (x_a - a)^2 - z_a^2 \right)^{\frac{1}{2}} \quad (3.10)$$

It is therefore possible to determine the position, and hence the shift, in three dimensions of a point by monitoring its distance from three fixed locations. Experimentally this can easily be achieved by using three L.V.D.T.'s to monitor the length of three cords which connect a single point on a specimen to the three reference points  $P_1, P_2$  and  $P_3$ .

To monitor all three possible rotations  $\theta_x, \theta_y$  and  $\theta_z$ , the  $x, y$  and  $z$  co-ordinates of a minimum of three non co-linear points must be known. Figure 3.4 shows how these three connection points  $A, B$  and  $C$  were located around the measurement point on the specimen. Points  $A$  and  $B$  were principally required to monitor the in-plane and out-of-plane rotations, whilst point  $C$  was required to monitor the twist. The distances  $h, l'$  and



$l$  were maximised to increase the relative displacement between the connection points, and hence improve the sensitivity of the device. The two rotation bars were fixed in the centre of the upper and lower flanges and as a result, their movement was less affected by any local flange distortions which may occur. This compares with the method used by Birnstiel, described previously, where the displacement of the section was monitored at the flange tips in which the presence of local flange distortions could be significant.

At first sight, it would appear that a total of nine L.V.D.T.'s would be required to derive the  $x$ ,  $y$  and  $z$  co-ordinates of the three attachment points  $A$ ,  $B$  and  $C$ , and hence the full 3-dimensional movement of point  $X$ . However, the distances between attachment points,  $h, l'$  and  $l$  and the subtended angles remain fixed. This constant geometric relationship effectively reduces the number of unknown co-ordinates, the number of equations to be solved and hence the number of L.V.D.T.'s required. This can be illustrated by considering figure 3.5 which shows a diagrammatic representation of the horizontal rotation bar. For a fixed armature length,  $l$ , the  $z$  offset of point  $B$  can be expressed as:-

$$z_B = b - z_A - \left( l^2 - (x_B - x_A)^2 - (y_B - y_A)^2 \right)^{\frac{1}{2}} \quad (3.11)$$

If the co-ordinates of point  $A$  are known, i.e. by adopting a three L.V.D.T. measurement device as discussed above, then the  $z$  co-ordinate at  $B$  can be determined directly from co-ordinates  $x_B$  and  $y_B$ . There are therefore only two unknown co-ordinates at  $B$ , and as a result only two further L.V.D.T.'s are required. A similar principle can be used to show that for a known in-plane member rotation, co-ordinates  $x_A, y_A$  and  $z_A$  and depth  $h'$ , it is theoretically possible to determine the twist of the member from a single L.V.D.T. reading at point ' $C$ '. It was evident however that by using just one L.V.D.T., the measurement of twist would be relatively insensitive and the resolution of the measurement device significant. The author therefore elected to use two L.V.D.T.'s at this particular location to provide a more accurate measurement of the co-ordinate  $x_C$ . This gave a total of seven L.V.D.T.'s for the measurement system as a whole, one more than

the theoretical minimum. Figure 3.6 shows how these seven L.V.D.T.'s were arranged around the specimen. The dimensions  $L_1$  to  $L_7$  represent lengths of cord which are each attached at one end to an L.V.D.T. and at the other to one of the attachment points  $A$ ,  $B$  or  $C$ . Each cord passes over a free running pulley,  $P_1$  to  $P_7$ , which is fixed in position.

The general expression for the cord lengths at point  $B$  can be written in the form:-

$$L_4^2 = (x + c)^2 + y^2 + z^2 \quad (3.12)$$

$$L_5^2 = (x - c)^2 + y^2 + z^2 \quad (3.13)$$

As at point  $A$ , these can be solved simultaneously to generate the  $x$  co-ordinate at  $B$ :-

$$x_B = \frac{L_4^2 - L_5^2}{4c} \quad (3.14)$$

By solving equations (3.11), (3.13) and (3.14), the  $y$  co-ordinate at  $B$  can be found as:-

$$y_B = \frac{-\beta + (\beta^2 - 4\alpha\mu)^{\frac{1}{2}}}{2\alpha} \quad (3.15)$$

where :-

$$\alpha = 4(y_A^2 + \chi^2)$$

$$\beta = -4y_A^2(\eta + 2\chi^2)$$

$$\mu = \eta^2 - 4\chi^2(l^2 - y_A^2)$$

$$\chi = b - z_A$$

$$\eta = L_6^2 - \alpha^2 - \chi^2 - l^2 + y_A^2$$

In a similar manner to that shown for points  $A$  and  $B$  the  $x$  co-ordinate at point  $C$  can be expressed as:-

$$x_C = \frac{L_6^2 - L_7^2}{4d} \quad (3.16)$$

The  $x_A, y_A, z_A, x_B, y_B, z_B$  and  $x_C$  co-ordinates can therefore be determined from the initial lengths of strings  $L_1$  to  $L_7$ , the shifts at these points being determined from

the subsequent movement of the seven L.V.D.T.'s. The co-ordinates can be processed further to generate the three-dimensional movement of a single reference point on the specimen:-

$$(\theta'_z) = \sin^{-1} \left( \frac{x_C - x_A}{h} \right) \quad (3.17)$$

$$(\theta_y) = \sin^{-1} \left( \frac{x_B - x_A}{l^2 - (y_B - y_A)^2}^{\frac{1}{2}} \right) \quad (3.18)$$

$$(\theta_x) = \sin^{-1} \left( \frac{y_B - y_A}{l^2 - (x_B - x_A)^2}^{\frac{1}{2}} \right) \quad (3.19)$$

$$(\delta_x) = \frac{(x_A + x_C)}{2} - l' \cos(\theta_y) \quad (3.20)$$

$$(\delta_y) = y_A - \frac{h}{2} \cos(\theta_x) \cos(\theta'_z) + l' \sin(\theta_x) \quad (3.21)$$

$$(\delta_z) = z_A - \frac{h}{2} \sin(\theta_x) \cos(\theta_y) - l' \cos(\theta_y) \cos(\theta_x) \quad (3.22)$$

where:-

$(\theta'_z)$  = Twist rotation.\*

$(\theta_y)$  = Minor axis rotation.

$(\theta_x)$  = Major axis rotation.

$(\delta_x)$  = x displacement.

$(\delta_y)$  = y displacement.

$(\delta_z)$  = z displacement.

\* Note:  $\theta'_z$  is the twist with respect to the local member axis.

Therefore, by applying equations (3.17) to (3.22) to the readings from a series of seven L.V.D.T.'s located around a specimen as shown in figure 3.6, it is possible to determine all six degrees of movement  $(\delta_x, \delta_y, \delta_z, \theta_x, \theta_y, \theta_z)$  for a particular measurement point on the specimen.

### **3.2.3 Construction and testing of a prototype measurement device.**

At an early stage in the research programme, a full size prototype of the proposed 3-dimensional measuring system was constructed. An investigation of the accuracy, sensitivity and repeatability of the prototype under controlled conditions, provided useful information on the feasibility and ease of operation of the system.

A frame constructed in 'Dexion' bolted framing angle, supported the L.V.D.T.'s and pulley mechanisms at the required points around the specimen, as indicated in figure 3.7. The test specimen was a 3.8m long 70 x 70 square hollow steel section. Threaded bolts 200mm long were passed through the section to form the attachment points on the upper and lower section surfaces. At one end, the specimen was supported on a lubricated ball joint (figure 3.7), point Y, and at the other end on a micrometer screw which displaced the specimen by a controlled distance, point X. A conventional dial gauge was used to give a direct measure of the displacement of the micrometer screw. The 3-dimensional measuring device was situated adjacent to the ball support, and monitored subsequent rotations of the specimen.

The L.V.D.T.'s used in the prototype tests had operating ranges of 25mm and 50mm. Data from the measuring device was recorded using an Orion Solatron Data Logging system, with data processing facilities, connected to an IBM PC compatible Opus computer. A computer program was written to process the output from the L.V.D.T.'s using the equations discussed above. This program was installed in the data logging system to provide continuous output of processed measurement data throughout the test.

From the outset, it was apparent that the device would have to be capable of measuring very small displacements and rotations. It was therefore essential that the cord which was used to connect the L.V.D.T.'s to points on the specimen was as near inextensible as possible. The cord which was used in the preliminary prototype tests was of a heavy gauge and was therefore relatively stiff. The tension in the cord produced by the return

spring mechanisms in the L.V.D.T.'s was of insufficient strength to fully remove any small kinks and deformations within the cord. Such kinks caused the cord to behave as though it were extensible and as a result, the data collected from the initial prototype tests tended to be inaccurate and of poor repeatability. When a low frequency vibrating source was attached to the measuring device frame, significant improvements were observed in the accuracy of measurement. It is assumed that such dynamic effects helped to remove the adverse effects of cord deformations. The use of a lighter gauge cord in subsequent tests resulted in a vast improvement in both the accuracy and the repeatability of the data.

The processing computer program automatically set all the initial offsets and rotations of the specimen to zero. Subsequent movements of the specimen were therefore measured relative to a zero datum irrespective of the initial specimen orientation. To carry out a rotation calibration of the device, scans were taken of the L.V.D.T. readings for 1mm increments of lateral displacement at point *X* on the specimen. These movements, actuated by the mechanical screw device, resulted in a rotation of the specimen about the ball support at *Y*. The magnitude of applied movement was measured using a dial gauge indicator with an accuracy of 0.01mm. As the distance between the point of movement, and the position of the ball support was 3505mm, a 1mm displacement movement produced an actual rotation of 0.000285 radians. An error in the measurement of the lateral movement of point *X* of 0.01mm would therefore result in an apparent error in the actual rotation of the specimen of only 0.000003 radians. Point *X* was moved in a lateral direction by up to 20mm, and then reversed back to its initial starting position. Calibration tests were also carried out for vertical movements of point *X*, resulting in in-plane rotation of the specimen and also for lateral movement of a vertical armature fixed to the specimen which induced twist rotations. The plots of the actual specimen rotations against the measured rotations are shown in figures 3.8 to 3.10.

To check the ability of the device to measure displacements, the ball joint at support *X* was replaced by a sliding roller bearing. The specimen was displaced laterally and

longitudinally by a specially adapted screw device in a similar manner to that described above. The magnitudes of the resulting displacements were measured directly by a dial gauge indicator. It was considered however that the rated accuracy of the gauge, 0.01mm, was sufficient for the purpose of deflection monitoring of the subassemblage. The resulting plots of actual against measured displacement are shown in figures 3.11 to 3.13.

It is evident from the calibration plots that the prototype device provided a very accurate measure of both displacement and rotation. The maximum apparent error for rotation measurement was 0.00005 radians whilst that for displacement was 0.05mm. The device was therefore developed further for use in the series of subframe tests.

#### **3.2.4 Development of the prototype for use in the subassemblage tests.**

The prototype testing of the measurement device used a temporary support frame constructed from proprietary 'Dexion' framing angle. For the actual subframe tests, the measuring device support frames were fabricated from 40 x 40 mm mild steel square hollow section. The frames were principally of welded construction; however a limited number of bolted connections were necessary to facilitate installation of the test specimen. The base-plates of the instrumentation frames were bedded in Plaster of Paris to eliminate any tendency for the frame to wobble during the course of a test. Figures 3.14 and 3.15 show photographs of the 3-dimensional measurement devices and supporting frames used in the subassemblage study.

Due to rolling tolerances, the opposite faces of the hollow section instrumentation frames were never truly parallel. The bearings used in the pulley mechanisms therefore had to be self aligning to prevent the shaft locking as a result of non-alignment. A total of 39 pulley mechanisms were fabricated, one for each of the L.V.D.T.'s used in the three-dimensional

measurement devices. A diagram of the pulley mechanisms is shown in Appendix A.

The L.V.D.T. cords were permanently connected to the measurement device rotation bars. To facilitate installation, the bars were temporarily bolted to the specimen and could therefore be connected to successive test subassemblages with relative ease.

### **3.2.5 Deflection components measured in the subassemblage tests.**

Section 3.2.2 described the development of a measurement device comprising seven L.V.D.T.'s capable of measuring all six degrees of three dimensional movement. This particular device was used at the column base and at the column end of each of the three beams. Simplified devices requiring a smaller number of L.V.D.T.'s were used at the remaining measurement locations. A six string measurement device was used at the mid-point of the column (figure 3.16). This particular device was capable of accurately monitoring the x, y and z displacements and twist rotations of the column. It was considered that values of the minor and major axis rotations at the column mid-point were not essential. A five string device was used at the head of the column (figure 3.17) which was capable of monitoring all displacements and rotations with the exception of column twist. The location of the various types of 3-dimensional measuring device around the subassemblage test specimen is shown in figure 3.18.

In addition to recording three-dimensional deformation, linear measurements were made using single L.V.D.T.'s of the displacement at the column head and at the remote end of each beam. A comprehensive summary of the deformation components which were monitored during a test are shown on the plan and elevation of the subassemblage in figure 3.19.

Before commencing a test, the initial lengths of the 39 strings forming the six 3-dimensional

measuring devices, were recorded. This data was used in the post processing to determine the initial absolute positions of the specimens, and hence the subsequent relative displacements.

### **3.3 Force measurement.**

As the columns used in the experimental subassemblage tests were to be deformed beyond their ultimate load capacity, it was inevitable that significant areas of material yielding would occur within the column section. The force measurement system therefore had to be capable of tracing the resulting complex 3-dimensional elastic-plastic stress distributions and of coping with the difficulties associated with experimental strain measurement in elastic-plastic material.

#### **3.3.1 Measurement of longitudinal strains.**

The column actions which were of particular interest produced longitudinal strains in the column. In principle, these strains could be measured easily using electrically energised, foil strain gauges. This particular type of gauge has been used by many experimental researchers in studies of the behaviour of structural steelwork. The thin construction of such gauges allows rapid heat dissipation thus limiting the effect of electrical energisation on the resistivity of the gauge. The specific type of gauge used in the subassemblage tests had a gauge length of 10mm and was of a form which was particularly insensitive to transverse strains [3.15]. The gauges were fixed using a cyanoacrylate adhesive which could be applied in a very thin layer and thus reduced to an absolute minimum the



residual stresses and post- cure shrinkage associated with certain types of adhesive [3.16].

### 3.3.2 Summation of the individual strain components.

The magnitude of longitudinal strains induced at any point on the column section equalled the sum of the individual strain components due to axial load,  $\epsilon_a$ , major axis bending moment,  $\epsilon_b$ , minor axis bending moment,  $\epsilon_c$ , and warping,  $\epsilon_d$ . The warping strains result from a bi-moment, which is a self- equilibrating system of moments that develop as a result of torsional deformations in flanged members [3.17]. A diagrammatic representation of the individual longitudinal strain components is shown in figure 3.20 [3.18].

In theory, only four measurements of strain are required at any one cross section to determine the four unknown force components. Four strain gauges could therefore have been used, one positioned close to the edge of each of the flange tips. For levels of load at which the section behaves wholly <sup>elastically</sup> elastic, the force components of axial load ( $P$ ), major axis moment ( $M_{xx}$ ), minor axis moment ( $M_{yy}$ ) and warping bi-moment ( $B$ ) could be derived using the following simple expressions:-

$$(P) = \frac{EA}{4}(\epsilon_1 + \epsilon_2 + \epsilon_3 + \epsilon_4) \quad (3.23)$$

$$(M_{xx}) = \frac{EZ_{xx}}{4}(\epsilon_1 + \epsilon_2 - \epsilon_3 - \epsilon_4) \quad (3.24)$$

$$(M_{yy}) = \frac{EZ_{yy}}{4}(-\epsilon_1 + \epsilon_2 + \epsilon_3 - \epsilon_4) \quad (3.25)$$

$$(B) = \frac{EZ_w}{4}(-\epsilon_1 + \epsilon_2 - \epsilon_3 + \epsilon_4) \quad (3.26)$$

where  $\epsilon_1, \epsilon_2, \epsilon_3$  and  $\epsilon_4$  represent the total strains at the four corners due to the individual load components:-

$$\epsilon_1 = \epsilon_a + \epsilon_b + \epsilon_c + \epsilon_d$$

$$\epsilon_2 = \epsilon_a + \epsilon_b - \epsilon_c + \epsilon_d$$

$$\epsilon_3 = \epsilon_a - \epsilon_b - \epsilon_c - \epsilon_d$$

$$\epsilon_4 = \epsilon_a - \epsilon_b + \epsilon_c + \epsilon_d$$

and:-

$A$  = Cross-sectional area.

$E$  = Young's modulus.

$Z_{xx}$  = Major axis elastic section modulus.

$Z_{yy}$  = Minor axis elastic section modulus.

$Z_w$  = Warping modulus.

For elastic-plastic behaviour, in which the stress is no longer directly proportional to the strain, the stress distribution can be determined by applying integration techniques which take account of yield across the section [3.18]. However, the straightforward application of such expressions in experimental stress analysis is complicated by difficulties associated with the measurement of strains in excess of yield. At the onset of plastic deformation, the strain tends to concentrate at regularly occurring, well defined slip planes which result in the well known Luders lines [3.19]. Due to the resulting alternating high and low strain distribution, the readings from strain gauges in yielded zones, which may bridge a number of such planes, tend to be unreliable. Moreover, in a force monitoring system employing only four gauges there is effectively zero redundancy of measurement. As a result, the 'loss' of one of the gauges in a yielded zone would prevent the correct interpretation of the four force components.

This problem of strain measurement in zones of discontinuous yield was recognised by Birnstiel in a study of biaxially loaded steel columns [3.5]. The solution which he adopted was to use long strain gauges (65mm gauge length) which straddled a significant number of adjacent slip planes. The resulting strain reading was then effectively an average plastic strain over the length of the gauge. Whilst this approach appeared to work well

in Birnstiel's studies, it was decided that an alternative method should be developed which utilised standard length gauges.

Due to the unreliable performance of strain gauges in yielded zones, it was evident that more than the absolute minimum of four gauges would be required. Work carried out by Lightfoot [3.20] has shown how so called 'redundant' gauges can be incorporated into strain data analysis to generate the strain profile in structural steel sections more accurately. Small experimental variations in the performance of strain gauges, principally due to variations in the material and the fixing procedure, were rationalised by applying a least squares error approximation to produce the linear strain profile. Although the procedure used by Lightfoot was restricted to strain measurement in the elastic region, it was considered that this approach could be extended to cover strain measurement in the elastic-plastic range. Spurious readings from gauges situated in yielded zones, towards the extremities of the section, were to be replaced by extrapolating the linear strain profile deduced from those gauges in the remaining elastic regions situated closer to the centroid.

### **3.3.3 Derivation of the elastic-plastic stress distribution.**

During a subassemblage test, the readings from the 10 strain gauges at each of the measurement locations, positioned as shown in figure 3.21, were recorded. Only upon completion of the test was the data processed to generate the force components acting at the measurement locations. This was done using a purpose written suite of FORTRAN programs on a PRIME mainframe computer. The method, developed to evaluate the elastic and the elastic-plastic actions of the section, is best illustrated by considering the principal sequence of program operations as outlined below.

1. Initially, a check was made of the four strain gauges on the upper flange of the section (gauges 1 to 4 on figure 3.22a) to determine if all strain readings were within the elastic limit of the material, thereby indicating that the gauges were situated within an 'elastic zone'. The readings and positions of the four gauges were then passed to a standard FORTRAN statistical utility module which generated the least squares error approximation to the linear strain profile through the gauge points. Readings from strain gauges which exceeded the strain at yield were ignored, the strain profile being determined only from those gauges which remain in elastic zones.
2. The above procedure was then repeated for the four gauges on the lower flange of the section (gauges 7 to 10).
3. The value of strain at the centre of the upper and lower flanges was then determined from the two flange strain profiles (figure 3.22b). The values at these two 'virtual' strain gauge positions were then combined with the measured values from the two gauges on the web (gauges 5 and 6), thus providing a total of four data points over the depth of the section. The strain gradient was then determined along the web in a similar manner to that described above for the flanges.
4. A mesh was constructed over the entire cross section resulting in an  $80 \times 2$  element array for each of the flanges and an  $80 \times 1$  array for the web. From the 3-dimensional strain gradients, a specific value of strain was assigned to each element in the mesh.
5. From these strains, the corresponding values of stress were determined for each mesh element across the whole section assuming a bi-linear stress strain distribution. In instances where the strain exceeded the yield strain, the resulting stress was limited to the yield stress of the material (figure 3.22c). The effect of post yield strain hardening was not taken into account.

In instances where excessive yielding of the section took place, usually as a result of excessive minor axis bending, it was possible for three of the four gauges along either of the flanges to be in a yielded zone. From the one remaining 'elastic' gauge it was therefore impossible to determine the slope of the linear strain gradient. In such cases, the processing program simplified the stress profile to an idealised fully plastic distribution (figure 3.22d). The neutral axis location used in this distribution corresponded to the last recorded position of the neutral axis determined from the elastic gauge readings. The 3-dimensional stress distribution could therefore be monitored at all levels of loading from elastic through to fully plastic by checking the spread of yielded material across the section. Figure 3.23 shows a typical 'spread of yield' output from the processing program for test S6 at a post failure level of load.

### 3.3.4 Derivation of the force components.

Each of the mesh elements across the section was of a finite area. From the stress assigned to each individual element, it was possible to derive a corresponding finite force. Vlasov's expressions [3.21] shown below were used:-

$$P = \int_0^A \sigma .dA \quad (3.27)$$

$$M_{xx} = \int_0^A \sigma .y.dA \quad (3.28)$$

$$M_{yy} = \int_0^A \sigma .x.dA \quad (3.29)$$

$$B = \int_0^A \sigma .x.y.dA \quad (3.30)$$

where:-

$A$  = Area of section

$\sigma$  = Stress assigned to each element

$x, y =$  Cartesian co-ordinates of the element  $dA$ ,  $(0,0)$  at centroid.

Figure 3.24 shows a plot of the column axial load generated from the processed strain gauge data, against the axial load measured from load cells, for subassemblage test number S5. The supports at the remote ends of each of the beams prevented in-plane rotation, but were free to displace in a direction parallel to the axis of the column, therefore offering no direct resistance to vertical load. All the applied beam load was therefore transferred, via flexure, to the column and thus the column axial load equalled the total load applied to the subassemblage. The strain gauge cluster used to generate the axial load data on the plot was situated at the centre of the column, where maximum plastic deformation occurred. It is evident that the plot is linear, even in the elastic-plastic range, and is very close to the line for which the column axial load is equal to the measured total applied. At the point of failure, the axial load derived from the strain gauges was very close to that of the actual loading, with an apparent error of less than 3%.

A plot of the measured minor axis moment at the centre of test column S5 is shown in figure 3.25. As a result of applying the approach described to the interpretation of experimental strain data, the curve shows a smooth transition from the moment measured in the elastic range right up to full section plasticity. The vertical portion on the far right of the plot denotes that the idealised fully plastic moment has been reached.

Figure 3.26 shows a plot of the 'as measured', and the corrected strains for two strain gauges,  $A$  and  $B$ , at the base of the column in test S5. The strain at  $A$  is initially compressive, becoming tensile as the column approaches failure. As strain  $A$  never exceeds the nominal yield strain of 1500 microstrain, very little correction is made to the measured strain. However, the strain at  $B$  is compressive for all levels of column load. For strains in excess of 1500 microstrain the divergence between the measured and the corrected strain, resulting from the interference of Luder's slip planes, is apparent.

It is interesting to note that although the degree of correction to each of the gauges is very different, the same linear strain gradient was used to correct each of the measured strains.

### 3.3.5 Overall subassembly force instrumentation.

The sophisticated 10 gauge elastic-plastic force monitoring system described in the preceding sections was adopted at the base, mid point and top of each column in the subassembly test series. Throughout the subassembly test series, load arrangements were specifically selected to prevent the stresses within the beam sections exceeding the yield stress of the material. As these particular sections remained wholly elastic, a more modest four gauge system (figure 3.27), which employed the principles previously described in section 3.3.2, was used to monitor the forces at each end of the beams. For a typical three beam subassembly, a total of 54 strain gauges was used for each test (30 fixed to the column and 8 fixed to each of the beams). The plan and elevation of the subassembly shown in figure 3.28 indicates the location of the different strain gauge clusters and summarises the force components which were recorded.

## 3.4 Data <sup>c</sup>quisition.

An Orion data logging system, linked to an I.B.M. P.C. compatible computer, was used to record the readings from the electrical instrumentation devices. A total of 154 logging channels was used, 108 for strain gauges (54 energising and 54 recording), 42 for the L.V.D.T.'s, 3 for monitoring the pressure in the hydraulic beam rams and a single

channel to monitor the column head load cell. The logging system was triggered manually and recorded the data at a rate of 100 channels/second. A computer program was incorporated into the logging system which processed the data from the 3-dimensional displacement device at the column centre. This enabled the load against minor axis deflection plot to be displayed continuously on the monitor as the test progressed. Due to the large amount of data recorded and the complex processing procedures, the majority of the data was processed after completion of the tests using a suite of purpose written FORTRAN programs on a PRIME mainframe computer.

## References.

- 3.1 Gibbons, C., Kirby P.A. and Nethercot D.A., *'The development of a device for measuring the 3-dimensional deformation of steel columns.'*, Journ. Strain Analysis. (to be published)
- 3.2 Gibbons, C., Kirby P.A. and Nethercot D.A., *'The experimental assessment of force components within thin walled structural steel members'*, Journ. Strain Analysis. (to be published)
- 3.3 Wang, Y.W. and Nethercot, D.A., *'Ultimate strength analysis of three-dimensional column subassemblages with flexible connections'*, Journ. Construct. Steel Res., No. 9, 1988, pp. 235-264.
- 3.4 Estuar, F.R. and Tall, L., *'Testing of pinned-end steel columns'*, Test Methods for Compression Members, Am. Soc. Testing Mats., STP 419, 1967, pp. 80-96.
- 3.5 Birnstiel, C., *'Experiments on H-Columns under biaxial bending'*, Journ. Struct. Div., Proc. Am. Soc. Civil Engrs., No. ST10, October 1968, pp. 2429-2449.
- 3.6 Aggarwal, A.K., Coates, R.C., *'Moment-rotation characteristics of bolted beam to column connections'*, Journ. Const. Steel Res., Vol. 6, No. 4, 1986, pp. 303-318.
- 3.7 Gent, A.R. and Milner, H.R., *'The ultimate load capacity of elastically restrained H-Columns under biaxial bending'*, Proc. Inst. Civil Engrs., No. 41, 1968, pp. 685-704.



- 3.8 Wood, R.H., Needham, F.H. and Smith, R.F., '*Test of a multi-storey rigid steel frame*', The Structural Engineer, Vol. 46(4), April 1968, pp. 107-119.
- 3.9 MacLachlan, D.F.A., Squire, A.M. and Planer, G.V., '*Remote indication of angular displacement*', The Engineer, Vol. 214, No. 559, 10 August 1962, pp. 235.
- 3.10 Davison, J.B., Kirby, P.A. and Nethercot, D.A. '*Column behaviour in PR construction: Experimental studies*', Journ. Struct. Div., Am. Soc. Civil Engrs., Vol.113, No.9, Sept. 1987, pp. 2032-2050.
- 3.11 Johnson, D.L., '*A method for the full-scale testing of roof systems*', Full-Scale Load Testing of Structures, Am. Soc. Testing Mats., STP 702, Ed. W.R. Shriever, 1980, pp. 78-87.
- 3.12 O'Heachteirn, P., '*An experimental investigation into the lateral buckling strength of plate girders*', Ph.D. Thesis, University of Sheffield, England, 1983.
- 3.13 Cuk, P.E., Rogers, D.F. and Trahair, N.S., '*Inelastic buckling of continuous steel beam-columns*', Journ. Const. Steel Res., Vol. 6, No. 1, 1986, pp. 21-50.
- 3.14 Eisenhart, L.P., '*Co-ordinate geometry*', Dower Publications Inc., 1939.
- 3.15 Holister, G.S., '*Experimental stress analysis - principles and methods*', Cambridge University Press, 1967.
- 3.16 Dally, J.W. and Riley, W.F., '*Experimental stress analysis - second edition*', McGraw-Hill, 1978
- 3.17 Randolph M.F. and Lightfoot, E., '*Analysis of strain gauge data from thin walled structural steel members subjected to eccentric longitudinal loading*', Proc. Inst. Mech. Engrs., Journal of Strain Analysis, Vol. 10, No. 2, 1975.
- 3.18 Chen, W.F. and Atsuta, T., '*Theory of beam-columns - Volume 2 space behaviour and design*', McGraw-Hill, 1977.
- 3.19 Nadai, A., '*Theory of flow and fracture of solids*', Vol. 1, 2nd. edition, McGraw-Hill, 1950.
- 3.20 Lightfoot, E., '*The statistical interpretation of strain gauge readings*', Proc. Inst. Mech Engrs., Journal of Strain Analysis, Vol. 1, No. 1, 1965, pp. 27-30.
- 3.21 Zbirohowski-Koscia, K., '*Thin walled beams - from theory to practice*', Crosby Lockwood & Son Ltd., London, 1967.

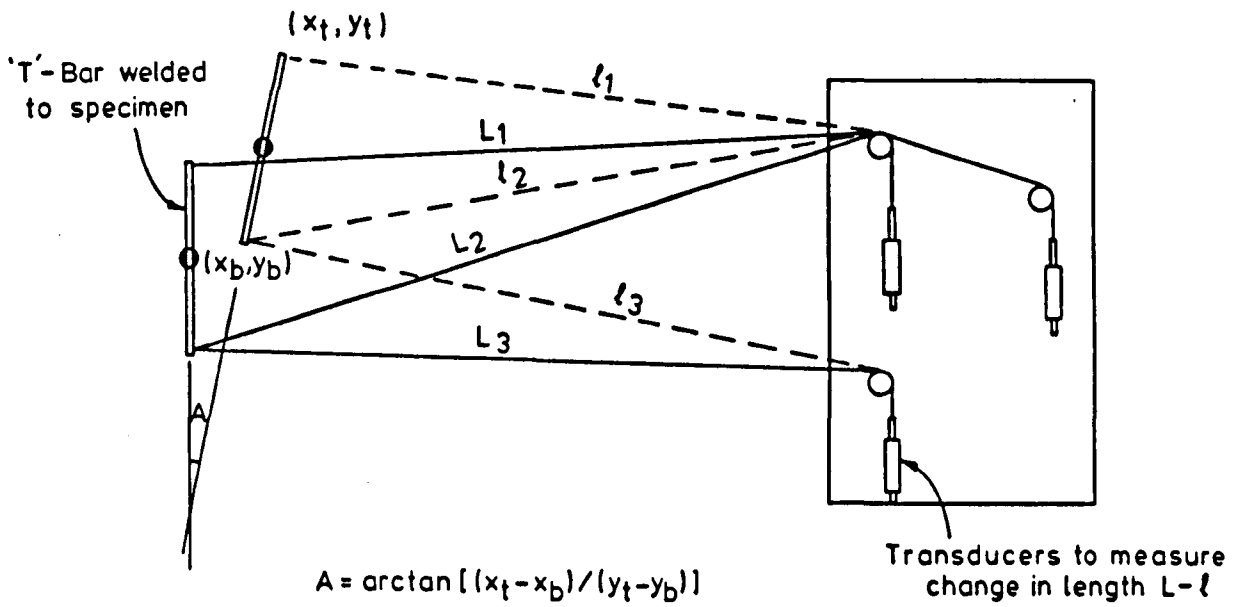


Figure 3.1: Two dimensional measurement device using three L.V.D.T.'s.

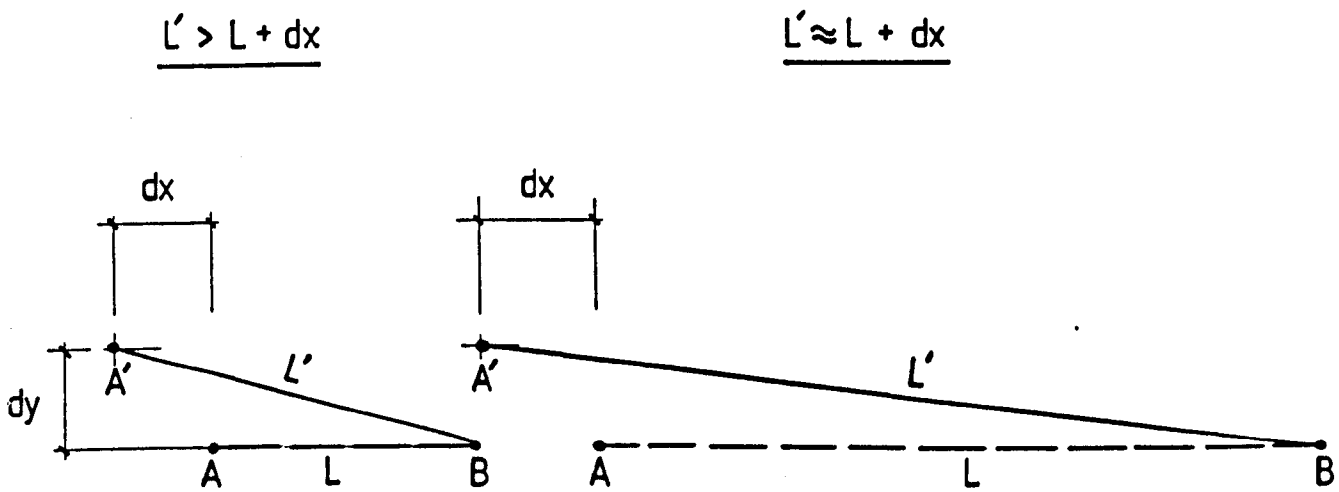


Figure 3.2: The effect of out-of-plane movement on the measurement of in-plane displacement.

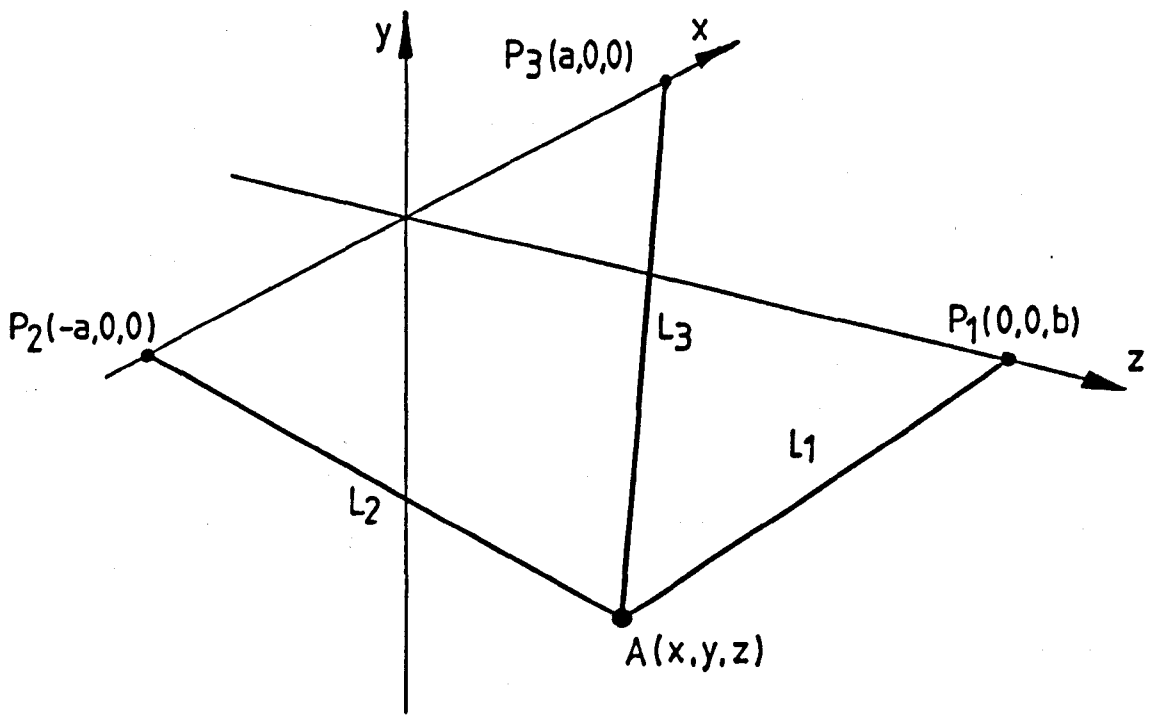


Figure 3.3: Three-dimensional co-ordinates of reference points  $P_1$ ,  $P_2$  and  $P_3$  from general point  $A$ .

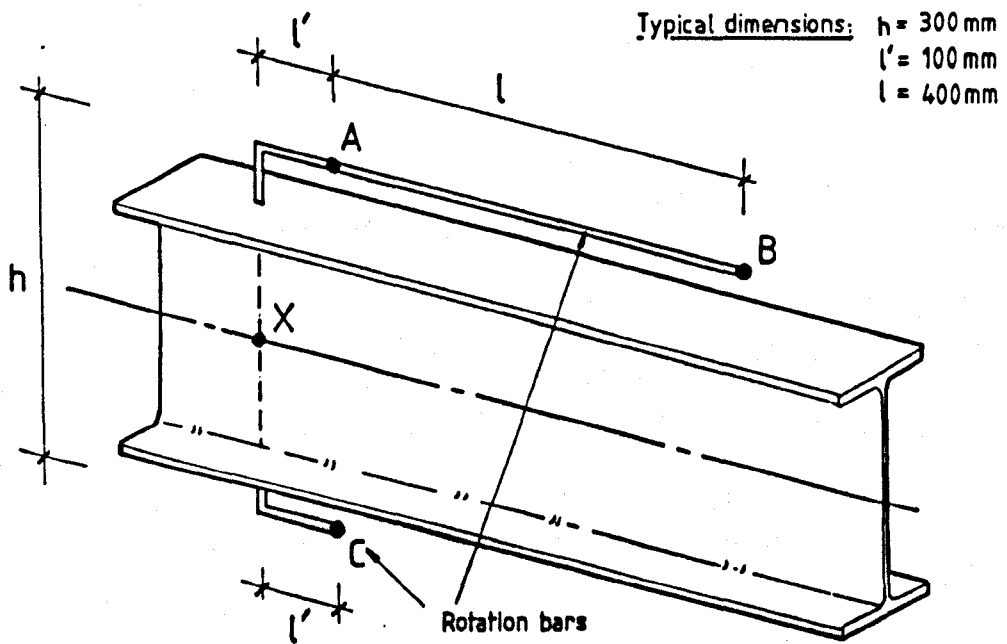


Figure 3.4: Location of the three connection points around the specimen.

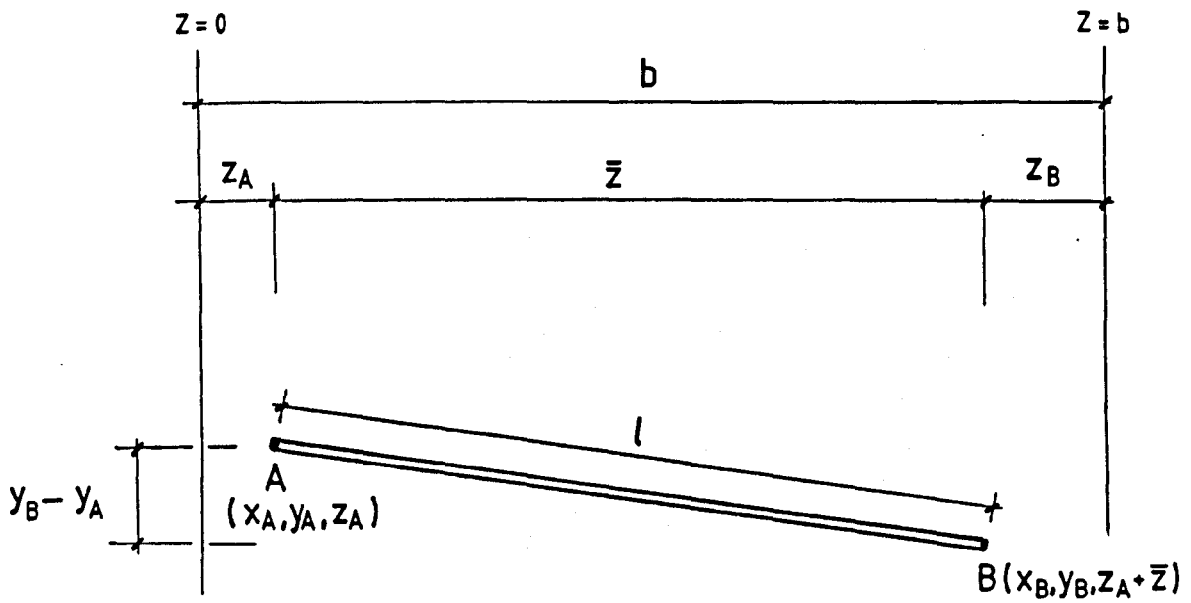


Figure 3.5: Co-ordinates of the rotation bar connecting reference points A and B.

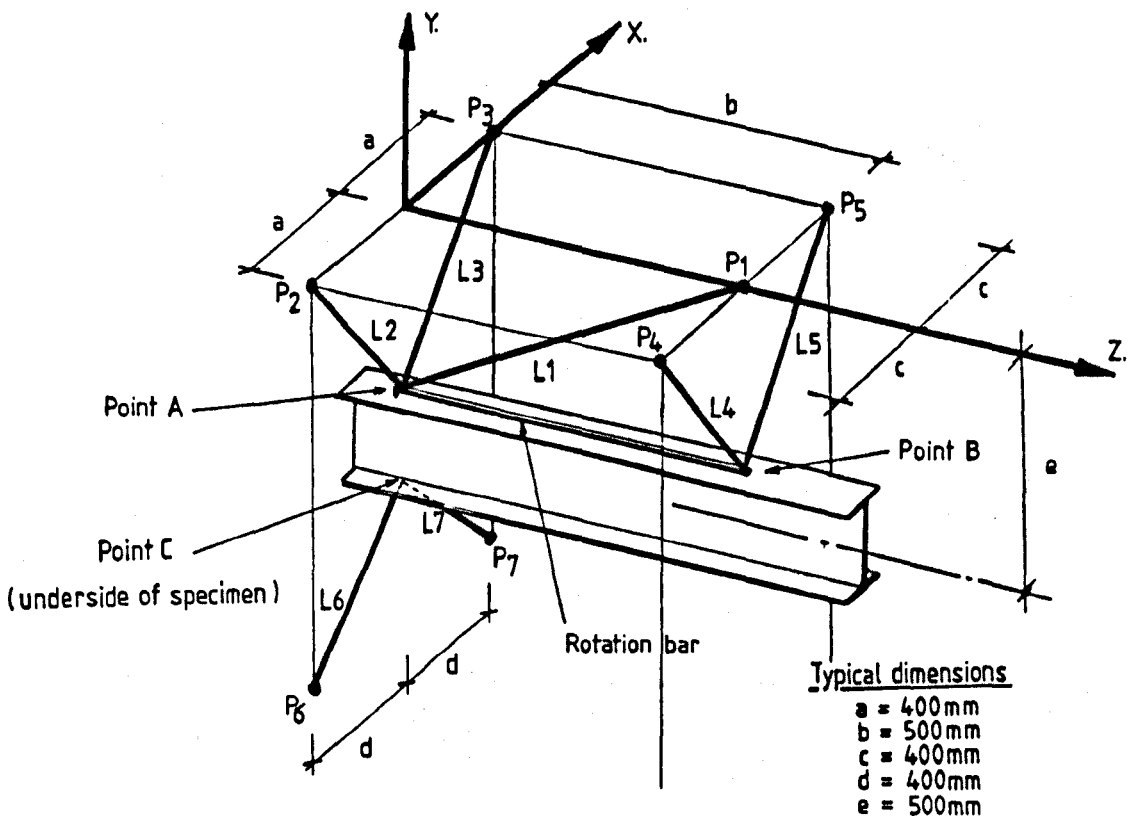


Figure 3.6: Arrangement of the three-dimensional measurement system.

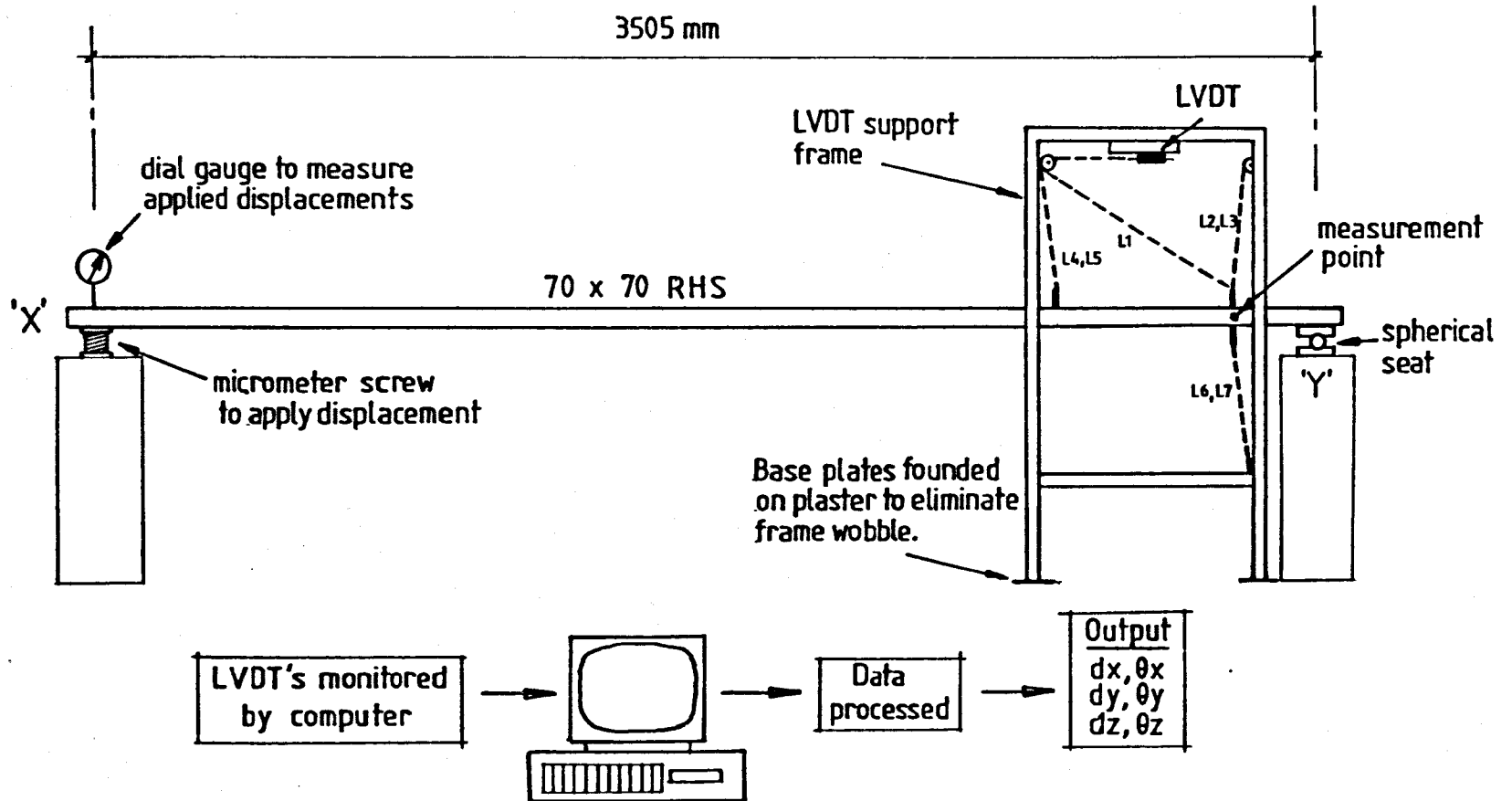


Figure 3.7: Experimental set-up used for testing a prototype of the 3-dimensional measurement system.

## MAJOR AXIS ROTATION

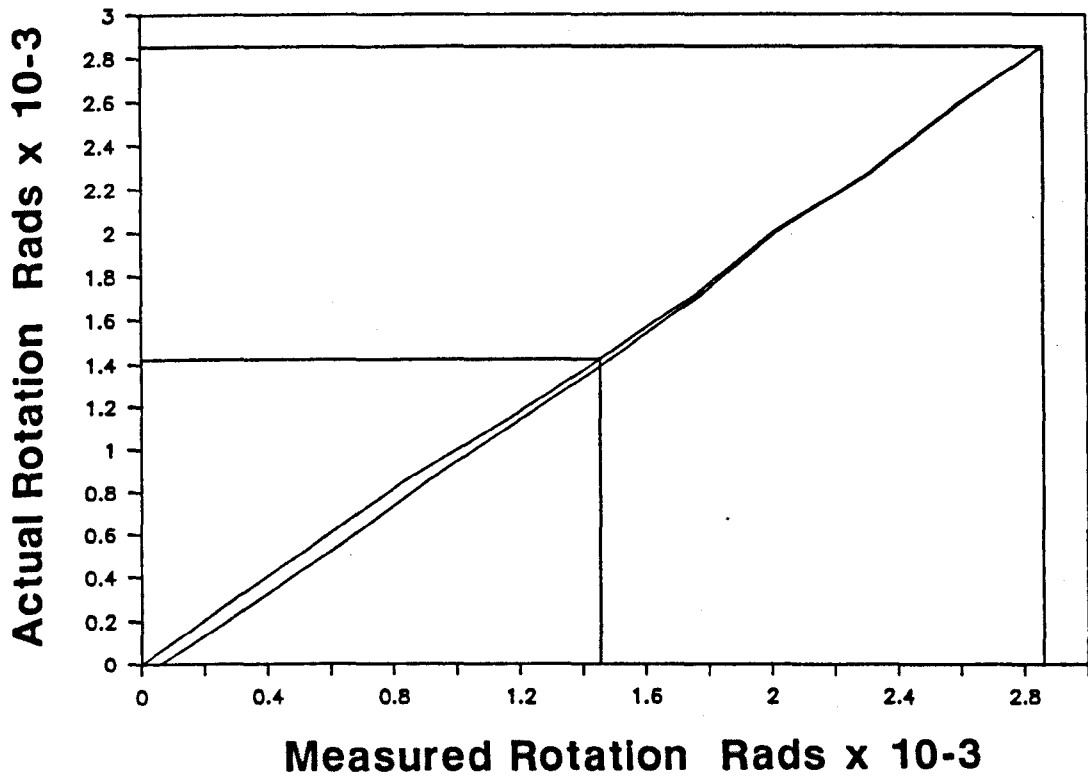


Figure 3.8: Plot of actual vs. measured major axis rotation.

## MINOR AXIS ROTATION

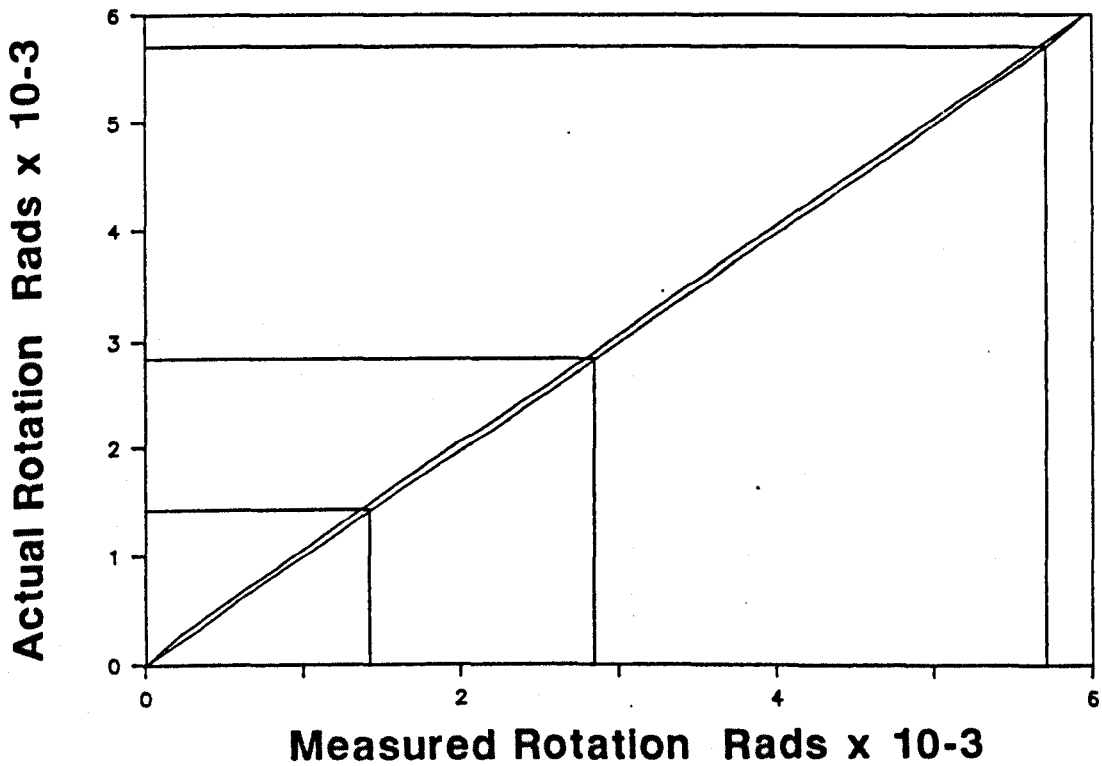


Figure 3.9: Plot of actual vs. measured minor axis rotation.

## TWIST ROTATION

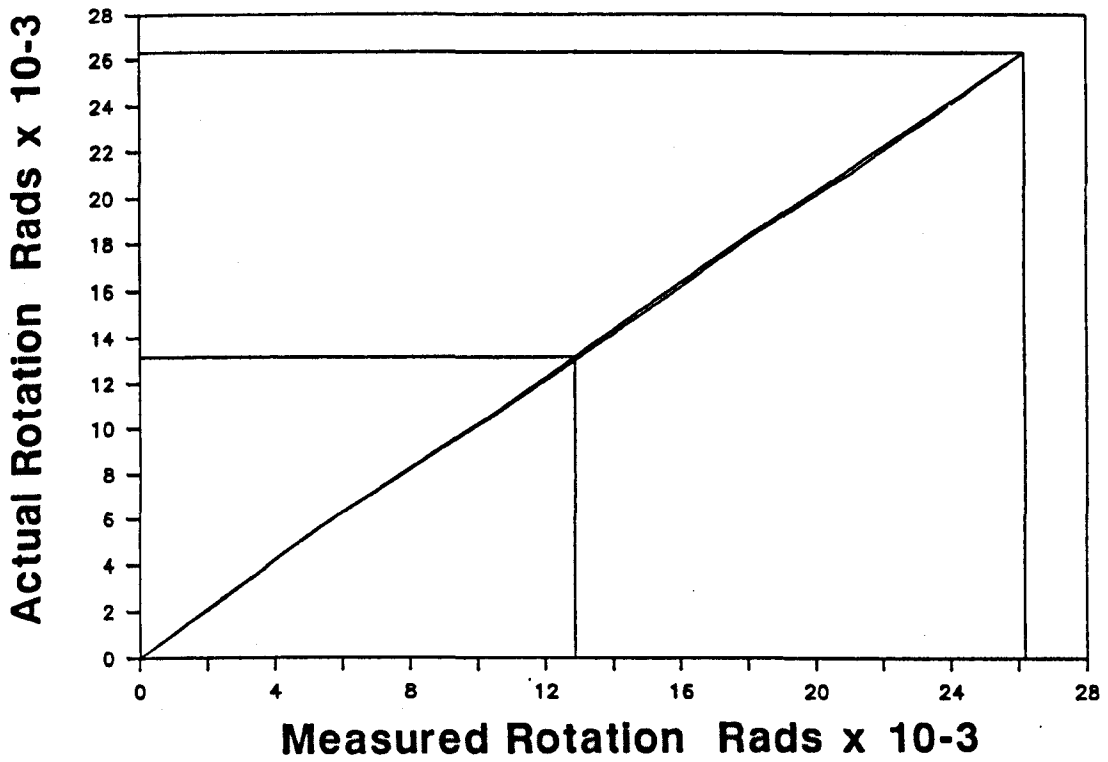


Figure 3.10: Plot of actual vs. measured twist rotation.

## X - DISPLACEMENT

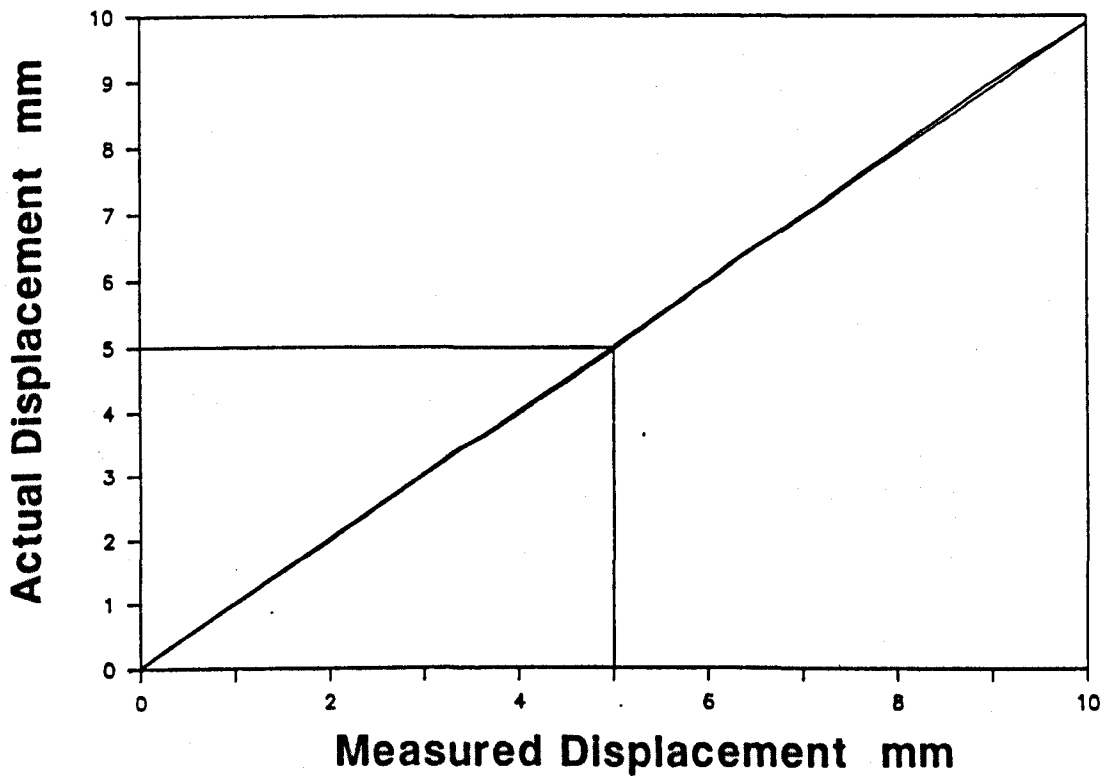


Figure 3.11: Plot of actual vs. measured 'x' displacement.

## Y - DISPLACEMENT

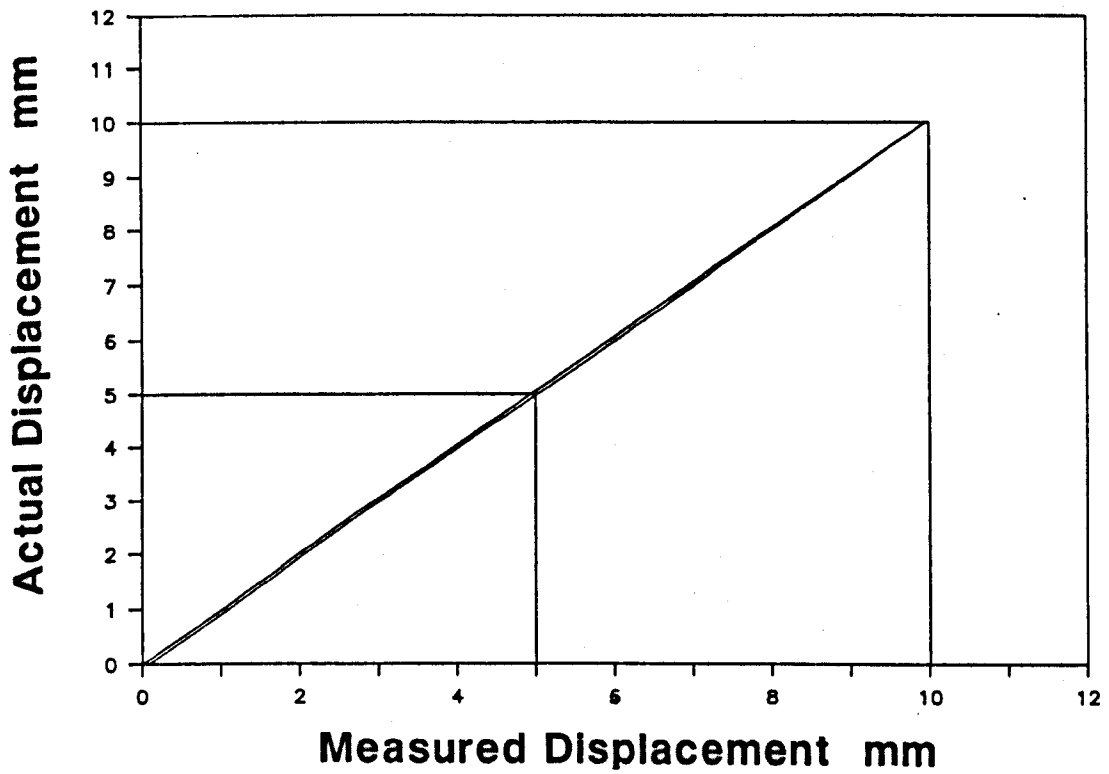


Figure 3.12: Plot of actual vs. measured 'y' displacement.

## Z - DISPLACEMENT

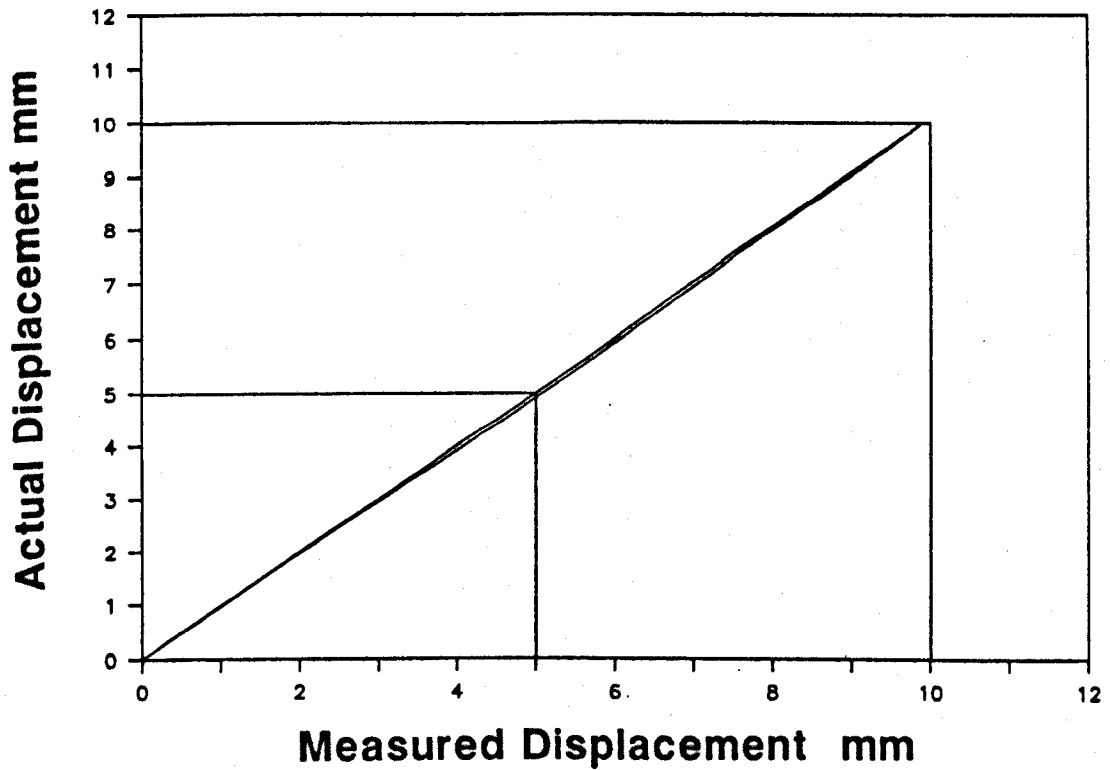


Figure 3.13: Plot of actual vs. measured 'z' displacement.



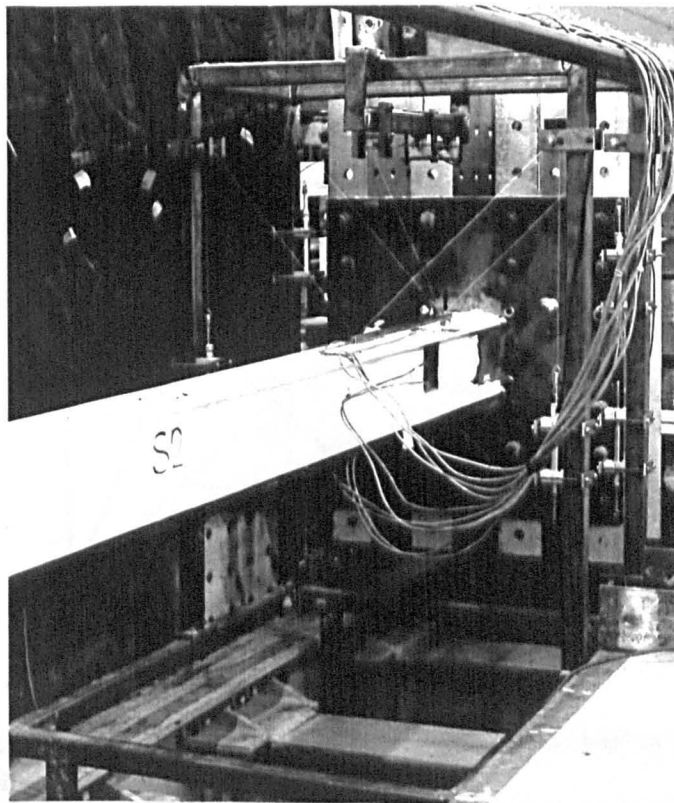


Figure 3.14: Measurement system used at the base of the column.

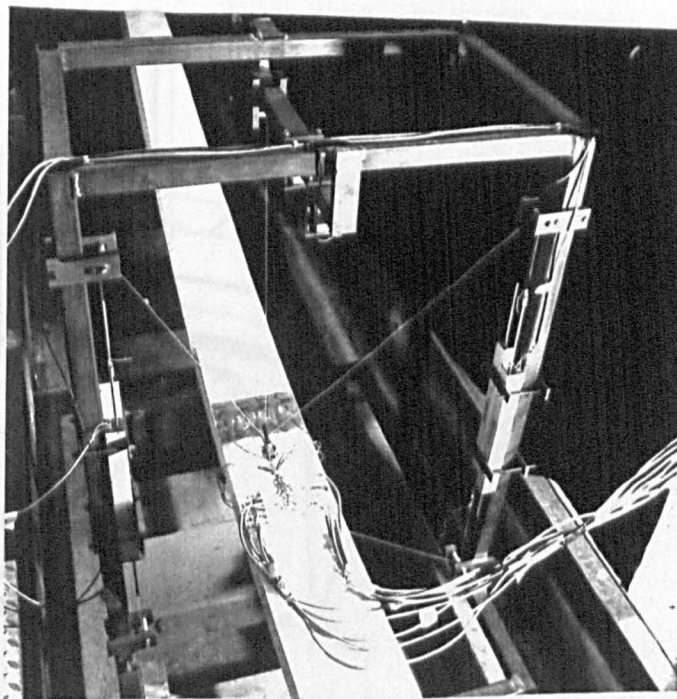


Figure 3.15: View along the column illustrating the measurement device at the column centre.

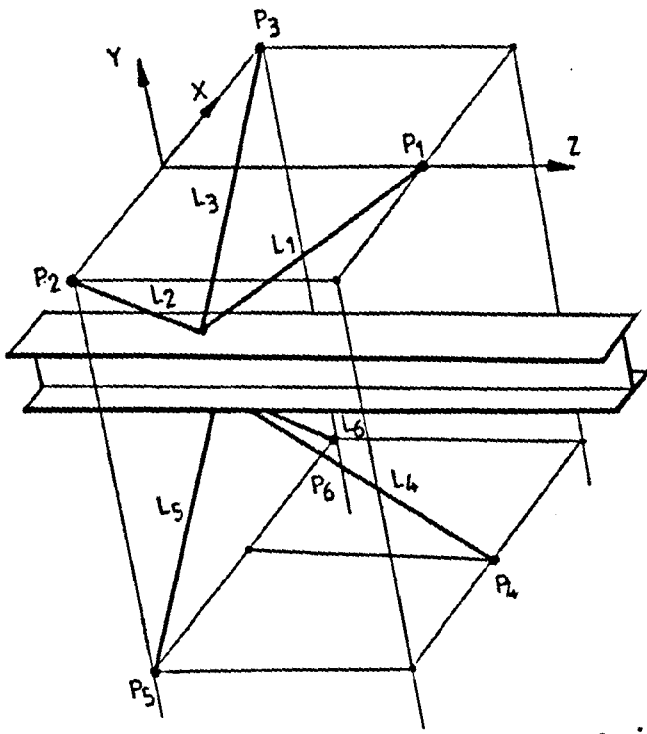


Figure 3.16: Schematic diagram of the six L.V.D.T. device used at the column centre.

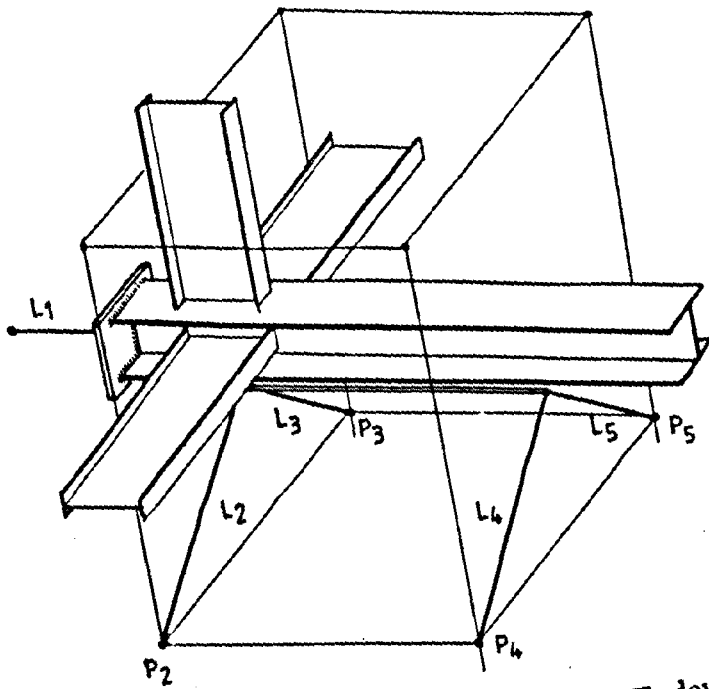


Figure 3.17: Schematic diagram of the five L.V.D.T. device used at the column head.

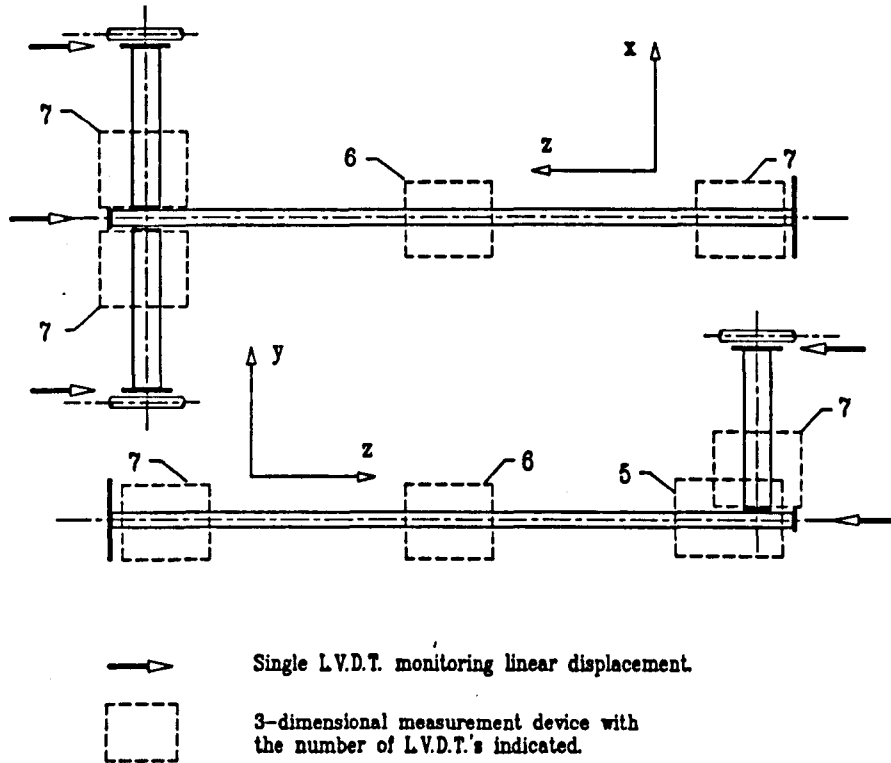


Figure 3.18: Location of three-dimensional measurement devices.

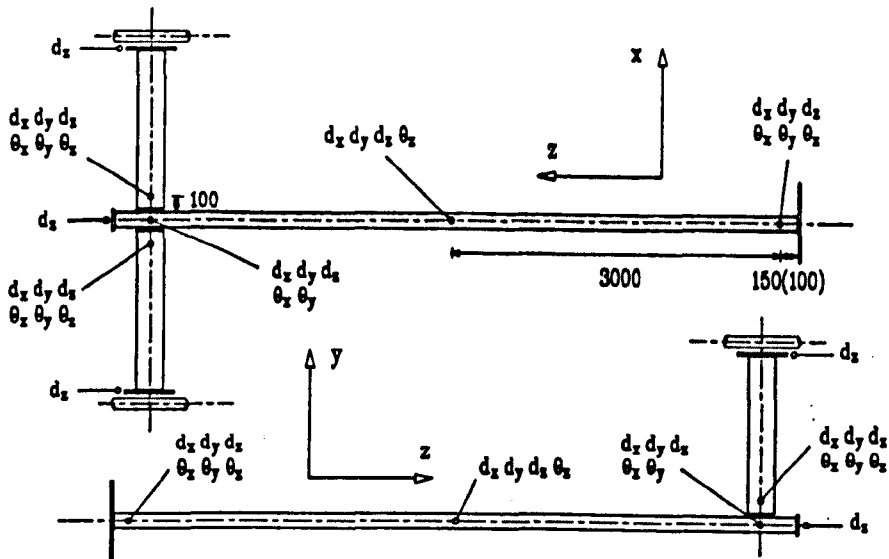
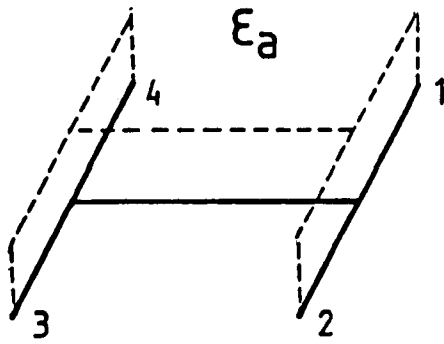
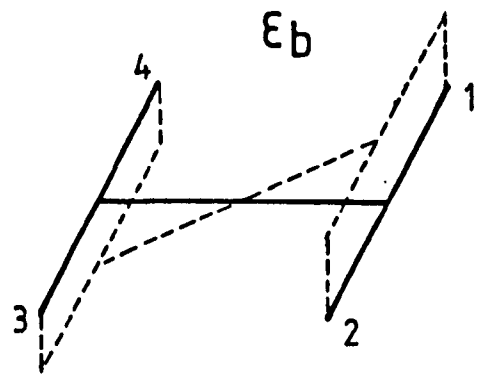


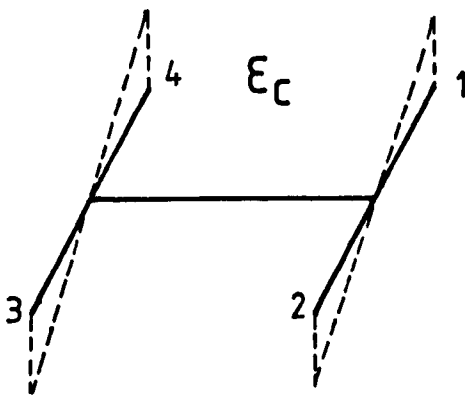
Figure 3.19: Deformation components measured in the subassembly tests.



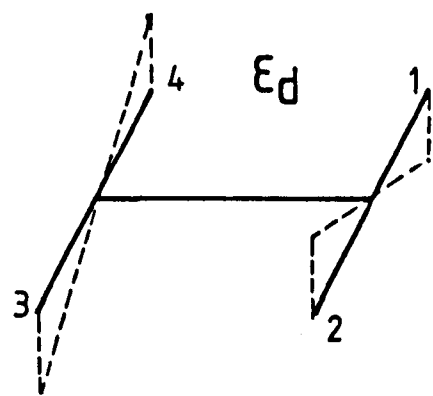
Axial Load



Major Axis Moment



Minor Axis Moment



Warping Torque

$$\left. \begin{aligned} \epsilon_1 &= \epsilon_a + \epsilon_b + \epsilon_c - \epsilon_d \\ \epsilon_2 &= \epsilon_a + \epsilon_b - \epsilon_c + \epsilon_d \\ \epsilon_3 &= \epsilon_a - \epsilon_b - \epsilon_c - \epsilon_d \\ \epsilon_4 &= \epsilon_a - \epsilon_b + \epsilon_c + \epsilon_d \end{aligned} \right\}$$

Strain Compatibility  
Equations

$$\left. \begin{aligned} P &= \frac{EA}{4} (\epsilon_1 + \epsilon_2 + \epsilon_3 + \epsilon_4) \\ M_x &= \frac{E Z_x}{4} (\epsilon_1 + \epsilon_2 - \epsilon_3 - \epsilon_4) \\ M_y &= \frac{E Z_y}{4} (-\epsilon_1 + \epsilon_2 + \epsilon_3 - \epsilon_4) \\ M_w &= \frac{\Gamma W_{ns}}{4} (-\epsilon_1 + \epsilon_2 - \epsilon_3 + \epsilon_4) \end{aligned} \right\}$$

Force  
Equations

Figure 3.20: Member actions resulting from longitudinal strains.

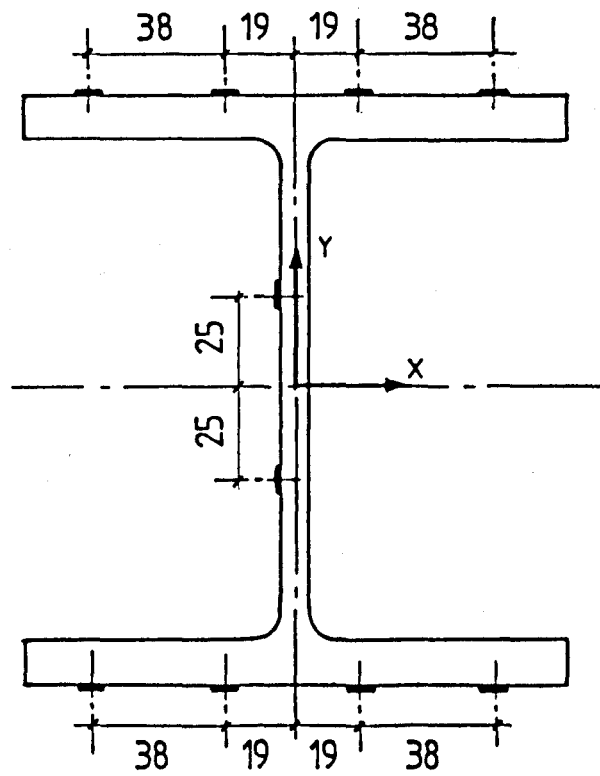


Figure 3.21: Arrangement of 10 strain gauges used at the column centre.

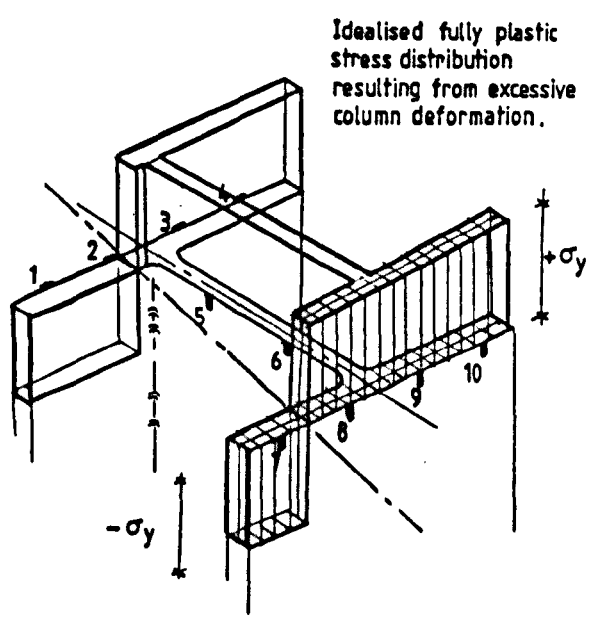
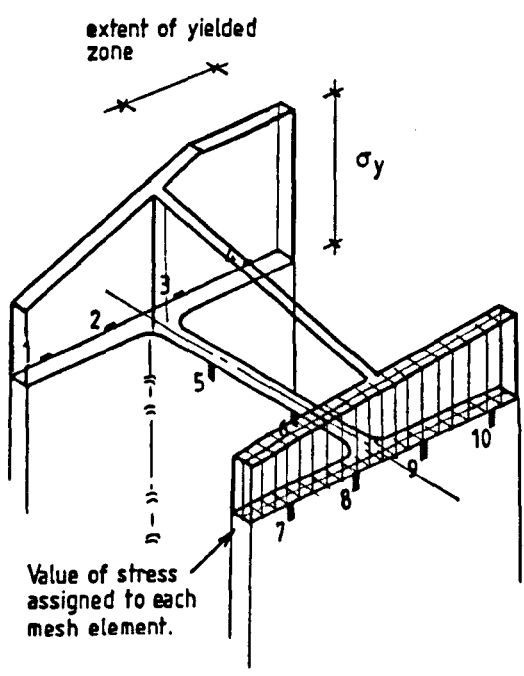
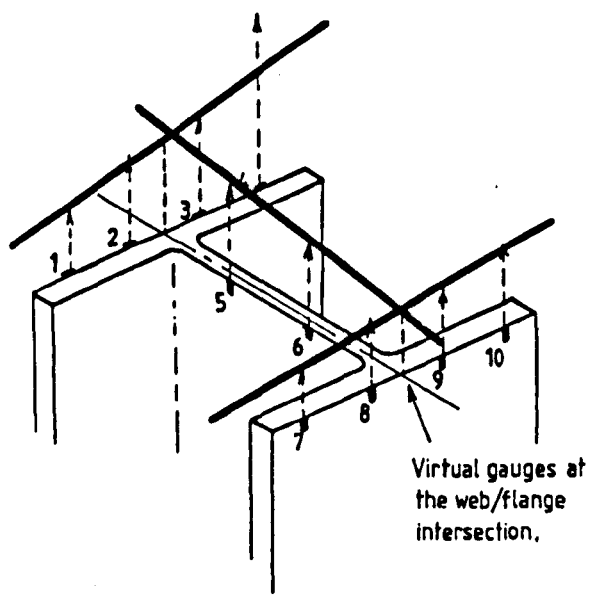
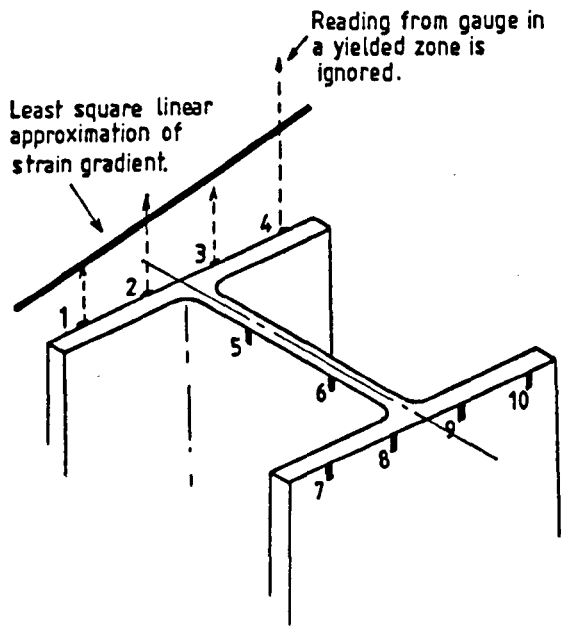
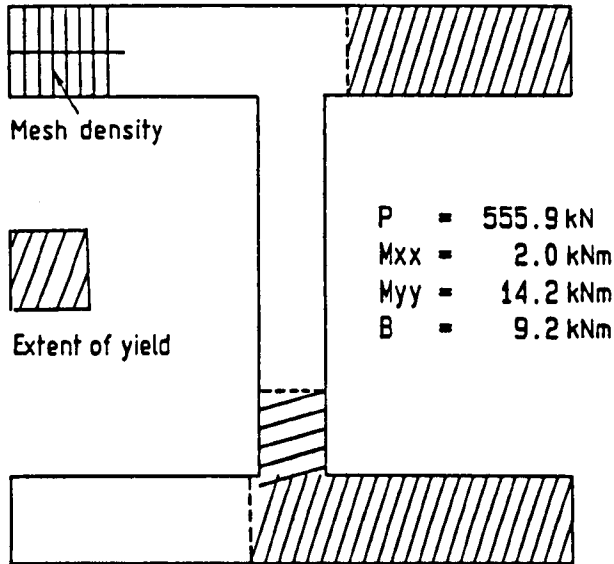


Figure 3.22: Derivation of the 3-D stress distribution from the measured strains.

Distribution of Yield Stresses in Column  
Subassemblage Test S6



Mid Column

Figure 3.23: Typical output from the processing program showing the extent of material yield.

Comparison of Applied and Measured Column Load      Test No : S5

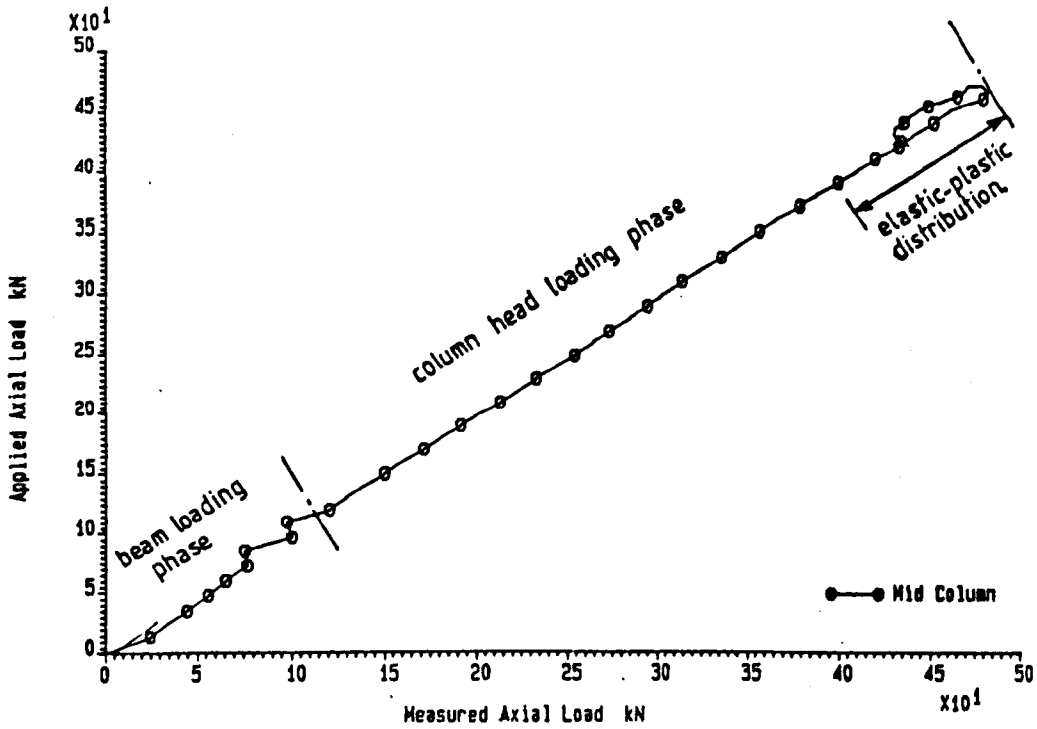


Figure 3.24: Plot of applied axial load against axial load measured from the strain gauges.

Axial Load v. Mid Column Moments

Test No : S5

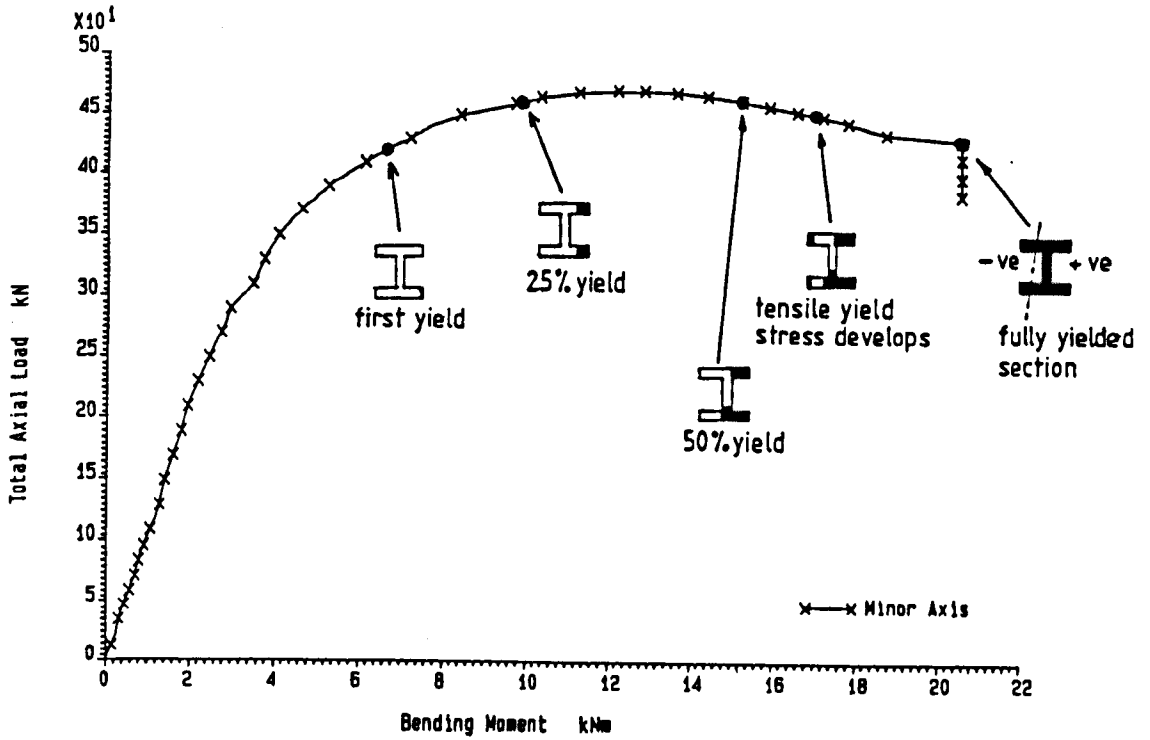


Figure 3.25: Plot of axial load vs. mid-column minor axis bending moment - test S5.

Comparison of the Measured and Corrected Strains Test No : S5

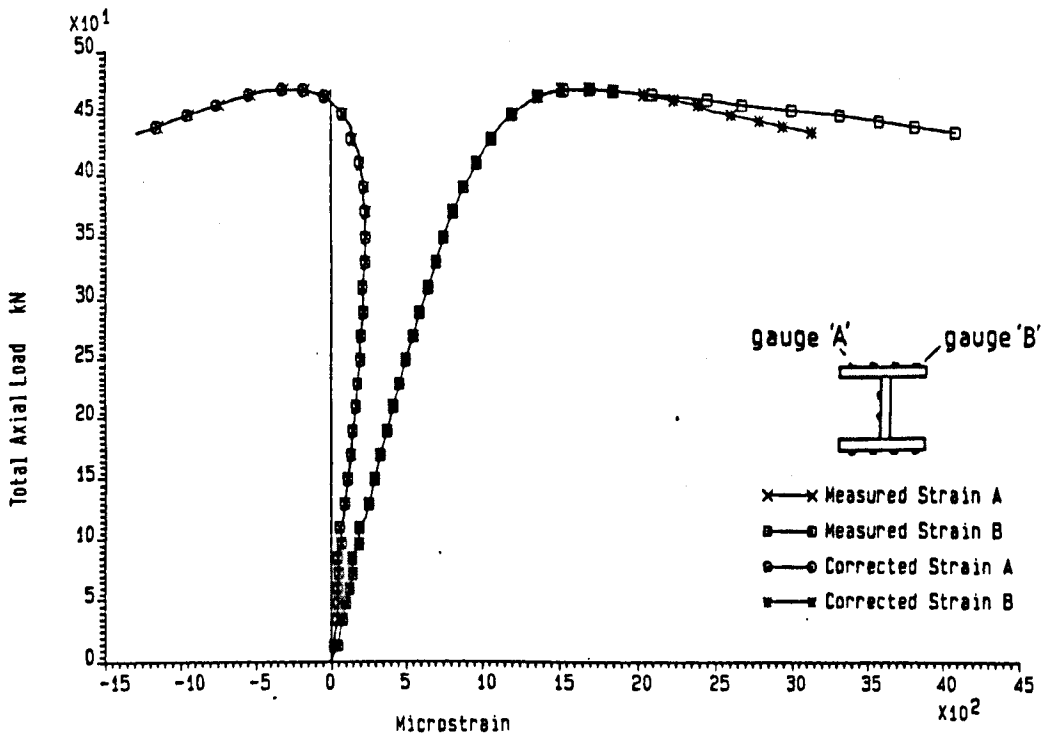


Figure 3.26: Plot of axial load vs. measured microstrain indicating the degree of correction made to different gauges.



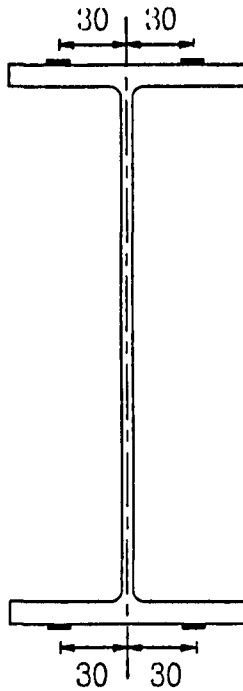
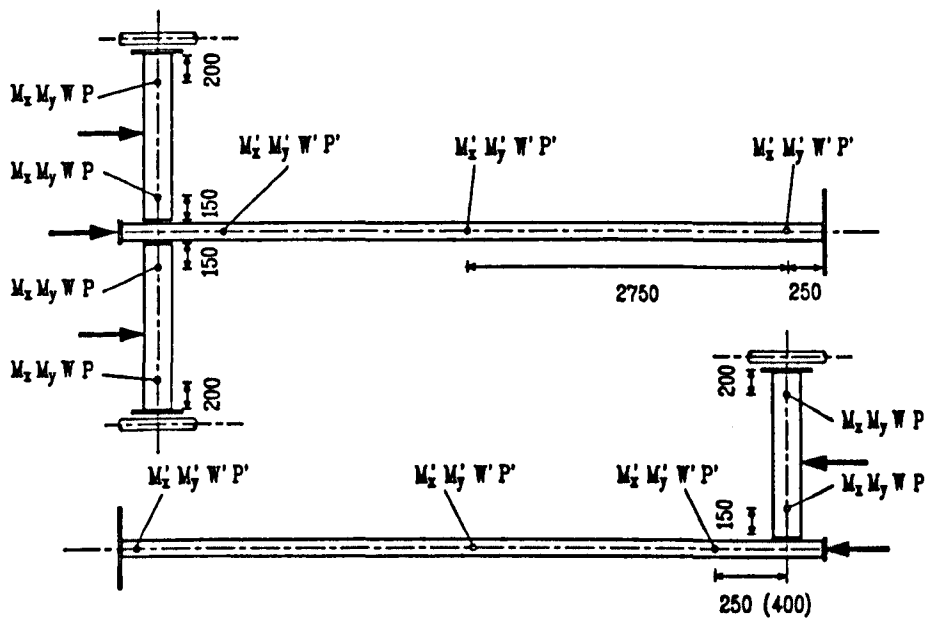


Figure 3.27: Arrangement of four strain gauges used to derive the elastic beam forces.



$M_x' M_y' W' P''$  Major axis moment, Minor axis moment, Warping bi-moment and axial load monitored up to full plasticity. ( 10 gauge cluster ).

$M_x M_y W P$  Major axis moment, Minor axis moment, Warping bi-moment and axial load monitored under elastic conditions only. ( 4 gauge cluster )

→ Externally applied loads.

( Dimensions in brackets refer to test numbers S2, S3, S8, S7, S9 and S10 )

Figure 3.28: Force components measured in the subassembly tests.

## Chapter 4

# Comparisons of Experimental and Analytically Predicted Subassemblage Behaviour

### 4.1 Introduction

One of the specific aims of the experimental subassemblage study was to validate the predictions of a sophisticated finite element analysis computer program capable of analysing 3-dimensional subassemblages. This section of the thesis describes how the computer program was used to model each of the ten subassemblage tests, and presents detailed comparisons of various aspects of the experimentally observed and analytically predicted behaviour.

## 4.2 The finite element analysis program.

The present version of the finite element computer program is the latest in a series of successively more complex enhancements to a program originally developed by Jones [4.1]. This original version of the program investigated the behaviour of isolated 2-dimensional beam-columns restrained by non-linear end conditions. The program was modified in the first instance by Rifai [4.2] to include the effect of beams framing into the column. This permitted the analysis of 2-dimensional beam column 'I' shaped subassemblages which incorporated the characteristics of semi-rigid connections.

In parallel, the original column program was reformulated by El-Kenfas [4.3]. Here, the restriction of the program to in-plane response was removed, thus permitting the analysis of isolated 3-dimensional beam-columns with non-linear end restraints. The latest major modification was carried out by Wang [4.4] who extended the work carried out by both Rifai and El-Kenfas to develop a program capable of analysing 3-dimensional beam-column subassemblages which incorporated semi-rigid beam to column connections. This latest version of the program, which was ultimately used to model the experimental subassemblage tests reported herein, was recently used to predict the behaviour of the small scale rigidly connected subassemblages [4.5] investigated experimentally by Gent and Milner [4.6].

The reader should refer to reference 4.4 for a comprehensive description of the program operation and the analysis techniques employed. However, as a means of introduction, a brief overview of the program is presented herein, the details of which have been extracted from the program user manual [4.7].

### 4.2.1 Brief overview of computer program analysis techniques.

The analysis program divides the beam-column member into a number of discrete elements, the stiffness of which is calculated in accordance with the formulation by Rajasekaran [4.8]. To save computer storage without sacrificing accuracy, the internal degrees of freedom are reduced using a static condensation technique. The overall stiffness matrix, the applied load vector and the resulting displacement vector are partitioned in the following form:

$$\begin{bmatrix} K_r & K_{rc} \\ K_{cr} & K_c \end{bmatrix} \begin{Bmatrix} d_r \\ d_c \end{Bmatrix} = \begin{Bmatrix} F_r \\ F_c \end{Bmatrix} \quad (4.1)$$

in which  $\{d_r\}$  and  $\{F_r\}$  are terms to be retained whilst  $\{d_c\}$  and  $\{F_c\}$  are those terms to be condensed out. In the analysis, the terms to be retained are those degrees of freedom at the ends of the member. A system of 7 degrees of freedom was adopted and as a result,  $[K_r]$  is a matrix of order 14.

From equation 4.1, the following relationship is obtained:

$$[K_r - K_{rc}K_c^{-1}K_{cr}]\{d_r\} = \{F_r - K_{rc}K_c^{-1}F_c\} \quad (4.2)$$

To incorporate various degrees of member restraint, the end reactions of each member must be known. This is achieved by considering the expression:

$$\{F_{endreaction}\} = \sum [K_{n-1}] \times \{\Delta d_{n-1}\} \quad (4.3)$$

in which  $[K_{n-1}]$  and  $\{\Delta d_{n-1}\}$  are the member stiffness matrix and the incremental displacement vector at the preceding step respectively.

Having obtained the end reactions of the member, the diagonal stiffness matrix of the non-linear semi-rigid connection attached to the member is calculated from the tangent of the connection's user defined multi-linear moment-rotation curve.

Having assembled the stiffness matrices of all the members in the subassemblage and ap-

plied the appropriate boundary conditions, load is then applied. The program considers a two stage loading sequence similar to that adopted in the experimental studies. Firstly, load is applied to the beam elements up to a pre-defined limit in pre-defined increments. This is followed by column head loading, again applied in pre-defined increments. Gaussian elimination methods are used to solve the linear equations and the Newton-Raphson iteration technique is used to follow the response of the subassemblage up to failure.

The principal features of the program are summarised below:-

1. The program uses a finite element technique to trace the full three dimensional deformation response of the column.
2. The spread of yield across the section is taken into account by considering an elastic-perfectly plastic stress-strain distribution.
3. In order to consider the spread of yield along the member as well as the non-uniform distribution of internal forces within, the member is divided into several longitudinal sections.
4. The beam to column connection is treated as a separate element. In instances where a beam frames into the column flange, the connection can be located at an offset from the column centreline to simulate column depth.
5. In the incremental analysis, the stiffness of the semi-rigid connection for the current beam end moment is taken from a simplified multi-linear  $M-\phi$  relationship defined by the user.
6. The effects of residual stress distributions, initial column deformations and eccentricity of applied loading are all considered in the program.

### **4.3 Modelling of the experimental parameters.**

A basic computer model of the subassemblage specimens was used to perform the pre-test parametric study discussed in section 2.2. The aim of that study was to quantify the effect on the subassemblage of applying various experimental boundary restraints and ultimately to develop an appropriate experimental test set-up. The basic model incorporated only nominal values for member size, strength and initial deformation. In the post-test verification of the program however, it was important that the actual properties of the experimental subassemblage specimens were used.

#### **4.3.1 Yield and residual stress.**

It is evident from the data presented in the supplementary volume to this thesis [4.9] that the measured residual stresses in the column sections were highly irregular and did not conform with the idealised residual stress pattern for hot rolled 'H' sections [4.10]. This was attributed to the effect of roller straightening and the relatively light sections used. From these measured stresses, it was impossible to apply a single residual stress pattern which would be valid along the entire length of the column. As a result, all the subassemblages were modelled assuming zero residual stress across the section.

The values of yield stress and Young's modulus,  $E$ , used for each column were those measured from stub column tests performed on the column sections [4.9]. It was considered that, in the case of the column, the yield stress derived from tensile coupon tests would be less representative. In addition, the stub column tests tended to rationalise the effect of the erratic residual stress distributions present in the sections. However, the yield stress and Young's modulus used for the beam elements were derived from tests on tensile coupons.

### **4.3.2 Initial deformations and geometric properties.**

The actual dimensions and geometric properties of each of the subassemblage members were used in the analytical modelling. The sizes and properties were extracted from the dimensional survey of steel sections presented under reference 4.9. The program allows the user to define the initial major and minor axis deformations and twists at five points along the length of the column. The measured values which were used in the analysis are summarised under section 2.4.

### **4.3.3 In-plane connection moment-rotation characteristics.**

A full appraisal of the moment-rotation characteristics measured in the experimental subassemblage tests is presented in chapter 6.

Ideally, the analytical model of a subassemblage specimen should have incorporated the moment-rotation characteristics of each of the connecting beams observed from that particular test. However, this was not always possible. Due to the very small connection rotations induced in the earlier tests, the resolution of the measurement devices became significant and hence the assessment of connection stiffness became very subjective. In the analytical modelling, this problem was overcome by considering the moment-rotation response of a similar connection, connected to the same column face but from another test in which the net connection rotations were larger. Figures 4.1 and 4.2 show typical multi-linear approximations to the true moment-rotation behaviour which were used in the analytical models.

#### 4.3.4 Out-of-plane and torsional moment-rotation responses.

Figure 4.3 shows that the net out-of-plane connection rotation is dependent on the magnitude of the absolute out-of-plane beam rotation relative to the twist of the head of the column. In the experimental tests however, the measured absolute out-of-plane beam rotation was almost negligible, typically less than 0.0015 radians. This was principally due to the short lengths of beam used, and the inevitable positional restraint from the beam loading jacks. In addition, the column head was effectively restrained against twist rotation due to the head load being applied eccentric to the column centreline. This was confirmed by the very small column head twist rotations which were observed in the tests. A situation therefore existed in which there was little potential for the development of significant out-of-plane connection rotations. Consequently, changing the out-of-plane connection characteristics in the analytical model had negligible effect on the predicted subassembly behaviour. The out-of-plane flexibility of the connection was therefore not considered in this analytical appraisal.

More important was the relationship between the major and minor axis column head rotations with respect to the twist rotations of the connecting beams (figure 4.4). Although the torsional constant ( $J$ ) of the beam section (254x102x22 UB) was relatively small, the torsional restraint from the beam was significant due to the short beam length and the warping restraint present at the beam support bearings. Depending on the precise restraint to beam twist offered by the beam loading ram, the calculated torsional stiffness of the beam at the connection was in the range 8.0 to 21.0 kNm/radian. The total restraint to the column head from a pair of beams would therefore be in the range 16.0 to 42.0 kNm/radian. It is evident that this restraint stiffness is significantly less than than the in-plane initial stiffness,  $C_i$  of even the most flexible semi-rigid connection. However, as the torsional stiffness is a linear relationship at relatively large rotations,



the component of torsional restraint will become significant when the in-plane connection stiffness tends to zero.

Figure 4.5 shows a comparison of the experimentally observed column head rotation and beam twist rotation, measured adjacent to the connection, for test S8 in which web cleats were used. The same data is also presented in figure 4.6 for the web and seat cleat connections of test S7. It is evident from the plots that the magnitude of beam twist was approximately equal to the rotation of the column and suggests therefore that the connections possessed a high torsional stiffness capable of transferring the full torsional action between the beams and the column. As a result, all the subassemblages were modelled assuming that the connections had infinite torsional stiffness. This apparent high connection torsional stiffness, also observed by Celikag [4.11], has formed the basis of possible areas of further investigation proposed by the author (chapter 9).

#### 4.3.5 Beam to column connection position.

In the computer model, beam elements are assumed to be connected to the column at the point of intersection of the member centrelines. The effect of column depth can be simulated by introducing a stiff panel zone to offset the position of the connections. For a beam connected to the flange of the column, as shown in figure 4.7, it would appear that the connection offset would need to be half the depth of the column section. However, it is proposed by the author that for certain types of connection the offset to the effective centre of beam support is significantly larger.

In the connection shown in figure 4.8, a large proportion of the vertical end reaction from the beam is transferred to the column via the angle cleat on the lower flange of the beam. In the region of the connection, the high in-plane stiffness of the beam's web effectively acts as a stiff shear panel. As a result, shear forces in zone 'A' resulting

from an applied beam load will tend to be resisted by diagonal strut action within the web of the beam. The component of the diagonal strut force to the lower cleat will be resisted by a diagonal tension force to the cleat on the upper flange and, in instances where the beam supports are fixed in position, by an axial compression in the beam. As a result, a point load applied close to the connection will tend to be resisted solely by strut action without necessarily inducing beam flexure. It is evident therefore that in a simplified 'centreline simulation' of such a connection, in which the beam is supported directly at the column face, larger beam span moments would be predicted than those observed experimentally. For this reason, the author proposes that the 'effective point of beam support' for a centreline simplified model is situated on the centreline of the beam at a point corresponding with the limit of diagonal strut action.

The magnitude and inclination of the diagonal strut force, and hence the position of effective beam support, is influenced by the stiffness of the 'tension cleat' on the upper flange, and the restraint to longitudinal translation of the beam ends. This is illustrated in figure 4.9 where structure type '1', in which both supports provide rigid positional restraint, resists the applied load solely by strut action. However in structure '2', where the right hand support permits longitudinal displacement, the diagonal strut force is zero and the load is resisted by flexure of the cranked member spanning over the full distance between the supports. For types of end support intermediate between those for structures '1' and '2', it is expected that the load will be resisted partly by strut action and partly by flexure.

In terms of the experimental tests, the nature of the positional restraint at the ends of the beams was influenced by the rotation of the column head. For a connection which was 'opening' as a result of column head rotation there was a corresponding small horizontal shift of the cleat on the bottom flange, equivalent to the supports of the structure shown in figure 4.9 moving apart. This reduced the capacity for generating axial beam forces to resist the diagonal strut force and thus increased the tendency for applied loads to be resisted solely by beam flexure. Conversely, for a 'closing' connection in which a horizontal

shift of the cleat simulated the supports shown in figure 4.9 moving closer together, there was a tendency to enhance the development of 'strut action'.

A secondary effect is the possible shift in the centre of beam support reaction acting on the bottom flange cleat (figure 4.10) and hence the precise location of any diagonal strut force. In a 'closing connection', the centre of force acting will tend to move away from the root of the angle as a hogging moment is induced into the cleat. It is anticipated that the opposite effect will be observed for an 'opening connection'. It is appreciated however, that this secondary effect would only be apparent in a connection employing a stiff supporting cleat subjected to large rotations.

To summarise, it is proposed that the effective centre of beam support for a 'centreline simplified model' acts at a distance away from the face of a supporting member. The offset distance is expected to be larger for a connection which is 'closing' as opposed to 'opening' and can therefore vary during the course of a test. However, in the present version of the computer program it is not possible to accurately model this phenomenon. The author has therefore made some reasoned assumptions to derive a consistent effective connection 'offset' for different connection types and different beam locations.

Typically, for a connection with a direct bearing support to the lower flange of the beam, the effective centre was considered to act at a distance of half the beam depth (125mm) away from the face of the support. This effectively assumed a 45 degree inclination for any strut force which may develop. For a web cleat connection, where there is no direct bearing support to the flange and consequently a reduced tendency for strut action, a nominal offset of 50mm was assumed. As shown in table 4.1, these offsets were modified in the case of a predominantly 'opening' or 'closing' connection to take into account the effects described above. For example, beam 2 in tests S5, S6 and S7 was a 'non-paired' beam connected to the minor axis of the column. In this arrangement there was the potential for large column head rotations resulting in a predominantly 'opening' connection. The offset to the connection with beam 2 was therefore specifi-

cally chosen to be less than that of the same connection type to either beam 1 or beam 3.

#### **4.3.6 Column end conditions.**

All the subassemblage test specimens incorporated a base support arrangement which prevented both major and minor axis column rotations. The adopted base-plate detail prevented any twist rotation at the base and was of a sufficient thickness to resist warping deformations. Warping of the section was also resisted at the head where load was applied to the column through a 25mm thick cap-plate fully welded to the member. These column boundary conditions were incorporated into the finite element models of the tests.

It has been shown in previous studies of biaxially loaded columns [4.12] that the presence of warping restraint at the ends of a column, and the resulting increase in the torsional stiffness, can increase the ultimate capacity by as much as 10%. This is confirmed in the following sections which show that only relatively small amounts of mid-column twist rotation occurred prior to column failure.

### **4.4 Comparisons of experimental and analytical behaviour.**

Table 4.2 presents a summary of the comparisons between experimental and analytically predicted ultimate capacities. It is evident that with the exception of test S5, the maximum error between the actual and predicted ultimate capacities is 7% and in the case of eight of the tests, the maximum error reduces to 4%. The following sections present graphical comparisons of more detailed aspects of the subassemblage behaviour for each

of the 10 tests. Salient features of the one-to-one comparisons are highlighted and possible explanations are proposed for any discrepancies which have been observed.

#### **4.4.1 Subassemblage test S1.**

Figures 4.11 and 4.12 show the predicted and observed deformation at the centre of column S1, whilst figures 4.13 to 4.15 show comparisons of the column bending moments.

As reported in section 2.3.1, the sliding support bearings to beam 1 locked part way through the test. In addition, it would appear from the dramatic change in slope of major axis moment shown in figure 4.13 that there was a shift in the major axis eccentricity of the column head load during the second phase of the test. This was partly attributed to not maintaining the initial 'nip load' at the head of the column during the beam loading phase of the test - a situation which was rectified in subsequent tests. It was not possible to model exactly these changes in the experimental boundary conditions and as a result, there are small discrepancies between the observed and predicted subassemblage behaviour.

#### **4.4.2 Subassemblage test S2.**

Figures 4.16 and 4.17 show comparisons of the predicted and observed deformation at the centre of column S2, whilst figures 4.18 to 4.20 show comparisons of the column bending moments. Figure 4.21 compares the span and connection major axis bending moments for subassemblage beam number 3.

It is evident that in this instance, the analytical model closely simulated all aspects of experimental behaviour. Of particular interest was the ability to predict the shedding of major axis moment at the column top illustrated in figure 4.18. Also of interest was the moment shedding at the connection of beam 3 illustrated in figure 4.21. As expected, the reduction in connection moment as failure approached resulted in an equal increase in the beam span moment, thus maintaining the 'depth' of the free bending moment.

#### 4.4.3 Subassemblage test S3.

Figures 4.22 to 4.26 show comparisons of the main components of column deformation and bending moment for subassemblage test S3. Figure 4.27 compares the predicted and observed major axis span and connection bending moments for subassemblage beam number 1.

As with test S2, the analytical model appeared to closely simulate all aspects of the observed experimental behaviour. Unlike the 'opening' connection of beam 3 discussed above for test S2, the 'closing' connection of beam 1 for test S3 shows a negligible change in bending moment after the application of the column loads. This can be explained by considering figure 4.28 which shows that the stiffness of an initially 'closed' connection which then 'opens', as in the case of beam 3 test S2, is significantly larger than the stiffness of a connection which continues to 'close', as in the case of beam 1 tests S3. For a given column head rotation, an 'opening' connection on one side of the column can therefore be expected to show a greater reduction in applied moment than the increase in moment experienced by the 'closing' connection on the opposite side of the column.

#### 4.4.4 Subassemblage test S4.

Figures 4.29 to 4.33 show comparisons of the main components of column deformation and bending moment for subassemblage test S4. This was the only subassemblage in the test series which was constructed with just two beams, thus representing a 'corner' column. It is evident from the plots that the analytically predicted data shows a good correlation with that measured in the experiment.

It is interesting to note that despite the high stiffness of the flush-end plate connection it is evident from the plots that only a very small minor axis moment was transferred to the head of the column. This was due to the relatively high flexibility of the column and the limited rotational capacity at the end of the short, stiff beams.

#### 4.4.5 Subassemblage test S5.

Figures 4.34 to 4.38 show comparisons of the main components of column deformation and bending for subassemblage test S5. In this particular test there appears to be a discrepancy between the observed and predicted ultimate capacity of the column.

Test S5 used web cleat connections throughout and was the first of a series of three tests in which Beam 2 framed into the web of the column. A situation therefore existed in which the minor axis of the column was restrained at the head by a single web cleat connection - the least stiff minor axis column restraint condition considered in the series of experimental tests. In hindsight, this was an unsatisfactory test arrangement. The parametric study reported in section 2.2.2, which investigated the effect of rotational restraint at the column base, had shown that small variations in the rotational stiffness of relatively flexible restraints had a considerable effect on column behaviour.

This particular subassemblage test was therefore very sensitive to possible experimental error in the rotational restraint provided to the column head. It is suggested that due to the relatively small restraint from the connections, the inevitable restraint from the spherical loading seat at the column head could have become significant and thus enhanced the performance of the experimental specimen.

#### **4.4.6 Subassemblage test S6.**

Figures 4.39 to 4.43 show comparisons of the main components of column deformation and bending for subassemblage test S6.

This particular subassemblage specimen was deliberately arranged with only a very small initial minor axis deformation at the column centre. The aim was to assess the ability of the program to predict the behaviour of a restrained column with a bifurcation type failure mode. It is evident from the plots that the computer has given a very close prediction of the ultimate column capacity. However, the comparisons of deformation at the column centre indicate a discrepancy which was attributed to malfunction of a particular displacement transducer. This is highlighted by two curious 'spikes' in the experimental data plot of twist rotation shown in figure 4.40. It is evident that without these 'data spikes', notably the one at the origin, the predicted and observed twist rotations would be very similar.



#### 4.4.7 Subassemblage test S7.

Figures 4.44 to 4.48 show comparisons of the main components of column deformation and bending for subassemblage test S7.

Again, the computer program gives a very close prediction of the ultimate capacity of the column. However, it is clear from the plots that there is a marked difference in both moment and deformation characteristics at loading levels greater than 65% of the failure load. This is characterised by the rapid increase in the experimental twist rotation observed at the column centre at a total applied load of 325kN (figure 4.45). This phenomenon coincided with an unusual distribution of bending moments at the column centre. Figure 4.46 shows that at a corresponding level of load, the minor axis moment at the column centre increased rapidly, deviating from the usual smooth curve. In addition, the major axis moment at the column centre increased rapidly, deviating from the expected 'nearly linear' path, only to revert to an expected value as failure approached. The behaviour was also accompanied by an unexpected large decrease in the major axis moment at the column head (figure 4.47).

The fact that this behaviour was monitored in terms of both force and deformation suggested that, rather than being the result of an instrumentation malfunction, the column did experience a sudden loss of stiffness. As mentioned in reference 4.9, measurements of residual stress had indicated that the column sections had been excessively 'roller straightened'. It is possible therefore that at some point along the length of the column there was a high concentration of residual stress which caused a rapid spread of material yield across the section at an applied load of 325kN. This would have the effect of reducing the column stiffness and causing the 'kink' in the minor axis moment plot of figure 4.46.

#### **4.4.8 Subassemblage test S8.**

Figures 4.49 to 4.53 show comparisons of the main components of column deformation and bending for subassemblage test S8.

This particular test employed web cleat connections. It is reassuring to note that the problems discussed above for test S5, which also employed web cleats connections, are not apparent in test S8. Figures 4.51 to 4.53 show that a good correlation has been achieved between the observed and predicted bending moments in the column.

#### **4.4.9 Subassemblage test S9 and S10.**

Figures 4.54 to 4.59 show comparisons of the main components of column deformation and bending for subassemblage column S9. Figures 4.60 to 4.65 show comparisons of the same parameters as for test S10. In the experimental tests, the total applied beam load for these two particular subassemblages was specifically chosen to represent a larger proportion of the total column failure load. The intention was to investigate the ability of the computer program to predict the behaviour of restrained columns with larger disturbing moments.

The plots indicate that there is a slight discrepancy between the observed and predicted minor axis column behaviour in the case of test S9 and the major axis behaviour in the case of test S10. However, in each case the form, slope and characteristic features of the predicted behaviour curves closely matches the experimental curves with only a slight shortfall in the predicted ultimate load capacity. The comments raised in section 4.4.2 regarding the shedding of connection moments are also applicable to beam 1 of test S9, the 'closing' connection, shown in figure 4.59 and beam 3 of test S10, the 'opening' connection, shown in figure 4.65.

#### **4.4.10 Investigation of the sensitivity of the predicted behaviour.**

It is evident from the preceding section that a close correlation has been achieved between the experimental and the analytical behaviour. However, it was considered prudent to carry out a further study which investigated the effect of small variations in the magnitude of the 'input parameters' used in the analytical model. The accuracy of these input parameters, e.g. yield stress, initial deflection, section area and moment rotation response, were themselves subject to possible experimental measurement errors. The aim was to assess whether the subassemblage models were 'over-sensitive' to 'acceptable' deviations in the measured parameters.

The analytical model for subassemblage test S2 was used in the study - this particular model gave the closest correlation with the experimental behaviour (section 4.4.2). This particular model was denoted S2A and was used as the datum for the study. The other models considered were as follows:-

- **Model S2B** - The initial minor axis central deflection was reduced from 9.0mm to 8.5mm. (The resolution of the method of initial deformation measurement was considered to be 0.5mm).
- **Model S2C** -The yield stress and Young's modulus were increased by 5% to  $327\text{N/mm}^2$  and  $217000\text{ N/mm}^2$  respectively.
- **Model S2D** - The sectional area of the column was increased by 5% to  $28.97\text{cm}^2$ . This was effected by increasing the flange thickness in the model from 6.45mm to 6.77mm.
- **Model 2DE** - The moment, and hence the loading and unloading stiffness, of the multi-linear moment rotation response used in the model was increased by 10%

(see figure 4.66).

Table 4.3 shows the predicted ultimate capacities and the minor axis bending moments at a load of 400kN for each of the above models. The table also gives an indication of the performance of the models with respect to the 'datum model' S2A.

It can be seen from the table that, as expected, experimental errors in the measurement of the column section area and material yield stress have a comparable effect on the ultimate capacity (models S2C and S2D). However, these particular parameters can be measured to a reasonable degree of accuracy, typically better than 3%, by following well established experimental procedures [4.13]. It was anticipated that the variation in thickness of the column material could affect the measurement of small initial deflections by up to 8% whilst the anticipated error in the measurement, and subsequent multi-linear simplification, of the connection moment rotation response could be as high as 10%. However, it is pleasing to note that models S2B and S2E show that variations in these particular parameters had only a very small effect on the performance of the subassemblage.

It can be concluded therefore that the subassemblage models do not appear unduly sensitive to inevitable errors in the experimentally measured input parameters which were studied.

#### **4.5 Conclusions on the comparisons of observed and predicted behaviour.**

In the previous section, the graphical comparison of subassemblage parameters shows that, in most cases, there is a very close agreement between the experimental and analytical data. In instances where there are numerical discrepancies between the sets of data, it is reassuring to note that the form and characteristic shape of the data plots are

very similar.

The principal objective of the experimental study has been achieved by verifying that the computer program can indeed predict the behaviour of flexibly connected subassemblages. The degree of correlation which has been achieved justifies the initial time and effort which was expended in the development of the experimental set-up. This included the extensive parametric study used to determine the optimum subassemblage configuration (section 2.2); a means of inducing predefined single curvature initial deformations (section 2.3.3); the development of a device for measuring 3- dimensional deformation (section 3.2) and also the development of a technique which improved the ability of strain gauges to monitor elastic-plastic behaviour (section 3.3).

## References.

- 4.1 Jones, S.W., '*Semi-rigid connections and their influence on steel column behaviour*', Ph.D. Thesis, Department of Civil and Structural Engineering, University of Sheffield, U.K., 1980.
- 4.2 Rifai, A.M., '*Behaviour of column subassemblages with semi-rigid connections*', Ph.D. Thesis, Department of Civil and Structural Engineering, University of Sheffield, U.K., June 1987.
- 4.3 El-Khenfas, M.A., '*Analysis of biaxial bending and torsion of open section beam columns*', Ph.D. Thesis, Department of Civil and Structural Engineering, University of Sheffield, U.K., 1987.
- 4.4 Wang, Y.C., '*Ultimate strength analysis of three-dimensional structures with flexible restraints*', Department of Civil and Structural Engineering, University of Sheffield, U.K., 1988.
- 4.5 Wang, Y.C. and Nethercot, D.A., '*Ultimate strength analysis of three-dimensional column subassemblages with flexible connections*', Journ. Construct. Steel Research, Vol. 9, No. 4, 1988, pp. 235-264.

- 4.6 Gent, A.R. and Milner, H.R., '*Ultimate load capacity of elastically restrained H-columns under biaxial bending*', Proc. Inst. Civil Engrs., Vol 43, December 1968, pp. 1685-1704.
- 4.7 Wang, Y.C., '*Ultimate strength analysis of three-dimensional structures with flexible restraints - Computer program*', User manual, Department of Civil and Structural Engineering, University of Sheffield, U.K., 1989.
- 4.8 Chen, W.F and Atsuta, T., '*Theory of beam-columns*', Chapter 12, Vol. 2, McGraw-Hill International Book Company, 1980.
- 4.9 Gibbons, C., '*The strength of biaxially loaded beam-columns in flexibly connected steel frames - Volume 2: A survey of the mechanical and geometric properties of structural steel sections*', Ph.D. thesis, Department of Civil and Structural Engineering, University of Sheffield, Dec. 1990.
- 4.10 Lay, M.G. and Ward, R., '*Residual stresses in steel sections*', Aust. Inst. Steel Construct., Steel Construction, 3 (3), 1969, pp. 2-20.
- 4.11 Celikag, M., '*Moment-rotation behaviour of steel beam-to-column connections.*', Ph.D. Thesis, Department of Civil and Structural Engineering, University of Sheffield, U.K., February 1990.
- 4.12 Birnstiel, C., '*Experiments on H-columns under biaxial bending*', Journ. Struct. Div., Am. Soc. Civil Engrs., Vol. 94, No. ST10, Oct. 1968, pp. 2424-2449.
- 4.13 '*Guide to stability design criteria for metal structures*', 4th Edition, Ed. T.V. Galambos, '*Technical Memorandum No.2: Notes on the compression testing of metals*', Wiley-Interscience, 1988, pp. 703-717.

Subframe Test	Beam to column connection type.	Connection offset (mm)		
		Beam 1	Beam 2	Beam 3
S1	Web Cleats	50.0	50.0	50.0
S2	Flange Cleats	125.0	125.0	125.0
S3	Web and Seat Cleats	125.0	125.0	125.0
S4	Flush End Plate	-	125.0	50.0
S5	Web Cleats	50.0	50.0	0.0
S6	Flange Cleats	125.0	50.0	125.0
S7	Web and Seat Cleats	125.0	50.0	100.0
S8	Web Cleats	50.0	25.0	50.0
S9	Flange Cleats	125.0	125.0	125.0
S10	Web and Seat Cleats (Beams 1 and 3) Flush End Plate (Beam 2)	125.0	125.0	125.0

Table 4.1: Offsets from the column face to the effective centre of beam support assumed for each model of the subassemblage tests.

Subframe Test	Ultimate column capacity (kN)		
	Pu(exp) (kN)	Pu(an1) (kN)	Pu(exp) Pu(an1)
S1	468.1	439.2	1.07
S2	503.0	510.1	0.99
S3	542.6	548.1	0.99
S4	494.7	473.0	1.04
S5	479.0	412.1	1.16
S6	614.0	614.3	1.00
S7	490.0	495.1	0.99
S8	482.2	490.2	0.98
S9	526.0	506.2	1.04
S10	520.1	514.9	1.01

Table 4.2: Comparison of the experimentally observed and analytically predicted ultimate column capacities.

Subframe Test	Minor axis moment at the column centre - P = 400kN		Ultimate column capacity	
	Myy (kNm)	Myy Myy(S2A)	Pu (kN)	$\frac{Pu}{Pu(S2A)}$
S2A	3.51	1.000	510.1	1.000
S2B	3.35	0.954	513.3	1.006
S2C	3.36	0.957	534.4	1.047
S2D	3.37	0.960	530.9	1.041
S2E	3.41	0.972	514.3	1.008

Table 4.3: Analytically predicted ultimate capacities and minor axis moments for supplementary models S2A to S2E.



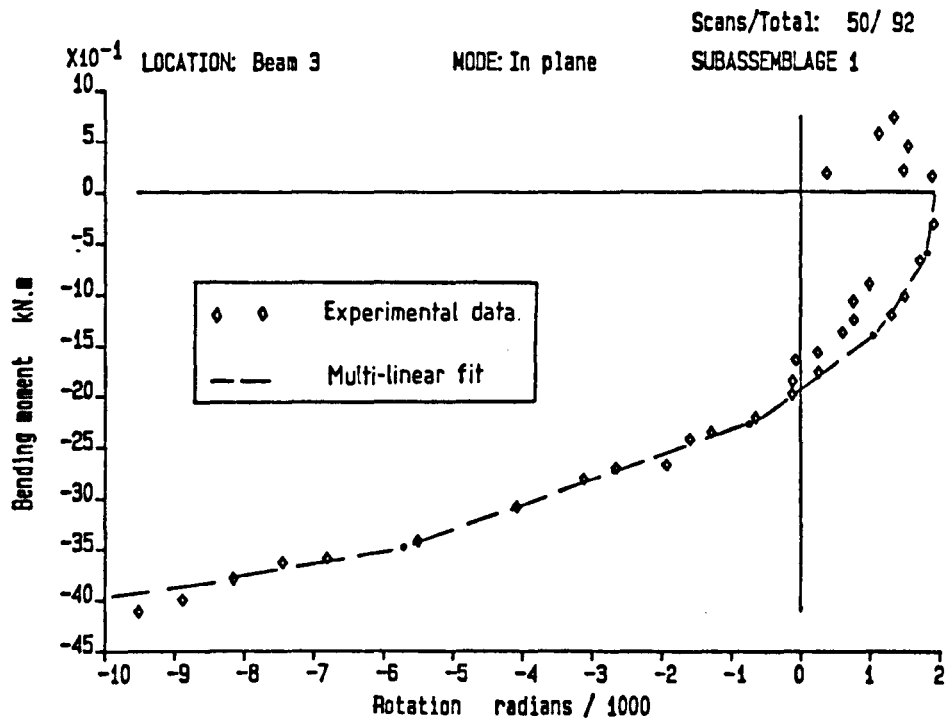


Figure 4.1: Multi-linear approximation to the  $M - \phi$  response of a web cleat connected to the minor column axis.

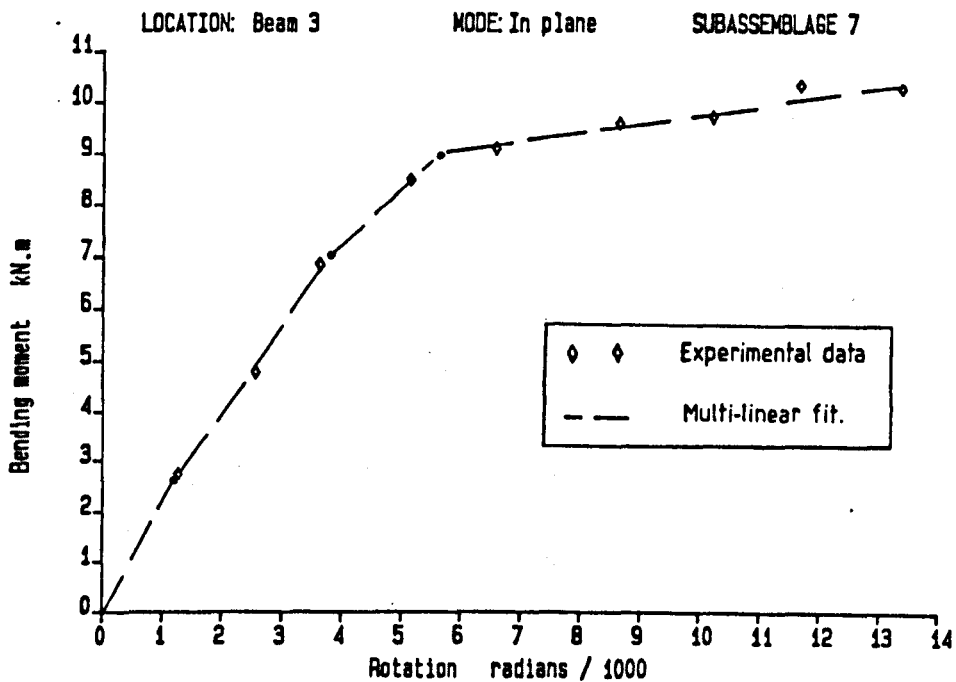


Figure 4.2: Multi-linear approximation to the  $M - \phi$  response of a web and seat cleat connected to the major column axis.

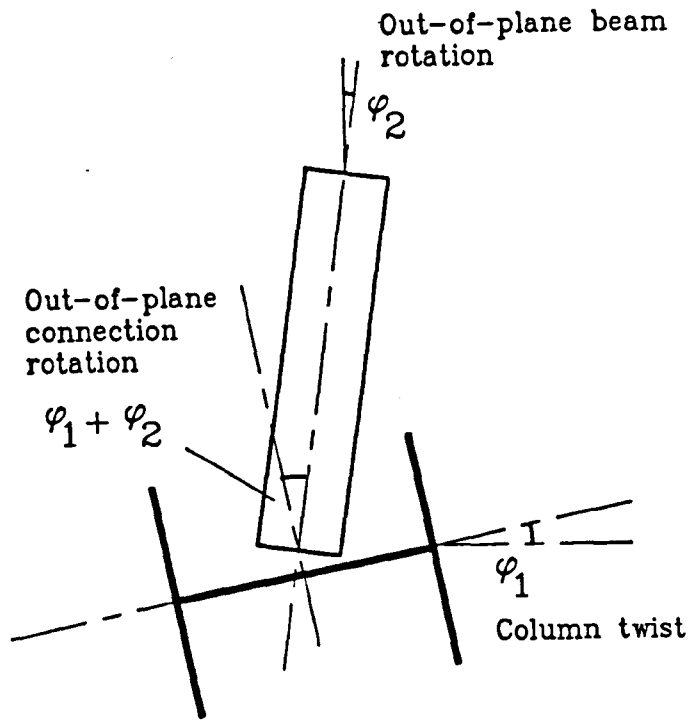


Figure 4.3: Components of out-of-plane connection rotation.

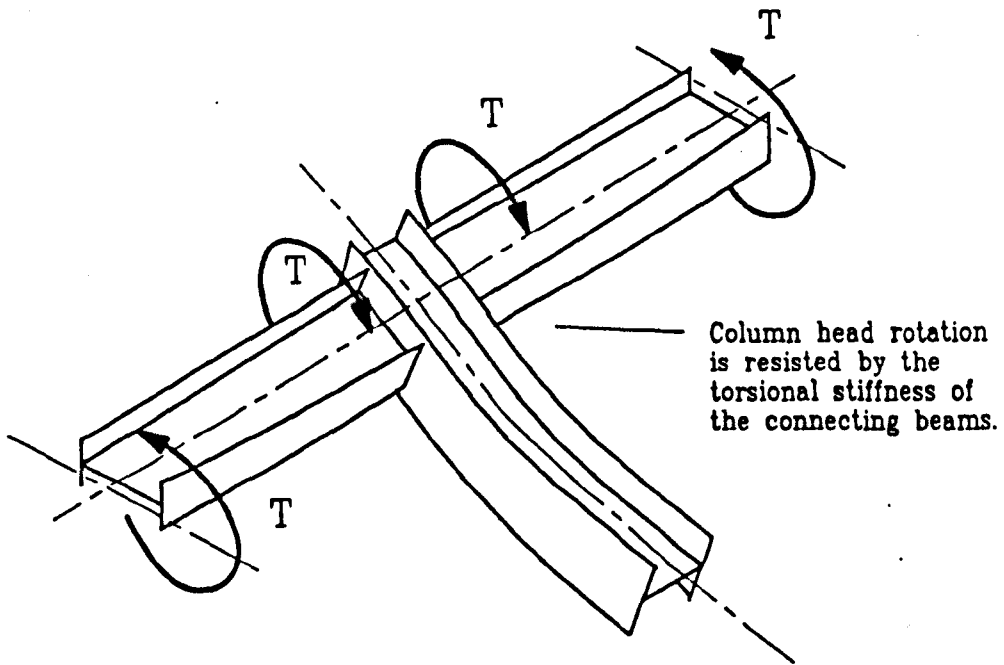


Figure 4.4: The effect of beam torsional stiffness on column head restraint.

Comparison of beam twist and column rotn. Test No : S8

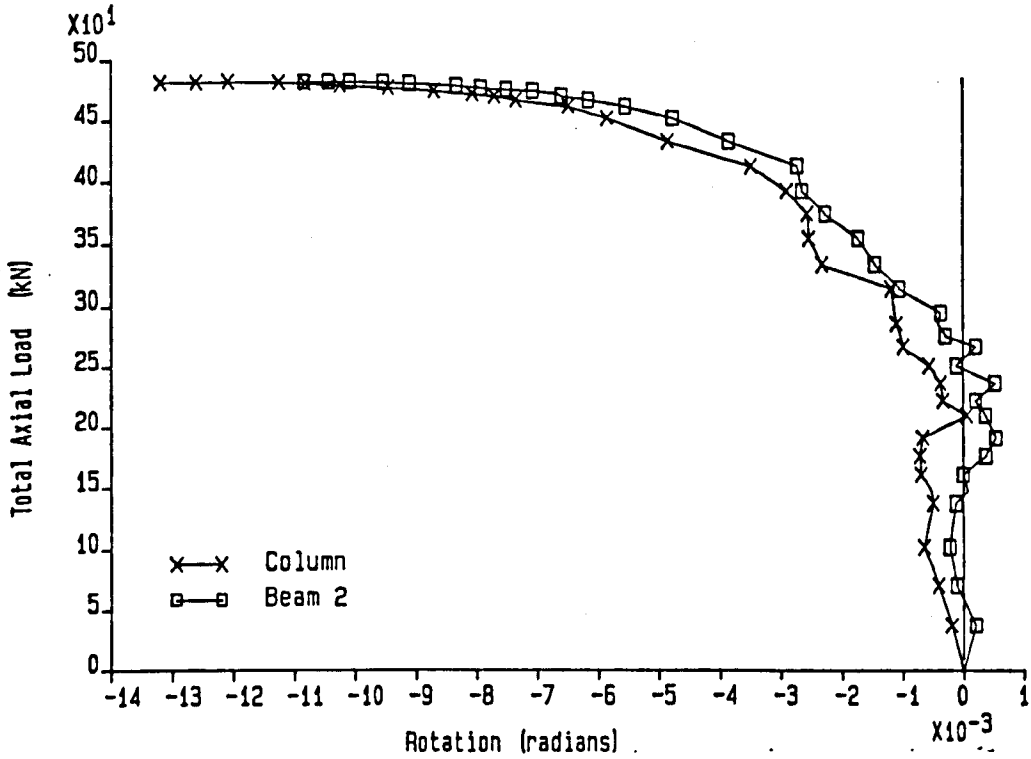


Figure 4.5: Comparison of the experimentally observed column head minor axis rotation and beam twist for a web cleat connection.

Comparison of beam twist and column rot Test No : S7

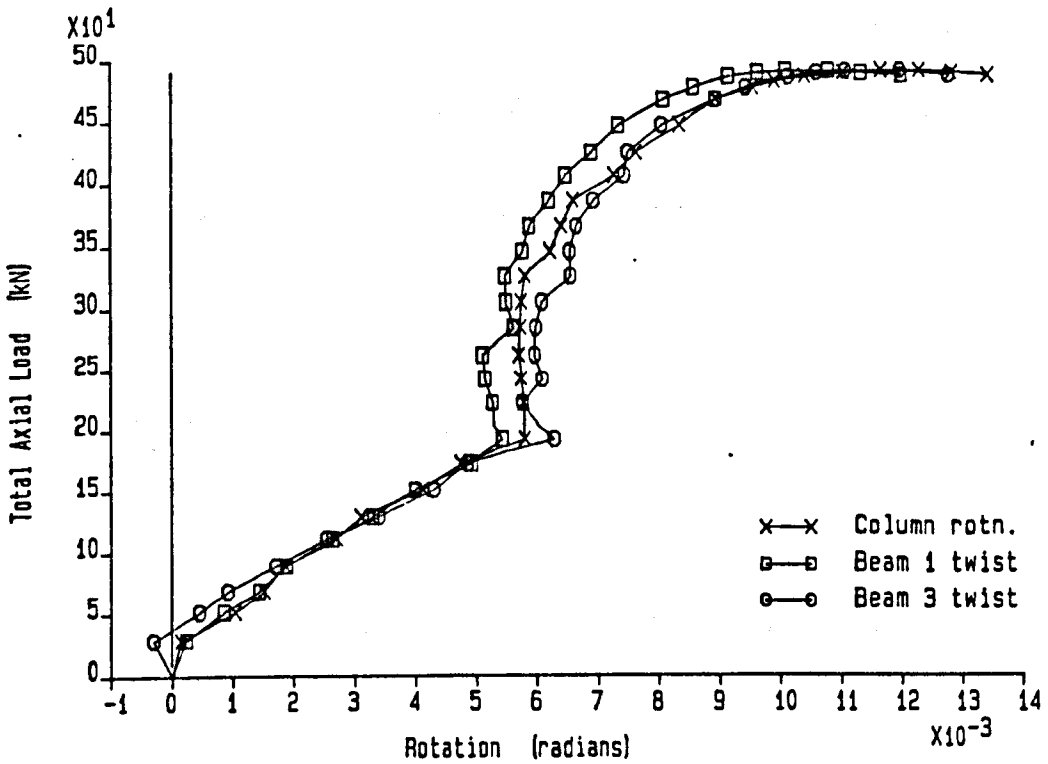
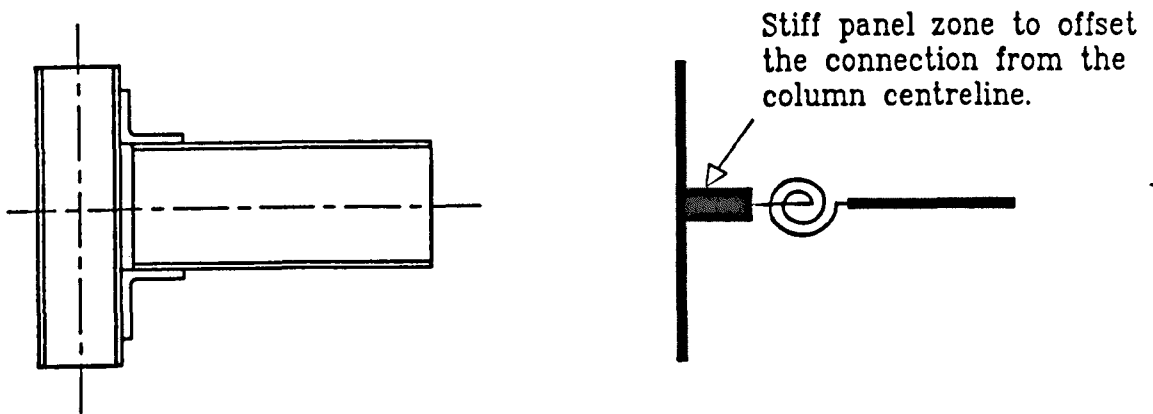


Figure 4.6: Comparison of the experimentally observed column head minor axis rotation and beam twist for a web and seat cleat connection.



Typical beam to column connection

Analytical model of the connection.

Figure 4.7: Offset required in the analytical model to simulate column depth.

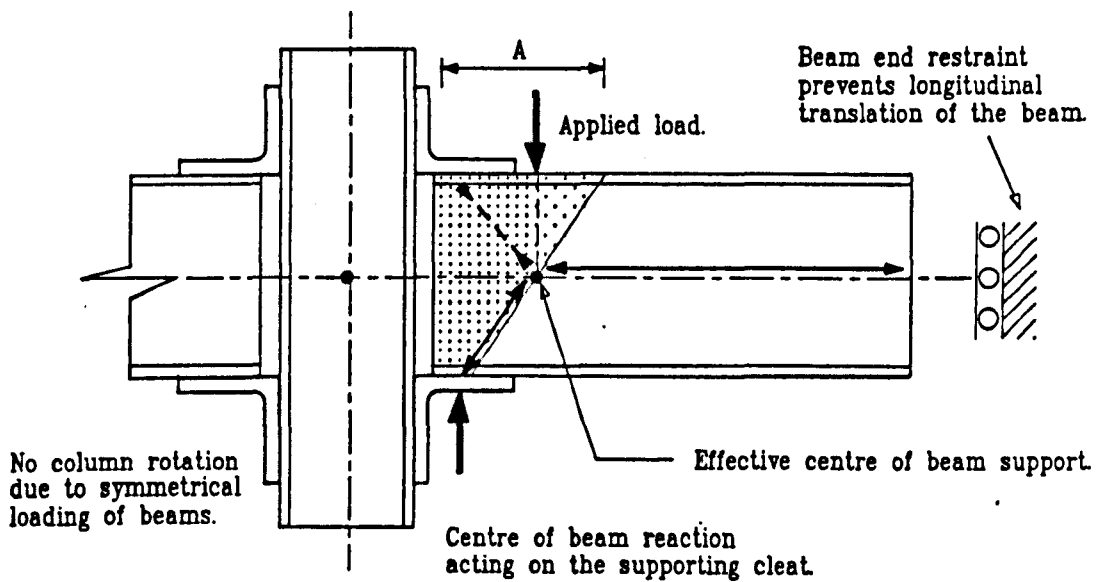
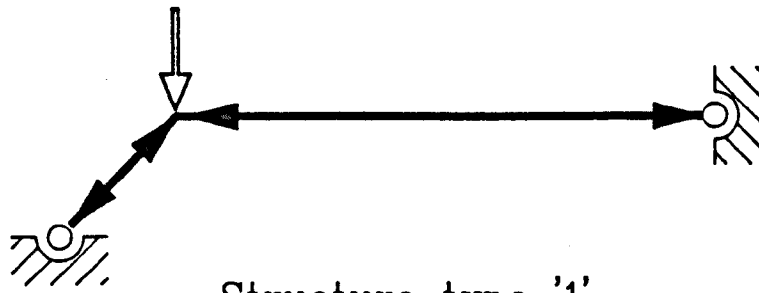
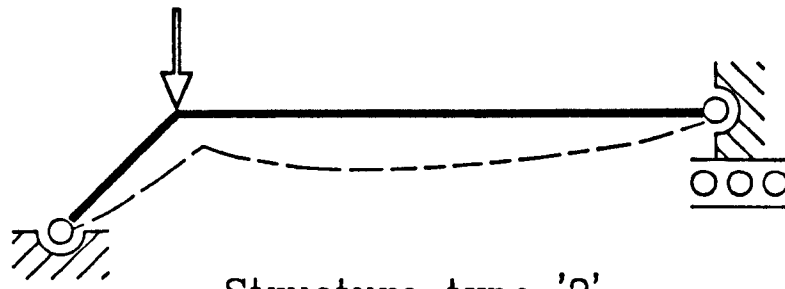


Figure 4.8: Typical connection showing the effect of 'strut action'.

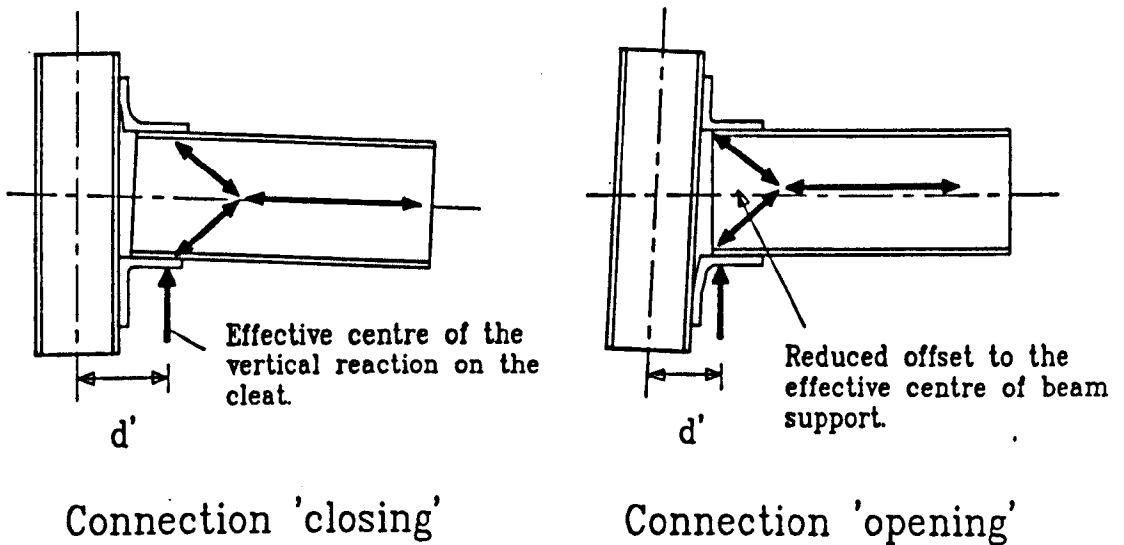


Structure type '1'



Structure type '2'

Figure 4.9: Two similar structures illustrating the effect of permitting support displacement.



Connection 'closing'

Connection 'opening'

Figure 4.10: Possible shift in the effective centre of beam support for an 'opening' and a 'closing' connection.

Deflections at the column centre.

Test No : S1

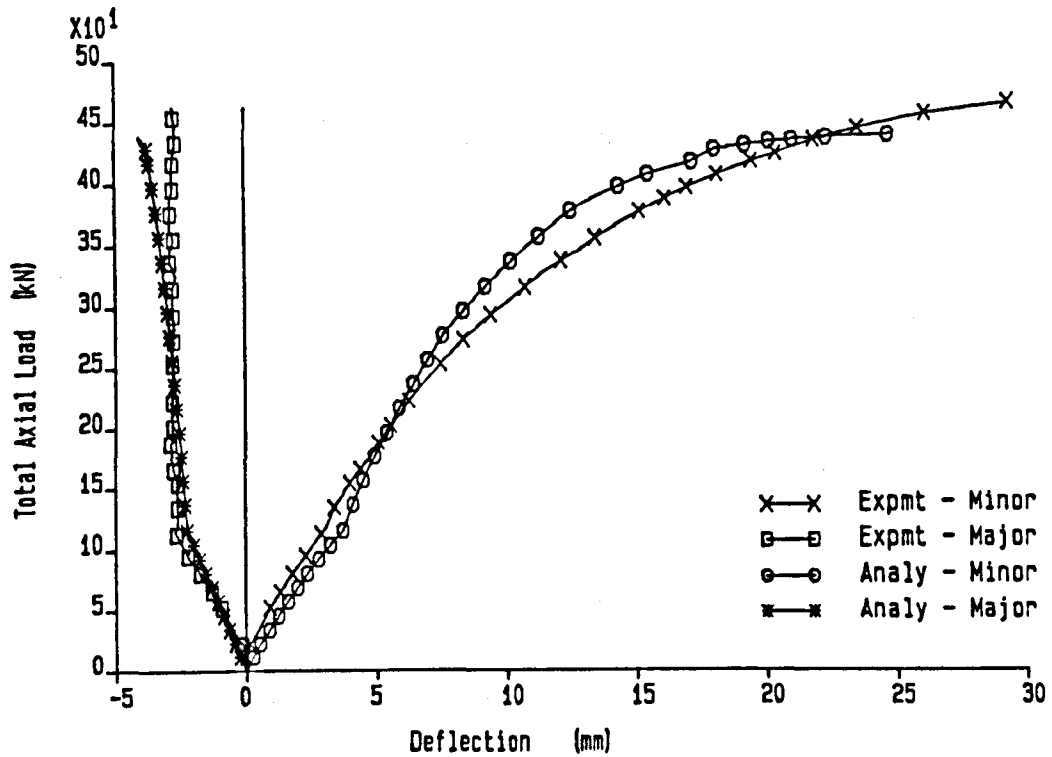


Figure 4.11: Experimental and analytical mid-column deflections, S1.

Twist rotations at the column centre.

Test No : S1

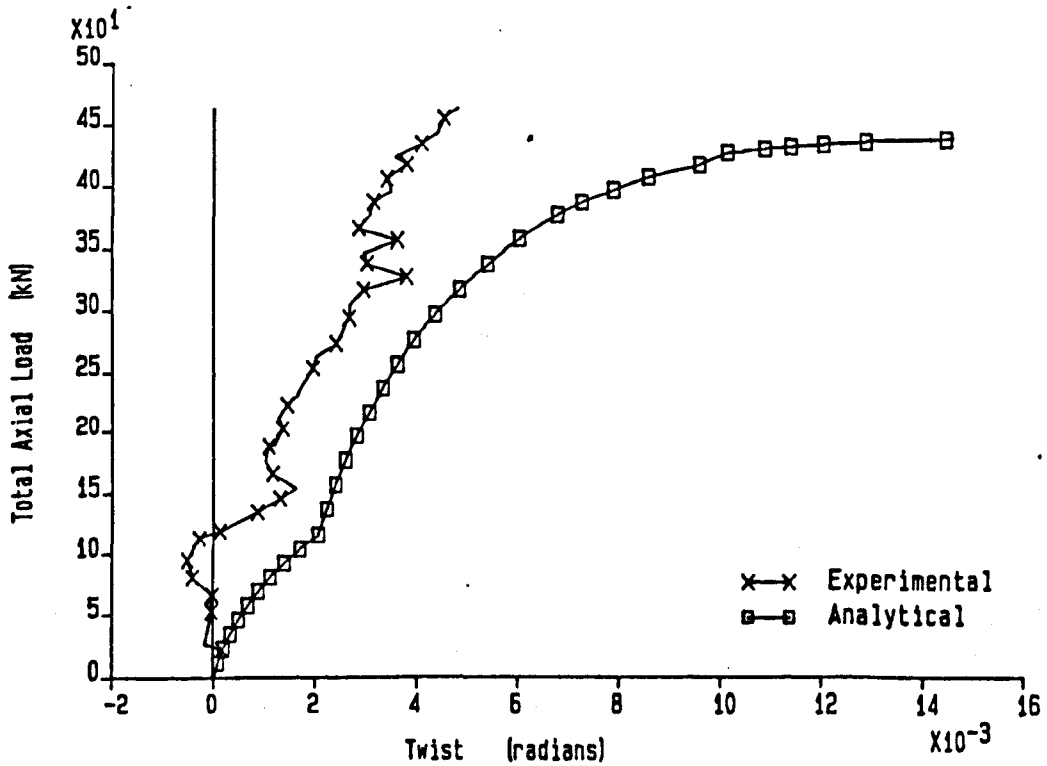


Figure 4.12: Experimental and analytical mid-column twist rotations, S1.

Bending moments at the column top.

Test No : S1

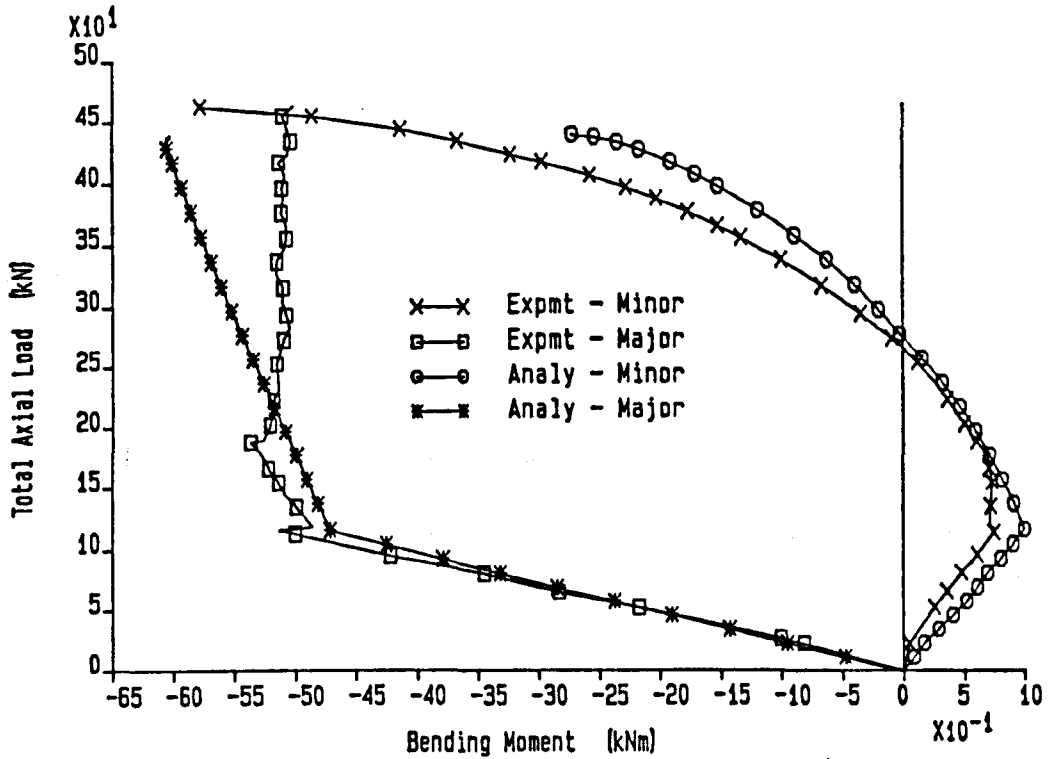


Figure 4.13: Experimental and analytical bending moments at the column head, S1.

Bending moments at the column centre.

Test No : S1

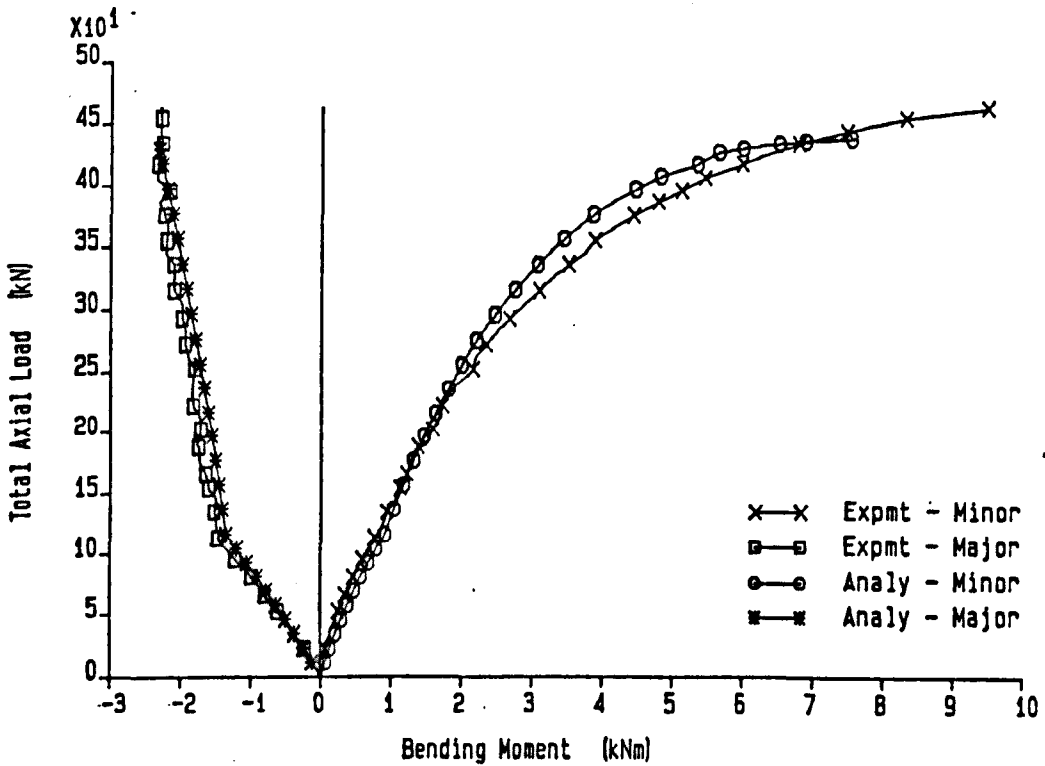


Figure 4.14: Experimental and analytical bending moments at the column centre, S1.

Bending moments at the column base. Test No : S1

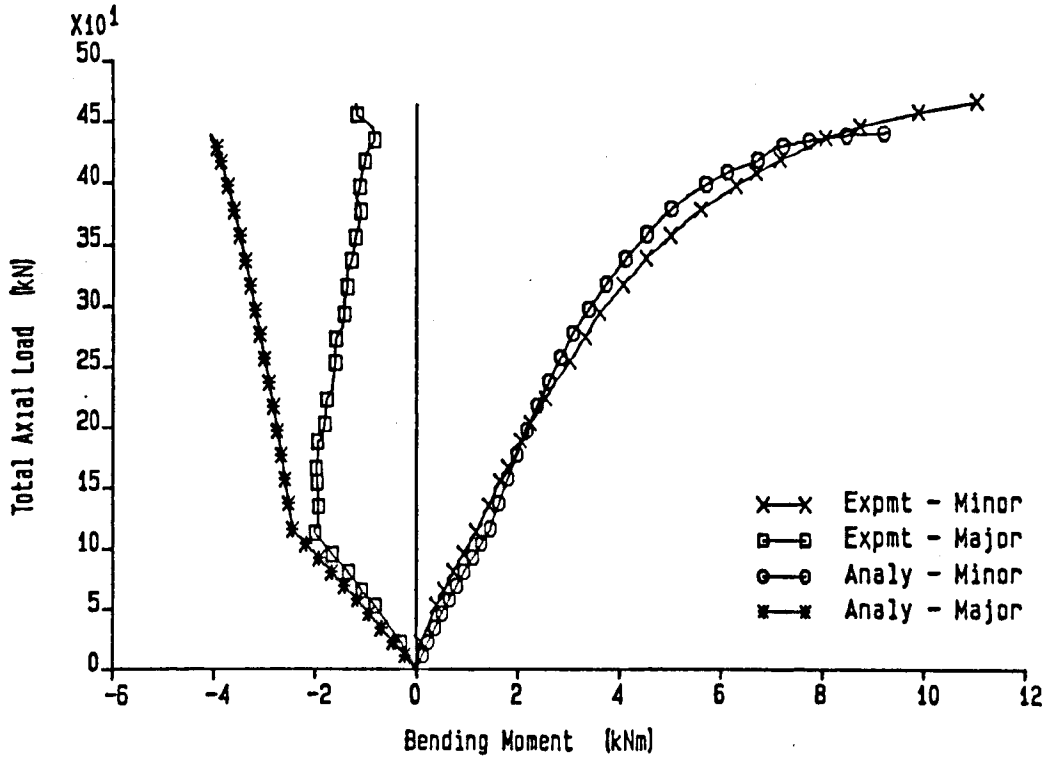


Figure 4.15: Experimental and analytical bending moments at the column base, S1.



Deflections at the column centre.

Test No : S2

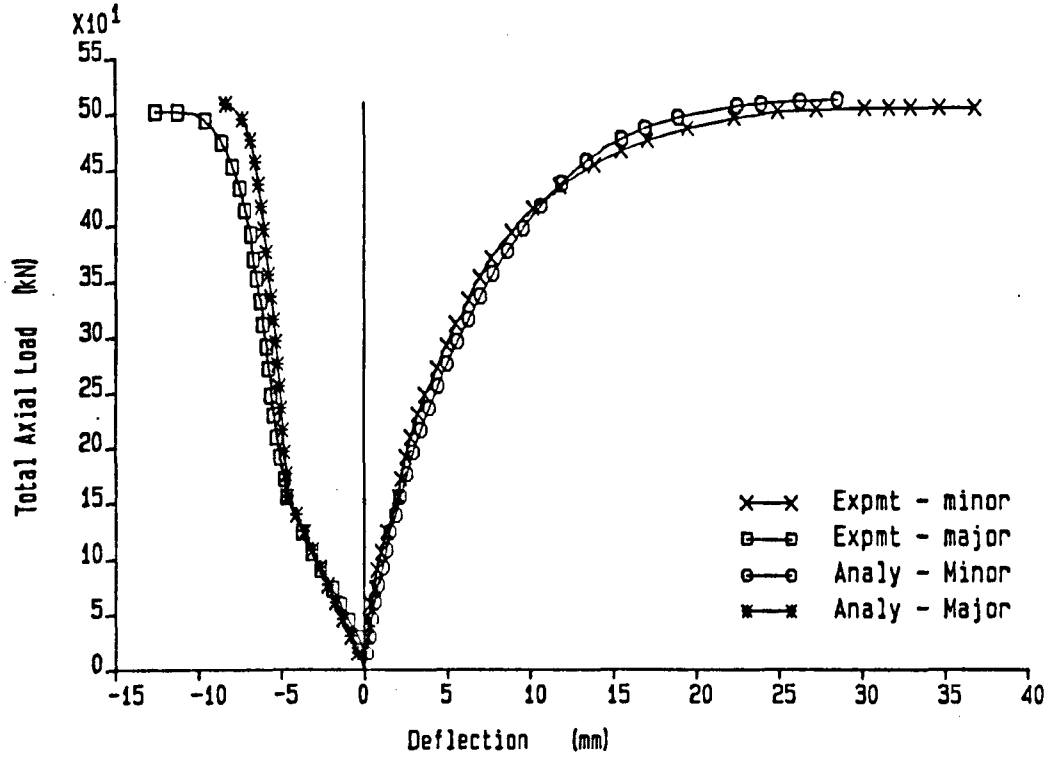


Figure 4.16: Experimental and analytical mid-column deflections, S2.

Twist rotations at the column centre.

Test No : S2

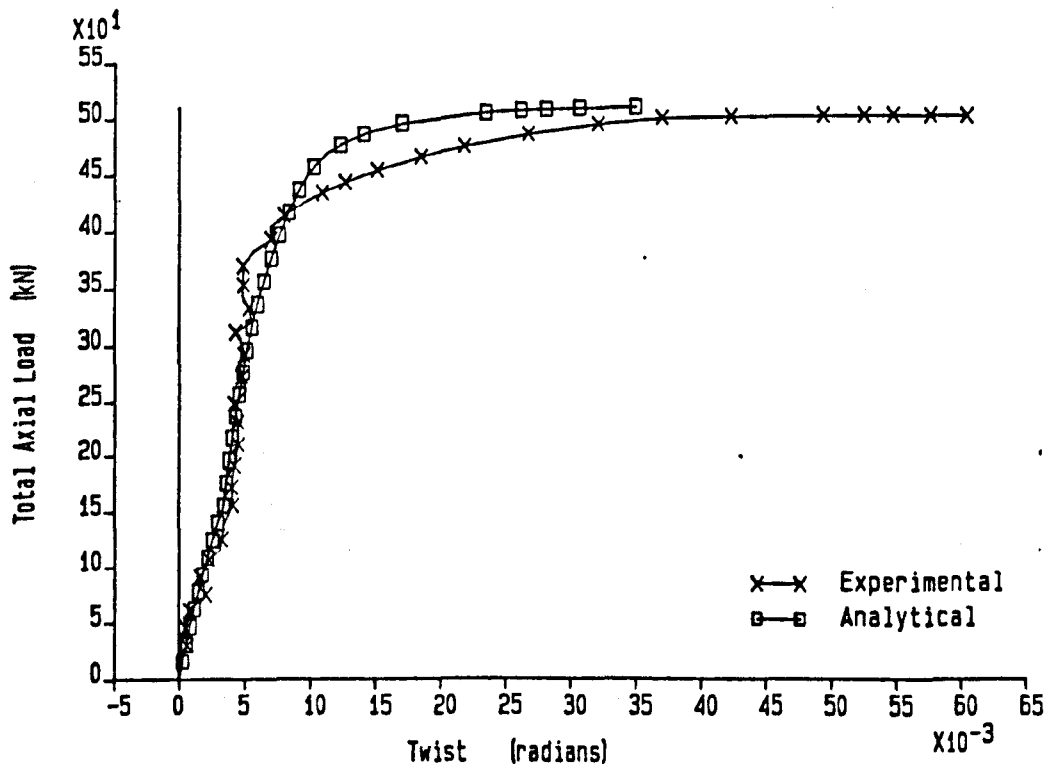
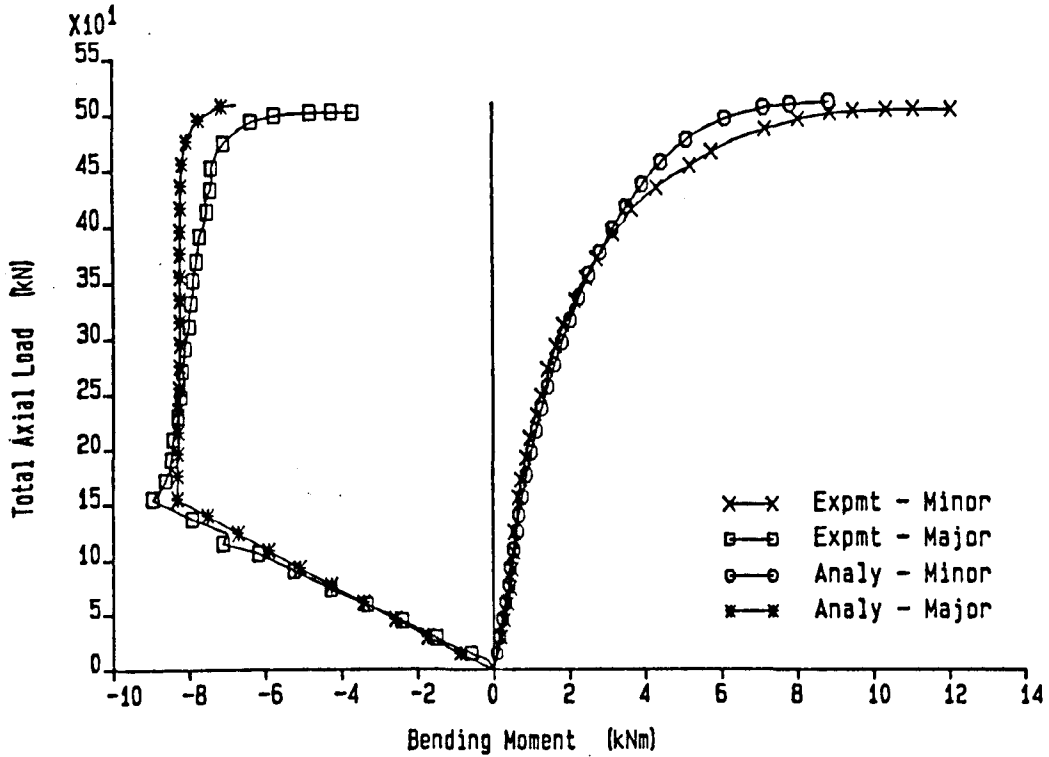


Figure 4.17: Experimental and analytical mid-column twist rotations, S2.

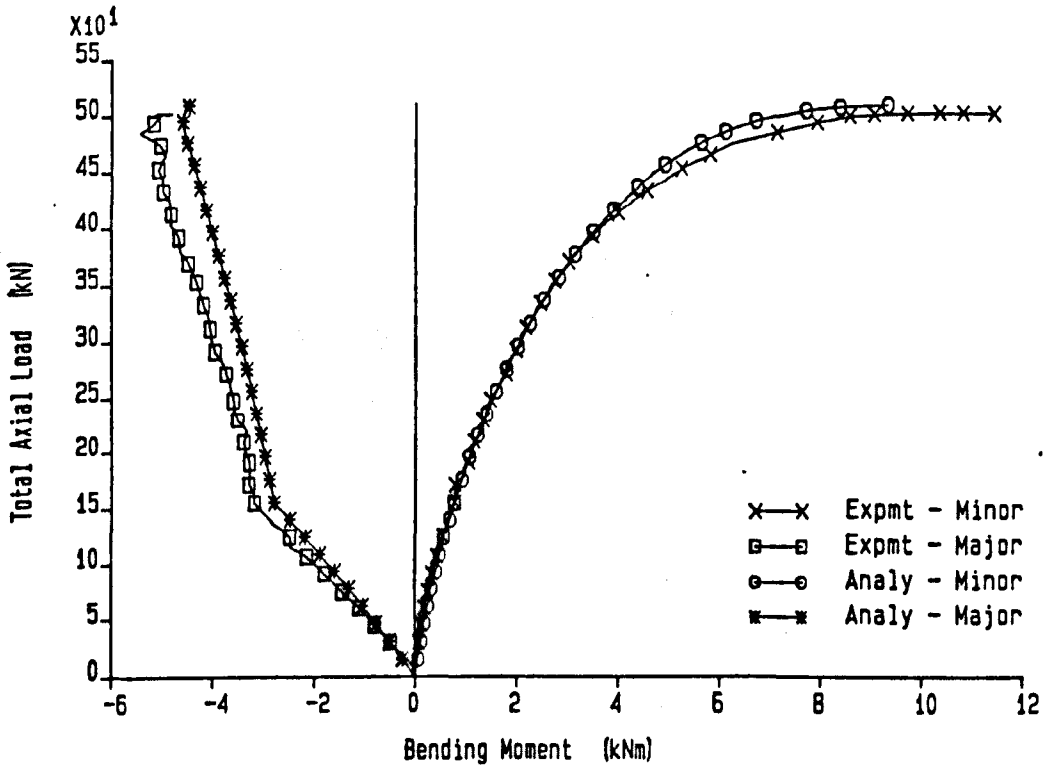
Bending moments at the column top.

Test No : S2



Bending moments at the column centre.

Test No : S2



Bending moments at the column base.

Test No : S2

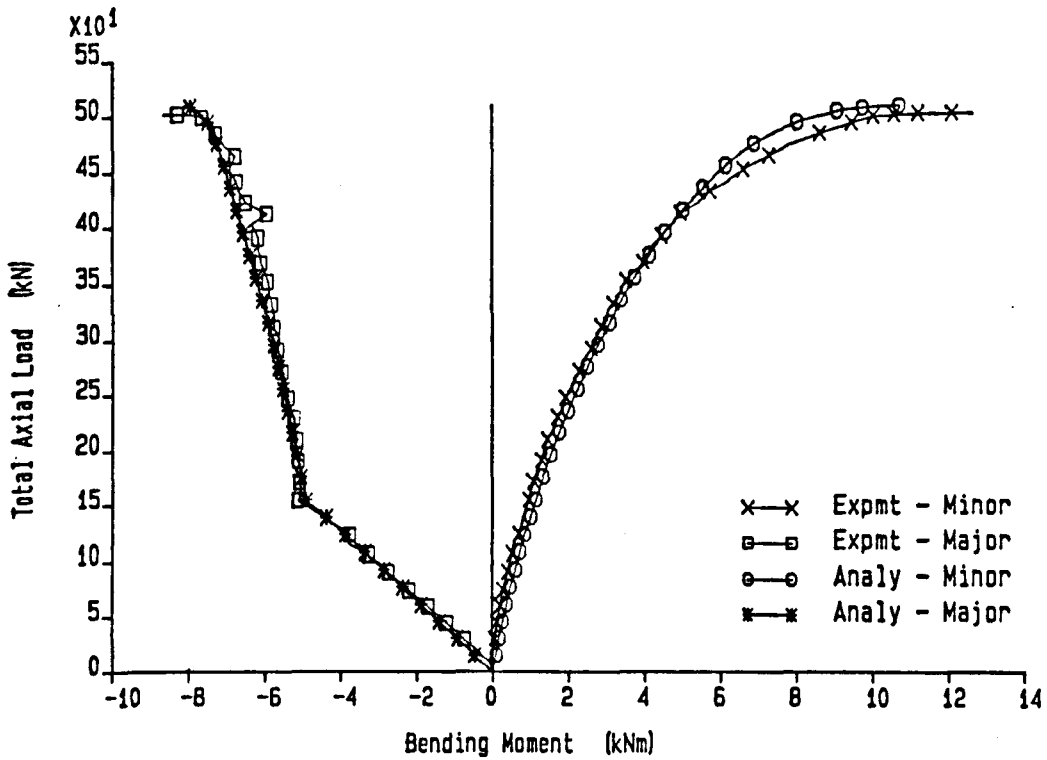


Figure 4.20: Experimental and analytical bending moments at the column base, S2.

Major axis bending moments - Beam 3

Test No : S2

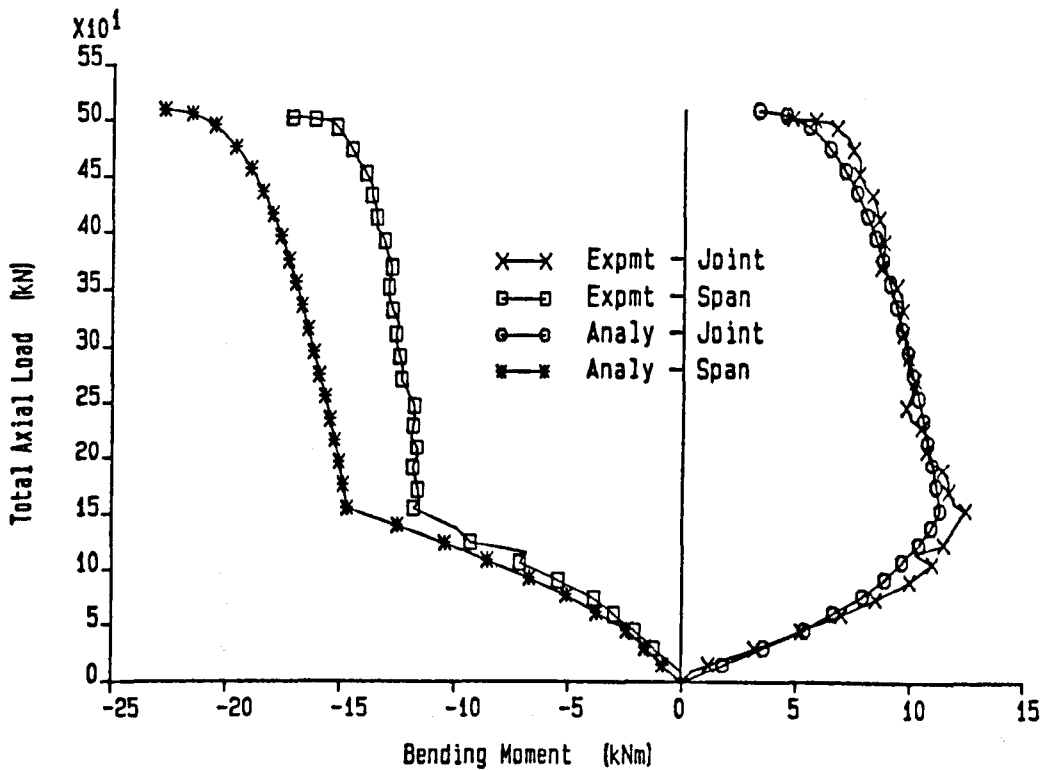


Figure 4.21: Experimental and analytical major axis moments for beam 3, S2.

Deflections at the column centre.

Test No : S3

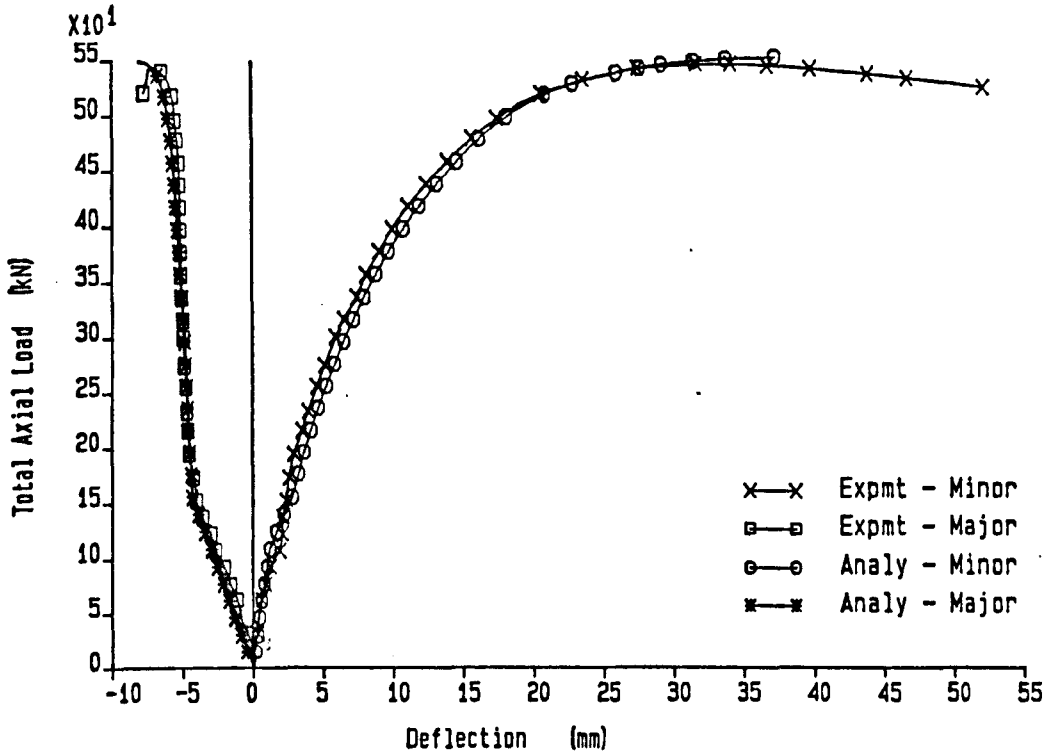


Figure 4.22: Experimental and analytical mid-column deflections, S3.

Twist rotations at the column centre.

Test No : S3

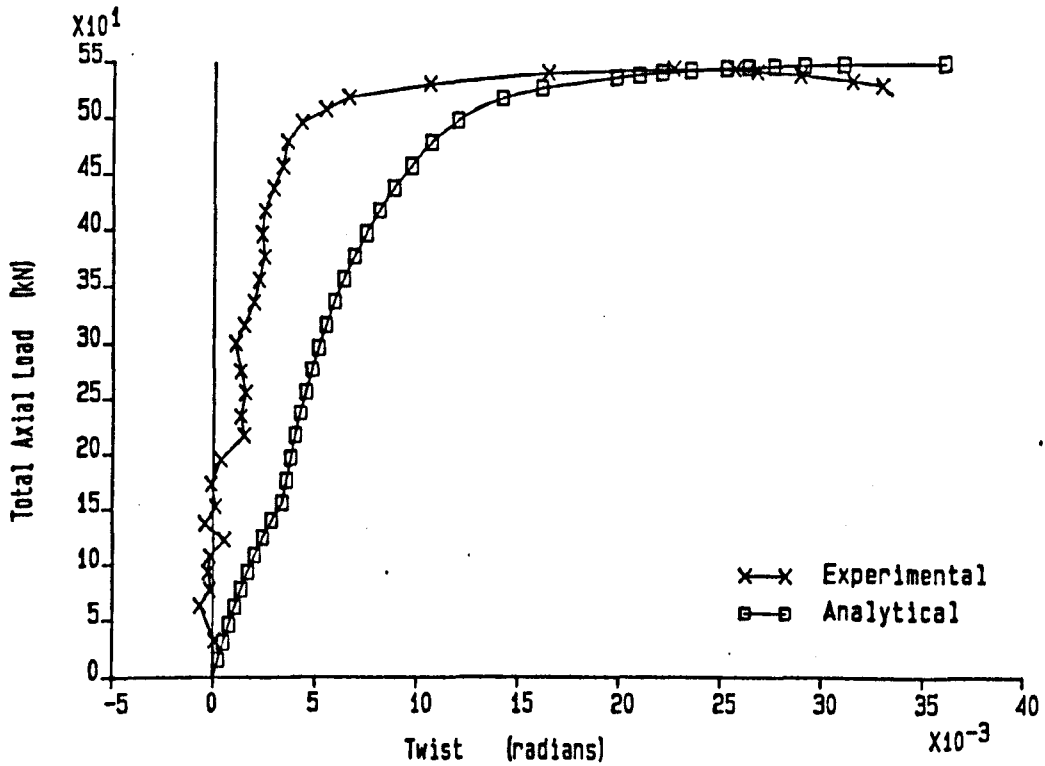


Figure 4.23: Experimental and analytical mid-column twist rotations, S3.

Bending moments at the column top.

Test No : S3

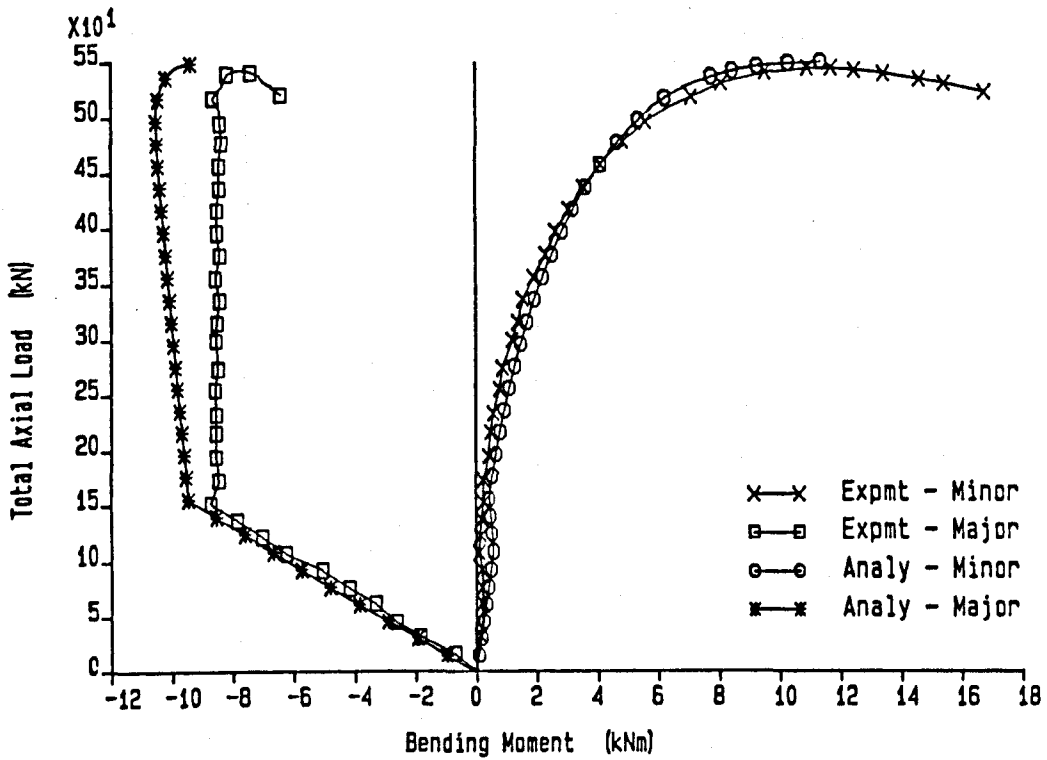


Figure 4.24: Experimental and analytical bending moments at the column head, S3.

Bending moments at the column centre.

Test No : S3

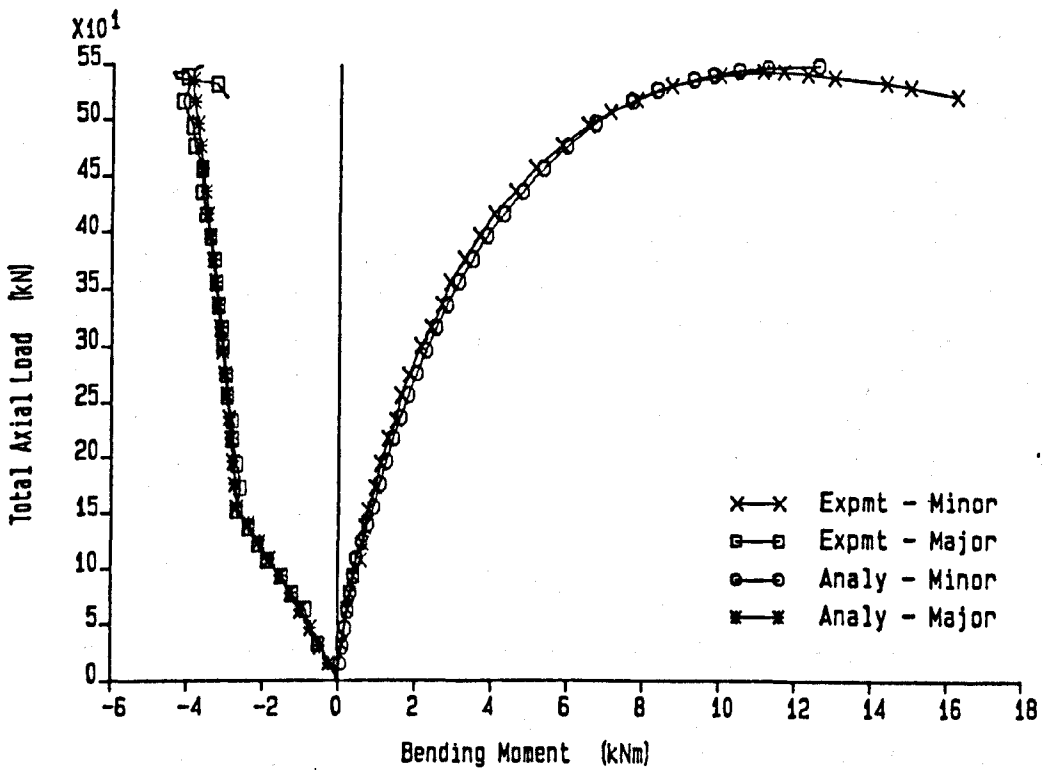


Figure 4.25: Experimental and analytical bending moments at the column centre, S3.

Bending moments at the column base.

Test No : S3

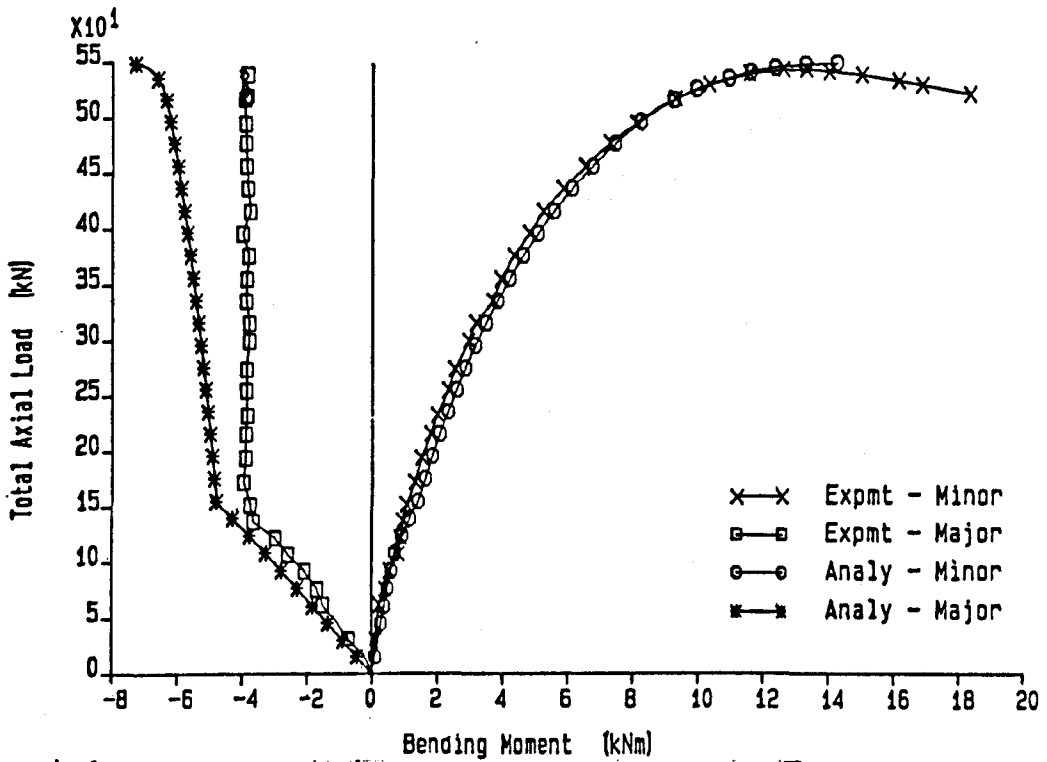


Figure 4.26: Experimental and analytical bending moments at the column base, S3.

Major axis bending moments - Beam 1

Test No : S3

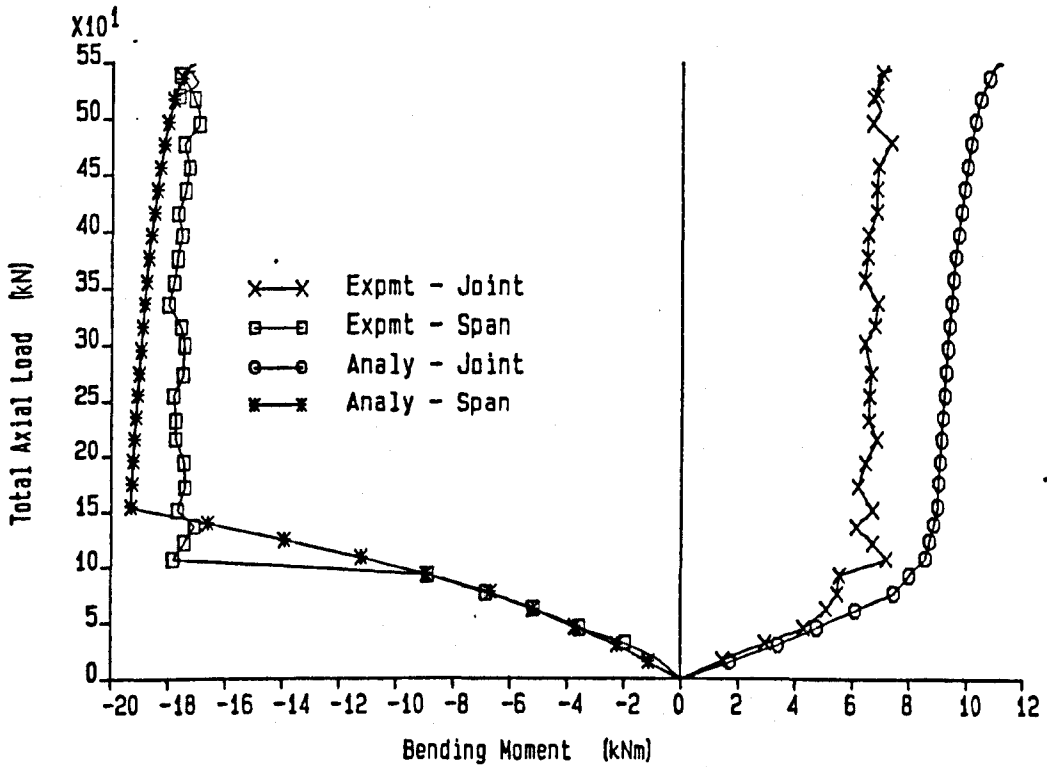


Figure 4.27: Experimental and analytical major axis moments for beam 1, S3.

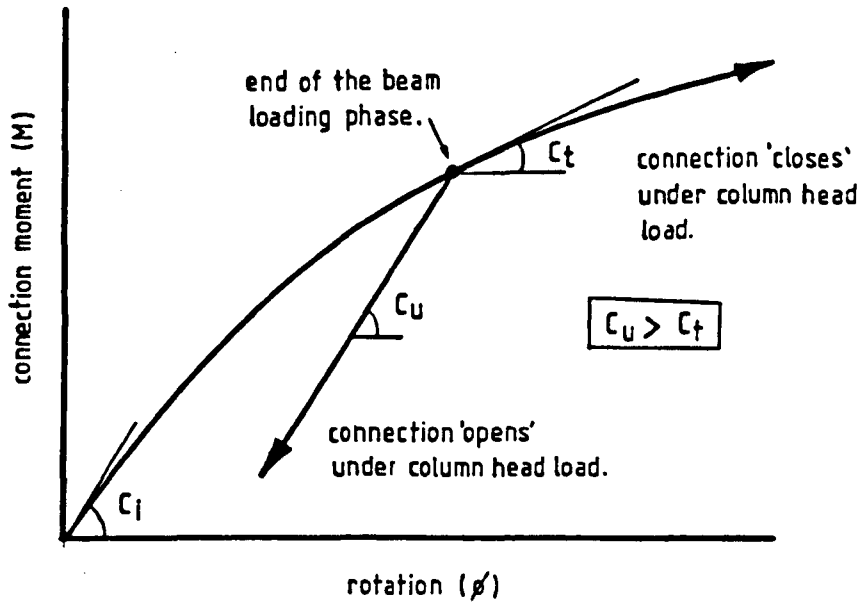


Figure 4.28: Typically  $M - \phi$  response for a 'closing - closing' connection and a 'closing - opening' connection.

Deflections at the column centre.

Test No : S4

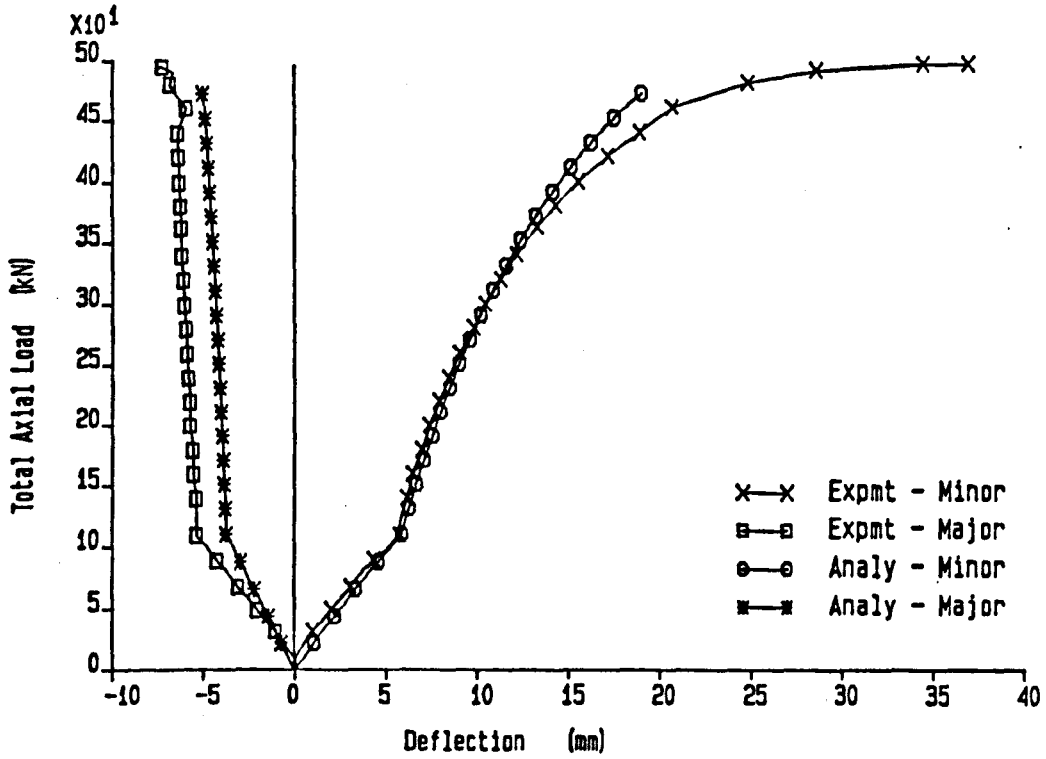


Figure 4.29: Experimental and analytical mid-column deflections, S4.

Twist rotations at the column centre.

Test No : S4

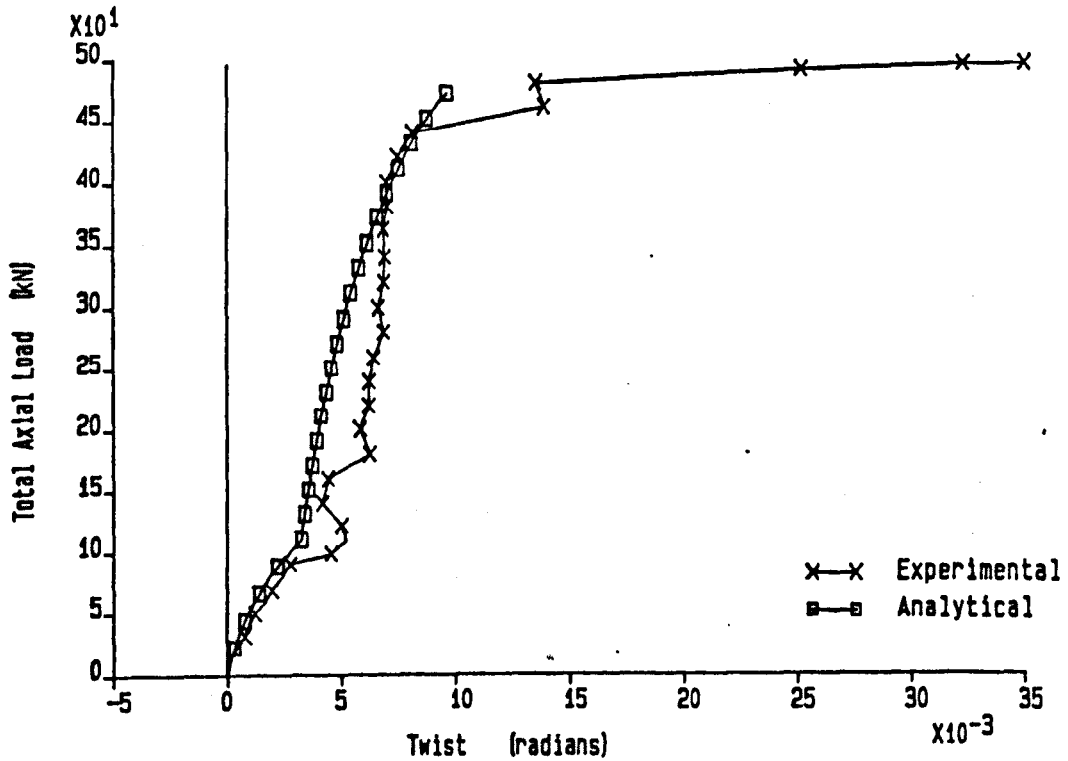


Figure 4.30: Experimental and analytical mid-column twist rotations, S4.



Bending moments at the column top.

Test No : S4

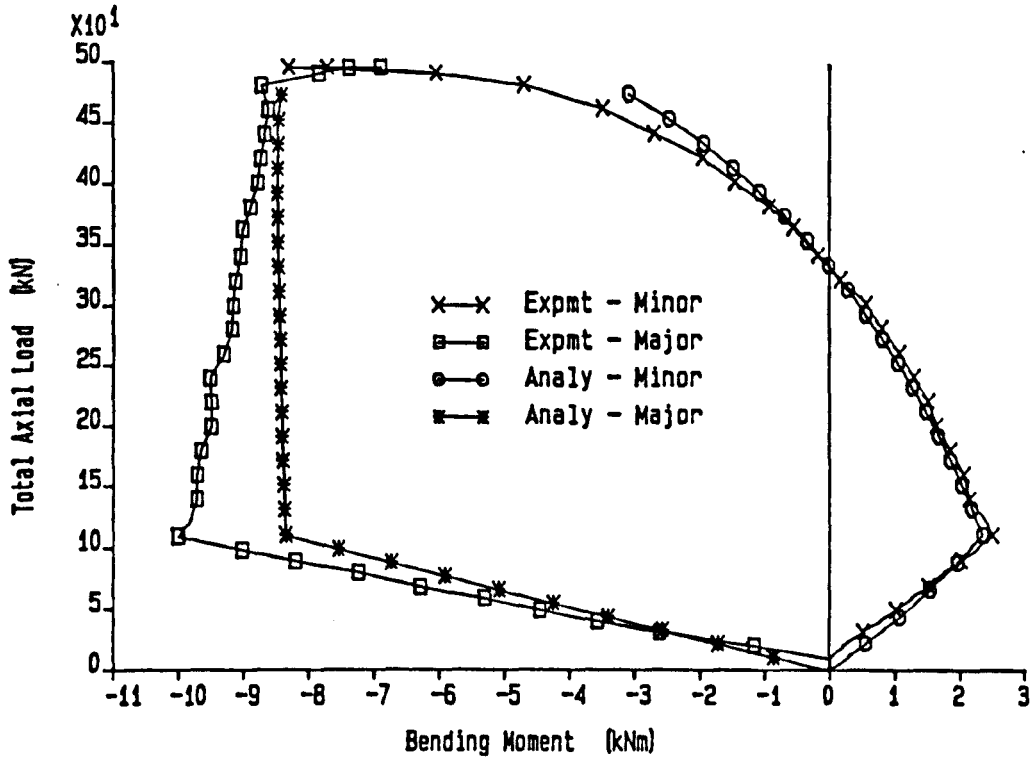


Figure 4.31: Experimental and analytical bending moments at the column head, S4.

Bending moments at the column centre.

Test No : S4

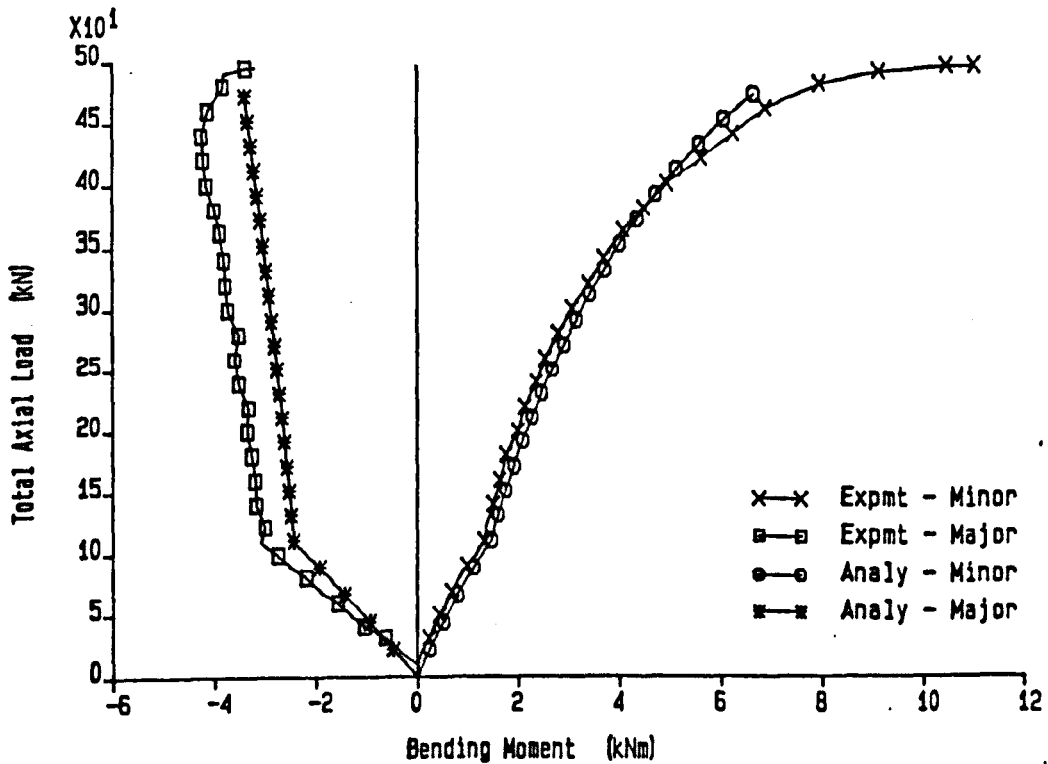


Figure 4.32: Experimental and analytical bending moments at the column centre, S4.

Bending moments at the column base.

Test No : S4

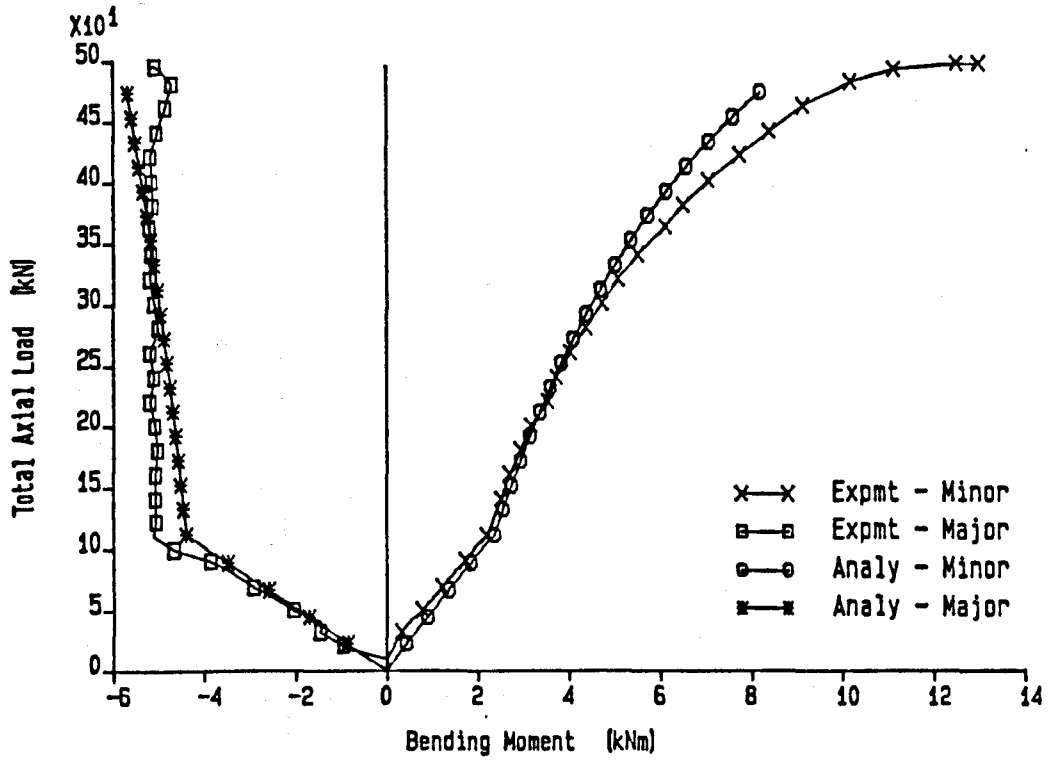


Figure 4.33: Experimental and analytical bending moments at the column base, S4.

Deflections at the column centre.

Test No : S5

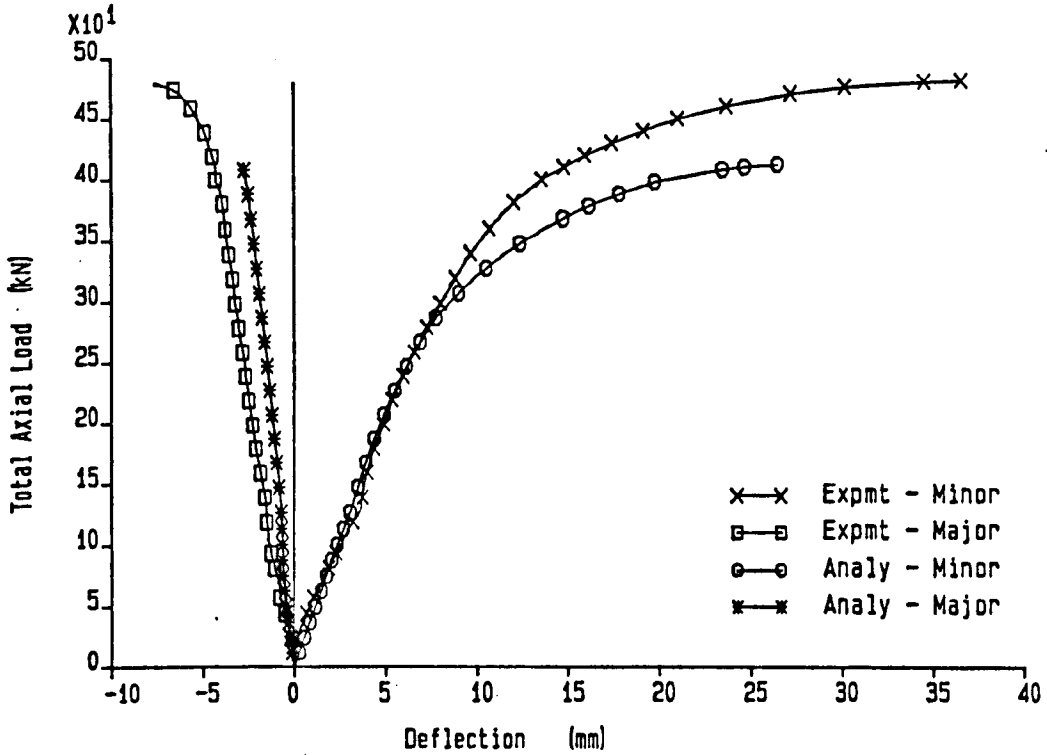


Figure 4.34: Experimental and analytical mid-column deflections, S5.

Twist rotations at the column centre.

Test No : S5

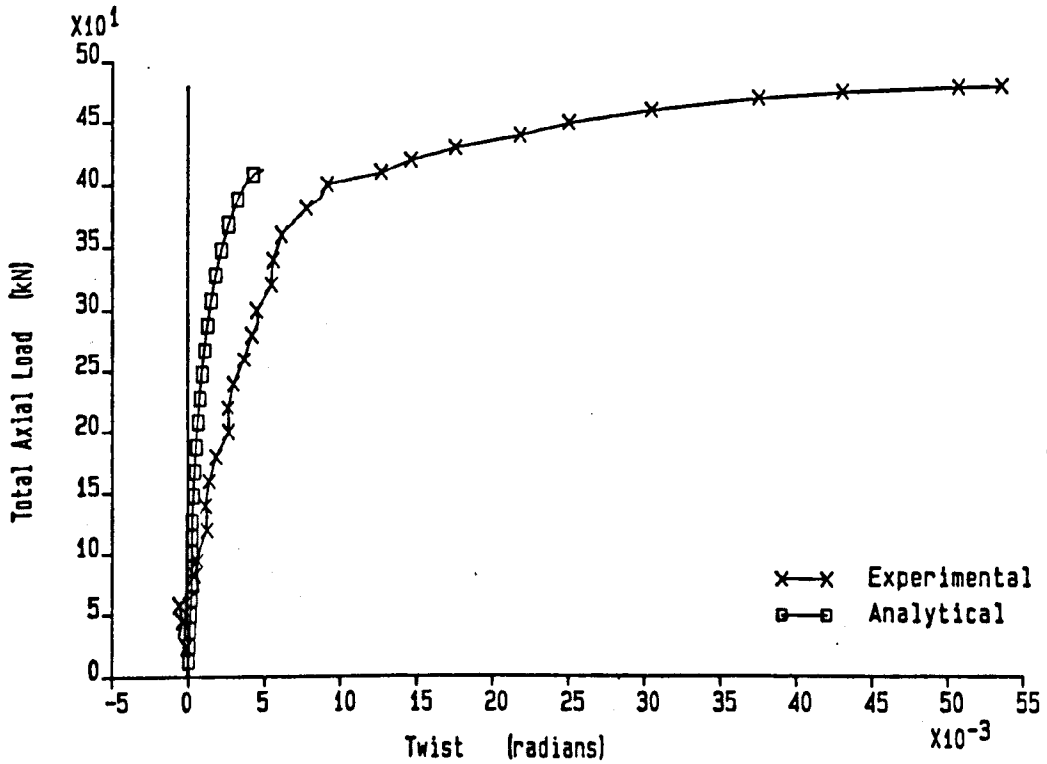


Figure 4.35: Experimental and analytical mid-column twist rotations, S5.

Bending moments at the column top.

Test No : S5

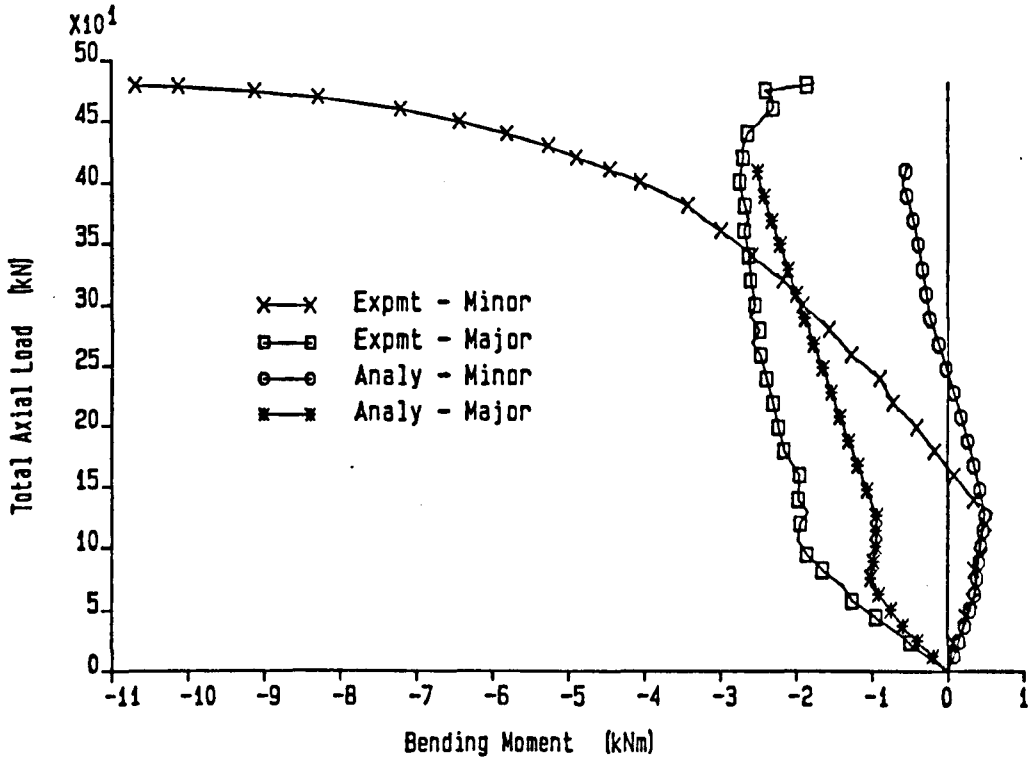


Figure 4.36: Experimental and analytical bending moments at the column head, S5.

Bending moments at the column centre.

Test No : S5

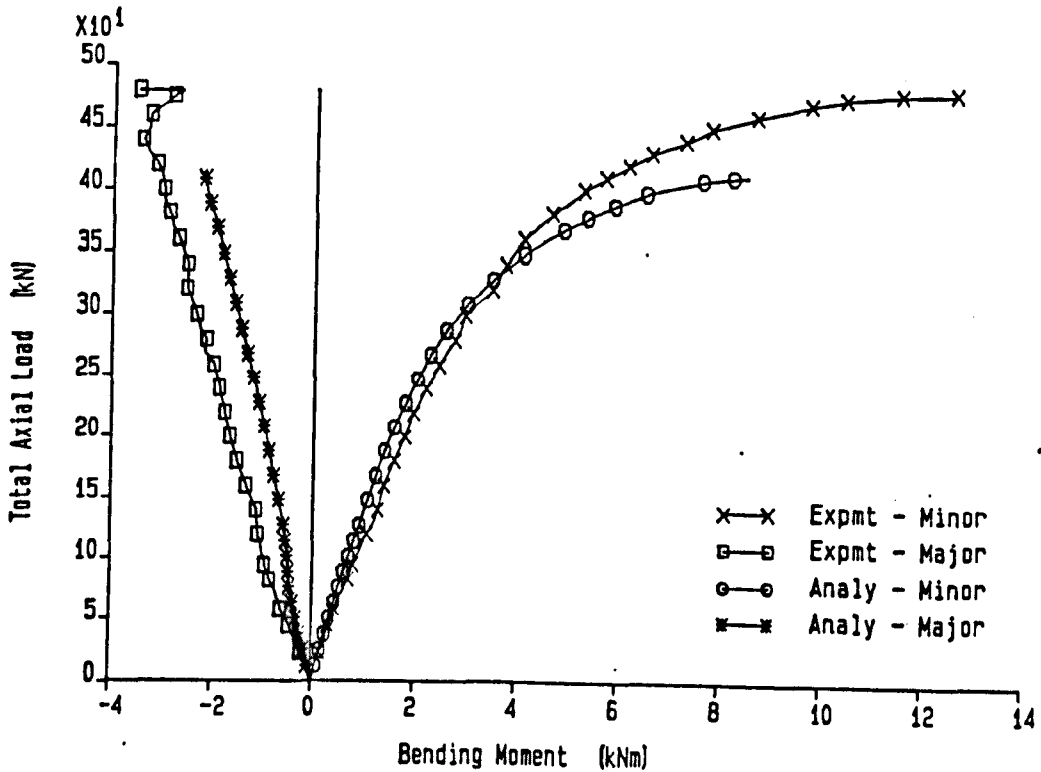


Figure 4.37: Experimental and analytical bending moments at the column centre, S5.

Bending moments at the column base.

Test No : S5

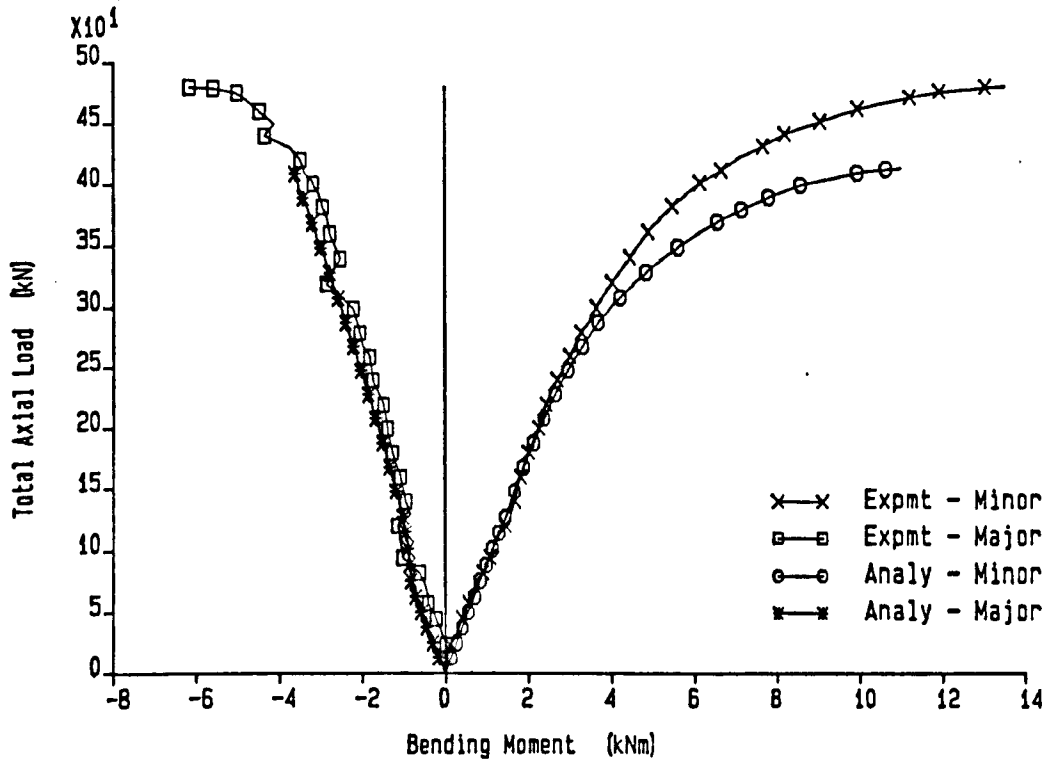


Figure 4.38: Experimental and analytical bending moments at the column base, S5.

Deflections at the column centre.

Test No : S6

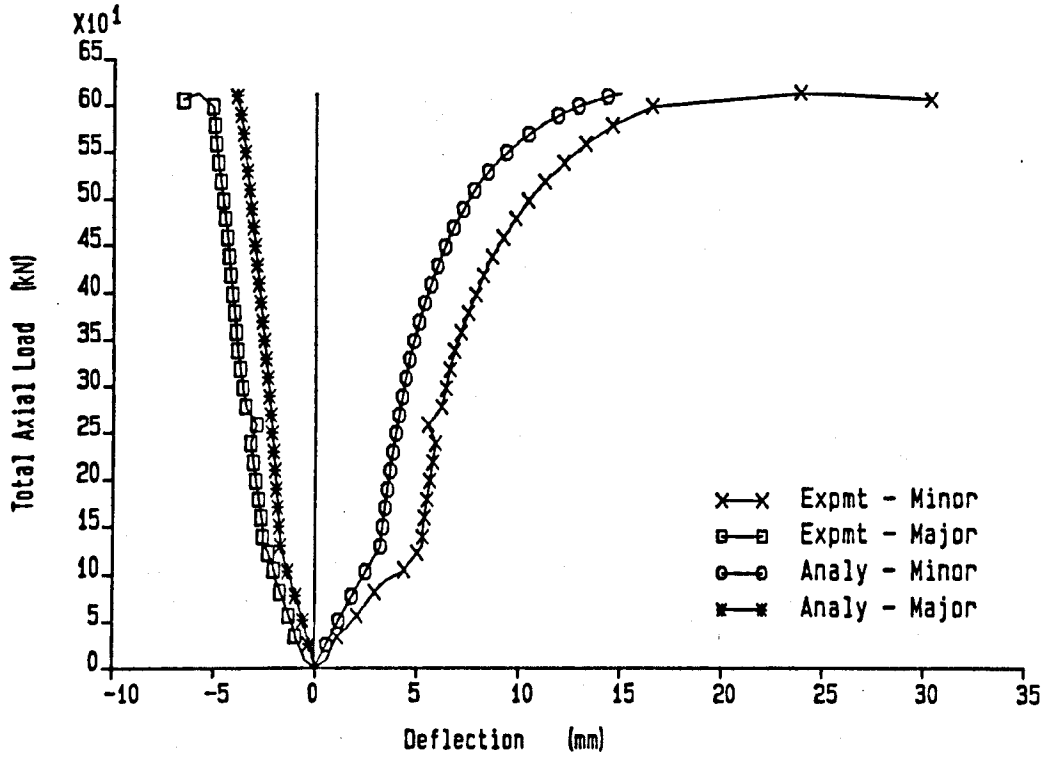


Figure 4.39: Experimental and analytical mid-column deflections, S6.

Twist rotations at the column centre.

Test No : S6

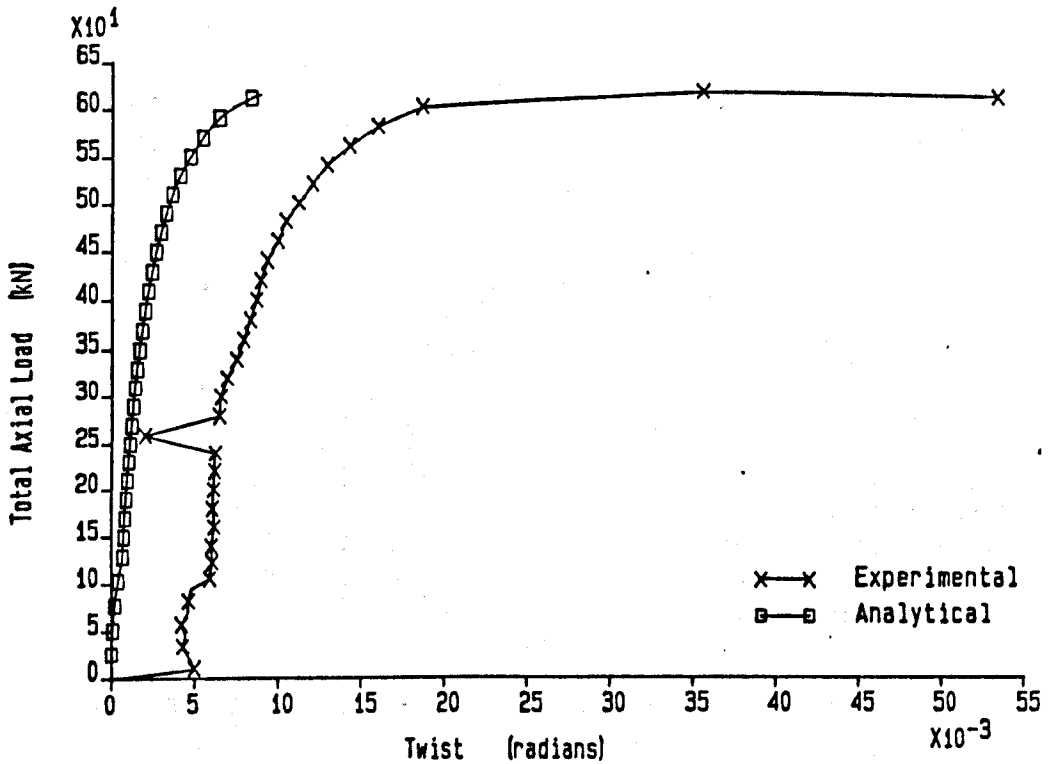


Figure 4.40: Experimental and analytical mid-column twist rotations, S6.

Bending moments at the column top.

Test No : S6

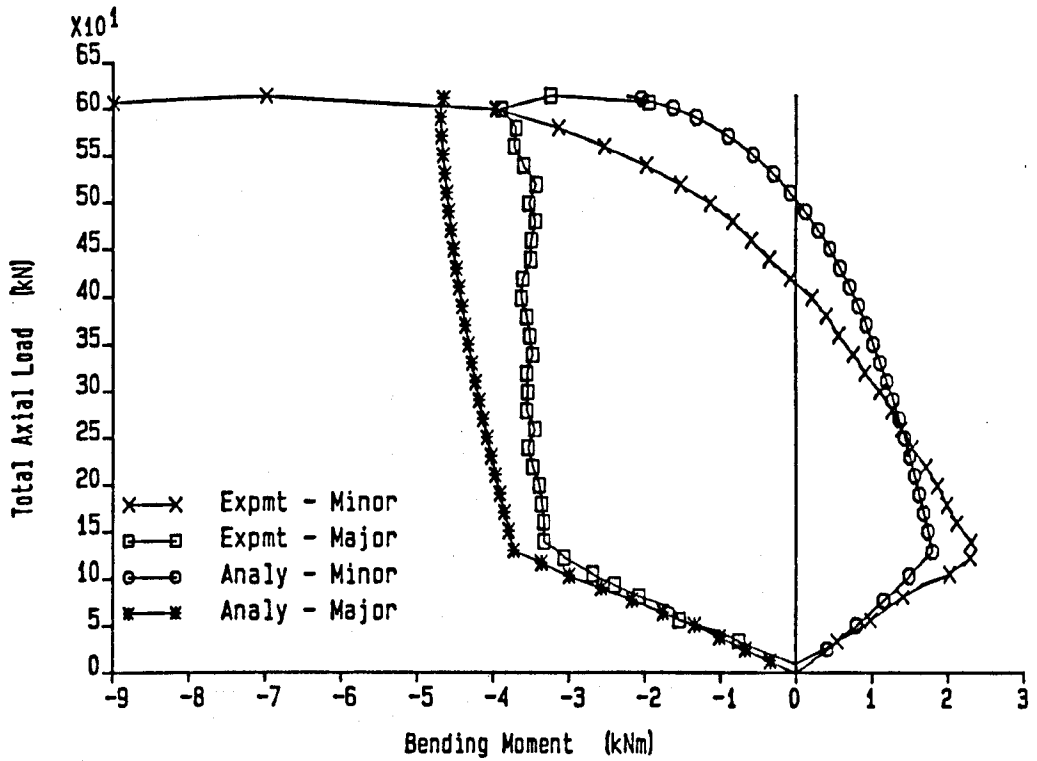


Figure 4.41: Experimental and analytical bending moments at the column head, S6.

Bending moments at the column centre.

Test No : S6

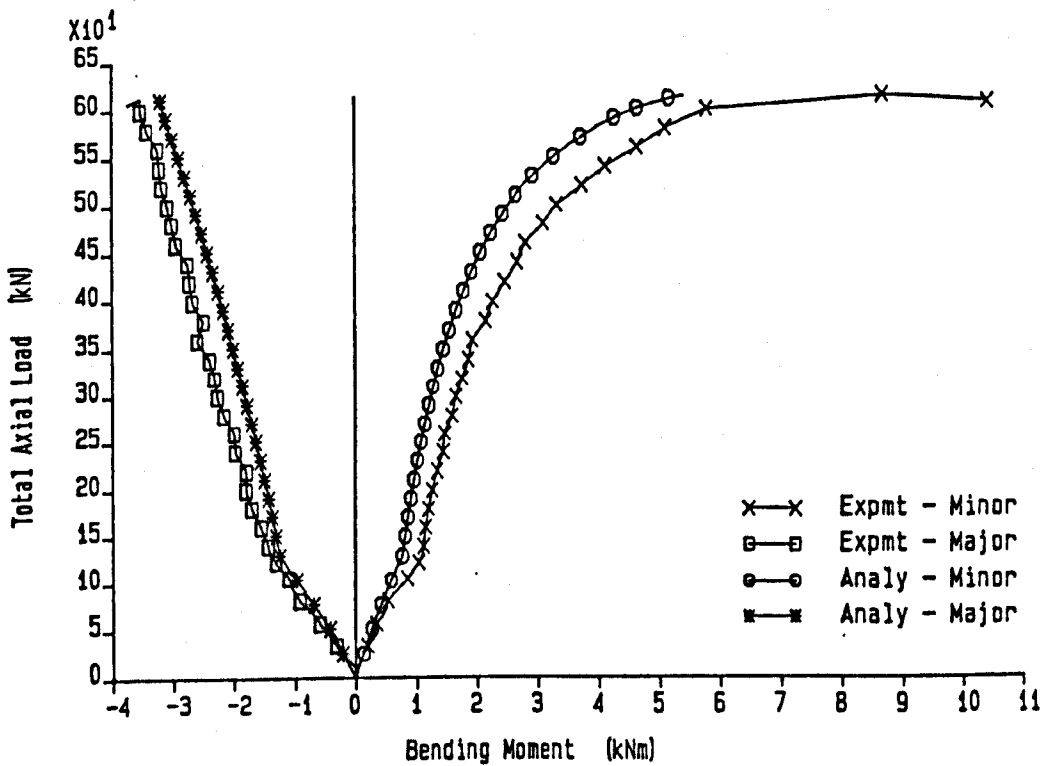


Figure 4.42: Experimental and analytical bending moments at the column centre, S6.

Bending moments at the column base.

Test No : S6

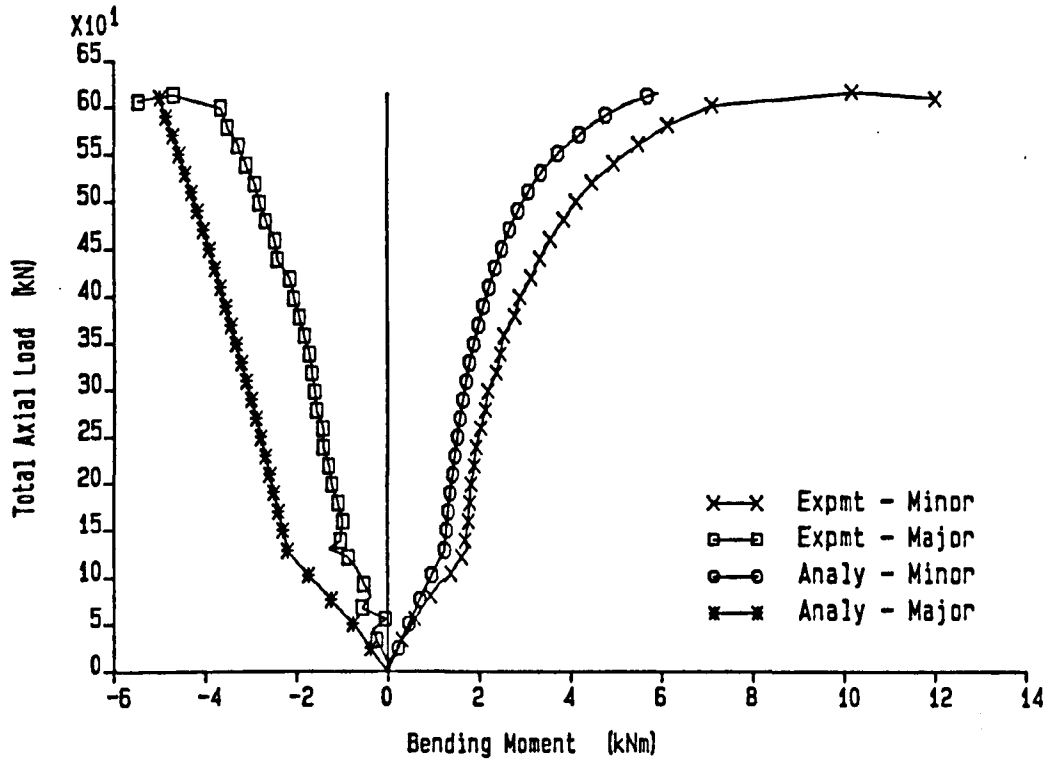


Figure 4.43: Experimental and analytical bending moments at the column base, S6.



Deflections at the column centre.

Test No : S7

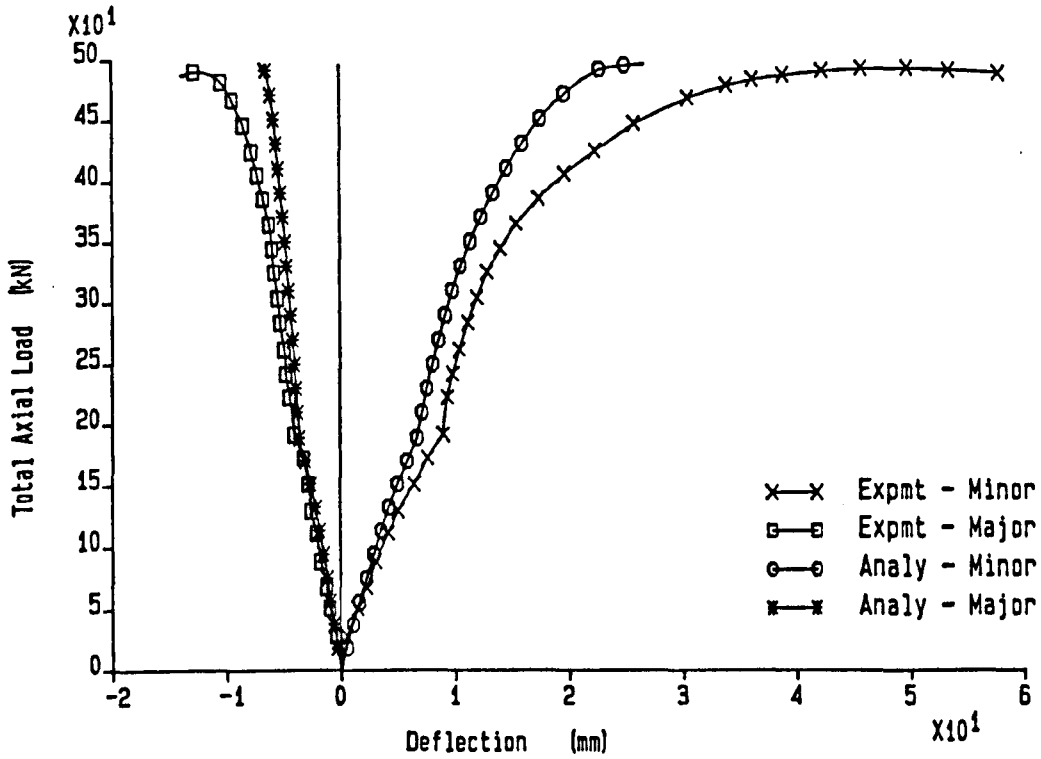


Figure 4.44: Experimental and analytical mid-column deflections, S7.

Twist rotations at the column centre.

Test No : S7

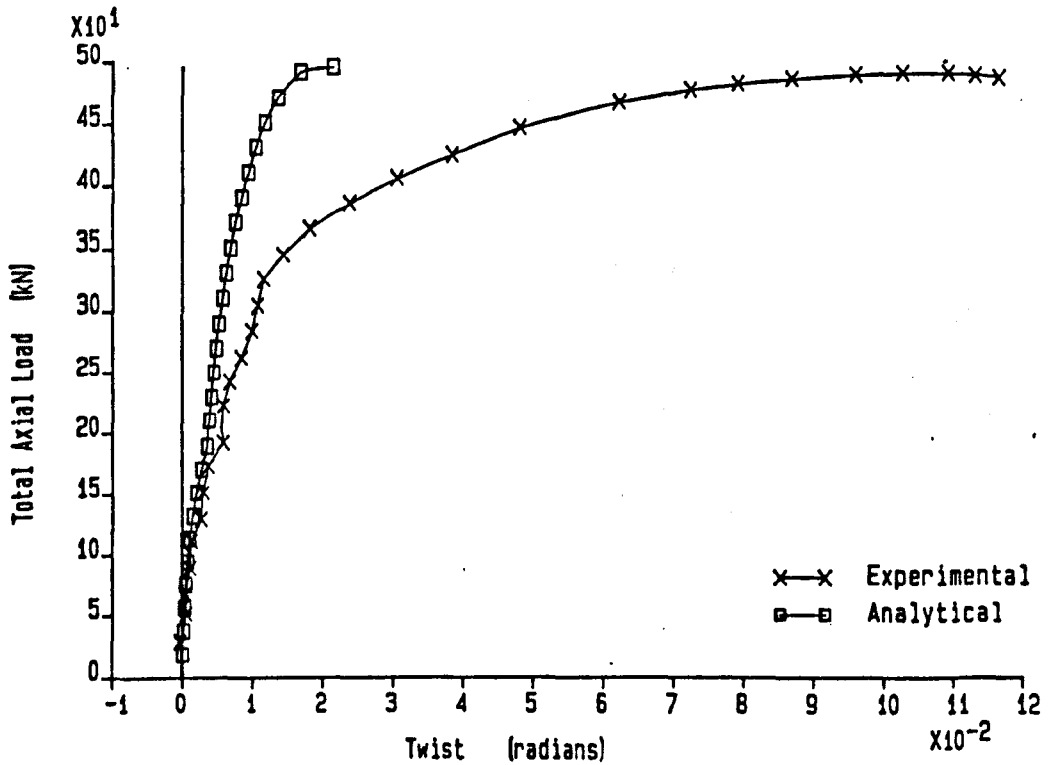


Figure 4.45: Experimental and analytical mid-column twist rotations, S7.

Bending moments at the column centre.

Test No : S7

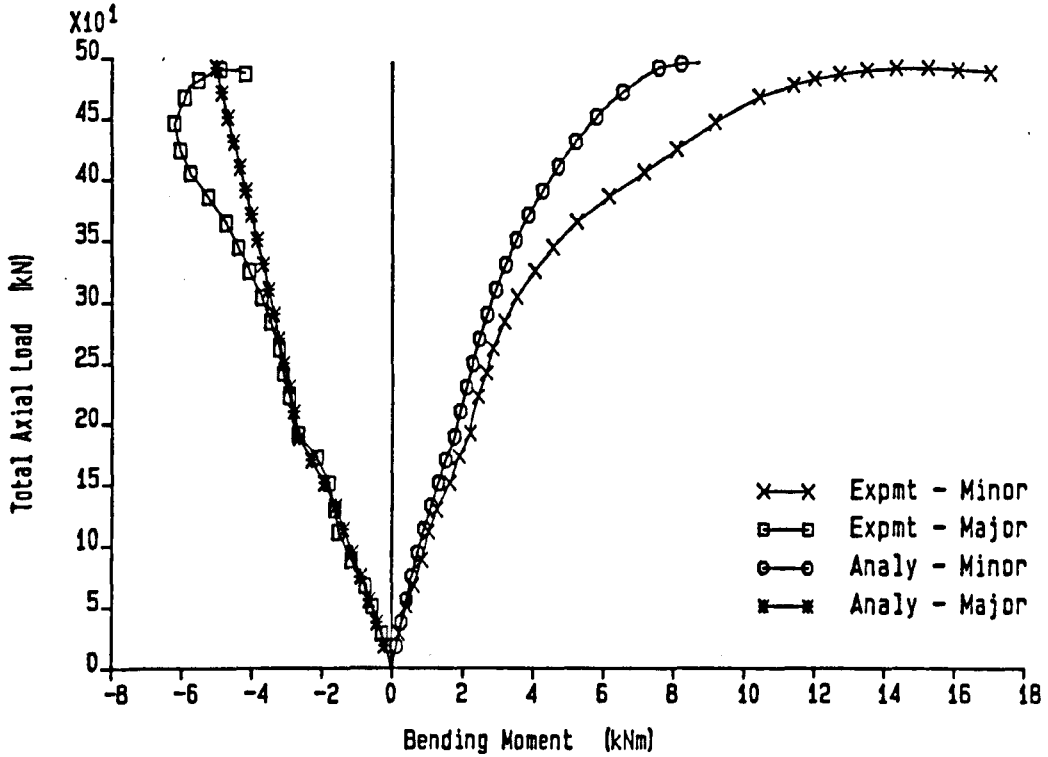


Figure 4.47: Experimental and analytical bending moments at the column centre, S7.

Bending moments at the column top.

Test No : S7

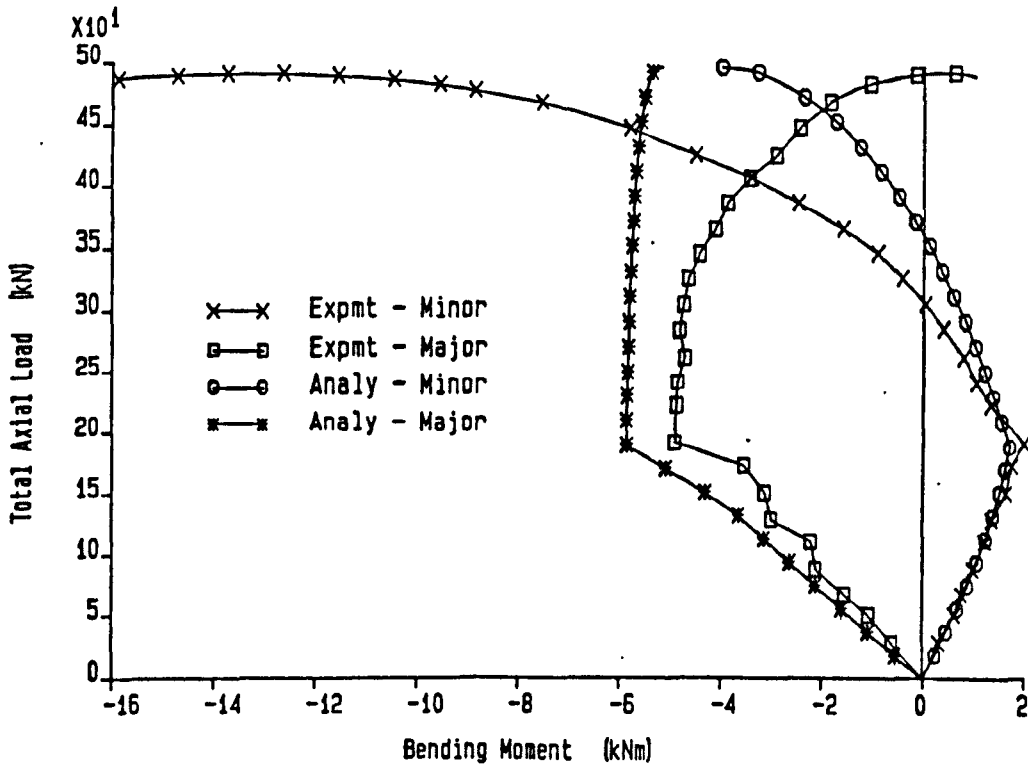


Figure 4.46: Experimental and analytical bending moments at the column head, S7.

Bending moments at the column base.

Test No : S7

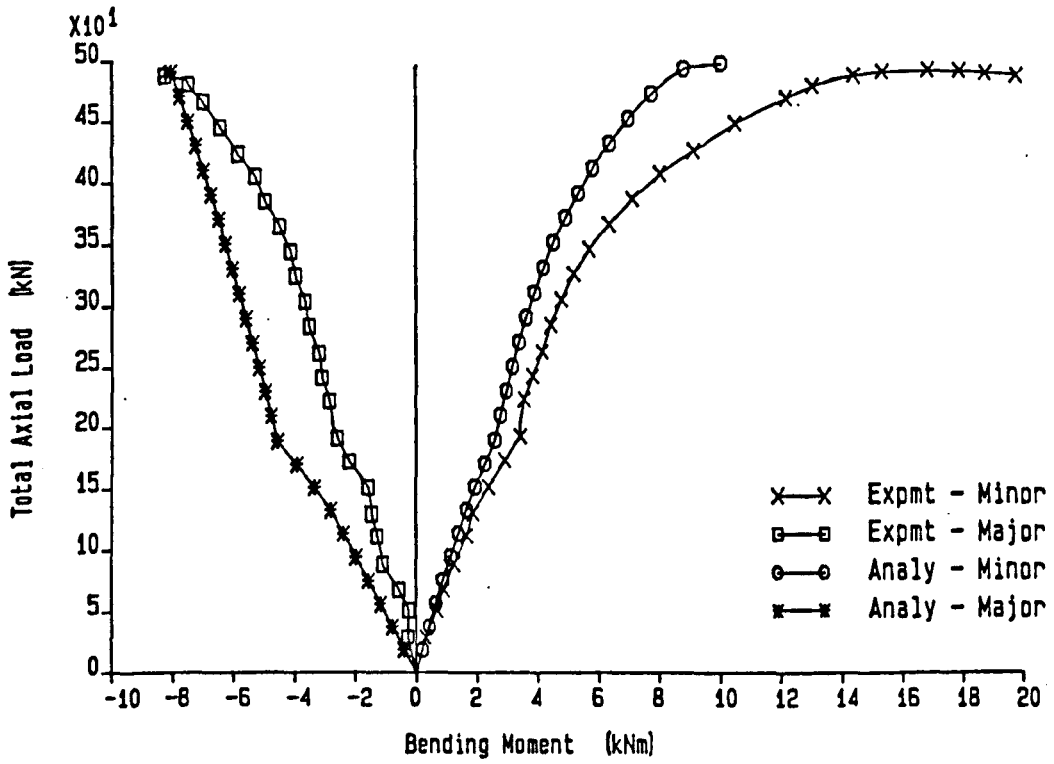


Figure 4.48: Experimental and analytical bending moments at the column base, S7.

Deflections at the column centre.

Test No : S8

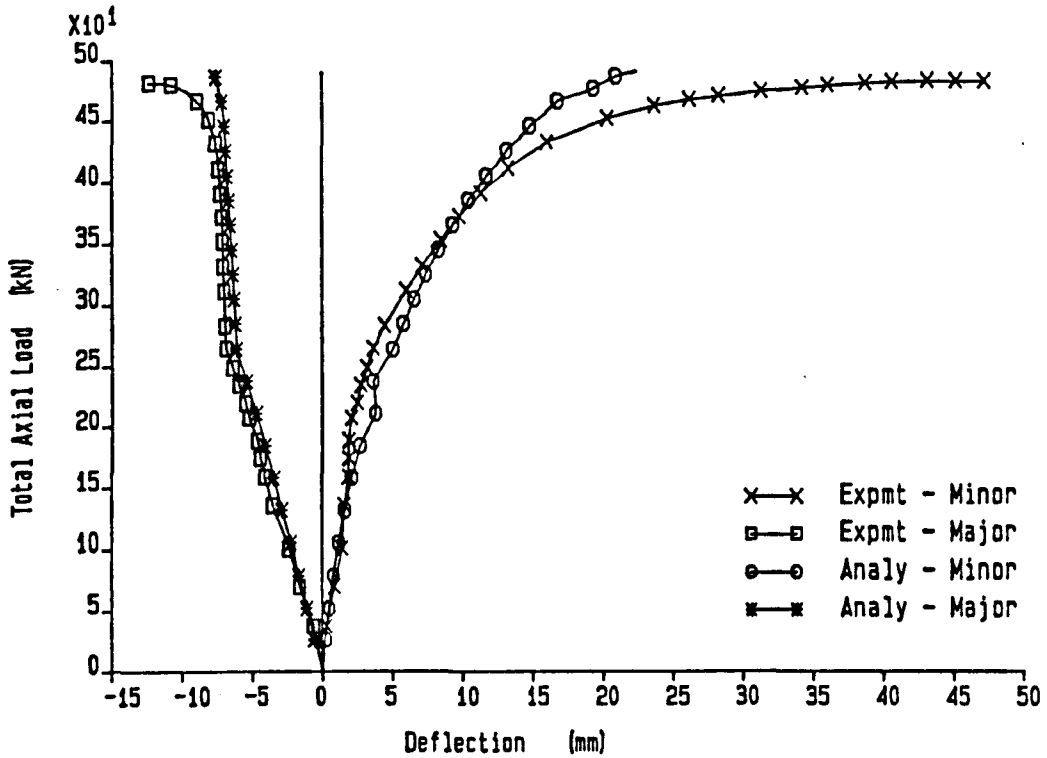


Figure 4.49: Experimental and analytical mid-column deflections, S8.

Twist rotations at the column centre.

Test No : S8

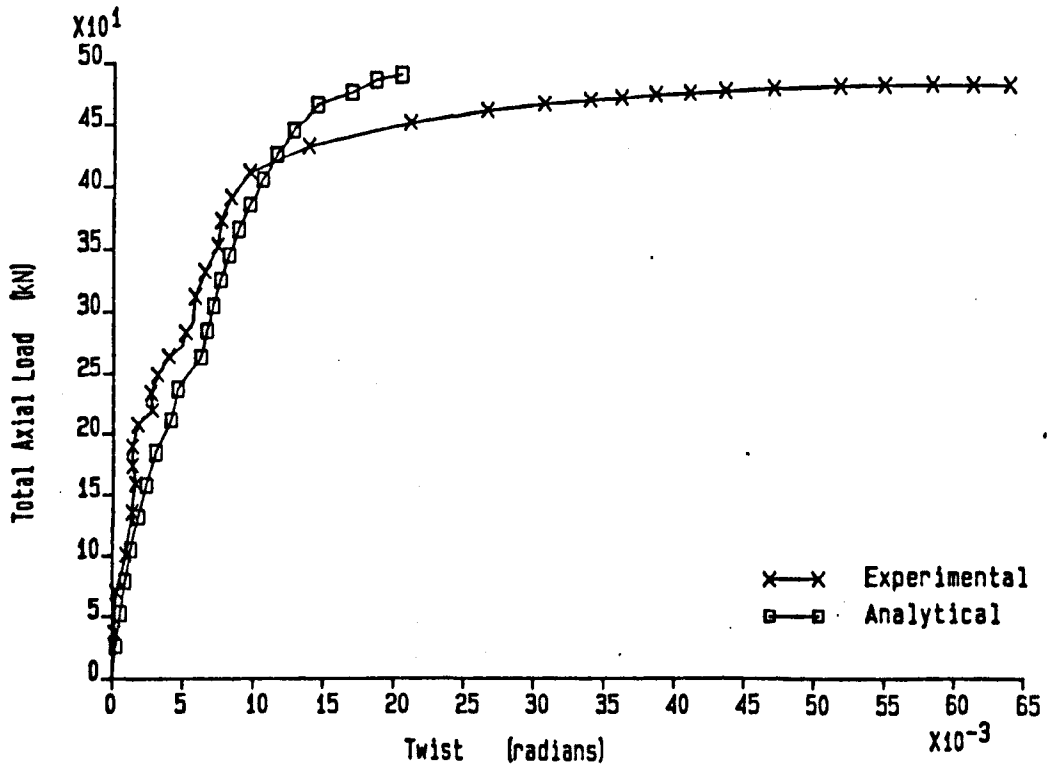


Figure 4.50: Experimental and analytical mid-column twist rotations, S8.

Bending moments at the column top.

Test No : S8

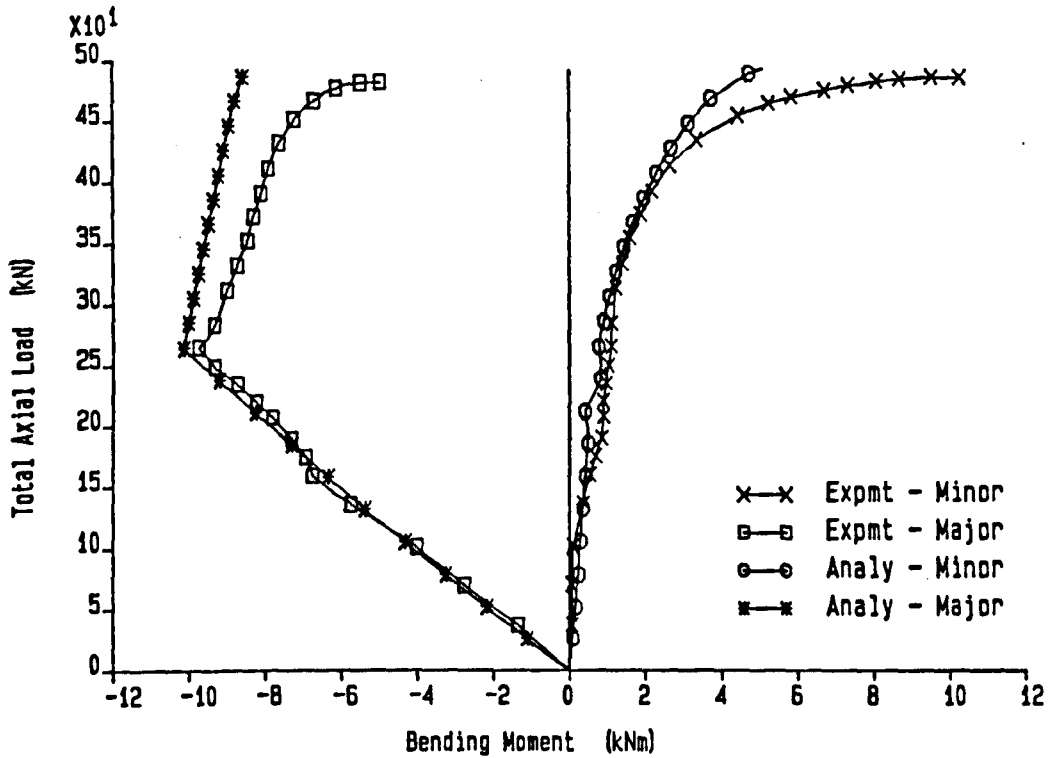


Figure 4.51: Experimental and analytical bending moments at the column head, S8.

Bending moments at the column centre.

Test No : S8

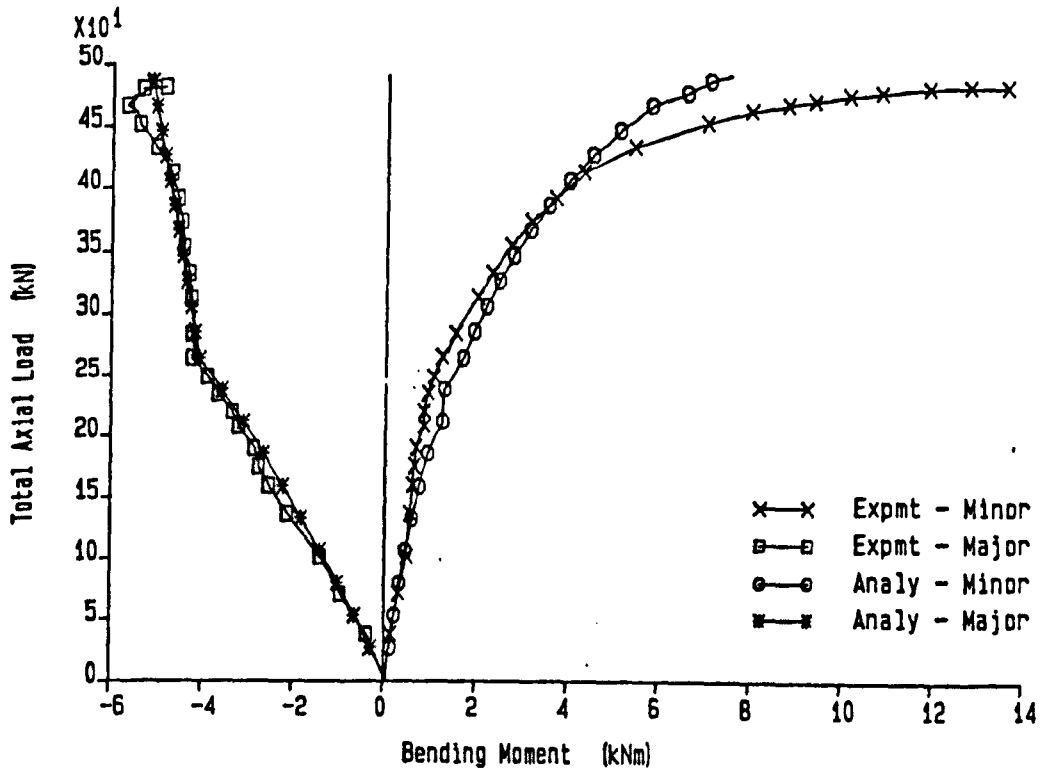


Figure 4.52: Experimental and analytical bending moments at the column centre, S8.

Bending moments at the column base.

Test No : S8

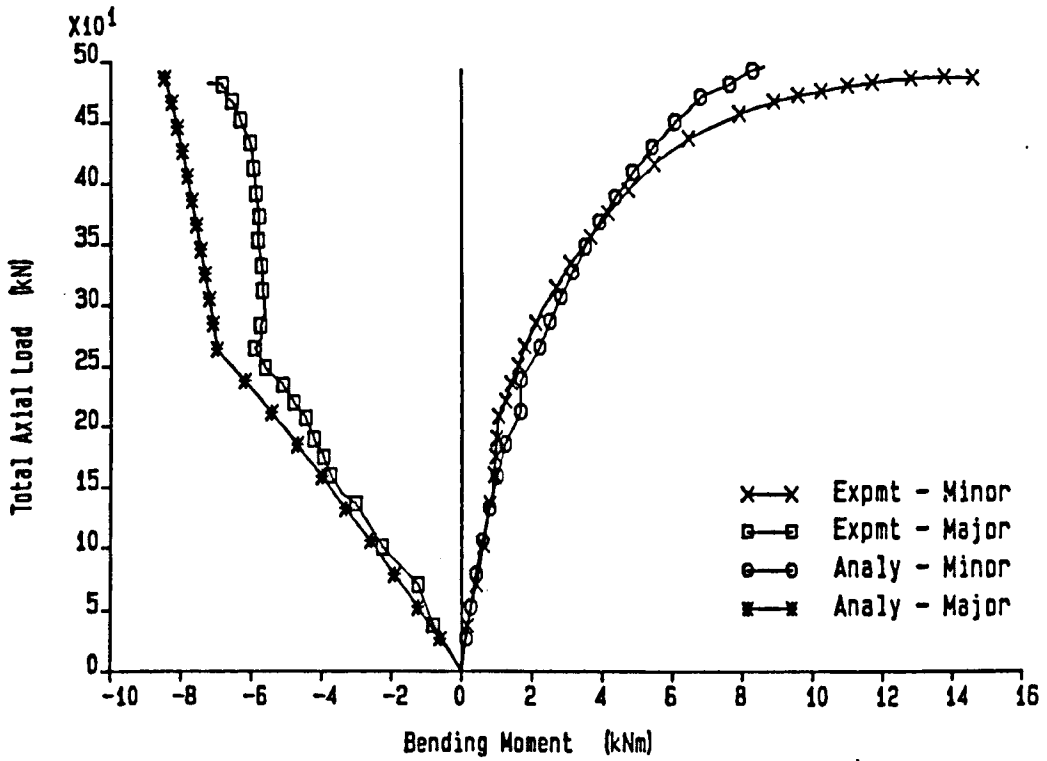


Figure 4.53: Experimental and analytical bending moments at the column base, S8.

Deflections at the column centre.

Test No : S9

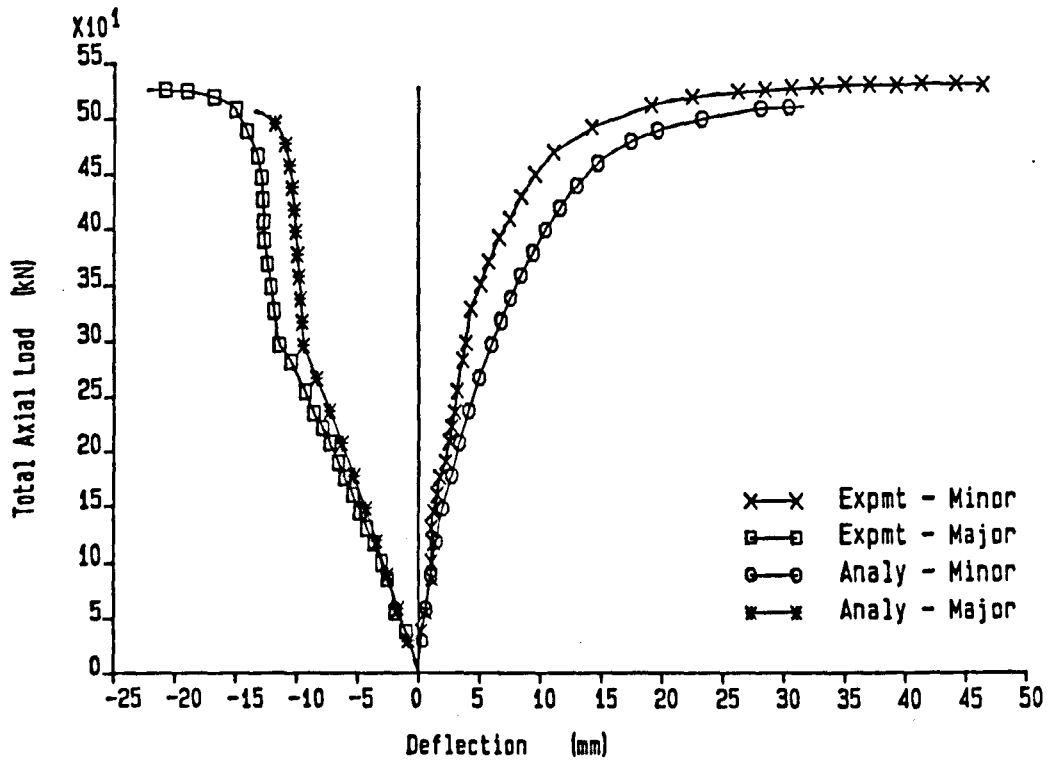


Figure 4.54: Experimental and analytical mid-column deflections, S9.

Twist rotations at the column centre.

Test No : S9

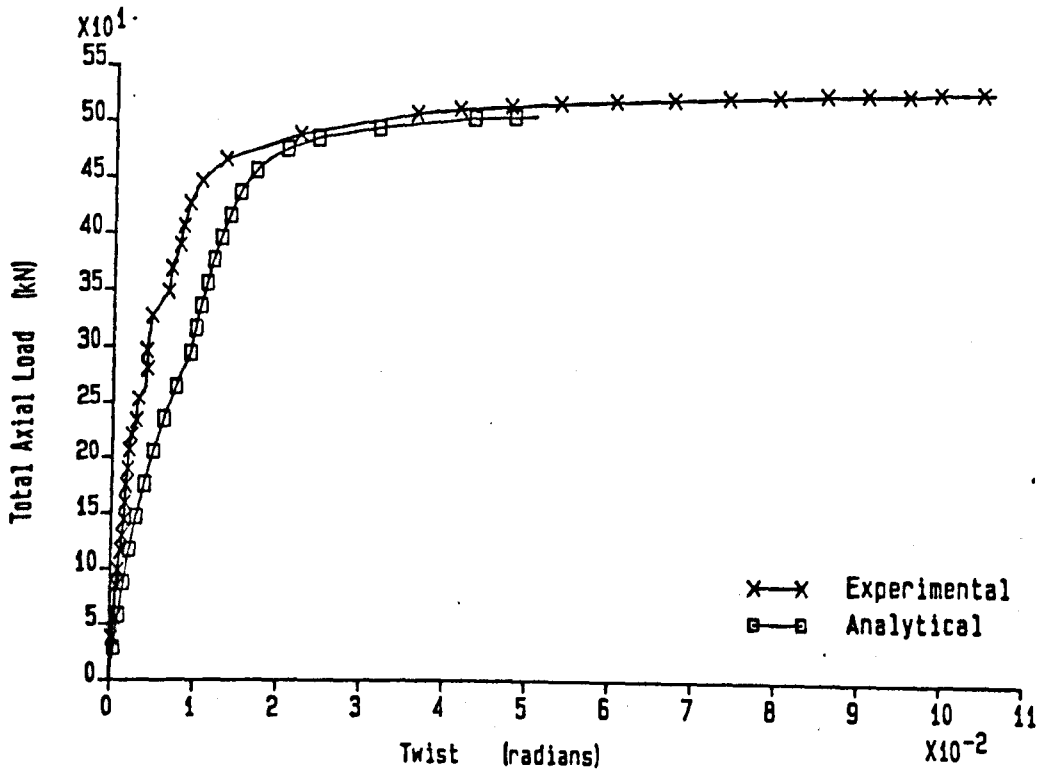


Figure 4.55: Experimental and analytical mid-column twist rotations, S9.

Bending moments at the column top.

Test No : S9

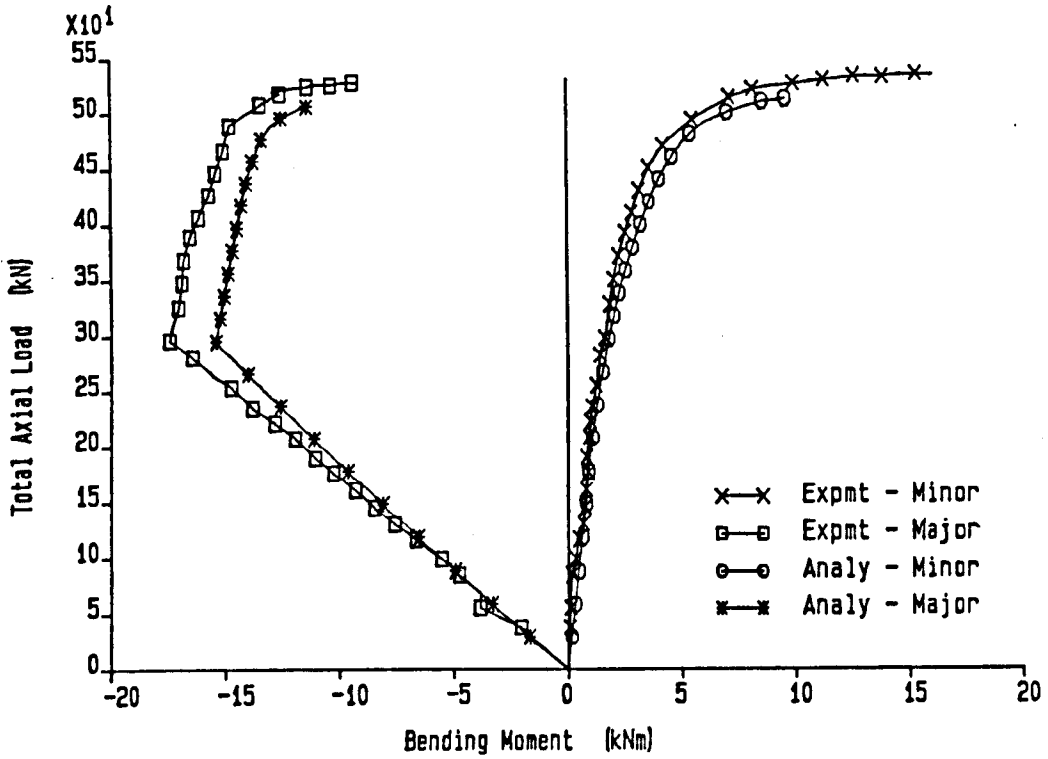


Figure 4.56: Experimental and analytical bending moments at the column head, S9.

Bending moments at the column centre.

Test No : S9

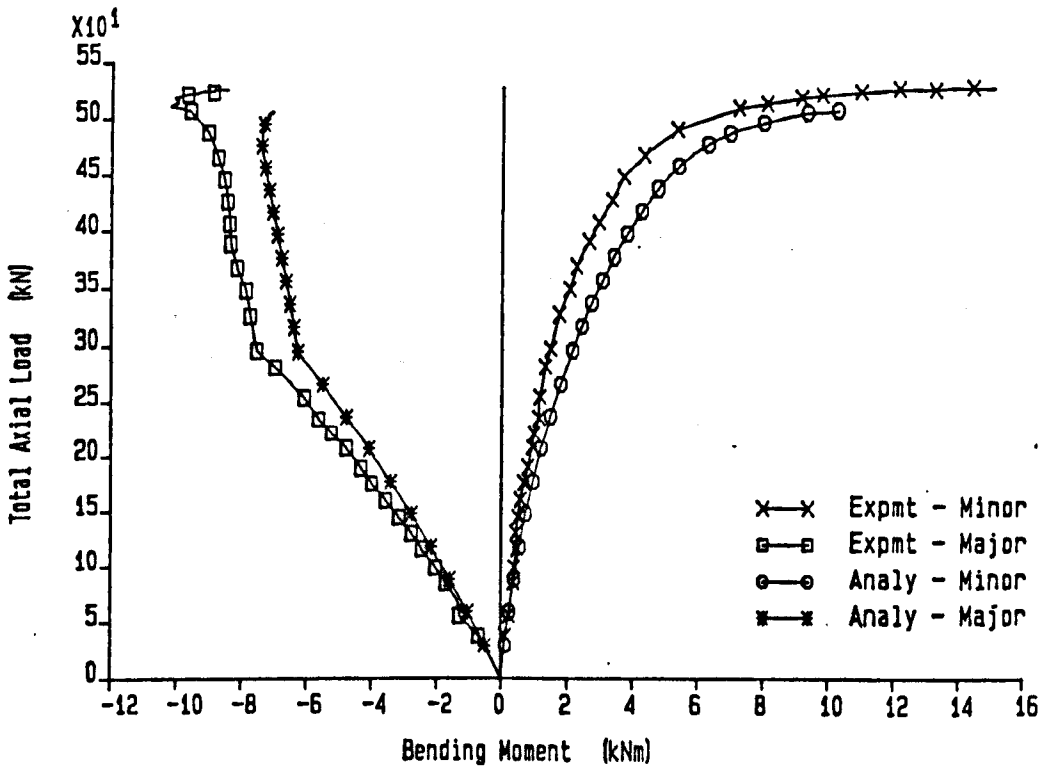


Figure 4.57: Experimental and analytical bending moments at the column centre, S9.



Bending moments at the column base.

Test No : S9

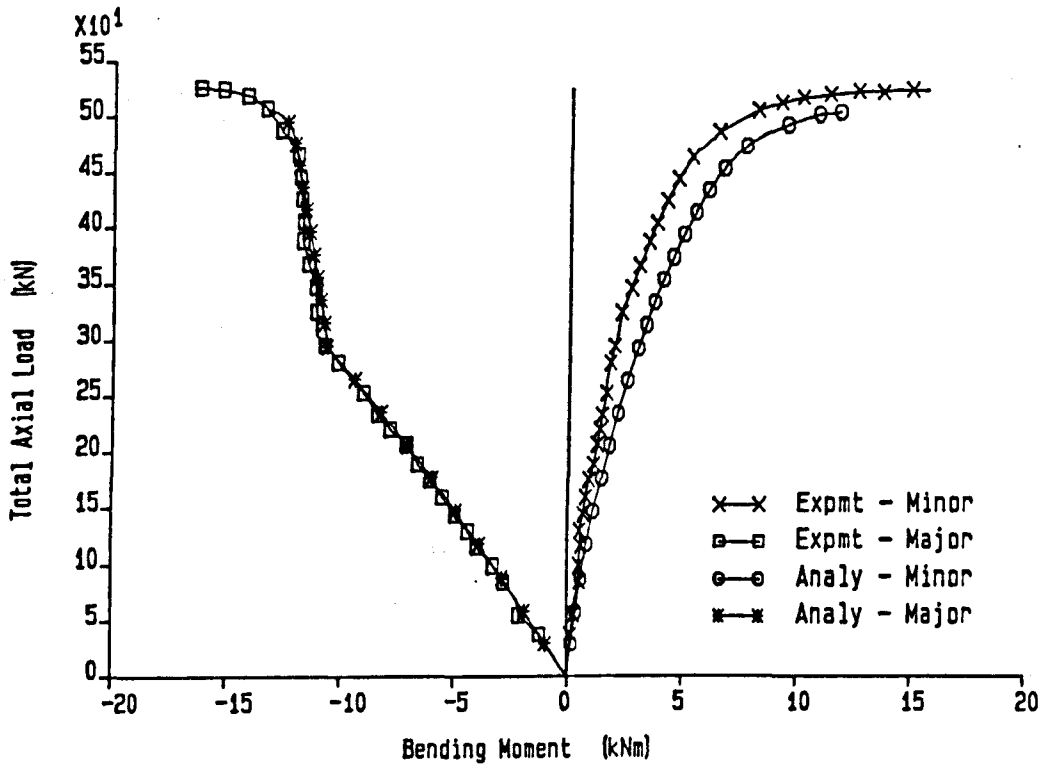


Figure 4.58: Experimental and analytical bending moments at the column base, S9.

Major axis bending moments - Beam 1

Test No : S9

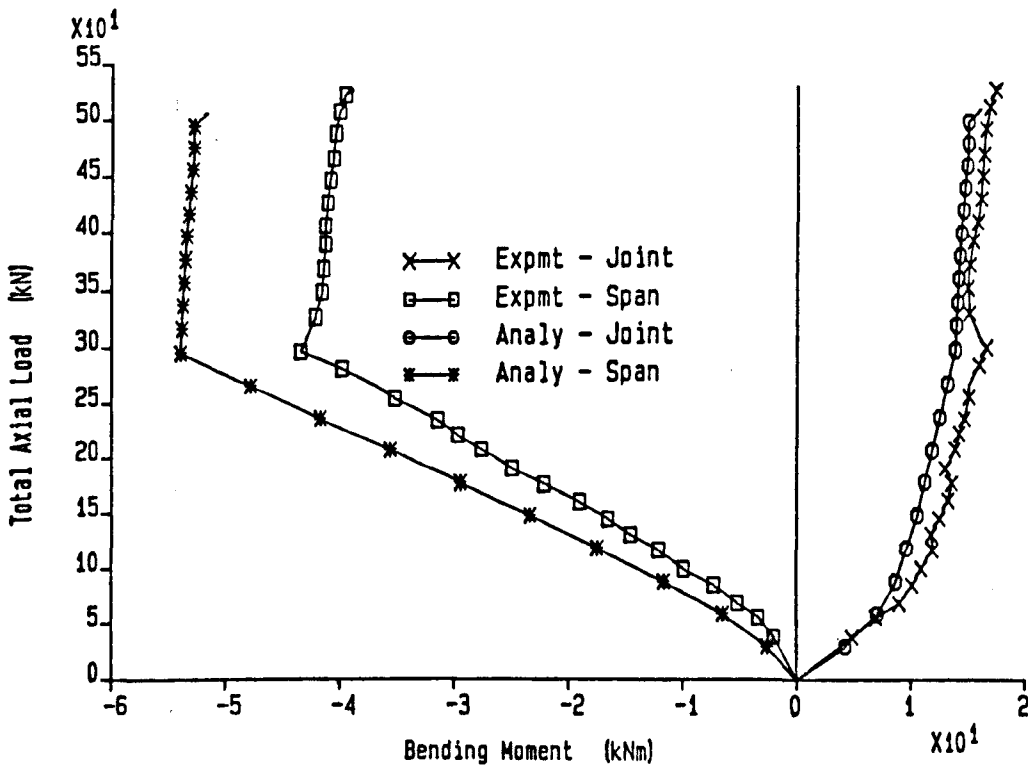


Figure 4.59: Experimental and analytical major axis moments for beam 1, S9.

Deflections at the column centre.

Test No : S10

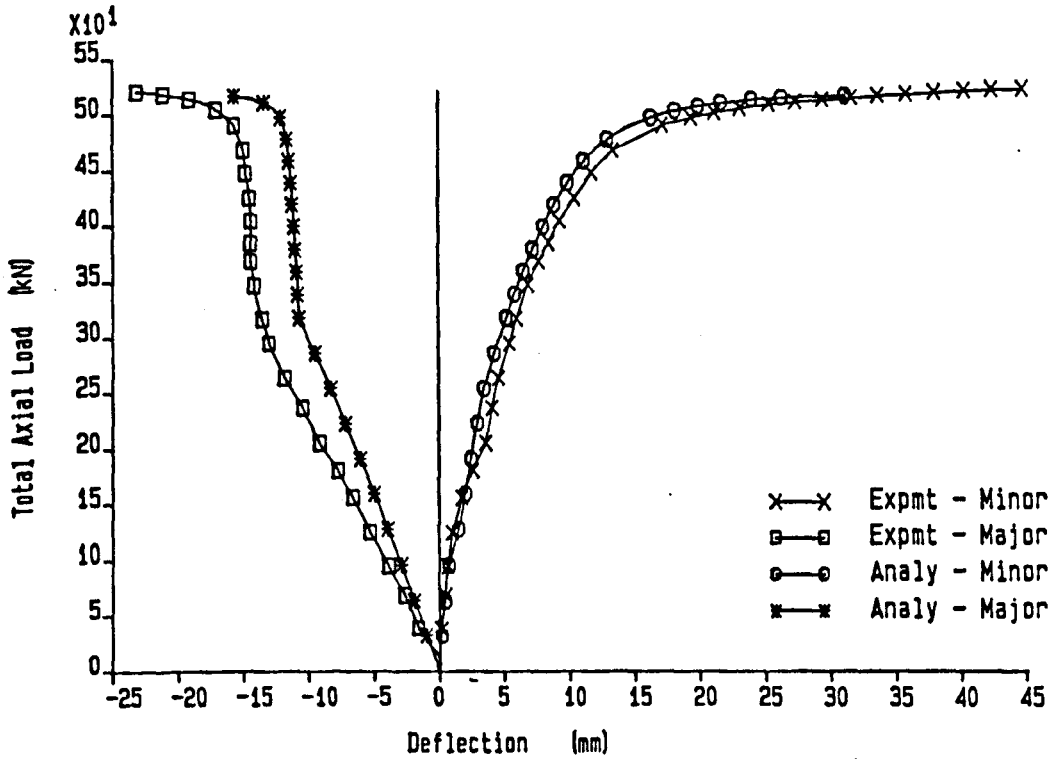


Figure 4.60: Experimental and analytical mid-column deflections, S10.

Twist rotations at the column centre.

Test No : S10

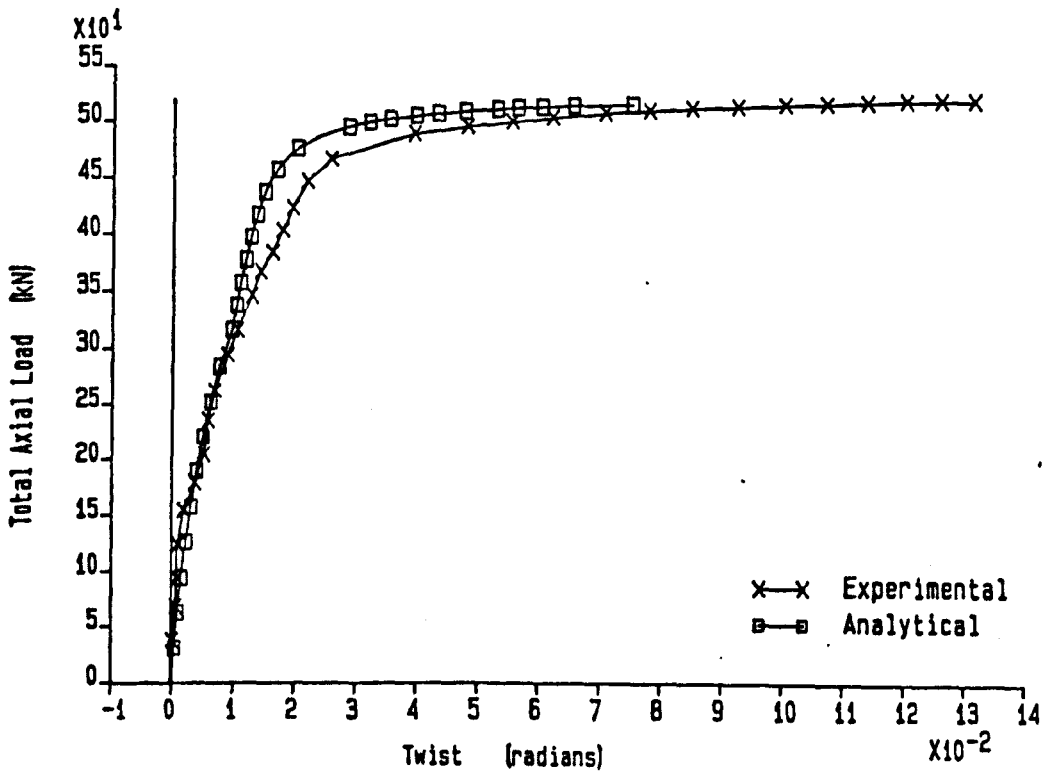


Figure 4.61: Experimental and analytical mid-column twist rotations, S10.

Bending moments at the column top.

Test No : S10

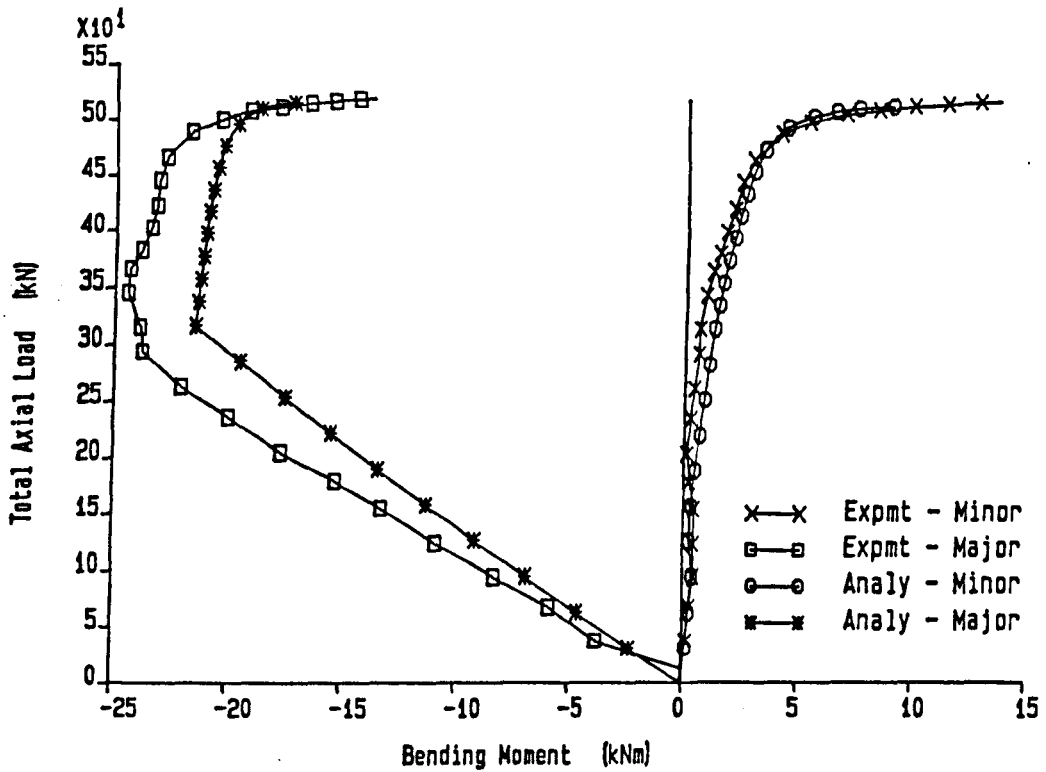


Figure 4.62: Experimental and analytical bending moments at the column head, S10.

Bending moments at the column centre.

Test No . S10

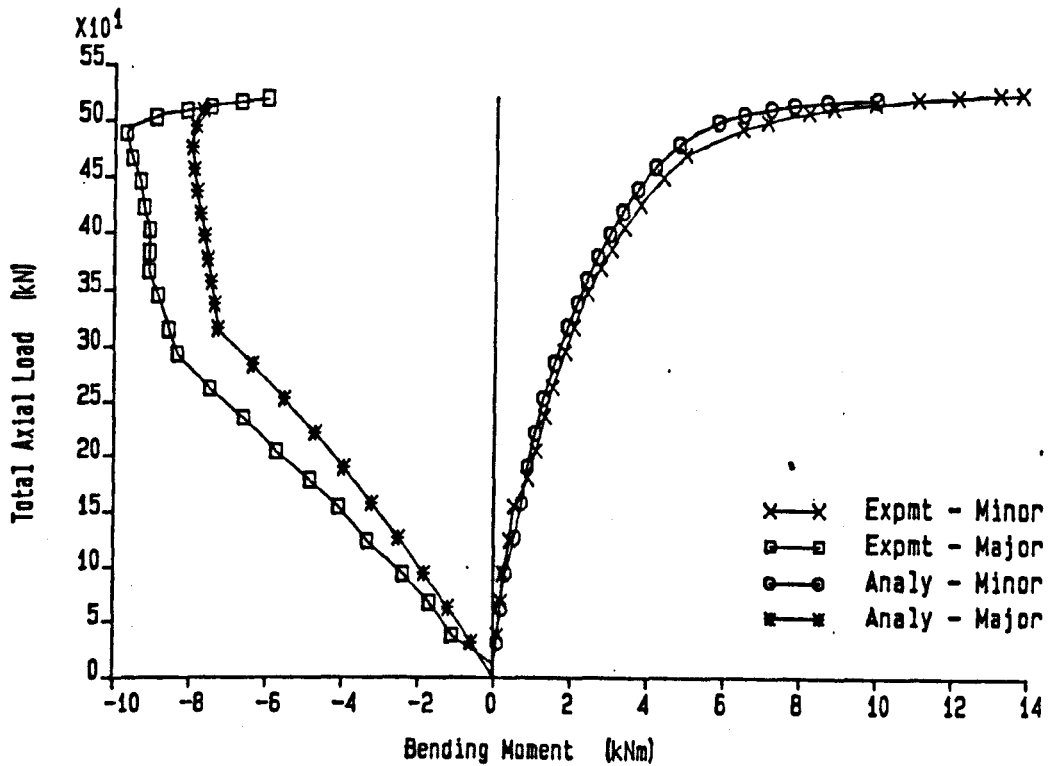


Figure 4.63: Experimental and analytical bending moments at the column centre, S10.

Bending moments at the column base.

Test No : S10

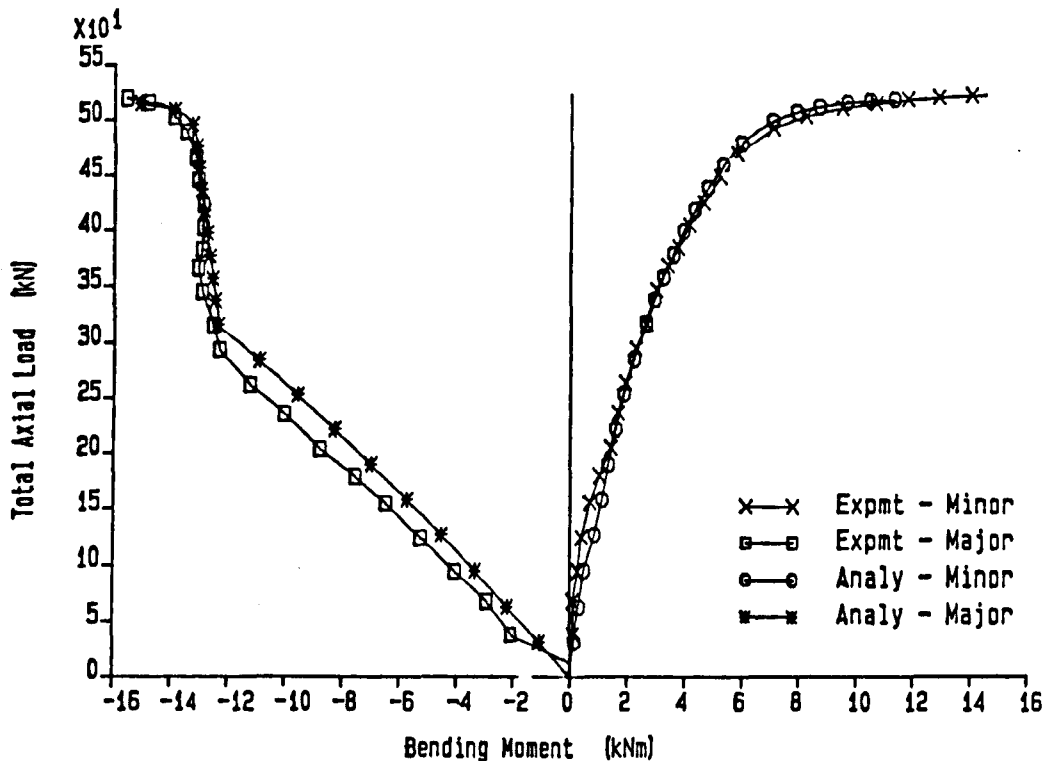


Figure 4.64: Experimental and analytical bending moments at the column base, S10.

Major axis bending moments - Beam 3

Test No : S10

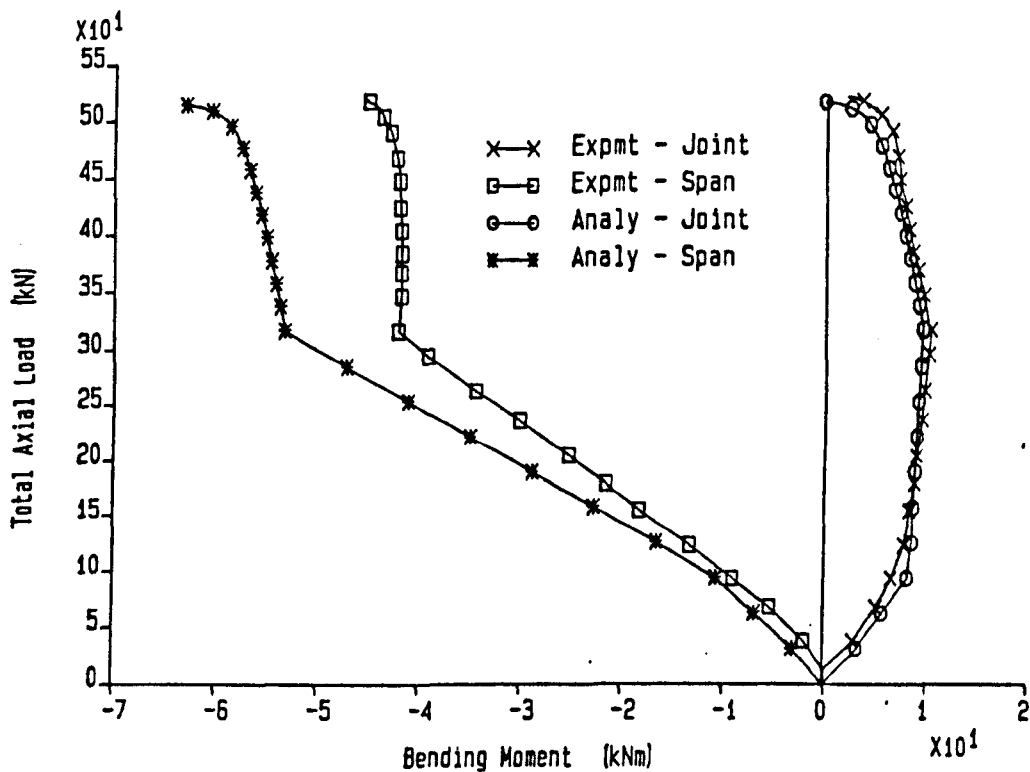


Figure 4.65: Experimental and analytical major axis moments for beam 3, S10.

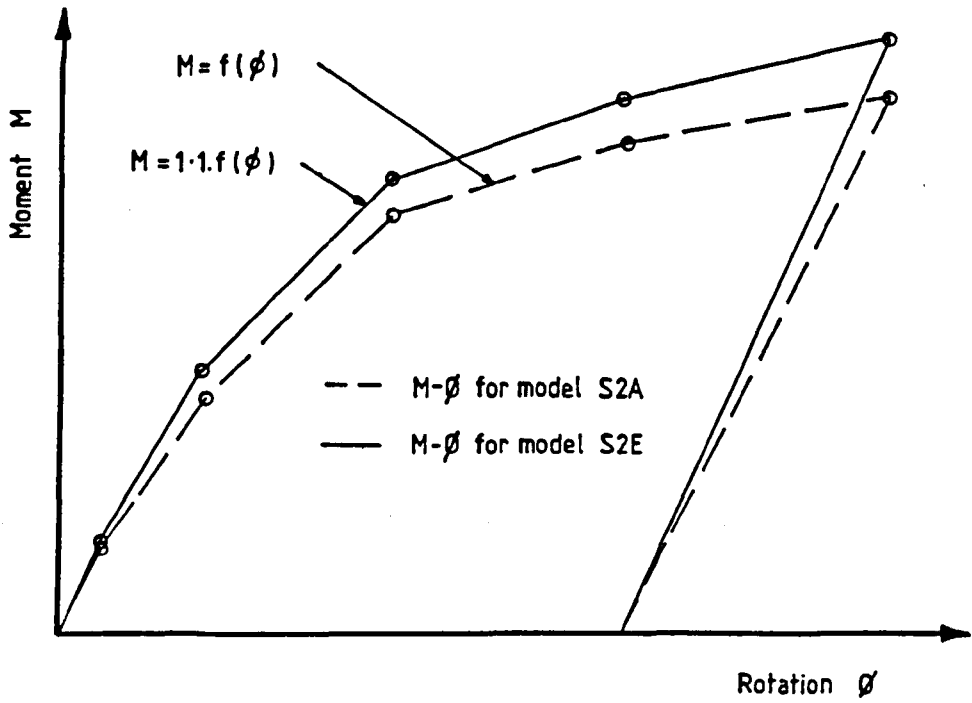


Figure 4.66: Adjustment to the  $M - \phi$  response of the connection characteristics in model 2DE.

# Chapter 5

## The full-scale frame tests.

### 5.1 Introduction.

The final phase of the research programme was devoted to the experimental investigation of two full-scale, 3-dimensional, non-sway, multi-storey frames. These frame tests formed an essential part of the experimental study. Firstly they enabled the effect of column continuity through a loading level to be investigated - a parameter not present in the subassemblage tests. Secondly they were undertaken to determine whether the experimentally observed behaviour of isolated joints and subassemblages was indeed representative of their 'in-frame' behaviour. This latter point is of particular importance if the extensive work on isolated elements carried out by the author and other researchers is to be incorporated into universally accepted methods of semi-rigid frame design.

There have been a number of previous experimental investigations of the performance of full scale, 3-dimensional, rectilinear steel frames. These include studies of both purpose made frames [5.1] and in-situ testing of existing structures [5.2]. However, as far as the author is aware, the frame tests described herein represent the first experimental study of a purpose made 3-dimensional, multi-storey, non-sway steel frame incorporating 'simple'

semi-rigid connections.

The frame tests were carried out in the large structures testing hall at the Building Research Establishment near Watford, England. A brief summary of the large scale testing facilities at the Building Research Establishment is presented in reference 5.3.

## **5.2 General arrangement of the full-scale test frames.**

For the purpose of description, each frame may be considered as comprising two parallel 2-dimensional frames each consisting of three columns and four primary beams, with six secondary beams connecting the two frames at the panel points. The two plane frames within the 3-dimensional structure have been termed the 'active' frame and the 'static' frame (figure 5.1 clarifies the terminology). Only the 'active' frame and the secondary beams were subjected to direct load and response monitoring, the 'static' frame simply provided the required 3-dimensional restraint. There were a number of reasons for considering the test frames in this manner:-

1. Testing only part of a large 3-dimensional frame to failure is significantly less hazardous than simultaneously testing the whole of the frame.
2. It reduced the amount of loading and instrumentation equipment required in any one test to an acceptable level.
3. As the 'static' frame from the first test was not loaded directly it did not sustain any permanent damage. The 'static' frame could therefore be re-used for the second test, thereby reducing both the time and the cost of fabrication.

Figure 5.2 shows the general arrangement of the first of these frames, F1. The configuration and overall dimensions of the second test frame, F2, were similar. The only difference between tests F1 and F2 was the orientation of the columns on the active frame and the detailing of the beam to column connection. In the case of the first frame test, the primary beams framed into the minor axis of the column whereas in test F2, the primary beams framed into the major axis. Figure 5.3 shows a typical plan highlighting the differences between the two tests. Prior to fabricating the subassemblage specimens, an in depth analytical study was carried out to ascertain the most appropriate dimensions for the test specimens. In the case of the frame tests however, the overall dimensions of the frames were dictated by the availability of loading and displacement measurement devices which were specially fabricated for a previous study of full-scale 2-dimensional frames [5.4].

Initially, it had been assumed that the frames would be limited to a two storey height. However, it was considered that the potential rotational restraint from the loading block acting directly at the head of the column would have had an unquantifiable effect on the behaviour of the second storey column segment. This problem was averted by introducing a third storey to the 'active' frame which effectively isolated the second storey column from any undesirable restraint effects. The height of the third storey (1.8m) was chosen as half that of the lower storeys (3.6m). As the positional bracing at the column head provided only a very small degree of rotational restraint (single bolt connection), the stiffness and distribution of moments within the third storey column were similar to that of a column of twice the length bending in double curvature. Edge columns in multi-storey structures with full floor loading, and internal columns with a non-symmetric floor loading arrangements often deform in this manner. Therefore, in terms of stiffness and moment distribution, the proposed arrangement for the third storey was representative of a full height storey in a more extensive multi-storey frame. The precise effect of the third storey column was evaluated by using appropriate instrumentation to determine the bending moments acting at the head of the second storey columns.



### 5.2.1 Frame members and connection type.

Both test frames were constructed using 152 x 152 UC 23 sections for the columns and 254 x 102 UB 22 sections for the beams. This maintained the common theme of similar section sizes which had been adopted throughout the research programme.

Flush end plate connections were used for all the beam to column connections in both test frames F1 and F2. There were a number of reasons for selecting this particular connection type in preference to other forms of simple connection. Firstly, recent surveys of British design and fabrication practice [5.5], have shown the flush end-plate to be the most popular. Secondly, connections which employ cleats are very often susceptible to bolt slip at relatively low moment levels. Once bolt slip has occurred, the moment rotation characteristics of the connection are usually irreversibly changed. The flush end plate connection however is not affected by bolt slip to the same degree and therefore exhibits similar moment-rotation behaviour under repeated moderate loading. Using such a connection, small levels of load could be applied to the frame without irreversibly deforming either the connections or the frame members. This was an important facility which allowed the loading devices and load control systems to be fully commissioned prior to carrying out a test to failure.

The particular flush endplate connection used in test F1 comprised a 12mm endplate and was fabricated in exactly the same manner as the flush end plate connections used in both the joint and subassembly studies (Chapter 6). The flush end plate connection used in test F2 was of a similar construction, but in this instance an 8mm end plate was used to increase the flexibility of the joint. In both cases, the end-plates were fixed to the beam with an 'all round' fillet weld. Although proposed initially, it was considered that using a partially welded end-plate connection would have increased the possibility

of an undesirable premature joint failure.

### **5.2.2 Frame construction details**

The test frames were fabricated and erected by the workshop at the Building Research Establishment. The fabrication drawings for each of the test frames are presented in Appendix B. Figures 5.4 and 5.5 show general views of the erected test frame F1 prior to testing, complete with instrumentation and loading devices.

Analytical studies of the effect of column base fixity reported in section 2.2.2 had shown that modest deviation in the actual, or as measured, stiffness characteristics of a fixed, or near fixed, base connection had a negligible effect on column behaviour. For this reason, and the much simplified erection procedure, all the columns in each of the two test frames were fabricated with a fixed base condition. It should be noted that in this instance the pre-compression method for inducing predefined initial column deformations, as described in section 2.3.3, was not used. Thus it was feasible to add welded stiffening plates to the column base to enhance the rigidity of the connection.

### **5.2.3 Prevention of column sway.**

The frame was prevented from swaying by a number of purpose made 'tie bars' which fixed the position of the structure with respect to the rigid concrete viewing balconies surrounding the test area. The principal ties were located at the node points of the columns to provide effective restraint in the two orthogonal directions. In addition, several restraints were provided to the compression flange of each of the four primary

beams to prevent premature failure by lateral torsional buckling of the beam. Although not necessary for member stability considerations, a single 'tie bar' was also provided at each level to the secondary beams adjacent to the viewing balcony. This was a safety precaution which fixed the position of the upper flange on the secondary beams at the points of applied load. Figure 5.6 shows a plan at a typical loading level illustrating the 'tie bar' arrangement . The restraints comprised a single length of threaded bar with a dowel pin connection at each end. This arrangement provided horizontal positional restraint, but permitted the small vertical movement arising from beam deflections and axial shortening of the columns to occur freely (figure 5.7).

### **5.3 Measurement of section properties.**

As in the subassemblage tests, measurements were made of the actual cross sectional dimensions of the all the principal beam and column elements to determine their true engineering properties. The material properties of the sections, yield stress and Young's modulus, were determined by performing tensile coupon tests and, in the case of the columns, by stub column tests. Tests were also carried out to determine the distribution of residual stresses within the column members. The results of these tests, together with a discussion of the test procedures, are presented in the supplementary volume to this thesis [5.6].

## 5.4 Method of load application.

Loads were applied to the frames by a series of hydraulic rams situated underneath the reinforced concrete floor slab of the test hall. High strength steel tendons and Macalloy bars, which passed through a regular grid of vertical ducts in the floor slab, transferred load from the rams to the frame via substantial 'saddle' and spreader beams. Each frame beam member was loaded by a pair of tendons tensioned by a pair of rams operating at the same pressure, thus providing a balanced arrangement of load to the saddle beams. The columns were loaded using a similar arrangement but Macalloy bars were used rather than tendons to enable large loads to be applied. Figure 5.8 clarifies the loading arrangement and shows the precise location of the loading points on the frame, whilst figure 5.9 shows a photograph of the hydraulic rams housed in the basement of the test hall.

As in the subassemblage tests, the beams were loaded first to a particular limiting value followed by loading of the column head to failure. Beam loading was 'load controlled' and therefore not influenced by the frame deformation resulting from column loading. As a safety precaution, and also to observe the 'post-failure' behaviour of the frame, the column head jacks were displacement controlled. Figure 5.10 shows a photograph of a typical column head load arrangement illustrating the cluster of three L.V.D.T.'s used to monitor the applied column head displacements.

The actual applied loads were measured by tension load cells which were coupled into the tendons and Macalloy bars. In the case of the beam loads, two cells were connected in series into each length of tendon. One cell was used to monitor the applied load and the second cell was used as a direct feedback signal to prevent the inadvertent application of excessive loads. In the case of the Macalloy bars, which applied load to the column head, a single cell was located in each bar to provide a direct measure of the applied load with the measurement of column shortening from the cluster of L.V.D.Ts. providing the necessary safety feedback signal.

## **5.5 Test frame instrumentation.**

Figure 5.11 summarises the various force and deformation components which were monitored during each of the frame tests.

### **5.5.1 Deformation measurement.**

Both primary and secondary beam deflections were measured at the quarter, mid, and three-quarter points relative to an aluminium box section supported at both ends of the beam. Deflections were therefore measured relative to any vertical displacements which may have occurred at the supports. This method of beam deformation measurement had been successfully used in a previous study of two-dimensional frame behaviour [5.4]. A photograph of the deflection monitoring system as used on the secondary beam SB1 of frame test F1 is shown in figure 5.12.

Column deformations were measured using a three-dimensional monitoring system comprising six L.V.D.T.'s, similar to that developed for the subassemblage tests (section 3.2) [5.7]. Using this device, the column deflections  $dx$ ,  $dy$  and  $dz$  were measured together with twist rotation. In total six such systems were used, one situated at the mid-point of each of the column segments on the active frame. Figure 5.13 shows a photograph of the 'free-standing' version of the device used to measure the deformation of the ground floor columns.

Rotations were measured by 'hanging dumb-bell' devices. This measurement system had also been used successfully in the previous study of 2-dimensional frame behaviour [5.4].

The dumb-bells were connected to the frame via a thin strip of spring metal. Measurement of the flexural strains in the spring metal as the frame rotated with respect to the dumb-bell (which maintained its orientation due to gravity), gave a precise and direct measure of the applied rotation. These rotation devices were located at each end of the four primary beams, at the active frame end of the secondary beams and on the major and minor axis of the column at the node points on the active frame - a total of 26 devices. Figure 5.14 shows a photograph of one of the secondary beam rotation devices fixed to the test frame.

### **5.5.2 Force measurement.**

A total of 244 adhesive fixed foil strain gauges was used in each of the frame tests to monitor the longitudinal strains, from which the member forces could be determined. As in the subassemblage tests, a cluster of ten gauges was provided at the mid height of the columns to enable the elastic-plastic response of the frames to be monitored. The merits of this particular strain gauge arrangement are discussed in section 3.3 and reference 5.8. Elsewhere, conventional four gauge clusters, capable of monitoring forces in the elastic range, were used. The precise location of strain gauges on the column and beam members are shown in figures 5.15 and 5.16 respectively.

### **5.5.3 Data logging and experimental control.**

Two Solatron Orion Data Loggers were used to provide the 667 data channels necessary to monitor the frame instrumentation. This comprised 488 channels to energise and record the 244 strain gauges; 26 for monitoring the rotation devices, 24 for monitoring

the applied loads; 63 for measuring bolt forces and 66 devoted to monitoring the displacements measured from the L.V.D.T.'s. Load was applied to the frame via two electric hydraulic pumps. A pair of dedicated servo-control amplifier units controlled the pressures, and hence loads, applied to the individual loading rams and monitored the safety feedback signals. Both the data loggers and the amplifier units were controlled directly from a remote minicomputer. Via the computer, it was therefore possible to specify an applied loading, initiate scanning of the instrumentation and view the recorded data. Figure 5.17 shows a schematic arrangement of the experimental set-up.

After a load increment had been applied to the frame, it was probable that the hanging dumb-bell rotation devices described in section 5.5.1, would tend to oscillate about the vertical gravity reference datum. To improve the accuracy of measurement, 50 consecutive scans were taken for each rotation device and the average value used. The interval between scans was specifically chosen as 0.4 seconds being approximately one half of the 0.8 seconds natural period of dumb-bell oscillation. At this interval, the alternating positive and negative errors in the measurement of the true rotation were approximately equal and therefore tended to cancel out when the readings were averaged, as indicated in figure 5.18.

#### **5.5.4 Processing of recorded data.**

The 'raw' data recorded in the test was processed on a Prime mainframe computer using a suite of purpose written FORTRAN programs. The processing software essentially converted the measured strains and gross displacements into member forces and net deflections. One important feature of the software was the calculation of the column axial forces from the applied loads and elastic shears resulting from the distribution of beam bending moments. This supplemented the direct measurement of axial force from the

column strain gauges which tended to become rather erratic as the column approached failure.

## **5.6 Test frame F1 - test parameters and experimental observations.**

Figure 5.19 shows an elevation and sections through the test frame indicating the nomenclature adopted for the members of frame F1. It should be noted that the different column segments have been identified with reference to the grid labels at the different frame levels. For example, C5/0-1 is the segment of column C5 between levels 0 and 1 - i.e. the ground floor column.

### **5.6.1 Selection of the loading configuration.**

As discussed previously, the basic sequence of loading was to apply the beam loads in increments up to a predefined limit and then, with the beam loads held constant, the columns were loaded to failure individually. It is evident therefore that the selected pattern of beam loading would have a significant effect on the behaviour of the columns during the second stage of the test.

One feature of particular interest was the behaviour of the second storey segment of column C5 as failure approached. A 'chequer-board' pattern of beam loads, representing an extreme distribution of minimum dead and maximum dead plus live loading, was therefore adopted, as shown in figure 5.20. It was intended that the more onerous



distribution of moments would cause the second storey segment to become more critical than the first storey despite the reduced axial loading. The proposed arrangement of beam loads would induce a positive disturbing moment at both the upper and lower ends of the second storey column. This was intended to clarify whether the reversal of moment associated with columns disturbed by end moments would occur at the upper end of the column, at the lower end or at both locations simultaneously.

Relatively large loads were applied to the secondary beams to induce significant major axis moments into the columns. The exceptions were beam SB1, which would remain unloaded due to the limited number of loading devices available, and beam SB5, in which a reduced load was necessary to limit the axial load applied to the first storey segment of column C5.

### **5.6.2 Measurement of initial frame deformations.**

The congestion of instrumentation and loading devices around the frame prevented the direct measurement of the initial column deformations. The major and minor axis column alignments were therefore measured by carrying out a detailed 'offset survey' using a theodolite. A summary of the measured initial column deformations of frame F1 is presented in figure 5.21.

### **5.6.3 Experimental test procedure and observations.**

Frame test F1 was carried out on 12 April 1990 in the Structures Test Hall at the Building Research Establishment.

Before applying any load to the frame, a series of four 'zero scans' were taken. The first zero scan was taken with the loading pumps switched off; the second with the pumps switched on; the third was with loading jacks advanced and the fourth was with the jacks taking up the slack in the loading cables. The beams were loaded first in 14 equal increments. However, after the first increment of loading, it became apparent that there was a malfunction with the loading rams to the secondary beam SB5. It should be noted that it had been the intention to limit the load applied to this particular beam to reduce the total axial load in the lower column segment C5/0-1. It was decided therefore that the application of this load was not crucial and that the test should proceed with the load to this beam removed. Table 5.1 summarises the total beam loads which were applied.

Load increment 14 represented the end of the beam loading phase. At this stage however the oscillation of applied load to secondary beam SB4, which had been evident throughout the test, began to worsen. In an attempt to correct the oscillation by modifying the input signal, a large instantaneous load was inadvertently applied to the beam. This resulted in a dramatic lateral-torsional failure of the beam with a large vertical deformation and twist rotation at the loading point. The load to this particular beam was immediately removed. An initial appraisal of the situation revealed that the effect of this localised member failure had not significantly affected the remainder of the frame. This was later confirmed in the subsequent analysis of the recorded data.

With the applied load on all four of the primary beams and three of the secondary beams held constant, the test continued to fail the columns. The columns were to be failed in sequence, rather than simultaneously, commencing with the centre column C5. The column loading was displacement controlled and was applied by specifying a required column shortening, typically in increments of 0.5mm. At the end of loading increment number 30, the column had been shortened by a total of 9.5mm, equivalent to an applied column head loading of 485.4 kN.

It was evident from the on-line processed force and deformation data that, at this incre-

ment, the centre segment of column C5 had very little residual stiffness and was therefore very close to failure. This was verified by the prominent bow observed in the column. On applying the next increment of column shortening, the hydraulic pumps, which maintained the applied load to both beams and columns, 'tripped out'. This caused all the applied loading to revert to zero and effectively brought a premature end to the testing of column C5. Subsequent analysis of the results showed that, as expected, the column was indeed very close to failure and that it was unlikely that further increments of shortening would have resulted in an appreciable increase in the supported load.

Having isolated the problem with the feedback signal to the hydraulic pumps, the beams were re-loaded to their pre-failure load configuration. Increments of axial shortening were then applied to column C6. The maximum applied column head load of 548.0 kN was achieved when the total applied column shortening was 9.5mm. The loading stage of the test was terminated when the total applied shortening was 10.0mm. It was evident from the large outward bow that in this instance, the lower section of column C6 had failed. The frame was unloaded by removing the column head load first, in two large increments, followed by the beam loads, again in two large increments. The frame test had commenced at 09.00 hrs. and was concluded at 23.15 hrs., a duration in excess of 14 hours.

## **5.7 Frame test F1 - Presentation and discussion of results.**

The results of the first frame test are presented and appraised in the following sections. For clarity, the frame behaviour at the three main stages in the test, i.e. at the end of beam loading, at the failure of column C5 and at the failure of column C6, are described separately. The reader should also refer to chapter 6, where the measured moment-rotation responses of the connections in the frame test are compared with the behaviour

measured from isolated connection tests, and also to chapter 8 in which the capacity of the frame is compared to various design predictions.

### 5.7.1 The beam loading phase.

Figure 5.22 shows the computer generated bending moment diagrams for the frame at the end of the beam loading phase. It should be noted that the beam support moments are the values computed at the face of the column. Throughout this appraisal of frame data a consistent bending moment sign convention has been adopted with the moment drawn on the tension side of the member. Examination of the diagrams show that they are markedly different from those which correspond to moment distributions for simply supported beams. It can be concluded therefore that the stiffness characteristics of the connection had a significant influence on the distribution of bending moments and consequently on the member deflections.

At the centre column, C5, the primary beams were connected to both sides of the column web. Recent studies of isolated connection behaviour have shown that this particular arrangement produces the stiffest moment rotation response for a given connection type [5.9]. This was confirmed by the relatively large maximum moment (48.9 kNm) attracted to the connection ( $M_{px}$  beam = 72 kNm).

It would appear from the bending moment diagram that the columns in the upper storey, C5/2-3, behaved as expected with zero moment at the juncture between the horizontal bracing member and the column heads. The approximately equal proportions with which the out of balance end moments from beams PB5 and PB6 were distributed between the upper and lower columns suggests that the stiffness of the third storey column segment was indeed representative of a full height column in double curvature.

A complete appraisal of the frame deflections observed during the beam loading phase is presented in chapter 8 in which frame test data is used to validate a deflection prediction technique developed by the author.

### 5.7.2 Loading of column C5.

Figure 5.23 shows the computer generated bending moment diagrams for the frame at the point of maximum load on column C5. It should be noted that there was zero load applied to beam SB4. However, due to the accidental failure of this particular beam and the resulting high plastic strains, the gauges on the member still recorded a net strain, thereby indicating a 'non-existent' moment.

Figure 5.24 shows the major and minor axis moments at the centre of column segments C5/0-1 and C5/1-2 plotted against the respective axial loads. It is evident from this plot that the minor axis of the second storey segment, C5/1- 2, shows the characteristic progressive loss of stiffness associated with columns subjected to initial disturbing moments. However, as the second storey segment reached the failure load the lower segment, C5/0-1, failed exhibiting a sudden loss of stiffness. This is illustrated more clearly in figure 5.25 which shows the same column bending moments plotted against the applied column load - which is common to both column segments. Prior to failure, the bending moments in the lower segment remained relatively constant during head loading phase. This suggested that the applied axial load was being resisted by direct axial compression and was not inducing member flexure associated with buckling. Figures 5.26 and 5.27 show plots of the mid- column deflections and twist rotations for the two column segments. The bifurcation type failure of the lower segment, which resulted from the lack of initial column deformation, a negligible major axis disturbing moment and the high degree of rotational restraint at head and base, explains the very high axial load capacity which

was observed.

It is considered that the simultaneous failure of the two column segments was not coincidental, but that the excessive deformation of the segment C5/1-2 as the ultimate capacity was approached initiated the failure of the lower segment. Such interaction between column segments at the point of failure has been observed in previous frame tests [5.1].

Figures 5.28 and 5.29 show plots of the minor and major axis moments at the top, mid-point and bottom of column segment C5/1-2. The corresponding data is presented in figures 5.30 and 5.31 for the lower column segment, C5/0-1. The minor axis plots for column C5/1-2 show that the moments at the top and bottom of the column segment were of the opposite sign (adopting the sign convention introduced in section 5.7.1) and therefore differed from the single curvature bending predicted for this particular column from consideration of the primary bending moments (figure 5.20). This discrepancy was due to the observed frame moments being a combination a small single curvature primary moment combined and a larger double curvature secondary moment resulting from column deformations.

It is evident from the plots of minor axis moment that the failure of the column caused the bending moment at the bottom of segment C5/1-2 to reverse whilst those at the top continued to increase in the same direction as the initial disturbing moment. The plots in figure 5.29 show that, unlike the minor axis, the major axis column moments remain relatively constant after application of the beam loads. Only when the failure load has been reached, at which point the column has negligible stiffness and therefore experiences large deformations, are there significant changes in the magnitude of the major axis moments.

The minor axis moments at the top, middle and bottom of column segment C5/0-1 (figure 5.30), show the sudden failure of the segment as discussed above. It would appear

however that at a load in this column of approximately 650kN, the minor axis moment at the base of the column segment begins to increase rapidly. This level of load corresponds with the large increase in the major axis moment at the base shown in figure 5.31. Up to the point of failure, the moments about both major and minor axes at the mid point of the column are relatively small. This would therefore suggest that the local capacity of the section at the base dictated the ultimate capacity of column segment C5/0-1. It is quite probable that this local failure was initiated by the increased residual stresses resulting from the welded fabrication of the fixed column base detail.

Figure 5.32 shows a plot of the in-plane connection moment of the secondary beam SB2, which was connected to the major axis of column C5, plotted against the axial load in column segment C5/1-2. The plot shows that a large proportion of the disturbing connection moment diminishes during the second phase of the loading sequence. This compares with figures 5.33 and 5.34 which show plots of axial load against the primary beam major axis moments at the connection with the minor axis of the centre column, C5. It is evident that in this instance, there is only a very small redistribution of the connection bending moments, particularly in the case of beams PB5 and PB6. The significance of this reduced beam to column interaction resulting from beam continuity, the surprising effect on the moment rotation characteristics of the connection and the implications for semi-rigid design are considered in detail in chapter 6 of the thesis.

### **5.7.3 Loading of column C6.**

It should be noted that all the data plots presented in this section have been edited to remove the re-loading of the beams resulting from the hydraulic pump failure which followed the test of column C5 (section 5.6.3). As a result, some of the plots indicate a slight discontinuity in the data at the end of the beam loading phase.

Figure 5.35 shows the computer generated bending moment diagrams for the frame at the point of maximum load on column C6. Figure 5.36 shows the major and minor axis bending moments at the centre of column segments C6/0-1 and C6/1-2 plotted against the corresponding axial column loadings. It is evident that unlike column C5, the minor axis of the lower column segment C6/0-1 experiences the progressive loss of stiffness associated with initially deformed columns. This is despite the anticipated increased capacity of this segment due to the close proximity of the rotation and warping restraint at the column base. The minor axis moment at the centre of the upper column, C6/1-2, remained relatively constant during the second stage of the test diminishing as the ultimate capacity of the lower segment was approached. However, the plateau on the plot of minor axis moment at the centre of segment C6/1-2 is not an indication of failure. Clearly, the summation of the co-existent components of axial load, minor and major axis moments is not sufficiently large to cause excessive yielding across the section. The plateau is a result of the continuing transfer of moment and node rotation from the lower column C6/0-1 in conjunction with the 'cut-off' in applied load due to the limited capacity of the lower column segment. This is similar to the interaction between column segments at the point of failure observed in column C5 (section 5.7.2). The rather dramatic shift in the magnitudes of bending moments at the point of failure is attributed to strain gauge failure at high levels of strain and is not, therefore, of any great significance.

Figure 5.37 shows the mid-column deflections for segments C6/0-1 and C6/1-2. It is interesting to note that these plots closely follow those of bending moment presented in figure 5.36 thus emphasising the relationship between deflected shape and column bending moment distribution. Despite the significantly reduced mid-column deflections, figure 5.38 shows that the twist rotation at the centre of column segment C6/1-2 was larger than that of the lower segment. Obviously, the small twist rotation of the lower column segment C6/0-1 was influenced by the high torsional restraint from the 'fixed' column base connection.



The minor and major axis bending moments at the top, middle and base of column segment C6/1-2 are shown in figures 5.39 and 5.40 respectively. The same data is presented for segment C6/0-1 in figures 5.41 and 5.42. It is evident that in the case of segment C6/1-2, the bending moment distribution is typical of that of a member in double curvature with the end moments approximately equal but of opposite sign, and with a very small moment at the column centre. The lack of redistribution of moment within this particular column segment during the second phase of loading is to be expected in view of the negligible column deformations which were observed (figure 5.37).

Surprisingly, the plot of minor axis moments for segment C6/0-1 in figure 5.41 shows that at the end of the beam loading phase, the column was in single curvature bending with positive moments at the top, mid-point and base of the column. Due to the relatively small disturbing moment from primary beam PB8, the minor axis column moments were very small. However, it is interesting to note that a simultaneous reversal of moment occurred at both the top and base of the column segment whilst the mid-point moment continually increased. As was observed in the test of column C5, the minor axis base moment increased rapidly, following reversal, during the later stages of the test. This tends to substantiate the explanation presented previously for column C5 regarding the effect of the increased residual stresses in the region of the base-plate connection on the local capacity of the column.

The major axis connection moments for secondary beams SB3 and SB6 are plotted against the axial load in column segment C6/1-2 in figure 5.43. The reduction in the initial disturbing moment during the second phase of the test is similar to that observed for beam SB2 during the test of column C5 (figure 5.32). Figure 5.44 shows the major axis moments at the connections of primary beams PB6 and PB8 plotted against the axial load in column C6/1-2. Unlike the primary beam connections to the internal column C5 (figure 5.33), here there is an appreciable change in the applied minor axis moment during the second stage of the test. This is principally due to the absence of beam continuity effects in the case of column C6 and hence a more direct relationship

between column deformation/head rotation and beam connection moment (see section 6.5). As expected, the largest reduction in the disturbing connection moment occurs at beam PB8 which is connected directly to the critical column segment C6/1-2. As expected from the reversal of moment observed at the head of column C6/0-1 (figure 5.41), the moment at the connection of beam PB8 to the same column segment is also seen to reverse.

## **5.8 Test frame F2 - test parameters and experimental observations.**

As discussed previously, the overall dimensions of test frame F2 were similar to those of frame F1. However, in terms of general arrangement and detailing there were two major differences between the two tests:-

1. The columns on the active frame of test F2 (C7, C8 and C9) were orientated such that the primary beams framed into the column flanges and the secondary beams framed into the column web.
2. In view of the very high connection stiffnesses observed in test F1, the thickness of the connection end plate was reduced in test F2 from 12mm to 8mm. However, all other aspects of the connection detail remained the same.

The member and joint nomenclature adopted for frame test F2 is detailed in figure 5.45. It should be noted that the referencing of the members follows a sequence similar to that of frame F1.

### **5.8.1 Selection of the loading configuration.**

Table 5.2 summarises the maximum total beam loads which were applied to frame F2. As in frame test F1, the primary beam loads were applied in a chequer-board pattern to give the most onerous distribution of primary column bending moments. Due to the reduced stiffness of the flush end plate connection and the revised column orientation, the maximum applied beam loads were purposely chosen to be less than those applied in test F1. This was particularly apparent in the case of the secondary beams where the support moments at the connection to the minor axis of the columns on the 'active' frame were expected to be relatively small.

### **5.8.2 Measurement of initial column deformations.**

As in the case of frame F1, an offset theodolite survey was performed to determine the initial major and minor axis deflections of the columns on the 'active' frame. The measured column deformations are summarised in figure 5.46. In view of the large initial deformations which were observed in test F1, particular care was exercised when aligning frame F2 to ensure that the deformations of columns C7 and C8, the columns which would subsequently be tested to failure, were not excessive.

### 5.8.3 Experimental test procedure and observations.

In the first instance, frame test F2 commenced on 12 October 1990. As previously, the beam loads were applied first in equal increments of fixed proportion up to the maximum loads summarised in table 5.2. At the end of the beam loading phase, columns C7 and C8 were to be failed in sequence commencing with the internal column C8. However, when the applied displacement to the head of column C8 was 3.5mm, equivalent to an applied load of 306 kN, a loud bang was heard and all the applied loads were automatically released. It was immediately apparent that one of the Macalloy bars, which was used to apply load to column C8, had failed at a coupling joint. Further investigation revealed that the threaded end of the bar had not been screwed far enough into the female coupler. As a result, the few threads which had engaged 'stripped' at a relatively low bar tension. Although it appeared that the frame had been unaffected by the failure, a number of instrumentation devices were disabled and the loading block at the head of column C8 had sheared its restraining bolts and was precariously balanced on the column head. It was clear that the test could not continue and that the adequacy of all the tendon couplers would have to be checked before any further load could be applied. The test was therefore temporarily postponed.

The re-test of the frame commenced at 09.00 hrs. on 17 October 1990. As in the initial test, the beam loads were applied in equal increments of fixed proportion up to the total loads presented in table 5.2. With the beam loads held constant, displacements were applied to column C8 in 0.5mm increments. When the applied column head displacement was 6.0mm, corresponding to the maximum applied load of 517 kN, a prominent minor axis bow was observed in column segments C8/0-1 and C8/1-2 in the directions shown in figure 5.47. At this increment it was noticed that the applied column head load was slowly decreasing with time ( the column head loading was displacement controlled rather than load controlled). A further two increments were applied, making the total displacement 7.0mm. Over a twelve minute period, the applied 'post- failure' load at

this increment decreased under a constant head displacement from 440 kN to 434 kN. The testing of this column was terminated at this increment of displacement.

With the beam loads held constant and the load applied to column C8 removed, displacements were applied to column C7 in 0.5mm increments. The maximum load applied to the column was 563 kN corresponding to an applied head displacement of 7.5mm. At the point of maximum load a prominent minor axis bow was observed in segments C7/0-1 and C7/1-2 but in this instance, the deformations were in the opposite directions to those observed for column C8 (figure 5.48). Closer examination of the lower column segment, C7/0-1, revealed that a large twist rotation had occurred being most pronounced at mid-height. The test continued until the total applied displacement was 8.0mm, corresponding to a post-failure applied load of 549 kN.

At the end of column loading, the applied displacement to column C7 was removed in four large increments. The beam loads were then removed in fixed proportion in three increments. The test was completed at 16.00hrs. and had therefore lasted almost nine hours.

## **5.9 Test Frame F2 - Presentation and discussion of results.**

This section presents and discusses the measured data obtained from the second frame test. As in the case of frame F1, the behaviour of the frame during the three key stages of the test, i.e. beam loading, loading of column C8 and loading of column C7, have been discussed separately.

### 5.9.1 The beam loading phase.

Figure 5.49 shows the distribution of frame bending moments present at the end of the beam loading stage. It should be noted that in the case of primary beam PB11 an error in the calibration of the feedback load cells resulted in an actual applied load of 76.4 kN - less than the intended nominal load of 83 kN. This is the reason for the slightly reduced depth of the free bending moment diagram for beam PB11 when compared with that of PB10 in which the correct beam loading had been applied.

It is evident that, as in the case of test F1, the stiffness characteristics of the connection had a significant influence on the distribution of moments. However, unlike test F1, the primary beam support moments were similar irrespective of whether the connection was to an external or an internal column. The reactant bending moment diagram for the primary beams was therefore almost horizontal. This can be explained by the increased major axis stiffness of the columns which resulted in a significantly reduced relaxation of the disturbing moment to the external column. In addition, the performance of all of the connections to column major axis was influenced by the deformation of the column flanges irrespective of whether the column was internal or external. This compares with test F1 in which the continuity of the beams connected to the web of the internal column cancelled out the effect of web panel flexibility and thereby produced a very large support moment. The distribution of moments presented in figure 5.49 therefore substantiates the observations discussed in chapter 6 in which the moment-rotation response of a column flange connection was similar for both an isolated cruciform (internal column) and cantilever (external column) test arrangement.

### 5.9.2 The loading of column C8.

Figure 5.50 shows the distribution of bending moments at the point of maximum applied load (517 kN) on column C8. It is clear that whilst the distribution of minor axis bending moments on column C8 confirms the direction of minor axis deflection observed during the test (figure 5.47) the major axis column moments show negligible change from those present at the end of the beam loading phase.

Figure 5.51 shows the major and minor axis bending moments at the centre of column segments C8/0-1 and C8/1-2 plotted against the respective axial loads. The dramatic shift in the major axis moment in segment C8/0-1 is not an indication of major axis failure, but is in fact due to the 'loss' of a number of strain gauges resulting from very high plastic strains as the column deformed about its minor axis. This is illustrated in figure 5.52 which shows the mid-column major and minor axis deflections for the two column segments. The large distance between the data points on the minor axis plot for column C8/0-1 at the point of maximum load clearly shows the negligible minor axis axial stiffness of the lower column segment and the dominance of the minor axis failure. Conversely, the 'near vertical' nature of the major axis deflection plot and the very small deflection at the point of maximum load clearly demonstrate the high resistance of the column to major axis failure.

The mid-column minor axis deflections for the two column segments, C8/0-1 and C8/1-2, have been plotted against the applied column head load (figure 5.53) which, unlike the axial column load used in figure 5.52, is the same for the two segments at any load increment. This particular diagram shows that whilst the load deflection characteristics for the two segments are similar below an applied load of 420 kN, above this load level the axial stiffness of the lower segment, C8/0-1, decreases rapidly. It is clear that it is this lower segment which fails and therefore controls the capacity of the column. As was discussed in section 5.7.3, the peak load and subsequent load reduction observed for the upper column C8/1-2 is not necessarily an indication of the failure of that column

segment, but is simply a characteristic of the 'cut-off' load and interaction between column segments tested in series. The twist rotations observed at the centre of the two column segments are plotted against the axial column loads in figure 5.54.

Figures 5.55 and 5.56 show the minor and major axis moments at the top, mid-point and bottom of column segment C8/1-2. It is interesting to note that in this instance there is a reversal of both the major and minor axis moments at the top of the column segment. Corresponding data is presented in figures 5.57 and 5.58 for the lower column segment C8/0-1.

The secondary and primary beam support moments at the connection with column C8 are plotted against axial load in figures 5.59 and 5.60 respectively. In the case of figure 5.59, it is clear that when the column head loading is applied, the connection to beam BS11 continues to 'close' causing an increase in the connection moment whilst that to beam BS8 starts to 'open' resulting in a reversal of moment. This response is commensurate with the observed shape of the minor axis of the column shown in figure 5.47 in which the mid-height of the two column segments deflected in opposite directions.

### 5.9.3 The loading of column C7.

The distribution of bending moments on column C7 at a load just below the ultimate capacity is shown in figure 5.61. The diagram clearly shows the minor axis failure of the lower column segment C7/0-1 and is in agreement with the observed deformed shape of the column shown in figure 5.48.

Figure 5.62 shows the major and minor axis bending moments at the centre of the two column segments plotted against their respective axial loads. As before, the dramatic shift in the major axis moment at the point of ultimate load is due to the inability of



the system to measure and convert the large strains from the limited number of gauges at mid-height and is not therefore representative of the actual column response. The failure criteria of the column is better illustrated in figure 5.63 which shows a plot of the mid-column major and minor axis deflections. It is clear from this diagram that, as in the case of column C8, it is the minor axis response of the lower segment, C7/0-1, which dictated the maximum applied load. The rapid increase in the minor axis deflection at a load of 475kN suggests that there was a corresponding reduction in the axial stiffness of the column at this load increment. In addition figure 5.64 shows that at this stage in the test, the twist rotation at the centre of the lower segment increased rapidly. Without doubt, these sudden changes in the load- deflection response are a result of the spread of plasticity across the column section. Depending on the nature of the initial residual stresses, this spread of yield can be rapid and relatively erratic.

Figures 5.65 and 5.66 show the minor and major axis moments at the top, mid- point and bottom of column segment C7/1-2. As discussed above, the plateaux portions of the minor axis plots are not necessarily an indication of failure of the segment. The increased minor axis moments in the latter stages of the test are a result of the moments, and deformation, induced by the failure of the lower column segment. The corresponding data for the lower column segment, C7/0-1, is plotted in figures 5.67 and 5.68. Here it is evident that during the initial stages of the column head loading phase, the minor axis moments at the top and bottom of the column segment reverse sign. However, when the axial load in the column was 475kN - the load at which twist rotation at the centre increased rapidly - the minor axis moment at the base changes sign once more. This corresponds with the load increment at which the column base major axis moment begins to reverse sign.

At first sight the double reversal of moment at the base of column C7/0-1 appears to be rather an unusual response. However it is simply an illustration of the relative dominance of primary disturbing moments from the beam connection and secondary moments arising from column deformation. In the initial stages of column head loading, the base

moment reduces at a similar rate to the disturbing moment applied at the head of the column segment. Due to the combination of the net column deflection with the initial column deformation, which was in the opposite direction to the direction of failure, the absolute displacement of the column is negligible. Consequently, the secondary moments arising from the axial load acting through a column eccentricity are also negligible - the primary moments therefore dominated. However, when the axial load was 475kN the observed increase in the lateral deformations caused a corresponding increase in the size of the secondary column moments. These effectively 'swamped' the reductions in the primary moments and changed the direction of base moment to one which was compatible with a large deformation at the mid-height of the column. It is clear that the non-symmetric loading and restraint conditions on this 'corner' column had a significant effect on the behaviour. Unlike the 'internal' column C8, it appears that, in this instance, the presence of relatively large disturbing moments has resulted in a lateral-torsional plastic failure of the column segment.

## **5.10 Summary of the observed column failure loads.**

Table 5.3 presents a summary of the column moments at the end of the beam loading stages and the measured ultimate capacities of columns from both the frame tests. Due to the different loading arrangements and connection types which were used, it is difficult to make a direct comparison between the behaviour of columns in test F1 (C5 and C6) with those from test F2 (C7 and C8). However, there are a number of interesting features which can be identified. Firstly, the non-dimensionalised failure loads show that despite the relatively large minor axis slendernesses, the columns failed at loads reasonably close to the squash load. The lowest failure load occurred in segment C5/1-2 in which the total column restraint was less than that of the other 'failed' columns, all of

which had fixed base connections. Despite the significant difference between the bending moment patterns in frame F1 and F2, it is interesting to note that the failure loads of the corresponding columns in the two tests were reasonably similar.

As expected, the lower column segment C7/0-1 failed at a lower load than the other frame test F2 column, C8/0-1, due to the increased minor axis disturbing moments from the beams. It must be remembered that each of these columns had the same single beam minor axis restraint at the first floor level. However, although column segment C5/0-1 was subjected to significantly larger minor axis disturbing moments than the other frame F1 column, C6/0-1, in this instance the column failed at a larger load. This is of course due to the increased minor axis restraint to the 'internal' column (C5) of frame test F1 from a pair of primary beam connections as opposed to the single beam minor axis restraint to the 'external' column (C6).

A significant part of the research project was devoted to the preparation of the two complex full scale frame tests and the subsequent acquisition of a large amount of experimental data. Unfortunately, this meant that the time available for analysing and appraising the data was limited, particularly in the case of the second frame test F2. The experimental data which has been presented in this chapter, chapter 6 (moment-rotation behaviour) and that in chapter 8 (frame deflection) considers only the basic response parameters. It is clear however that in view of the large amount of data which was collected, there remain a number of other more detailed aspects of frame response which need to be investigated. There are at present plans for others at the University of Sheffield to extend the appraisal which has been conducted by the author.

## **5.11 Concluding comments on the full-scale frame tests.**

- 1. Two full-scale frame tests have been conducted at the Building Research Establishment. Analysis of the recorded data has shown that the moment-rotation characteristics of the connections used had a significant influence on the distribution of frame forces and deflections.**
- 2. The high column failure loads and the minor axis moment reversal which has been observed clearly illustrate the benefit of connection restraint on column capacity.**
- 3. The significant difference between the distributions of bending moments observed in test F1 and F2 clearly substantiates the differences which have been observed in 'isolated' connection tests on the behaviour of connections to a column flange and those to a column web.**
- 4. It is evident that at the point of ultimate load there is interaction between adjacent segments in a series of columns.**
- 5. In one particular instance, it has been shown how the large thermal residual stresses present at a substantial welded base plate connection influenced the failure of a column segment.**

## References.

- 5.1 Wood, R.H., Needham, F.H. and Smith, R.F., '*Tests on a multi-storey rigid steel frame*', The Structural Engineer, Vol. 46, No. 4, April 1968, pp. 107-120.
- 5.2 Baker, J.F., '*An investigation of the stress distribution in the steel framework of a modern hotel building*', Final report of the Steel Structures Research Committee, H.M.S.O., London, 1936, pp. 8-139.
- 5.3 Weeks, G., '*Laboratory testing of large structures*', I.A.T.R.L.M.S., Methodology and testing of structures No. 3 - Tests on full-scale structures, International Colloquium, Rilem, Bucharest, 1969, pp. 204-222.
- 5.4 Davison, J.B., '*Strength of beam-columns in flexibly connected steel frames*', Ph.D. Thesis, Department of Civil and Structural Engineering, University of Sheffield, U.K., June 1987.
- 5.5 Jenkins, W.M., '*Local failures in steelwork structures.*', research report F3/2/256 No.2, Division of Civil Engineering, Hatfield Polytechnic, U.K., March 1984, pp.1-60.
- 5.6 Gibbons, C., '*The strength of biaxially loaded beam-columns in flexibly connected steel frames - Volume 2: A survey of the mechanical and geometric properties of structural steel sections*', Ph.D. thesis, Department of Civil and Structural Engineering, University of Sheffield, Dec. 1990.
- 5.7 Gibbons, C., Kirby P.A. and Nethercot D.A., '*The development of a device for measuring the 3-dimensional deformation of steel columns.*', Journ. Strain Analysis. (to be published)
- 5.8 Gibbons, C., Kirby P.A. and Nethercot D.A., '*The experimental assessment of force components within thin walled structural steel members*', Journ. Strain Analysis. (to be published)
- 5.9 Davison, J.B., Kirby, P.A. and Nethercot, D.A., '*Rotational stiffness characteristics of steel beam-to-column connections*', Journ. Construct. Steel Research, No.8, 1987, pp. 17-54.

Primary beam reference	Total beam load (kN)	Secondary beam reference	Total beam load (kN)
PB5	69	SB1	-
PB6	139	SB2	101
PB7	138	SB3	96
PB8	70	SB4	98
		SB5	0
		SB6	101

Table 5.1: Total loads applied to the beams in test F1.

Primary beam reference	Total beam load (kN)	Secondary beam reference	Total beam load (kN)
PB9	131	SB7	-
PB10	84	SB8	62
PB11	76	SB9	69
PB12	132	SB10	63
		SB11	20
		SB12	65

Table 5.2: Total loads applied to the beams in test F2.

Summary of column failure loads observed in the frame tests.					
Column ref.	Minor axis moments top/bottom (kN.m)	Major axis moments top/bottom (kN.m)	Maximum axial load $P_{max}$ (kN)	$\frac{P_{max}}{P_{squash}}$	Notes on failure mode.
C5/1-2	-1.7 3.4	14.7 6.2	660	0.69	minor axis failure with modest twist.
C5/0-1	5.2 -2.7	2.1 0.3	779	0.82	Bifurcation type failure of minor axis including a local failure at column base.
C6/1-2	15.1 9.8	15.8 14.6	675	-	n/a
C6/0-1	1.8 0.6	8.8 3.9	756	0.81	minor axis failure with negligible twist
C7/1-2	1.5 4.2	18.5 12.3	626	-	n/a
C7/0-1	5.1 3.4	9.5 8.2	698	0.75	minor axis failure with very large twist
C8/1-2	6.6 5.0	1.1 2.7	659	-	n/a
C8/0-1	2.0 0.5	6.1 4.2	776	0.83	minor axis failure with small twist.

Table 5.3: Summary of the column bending moments at the end of the beam loading phase and the ultimate capacities measured in frame tests F1 and F2.

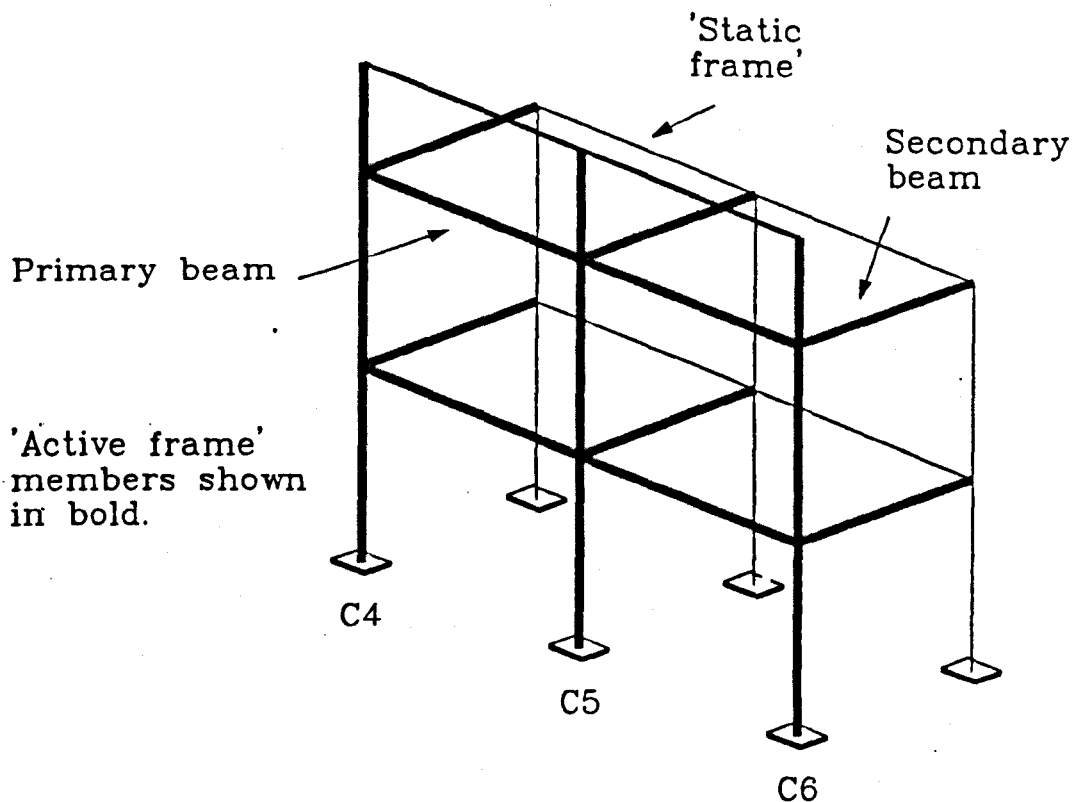


Figure 5.1: Isometric view indicating the 'active' and 'static' parts of the test frame.

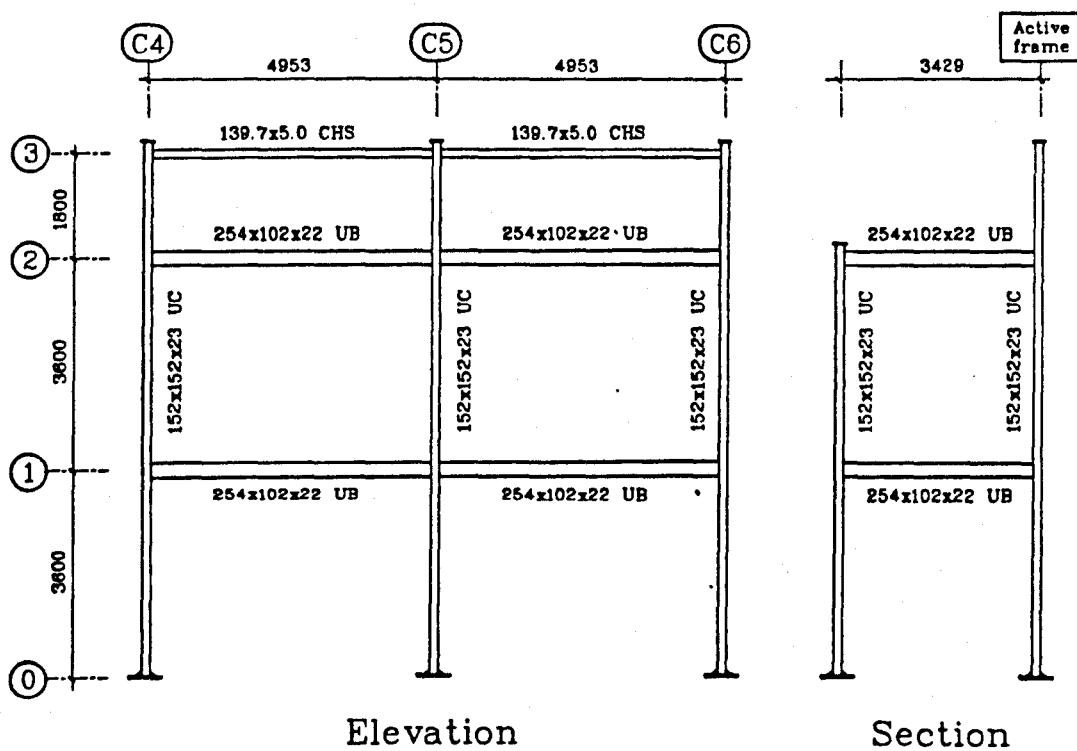
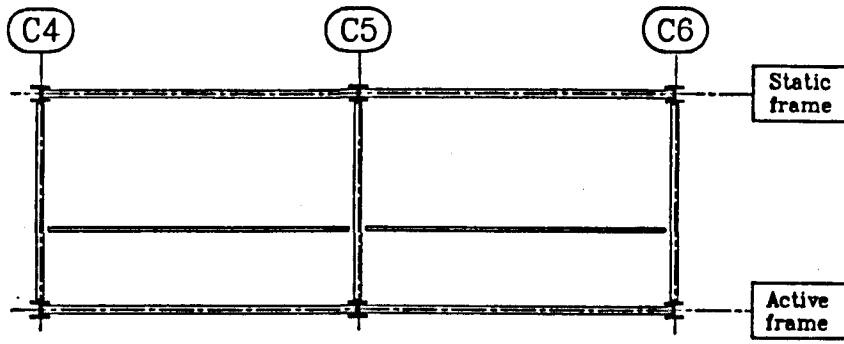
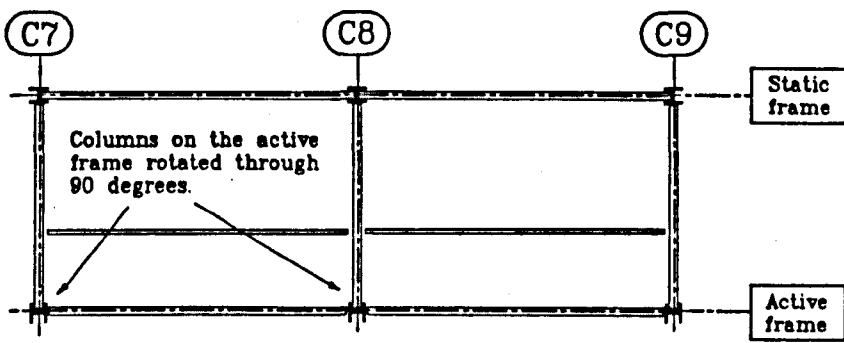


Figure 5.2: General arrangement of test frame F1, (F2 similar).





Frame F1



Frame F2

Figure 5.3: Plan views indicating the different column orientations adopted for frame test F1 and F2.



Figure 5.4: Photograph of test frame F1 prior to testing (active frame at rear).

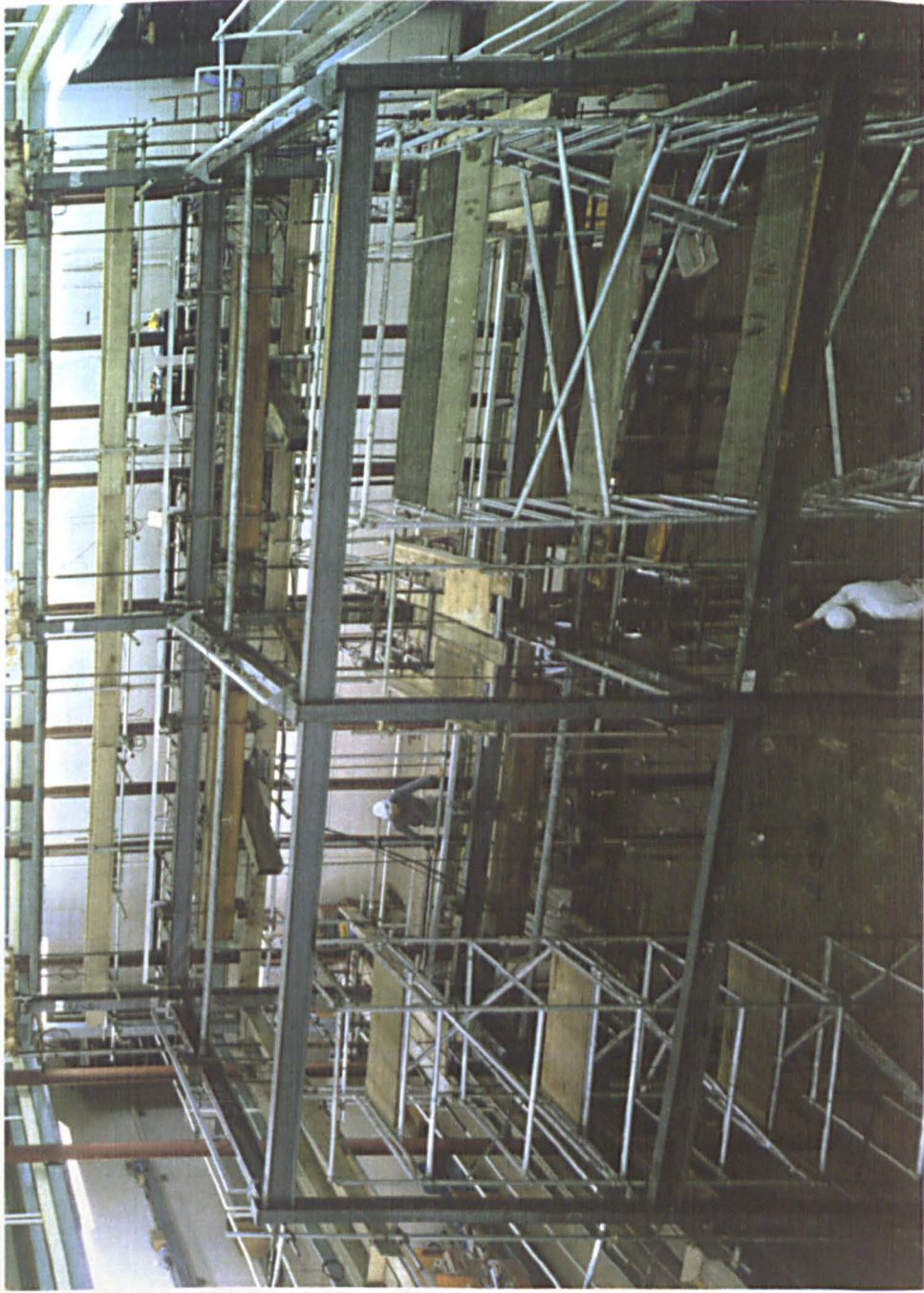


Figure 5.5: Photograph of test frame F1 prior to testing.

Figure 5.7: Typical "in bar" used to prevent column work.

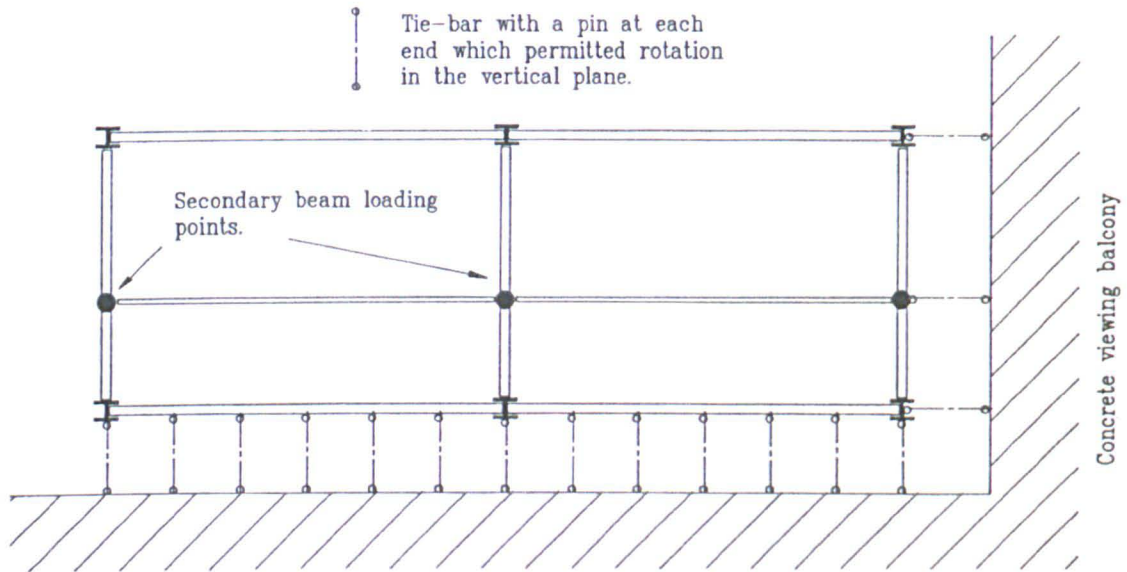


Figure 5.6: Typical plan view of frame indicating the position of restraint bars.

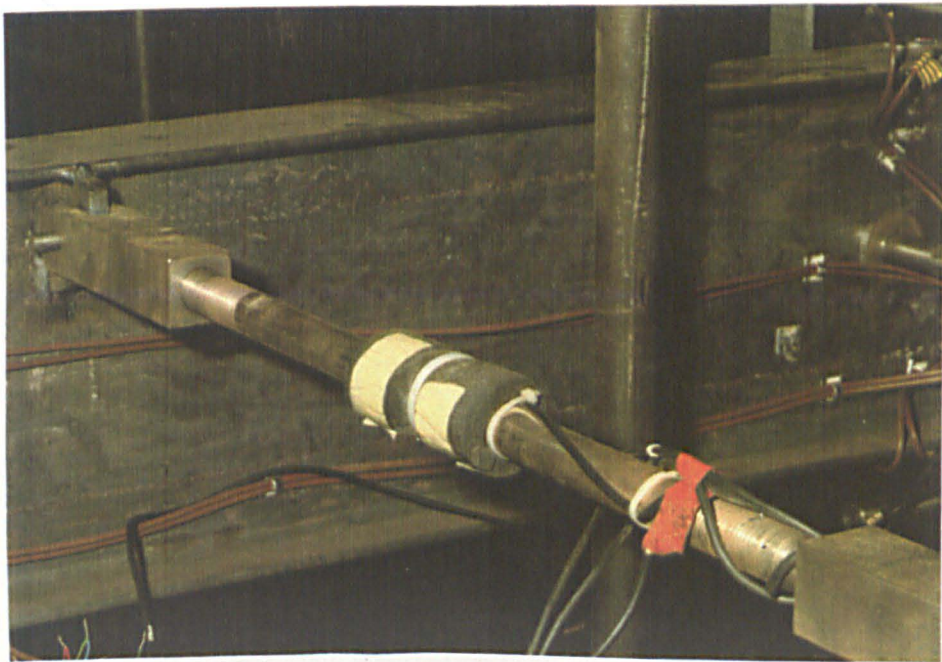


Figure 5.7: Typical 'tie bar' used to prevent column sway.

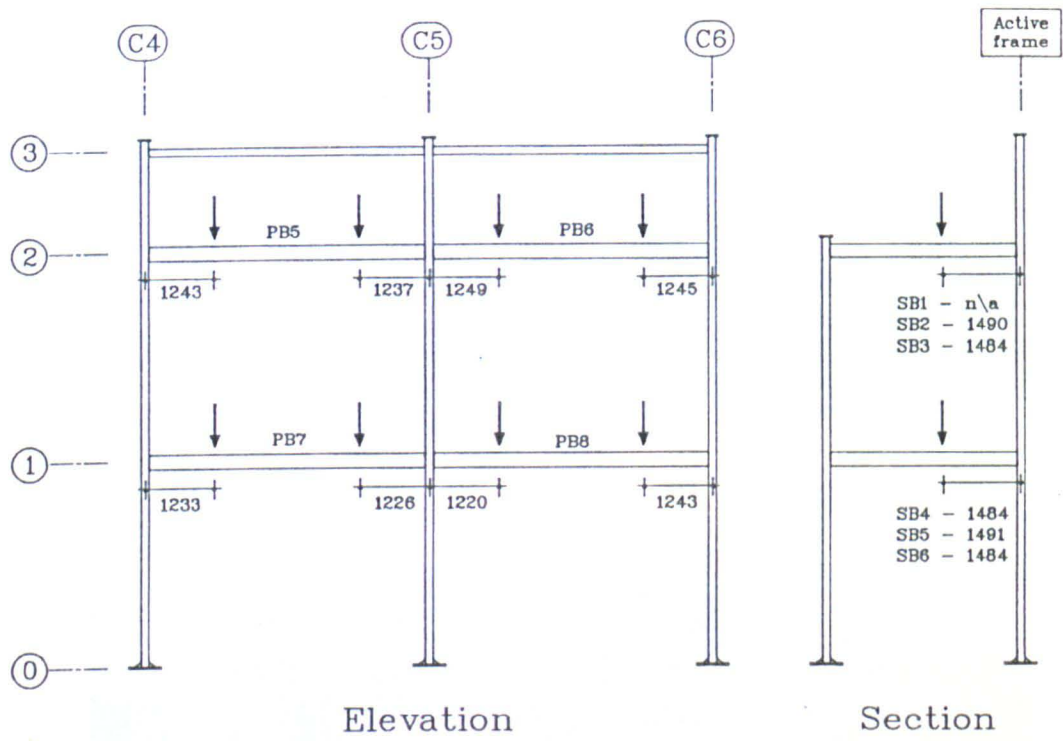


Figure 5.8: Elevation and section through the frame illustrating the location of the beam loading points.



Figure 5.9 : View of the hydraulic loading rams housed in the basement beneath the test area.

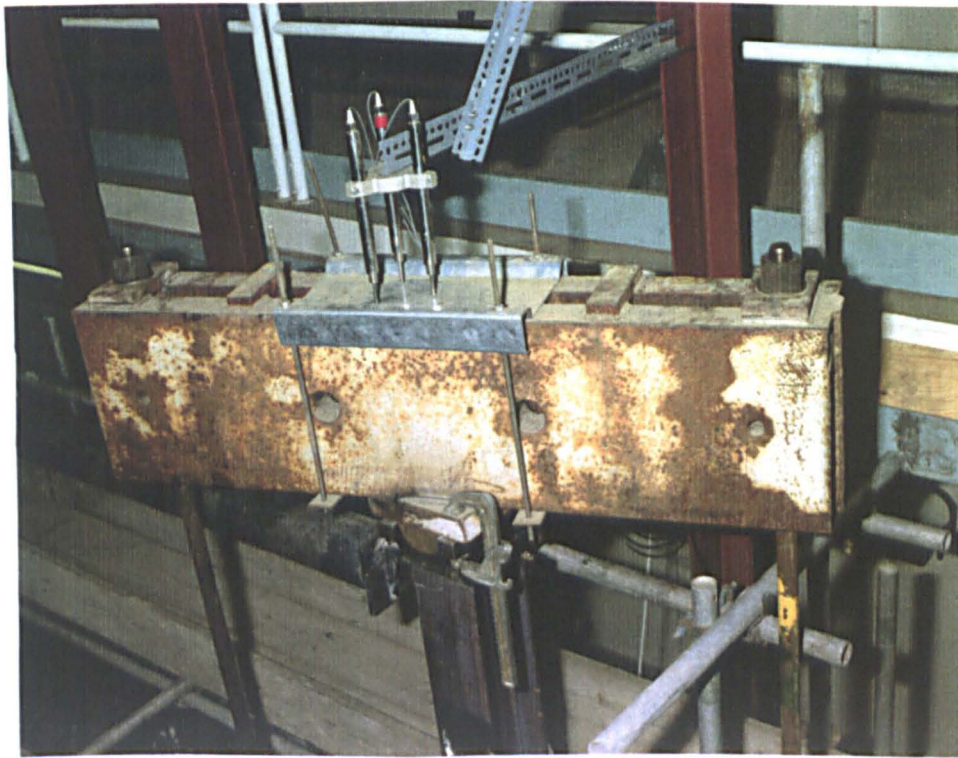
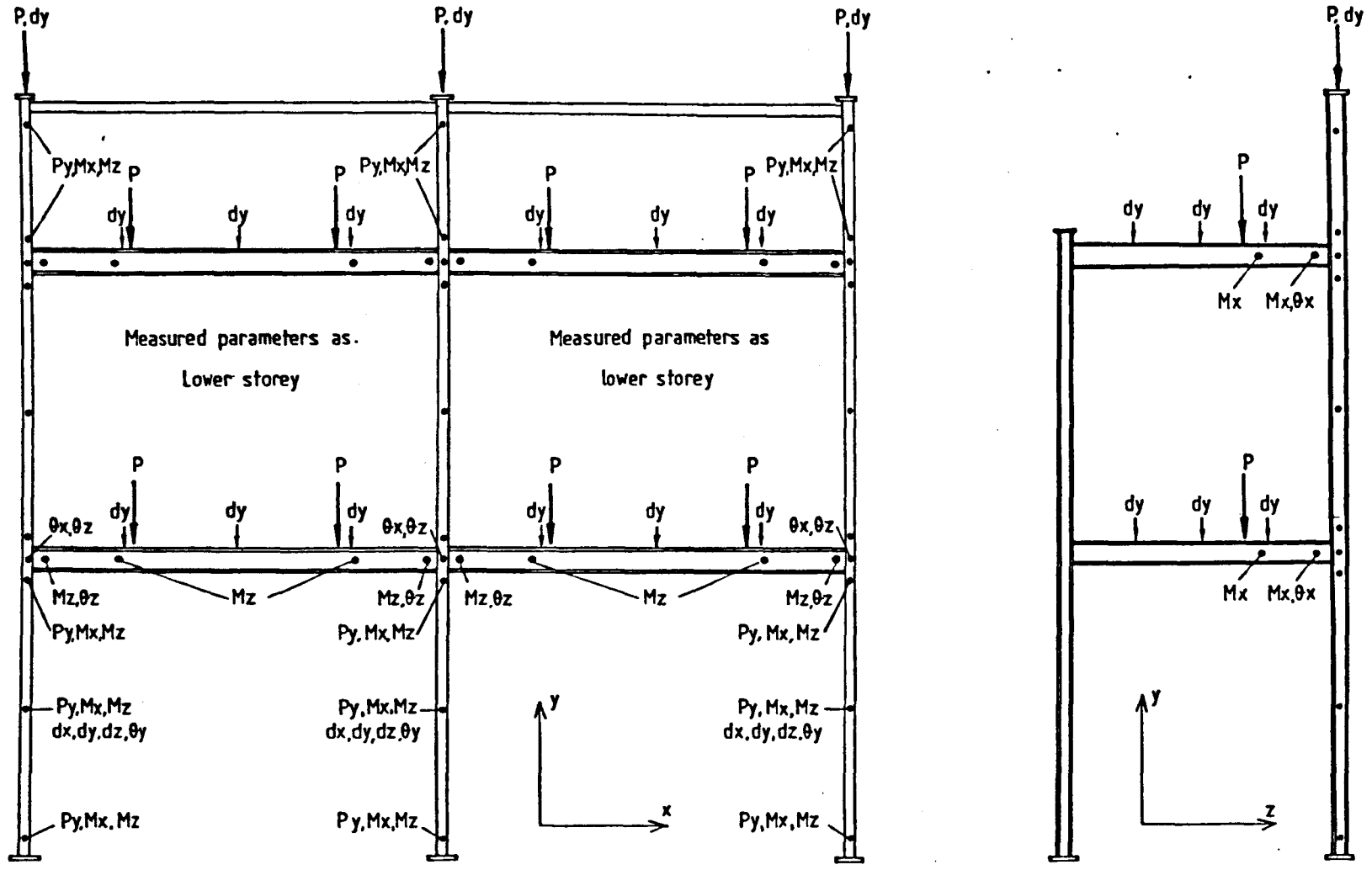


Figure 5.10: Arrangement used to apply load at the column head.



Figure 5.11: Summary of the various force and deformation components which were measured.

Figure 5.11: Summary of the various force and deformation components which were measured.



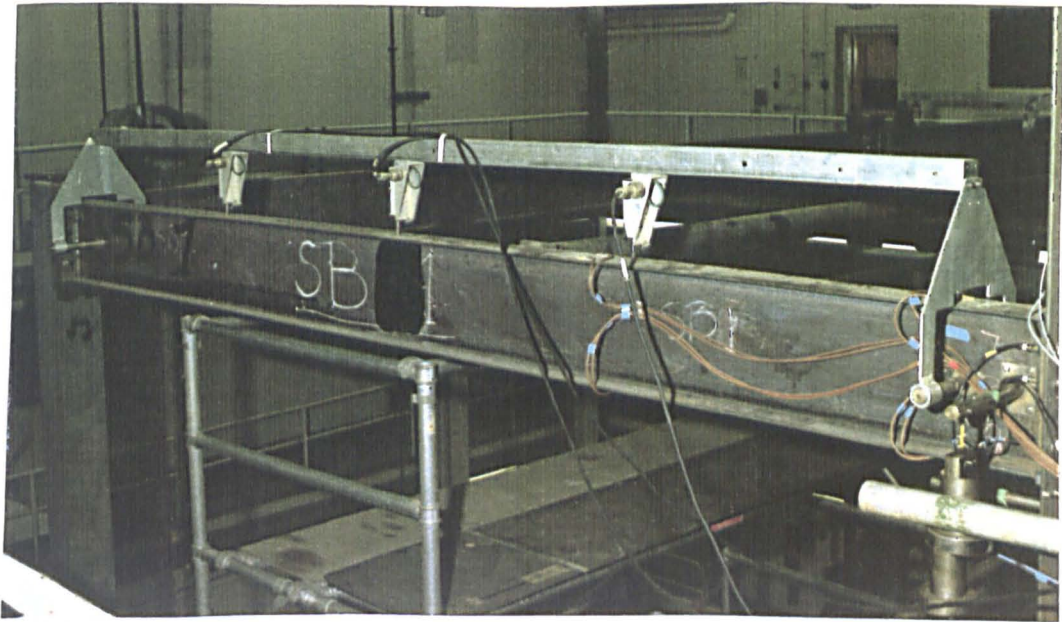


Figure 5.12: System used to monitor beam deflection.



Figure 5.13: Three-dimensional measurement device used to monitor the deformations at the column centre.



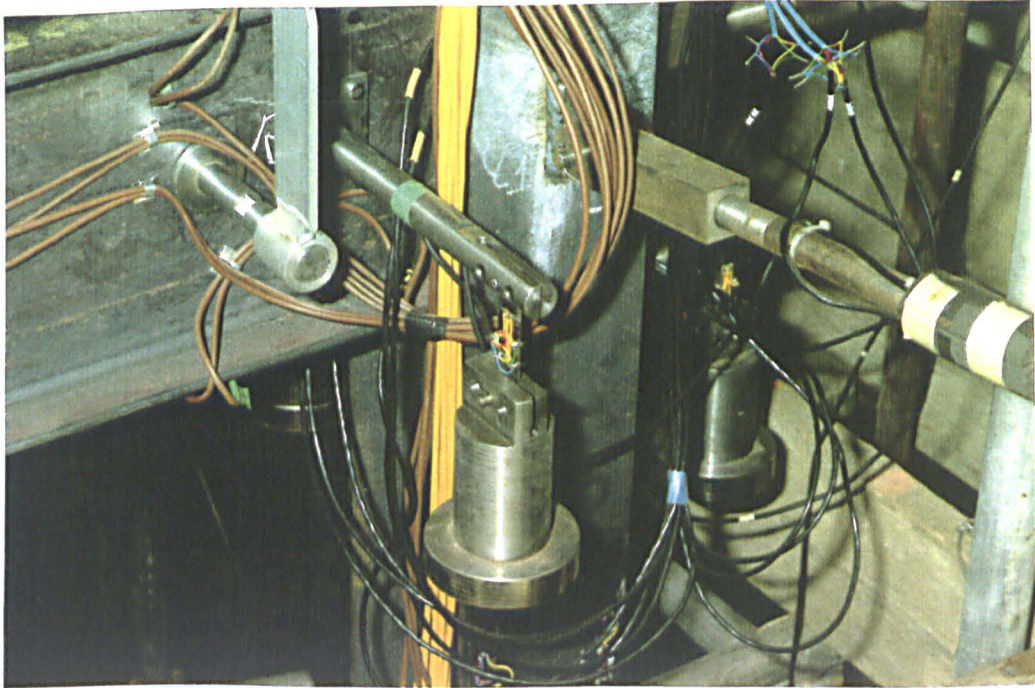


Figure 5.14: The 'hanging dumb-bell' rotation measurement device.

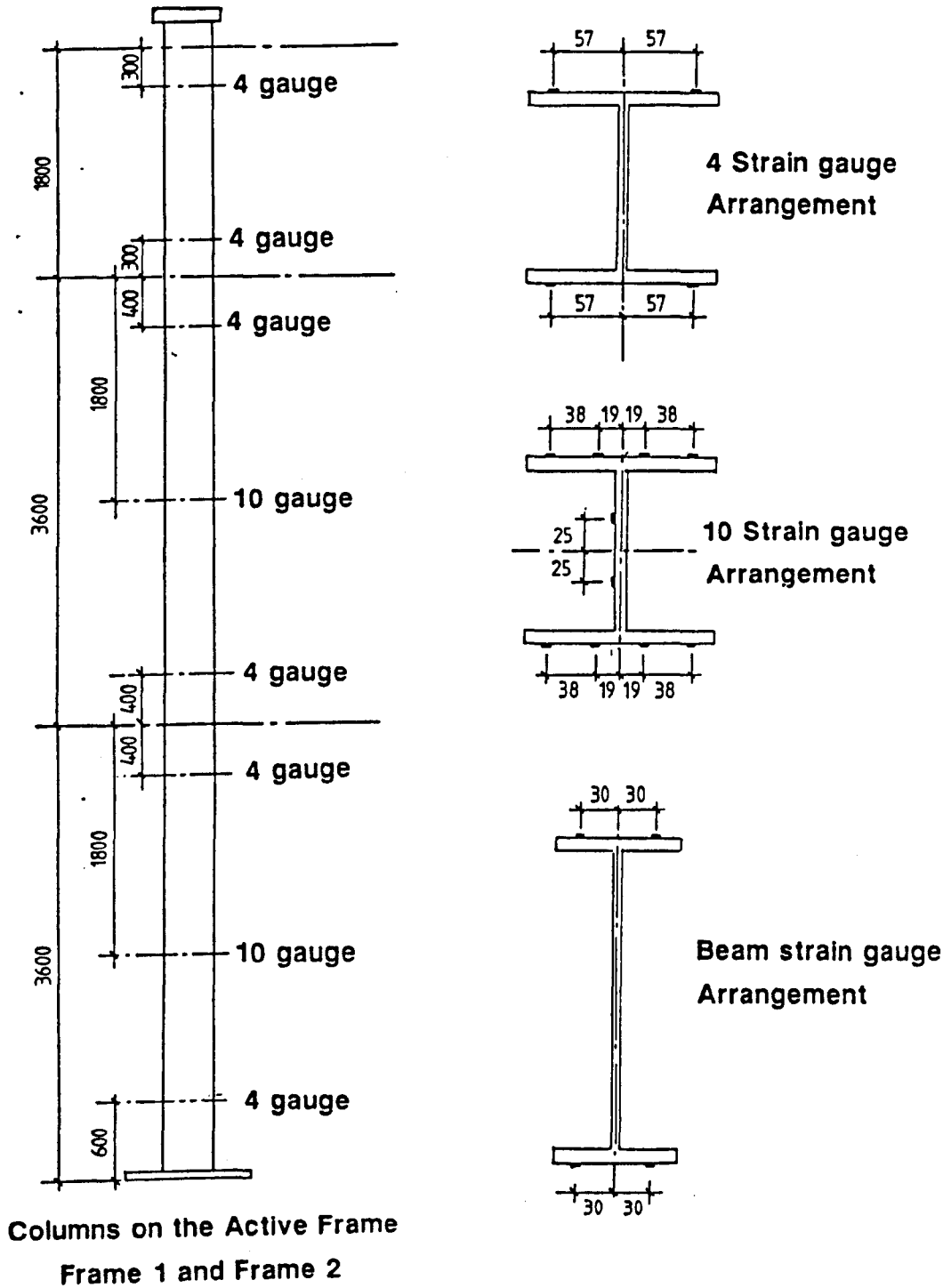


Figure 5.15: Location of strain gauges on the column members.

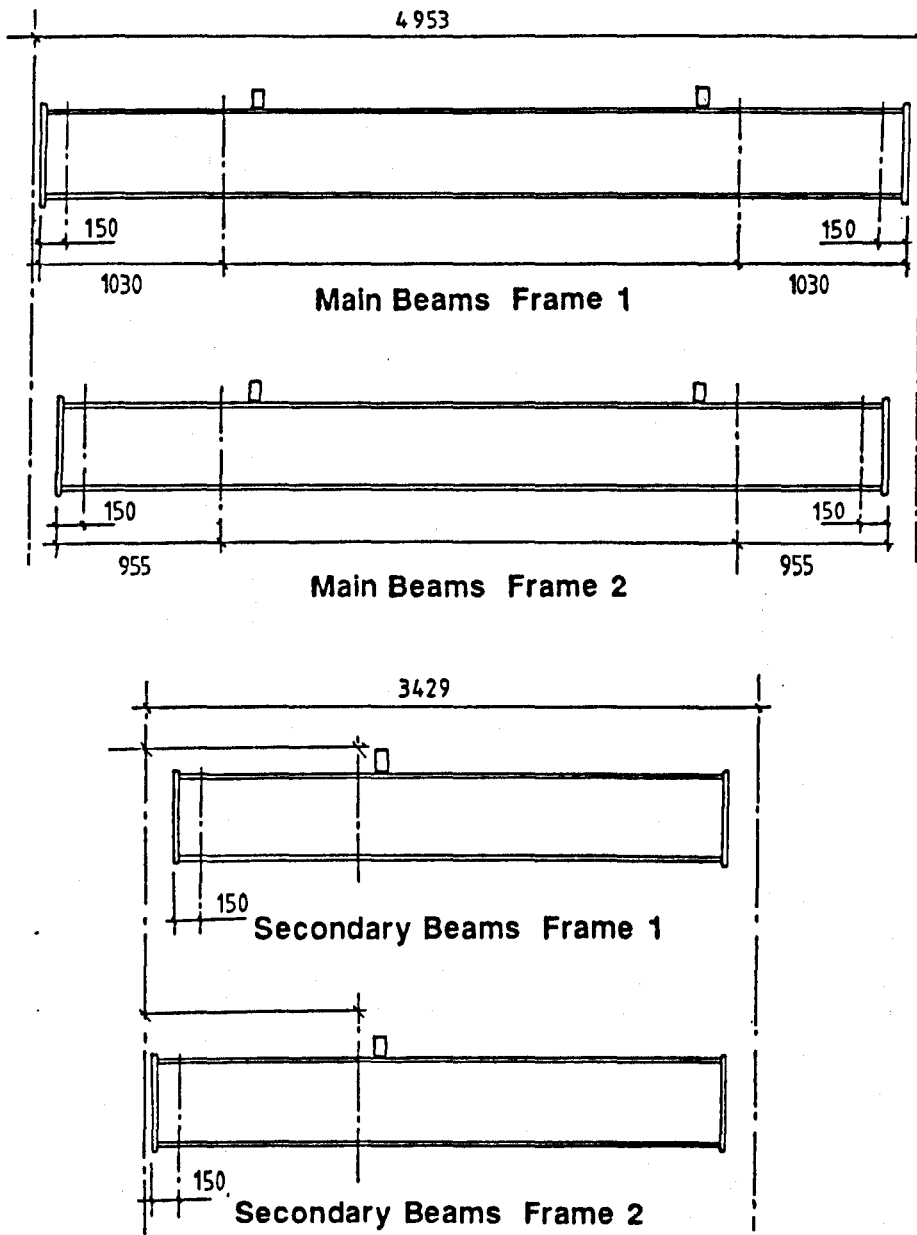


Figure 5.16: Location of strain gauges on the beam members.

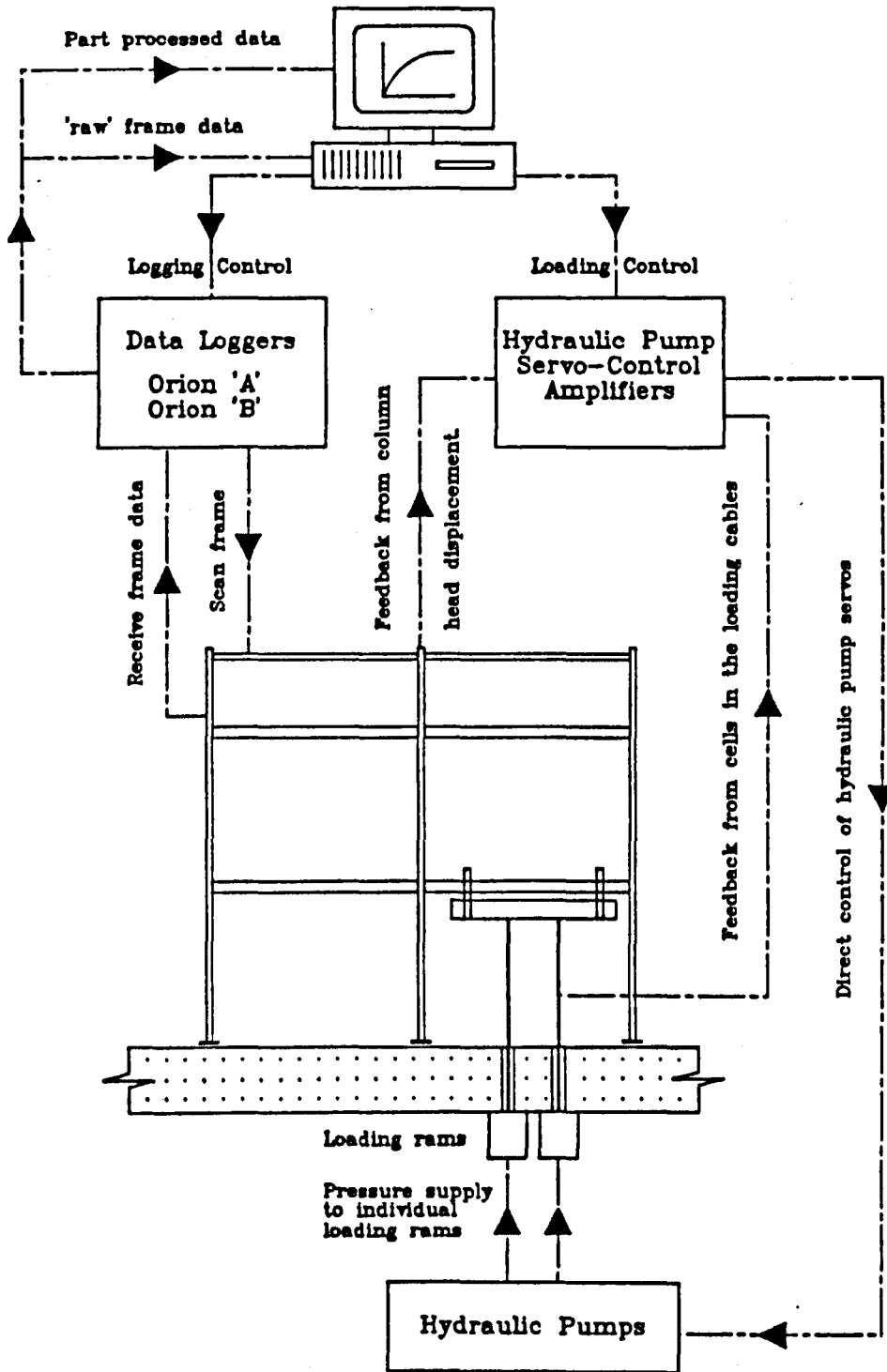


Figure 5.17: Schematic diagram showing the experimental set-up.

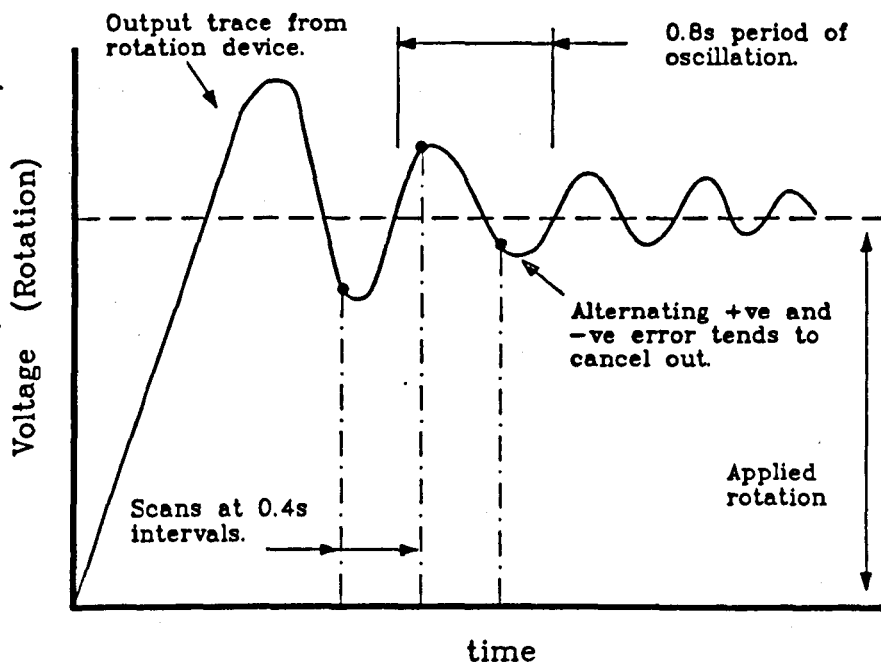
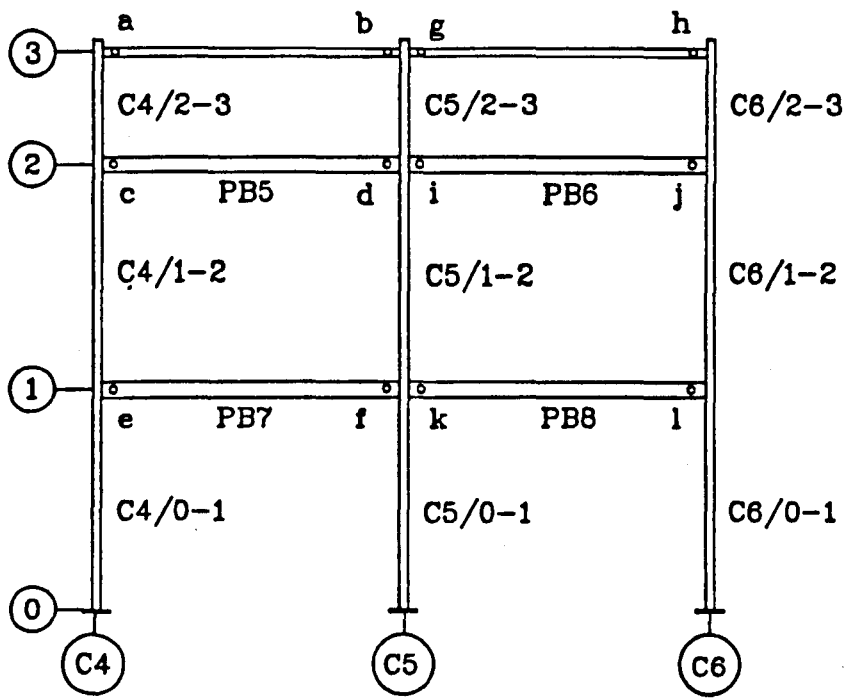
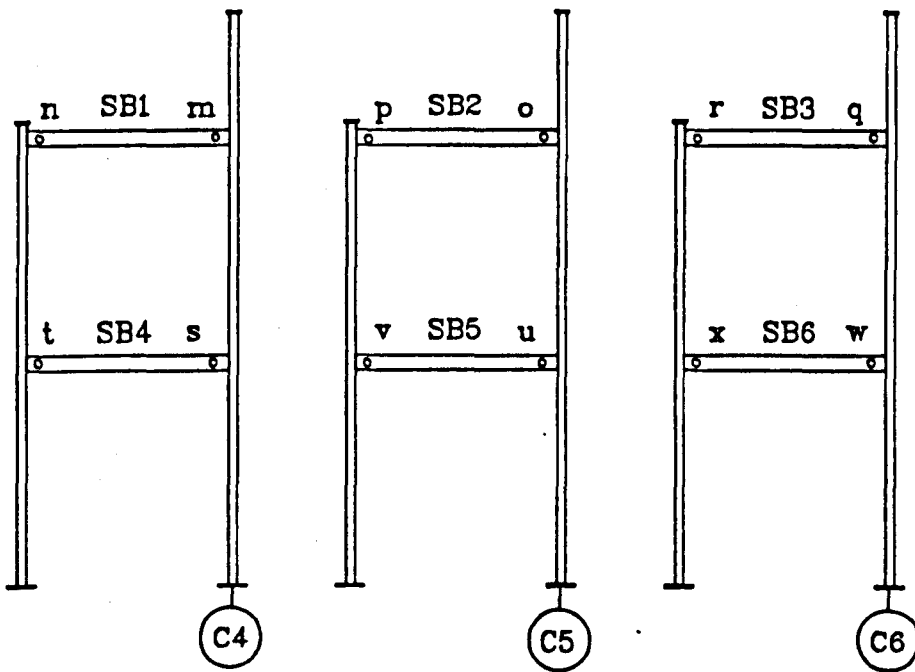


Figure 5.18: A plot of measured rotation against time for one of the 'hanging dumb-bell' rotation devices.



Elevation of the 'active' frame



Sections at secondary beam locations

Figure 5.19: Elevation and section through test frame F1 indicating the member nomenclature.

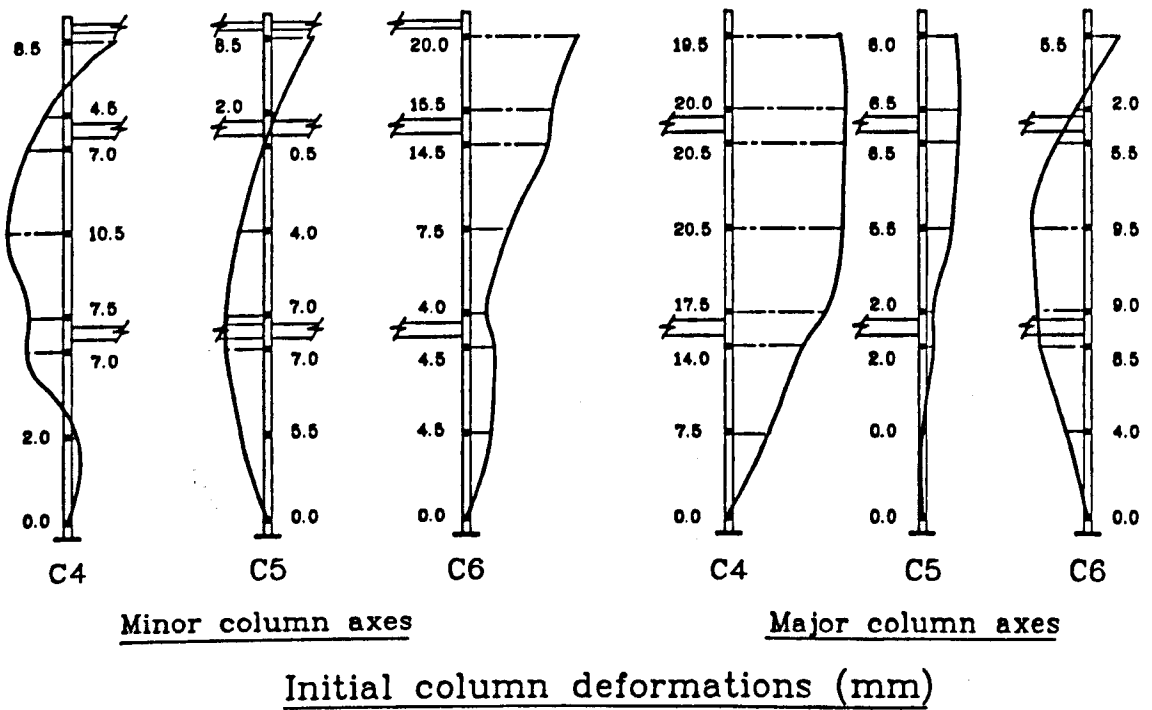
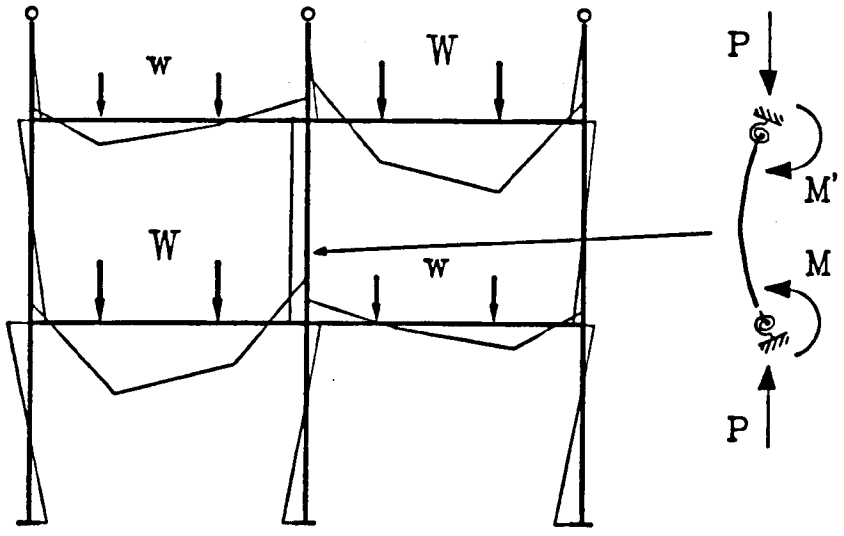
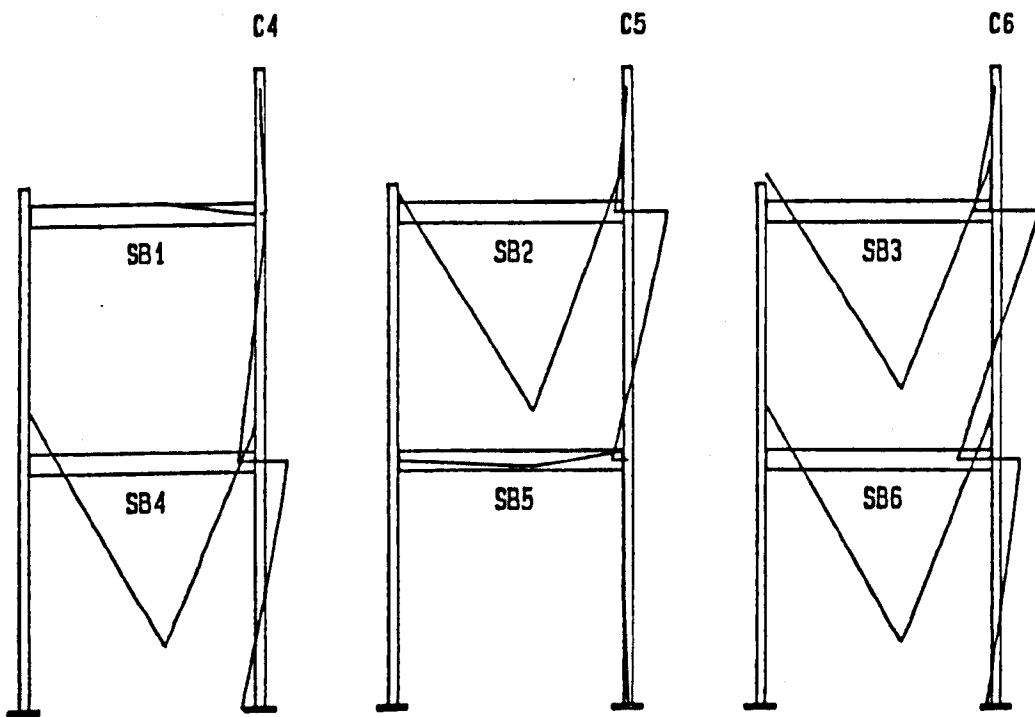
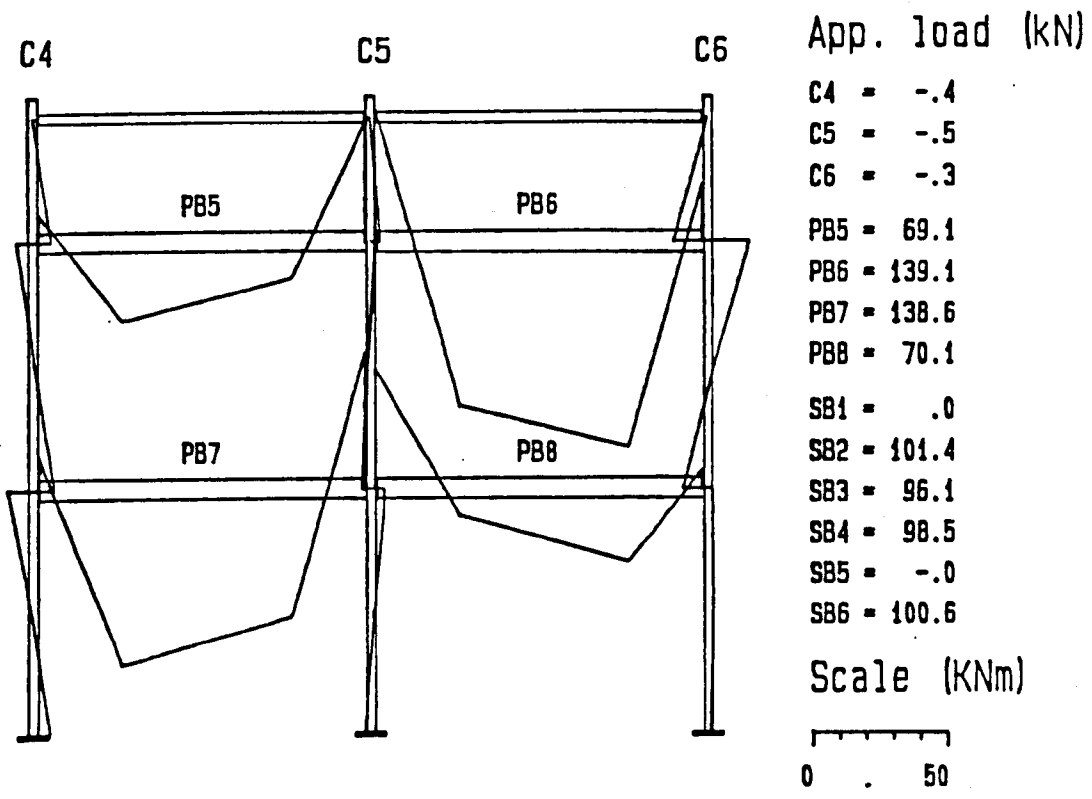


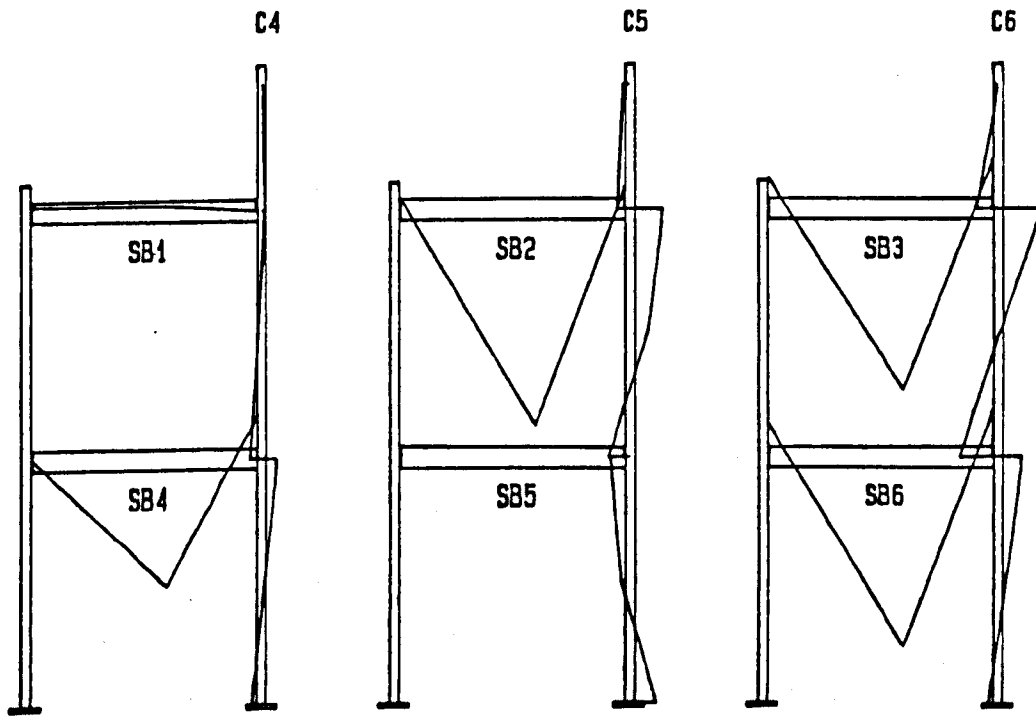
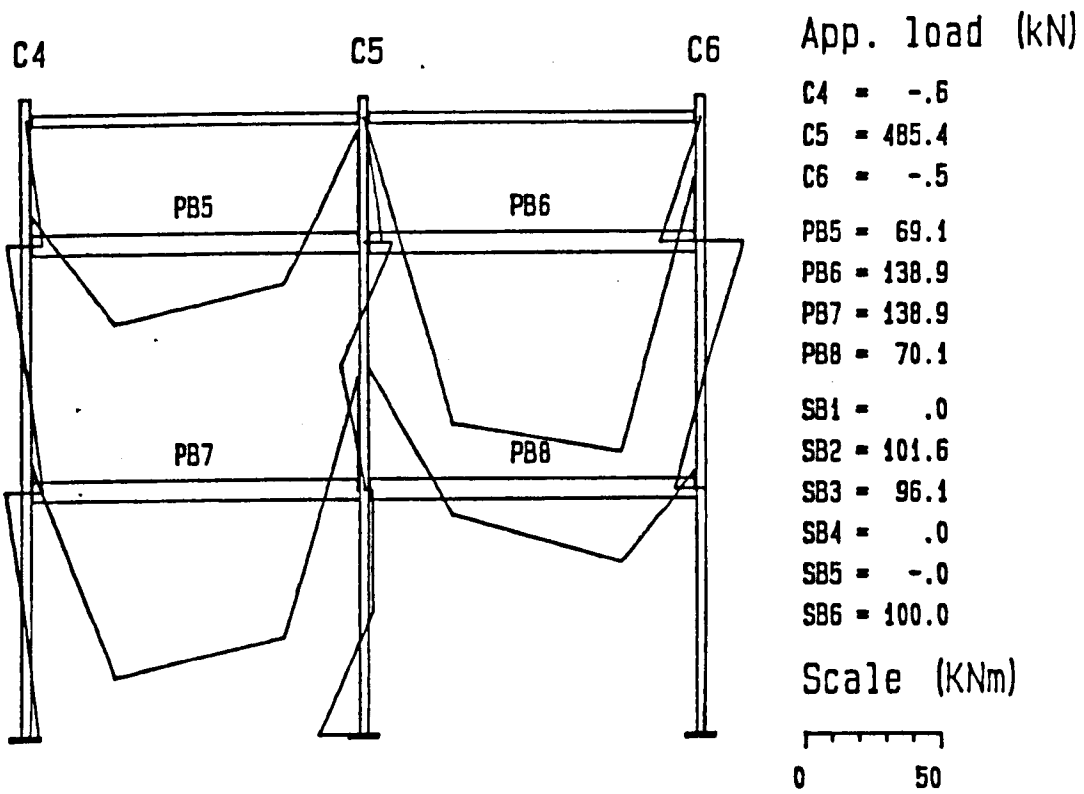
Figure 5.21: Initial column deformations for test F1.



Bending Moment Diagram - Test Frame 1

Figure 5.22: Computer generated frame bending moments at the end of the beam loading phase - test frame F1.





Bending Moment Diagram - Test Frame 1

Figure 5.23: Computer generated frame bending moments at the point of maximum load on column C5.

Mid-column bending moments.

Frame test F1

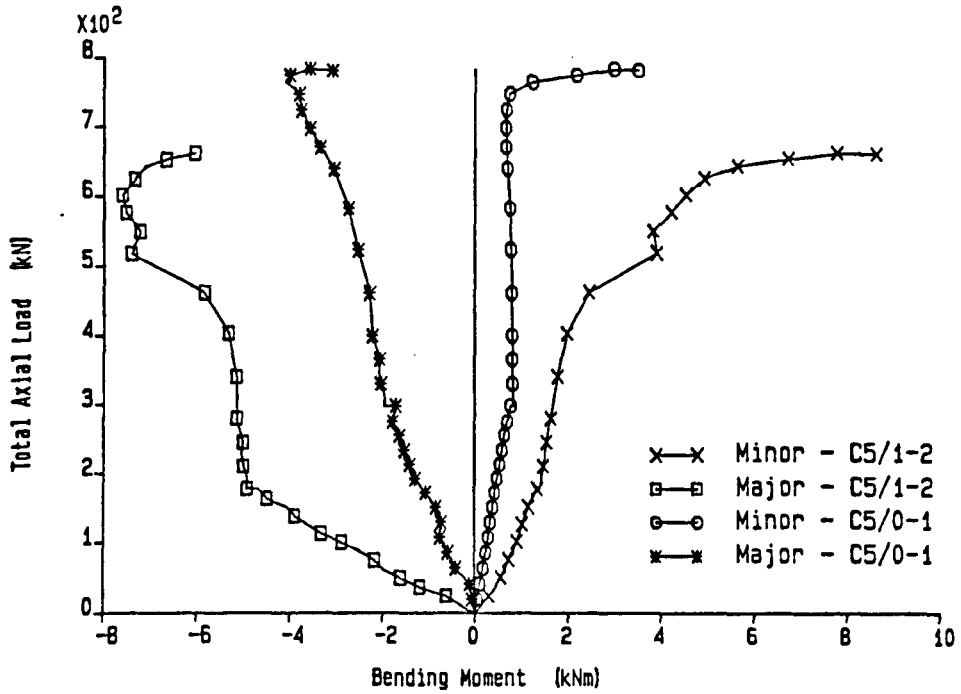


Figure 5.24: Axial load vs. mid-column moments for C5/0-1 and C5/1-2.

Mid-column bending moments.

Frame test F1

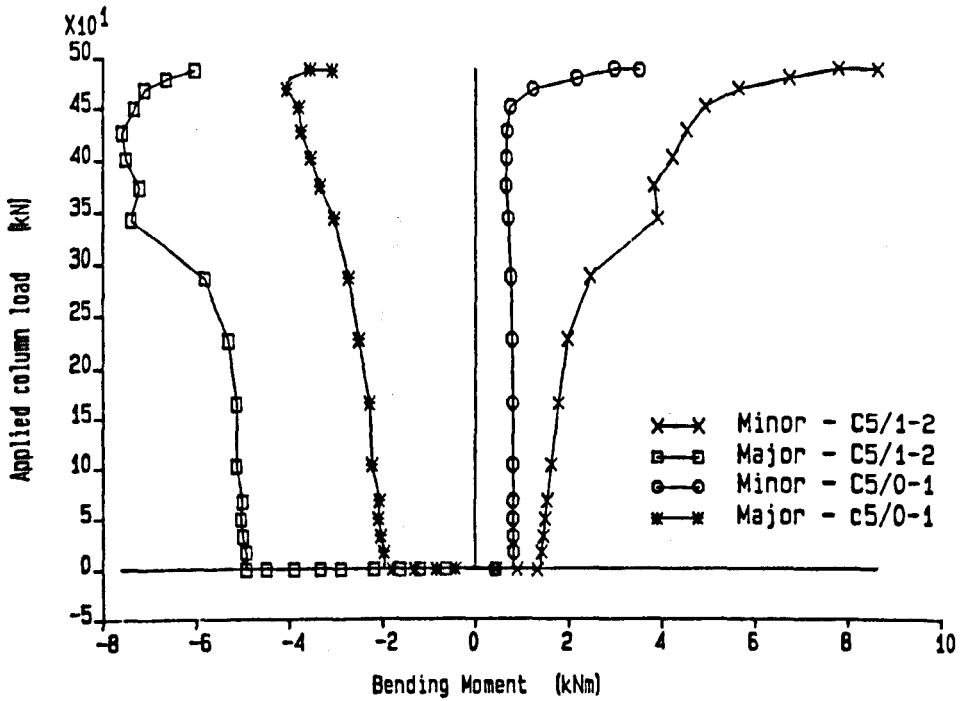


Figure 5.25: Applied column head load vs. mid-column moments for C5/0-1 and C5/1-2.

Mid-column deflections.

Frame test F1

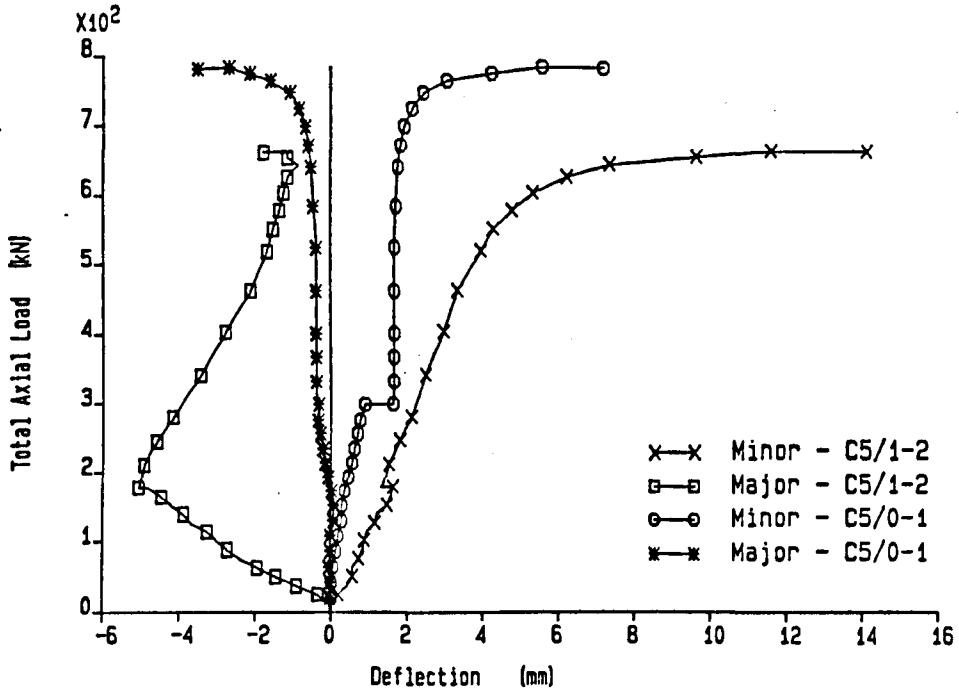


Figure 5.26: Axial load vs. mid-column deflections for C5/0-1 and C5/1-2.

Mid-column twist rotations.

Frame test F1

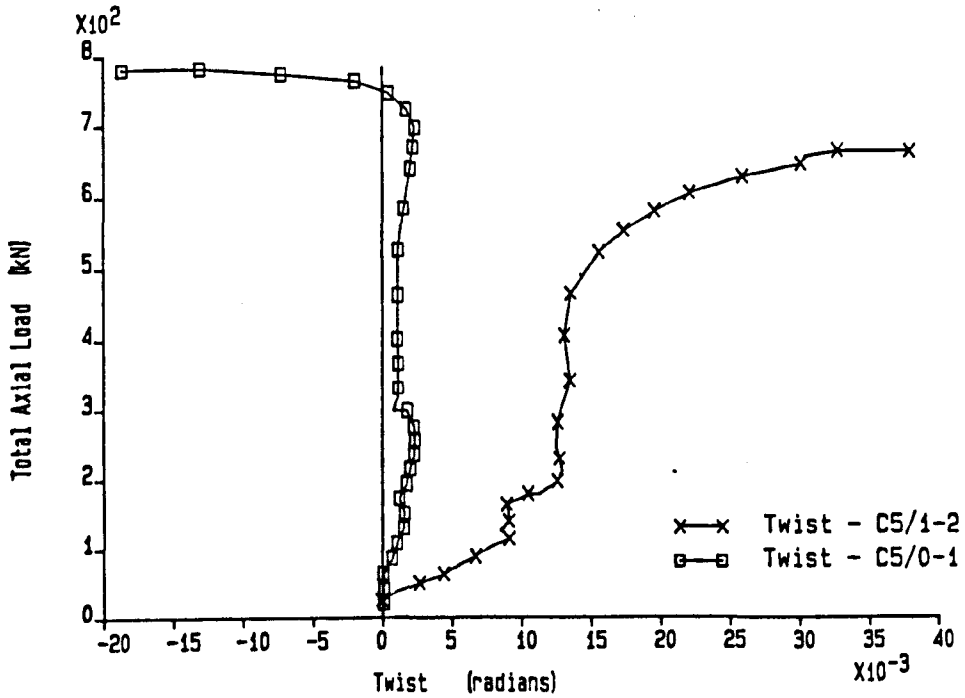


Figure 5.27: Axial load vs. mid-column twist rotation for C5/0-1 and C5/1-2.

Minor column axis bending moments.

Frame test F1

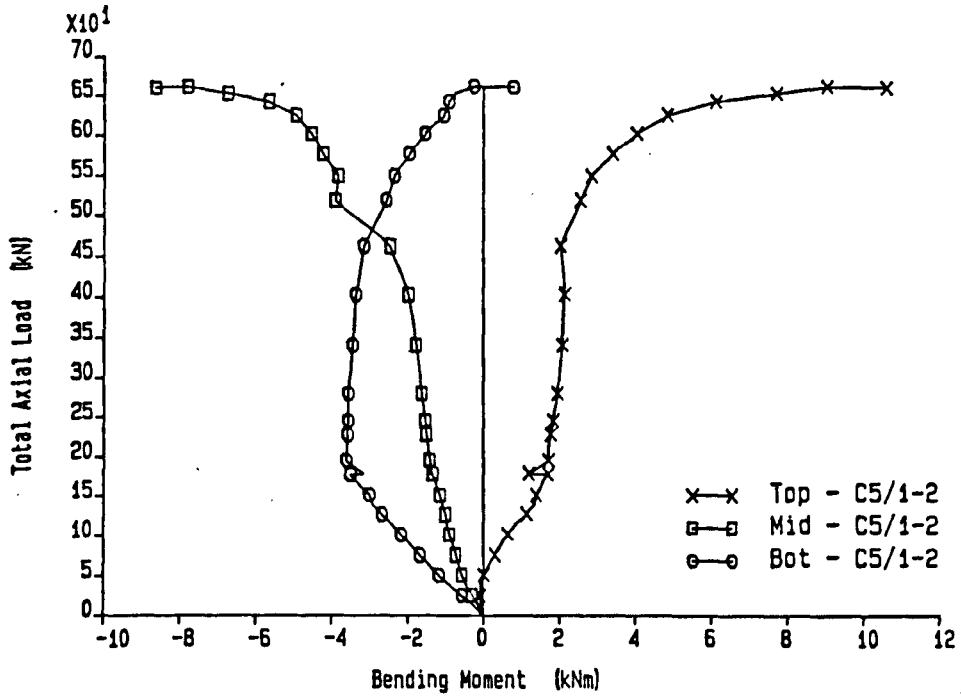


Figure 5.28: Axial load vs. minor axis moment at the top, mid-point and bottom of C5/1-2.

Major column axis bending moments.

Frame test F1

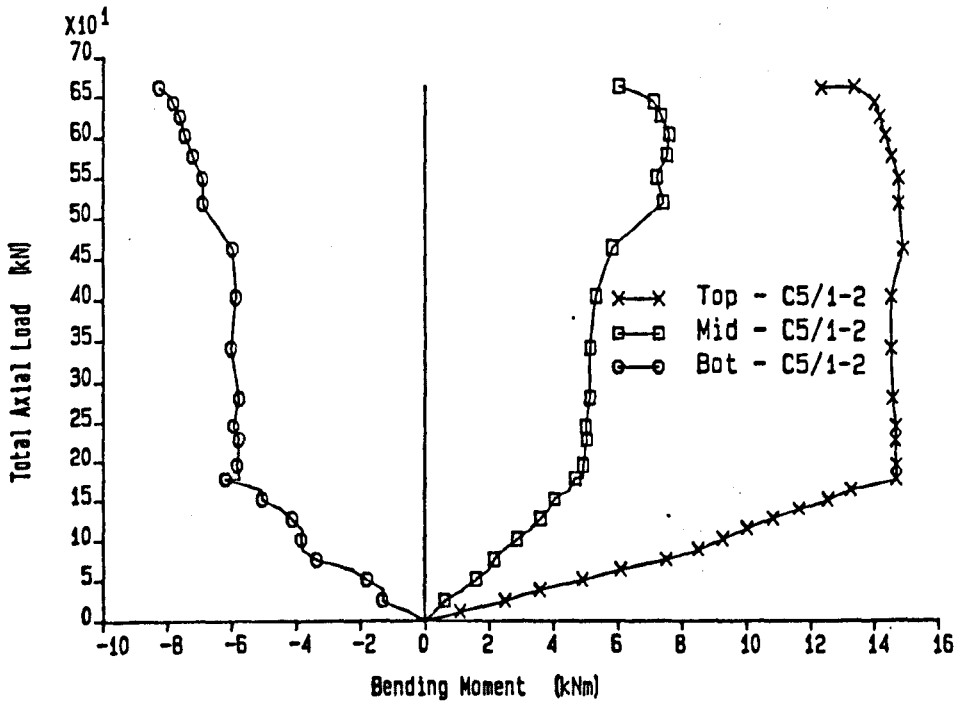


Figure 5.29: Axial load vs. major axis moment at the top, mid-point and bottom of C5/1-2.

Minor column axis bending moments.

Frame test F1

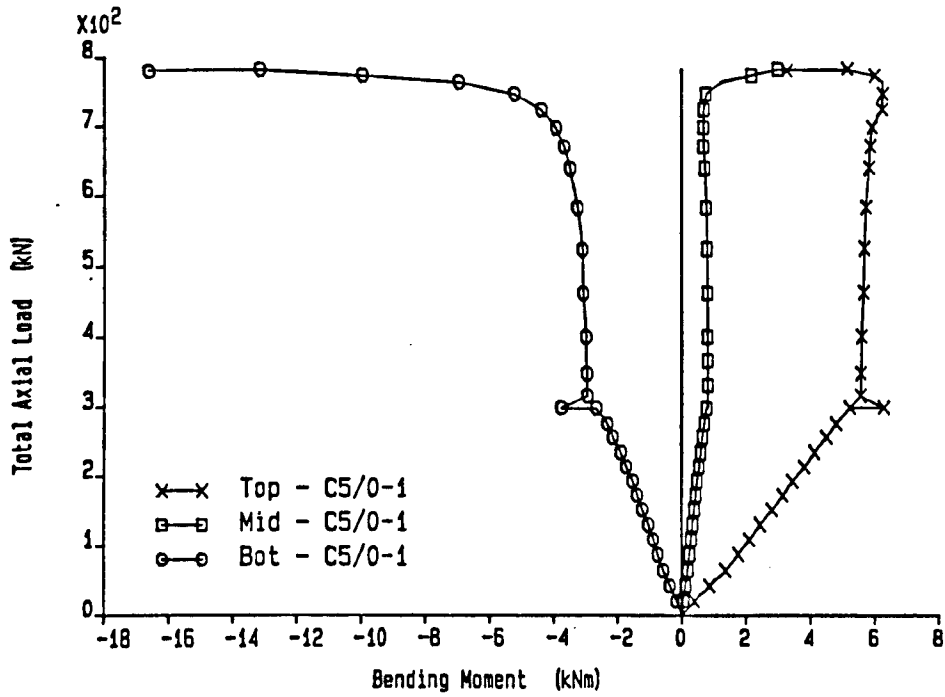


Figure 5.30: Axial load vs. minor axis moment at the top, mid-point and bottom of C5/0-1.

Major column axis bending moments.

Frame test F1

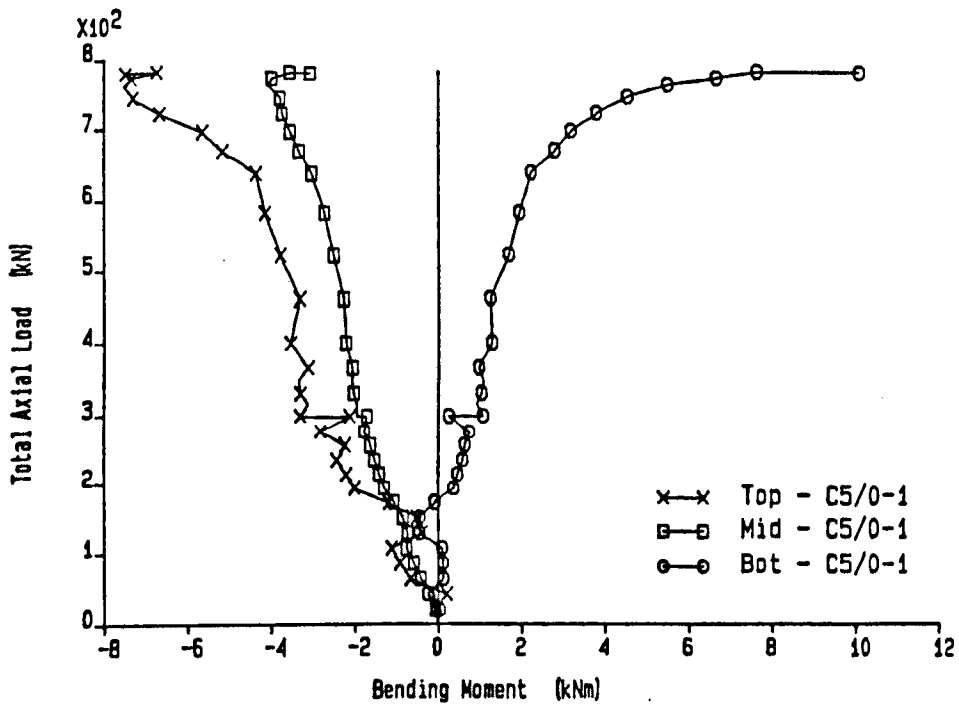


Figure 5.31: Axial load vs. major axis moment at the top, mid-point and bottom of C5/0-1.

Secondary beam connection moment.

Frame test F1

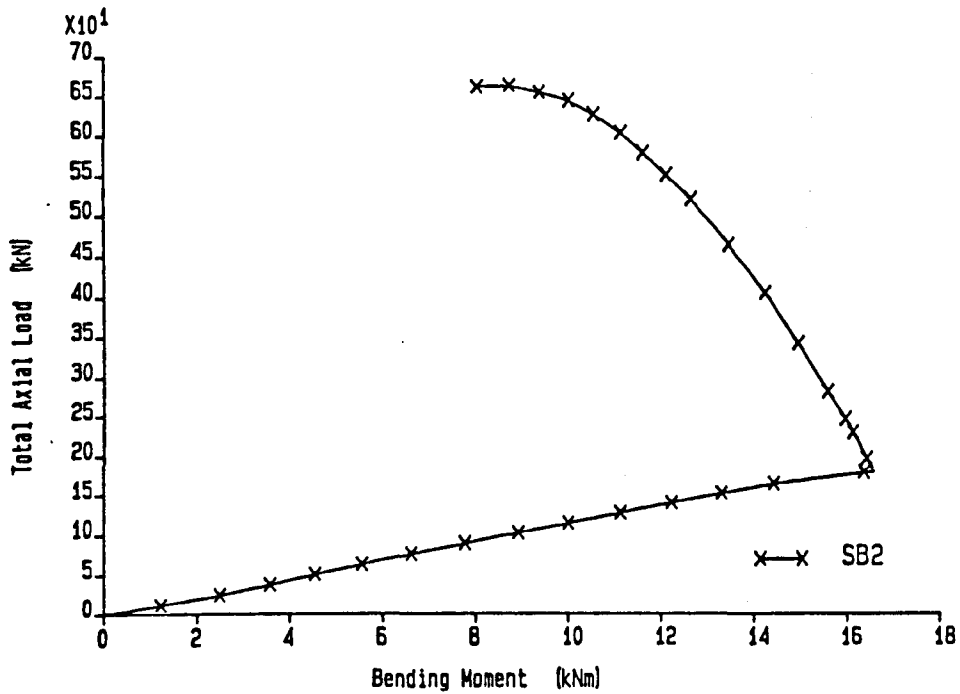


Figure 5.32: Axial load vs. moment at the connection of beam SB2 to column C5/1-2.

Primary beam connection moments.

Frame test F1

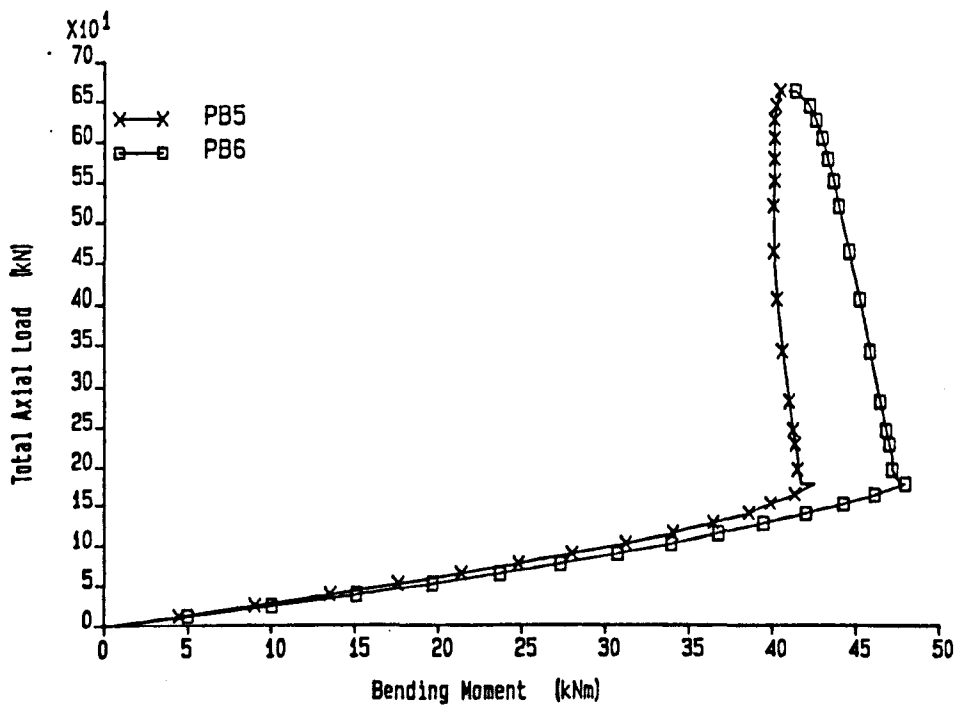


Figure 5.33: Axial load vs. moment at the connection of beams PB5 and PB6 to column C5/1-2.

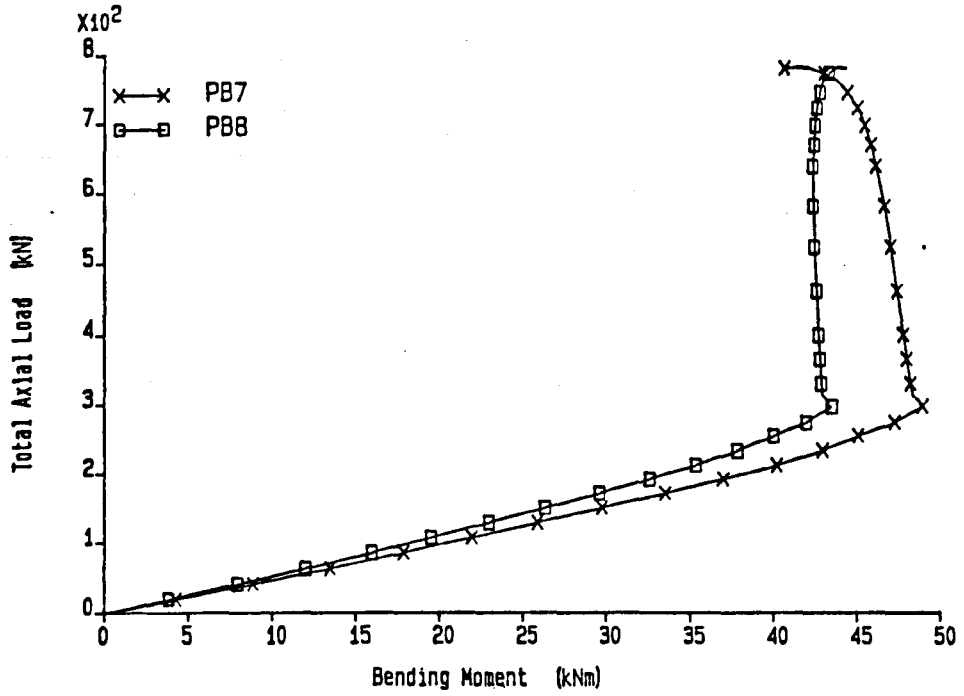
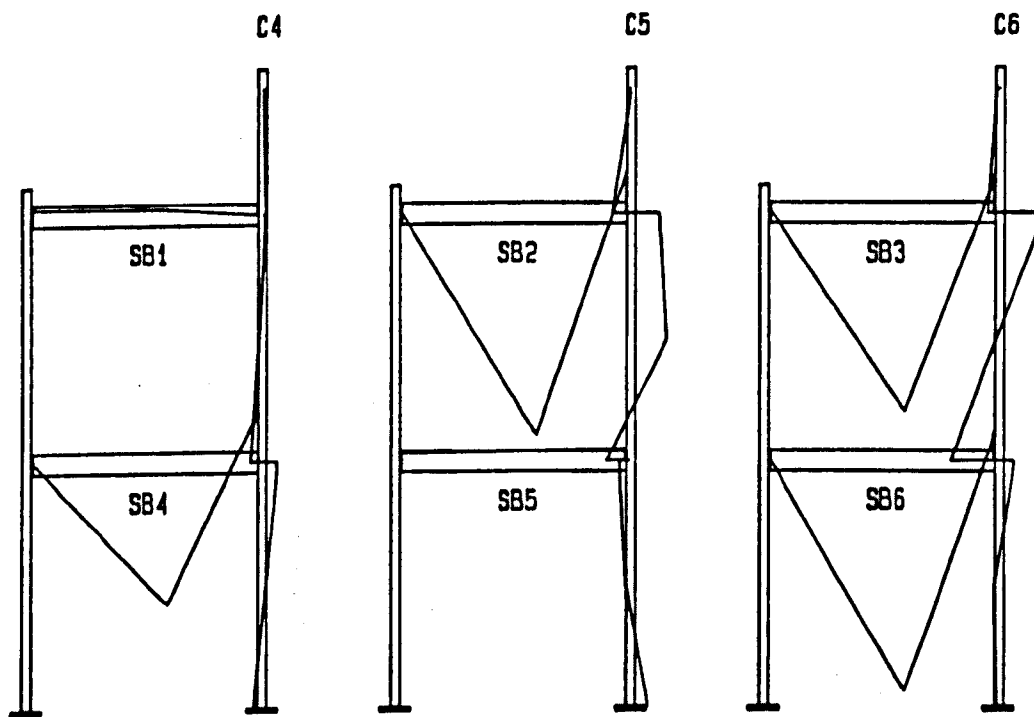
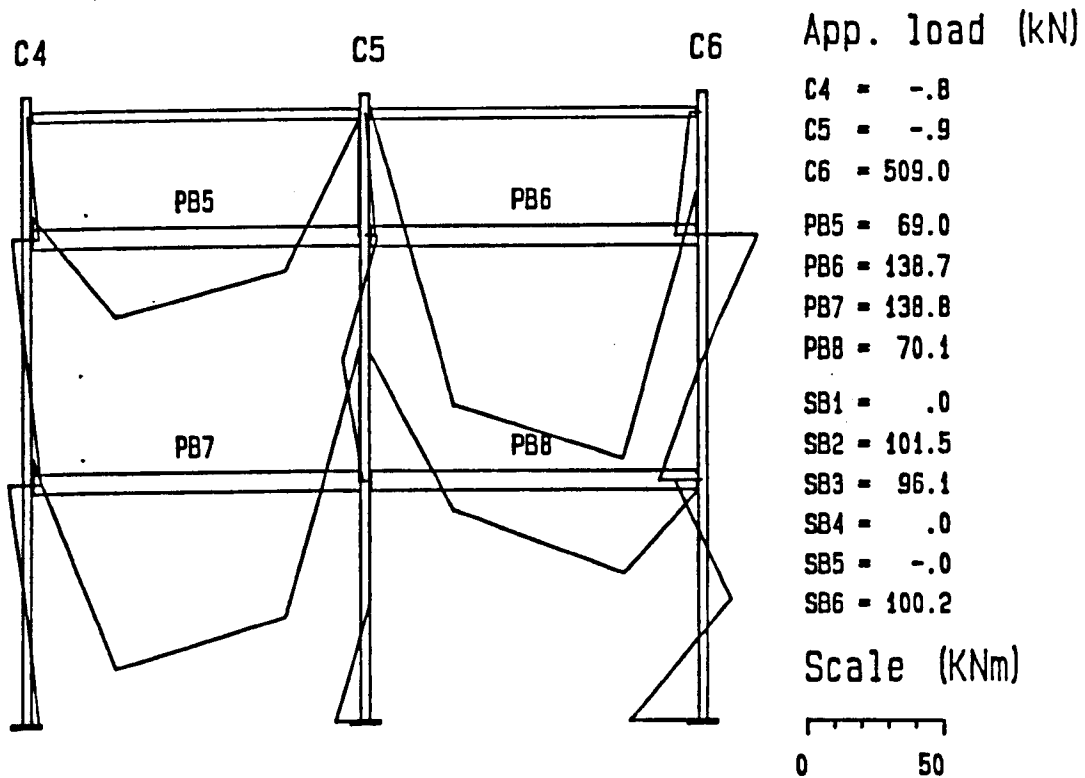


Figure 5.34: Axial load vs. moment at the connection of beams PB7 and PB8 to column C5/0-1.



Bending Moment Diagram - Test Frame 1

Figure 5.35: Computer generated frame bending moments at the point of maximum load on column C6.



Mid-column bending moments.

Frame test F1

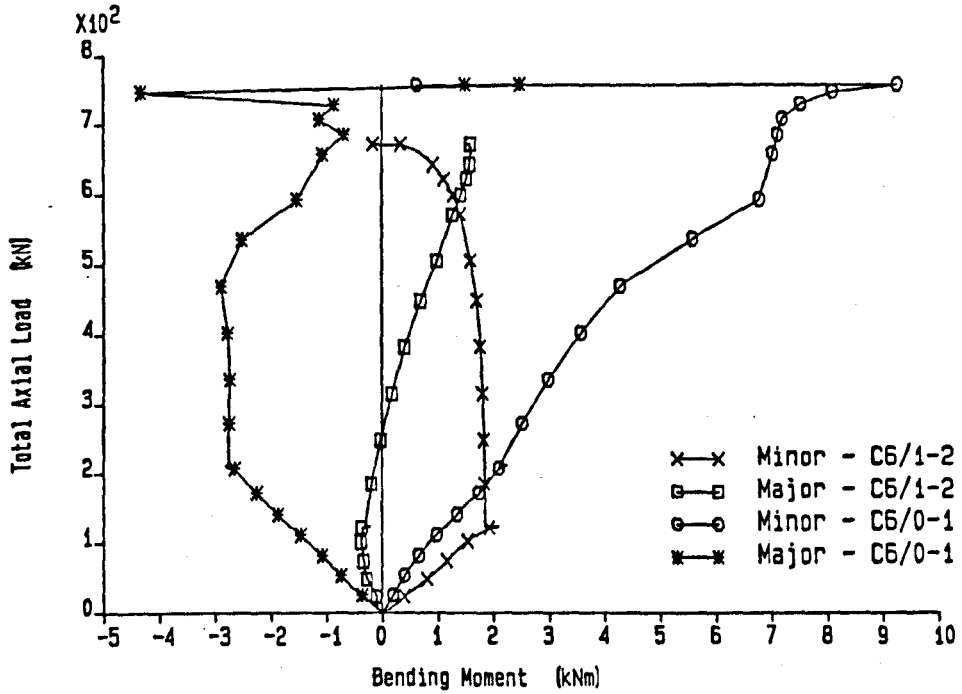


Figure 5.36: Axial load vs. mid-column moments for columns C6/0-1 and C6/1-2.

Mid-column deflections.

Frame test F1

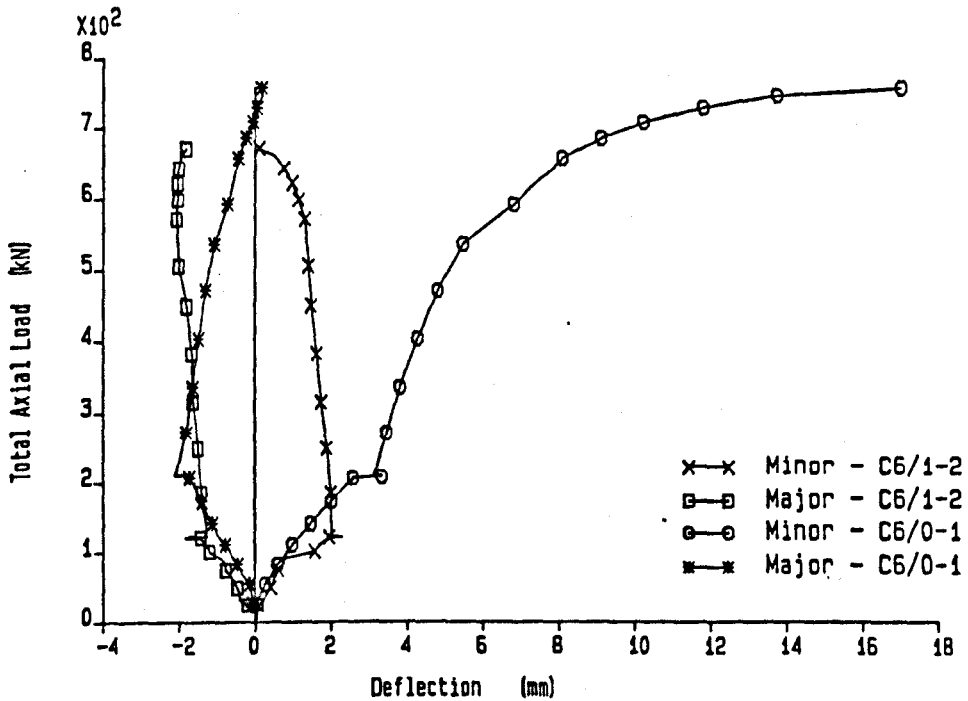


Figure 5.37: Axial load vs. mid-column deflections for columns C6/0-1 and C6/1-2.

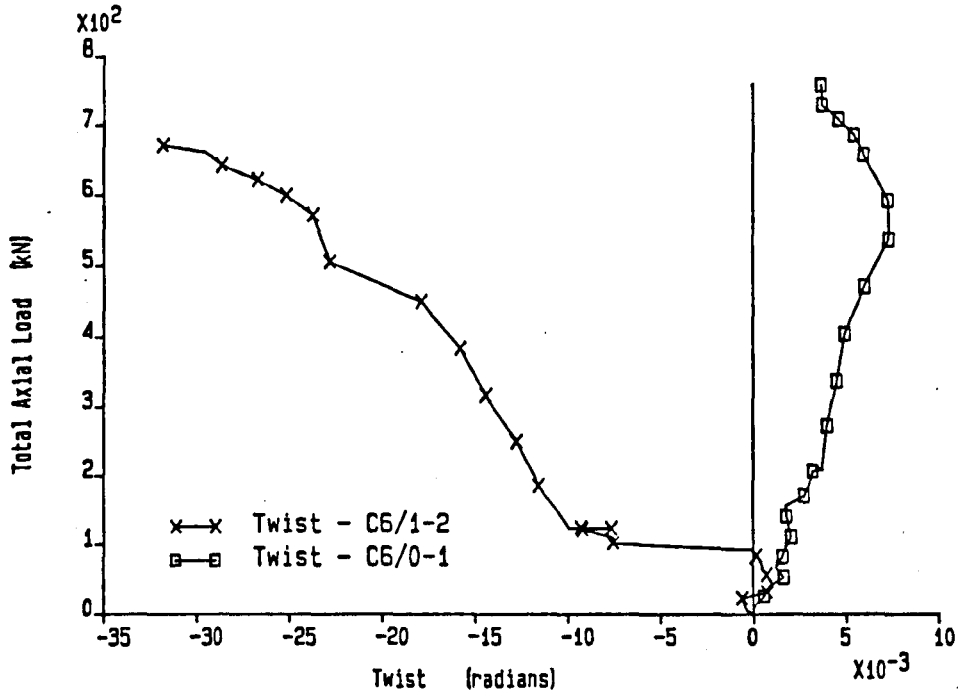


Figure 5.38: Axial load vs. mid-column twist rotation for columns C6/0-1 and C6/1-2.

Minor column axis bending moments.

Frame test F1

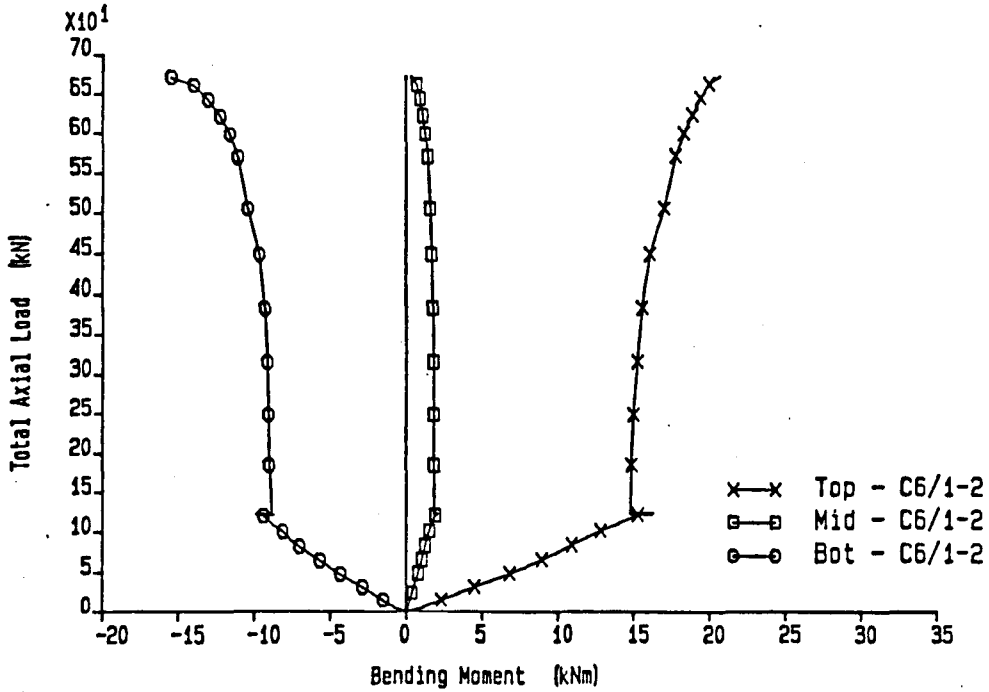


Figure 5.39: Axial load vs. minor axis moment at the top, mid-point and bottom of column C6/1-2.

Major column axis bending moments.

Frame test F1

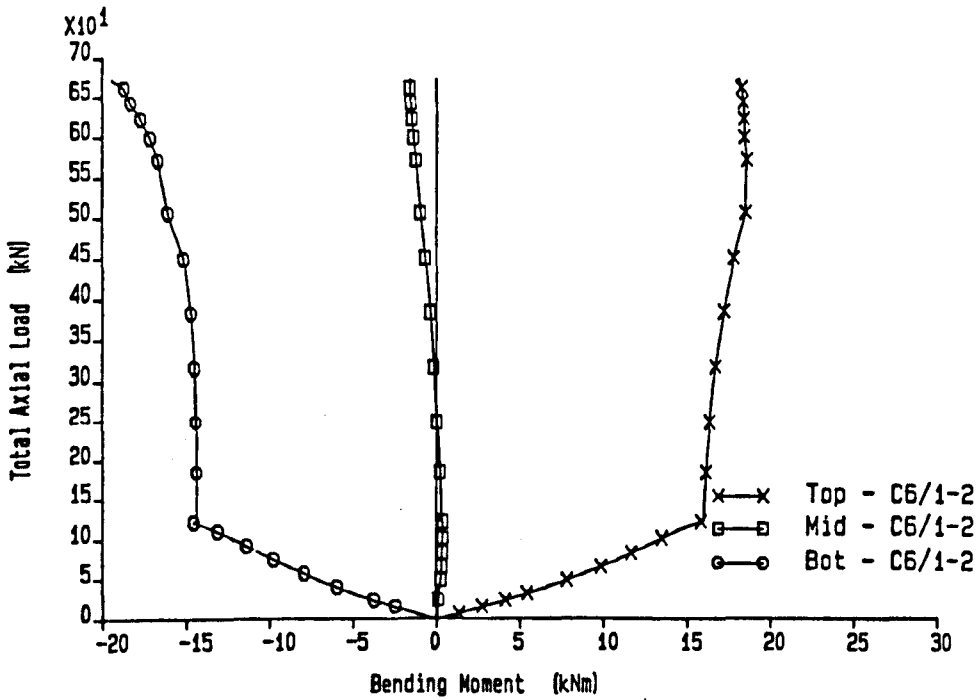


Figure 5.40: Axial load vs. major axis moment at the top, mid-point and bottom of C6/1-2.

Minor column axis bending moments.

Frame test F1

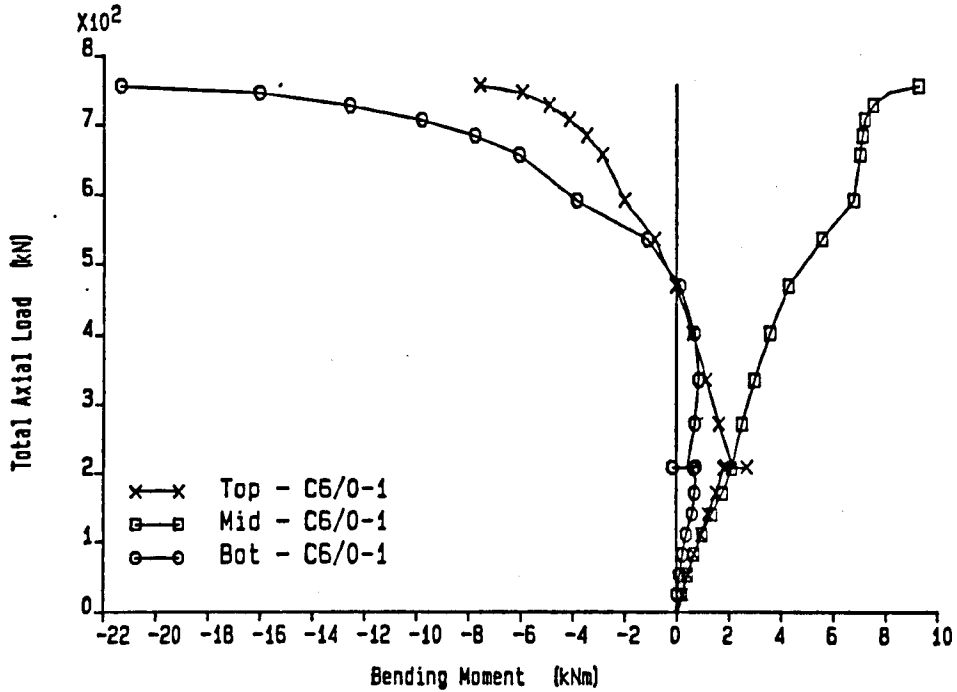


Figure 5.41: Axial load vs. minor axis moment at the top, mid-point and bottom of column C6/0-1.

Major column axis bending moments.

Frame test F1

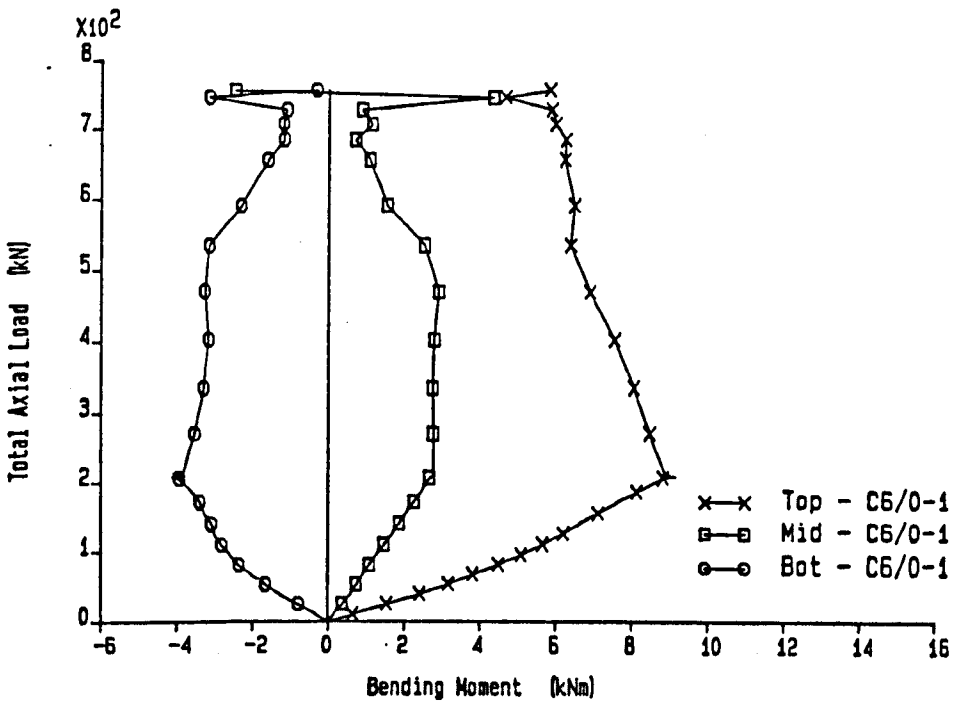


Figure 5.42: Axial load vs. major axis moment at the top, mid-point and bottom of column C6/0-1.

Secondary beam connection moments.

Frame test F1

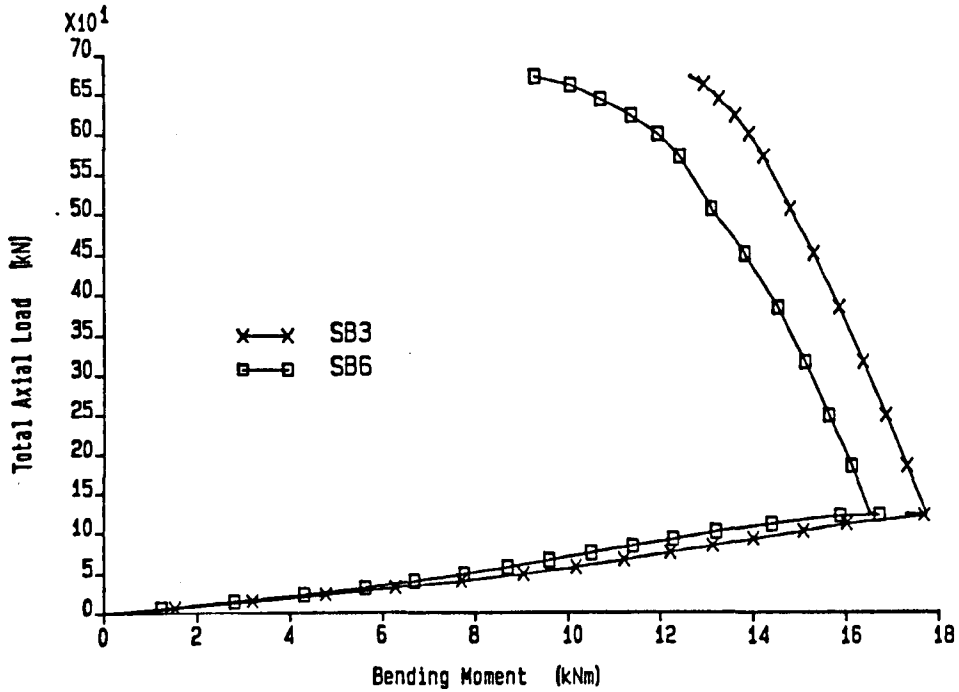


Figure 5.43: Axial load vs. moment at the connection of beams SB3 and SB6 to column C6/1-2.

Primary beam connection moments.

Frame test F1

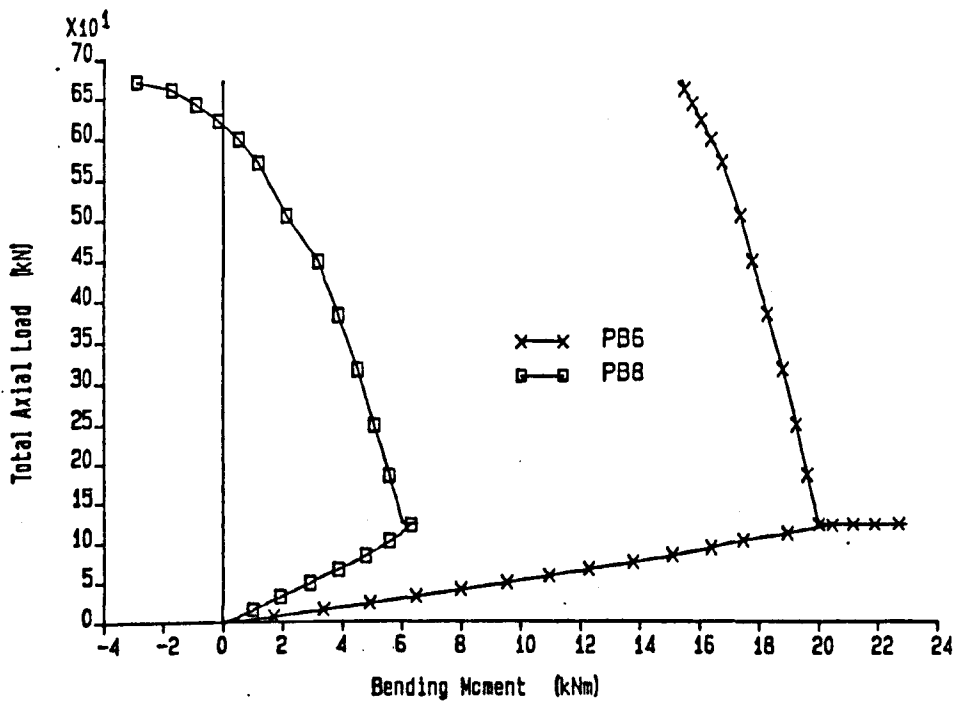
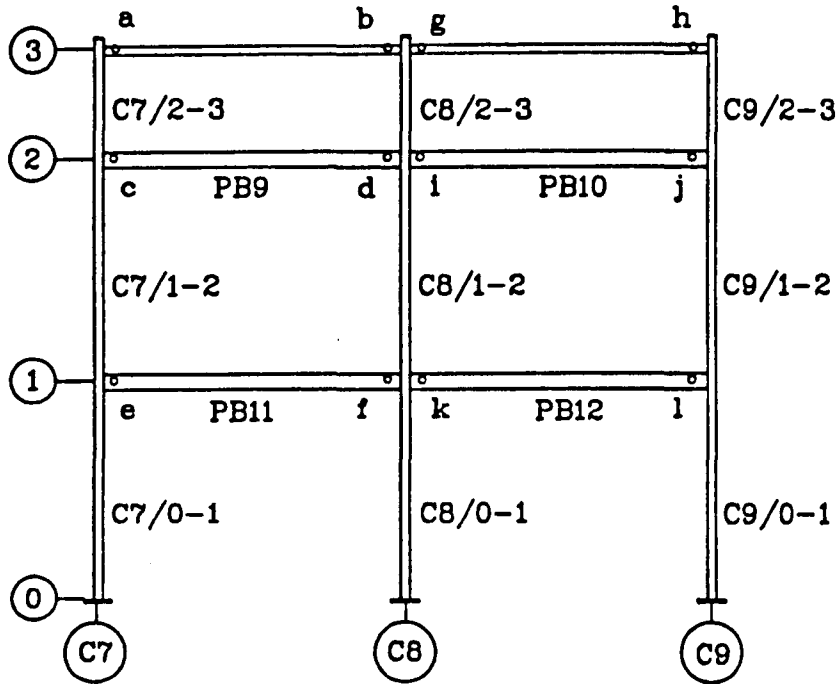
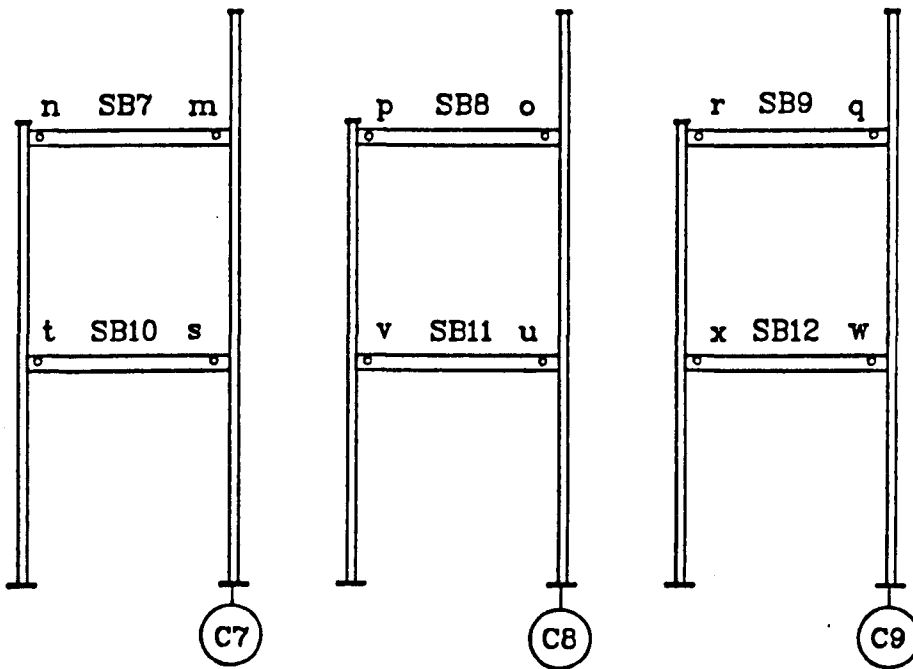


Figure 5.44: Axial load vs. moment at the connection of beams PB6 and PB8 to column C6/1-2.

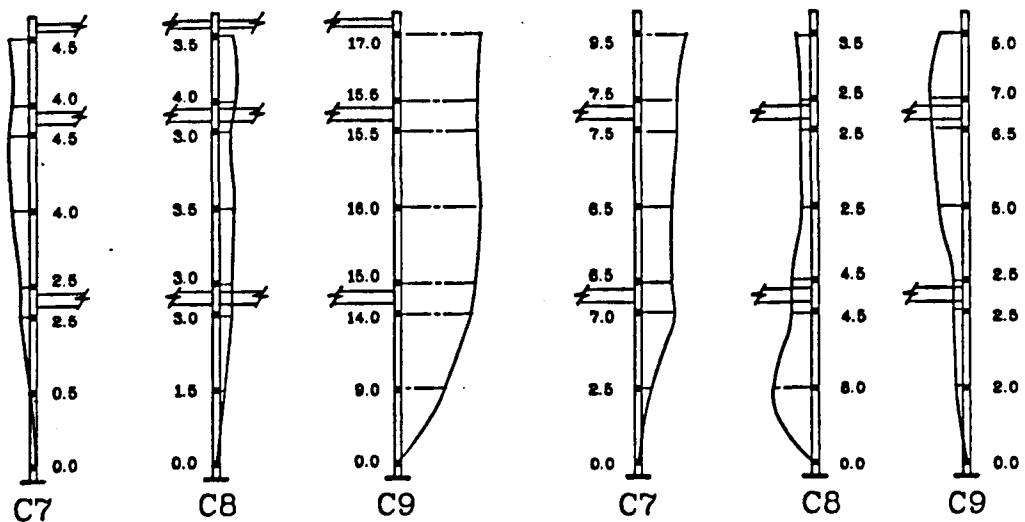


Elevation of the 'active' frame



Sections at secondary beam locations

Figure 5.45: Elevation and section through test frame F2 indicating the member nomenclature.



Major column axes

Minor column axes

Initial column deformations (mm)

Figure 5.46: Initial column deformations for test F2.

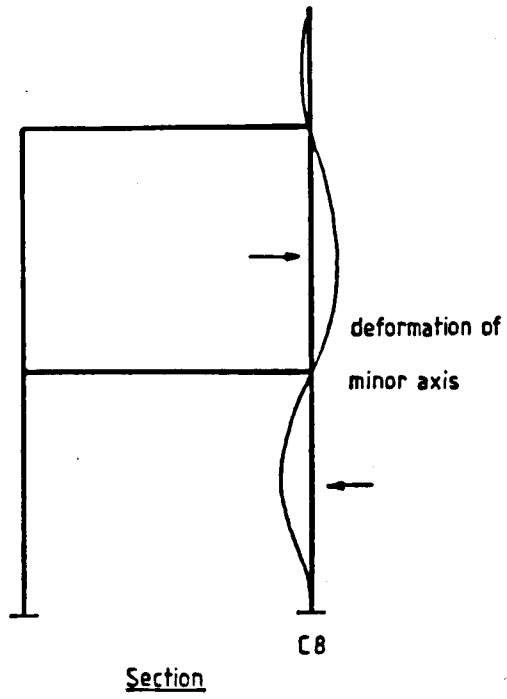


Figure 5.47: Observed deformed shape of the minor axis of column C8.

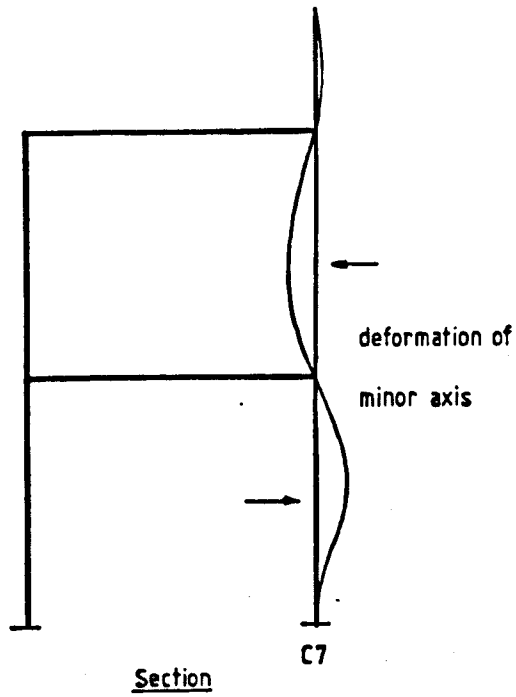
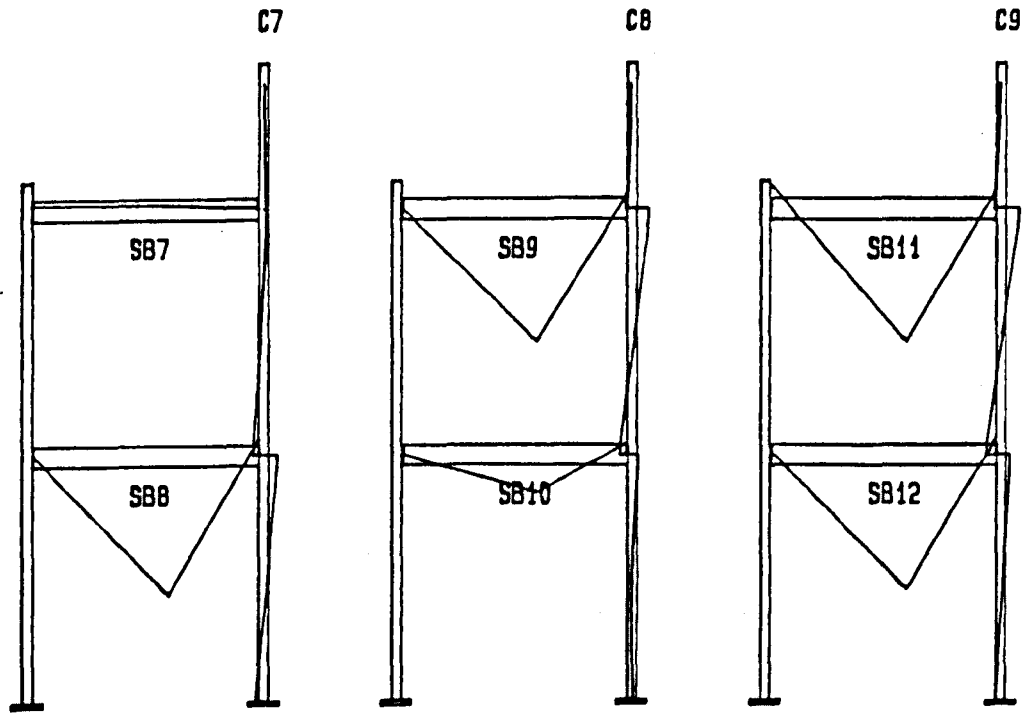
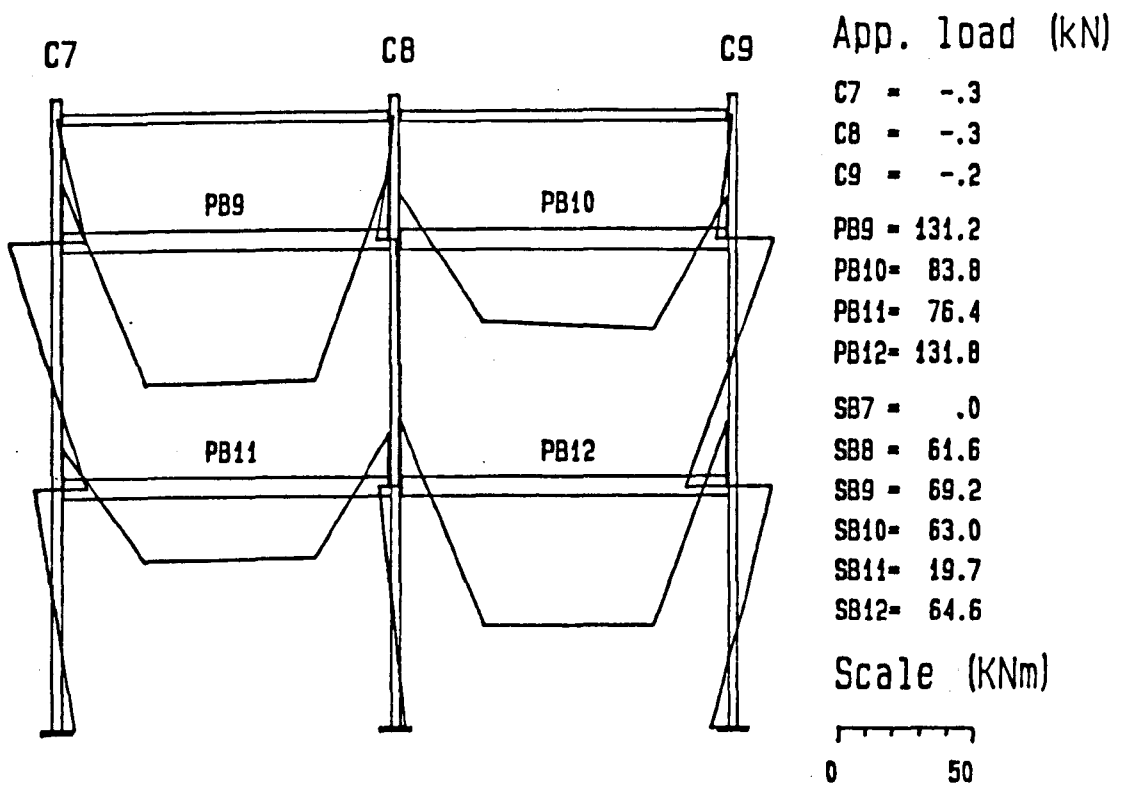


Figure 5.48: Observed deformed shape of the minor axis of column C7.





Bending Moment Diagram - Test Frame 2

Figure 5.49: Computer generated frame bending moments at the end of the beam loading phase - test frame F2.



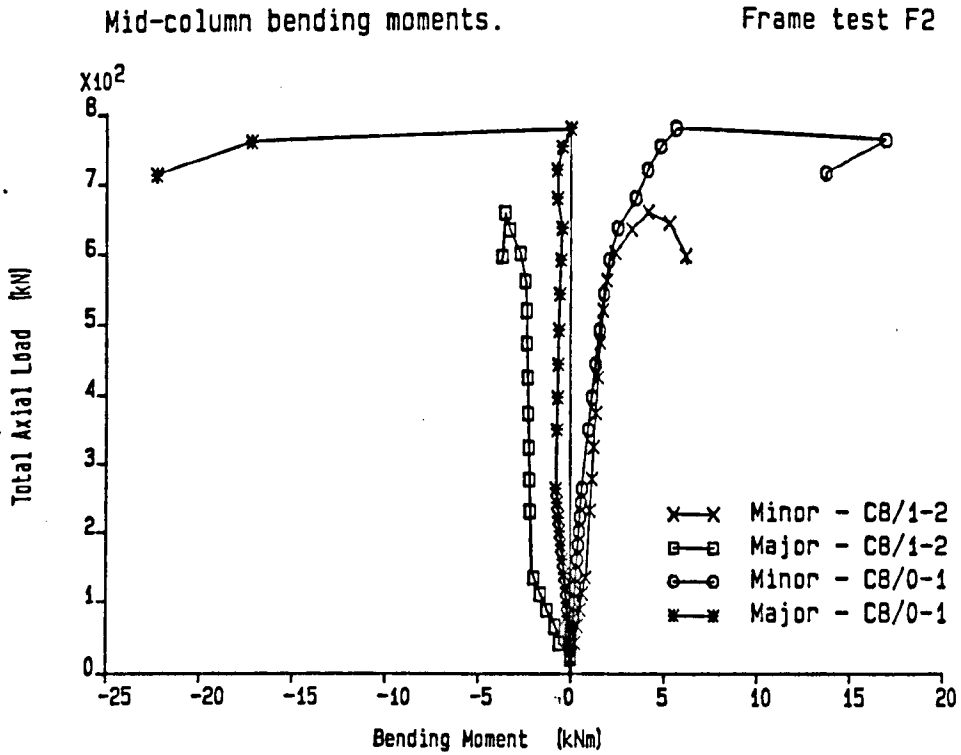


Figure 5.51: Axial load vs. mid-column moments for C8/0-1 and C8/1-2.

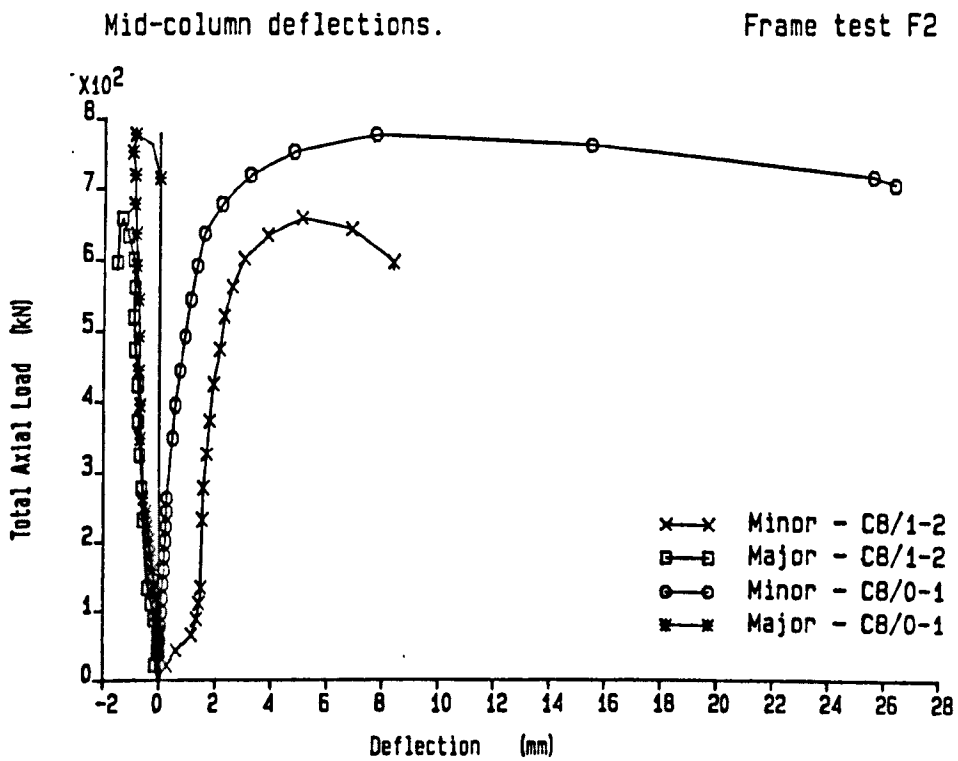


Figure 5.52: Axial load vs. mid-column deflections for C8/0-1 and C8/1-2.

Mid-column deflections.

Frame test F2

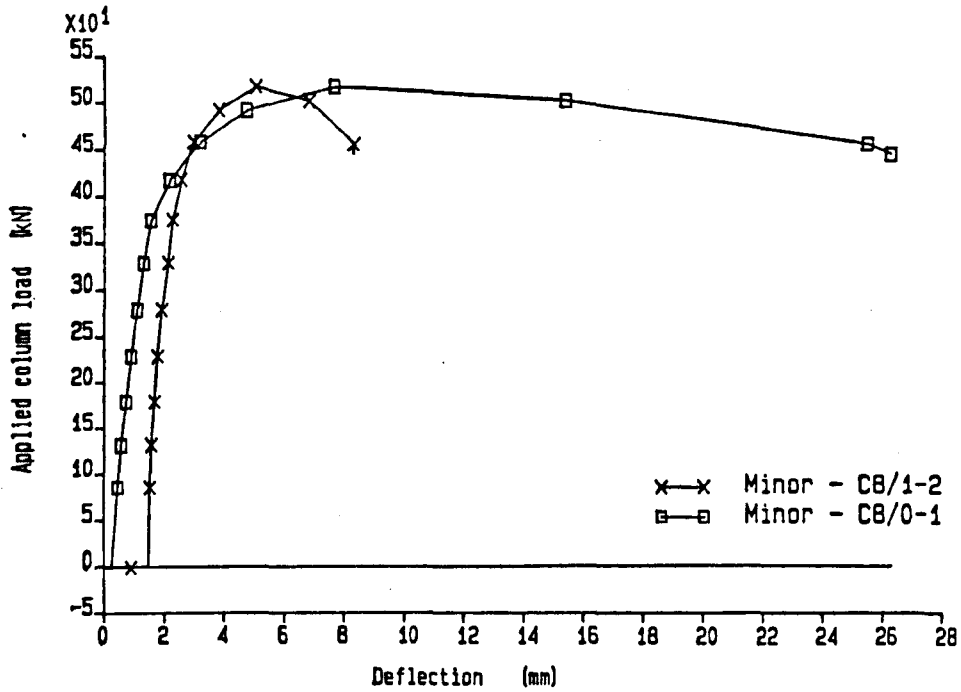


Figure 5.53: Applied load vs. mid-column deflections for C8/0-1 and C8/1-2.

Mid-column twist rotations.

Frame test F2

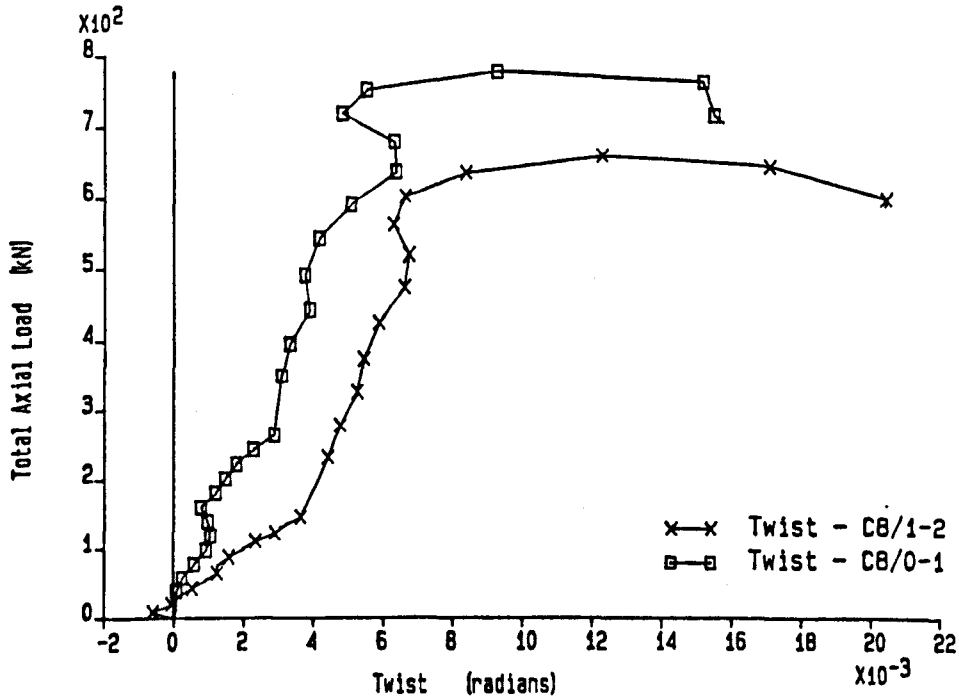


Figure 5.54: Axial load vs. mid-column twist rotation for C8/0-1 and C8/1-2.

Minor column axis bending moments.

Frame test F2

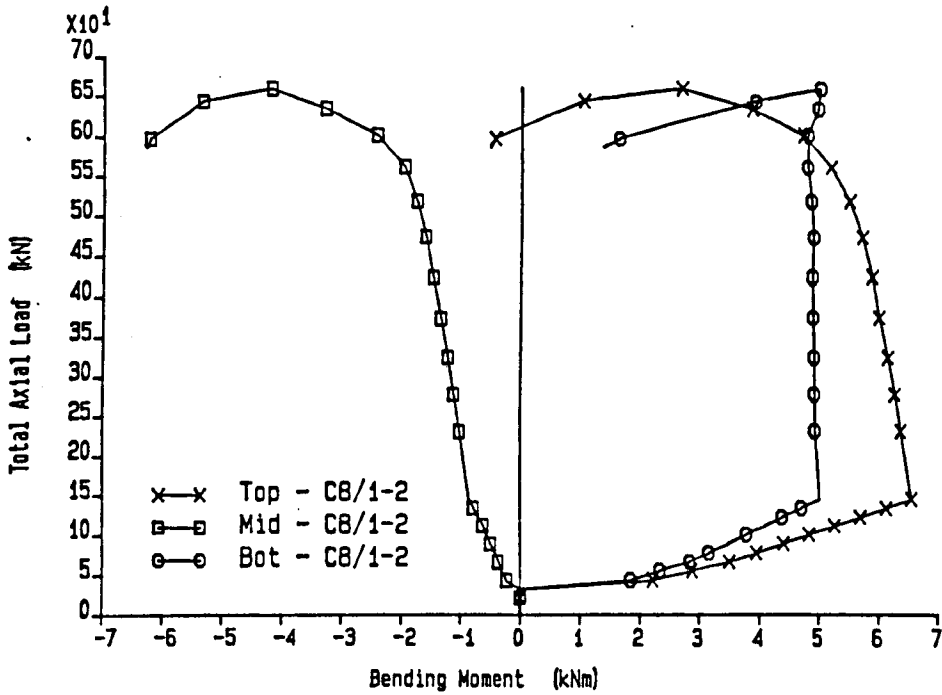


Figure 5.55: Axial load vs. minor axis moment at the top, mid-point and bottom of C8/1-2.

Major column axis bending moments.

Frame test F2

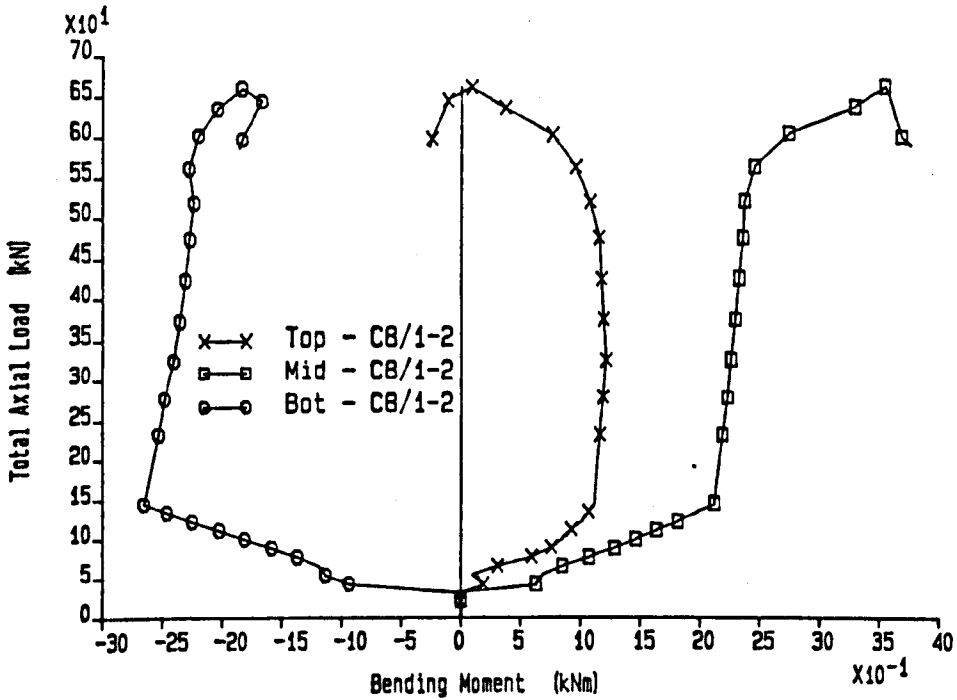


Figure 5.56: Axial load vs. major axis moment at the top, mid-point and bottom of C8/1-2.

Minor column bending moments

Frame test F2

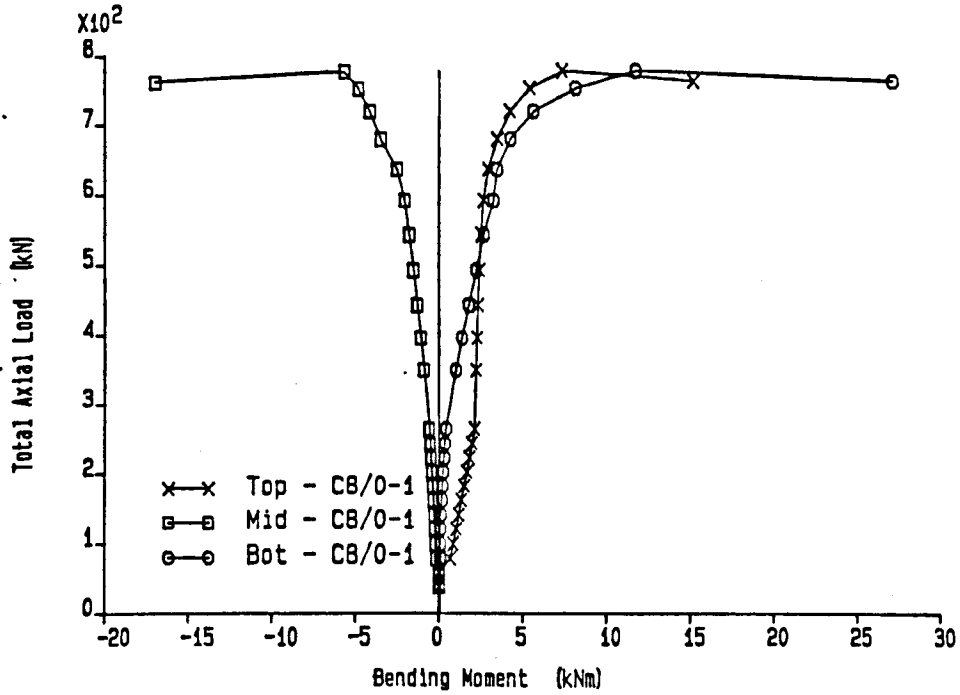


Figure 5.57: Axial load vs. minor axis moment at the top, mid-point and bottom of C8/0-1.

Major column axis bending moments.

Frame test F2

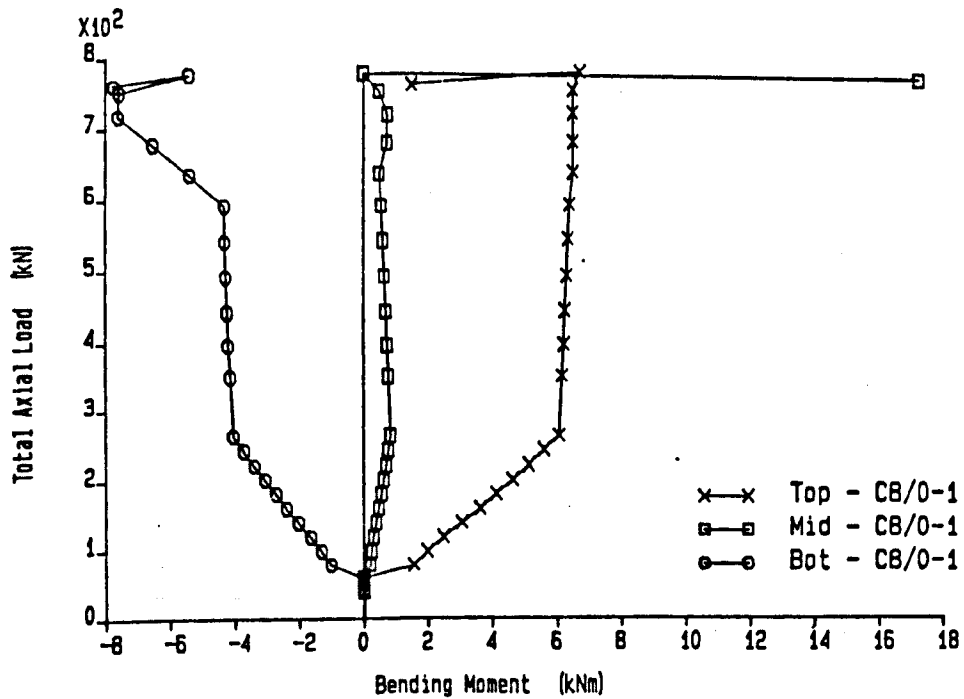


Figure 5.58: Axial load vs. major axis moment at the top, mid-point and bottom of C8/0-1.

Secondary beam connection moments.

Frame test F2

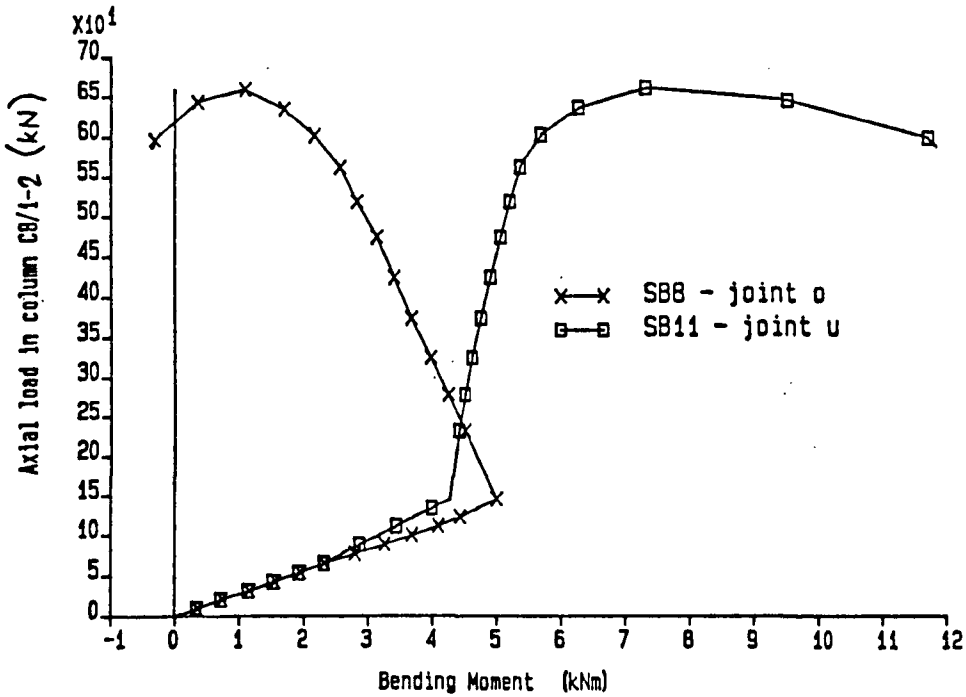


Figure 5.59: Axial load vs. moment at the connection of beams SB8 and SB11 to column C8/1-2.

Primary beam connection moments.

Frame test F2

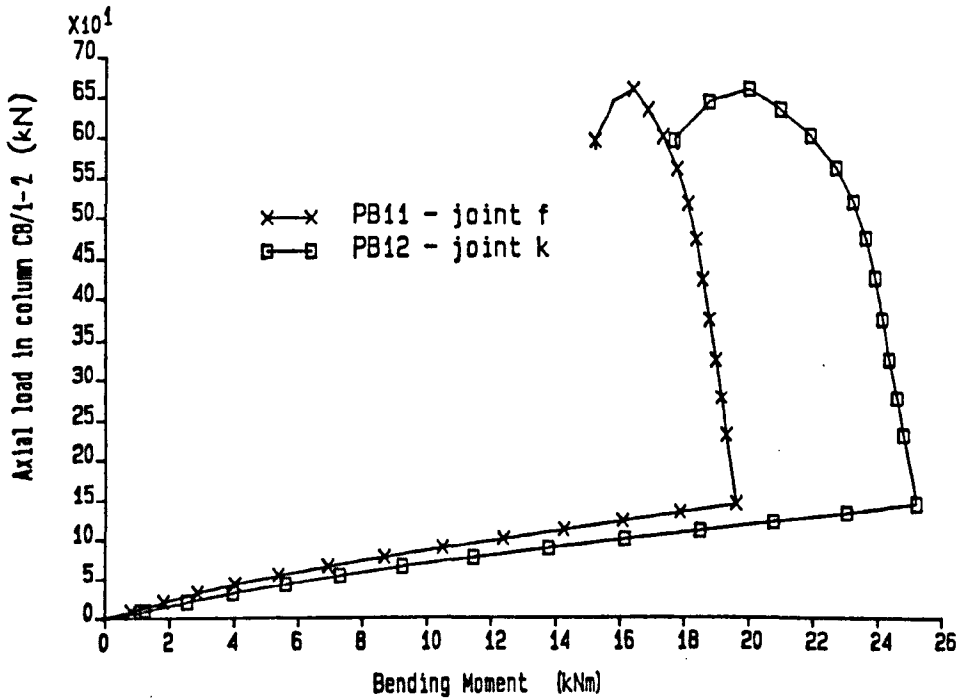
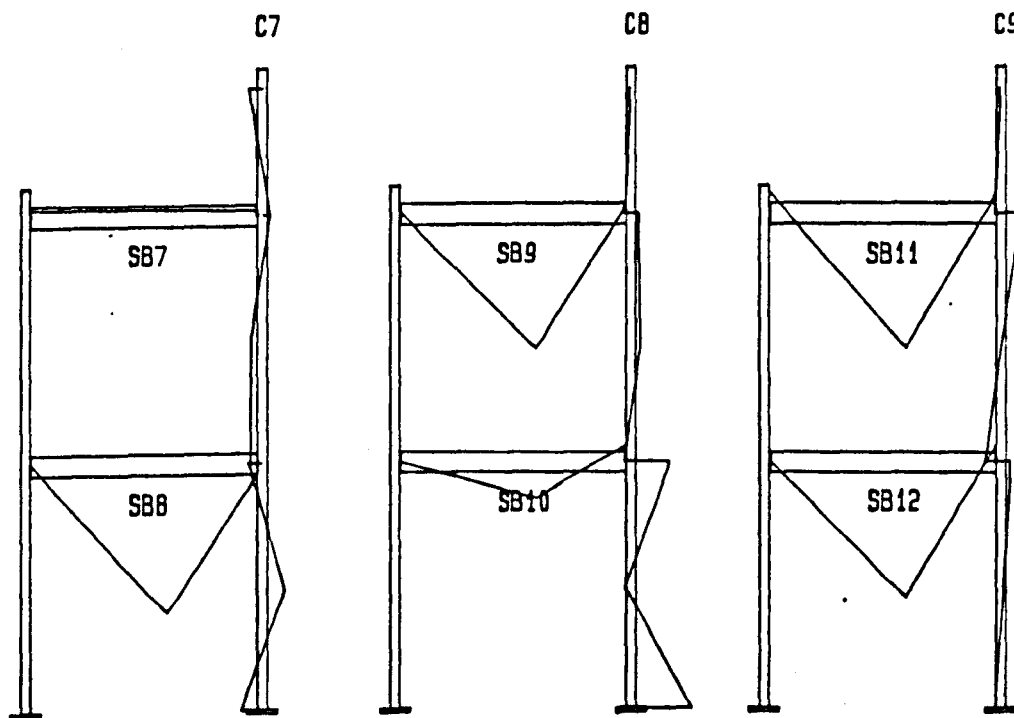
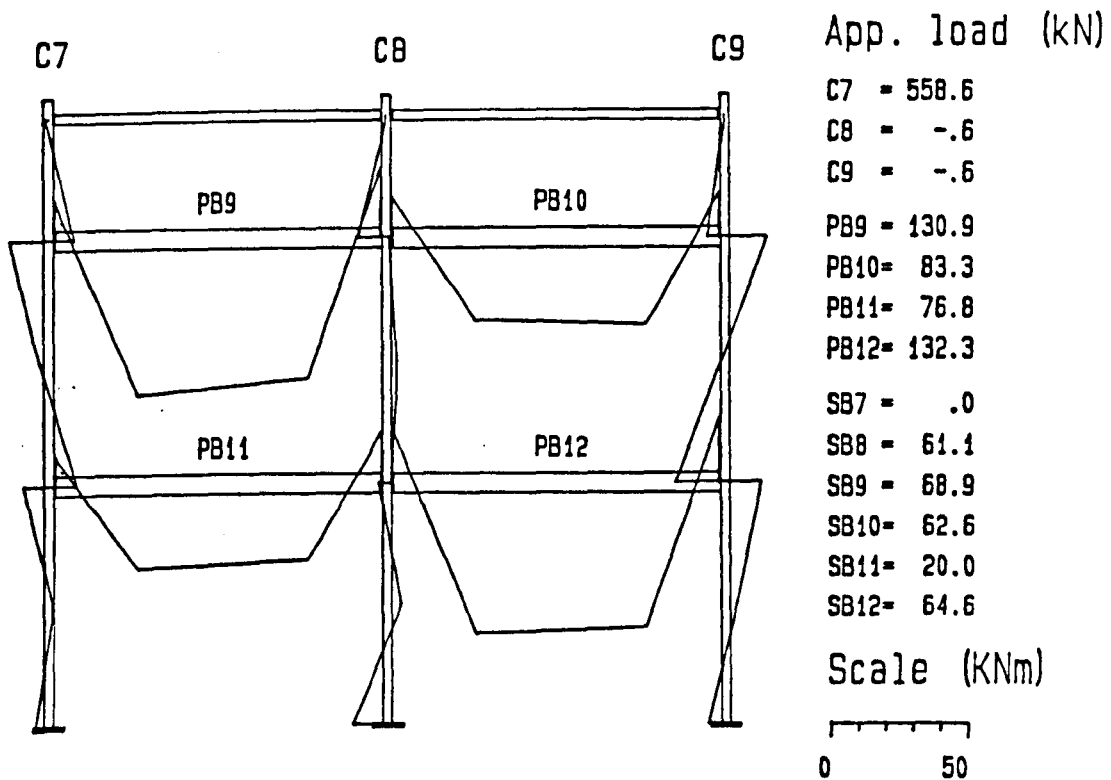


Figure 5.60: Axial load vs. moment at the connection of beams PB11 and PB12 to column C8/1-2.



Bending Moment Diagram - Test Frame 2

Figure 5.61: Computer generated frame bending moments on column C7 at the penultimate increment before the ultimate load was achieved.



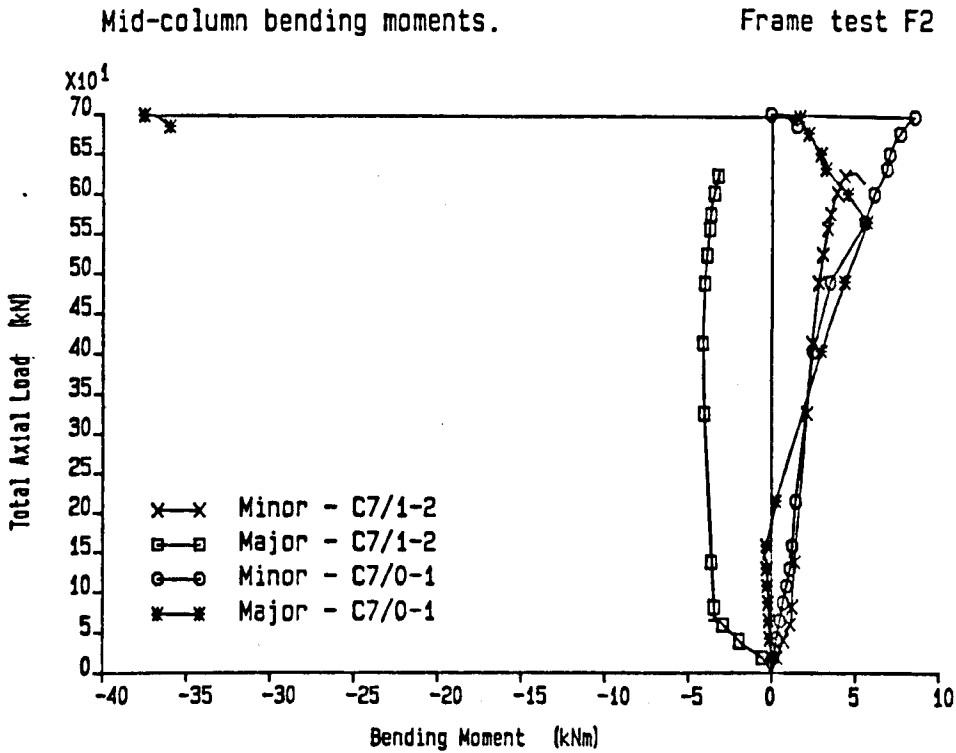


Figure 5.62: Axial load vs. mid-column moments for columns C7/0-1 and C7/1-2.

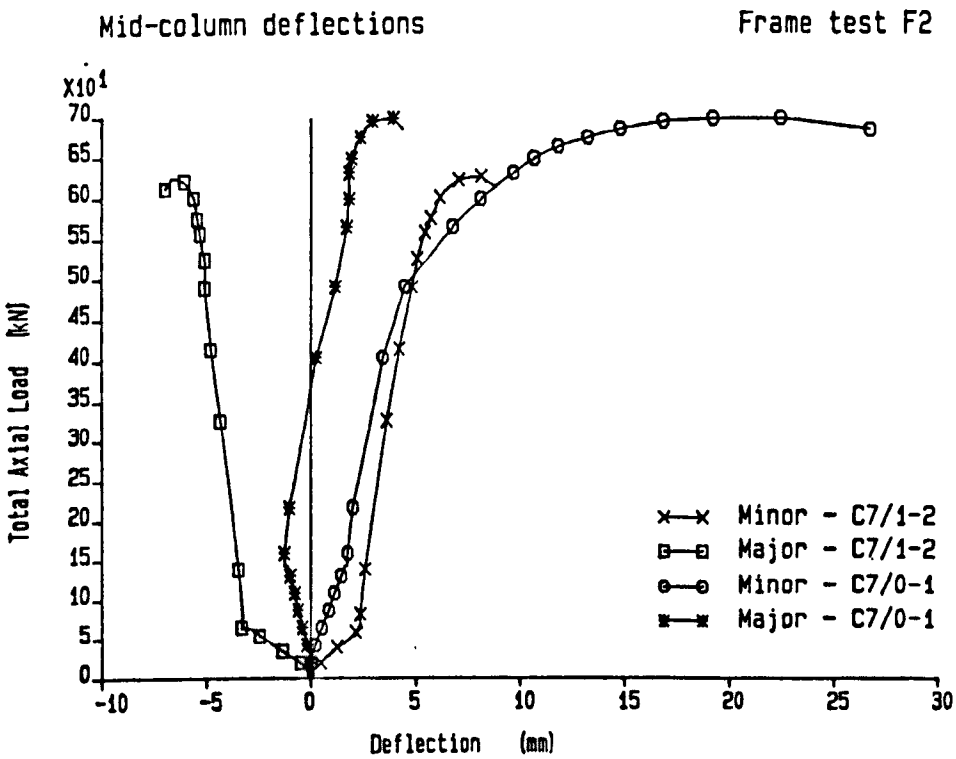


Figure 5.63: Axial load vs. mid-column deflections for columns C7/0-1 and C7/1-2.

Mid-column twist rotations.

Frame test F2

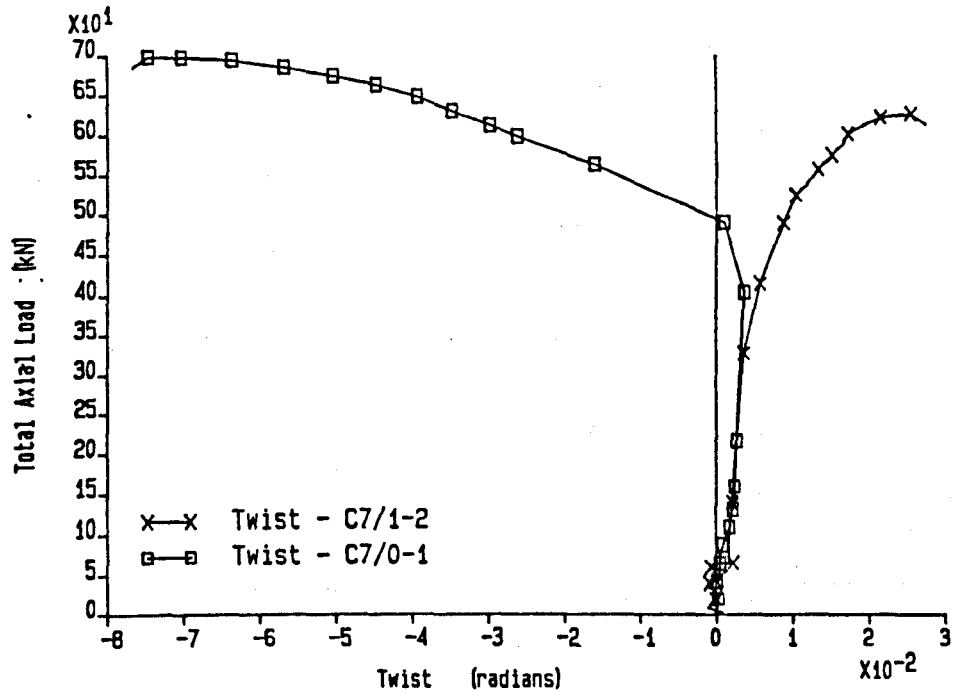


Figure 5.64: Axial load vs. mid-column twist rotation for columns C7/0-1 and C7/1-2.

Minor column axis bending moments.

Frame test F2

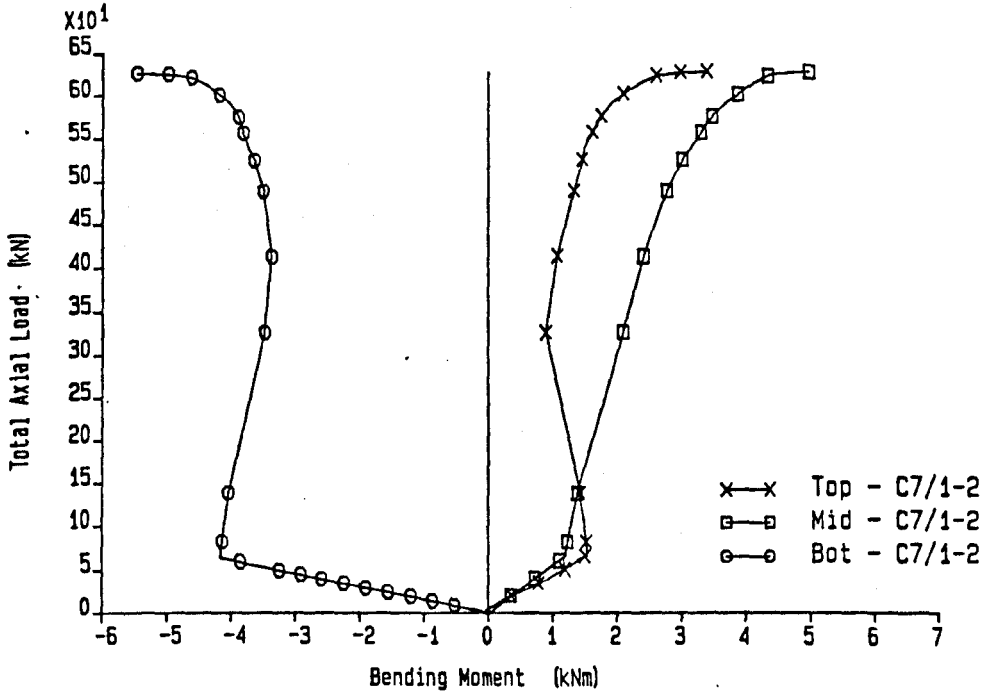


Figure 5.65: Axial load vs. minor axis moment at the top, mid-point and bottom of column C7/1-2.

Major column axis bending moments.

Frame test F2

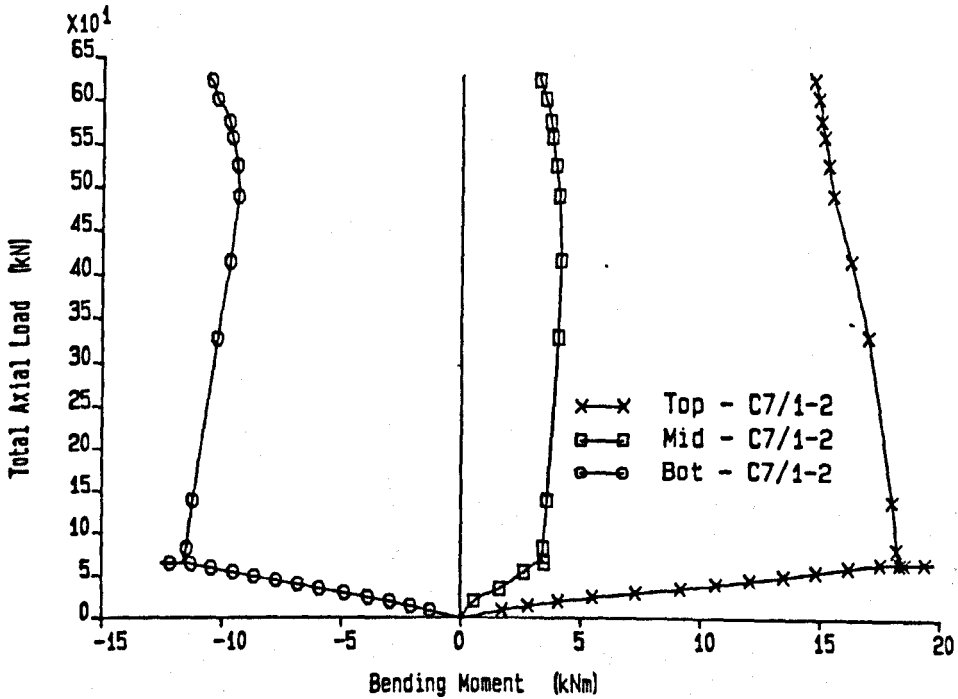


Figure 5.66: Axial load vs. major axis moment at the top, mid-point and bottom of C7/1-2.

Minor column axis bending moments.

Frame test F2

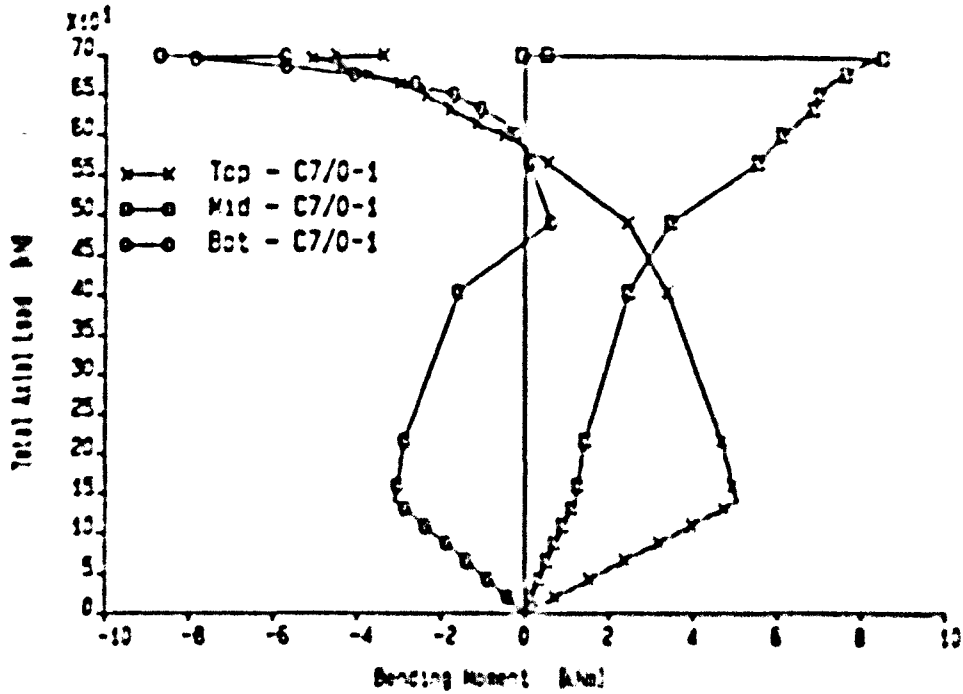


Figure 5.67: Axial load vs. minor axis moment at the top, mid point and bottom of column C7/O-1.

Major column axis bending moments.

Frame test F2

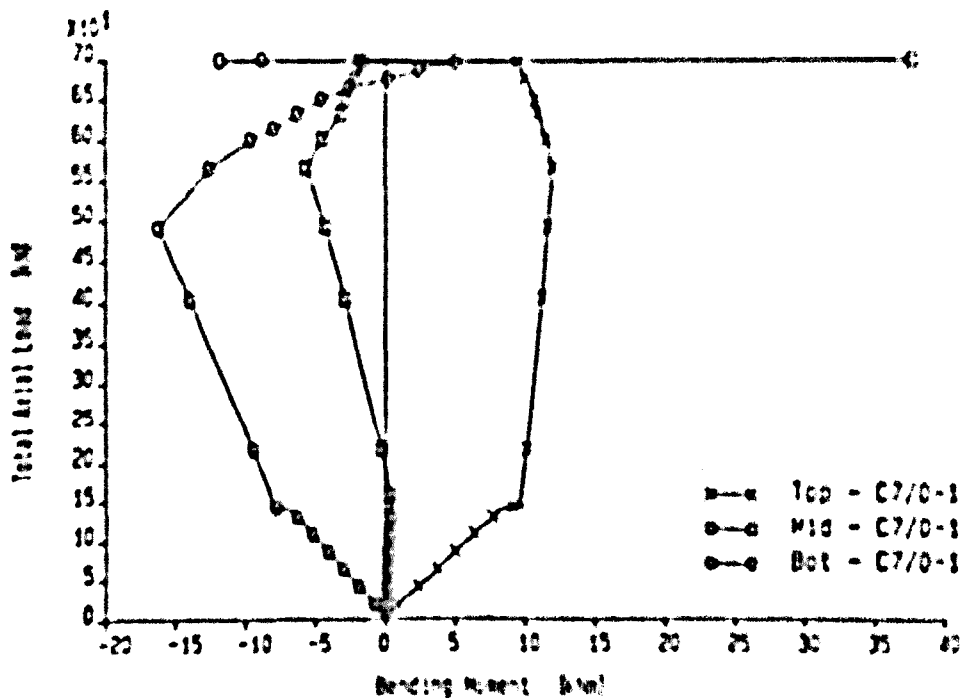


Figure 5.68: Axial load vs. major axis moment at the top, mid point and bottom of column C7/O-1.

## Chapter 6

# Connection Moment-rotation Behaviour.

### 6.1 Introduction

The moment rotation characteristic of a connection is one of the most fundamental parameters used in the study of semi-rigid frame behaviour. The diversity of the  $M - \phi$  response for different connection types, and the equally diverse effect on the behaviour of the connected elements, means that a measure of the connection stiffness will be an important feature in any design or analysis technique developed for semi-rigid frames. As a consequence, there has been much research activity in recent years devoted to quantifying the  $M - \phi$  behaviour by experimentation, and by analytical means. As was discussed in chapter 1, analytically predicted moment-rotation behaviour tends to be unreliable and the various analysis programs which have been developed have a limited range of application. For this reason, the experimental assessment of connections remains the most reliable means of determining connection response.

This chapter presents a brief overview of a series of isolated connection tests which were

performed at the University of Sheffield. The tests, performed by others, considered nominally identical connection details to those adopted in the subassemblage test series and frame test F1. Throughout this chapter, the behaviour of these 'isolated' connections has been compared to the response of the corresponding subassemblage and frame connections. The chapter concludes by investigating an apparent anomaly which was observed in some of the frame test connections and highlights the possible ramifications for design and future experimental connection studies.

## **6.2 The 'isolated' connection tests.**

At the time of this research project, a study was being conducted at the University of Sheffield into the in-plane and out-of-plane response characteristics of 'simple' isolated bolted steelwork connections under slow cyclic loading [6.1]. It was proposed that a series of additional connection specimens should be appended to this test programme which were nominally similar to those subsequently used by the author in the subassemblage tests and frame test F1. The aim was to provide a direct correlation between isolated connection response and connection behaviour in extensive three-dimensional structures.

The details of the four different connection types studied; namely web cleats, flange cleats, web and seat cleats and flush end plates, are presented in figure 6.1. Figure 6.2 shows the basic experimental set-up used for the connection tests and illustrates the principal components. It is evident that the test was a 'cantilever' arrangement in which one beam only was connected to the column. This compares with the commonly used alternative 'cruciform' arrangement in which two beams are connected one on each side of the column. The merits of these two types of connection test are discussed in section 6.5.

The specimens comprised a 650mm length of beam, 254x102x22 UB, connected to a 650mm long 152x152x23UC column. The column section was clamped along its length to a stiff mounting plate bolted to the test rig. Two one-way acting hydraulic rams applied a moment, and hence rotation, to the connection in an alternating clockwise and anti-clockwise direction, with progressively increasing magnitude, to develop the full cyclic  $M - \phi$  envelope.

To achieve maximum similarity between the isolated connection tests and the subsequent subassembly tests, the beam, column and cleat angle sections were cut from the same stock lengths of steel used to fabricate the subassembly specimens. The assumption was that there would be only a marginal variation in the steel properties used in the two types of test. A summary of the location of the connection test offcuts, together with measured material properties, is presented in the supplementary volume to this thesis [6.2].

Each of the four different connection types was tested to determine the in-plane and the out-of-plane response when connected to either the column web or the column flange. This resulted in a total of 16 tests, a summary of which is presented in table 6.1. Those tests with a suffix 'a' (see table), denote secondary tests which were performed to investigate the out-of-plane connection response when the beam was connected to the column flange and 'redundant' cleats were connected to the column web. These 'redundant' cleats simulated the stiffening effect of the column web panel due to the presence of an adjacent interconnecting beam.

For a comprehensive description of these tests and a discussion of the results, the reader should refer to reference 6.1. However, a number of the measured in-plane connection responses are presented in the following sections and compared with the observed connection behaviour in the subassembly tests and frame test F1.

### 6.3 The subassemblage tests.

Although four different connection types were studied in the subassemblage tests (chapter 2), only the web cleat, flange cleat and the web and seat cleat connections will be discussed in this section. The behaviour of the flush-end plate connection is discussed at length in section 6.4 which concentrates on the experimental frame test data.

A selection of the moment-rotation responses observed in the subassemblage tests is presented in figures 6.4 to 6.8. A consistent plot scale has been adopted throughout to enable a direct comparison between the relative performances of the different connection types. The moment-rotation data derived from 'isolated' connection tests have been shown on the plots. This includes the 'cantilever' connection data from the tests described in section 6.2, together with that from 'cruciform' connection tests performed by Davison [6.3]. As the name suggests, the 'cruciform' test comprises two beams connected to either side of a single length of column. A symmetrical beam loading is applied and the moment-rotation response of the two connections is measured simultaneously. Figure 6.3, extracted from reference 6.3, shows the experimental set-up used for the 'cruciform' connection tests. The particular 'cruciform' specimens investigated by Davison were fabricated using similar member sizes and connection details to those studied in the 'cantilever' tests and the subsequent subassemblage tests. It should be noted that to improve the clarity, all of the 'isolated' connection test data has been shown as smooth fitted curves.

The  $M - \phi$  response of the web cleat connection to the column flange, shown in figure 6.4, illustrates the relatively small stiffness and moment capacity of this particular connection. It is evident that the behaviour of the subassemblage connection is similar to that from the 'isolated' tests at small rotations. Figure 6.5 shows the  $M - \phi$  curves for a flange cleat connection to the column web. Again, the behaviour of the subassemblage connections corresponds quite closely with that observed in the 'isolated' connection tests. However, the negative slope of the moment-rotation curve observed for two of the



three subassemblage joints in the early stages of loading does suggest a small degree of experimental error.

The  $M - \phi$  response for flange cleat and web and seat cleat connections to the column flange are shown in figures 6.6 and 6.7 respectively. It is evident that in the case of figure 6.6, the subassemblage connection behaviour closely resembles that of the 'isolated' tests if the initial experimental data offset is ignored.

Figure 6.8 shows the  $M - \phi$  response for web and seat cleat connections to the column web. It is noticeable that in this instance there is a significant difference in the behaviour of the two 'isolated' test connections. This is due to the effects of column web flexibility which are included in a 'cantilever' connection test but which are nullified in a 'cruciform' test due to the symmetrical arrangement of beam loads (see section 6.5). This explains the reduced stiffness and moment capacity observed for the 'cantilever' test connection. Due to the relatively small lever arm between the cleats in a web and seat cleat connection, the tension and compressive forces acting on the cleats will, for a given moment, be significantly larger than those in a flange cleat connection where the lever arm between cleats is significantly larger. Consequently, the behaviour of the web and seat cleat connection is very much more susceptible to the effects of column web flexibility. This is verified in figure 6.5 in which the behaviour of a flange cleat connected to the column web in the 'cantilever' test is almost identical to that from the 'cruciform' test. It is evident from figure 6.8 that the behaviour of the three subassemblage connections are similar and that they are intermediate between the behaviour of the 'cantilever' and 'cruciform' test specimens.

For clarity, only those subassemblage connections which exhibited a continual 'closing' throughout both the beam loading and column loading phases of the test, a 'loading-loading' response, have been presented in figures 6.4 to 6.8. However, there were a number of instances in which connections applied a disturbing moment to the column during the beam loading phase which was subsequently reduced, or in some cases reversed, when the

column head load was applied. This is often referred to as 'loading-unloading' connection behaviour. Figure 6.9 shows the moment-rotation response for three subassemblage connections, a web cleat, flange cleat and a web and seat cleat, where this phenomenon was observed.

## 6.4 Frame test F1.

A 12mm thick flush end plate connection, similar to that shown in figure 6.1, was used for all the connections in the first full scale frame test, F1. There were three different arrangements of beam to column connection to be considered, namely:-

1. A secondary beam connected to column flange on one side only - joints 'o', 'q' and 's'.
2. A primary beam connected to one side only of the column web (i.e. primary beam/'corner' column) - joints 'j', 'e' and 'c'.
3. A primary beam connected to both sides of the column web (i.e. primary beam/internal column) - joints 'd', 'f', 'i' and 'k'.

The multiple moment-rotation plots for these three structural arrangements are shown in figures 6.10 (case 1), 6.11 (case 2), 6.12 (case 3 - joints 'f' and 'i') and 6.13 (case 3 - joints 'd' and 'k'). The moment-rotation characteristics of the same flush-end plate connection observed in isolated joint tests by Davison (cruciform tests) [6.3] are shown on the plots for comparison together with those observed in the 'cantilever' tests described in section 6.2.

It is quite apparent from figure 6.10 that the  $M - \phi$  response of the secondary beam connections 'o' and 'q' is very similar to that observed in both the isolated connection tests, whereas that for connection 's' is markedly different. It should be noted however, that this connection was at the 'active' frame end of beam SB4 which experienced a loading malfunction during the course of the frame test (see chapter 5). The inadvertent premature failure of this particular beam corresponds with the large distance between the penultimate data points on the plot for joint 's' shown in the figure.

Figure 6.11 shows the  $M - \phi$  response of the primary beam connections with the web of the 'corner' columns. The unusual 'shift' in the data points at the end of the beam loading phase for joint 'e' was a result of the accidental failure of the adjacent beam, SB4, described above. The large discrepancy between the behaviour of the 'cruciform' and 'cantilever' tests data is a result of the effects of web flexibility described in the previous section. Not surprisingly, the observed  $M - \phi$  behaviour of the frame connections was very much closer to that observed in the isolated 'cantilever' joint test when compared to that from the 'cruciform' test. This is of course due to the similarity of structural configuration between the 'cantilever' specimens and these particular frame connections. It is interesting to note that whilst there appears to be a discrepancy between the measured initial stiffness and moment capacity of the three frame connections, the unloading stiffness of the connections are approximately equal.

Figure 6.12 shows the moment-rotation plots for the primary beam connections to the internal column at joints 'f' and 'i', which exhibited a 'loading-unloading' response, whilst those for joints 'd' and 'k', which exhibited a 'loading-loading' response, are shown in figure 6.13. It is evident that the behaviour of all four connections is similar during the beam loading phase and, unlike the connection to the 'corner' columns discussed above, has a similar stiffness and ultimate capacity to that observed in the isolated 'cruciform' test. The high stiffnesses which have been observed explain the large primary beam moments which were attracted to the centre column support.

The most interesting feature of the plots shown in figure 6.12 is the unexpected response of the connections during the column head loading phase in which both connections 'f' and 'i' exhibited a significantly reduced unloading stiffness. This implied that modest rotations at the head of the column had a negligible effect on the beam connection moments. However, when the applied loads were instantaneously removed at the point of maximum load on the centre column, C5, the connections exhibited an unloading stiffness comparable with the initial tangent stiffness,  $C_i$ . The magnitude of the unloading stiffness therefore depended on whether the rotations induced at the connection were induced as a result of column deformation or due to a reduction in the applied connection moment. It is the author's opinion that this particular phenomenon was one of the most important observations from the entire research study. The following section has therefore been devoted to proposing an explanation for this behaviour as well as highlighting the possible ramifications for semi-rigid frame design and future experimental connection tests.

## 6.5 The behaviour of semi-rigid connections in frames.

The generally accepted moment rotation response of a semi-rigid connection is shown in figure 6.14 [6.4]. The plot comprises a non-linear loading phase followed by a linear unloading phase of equivalent slope to the initial tangent stiffness  $C_i$ . The usefulness of this correlation between the loading and unloading phases of connection response has been realised by many researchers and has formed the basis of a number of semi-rigid design techniques [6.5].

The previous section presented some observations of connection moment-rotation response from frame test F1 and showed that in some instances the unloading stiffness of the connection can be significantly less than  $C_i$ ; thus representing a deviation from the ac-

cepted theory. Figure 6.15 shows the behaviour of the particular frame connection where this phenomenon was most prevalent highlighting the various stages of loading. It is clear that if this behaviour occurs in a wide range of practical situations, the ramifications for semi-rigid design may be far reaching.

It is envisaged that this 'unusual' connection response will only occur when a pair of beams are attached to both sides of the column web via relatively stiff connections. Therefore, in section 6.5 the author has proposed a possible explanation of the response which concentrates on the combined effect of column web panel flexibility and beam continuity. In addition, the author has extended these observations to propose a method which enables this kind of connection response to be predicted for a wide range of beam and column combinations. However, it should be appreciated that the proposed prediction method is based on a limited number of observations of the phenomenon from a single experimental frame test. Clearly, further experimental observations of this type of connection behaviour are required to fully validate the proposed concept.

### 6.5.1 The influence of column web panel flexibility.

Figure 6.16 shows a hypothetical situation in which a beam frames into one side of a column web. On applying a load to the beam, the resulting fixed end moment is distributed between the connected parts in the proportions shown in the figure. The column web panel transfers the connection moment to the relatively stiff column flanges and deforms accordingly. When a load is applied to the column head, the column deforms in the same direction as the initial disturbing moment thus causing a reversal of the column head moment, the connection moment and the column web deformation.

Observation of the effect of column web flexibility on connection behaviour is not new. Indeed, it was this phenomenon which led a number of researchers to develop cantilever

tests, similar to those described in section 6.2, which determined the  $M - \phi$  connection response in the presence of local column deformations. In such arrangements in which the beam is connected to the minor axis of the column, there is a direct relationship between the moment which can be sustained and the flexibility of the column web. The differences between the 'cantilever' and the 'cruciform' connection tests reported in section 6.4 highlighted the importance of web flexibility effects on the performance of connections.

### 6.5.2 The influence of beam continuity.

The hypothetical arrangement shown in figure 6.16 is repeated in figure 6.17 but, in this instance, a beam is connected to either side of the column web. If, as before, a load is applied to the beam on the left hand side of the column, the fixed end beam moment will be distributed between the connected parts in relation to their bending stiffness. Unlike the cantilever arrangement however, only a small proportion of the applied disturbing moment is transferred to the column. Obviously, the total stiffness of the components at this connection is greater than that of the cantilever arrangement and consequently, the moment attracted to the beam connection will be significantly larger. The magnitude of the smaller proportion of moment transferred to the column may therefore, depending on the stiffness of the beams, be comparable with that observed in the cantilever arrangement shown in figure 6.16.

As before, the column web deforms as the disturbing connection moment is transferred, via the web panel, to the stiff column flanges. On subsequently applying the column head load the column deforms, as in the cantilever arrangement, in the same direction as the disturbing moment. This causes a reversal of both the column head moment and the column web deformations. However, due to the continuity of the beam and the

relatively low stiffness of the column, rotation at the column head will have only a very small effect on the moment at the beam to column connections. The connection moment will therefore remain approximately constant despite the possibility of a complete reversal of moment at the column head.

This effect of beam continuity on the moment-rotation response of a connection is illustrated by considering an extreme example. Figure 6.18 shows a pair of small, compact beams connected to either side of a large, thin column web panel via stiff semi-rigid connections. If the web panel is assumed to be sufficiently flexible and its ability to resist rotation ignored, then the column may be treated as a simple pinned prop to a continuous beam. This structural arrangement is shown in figure 6.19. If the beams are loaded symmetrically, a pattern of beam bending moments will result and a conventional non-linear 'loading' moment-rotation response will be observed at the connections. If at the end of the beam loading phase load is applied directly to the column head, the column will deform laterally inducing a rotation at the head of the column. Due to the negligible bending stiffness of the column web panel, the column head rotation will not have any effect on the distribution of beam bending moments. The unloading stiffness of the arrangement at the column head will therefore be zero producing a horizontal line on the moment-rotation plot. The resulting 'loading-loading' and 'loading-unloading' moment-rotation plots for the connections on either side of the column are shown in the figure.

It is evident that these moment-rotation plots are hybrids of the expected moment-rotation response measured from a 'cruciform' test and that from a 'cantilever' test, as shown in figure 6.20. The 'cruciform' test is representative of the beam loading phase, whilst the unloading 'cantilever' test response is representative of the connection behaviour when 'unloading' due to column deformation. This is verified in figure 6.21 which compares the response of frame test joint 'f', a minor axis connection to the internal column (similar arrangement to a cruciform test), with that of joint 'j', a minor axis connection to a 'corner' column (similar arrangement to a cantilever test). As

discussed previously, these two structural arrangements exhibit a significantly different stiffness during the loading phase. However, it is evident that the unloading stiffness at joint 'f', resulting from column deformation, is approximately equal to that of the cantilever arrangement at joint 'j' when the beam loads are removed.

It is clear therefore that situations can arise in which the unloading stiffness of a beam to column web connection in a frame is not equal to the initial tangent loading stiffness.

### **6.5.3 The validity of isolated connection tests.**

As discussed in the previous section, the total loading-unloading response of some of the frame test connections appears to be a combination of the response expected from a cruciform joint test and that from a cantilever test. This would suggest therefore that the data from these two types of test could be used to 'construct' the total response of a connection in a frame with the 'loading' cruciform data representing the non-linear 'loading' stiffness and the 'unloading' cantilever response representing the 'unloading' stiffness. It is clear however that the arrangement of the isolated connection tests must accurately simulate the boundary conditions which are present in the frame. In the case of the cantilever test, the column length must be supported at its ends and be of sufficient length to enable local web and flange deformations to fully develop at the location of the beam connection. It should be noted that this was not the case in the cantilever tests reported in section 6.2 in which the column flanges were rigidly clamped to a stiff backing plate along the full length of the section.

It would appear from the arguments presented above that the unloading stiffness derived from the numerous cruciform tests on beam connections to the column web is of little use. The exception would of course be cruciform tests on very flexible connections connected



to stiff web panels where the potential for web deformation is very small. In terms of semi-rigid design, extreme caution should be exercised when applying an unloading stiffness which is equivalent to the initial tangent stiffness derived from a cruciform test.

Due to the symmetrical nature of the cruciform test, the two connections which are assessed in any one test are invariably of the same type using similar sized beams. It would therefore be difficult to apply the principles discussed above to a situation in which beams of different stiffness were connected to either side of the column web by different connection types - a situation which occurs frequently in practice (figure 6.22). It is evident that due to the anti-symmetry of this arrangement, the precise role of the column web flexibility and beam continuity would be less certain. It is quite probable that in this situation the behaviour of both connection types will be dissimilar, both during loading and unloading, to that derived from either a cruciform or cantilever connection test.

In the 'cruciform' and 'cantilever' joint tests, the unloading stiffness of a connection is determined by monitoring the connection rotation as the applied beam loads are reduced. Clearly, this is an unsatisfactory approach if the connection data is to be used to define a total restraint stiffness to the head of a column. Firstly, the load history is not compatible with real behaviour - internal columns in frames do not fail when the applied beam loading is reduced. Secondly, it is evident from the frame test data that where a stiff beam is connected to a flexible column web, the beam connection moments remain approximately constant - the connection rotation being a result of column deformation. Ideally, an alternative test arrangement is required which includes the effects of both beam continuity and column web deformation and which enables the connection rotations to be induced from column deformations.

The author has presented a possible test arrangement in figure 6.23 which satisfies these criteria. Initially, the tie bars at each end of the saddle beam would be tensioned, possibly by turnbuckles, to pre-load the column section. The beam loading rams, which react

against the saddle beam, would then be activated to load the beams and thereby induce a moment at the connections with the central column. Assuming that the beam loading rams are displacement controlled with a load monitoring facility, the extension of the rams will, once the required beam load has been applied, remain constant throughout the remainder of the test. To simulate the effect of column deformation in the second stage of the test, the turnbuckles to the two tie bars would be turned in opposite directions to rotate the saddle beam, and hence the axis of the beam sections with respect to the column. It is envisaged that this method of simulating column deformation will result in a much simplified experimental set-up when compared to an arrangement in which the column can be rotated directly. By using appropriate instrumentation to monitor the beam and column rotations and the connection moments, the unloading stiffness of the both connections could therefore be derived by rotating the saddle beam in a clockwise and then an anti-clockwise direction.

It is appreciated that whilst the measurement of the various parameters is relatively straightforward, the proposed experimental set-up is extremely complex and cumbersome. The author therefore proposes an alternative semi-empirical approach which determines the unloading connection stiffness from readily available existing cruciform and cantilever beam to column web connection data.

#### **6.5.4 A semi-empirical approach for determining $M - \phi$ response.**

If a stiff column web panel is used in conjunction with a relatively flexible connection then the behaviour of the connection will dominate the combined response. The total effective unloading stiffness will therefore be equivalent to the unloading stiffness of the connection irrespective of the web stiffness. Conversely, if a stiff connection is connected to a flexible column web panel then the flexibility of the web panel will dominate. This

appraisal of the combined effects of different actions is similar to that between beam stiffness and connection stiffness discussed in chapter 2. Galambos [6.6], proposed the following equation for the combined column restraint ( $K_{tot}$ ) due to these effects:-

$$K_{tot} = \frac{K_{beam}K_{joint}}{K_{beam} + K_{joint}} \quad (6.1)$$

where:

$K_{beam}$  = bending stiffness of the beam.

$K_{joint}$  = stiffness of the joint.

The value  $K_{joint}$  is the total beam to column joint stiffness and therefore includes the components of connection stiffness and local column deformation. From the appraisal presented above, the author proposes that the total joint stiffness can be expressed as follows:-

$$K_{joint} = \frac{K_{con}K_{web}}{K_{con} + K_{web}} \quad (6.2)$$

where:

$K_{con}$  = actual stiffness of the connection.

$K_{web}$  = stiffness of the web panel.

The total column restraint can therefore be expressed in terms of the individual components of beam stiffness, connection response and column web flexibility:-

$$K_{tot} = \frac{K_{beam}K_{con}K_{web}}{K_{beam}(K_{con} + K_{web}) + K_{con}K_{web}} \quad (6.3)$$

It is expected therefore that by using this equation, the loading restraint to a column with a single beam connection (as in figure 6.24) could be derived using the unloading

connection stiffness determined from a cruciform test in which the effects of local column deformation are ignored.

If an internal column arrangement is considered, there are two beams and two connection types to be taken into account when determining the total column restraint. The web panel flexibility will of course remain a single component for this arrangement. It is important when combining all of these stiffness components that the two beams are considered individually with their respective connections. The author therefore proposes an equation for determining the total effective column restraint for the arrangement shown in figure 6.25 as follows:-

$$K_{tot} = \frac{K_{web}(K_{bc1} + K_{bc2})}{K_{web} + (K_{bc1} + K_{bc2})} \quad (6.4)$$

where:

$K_{bc1}$  = The total stiffness of the beam and connection for beam 1.

$$K_{bc1} = \frac{K_{beam1} K_{con1}}{K_{beam1} + K_{con1}} \quad (6.5)$$

and

$K_{bc2}$  = The total stiffness of the beam and connection for beam 2.

$$K_{bc2} = \frac{K_{beam2} K_{con2}}{K_{beam2} + K_{con2}} \quad (6.6)$$

In the case of an internal column with beams connected to either side of the column web, the stiffness of the 'opening' connection ( $K_{con1}$ ) would be equivalent to the unloading stiffness. The stiffness of the 'closing' connection ( $K_{con2}$ ) would be equivalent to a secant stiffness at an appropriate level of moment on the 'loading' portion of the  $M - \phi$  plot.

Depending on the level of accuracy required, the contribution of the smaller stiffness contribution from the 'closing' connection ( $K_{con2}$ ) could be ignored. It is clear that this simplification implies that the total column head restraint is similar to that of a column with a single beam connection.

The web panel stiffness  $K_{web}$  is prominent in the above equations. It is this particular component which, at present, would be difficult to quantify. However, the author hopes that future research could be conducted to quantify the web panel stiffness for a range of column sections. It is envisaged that by creating a relatively simple linear elastic finite element model a direct relationship could be derived between the aspect ratio of the bolt group compared to the web panel dimensions and the bending stiffness  $K_{web}$  of the panel. The author expects that such a numerical model would be significantly less complicated, and possibly more reliable, than those which have been created to study the full semi-rigid response of connections.

Assuming that the finite element study of web flexibility was successful, equation 6.4 would comprise terms derived from standard experimental cruciform connection tests ( $K_{con}$ ), conventional stiffness considerations ( $K_{beam}$ ) and numerically modelled linear-elastic relationships ( $K_{web}$ ). Using the equation, the large amount of existing moment-rotation data derived from cruciform tests could be modified to include web flexibility effects and thereby predict the effective restraint to wide range of columns used in multi-storey semi-rigid frames.

A convenient means of checking the reliability of the approach would be to predict the unloading stiffness of a cantilever connection arrangement from the measured response of a cruciform connection test which used the same beam section and connection type. If found reliable, the use of equations 6.3 and 6.4 would effectively fulfil the function of the alternative connection test method proposed by the author in figure 6.23.

An in-depth appraisal of the proposals discussed above is outside the scope of this thesis. However, it is hoped that the thoughts and proposals presented herein by the author will be pursued by others to ultimately develop a more complete understanding of the complex behaviour of semi-rigid beam to column connections.

## **6.6 A summary of observations on connection $M - \phi$ response.**

1. Due to the effects of column web flexibility, there is a significant difference in the performance of stiffer connections, e.g. flush end plate and web and seat cleat, in the two types of 'isolated' connection tests.
2. The 'loading-loading' connection behaviour observed in both the subassemblage and frame tests appears to be similar to that observed in the corresponding 'isolated' connection test.
3. It was concluded that due to the combined effects of beam continuity and web panel flexibility that the unloading stiffness of beam connections to either side of the minor column axis is not necessarily equal to the initial tangent stiffness.
4. The author has proposed a method by which the effects of column web flexibility can be taken into account. The method can be applied to predict the performance of connections in which the beam loading, beam sizes and connection type are dissimilar on each of the opposite column faces.

## References.

- 6.1 Celikag, M., '*Moment-rotation behaviour of steel beam-to-column connections.*', Ph.D. Thesis, Department of Civil and Structural Engineering, University of Sheffield, U.K., February 1990.
- 6.2 Gibbons, C., '*The strength of biaxially loaded beam-columns in flexibly connected steel frames - Volume 2: A survey of the mechanical and geometric properties of structural steel sections*', Ph.D. thesis, Department of Civil and Structural Engineering, University of Sheffield, Dec. 1990.
- 6.3 Davison, J.B., '*Strength of beam-columns in flexibly connected steel frames*', Ph.D. Thesis, Department of Civil and Structural Engineering, University of Sheffield, U.K., June 1987.
- 6.4 Davison, J.B., Kirby, P.A. and Nethercot, D.A., '*Rotational stiffness characteristics of steel beam-to-column connections*', Journ. Construct. Steel Research, No.8, 1987, pp. 17-54.
- 6.5 Bjorhovde, R., '*Effect of end restraint on column strength - practical applications.*', A.I.S.C. Engineering Journal, Vol. 20, No. 1, First quarter, 1984, pp. 1-13.
- 6.6 Galambos, T.V., '*Discussion of small end restraint effects on the strength of H-columns.*', Journ. Struct. Div., Am. Soc. Civil Engrs., Vol 109, ST4, April 1982, pp. 1067-1077.

Joint Test	Beam to Column Connection Type	Beam connected to Web/Flange	Test type
JT1	Web cleat	Web	In-plane
JT2	Web cleat	Web	Out-of-plane
JT3	Web cleat	Flange	In-plane
JT4	Web cleat	Flange	Out-of-plane
JT5	Flange cleat	Web	In-plane
JT6	Flange cleat	Web	Out-of-plane
JT7	Flange cleat	Flange	In-plane
JT7A	- JT7 with added cleats		
JT8	Flange cleat	Flange	Out-of-plane
JT8A	- JT8 with added cleats		
JT9	Web and seat cleat	Web	In-plane
JT10	Web and seat cleat	Web	Out-of-plane
JT11	Web and seat cleat	Flange	In-plane
JT11A	- JT11 with added cleats		
JT12	Web and seat cleat	Flange	Out-of-plane
JT12A	- JT12 with added cleats		
JT13	Flush end plate	Web	In-plane
JT14	Flush end plate	Web	Out-of-plane
JT15	Flush end plate	Flange	In-plane
JT15A	- JT15 with added plates		
JT16	Flush end plate	Flange	Out-of-plane
JT16A	- JT16 with added plates		

Table 6.1: Summary of the 'cantilever' connection test series.



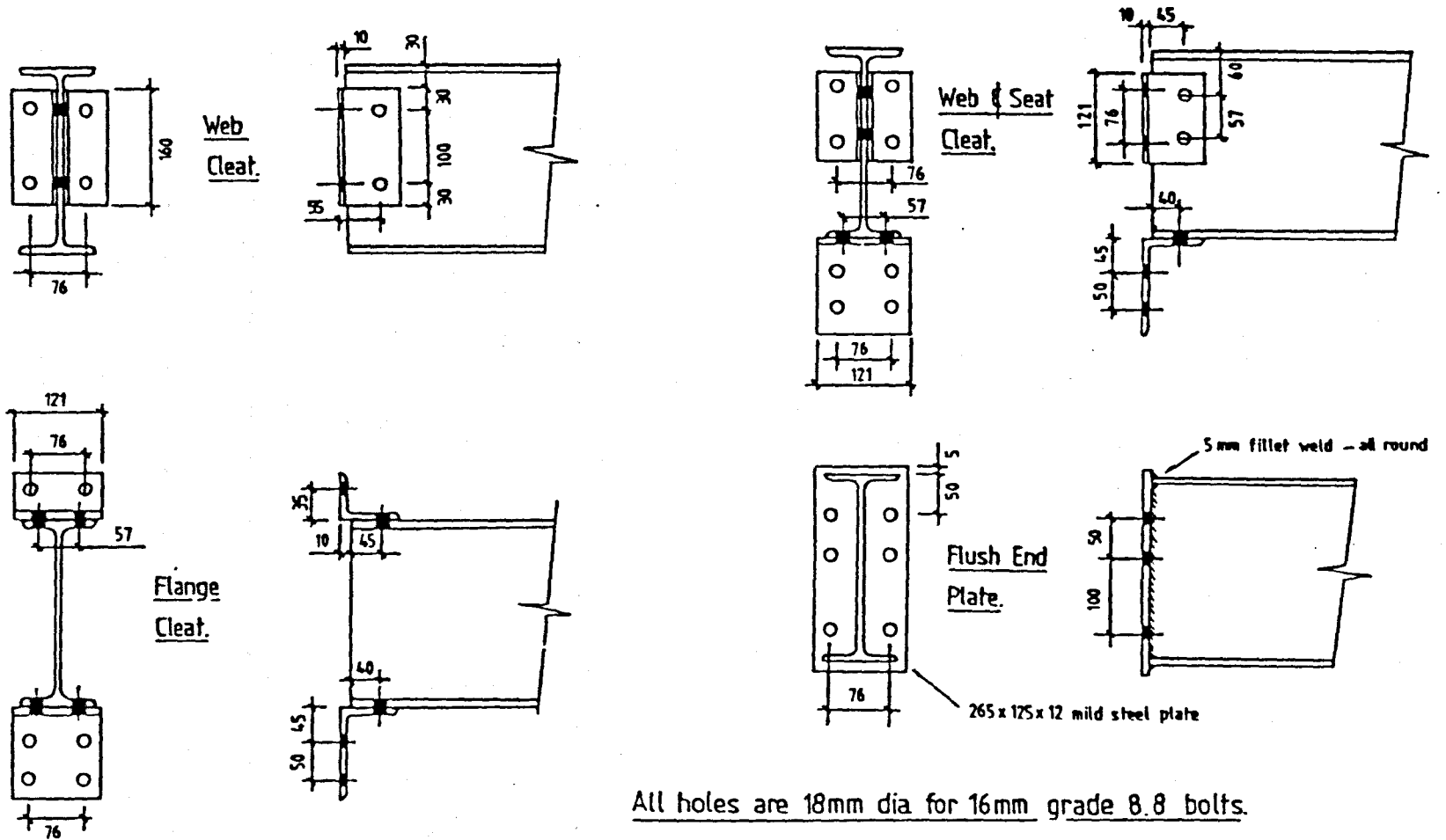


Figure 6.1: Fabrication details of the connections used in the study.

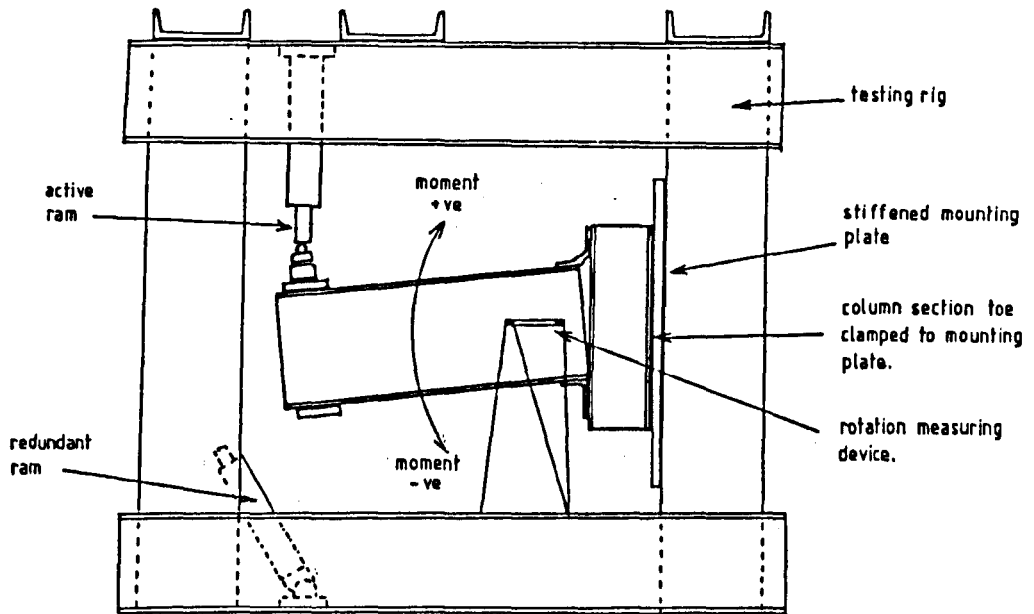


Figure 6.2: Experimental set-up of the 'cantilever' connection test.

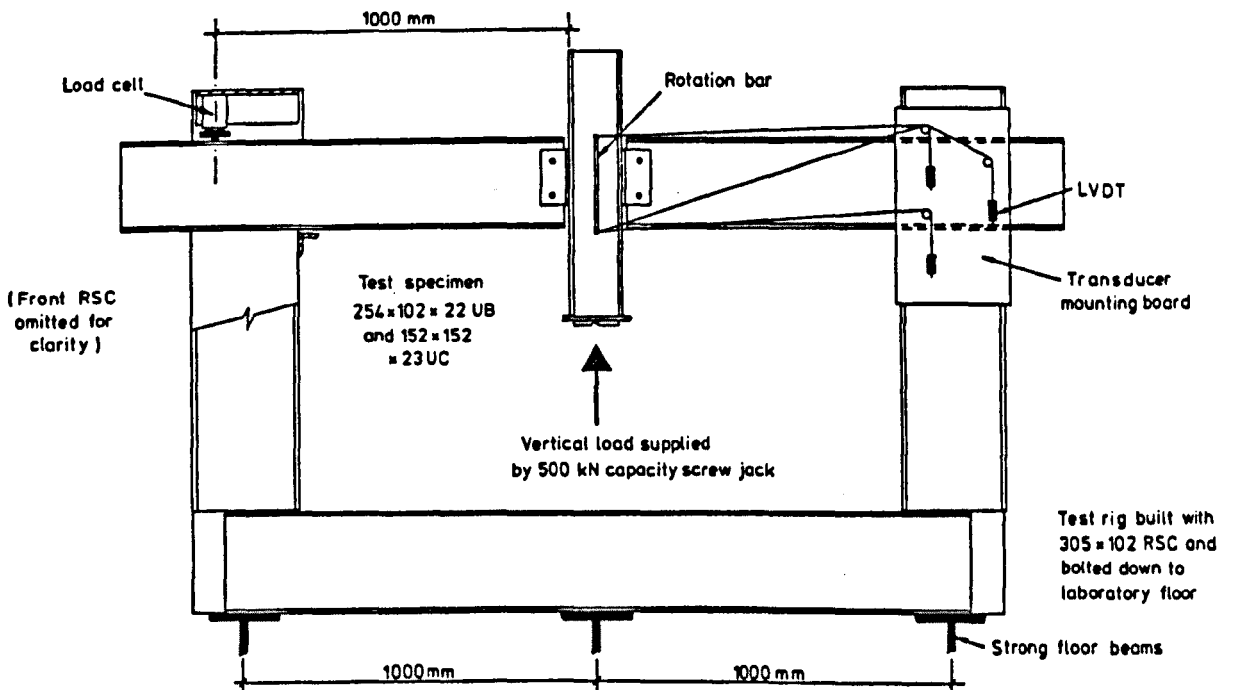


Figure 6.3: Experimental set-up of the 'cruciform' connection test.

Subassembly test moment-rotation data

Web cleat to column flange.

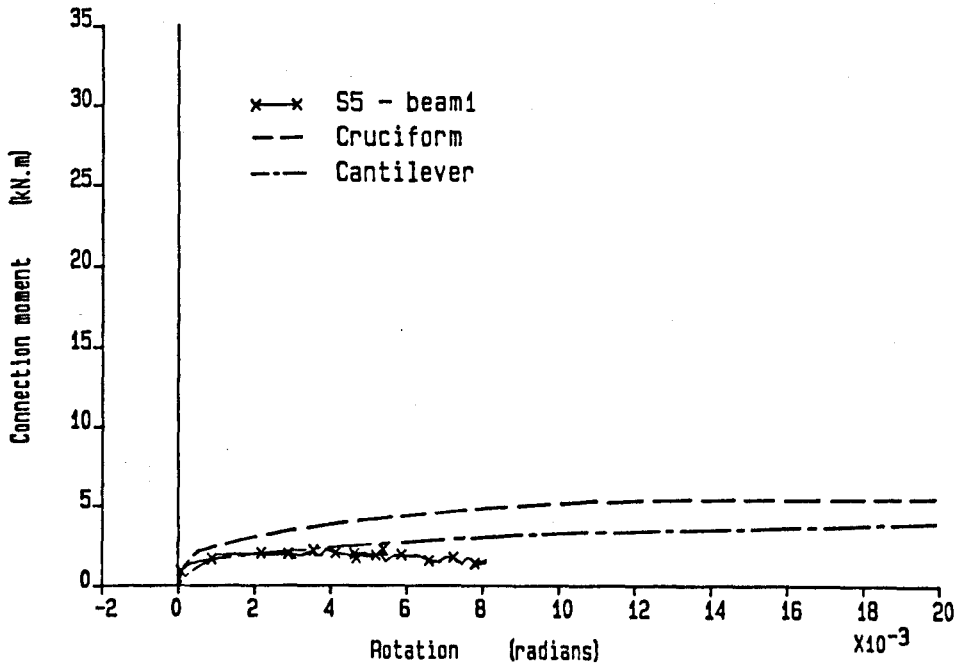


Figure 6.4: Moment-rotation response of web cleat connections to the column flange.

Subassembly test moment-rotation data

Flange cleat to column web.

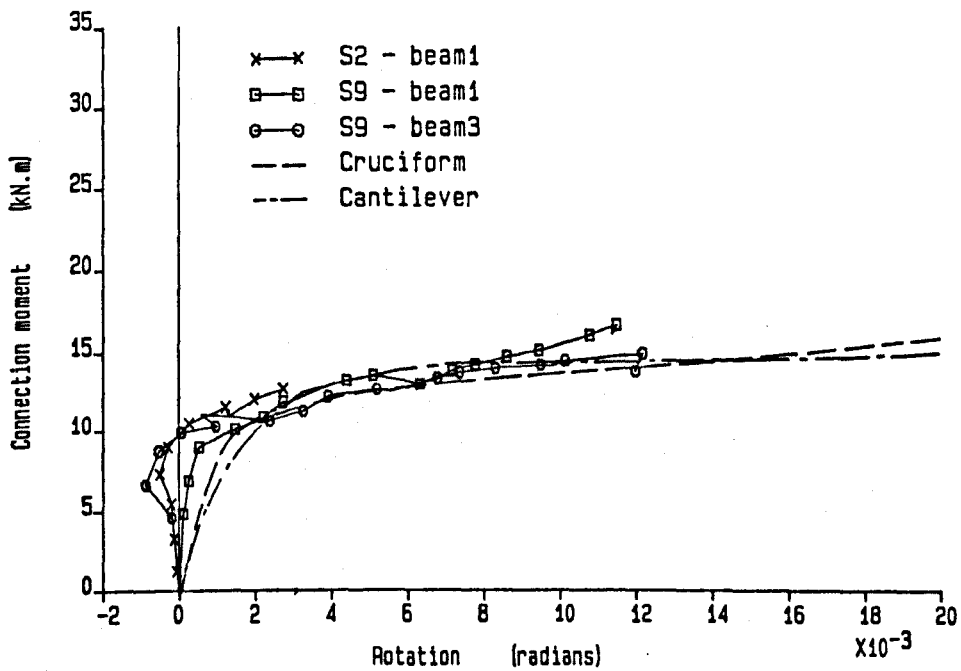


Figure 6.5: Moment-rotation response of flange cleat connections to the column web.

### Subassemblage test moment-rotation data

Flange cleat to column flange.

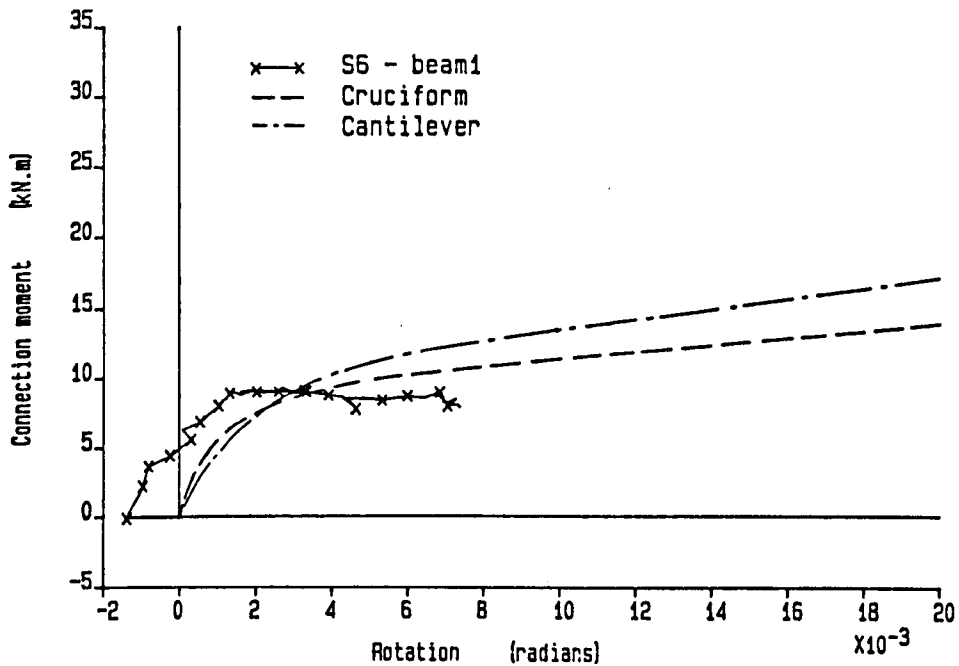


Figure 6.6: Moment-rotation response of flange cleat connections to the column flange.

### Subassemblage test moment-rotation data

Web and seat cleat to column flange.

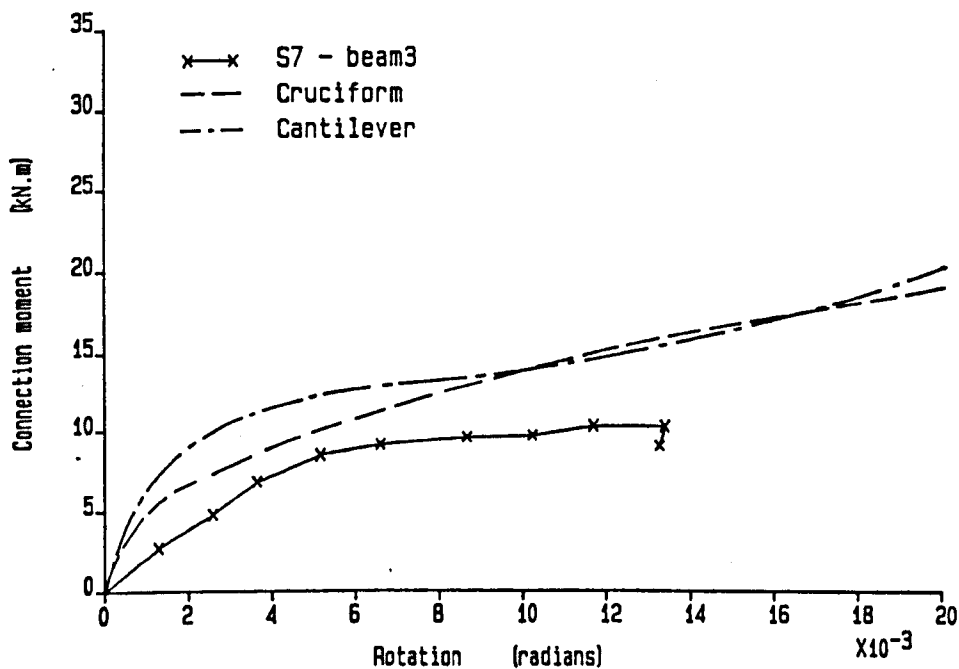


Figure 6.7: Moment-rotation response of web and seat cleat connections to the column flange.

Subassembly test moment-rotation data

Web and seat cleat to column web.

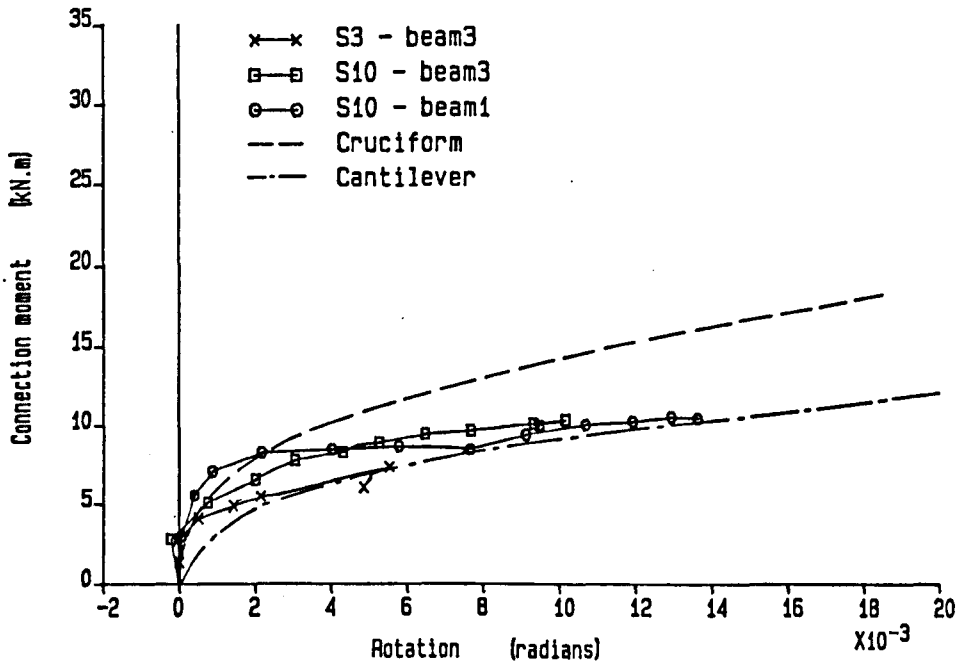


Figure 6.8: Moment-rotation response of web and seat cleat connections to the column web.

Subassembly test moment-rotation data

Connections to column web.

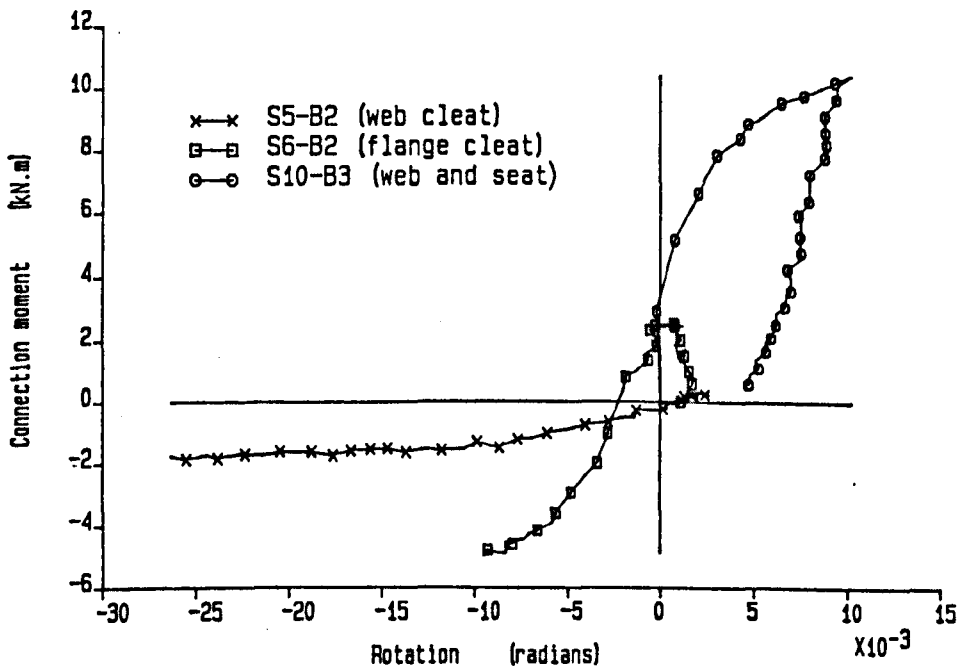


Figure 6.9: Moment-rotation response of different connections to the column web illustrating the 'loading-unloading' response.

Connection Moment Rotation

Frame test F1

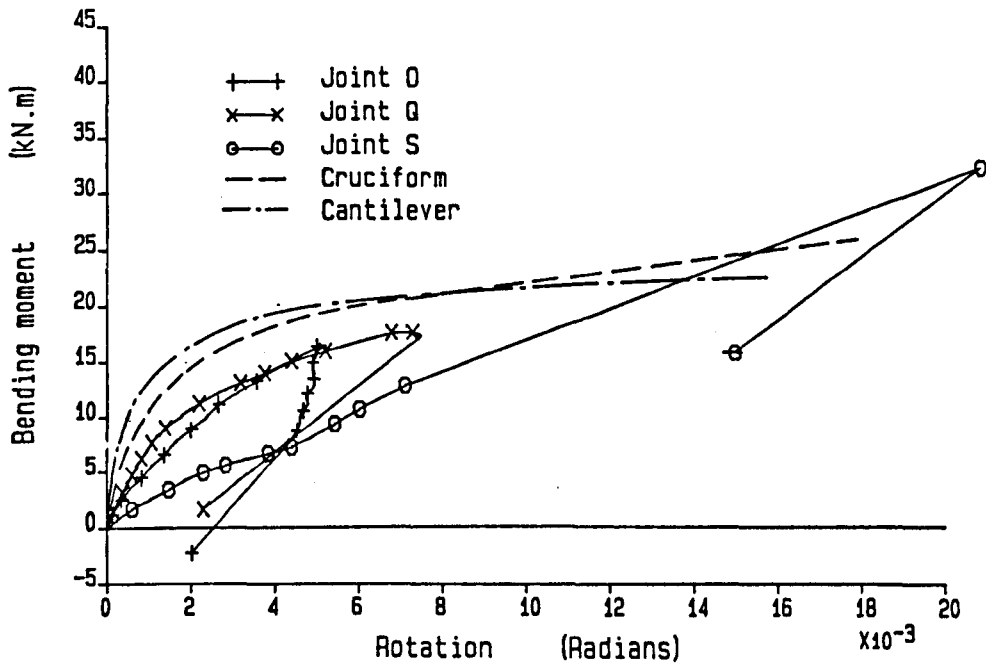


Figure 6.10 Moment-rotation response of flush end plate connections to the column flange.

Connection Moment Rotation

Frame test F1

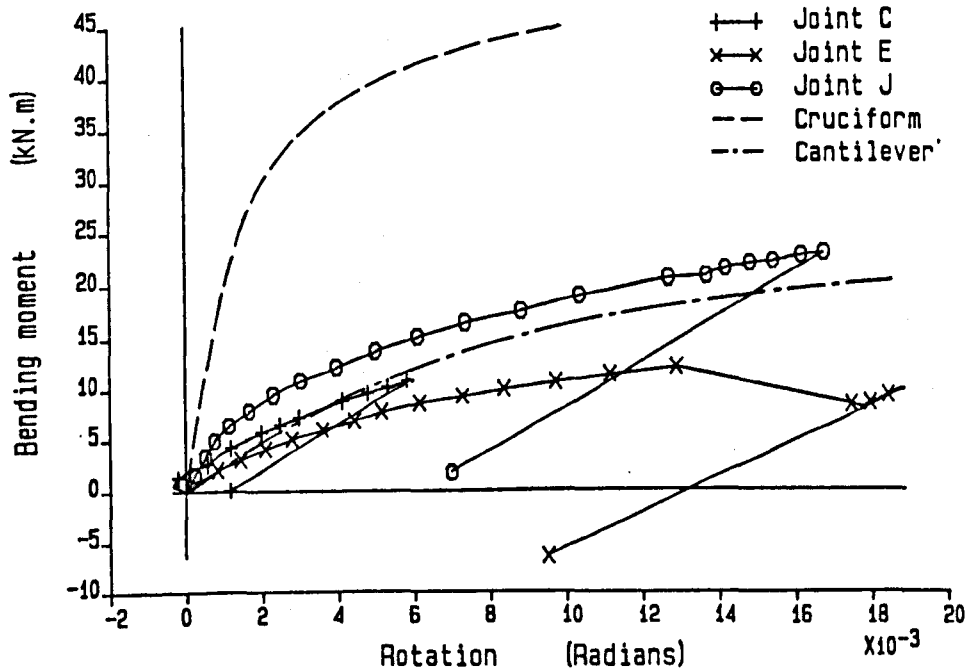


Figure 6.11 Moment-rotation response of flush end plate connections to the web of a 'corner' column.

Connection Moment Rotation

Frame test F1

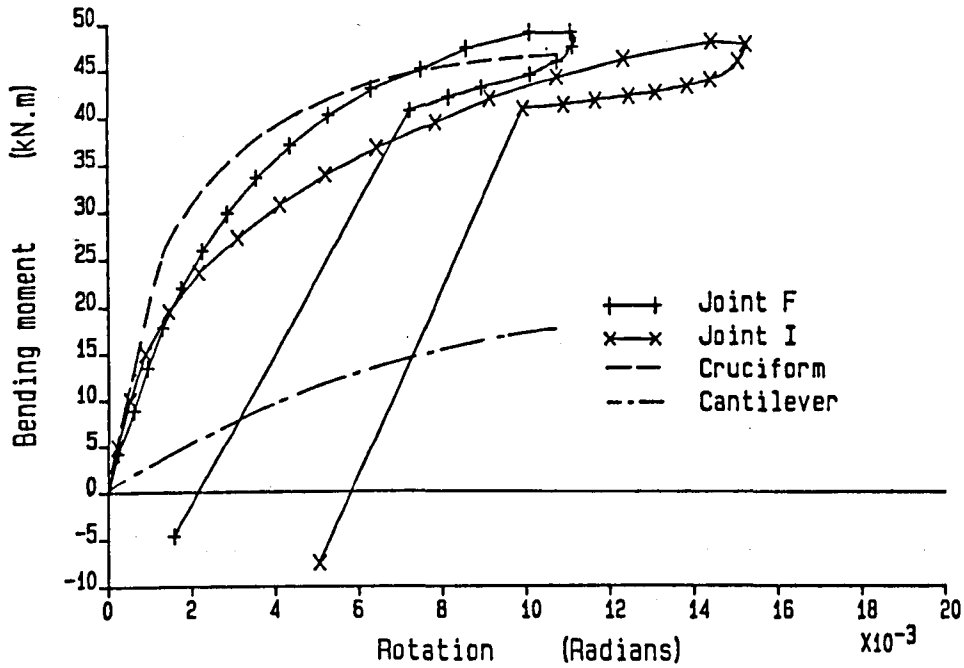


Figure 6.12 Moment-rotation response ('loading-unloading') of flush end plate connections to the web of the 'internal' column.

Connection Moment Rotation

Frame test F1

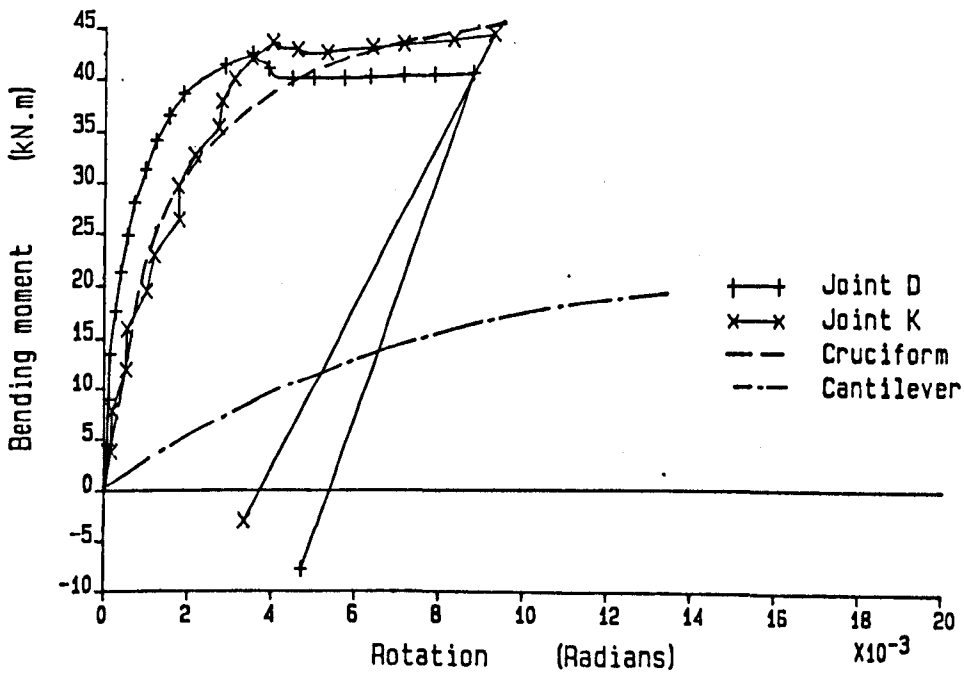


Figure 6.13 Moment-rotation response ('loading-loading') of flush end plate connections to the web of the 'internal' column.

Idealised connection response

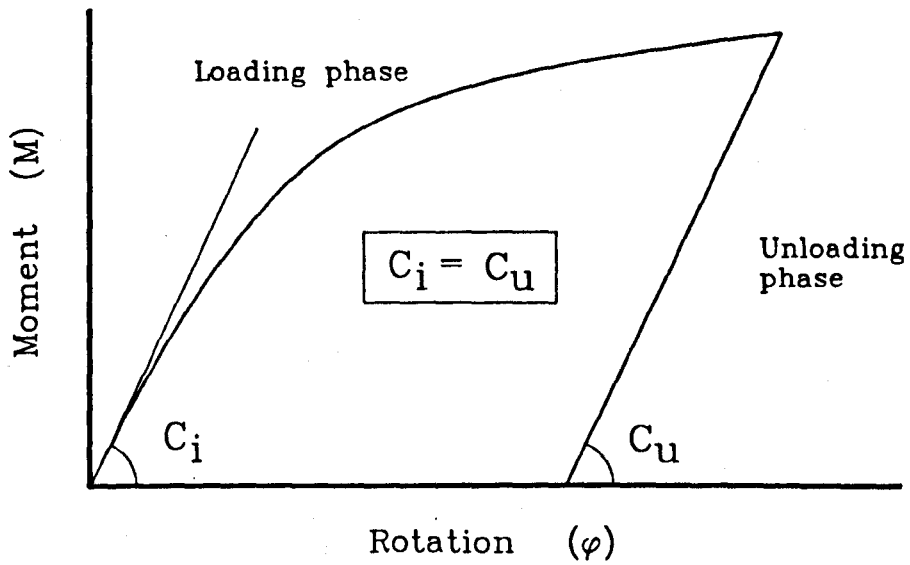


Figure 6.14 Idealised connection moment-rotation response.

Frame test F1 - joint 'f'.

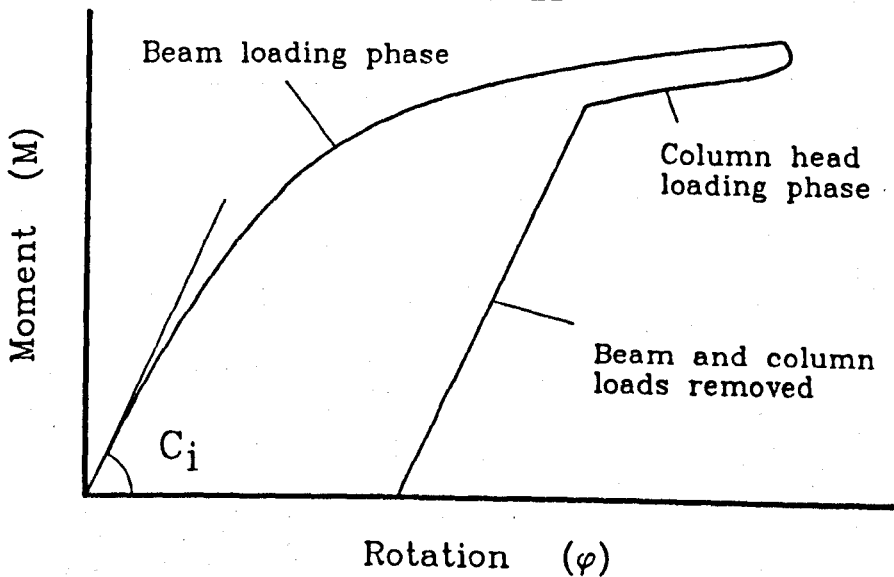
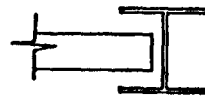
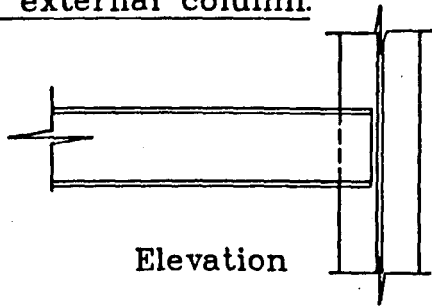


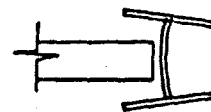
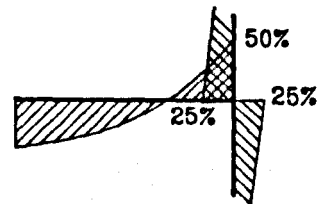
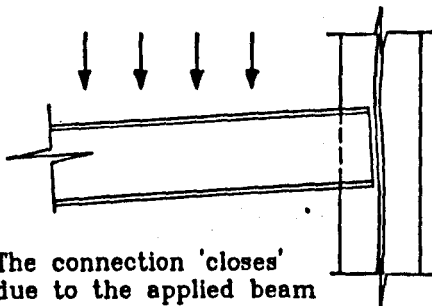
Figure 6.15 Frame test moment-rotation response illustrating the reduced unloading connection stiffness.



Beam connected to the web of an external column.



Beam loading applied.



Column load applied

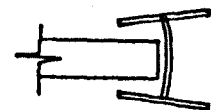
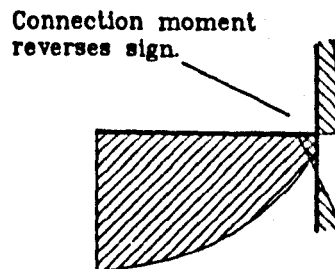
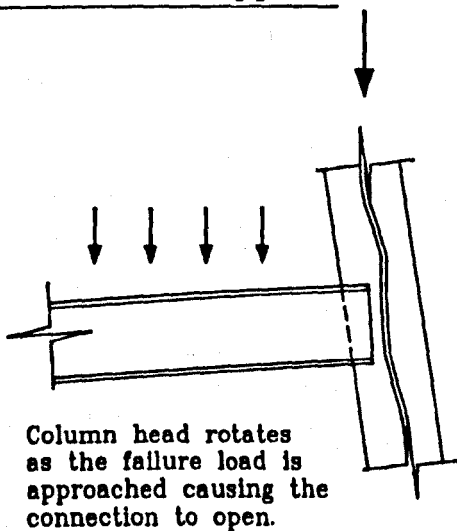
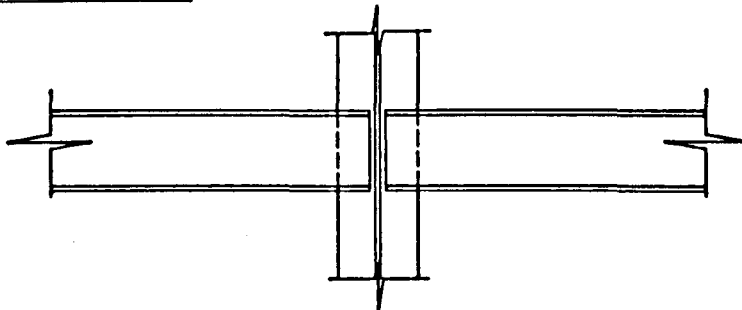


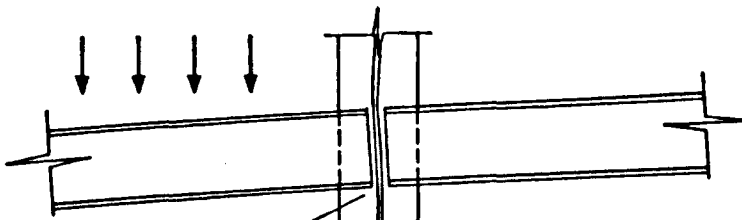
Figure 6.16 Deformation of a connection to the web of a 'corner' column.

Beam connected to the web of an internal column.



Elevation

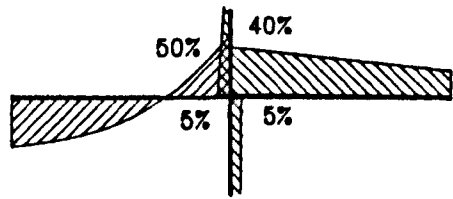
Beam loading applied.



The connection 'closes' due to the applied beam load.

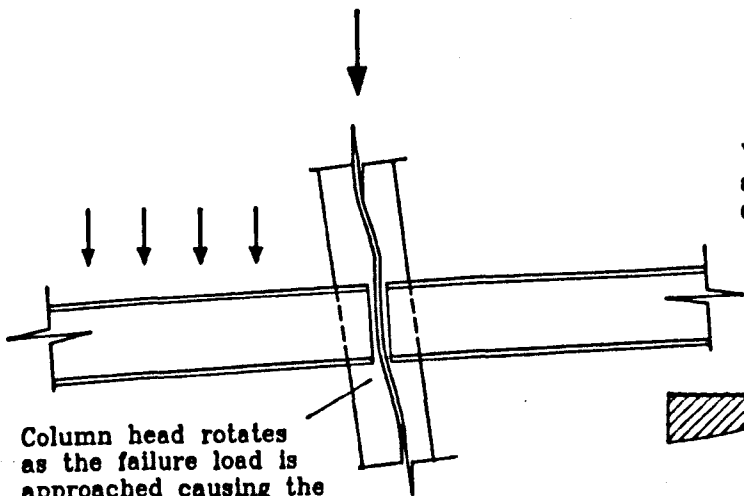


Column web deforms as in the external column.



Bending moment distribution

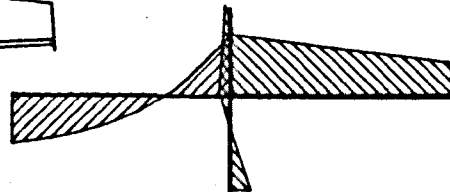
Column load applied



Column head rotates as the failure load is approached causing the connection to open.



Web deformations reverse as the moment at the column head reverses.



Bending moment distribution

Figure 6.17 Deformation of a connection to the web of an 'internal' column.

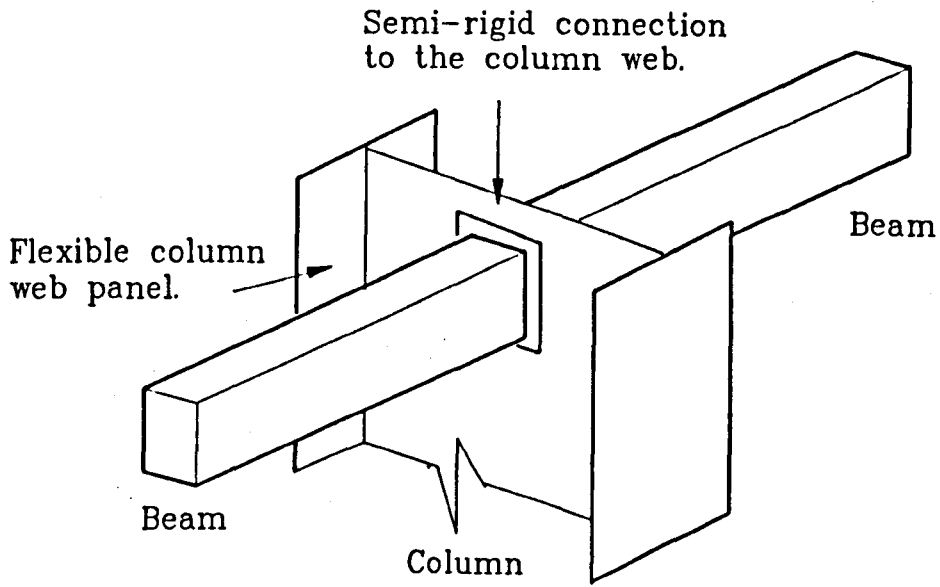


Figure 6.18: Small beams connected to a flexible web panel via stiff connections.

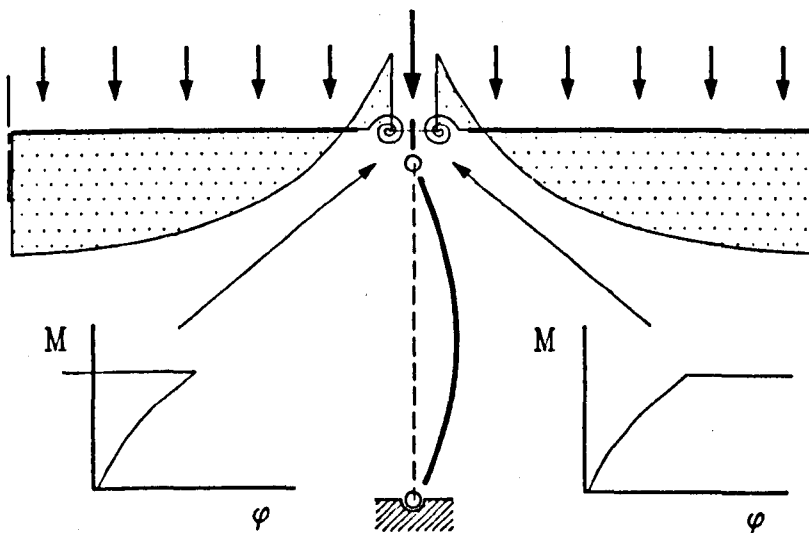


Figure 6.19: Column supporting a pair of beams using the connection shown in figure 6.18.

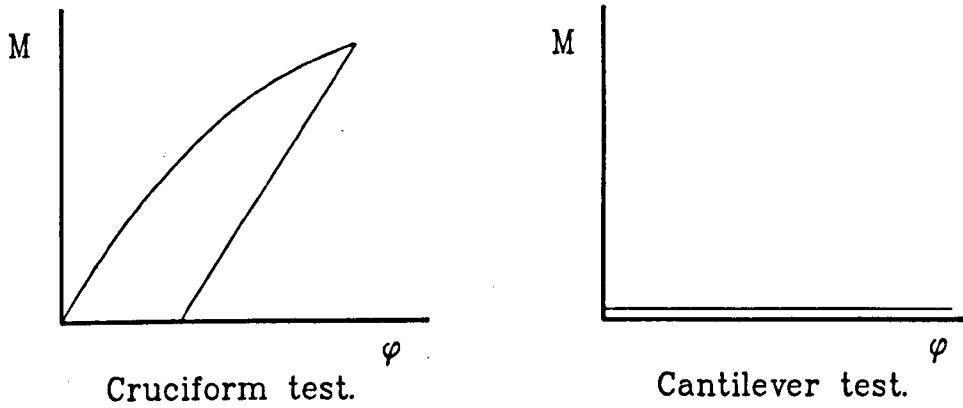


Figure 6.20: Moment-rotation plots from 'isolated' tests of the connection shown in figure 6.18.

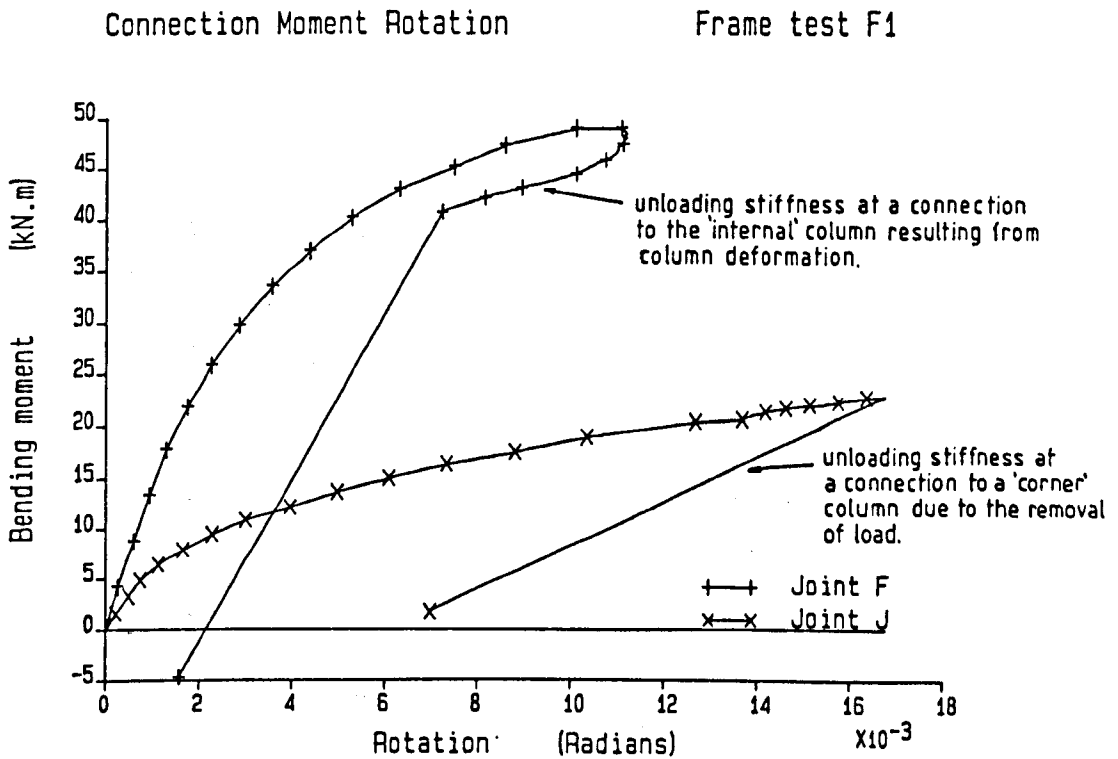


Figure 6.21: Comparison of the unloading stiffness of a frame connection to the 'internal' column resulting from column deformation, and that from a 'corner' column connection when the loading is removed.

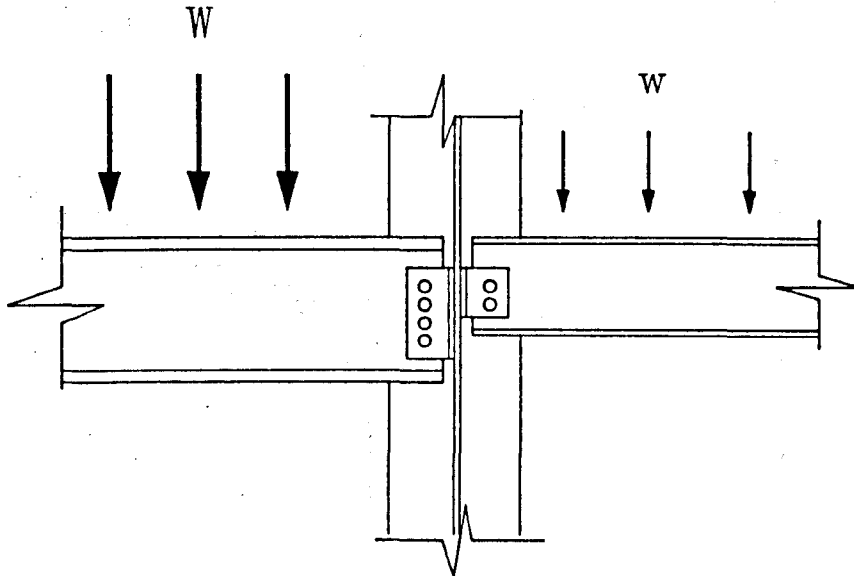


Figure 6.22: Internal column with a non-symmetrical arrangement of beams and connection types.

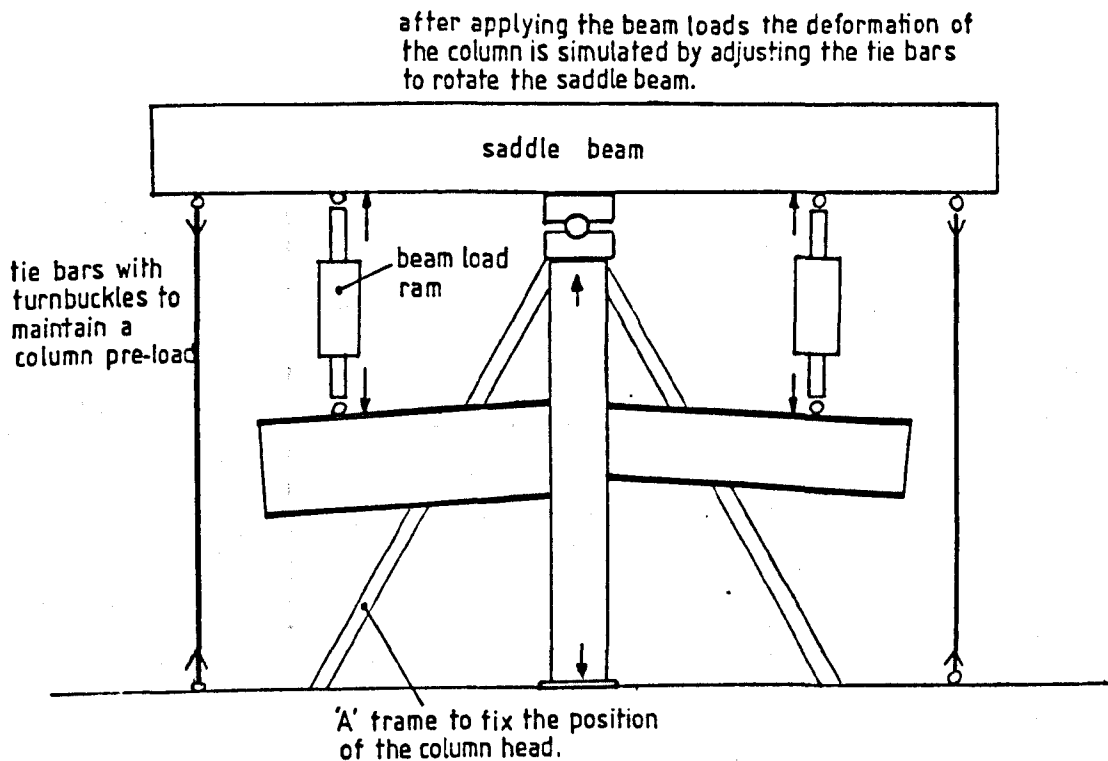


Figure 6.23: Possible connection test arrangement which would permit connection rotations resulting from column deformation.

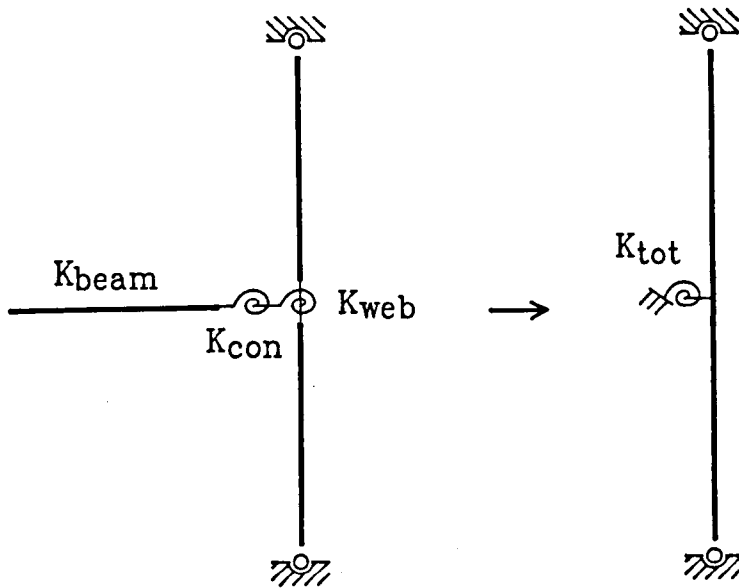


Figure 6.24: The individual stiffness components of a beam connection on one side of a column.

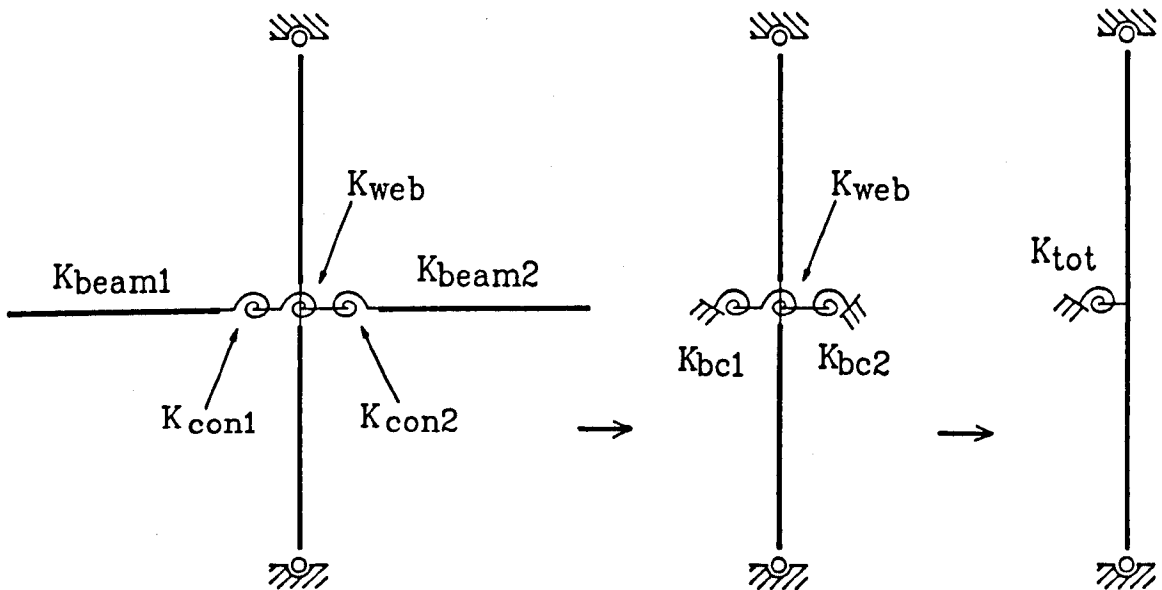


Figure 6.25: The individual stiffness components of connections to both sides of a column.

## Chapter 7

# A Parametric Study of Subassemblage Behaviour.

### 7.1 Introduction

Chapter 2 described the experimental investigation of a series of 10 subassemblage specimens and presented an in depth appraisal of the results obtained. In chapter 3, a detailed comparison was made between these results and the predictions of a sophisticated, purpose written finite element computer program [7.1]. It was evident that the analytical models of the subassemblage tests gave accurate predictions of the observed experimental behaviour. It was therefore concluded that the experimental results had verified the ability of the computer program to predict the behaviour of 3- dimensional beam columns restrained by semi-rigid connections. This supplemented a previous verification in which the program was used to predict the behaviour of 3-dimensional column subassemblages restrained by fully rigid connections [7.2].

The series of experimental subassemblage tests were designed with the primary aim of validating the finite element analysis techniques and therefore did not necessarily

conform, in terms of member size and loading, with subassemblages encountered in general steelwork practice. The purpose of the parametric studies described herein was to use the validated analysis software to examine subassemblage configurations and loading arrangements which are of a more direct practical significance. The studies were designed with the following objectives in mind:-

1. To investigate the influence of semi-rigid connections on the performance of subassemblages with a range of beam and column stiffness ratios comparable with those encountered in practice.
2. To investigate how the different distributions of beam loading resulting from different types of floor construction could affect subassemblage behaviour.
3. To investigate the potential benefits of adopting a 'preferred column orientation'.
4. To quantify the adverse effect, if any, of the transferred moment from a semi-rigid connection to an edge or corner column subassemblage.
5. To accumulate a body of data on the behaviour of a range of subassemblages under different loading conditions from which comparisons could be made with present methods of design.

The results of the first stages of this study were presented at an international conference [7.3] and have been published in a technical journal [7.4].

## **7.2 Formation of the study.**

The study was conducted in three stages. Firstly, a large number of models were analysed to investigate the effect of load distribution, column orientation and floor construction for



three different subassemblage types which employed the same beam and column member sizes. This was followed by a second series of tests in which a limited number of load cases from the initial study were repeated on a range of subassemblages which employed different beam and column stiffness ratios. The final stage of the study examined the effect of increasing the floor loading on larger, stiffer beams. For clarity, the discussion of these three related studies, and the resulting conclusions, have been reported separately in sections 7.5, 7.6 and 7.7 respectively.

### **7.3 Subassemblage configurations.**

The parametric study involved the analysis of a series of isolated subassemblages which represented parts of a rectilinear, non-sway steel framed structure. Subassemblages incorporating two, three and four beams were considered representing corner, edge and interior columns respectively. Figure 7.1 shows the arrangement of the four beam subassemblage modelled in the study indicating the sections used in the initial phase.

The effect of column continuity through the floor level was not investigated in this particular study. It is clear that such continuity would tend to distribute the applied connection moments, thereby reducing the maximum disturbing moment on the column. As one of the aims of this study was to investigate the extent of the adverse effects of moment transfer associated with semi-rigid design, only the more onerous non-continuous case has been considered.

A column height of 3.8m was adopted throughout. Whilst this is a fairly typical dimension, the primary and secondary beam spans of 5.5m and 4.0m are slightly smaller than would be encountered in practice. However, this restriction on floor span enabled the smaller British Standard beam sections to be considered so that direct use could be

made of connection performance data from previous studies [7.5].

All the subassembly models included an initial sinusoidal column deformation with a maximum amplitude  $L/1000$  (3.8mm) about both the major and minor axes. The yield stress of the steel was assumed to be  $275 \text{ N/mm}^2$  and the analytical model of the column incorporated a pattern of residual stress similar to that shown in figure 7.2.

To determine the response range for a particular subassembly, the performance of each subassembly model was investigated using two types of connection, one from each end of the connection stiffness range. The flexible connection was taken as a web cleat whilst the very stiff connection was taken as fully rigid (i.e. infinite rotational stiffness). Figure 7.3 shows the assumed multi-linear moment rotation characteristics of the web-cleat connection, non-dimensionalised with respect to the fully plastic moment  $M_{px}$  capacity of the primary beam. In this particular study, the same connection type was used on all the beams of any one subassembly, the effect of 'mixed connections types' on the behaviour of the column was not considered.

#### **7.4 Loading sequence.**

In all cases, beam loads were applied proportionally in 10 equal increments up to the prescribed limiting values. This was followed by a concentric loading at the column head applied in small increments until the maximum supported load, and hence column failure, was achieved. The loading sequence was therefore similar to that adopted in the experimental subassembly study reported in chapter 2.

## 7.5 Parameters investigated in the initial phase of the study.

The initial phase of the study investigated the influence of moment transfer on the performance of the subassemblages by considering various load arrangements for both one-way and two-way spanning floor systems. The former is analogous to precast concrete floor planks spanning between primary beams, whilst the latter corresponds to an in-situ reinforced concrete slab supported on both the primary and secondary beams. Figure 7.4 shows the assumed distribution of floor loading on each of the supporting beams for both types of floor construction. To allow an effective comparison between the moment transfer effects of the two floor systems, each was considered to have the same characteristic dead weight of  $3.8 \text{ kN/m}^2$ . Table 7.1 shows how this value was derived.

Figure 7.5 shows the distribution of floor loading for each of the nine load cases which were considered in the study. A typical office floor live loading of  $4.0 \text{ kN/m}^2$  was used [7.6]. The design loads on the beams were derived by applying factors to the dead and live loads in accordance with the current British Steelwork Design Code [7.7]. In instances where there was an imbalance of beam loads on either side of the column, the load factors were proportioned to accentuate the effect of the imbalance. In a number of instances, the imbalance was maximised by considering zero load acting over parts of the floor area. Whilst it is appreciated that this not a likely design consideration, except for construction conditions in which a reduced live load would be considered, it does represent an 'upper bound' to the effect of the disturbing moment.

The effect of the column orientation on the behaviour of the subassemblage was also investigated in the initial study. In orientation type *A* the primary beams framed into the web of the column whilst for orientation *B* the primary beams framed into the column flanges.

### 7.5.1 Discussion of the result from the first phase of the study.

The non-bracketed values in table 7.2 presents the total column load at failure, for the 9 load cases, 2 forms of connection, 2 column orientations and 2 floor systems considered in the initial study - a total of 72 different analytical models. The tabulated failure loads are presented in terms of a non-dimensionalised factor  $\alpha_{pin}$  where:-

$$\alpha_{pin} = \frac{\textit{Ultimate load of the subassemblage column } (P_{ult})}{\textit{Ultimate load of the column pin connected at each end } (P_{pin})} \quad (7.1)$$

The non-dimensionalised factor,  $\alpha_{pin}$ , therefore gives an indication of the benefit of the restraint from the beam to column connections after incorporating the potentially disadvantageous influence of moment transferred through the joint. The value of the lower bound failure load,  $P_{pin}$ , was calculated using the program, and had a value of 409 kN for a 3.8m long 152x152x23UC section.

The failure loads presented in table 7.2 are repeated in table 7.3, but in this instance the values are presented in terms of an  $\alpha_{res}$  factor in which the ultimate load is non-dimensionalised with respect to an upper bound failure load  $P_{res}$ .  $P_{res}$  is the failure load of the restrained column, in the four possible column arrangements when loaded at the column head only (table 7.4). The factor  $\alpha_{res}$  is therefore expressed as:-

$$\alpha_{res} = \frac{\textit{Ultimate load of the subassemblage column } (P_{ult})}{\textit{Ultimate load of subassemblage when loaded at the head only } (P_{res})} \quad (7.2)$$

The extent to which the factor  $\alpha_{res}$  falls below unity thus quantifies the amount by which the moment transferred from the beams erodes the benefit of column end restraint.

The results shown bracketed in tables 7.2 and 7.3 represent additional solutions in which the sign of the initial column deflections has been reversed. For type *B* arrangements, the reversed deflections are in the same direction as the dominant column bending,

thus resulting in a reduced failure load. In arrangement type *A* however, the reverse deflections are in the opposite sense to the dominant bending, therefore resulting in a higher failure load. The difference between these results and the corresponding original  $\alpha_{res}$  values provides an indication of the variation in failure load which may be expected depending on the direction of the initial column deformations. Since it is not, of course, reasonable to expect any design method to be able to cater for such inherent variability, the magnitude of these differences provides a guide to the level of accuracy for which design methods should aim.

Figure 7.6 presents the load-deflection curves for one of the axially loaded columns without disturbing moments shown in table 7.4. As expected, the plots show that the dominant column deformation is minor axis bending. A similar response was observed for all the 72 cases considered, with minor axis deformation becoming even more dominant with increased applied minor axis moment. This is illustrated in figure 7.7 which shows the mid-column minor axis deflection for a number of cases with column orientation *A* and a one-way spanning floor system.

The general pattern of results presented in tables 7.2 and 7.3 is very similar for both web cleat and rigid connection types. The smaller failure loads for the web cleat condition reflect the smaller degree of column end restraint provided by the connection. However, in certain cases of predominantly major axis bending (cases 6, 7 and 8B), a slightly higher failure load is observed for the web cleat connection. This is explained by the reduced major axis moment transferred into the column by the relatively flexible web cleat connection, permitting a greater capacity for axial load. Consideration of the type *B* arrangement, where the primary beams frame into the column flange under one way spanning floor conditions (category *B1*), show that the  $\alpha_{res}$  values in table 7.3 are approximately equal to 1.0 for the web cleats in all load cases, i.e. are virtually unaffected by the applied moment from the beams, whilst those for the rigid connection vary by up to 14%.

What is perhaps of greatest interest, is that for all of the 36 different cases considered for the web cleat condition, the  $\alpha_{pin}$  values shown in table 7.2 are greater than unity. This shows that for the particular column subassemblages in this study, the benefits of column end restraint outweigh the detrimental effects of moment transfer and, as a result, the failure loads are greater than that of the equivalent pinned-end column. The lowest  $\alpha_{pin}$  value is 1.03 for load case 6A and a one way spanning floor system. However, such a figure compares favourably with the figure of 1.06 for the fully rigid connection under the same load arrangement.

It is interesting to note that, in practice, there are not usually any restrictions placed on the orientation of the column. As a result many of the low  $\alpha_{pin}$  values in table 7.2 could be avoided by adopting the most appropriate column orientation. In such a situation, the minimum value of  $\alpha_{pin}$  for an interior column subassemblage employing web cleat connections increases from 1.17 to 1.25, for an edge column the value increases from 1.03 to 1.24 and for a corner column the value increases from 1.12 to 1.14. Therefore, for different numbers of intersecting beams subjected to a range of practical floor loading arrangements, and without a restriction on column orientation, the capacity of the column considered in the study was increased by a minimum of 14% over the corresponding pinned-end column due to the restraint of web cleat connections.

For each load case, a larger failure load was observed when the column was orientated such that the primary beams framed into the column flange. This was despite a reduced restraint to the minor column axis from the smaller secondary beams (connection response related to  $M_{px}$  of the beam). Also, for a given column orientation, a higher failure load was observed when the floor load was distributed such that the load on the beam connected to the column web was minimised, whilst the load on the beam connected to the column flange was maximised. This is illustrated by the higher failure load observed for a two-way spanning floor condition for orientation A, and a one-way spanning floor condition for orientation B.

When the above appraisal is repeated, retaining the freedom of column orientation but with the restrictions on floor construction removed, an even greater improvement in the failure loads is observed. The value of  $\alpha_{pin}$  now increases from 1.17 to 1.38 for an interior column, from 1.03 to 1.35 for an edge column and from 1.12 to 1.28 for a corner column. The minimum increase in the capacity of the column for all loading conditions is therefore doubled from 14% to 28%. These enhanced  $\alpha_{pin}$  values for the web cleat connected subassemblage approach the corresponding values for the rigidly connected subassemblage. Indeed, in the case of the edge column arrangement, the 'unrestricted'  $\alpha_{pin}$  value of 1.35 for the web cleat connection is exactly the same as the 'unrestricted'  $\alpha_{pin}$  value for the rigid condition.

### 7.5.2 Conclusions from the first phase of the study.

For the particular subassemblage studied above it can be concluded that:-

1. In all of the 36 cases studied for the subassemblage employing web cleat connections, the failure load was greater than the failure load of the pinned end column.
2. All the subassemblages in the study failed as a result of excessive minor axis bending.
3. It was evident that higher failure loads were observed when the load applied to beams connected to the column flange was maximised whilst the load on the beams connected to the column web was minimised.
4. By adopting a preferred column orientation, the minimum  $\alpha_{pin}$  factor was increased from 1.03 to 1.14. If, in addition, a preferred distribution of beam loads was adopted, the  $\alpha_{pin}$  factor was increased to 1.28.

## 7.6 Parameters investigated in the second phase of the study.

The second phase of the study concentrated on investigating the ultimate load capacities and distribution of moments for subassemblages with different connection stiffnesses and beam/column stiffness ratios. The initial study had shown that for a large range of different load cases,  $\alpha_{pin}$  was always greater than unity. This implied that the benefit of connection restraint was greater than the detrimental effect of the transferred disturbing moment. One of the principal objectives of this second phase of the study was to examine the range of application of this particular aspect of semi-rigid behaviour in greater detail.

It was evident from the first study that the most onerous configuration was a one-way spanning floor construction in which the primary beams framed into the web of the column (arrangement *A1*). The second phase of the study therefore concentrated solely on this particular arrangement and, to optimise the use of computer processing time, only load cases 1, 2 (interior column), 6 (edge column) and 9 (corner column) were considered.

A total of three different primary beam sections was investigated in conjunction with three different column sections, giving a total of nine different beam to column stiffness ratios. The sections used are presented in table 7.5 whilst table 7.6 summarises the stiffness ratios for each primary beam and column combination. The values presented in these two tables were computed using the minor axis values for the column extracted from published tabulated data [7.8]. In all cases, the secondary beam section was the same as that used in the initial study. Table 7.7 shows the squash load ( $A \times p_v$ ) and the



pinned-end failure load,  $P_{pin}$ , determined from the finite element program, for each of the three different column sections. All the parameters relating to beam loading, material properties, initial deflection and residual stress remained the same as those which had been used in the previous study as described in section 7.5.

In the first instance, the web cleat connection characteristics remained exactly the same as those used in the initial study so that a direct appraisal could be made of the influence of beam stiffness. For completeness however, a series of supplementary models was also studied in which the stiffness's of the web cleat connections were directly related to the size of the primary beam, thus representing a more realistic arrangement. The connection characteristics used in the initial study, which have been termed the 'nominal web cleat connections' and which remained constant irrespective of the primary beam type, have been treated as a reference datum. The moment and stiffness characteristics of the connections in the supplementary tests were derived by multiplying the stiffness and capacity, both loading and unloading, of the nominal web cleat connection by:-

$$M_{px2}/M_{px1} \text{ - in the case of beam 2}$$

and  $M_{px3}/M_{px1} \text{ - in the case of beam 3.}$

Connections with these particular moment-rotation characteristics will be referred to as 'enhanced web cleat' connections. As in the initial study, models were also studied with a fully rigid, infinitely stiff, connection - making a total of three different connection types.

### 7.6.1 Discussion of the results from the second phase of the study.

The non-dimensionalised failure loads,  $\alpha_{pin}$ , for the four load cases, three beam sizes, nominal web cleat and rigid connection types are presented respectively in tables 7.8a, 7.8b and 7.8c for the three different column types *C1*, *C2* and *C3*. The corresponding results from the models employing enhanced web cleat connection characteristics are shown in parentheses.

As before (table 7.2), the  $\alpha_{pin}$  factors presented in table 7.8 for the web cleat connected subassemblages exhibit a similar pattern to those which are rigidly connected. As expected, increasing the stiffness of the beam resulted in an increase in the column failure load. In the case of the nominal web cleat and rigid connections, this can be explained by the reduced rotations subtended at the support of the stiffer beam. As the moment-rotation characteristics of these two particular types of connection remains constant irrespective of beam type, the reduced rotation results in a reduced disturbing moment being applied to the column, thereby increasing the capacity for axial loading. A similar effect also explains the increase in the failure loads of the columns with enhanced web cleat connections. However, as the moment-rotation response of these particular connections is related to the  $M_{px}$  of the primary beam, there is of course the additional effect of increased column restraint from the stiffer connections.

The other obvious feature of the results is that the percentage increase in the failure loads of both the web cleat and rigidly connected subassemblages decrease as the size of the column is increased. This is a direct consequence of the decreased slenderness of the progressively larger columns and the resulting increase in the  $P_{pin}/P_{squash}$  ratio, thereby reducing the potential for enhanced failure loads. If the nominal web cleat data in tables 7.8a to 7.8c is repeated in table 7.9 in the form of a non-dimensionalised parameter  $\beta_{pin}$ , the 'swamping effect' of the different buckling criteria of the columns tends to be

negated.

$$\beta_{pin} = \frac{P_{nwc} - P_{pin}}{P_{rgd} - P_{pin}} \quad (7.3)$$

where:-

$P_{nwc}$  = Ultimate load of the nominal web cleat connected subassemblage.

$P_{rgd}$  = Ultimate load of the rigidly connected subassemblage.

$P_{pin}$  = Capacity of the pinned-end column.

It is evident from the above equation that  $\beta_{pin}$  will equal 0.0 for a column restrained by beams with pin connections and will equal 1.0 when fully rigid connections are used. The factor  $\beta_{pin}$  therefore gives an indication of the enhanced column capacity when using a nominal web cleat connection compared to that achieved using a fully rigid connection, irrespective of the column  $P_{ult}/P_{squash}$  ratio. The results presented in table 7.9 clearly show that the effect of the restraint from the web cleat connection, when compared to that of a fully rigid connection, diminishes as the slenderness of the column is reduced - the connection may be considered as acting less efficiently.

Comparing the values in parentheses in table 7.8, which are the failure loads of the subassemblages using enhanced web cleat connections, with the corresponding non-bracketed values shows a slight improvement in the failure loads compared with those obtained using columns employing the constant nominal web cleat characteristics. This is primarily due to the increased connection restraint offered to the column. However, it is interesting to note that when the enhanced web cleat characteristics are used in conjunction with beam B3, the improvement in failure load is similar to that achieved with fully rigid connections.

Unlike the initial study, there are a few instances where the  $\alpha_{pin}$  factor for subassemblages employing nominal web cleat connections is marginally less than unity - load case 6, for

combinations *B1C2* and *B1C3* of tables 7.8(b) and 7.8(c). This implies that the onerous effect of the disturbing moments from the connection is marginally greater than the enhancing restraint effect as the column fails. This is particularly apparent in the case of the rigidly connected subassembly where the disturbing moment from the beams is significantly larger than for the equivalent subassembly employing nominal web cleats. It is interesting to note however that this behaviour has been observed in instances where the column size has been increased (*C1* to *C3*) and the beam size held constant (*B1*). This suggests a conflict with the generally accepted view that the disturbing moments from deep beams has a more onerous effect on smaller, more slender edge columns.

The apparent vulnerability of stocky columns to disturbing moments can be explained by considering figure 7.8 which shows a non-dimensionalised plot of axial load verses minor axis bending moment for columns *C1*, *C2* and *C3* under load case 6 when rigidly connected to beam type *B1*. The 'near vertical' slope of the mid-column moment plot for *C3* during the head loading phase indicates that the applied load is resisted almost entirely by compression with only a small amount of member flexure. This behaviour is typical of a stocky member with a high  $P_{ult}/P_{squash}$  ratio and a high minor axis bending stiffness. One ramification of this is that there is a reduced tendency for rotation at the upper end of the column as the column head load is applied. Consequently, the column is unable to fully benefit from the potential restraint available from the connecting beams. This is illustrated by the inability of the column head moment for column *C3* to reverse sign. The axial capacity of the column is therefore dictated by the yield strength of steel, or more precisely the net stress in the presence of the small disturbing moment, as opposed to overall buckling considerations. This compares with the relatively slender column *C1* in which the increased minor axis flexibility promoted larger column deformations, increased flexural action and consequently increased column head rotation - thus causing an appreciable reversal of head moment.

Figure 7.9 shows the distribution of minor axis moments on the columns *C1*, *C2* and *C3* at the point of failure for the same load case discussed above. Obviously, in the case of

column *C3* in which the head moment is of the same sign as the mid column moment, due to the incomplete reversal of the initial disturbing moment, a more onerous distribution of moments occurs when compared to the pinned-end column at failure. As a result, the  $\alpha_{pin}$  value for this particular 'stocky' column will be less than unity. Conversely, column *C1* exhibits an appreciable reversal of moment at the column head, thereby producing a more advantageous distribution of minor axis moment. As a result, the  $\alpha_{pin}$  factor for this particular column is, as expected, greater than unity.

Of particular interest is the distribution of moments for column *C2*. Although there was a small reversal of moment at the column head, the  $\alpha_{pin}$  factor was less than unity - i.e. the failure load of the column was less than that of the pinned-end column. However, the predicted  $\alpha_{pin}$  value of 0.97 was only marginally less than 1.0. It is quite possible therefore that this surprising result was due to a convergence error in the computer program as the failure load was approached. If, on the other hand, the predicted  $\alpha_{pin}$  value is correct, then a possible explanation could be the second-order nature of the  $P - \delta$  effect on the increased mid column deflection,  $\delta_b$ , arising from the initial disturbing moment when zones of plasticity are present in the column. This phenomenon is best illustrated by considering figure 7.10 which shows plots of load verses mid-height deflection for a pinned-end column and a similar column subjected to an initial disturbing moment.

Applying a disturbing moment to the head of the column results in a deflection at the column centre of  $\delta_o + \delta_b$ , where  $\delta_o$  is initial column deformation. Due to the increased bow of the column, the slope of the load- deflection plot is less than that of the undisturbed column. If at a subsequent stage of loading the combination of axial load and moment (both primary and secondary) causes partial plasticity of the column section, then removal of the moment results in a total deflection at the column centre,  $\delta'_o$ , which is greater than that of the undisturbed column at the same loading level. Although at this stage the load applied to both the undisturbed and initially disturbed columns is similar, the increased deflection at the centre of the initially disturbed column represents a more onerous condition and consequently fails at a lower load. It is evident therefore

that where plasticity of the column section occurs, the principles of superposition do not apply and the behaviour is dependent on the loading history. In such a situation, a small reversal of moment at the column head, as observed in column C2, may not be sufficient to counteract the effect, resulting in an  $\alpha_{pin}$  value less than unity. It is appreciated that in the column subassemblages the reduction in the column head moment was gradual and commenced at the instant the column head loading was applied. However, the principles illustrated in figure 7.10 will still apply but to a lesser extent.

### 7.6.2 Conclusions from the second phase of the study.

1. The reduced support rotations of stiffer beams subjected to the same load increases the axial load capacity of the column.
2. In instances where an 'enhanced web cleat' connection is used, i.e. the stiffness of the connection is related to the moment capacity of the beam, the increase in the column failure load is greater than that observed using 'nominal web cleats', but less than or equal to that obtained when the beams are rigidly connected.
3. The enhancing effect of a web cleat connection on the ultimate capacity of a column decreases as the size and stiffness of the column increases.
4. It would appear that stocky columns, in which strength rather than buckling criteria dictates the ultimate capacity, are more susceptible to the detrimental effect of small disturbing moments from semi-rigid beam connections.
5. Moment reversal at the column head does not necessarily result in an  $\alpha_{pin}$  factor which is greater than unity.

## 7.7 Parameters investigated in the third phase of the study.

The conclusions which can be drawn from the above study regarding the effect of the larger beams *B2* and *B3* are limited. A particular arrangement of floor loading was assumed throughout which produced a maximum 'safe' bending moment on primary beam *B1*. Obviously, applying the same loading to stronger, stiffer beams will produce a reduced beam support rotation thereby reducing the disturbing effect on the column. It was proposed therefore that further models were studied in which the primary beams *B2* and *B3* were subjected to significantly greater loading, thereby increasing the induced rotation at the beam support.

It is appreciated that these additional studies represent a departure from the practical considerations of load and member sizes which the study aimed to investigate initially. However, the results of these models will help to discriminate between the separate effects of load, beam flexibility and connection response which are undoubtedly interrelated.

A maximum beam loading of 46.8 kN/m (*w1*) was applied to the primary beam in load case 6A of the subassemblages reported under sections 7.3 and 7.4. Increased loadings of 90.0kN/m (*w2*) and 160.0 kN/m (*w3*) were considered in this phase of the study. The *w3* load was specifically limited to 160kN/m to prevent a failure of column *C1* during the beam loading phase of the analysis. The effect of these load intensities on beams *B1*, *B2* and *B3* over a simply supported span of 5.5m are summarised in table 7.10.

From the results of the second phase of the study, it was evident that the column failure loads achieved using an 'enhanced' web cleat connection were, not surprisingly, intermediate between those using a 'nominal' web cleat connection and a rigid connection.

Therefore, to save computation, only the extremes of the 'nominal' web cleat and the rigid connection types have been considered in this stage of the study.

### 7.7.1 Discussion of the results from the third phase of the study.

Tables 7.11a, 7.11b and 7.11c show the failure loads in the form of  $\alpha_{pin}$  factors for the different combinations of loading, connection type, beam and column size. Part of the data in these tables has been presented in a series of graphical plots which illustrate a number of distinct trends despite the limited number of data points which are available.

Figure 7.11 shows a plot of non-dimensionalised failure load against beam stiffness when a beam load  $w1$  is applied. As discussed in section 7.6.1, the plot illustrates that the effect of a disturbing beam moment on a more stocky column can result in an  $\alpha_{pin}$  factor slightly less than unity. In addition, it highlights the difference between the behaviour of the rigidly connected subassembly and that using web cleats, particularly where a beam of low stiffness is used. As discussed previously, this is a result of the increased potential for rotation at the beam support. In the case of the rigid connection, this translates to a corresponding increase in the disturbing moment applied to the column and hence a decrease in the ultimate capacity. In the case of the web cleat connection however, the non-linear nature of the  $M - \phi$  response results in a decreasing increase in the disturbing moment and hence a less onerous effect on column capacity.

The same effect is illustrated in figure 7.12 which shows a plot of non-dimensionalised failure load against beam stiffness when a beam load  $w2$  is applied. There are only two data points on this plot as the intensity of the  $w2$  loading exceeded the capacity of beam  $B1$ . As expected, the increased loading, and hence beam support rotation, results in a reduction in the failure load for a given beam stiffness. The characteristic 'cross-over' of the rigid and web cleat plots for column  $C3$  therefore occurs at a slightly lower



beam stiffness. In both cases, the 'near horizontal' nature of the plots for the web cleat connection to column *C3* demonstrates the apparent difficulty of producing an  $\alpha_{pin}$  value less than unity, irrespective of the beam stiffness. This is particularly reassuring as it was concluded from the second phase of the study that the stocky *C3* column was the most sensitive to the detrimental effect of an initial disturbing moment from the beams. It must be remembered however that the use of a stiffer nominal semi-rigid connection would result in failure loads closer to those obtained from the rigid connection with the possibility of achieving a  $\alpha_{pin}$  value as low as 0.94 in extreme cases.

Figures 7.13 and 7.14 show plots of the failure load against the applied beam load when using beams *B3* and *B2* respectively. The gradient of the plots illustrate the potentially onerous effect of increased beam loading on the capacity of the column. The steeper gradient in the case of beam *B2* is a direct consequence of the increased beam flexibility and the larger rotations induced at the support for a given beam load. The convergence, and in some instances intersection, of the plots for the rigid and web-cleat beam connections clearly illustrate the less onerous effect of the reduced moment transferred from nominal semi-rigid connection.

### 7.7.2 Conclusions from the third phase of the study.

1. Increasing the applied beam load reduces the axial carrying capacity of the column. The effect is more pronounced in the case of rigidly connected sub-assemblages.
2. For the particular subassemblage parameters which have been considered, the gradients of the plots of beam load against failure load decrease as the size and stiffness of the column increases.

## 7.8 Concluding remarks on the parametric study.

From the results which have been obtained, the author has made a number of observations regarding 3-dimensional subassemblage behaviour. Perhaps the most significant finding was that for the cases considered, the influence of the restraint to the column from the semi-rigid beam connections generally exceeded the detrimental effect of the moment transferred. This was certainly true in all cases where a beam framed into each side of minor column axis, the only exception being an edge column arrangement in which a 'small' beam framed into the minor axis of a 'large' column. As the  $\alpha_{pin}$  factor was greater than unity for most cases, the results suggests that the columns in the study could have been designed assuming a pinned-end condition at the top and base of the column. Economies would thus arise in two ways. Firstly, there would be a reduction in the design effort, even when compared to current simple design methods, and secondly, for cases in which there is an appreciable net primary disturbing moment resulting from non-symmetric floor load distributions, there would be a reduction in steel weight. In chapter 8 of the thesis the author has investigated these simple concepts and compared the performance of the subassemblages in this study with design predictions.

It is appreciated that although a large number of analytical models have been studied, when compared to the variety of structural forms encountered in practice the applicability of the results is clearly limited. However, the author hopes that the parameters studied herein and the general trends which have been observed will be extended by other researchers to provide a more extensive appraisal of semi-rigid behaviour on the performance of three-dimensional subassemblages. Typical studies could concentrate on the effects of long span beams and the effect of different beam and connection types on each side of the column.

## References.

- 7.1 Wang, Y.C., '*Ultimate strength analysis of 3-D beam columns and column subassemblages with flexible connections*', Ph.D. thesis, The Department of Civil and Structural Engineering, University of Sheffield, U.K., 1988.
- 7.2 Wang, Y.C. and Nethercot, D.A., '*Ultimate strength analysis of three-dimensional column subassemblages with flexible connections*', J. Construct. Steel Research, Vol 9, 1988, pp. 235-264.
- 7.3 Gibbons, C., Wang, Y.C. and Nethercot, D.A., '*The influence of connections on the behaviour of 3-dimensional steel frames*', presented at the 3rd. Joint A.S.C.E./A.S.M.E. Mechanics conference, San Diego, U.S.A., July 1989.
- 7.4 Gibbons, C., Wang, Y.C. and Nethercot, D.A., '*The influence of connections on the behaviour of 3-dimensional steel frames*', Journal of the Singapore Steelwork Society. (to be published).
- 7.5 Davison, J.B., Kirby, P.A. and Nethercot, D.A., '*Rotational stiffness characteristics of steel beam to column connections*', J. Construct. Steel Research, Vol 8, 1987, pp. 17-54
- 7.6 British Standard BS 6399, '*Design loading for building*', Part 1, Code of practice for dead and imposed loads, London, British Standards Institution, 1984.
- 7.7 British Standard BS 5950, '*The structural use of steelwork in buildings, Part 1: Code of practice for design in simple and continuous construction: Hot rolled sections*', London, British Standards Institution, 1985.
- 7.8 '*Steelwork design guide to BS5950: Part 1: 1985, Volume 1 - Section properties and member capacities*', 2nd. edition, The Steel Construction Institute.

Floor construction	Dead load components	kN/m <sup>2</sup>
One way spanning	Cement screed	0.80
	Precast floor planks	2.70
	Battens	0.05
	Ceiling board	0.15
	<b>Total</b>	<b>3.80</b>
Two way spanning	Non-cement screed	0.05
	150mm R.C. slab	3.55
	Battens	0.05
	Ceiling board	0.15
	<b>Total</b>	<b>3.80</b>

**Table 7.1: Assumed dead load components for the two types of floor construction.**

Connection Type	WEB CLEAT				RIGID			
	A		B		A		B	
Column Orientation	A		B		A		B	
Slab Span	1	2	1	2	1	2	1	2
1	1.28	1.29	1.38	1.27	1.44	1.44	1.42	1.42
2	1.17	1.20	1.37 (1.35)	1.30 (1.28)	1.26	1.29	1.34 (1.33)	1.37 (1.36)
3	1.22 (1.40)	1.24 (1.39)	1.38	1.30	1.31	1.34	1.38	1.40
4	1.24	1.25	1.38 (1.36)	1.25 (1.24)	1.34	1.35	1.40 (1.39)	1.33 (1.33)
5	1.26 (1.36)	1.27 (1.35)	1.38 (1.37)	1.35 (1.26)	1.37	1.38	1.41 (1.40)	1.47 (1.36)
-----	---	---	---	---	---	---	---	---
6	1.03 (1.23)	1.06	1.35	1.29	1.06	1.18	1.23	1.28
7	1.14	1.16	1.37	1.24	1.25	1.27	1.35	1.31
8	1.08	1.12	1.37	1.25	1.21	1.24	1.31	1.30
-----	---	---	---	---	---	---	---	---
9	1.12	1.14	1.28	1.14	1.25	1.25	1.33	1.22

Table 7.2: Failure loads ( $\alpha_{pin}$ ) of the models in the initial study.

Connection Type	WEB CLEAT				RIGID			
Column Orientation	A		B		A		B	
Slab Span	1	2	1	2	1	2	1	2
1	0.92	0.93	1.00	0.92	1.00	1.00	1.00	1.00
2	0.84	0.86	1.00 (0.97)	0.94 (0.93)	0.88	0.90	0.94 (0.93)	0.97 (0.95)
3	0.88 (1.00)	0.89 (0.97)	1.00	0.94	0.91	0.93	0.97	0.98
4	0.89	0.90	1.00 (0.99)	0.90 (0.89)	0.93	0.94	0.99 (0.98)	0.94 (0.93)
5	0.90 (0.97)	0.91 (0.96)	1.00 (0.99)	0.98 (0.91)	0.95	0.96	0.99 (0.99)	1.03 (0.96)
- - - - -	- -	- -	- -	- -	- -	- -	- -	- -
6	0.79 (0.95)	0.82	0.98	0.93	0.74	0.83	0.86	0.90
7	0.88	0.89	1.00	0.90	0.88	0.90	0.95	0.92
8	0.83	0.86	1.00	0.91	0.85	0.88	0.92	0.92
- - - - -	- -	- -	- -	- -	- -	- -	- -	- -
9	0.86	0.88	1.00	0.90	0.89	0.90	0.95	0.88

Table 7.3: Failure loads ( $\alpha_{res}$ ) of the models in the initial study.

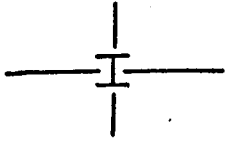
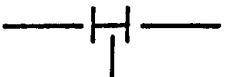

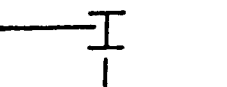
Column Arrangement	WEB CLEAT	RIGID
	1.40	1.44
	1.30	1.43
	1.38	1.42
	1.30	1.43

Table 7.4: Failure loads ( $\alpha_{pin}$ ) of the subassemblages when loaded at the column head only.

Section reference	Section serial size	M <sub>px</sub> (kNm)	M <sub>py</sub> (kNm)
B1	305x127x48 UB	194.0	24.0
B2	406x178x74 UB	412.0	56.0
B3	686x254x140 UB	1210.0	130.0
C1	152x152x23 UC	45.0	14.0
C2	203x203x46 UC	137.0	49.0
C3	305x305x97 UC	396.0	131.0

Table 7.5: Plastic moment capacities of the sections used in the second phase of the study.

Stiffness ratios $K_{bx}/K_{cy}$ ( $I_{bx}.L_c/I_{cy}.L_b$ )			
Section reference	C1	C2	C3
B1	16.2	4.6	0.9
B2	46.8	12.2	2.6
B3	233.2	61.0	12.9

Table 7.6: Stiffness ratios for the different beam and column combinations.

Column Ref	Column serial size	$L/r_{yy}$ ( $L = 3.8m$ )	Squash load $P_{sq}$ (kN)	Pinned-end axial load capacity $P_{pin}$ (kN)
C1	152x152x23 UC	103.3	820.0	409.0
C2	203x203x46 UC	74.4	1620.0	1133.0
C3	305x305x97 UC	49.5	3380.0	2894.0

Table 7.7: Nominal column squash loads and ultimate capacities determined from the finite element program.



Beams connected to COLUMN C1 $P_{ult}/P_{pin}$						
Load case	Web Cleat Connection			Rigid Connection		
	B1	B2	B3	B1	B2	B3
1	1.28	1.35 (1.39)	1.40 (1.43)	1.44	1.44	1.45
2	1.17	1.32 (1.34)	1.39 (1.42)	1.26	1.37	1.43
6	1.03	1.25 (1.27)	1.37 (1.40)	1.06	1.32	1.41
9	1.12	1.26 (1.32)	1.34 (1.41)	1.25	1.37	1.43

Table 7.8a: Values of  $\alpha_{pin}$  for column C1 with different beam sizes.

Beams connected to COLUMN C2 $P_{ult}/P_{pin}$						
Load case	Web Cleat Connection			Rigid Connection		
	B1	B2	B3	B1	B2	B3
1	1.09	1.13 (1.16)	1.16 (1.20)	1.20	1.21	1.21
2	1.04	1.11 (1.14)	1.16 (1.19)	1.10	1.18	1.20
6	0.98	1.08 (1.09)	1.14 (1.18)	0.97	1.14	1.20
9	1.01	1.07 (1.12)	1.11 (1.18)	1.09	1.18	1.20

Table 7.8b: Values of  $\alpha_{pin}$  for column C2 with different beam sizes.

Beams connected to COLUMN C3 $P_{ult}/P_{pin}$						
Load case	Web Cleat Connection			Rigid Connection		
	B1	B2	B3	B1	B2	B3
1	1.02	1.03 (1.04)	1.04 (1.06)	1.05	1.07	1.07
2	1.00	1.02 (1.03)	1.04 (1.05)	1.00	1.05	1.06
6	0.99	1.01 (1.01)	1.03 (1.04)	0.94	1.03	1.06
9	1.00	1.01 (1.02)	1.02 (1.05)	1.00	1.05	1.07

Table 7.8c: Values of  $\alpha_{pin}$  for column C3 with different beam sizes.

COLUMN C1 Web cleat performance indicator $\beta_{pin}$			
Load case	B1	B2	B3
1	0.63	0.79	0.89
2	0.65	0.84	0.91
6	0.50	0.79	0.89
9	0.43	0.71	0.81

COLUMN C2 Web cleat performance indicator $\beta_{pin}$			
Load case	B1	B2	B3
1	0.45	0.61	0.76
2	0.41	0.64	0.80
6	*	0.60	0.73
9	0.11	0.39	0.52

COLUMN C3 Web cleat performance indicator $\beta_{pin}$			
Load case	B1	B2	B3
1	0.27	0.40	0.58
2	0.0	0.39	0.55
6	*	0.38	0.47
9	0.0	0.20	0.37

Table 7.9: Web cleat performance indicator ( $\beta_{pin}$ ) for different beam and column combinations.

Effect of beam loading on simple 5.5m spans						
Beam load kN/m	B1		B2		B3	
	M/Mpx kNm	∅sp mRads	M/Mpx kNm	∅sp mRads	M/Mpx kNm	∅sp mRads
46.8 (w1)	0.91	16.2	0.43	5.6	0.15	1.1
90.0 (w2)	-	-	0.83	10.9	0.28	2.2
160.0 (w3)	-	-	-	-	0.50	3.8

Table 7.10: Effect of the different loading intensities  $w_1$ ,  $w_2$  and  $w_3$  on the beams  $B_1$ ,  $B_2$  and  $B_3$  over a simple 5.5m span.

COLUMN C1 - LOAD CASE 6A Failure loads $\alpha_{pin}$						
Beam load	Web cleat connection			Rigid connection		
	B1	B2	B3	B1	B2	B3
w1	1.03	1.25	1.37	1.06	1.32	1.41
w2	-	1.19	1.35	-	1.22	1.38
w3	-	-	1.33	-	-	1.33

Table 7.11a: Failure loads ( $\alpha_{pin}$ ) of column C1 employing web cleat connections.

COLUMN C2 - LOAD CASE 6A Failure loads $\alpha_{pin}$						
Beam load	Web cleat connection			Rigid connection		
	B1	B2	B3	B1	B2	B3
w1	0.98	1.08	1.14	0.97	1.14	1.21
w2	-	1.05	1.14	-	1.07	1.18
w3	-	-	1.13	-	-	1.15

Table 7.11b: Failure loads ( $\alpha_{pin}$ ) of column C2 employing web cleat connections.

COLUMN C3 - LOAD CASE 6A Failure loads $\alpha_{pin}$						
Beam load	Web cleat connection			Rigid connection		
	B1	B2	B3	B1	B2	B3
w1	0.99	1.01	1.03	0.94	1.03	1.06
w2	-	1.01	1.03	-	0.99	1.05
w3	-	-	1.02	-	-	1.04

Table 7.11c: Failure loads ( $\alpha_{pin}$ ) of column C3 employing web cleat connections.

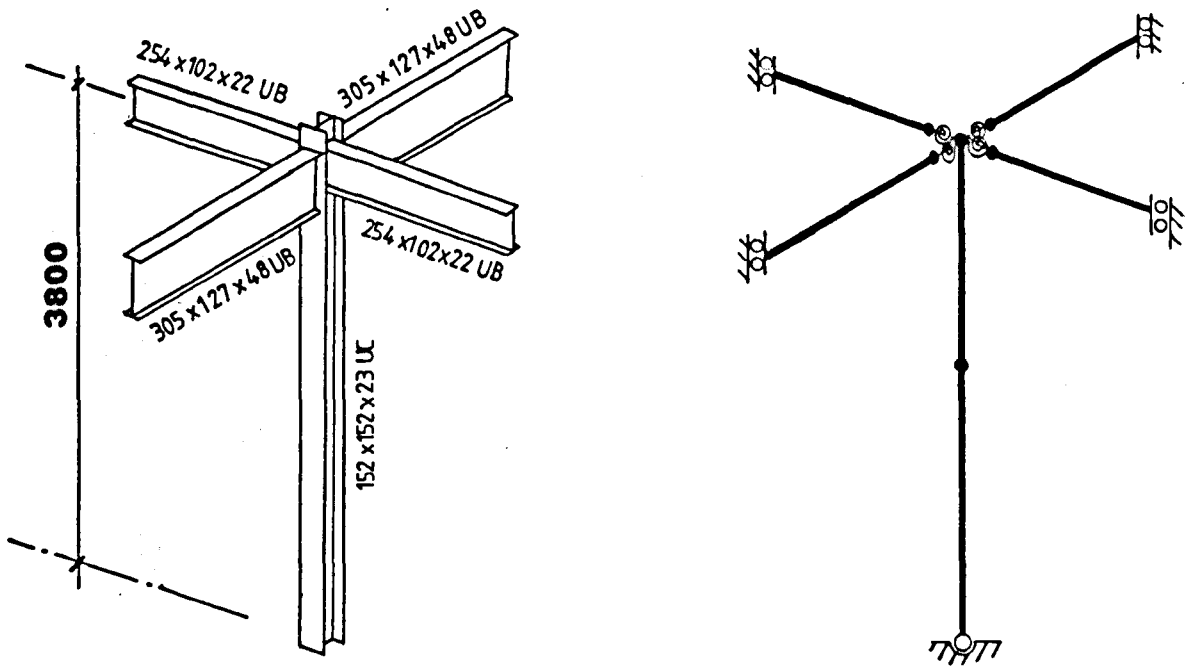


Figure 7.1: Arrangement of the subframe and subframe model used in the study.

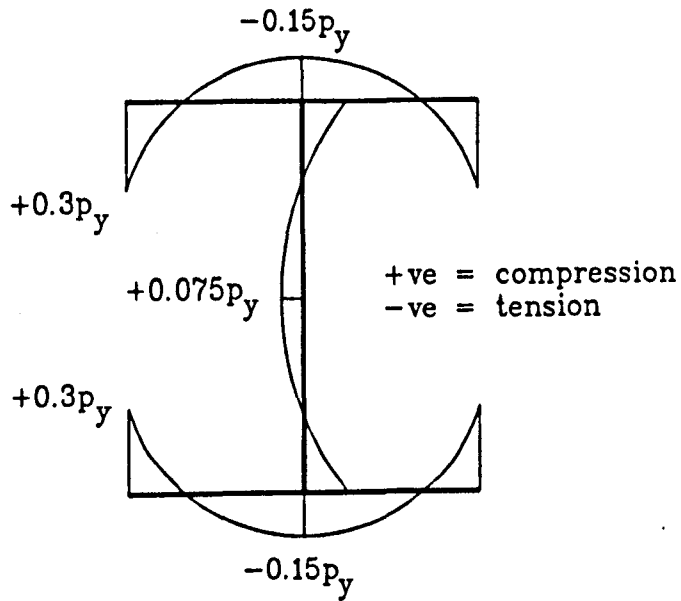


Figure 7.2: Assumed pattern of column residual stresses.

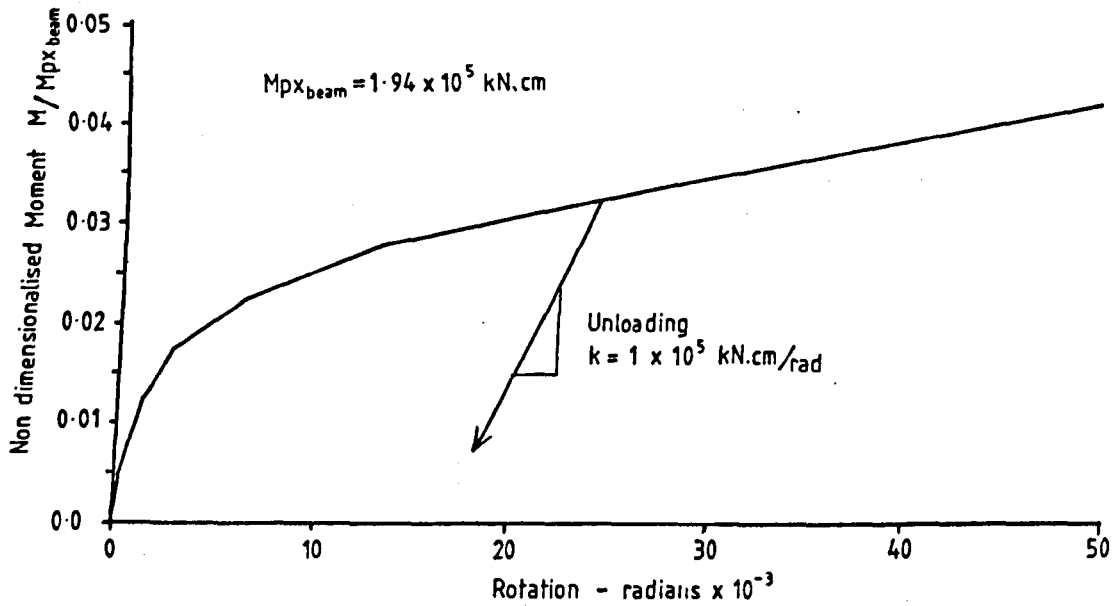


Figure 7.3: Moment-rotation characteristics assumed for the nominal web cleat connection.

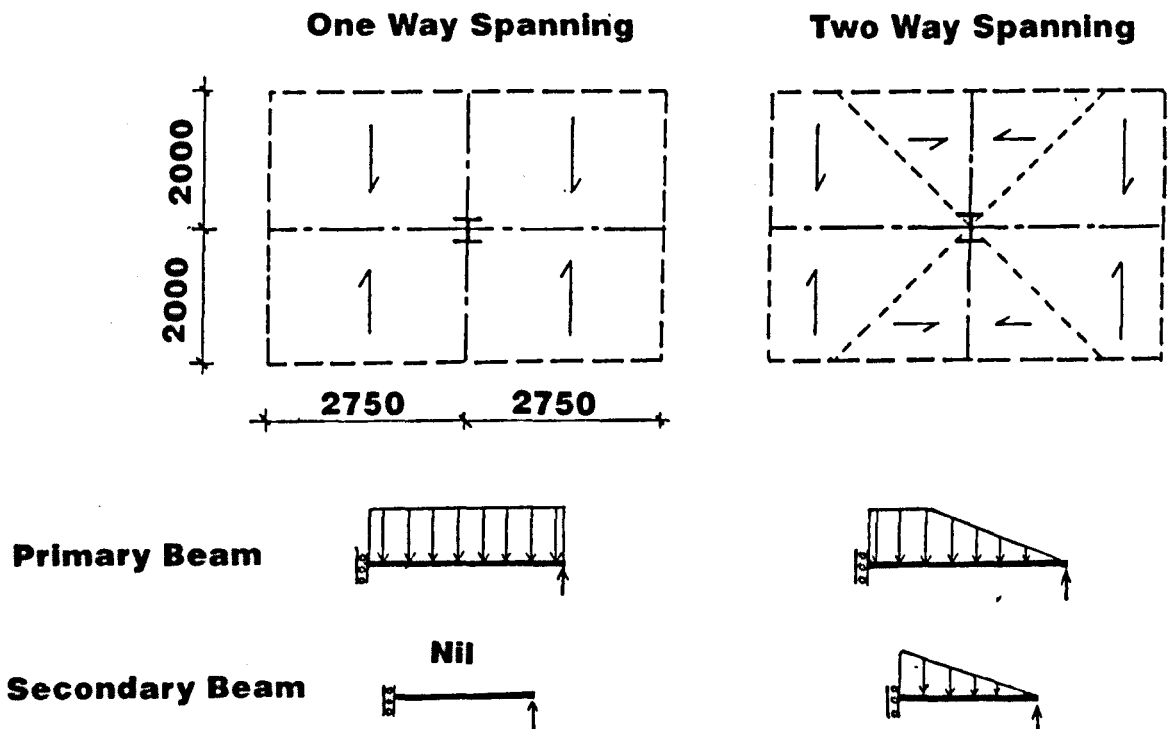


Figure 7.4: Assumed distribution of beam loading for one-way and two-way spanning types of floor construction.

**Extent of loaded area**

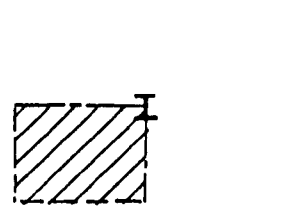
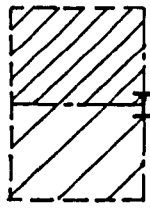
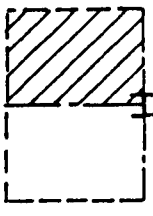
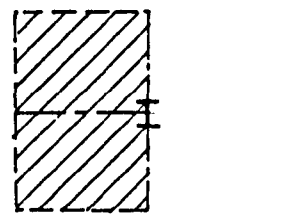
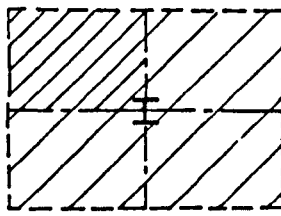
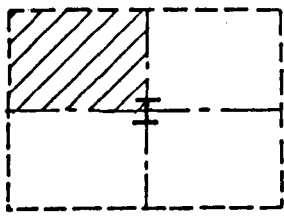
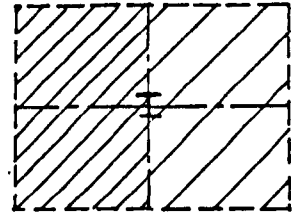
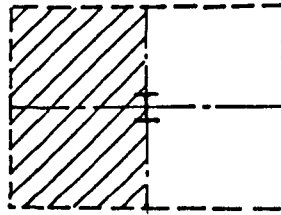
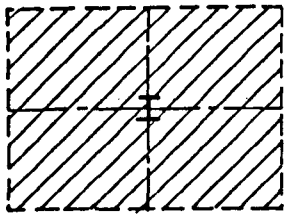
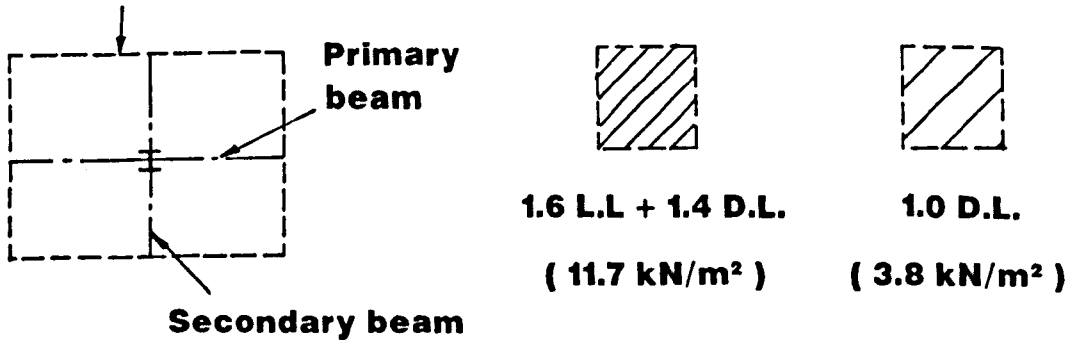


Figure 7.5: Arrangement of floor loading for load cases 1 to 9.



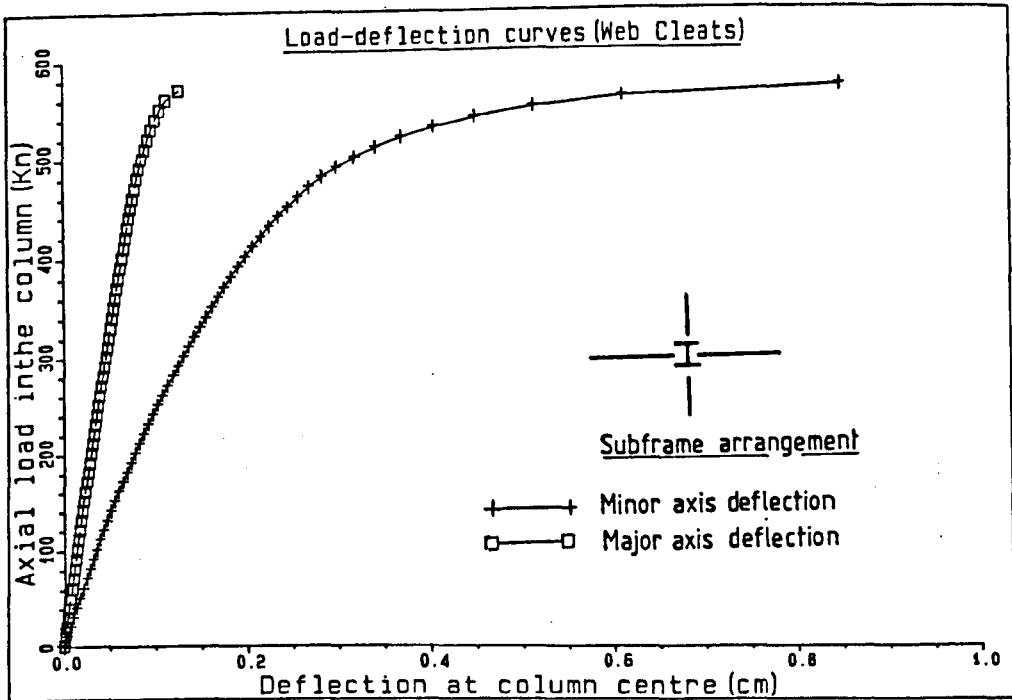


Figure 7.6: Load vs. mid-column deflection plot for the four beam subassemblage when loaded at the column head only.

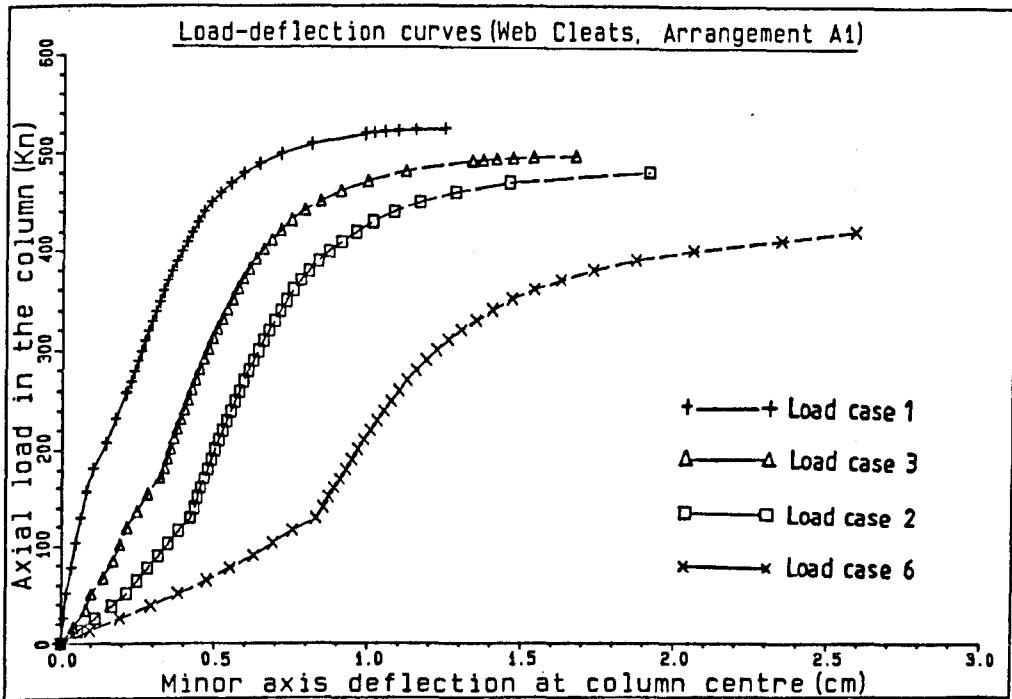


Figure 7.7: Load vs. mid-column minor axis deflection for load cases 1,2,3 and 6 and loading arrangement A1.

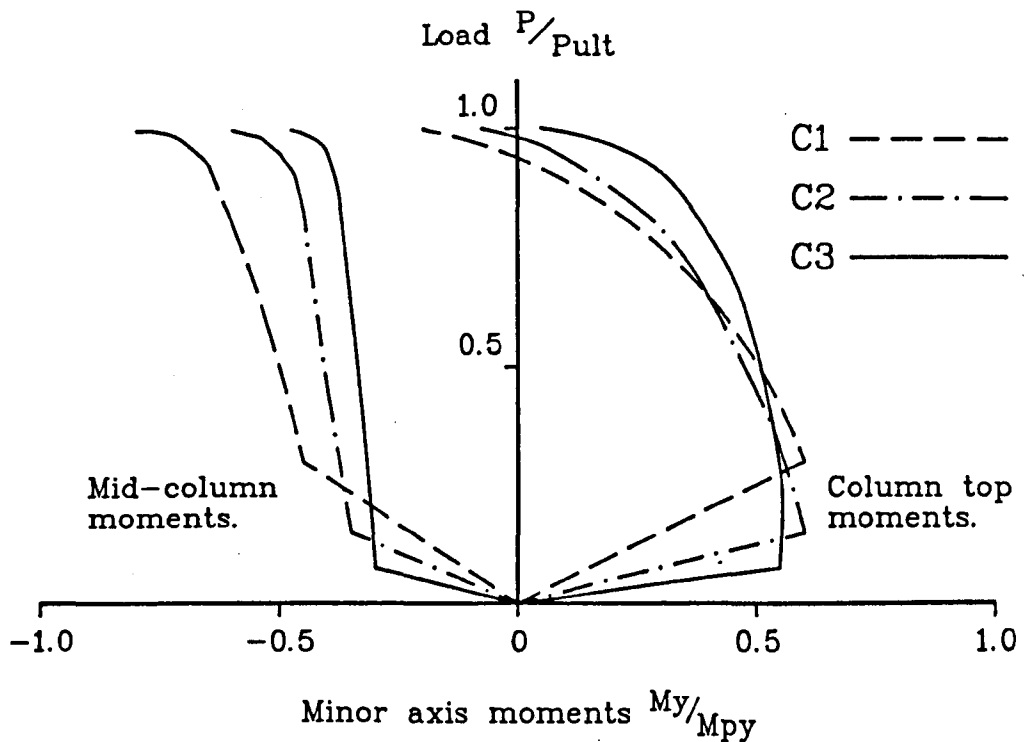


Figure 7.8: Plot of the top and mid-column minor axis bending moments for load case 6A with beam B1 and a rigid connection.

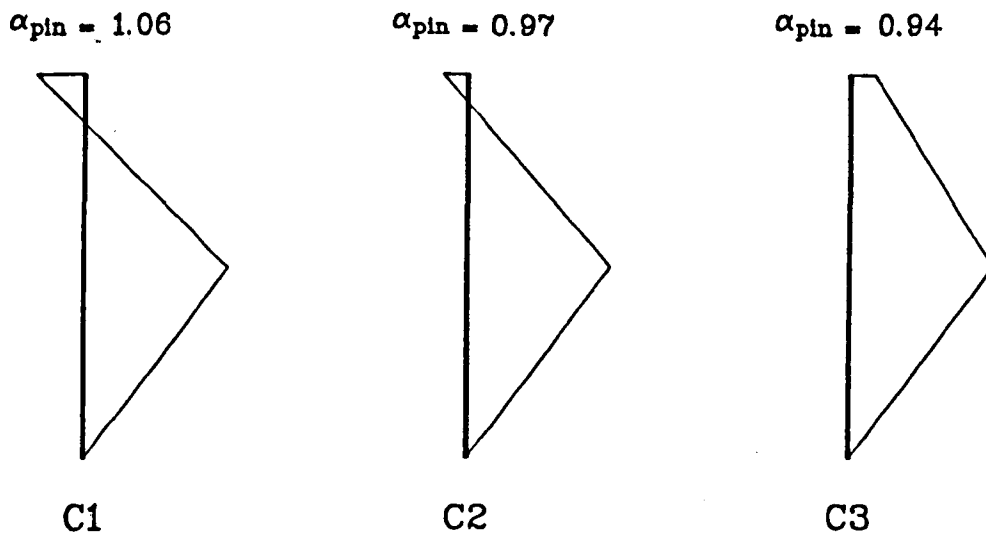


Figure 7.9: Minor axis bending moments at the point of failure for load case 6A with beam B1 and a rigid connection.

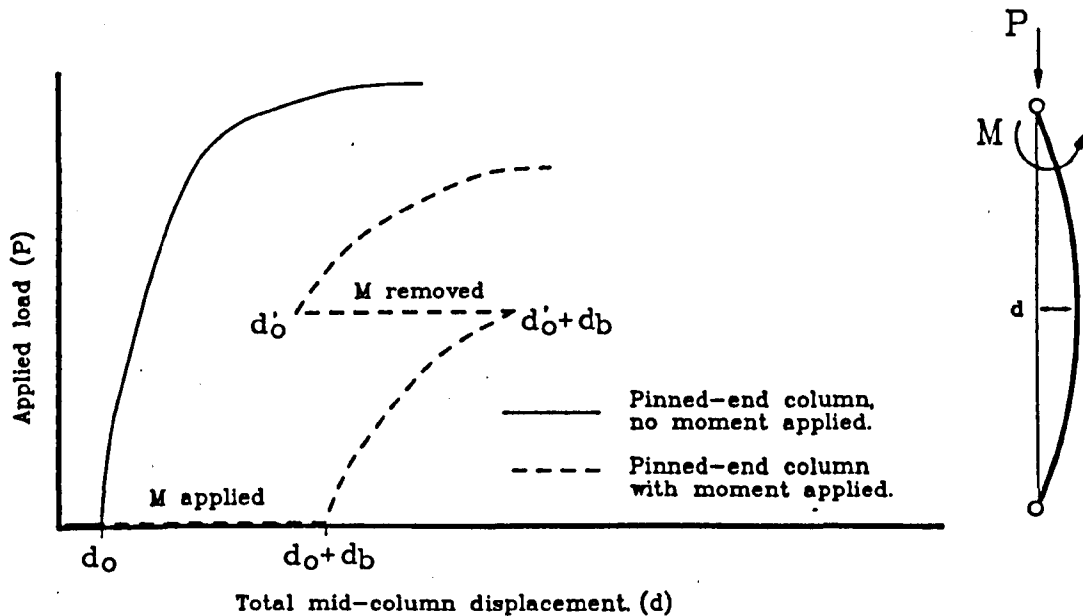


Figure 7.10: Plot of load vs. minor column axis displacement for a illustrating the adverse effect of the P- $\delta$  effect on initial disturbing moments.

Loading w1 — Columns C1,C2 and C3

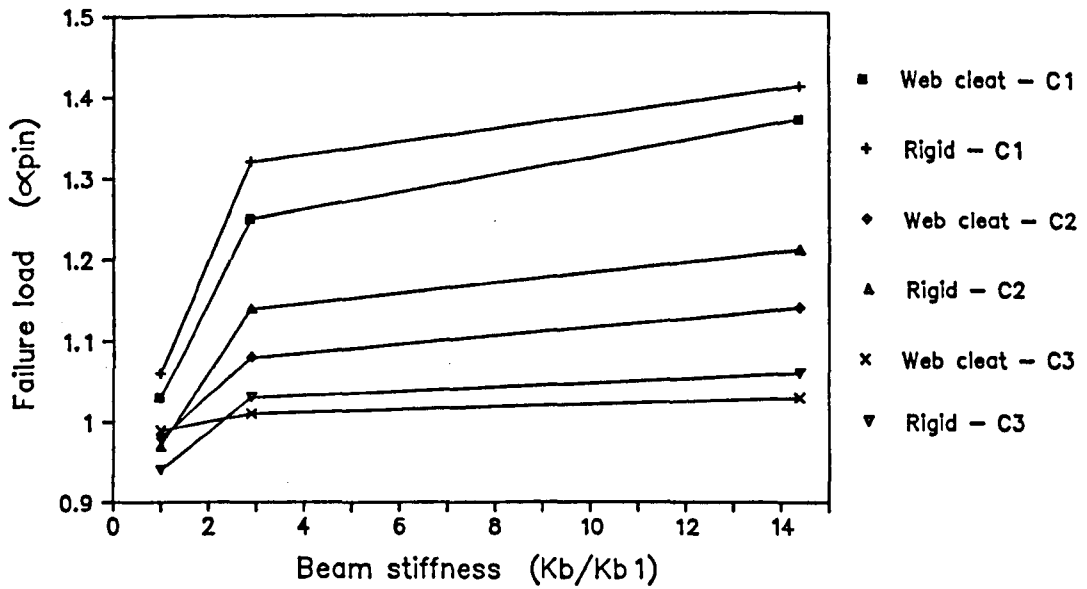


Figure 7.11: Plot of failure load ( $\alpha_{pin}$ ) vs. beam stiffness for load intensity w1.

Loading w2 — Columns C1,C2 and C3

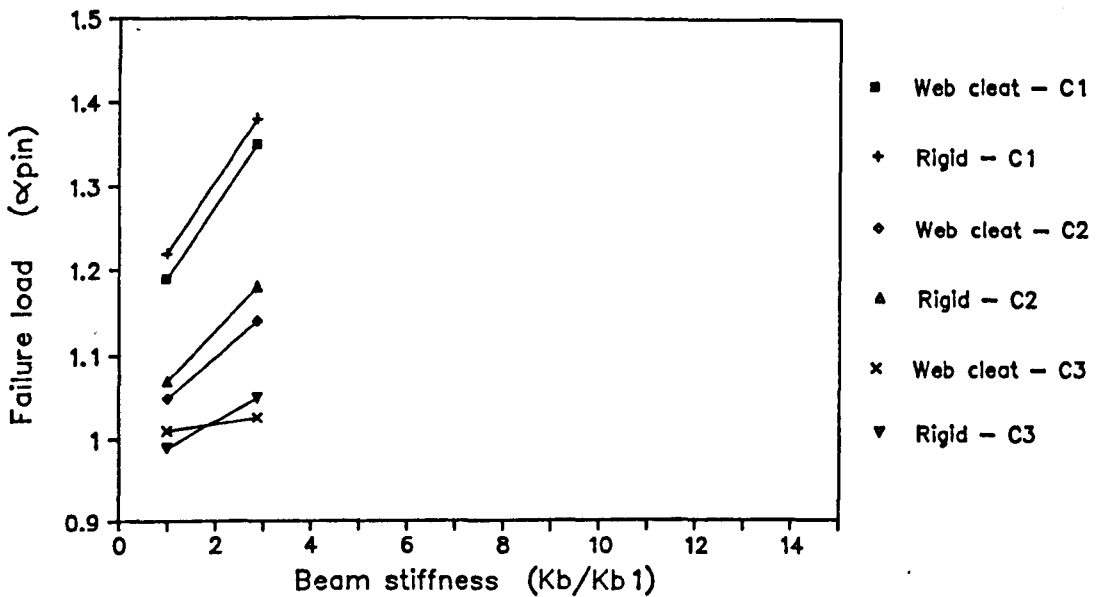


Figure 7.12: Plot of failure load ( $\alpha_{pin}$ ) vs. beam stiffness for load intensity w2.

Beam 3 - Columns C1,C2 and C3

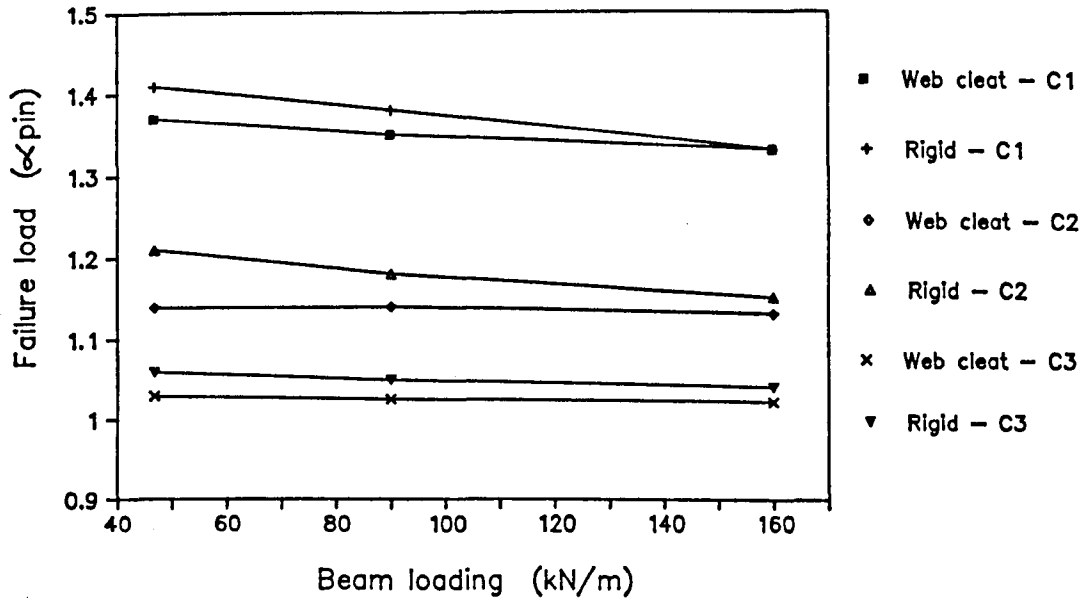


Figure 7.13: Plot of failure load ( $\alpha_{pin}$ ) vs. beam load intensity for a type B3 beam.

Beam 2 - Columns C1,C2 and C3

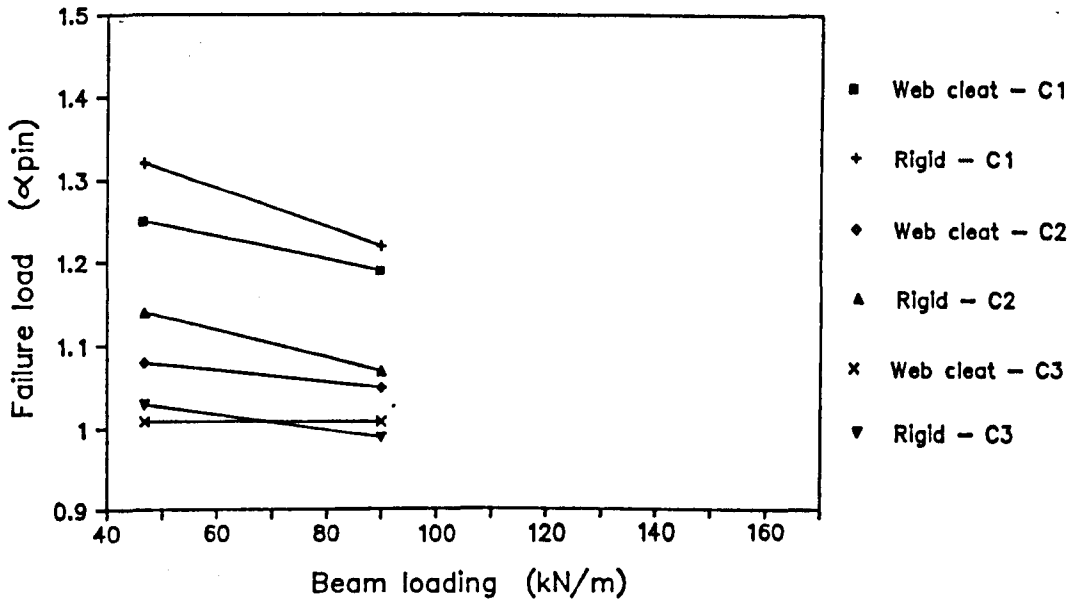


Figure 7.14: Plot of failure load ( $\alpha_{pin}$ ) vs. beam load intensity for a type B2 beam.

## Chapter 8

# The Design of Non-sway Frames with Semi-Rigid Connections.

### 8.1 Introduction

One of the principal objectives of this research project was to use the observations on semi-rigid frame behaviour from both experimental and numerical studies to investigate, and where appropriate enhance, existing methods of design. This chapter of the thesis is devoted to this objective.

Included in this chapter is a comprehensive historical review of the development of present 'codified' methods of isolated column design and 'state of the art' methods for the design of semi-rigid frames. Also included are the author's own proposals for semi-rigid design under both ultimate and serviceability loading conditions. In each case, the proposed design techniques have been verified against the response of the full scale frame tests F1, reported in chapter 5. In line with the need to provide steelwork designers with the option of performing relatively conservative designs requiring only the minimum of effort, the author has supplemented his proposed in-depth technique with possible alternative

simplified methods of design.

## **8.2 The deformation of semi-rigid frames under serviceability loads.**

It is appreciated that in steelwork design practice, the consideration of member deformations under a serviceability, or 'working', load condition, in which the response remains wholly elastic, is often of secondary importance to strength and stability considerations under ultimate loads. However, from the author's experience, it would appear that practising steelwork designers are prepared to accept unreservedly that the inherent rotational stiffness of nominal connections produces 'real structures' which are stiffer than those predicted from simple design methods. This compares with the potential benefit of connection restraint on the ultimate capacity which is generally viewed by designers with some scepticism. It is the author's opinion that the application of semi-rigid analysis/design principles to the less critical serviceability condition would, initially, be more readily accepted by steelwork designers and would act as a precursor to the universal acceptance and everyday use of ultimate load semi-rigid design techniques.

The benefit of end restraint on the deflection of beams is illustrated in figure 8.1 which shows the well known central deflection equations for the extreme support conditions of simply supported and fixed ends. It is evident that under elastic conditions, the central deflection of the fixed end beam is one fifth that of the same beam over a simply supported span. Unlike the ultimate load considerations described in Chapter 7, in which the benefit of column restraint was seen to decrease with decreasing column slenderness, this reduction in the deflection of beams loaded elastically will always apply irrespective of beam length. The following section describes a deflection prediction technique,

which enables this large potential for reduced beam deflections to be applied to non-sway frames with semi-rigid connections under serviceability loading conditions.

### 8.2.1 Development of the deflection equations.

Figure 8.2 shows a beam subjected to a uniform load with non-linear restraints at the supports. The support rotation  $\phi_b$  can be expressed as:-

$$\phi_b = \frac{wL_b^3}{24 EI_b} - \frac{M_{sr}L_b}{2 EI_b} \quad (8.1)$$

where:

$w$  = Intensity of applied load.

$E$  = Young's modulus.

$I_b$  = Second moment of area of the beam.

$L_b$  = Beam span.

$M_{sr}$  = Bending moment at the beam support  
assuming a semi-rigid connection.

If the beam is now considered as part of a non-sway subframe, as in figure 8.3 then the connection moment will induce a rotation at the node point of the column of:-

$$\phi_c = \frac{M_{sr}}{3 E \left( \frac{I_{cu}}{L_{cu}} + \frac{I_{cl}}{L_{cl}} \right)} \quad (8.2)$$

where:

$I_{cu}$  = Second moment of area of the upper column segment.

$I_{cl}$  = Second moment of area of the lower column segment.

$L_{cu}$  = Length of the upper column segment.



$L_d$  = Length of the lower column segment.

If the upper and lower column segments are the same length and section size then this equation reduces to:-

$$\phi_c = \frac{M_{sr} L_c}{6 EI_c} \quad (8.3)$$

It should be noted that the column node rotation has been derived assuming that the remote ends of the column segments to be pinned. This will of course result in a lower column stiffness than that of a column with more realistic boundary conditions, but will produce a conservative over-estimation of the beam deformations.

The net rotation of the connection ( $\phi_b - \phi_c$ ) can therefore be expressed in terms of the connection moment and the frame geometry:-

$$(\phi_b - \phi_c) = \frac{w L_b^3}{24 EI_b} - \frac{M_{sr} L_b}{2 EI_b} - \frac{M_{sr} L_c}{6 EI_c} \quad (8.4)$$

The linear relationship between connection moment and connection rotation in the above equation has been plotted in figure 8.4 as the frame response line. It evident from the figure that when the connection moment is zero, equation 8.4 intersects the abscissa at a rotation equivalent to that of a simply supported beam,  $\phi_{pin}$ . When the connection rotation is zero, the equation intersects the ordinate at a value equivalent to the rigid frame connection moment,  $M_{rigid}$ .

As in beam line theory [8.1], the non-linear moment-rotation characteristics of a connection can be superimposed onto the plot as in figure 8.4. The intersection point of the moment-rotation curve with the plot of equation 8.4 represents the connection moment and corresponding rotation which is compatible with the stiffness characteristics of the beam and column members. By substituting this connection moment,  $M_{sr}$ , into equation 8.1 the support rotation, the distribution of bending moments and hence the deflected shape of the beam shown in figure 8.3 can be determined. It is clear however,

that the inclusion of the non-linear characteristics of the connection in this approach is not appropriate for 'everyday' design calculations.

Bjorhovde, in a recent appraisal of end restraint on column strength [8.2], stated that the support rotations of simply supported beams of practical dimensions, subjected to their maximum allowable uniform load, were generally less than 0.0092 radians. That is:-

$$\frac{wL_b^3}{24 EI_b} \leq 0.0092 \quad (8.5)$$

At this rotation, he proposed that there was only a small overestimation of the restraining moment calculated using the linear initial tangent stiffness of the connection,  $C_i$  (figure 8.5) - the non-linear characteristics of typical connections only becoming significant at larger rotations. For a beam in a semi-rigid frame, the maximum connection rotation under serviceability conditions will obviously be less than that of a similar beam acting over a simple span. It suggests therefore that in this instance, in which serviceability loading has been considered, the linear representation of the non-linear moment-rotation connection response will result in a more accurate assessment of connection moment than that assumed by Bjorhovde.

From figure 8.6 the overestimation of the apparent connection moment,  $M'_{sr}$ , based on the assumption of a linear connection stiffness, compared to the actual connection moment,  $M_{sr}$  is evident. It is interesting to note however that as the gradient of the plot of equation 8.4 becomes smaller, i.e. long span beams connected to slender columns, the overestimation of the connection moment reduces. This implies that certain frame geometries will be relatively insensitive to the linear simplification of the non-linear connection moment rotation response. It also suggests that, when applied to frames, there is the potential for further reductions in the inaccuracies accepted by Bjorhovde for the restraining moment due to semi-rigid connections.

By adopting a linear connection stiffness, the moment at the connection can therefore be estimated quite accurately from:-

$$M'_{sr} = \frac{wL_b^3}{24 EI_b \left( \frac{1}{C_i} + \frac{L_b}{2 EI_b} + \frac{L_c}{6 EI_c} \right)} \quad (8.6)$$

The above equation is applicable to a limited subframe analysis in which the remote ends of the column are pinned and the beam is subjected to a uniformly distributed load. However, it is evident from figure 8.6 that for known end points of  $M_{rigid}$  and  $\phi_{pin}$ , a more general form of the equation, applicable for any beam load type and column end conditions, can be determined. The semi-rigid connection moment can therefore be expressed as:-

$$M'_{sr} = \frac{M_{rigid}}{\left( 1 + \frac{M_{rigid}}{\phi_{pin} C_i} \right)} \quad (8.7)$$

If a dimensionless semi-rigid stiffness factor,  $\mu$ , is introduced such that:-

$$\mu = \frac{M_{sr}}{M_{rigid}} = \frac{1}{1 + \frac{M_{rigid}}{\phi_{pin} C_i}} \quad (8.8)$$

where:

$$\mu = 0.0 \text{ when } M_{sr} = 0.0$$

$$\mu = 1.0 \text{ when } M_{sr} = M_{rigid}$$

Then, from consideration of elastic principles, the deflection at any point on the beam is given by:-

$$\delta_{sr} = \delta_{rigid} + (1 - \mu)(\delta_{pin} - \delta_{rigid}) \quad (8.9)$$

where:

$\delta_{sr}$  = Deflection of the beam in a semi-rigid frame.

$\delta_{rigid}$  = Deflection of the beam in a fully rigid frame.

$\delta_{pin}$  = Deflection of the beam with simple supports.

From equations 8.7, 8.8, and 8.9, the deflection of the beam can therefore be determined with relative ease. The parameters relating to rigid behaviour,  $M_{rigid}$  and  $\delta_{rigid}$ , could be determined from a relatively simple elastic plane frame analysis computer program, moment distribution principles on limited subframes or from Kleinlogel equations [8.3] - all of which are familiar to practising steelwork designers. The simple end rotation of the beam,  $\phi_{pin}$ , would be derived from well known beam bending equations.

### 8.2.2 Linear simplification of the connection moment-rotation response.

In the development of the semi-rigid frame deflection equation reported above a linear initial tangent stiffness was used to represent the characteristics of the connection. Researchers have made extensive use of the initial tangent stiffness,  $C_i$ , in the analysis of flexibly connected frames [8.2, 8.4, 8.5, 8.6] because of the relative ease of determining the value by both graphical and analytical means. However, it has been shown [8.7] that using the connection stiffness,  $C_i$ , can produce an unacceptable overestimation of the connection performance. In terms of the analysis method described in section 8.2.1, any slight overestimation of the connection stiffness would produce an unconservative shortfall in the prediction of frame deflections. A more conservative approach is to consider a less stiff connection response in the form of a linear secant stiffness.

As described in section 8.2.1, it is apparent that the maximum rotation which is likely to occur at the connection between members of practical proportions is 0.0092 radians. It would, therefore, seem reasonable to use a conservative lower bound connection secant stiffness for the serviceability condition of  $C_{10}$  - i.e. the linear stiffness corresponding to a rotation of 0.010 radians (figure 8.7). An approach which has been used in the current draft of EC3 [8.8], assumes a linear secant stiffness,  $C_M$ , corresponding to the design moment capacity of the connection. The relative magnitudes of the stiffnesses derived

using these two techniques would of course depend on the nature of the connection. For a very stiff connection, it is likely that the moment capacity would be achieved at a rotation less than 0.010 radians. However, for a moderately stiff connection to a flexible column web panel, the deformation dependent  $C_{10}$  secant stiffness will be close to the initial tangent stiffness and the reverse may well be true.

An alternative linear representation of connection stiffness has been proposed by Barakat and Chen [8.7] for use in a simplified method of semi-rigid frame analysis. They propose a linear secant stiffness,  $C_{k_o}$ , corresponding to the rotation of the connection,  $\phi_o$ , at the intersection point of the initial tangent stiffness,  $C_i$ , with the ultimate moment capacity of the connection. The procedure is illustrated in figure 8.8.

It is clear that there are a number of different ways of producing a linear stiffness 'equivalent' to the non-linear connection response. It would suggest therefore that this is an area which warrants further research to determine a single universally accepted linear representation of connection stiffness which is appropriate for design under serviceability and ultimate load conditions. In terms of the serviceability condition, this could be achieved by conducting a parametric study using a non-linear semi-rigid frame analysis program [8.9] to investigate the size of connection rotations for a range of practical beam and column sizes under 'working' loads. The aim would be to 'add more weight' to the maximum rotation proposed by Bjorhovde, on which the linear stiffness  $C_{10}$  was based, and to quantify the limits of application.

### 8.2.3 Validation of the semi-rigid frame deflection equations.

This section presents a comparison of the predicted deformations from the equations reported in section 8.2.1 with the observed deflections of the full scale frame test F1 reported in chapter 5. Figure 8.9 shows the arrangement of the test frame indicating the

particular increment of beam loading which closely approximated to the serviceability limit state assuming simple beam spans, i.e.

$$w_{serv} = \frac{w_{ult}}{1.5} \quad (8.10)$$

where:

$w_{serv}$  = Serviceability load.

$w_{ult}$  = Ultimate design load.

The observed experimental deflection measurements at this particular load increment were used throughout the comparative study. An elastic plane frame analysis computer program was used to determine the bending moments and deflections of the same frame with fully rigid connections subjected to the same loading conditions. Table 8.1 presents a summary of the measured experimental semi-rigid moments and the calculated fully rigid moments at each of the joints on the frame.

The predicted semi-rigid frame deflections were calculated assuming the range of different linear connection stiffnesses introduced in section 8.2.2. namely the initial tangent stiffness ( $C_i$ ), the secant stiffness at a rotation of 0.010 radians ( $C_{10}$ ), the secant stiffness corresponding with the design moment of the connection ( $C_M$ ) and that proposed by Barakat and Chen ( $C_{k_0}$ ). In each case, the stiffnesses were determined from the measured moment-rotation plots of the individual frame connections reported in Chapter 6. A design moment of 21.75 kN.m for the 12mm thick end-plate connection, extracted from reference 8.10, was used in determining the  $C_M$  secant stiffness. The ultimate moment capacities  $M_{ult}$  of the connections, used to determine  $C_{k_0}$ , were those observed in the isolated connection tests reported in Chapter 6.

Table 8.2 contains a summary of the different linear connection stiffnesses whilst table 8.3 presents a summary of the predicted semi-rigid connection moments calculated using equation 8.7 and the corresponding ' $\mu$ ' factors from equation 8.8. It should be noted that,

due to a faulty rotation measurement device, the experimental moment-rotation data for joint 'l' is not available. It has therefore been assumed that the measured stiffness of this particular connection is equal to that of joint 'c' - a geometrically similar connection arrangement subjected to a similar disturbing moment. In addition, the ultimate design connection moment of 21.75 kN.m. was only achieved at joint 'j' of those nodes on the external columns. As a result, the  $C_M$  secant connection stiffness for the remaining external column connections, 'l', 'e' and 'c', was assumed equal to that of joint 'j'.

An appraisal of the data in table 8.2 shows that, as discussed in chapter 6, there is a large difference between the stiffness of connections located on the minor axis of internal and external columns. This was attributed to the effects of beam continuity and column web flexibility as have been discussed in chapter 6. In addition, it also appears that large differences can occur between the stiffness of nominally similar connection types with the same beam and column arrangement (e.g. joint 'd' and joint 'f'). However, what is perhaps of most significance is that whilst the initial tangent stiffness,  $C_i$ , of joint 'd' is 600% larger than the secant stiffness,  $C_{10}$ , for the same connection and moment-rotation response, the resulting ' $\mu$ ' factor, and hence semi-rigid connection moment (table 8.3), is only 13% larger. It would appear therefore that this particular frame is relatively insensitive to large variations in the assumed linear stiffness of the beam to column connections - the most difficult parameter to determine accurately.

Due to the obvious difference in the nature and response of connections at either end of the primary beams in this particular frame, an average ' $\mu$ ' factor has been derived for each beam (table 8.4). The factor  $\mu_{ave}$  is effectively the numerical mean of the two ' $\mu$ ' factors at the beam supports. Table 8.5 presents a summary of the predicted semi-rigid frame mid-beam deflections, calculated using equation 8.9 and the data in table 8.4, for each of the four different linear connection stiffnesses. The simply supported span, rigid frame and actual experimental mid-beam deflections are also presented in the table for comparison. Table 8.6 presents a direct comparison between the predicted semi-rigid deflections and those measured in the full scale frame test, whilst table 8.7 compares the

predicted deflections with those calculated assuming simple beam supports.

It is evident from tables 8.5 and 8.6 that the predicted semi-rigid deflections compare favourably with those observed in the experimental frame test. As expected, there is a very close agreement when an initial linear stiffness,  $C_i$ , is assumed, with only a small under estimation of deflection on two of the four primary beams. Using the lower bound linear secant stiffness,  $C_{10}$ , all the predicted deflections are higher than actual, however the correlation is still reasonably close. In all cases, the predicted deflection of beam B8 produced the largest discrepancy. It should be noted however that the applied load to this particular beam produced very small deflections and that, in the absence of experimental data, an assumed moment-rotation response had been used for joint '1'.

The deflections predicted using the  $C_M$  linear secant stiffness are close to those obtained using a  $C_{10}$  stiffness. As discussed in chapter 6, beam continuity negated the effect of column web flexibility thus producing a stiff connection with the internal column. At this location therefore, the  $C_M$  stiffness was significantly larger than the deformation dependent stiffness  $C_{10}$ . At the opposite end of the beam, where continuity effects were not present, the  $C_M$  stiffness was smaller than  $C_{10}$ . These two reverse trends cancelled out when the factor ' $\mu_{ave}$ ' was determined, thereby predicting similar deflections. Table 8.7 shows that even by adopting a conservative estimation of the linear secant connection stiffness, there is a significant reduction in the predicted deflections compared with those derived from simple calculations. Using a linear secant stiffness,  $C_{10}$ , the minimum improvement resulted in a 39% reduction of the deflection of the corresponding simply supported beam.

It is the author's opinion that the close correlation which has been achieved with the experimental data from the full-scale frame test verifies the ability of the proposed serviceability design/analysis technique to accurately predict the deflections of beams in semi-rigid, non-sway frames. In addition, the apparent insensitivity of the technique to variations in the selection of the linear connection stiffness suggests that it is a method



suitable for use in practical steelwork design.

#### 8.2.4 Summary of the serviceability design technique.

This section presents a brief summary of the principal steps involved in carrying out the above serviceability check.

1. Determine the serviceability loading ( $1.0G_k + 1.0Q_k$ )
2. Perform a linear elastic analysis of the frame assuming fully rigid joints (member sizes having been determined from an ultimate load design).
3. Assuming a similar connection type throughout, extract the rigid central deflections,  $\delta_{rigid}$ , and rigid connection moments,  $M_{rigid}$ , for a critical 'internal' beam and an 'end-bay' beam.
4. Determine the end rotations of the two beam types assuming simple supports,  $\phi_{pin}$ .
5. Use an appropriate linear connection stiffness,  $C$ , and equation 8.7 to determine the semi-rigid connection moments,  $M'_{sr}$ .
6. Determine the  $\mu_{ave}$  factor for the two beams from equation 8.8. and use equation 8.9 to determine the central deflection of the beams.

In the validation of the method described in section 8.2.3, it was necessary to derive an average  $\mu$  factor because of the dramatic difference in the moment-rotation response of connections to the minor axis of internal and external columns. Where beams frame into the major column axis, in which the same connection produces a similar moment-rotation response irrespective of presence of beam continuity, it is proposed that a single  $\mu$  factor from any one joint would be applicable throughout the whole frame. This would result in a substantial simplification of the technique. The author suggests that the analysis technique, together with this proposal, should be validated, by others, against the experimental data from the second frame test F2 (Chapter 6), in which the primary beams were connected to the major column axis.

### 8.2.5 The potential benefits of predicting reduced deflections.

In the current British steelwork design code [8.11], the maximum permissible deflection of beams, when subjected to live loading only, is limited to span/360. Therefore, for a given beam type, there is a particular combination of applied load and beam span for which the above deflection restriction is more critical than ultimate strength considerations. This is particularly common in the case of long span beams supporting relatively light roof coverings where there is a high ratio of live to dead loading. Figure 8.10 shows a plot of the maximum permissible simple beam spans which satisfy both the strength and deflection requirements in BS5950: Part 1 [8.11] for two grade 43 steel beams subjected to different characteristic loads. The shaded zones on the plot represent the combinations of load and beam span which satisfy the strength requirements, but which exceed those for deflection. It should be noted that if higher material strengths had been considered, e.g. grade 50, these shaded zones would have been more extensive. Clearly, adopting a method of deflection prediction which incorporates the beneficial effects of semi-rigid joint action would produce economies for structural arrangements situated within these

zones. For the particular member sizes and live load ratio which have been considered, the transition from strength to deflection control occurs at a relatively large span to depth ratio of 25. However, in situations where the live load ratio was significantly larger, this transition point would occur at a much reduced span to depth ratio.

One other area where the inclusion of semi-rigid joint characteristics would produce economies is in the field of composite construction. Experimental studies have shown that the action of the concrete floor slab causes a dramatic increase in the connection stiffness compared with that of the bare steel frame [8.12]. This suggests that restrictions on the deflection of composite beams in frames could be relaxed and thus make more effective use of the potentially large resistance moments. Accurate prediction of the actual deflections of bare steel frames could have significant cost benefits when applied to composite frames during the construction stage. In certain circumstances of large spans, prudent use of the bare steel connection stiffness in the deflection prediction could alleviate the need for propping during the concreting operation [8.13].

It is hoped that the possible economies discussed above could be explored by others to assess the feasibility of the deflection prediction method for use in practical steelwork design. Whatever economies are shown to be possible, it is the author's belief that relatively simple analytical tools should be available to practising steelwork designers to enable a more accurate, and confident, prediction of 'real frame' behaviour.

### **8.3 The ultimate design strength of beam-columns.**

Previous research into the analysis and design of semi-rigid frames has concentrated almost entirely on the ability to predict the behaviour under ultimate loads. This section of the thesis contains a brief review of design methods, past and present, for both re-

strained and unrestrained beam-columns and includes the author's proposals for possible future developments. For a comprehensive historical review of past research in this area, the discerning reader should consult references 8.14 and 8.15.

### **8.3.1 The beam-column problem.**

The loading conditions on beam-column members with open sections can be categorised into three separate cases (figure 8.11):-

1. With the thrust applied eccentric to the minor axis (or if eccentric to the major axis, then the column is prevented from deflecting out of this plane by appropriate bracing), in which case the member will collapse by excessive deformation in this plane.
2. The thrust is applied with an eccentricity about the major axis, in which case the column will collapse by deflecting in the minor axis and twisting (i.e., similar to lateral-torsional beam buckling).
3. The thrust is applied with an eccentricity about both axes, in which case the member will collapse by biaxial bending and twisting.

Case 1 represents an interaction between column buckling and simple uniaxial beam bending, case 2 represents an interaction between column buckling and beam buckling whilst case 3 represents the interaction of column buckling and biaxial beam bending. Clearly case 3 represents the more general case, with the other cases being more limited versions.

The magnitude of the actions applied to beam-columns,  $P$ ,  $M_x$  and  $M_y$ , can be expressed conveniently as a single point on a three-dimensional interaction diagram. Likewise, the combinations of loading which meet the failure criteria can also be expressed as a series of points on the diagram in the form of an interaction failure surface (figure 8.12). Clearly combinations of loading which fall outside the appropriate interaction surface will result in an unsafe column design. In the case of a stocky member, in which instability phenomena are not present, the limiting load components are dictated by material strength considerations. The end points of the interaction surface for stocky columns are therefore well defined. However, depending on the geometrical properties, unbraced length and support conditions, the end points of the interaction for more slender columns will fall short of those dictated by material yield. The problem is therefore to define the end points of the appropriate interaction surface and to take due account of the effects of residual stress, member imperfections and variation in material properties which will have a direct influence on the concavity or convexity of the interaction surface.

The general form of the interaction surface can be expressed as:-

$$f\left(\frac{P}{P_u}, \frac{M_x}{M_{ux}}, \frac{M_y}{M_{uy}}\right) \leq 1.0 \quad (8.11)$$

Equations of this type represent by far the most common method of beam-column design specified in international steelwork design codes. The author has therefore presented a brief overview of the development of explicit forms of this equation which are widely used in North American design practice.

### 8.3.2 The development of interaction equations.

A starting point for many design equations considers the uniaxial bending condition (case 1 in section 8.3.1) with interaction being of the form:-

$$\frac{P}{P_u} + \frac{M}{M_u} \leq 1.0 \quad (8.12)$$

where:

$P$  = Axial thrust at failure.

$P_u$  = Ultimate load for a centrally loaded column for buckling in the plane of the applied load.

$M$  = Maximum bending moment at failure.

$M_u$  = Ultimate moment capacity in the absence of axial load.

The value of  $M$  can be taken as the maximum primary moment for the case of a stocky column. However, the maximum moment in the case of slender columns will be dependent on the applied primary moment and secondary effects due to member deformation (figure 8.13). To take account of this effect, the maximum moment at the mid-height of a column subjected to an axial load,  $P$ , and equal and opposite end moments,  $M_o$ , can be expressed approximately by [8.16]:-

$$M_{max} = M_o \left( \frac{1}{1 - \frac{P}{P_e}} \right) \quad (8.13)$$

in which  $P_e$  is the elastic critical load of the member. Substituting into equation 8.12 gives the design formula

$$\frac{P}{P_u} + \frac{M_o}{M_u \left( 1 - \frac{P}{P_e} \right)} \leq 1.0 \quad (8.14)$$

which was first recommended by the S.S.R.C. and which has been included in several codes. A direct comparison of this equation and the early numerical studies by Galambos and Ketter [8.17] is presented in reference 8.18. Comparisons based on more recent numerical studies are presented in reference [8.19].

Equation 8.14 was considered to be unduly conservative in instances where the member was in double curvature. The equation was therefore refined to take account of unequal end moments and/or transverse loading between the points of support in the plane of bending. The maximum value of end moment  $M_o$  was replaced by an equivalent uniform moment  $M_{eq}$  given by:-

$$M_{eq} = M_{max} C_m \quad (8.15)$$

Studies of the in-plane problem [8.15, 8.20] and the lateral torsional buckling problem [8.21], have shown that a simple and reasonably accurate correlation results if  $C_m$  is given by:-

$$C_m = 0.6 + 0.4\beta \quad \not\leq 0.4 \quad (8.16)$$

where:

$\beta =$  the ratio of the smaller end moments to the larger.

$$(-1.0 \leq \beta \leq +1.0)$$

This led to the modified design form of interaction equation 8.14:-

$$\frac{P}{P_u} + \frac{C_m M_o}{M_u \left(1 - \frac{P}{P_c}\right)} \leq 1.0 \quad (8.17)$$

Work by a number of researchers [8.15, 8.21, 8.22] on the effects of lateral-torsional buckling on the strength of members loaded about the strong axis of bending, case 2 in section 8.3.1, resulted in an expression for the elastic critical load of:-

$$\frac{M_o}{M_E} = \left[ \left(1 - \frac{P}{P_{ey}}\right) \left(1 - \frac{P}{P_\phi}\right) \right]^{\frac{1}{2}} \quad (8.18)$$

where:

$M_E =$  Elastic critical moment for lateral-torsional buckling.

$P_{ey} =$  Elastic critical load for minor axis flexural buckling.

$P_\phi =$  Elastic critical load for pure torsional buckling.

This led to the general design equation:-

$$\frac{P}{P_u} + \frac{C_m M_o}{M_u(1 - \frac{P}{P_{ez}})} \leq 1.0 \quad (8.19)$$

where:

$P$  = Applied load.

$P_{uy}$  = Axial load producing failure in the absence of bending moment, computed for weak axis bending.

$M_o$  = Maximum applied first order moment.

$M_u$  = Moment producing failure in the absence of axial load, allowing for lateral torsional buckling.

$C_m$  = Moment reduction factor.

This equation is of a similar form to that of equation 8.17, which deals with member deformation in the plane of the applied moment. However, the terms in the denominator now take account of the out-of-plane effects. Comparisons of equation 8.19 with numerical data have been performed by Vinnakota [8.23].

Equations 8.17 and 8.19 are special cases of the more general beam-column problem, case 3 in section 8.3.1. It has been shown that these two particular equations provide good descriptions of the  $P - M_y$  and  $P - M_x$  interaction for 'I' and 'H' sections. It was suggested that the general case can be derived from an empirical combination of these two equations to give:-

$$\frac{P}{P_u} + \frac{C_{mx} M_x}{M_{ux}(1 - \frac{P}{P_{ex}})} + \frac{C_{my} M_y}{M_{uy}(1 - \frac{P}{P_{ey}})} \leq 1.0 \quad (8.20)$$

It should be noted that under the appropriate loading conditions, this equation reduces to the uniaxial bending equations presented above (eqns. 8.17 and 8.19). This particular formula is that currently used in North American design practice and forms the basis of



many commonly used biaxial interaction design equations in other international design codes. However, comparisons with numerical studies by Chen and Atsuta [8.15] as shown in figure 8.14 have demonstrated that due to the convex nature of the true interaction, equation 8.20 is highly conservative under certain loading conditions. Based on his work on the behaviour of short columns, Tebedge [8.24] proposed that the following non-linear expression could be applied to intermediate and slender columns:-

$$\left(\frac{C_{mx}M_x}{M_{ucx}}\right)^\eta + \left(\frac{C_{my}M_y}{M_{ucy}}\right)^\eta \leq 1.0 \quad (8.21)$$

where:

$M_{ucx}$  = Ultimate moment capacity from eqn. 8.19

$M_{ucy}$  = Ultimate moment capacity from eqn. 8.17

$\eta$  = Factor depending on B/D ratio of section.

A quantitative assessment of the accuracy of equations 8.20 and 8.21 was performed by Pillai [8.25] on experimental data from tests by Birnsteil [8.26], Chubkin [8.27] and Kloppel and Winkelmann [8.28]. He concluded that equation 8.21 was an almost perfect predictor in terms of the mean value for  $P_{test}/P_{calc}$  of 1.05. However, with a standard deviation of 0.101, this meant that 31% of the results were overpredicted, i.e. unsafe.

### 8.3.3 The interaction equations in BS 5950: Part 1.

The British Steelwork Design Code, BS5950: Part 1 [8.11], uses the following interaction equations in clause 4.8.3.3.1 for the buckling criteria of beam- columns.

$$\frac{F}{A_g p_c} + \frac{m_x M_x}{M_b} + \frac{m_y M_y}{p_y Z_y} \leq 1.0 \quad (8.22)$$

$$\frac{m_x M_x}{M_{ax}} + \frac{m_y M_y}{M_{ay}} \leq 1.0 \quad (8.23)$$

where:

$F$  = Applied axial load.

$p_y$  = Design strength of the material.

$M_b$  = Buckling resistance moment.

$m_{x,y}$  = Equivalent uniform moment factor.

$A_g$  = Gross cross-sectional area.

$Z_y$  = Minor axis elastic section modulus.

$M_{ax}$  = Maximum buckling moment about the major axis  
in the presence of axial load.

$M_{ay}$  = Maximum buckling moment about the minor axis  
in the presence of axial load.

Equation 8.22, which is of a similar format to equation 8.20 in the above section, has been developed specifically as a simple design method. In instances where significant moments are applied, a less conservative solution requiring more design effort can be derived from equation 8.23, the so called 'more exact approach'.

### 8.3.4 The application of interaction equations to steel frame design in BS 5950: Part 1.

The interaction equations described above have been derived, and subsequently verified, by considering known end forces and end conditions on isolated structural elements. This is of course an idealistic simplification as beam- columns are, in reality, component parts

of real structures in which the forces and end conditions are dictated by interconnecting members. However, there are approximate methods within BS 5950 for incorporating frame response characteristics into isolated member design.

For multi-storey non-sway frames designed using the 'simple design' technique in BS 5950, in which the connections are assumed to act as true pins, the moment applied to the column is derived by considering the vertical end reaction of interconnecting beams acting at an eccentricity of 100mm from the column face, or at the centre of stiff bearing - whichever is the greater. Recent experimental studies of two-dimensional steel frame behaviour [8.10] have shown this eccentricity, which has a value of 100mm irrespective of connection type, beam size or frame configuration, to be grossly in error. Despite this, and the lack of a theoretical background to the method, it remains today one of the most commonly used methods of determining the column moments in simple frames since it was first introduced in the 1930's.

In BS 5950, the rotational restraint which is present at the ends of column segments due to the stiffness of adjoining members, is catered for in isolated column design by use of the effective length concept. By using appropriate effective length factors, the length of an equivalent pinned-end column can be determined which has the same critical load as the full height restrained column. For non-sway frames with positive end restraint, the effective length factor is usually less than unity. Use of the 'standard' cases for known end conditions in clause 4.7.2 of the code results in effective length factors which are typically in the range 0.8 to 1.0. This has a direct effect on the design column capacity by increasing the ultimate axial capacity,  $P_u$ , and where restraint to lateral-torsional buckling is present, the buckling resistance moment,  $M_b$ , both of which are terms in the denominator of the interaction equation (eqn. 8.22).

The effective length concept, which has its origins in the work carried out by Euler in the eighteenth century, has formed the basis of strut design for many years. However, the selection of appropriate effective length factors is very much based on the intuition,

and in some instances courage, of the individual engineer, particularly in the case of non-standard structural arrangements. This compares with the more exact approach given in appendix E of BS5950 for determining the effective lengths of columns in rigid frames. Here, the total restraint at the upper and lower ends of a column, derived from consideration of the adjoining members, are used to derive the column's critical load (effective length ratio) from alignment charts.

### **8.3.5 Beam-column design allowing for semi-rigid connection response.**

The recently superseded British Standard for steelwork design, BS 449 Part 1 [8.29], permitted the use of semi-rigid design principles. A detailed description of the technique was issued as supplement No. 1 to the code, denoted as document PD 3343, and was effectively a re-print of reference 8.30. The method included the use of design charts derived from the moment-rotation response of four classes of simple connection A, B, C and D. It is interesting to note that the stiffnesses of these four classes of connection were assumed to be directly proportional to the beam depth. This enabled a prediction of the connection response for beam depths which fell outside the bounds of the limited experimental work on which the standard curves were based. Using the appropriate charts the beam support moments, and hence the reduced span moments, could be determined with relative ease. Columns were then designed to resist the out-of-balance beam moments at any one level, in addition to those moments resulting from the eccentricity of beam reaction. However, to prevent potentially large moments being assumed in the column design, which would result in significant increases in the weight of column steel, the beam restraint moments were restricted to 10% of the free bending moment.

In BS 5950, the current version of the code, a simplified method of semi-rigid design is stated by which 10% of the free beam bending moment can be transferred, via the

connection, to the column. However, in this latest version, the guidance on 'standard' connection response has been omitted. Instead, the onus is now placed on the designer to ensure that the connection is capable of withstanding the transferred moment.

Whilst the above methods incorporate the beneficial distributions of bending moments associated with semi-rigid connection behaviour, guidance on the beneficial effects on column stability is clearly limited. In addition, the methods do not appear to take into account the frame, or subframe, geometry. Using such methods, caution should be exercised when designing long span beams supported on slender columns as the moment transferred through a fully rigid connection may well be less than 10% of the free beam bending moment.

The problem of developing a simplified design method which incorporates the beneficial effects of semi-rigid connection behaviour on column stability, was addressed by Lui and Chen [8.31]. Based on the results from tests on 83 isolated end restrained columns, they proposed that the effective length of a column member could be expressed as:-

$$L_e = k L \quad (8.24)$$

where:

$$k = 1.000 - 0.017 \alpha \quad (\text{for } \alpha < 23)$$

$$k = 0.600 \quad (\text{for } \alpha > 23)$$

and

$$\alpha = \frac{C}{M_{pc}}$$

$M_{pc}$  = Plastic moment capacity of the column.

$C$  = Linear connection stiffness.

For design purposes, the researchers then suggested a simpler and more conservative approach by recommending fixed  $k$  values that depended on the axis of bending as well as the column slenderness. Although a reasonable assumption, the suggested  $k$  values,

typically in the range 0.9 to 1.0, were considered by many to be too conservative.

As part of a method developed for semi-rigid frame design, Bjorhovde [8.2] suggested that the above treatment of an individual column member could be refined by replacing the  $\alpha$  factor with  $\alpha^*$ , where:

$$\alpha^* = \frac{C^*}{M_{pc}} \quad (8.25)$$

and where:

$$C^* = \frac{\beta^* EI_g}{L_g}$$

$$\beta^* = \frac{2\beta}{\beta + 2}$$

$$\beta = \frac{C_b}{EI_b}$$

This refined method effectively reduced the value of  $\alpha$  by considering the stiffness of the connection in conjunction with that of the connected beam.

Bjorhovde went on to develop a more exact approach applicable to frames which determined the effective lengths from consideration of the elastic critical load. It is the author's opinion that this particular approach presents the most fundamental treatment of semi-rigid frame behaviour. The merits of the technique have therefore been discussed in detail.

Figures 8.15 and 8.16 show an internal and an external column arrangement from a non-sway, semi-rigid frame. The characteristic buckling equation for the column sub-assembly shown in figure 8.16 is given by:-

$$\left(\frac{G_A G_B}{4}\right) \left(\frac{\pi}{k}\right)^2 + \left(\frac{G_A + G_B}{2}\right) \left(\frac{1 - \frac{\pi}{k}}{\tan(\frac{\pi}{k})}\right) + \frac{2 \tan(\frac{\pi}{2k})}{(\frac{\pi}{k})} = 1.0 \quad (8.26)$$

where  $G_A$  and  $G_B$  are the stiffness distribution factors for the column ends A and B. They are defined by:

$$G = \frac{\sum(\frac{EI_c}{L_c})}{\sum(\frac{EI_b}{L_b})} \quad (8.27)$$

$G$  therefore expresses the relative stiffness of the columns with respect to the beams at a particular node point. A higher value of  $G$  reflects the reduced rotational restraint at a column node point from smaller, less stiff, beams. To take account of the end-restraint from semi-rigid connections, the modified restrained distribution factor is given by:

$$G = \frac{\sum \left( \frac{EI_c}{L_c} \right)}{C^*} \quad (8.28)$$

The value of  $C^*$ , defined in equation 8.28, effectively reduces the total stiffness of the beams by including the stiffness characteristics of the connection.

In the case of the interior column (figure 8.15), the moment-rotation plots for the two connections on either side of the column at the same level are shown in figure 8.17. As the column fails by buckling, one of the connections will continue to 'close', whilst the adjacent connection on the opposite side of the column will start to 'open'. It is clear that the tangent stiffness of the closing connection ( $C_t$ ) will be significantly less than the stiffness of the unloading connection ( $C_u$ ). Bjorhovde assumed that the total restraint at the column node was that due solely to the unloading connection, conservatively ignoring any contribution from the 'closing' connection. In terms of the external column, this assumption meant that the total restraint at the base of the column shown in figure 8.16 was taken as zero.

Having determined the appropriate reduced distribution factors for the particular sub-assembly arrangement, the column effective length factors were determined from alignment charts, similar to those in appendix E of BS 5950: Part 1. Preliminary calculations by Bjorhovde have shown that by using this technique, there was the potential saving of 15%-20% in the weight of materials.

Whilst the above technique presents an in-depth appraisal of column stability, Bjorhovde makes no mention of the effect of bending moments resulting from semi-rigid joint action. Recently however, Barakat and Chen [8.7] proposed a practical method of semi-rigid frame analysis which combined the appraisal of column stability by Bjorhovde with a linear elastic frame analysis to determine the distribution of design column moments.

The linear connection stiffness used in the linear elastic model,  $C_{ko}$ , was a conservative modification of the initial tangent stiffness,  $C_i$ , which takes into account the ultimate moment capacity of the section. This particular linear approximation of connection response was introduced in section 8.2.2. Comparisons with 'exact' second order numerical studies had shown that the assumed linear connection stiffness,  $C_{ko}$ , gave a very close prediction of the semi-rigid frame bending moments.

The method proposed by Barakat and Chen required the use of a linear elastic computer program which had the facility for including the linear stiffness response of the connections. Although computer software with this facility is becoming increasingly popular, it is not at present widely available in this country. As an alternative, the computer analysis could be replaced by the method developed by the author for serviceability design described in section 8.2.3. Using this approach the semi-rigid frame moments can be determined from a more widely available simple rigid frame analysis computer program or, alternatively, from conventional rigid subframe manual computation techniques. The design sequence could therefore be summarised as follows:-

1. Determine the ultimate loading on the frame.
2. Assume appropriate member sizes, i.e. as in rigid frame design.
3. Assume an appropriate linear connection stiffness, e.g.  $C_M$ ,  $C_{ko}$ .
4. Perform an elastic frame analysis using the method described in section 8.2.3 to determine the distribution of semi-rigid moments.
5. Determine the distribution factors ( $G$  factors) at the upper and lower ends of the column including the contribution from the linear connection stiffness. These can be conveniently derived from the linear elastic analysis. e.g.



$$G^* = \frac{\sum(\frac{I_c}{L_c})}{\sum \mu \cdot (\frac{I_b}{L_b})} \quad (8.29)$$

or, for use in the alignment charts in BS 5950,

$$K^* = \frac{\sum(\frac{I_c}{L_c})}{\sum \mu \cdot (\frac{EI_b}{L_b}) + \sum(\frac{I_c}{L_c})} \quad (8.30)$$

(Note that  $\mu \cdot I_b/L_b$  is the stiffness of one beam only,  
the less stiff of the two on either side of an interior column)

7. From alignment charts, determine the critical load (effective length) of the column.
8. Check the adequacy of the column using the appropriate interaction formula.
9. Divide the semi-rigid frame moments by 1.5 and perform a serviceability beam deflection check using eqn. 8.9.

In the above procedure the effect of the out-of-plane, secondary beam, moments is only taken into account at the end of the design process when the different components in the interaction equation are summed. The assumption is, therefore, that the out-of-plane moments have no effect on the in-plane stiffness of the frame. One other major simplification, common to all methods which rely on the use of alignment charts, is that the restraint factors,  $K$  and  $G$ , are based on the elastic stiffness of the members intersecting at a column node. It should be noted however that at the point of ultimate load, the individual member stiffnesses will be significantly different due to the presence of plastic zones.

Appendix C contains a set of 'hand' calculations which were performed using this method to predict the ultimate capacity of the lower column C6/0-1 in frame test F1 (Chapter

5). The ultimate column capacities were derived by considering both the 'simplified' (pages C1 to C5) and the 'more exact' (pages C6 and C7) interaction equations in BS5950 Part 1. The linear connection stiffness assumed in the derivation of the semi-rigid connection moments,  $C_{ko}$ , is that proposed by Chen as discussed in section 8.2.2. This same stiffness has been used to derive the column restraint in the calculation of the critical load (effective length factors) from the alignment charts. It is appreciated that when considering column stability, the unloading stiffness of the connection ( $C_u = C_i$ ), as proposed by Bjorhovde would be more appropriate. However, it is quite probable that the increased design effort, and confusion, involved in considering two different stiffnesses for the same connection, i.e. one for moment distribution and one for stability, could not be justified.

The connection stiffnesses used in the 'hand' calculation were those determined directly from the plots of the measured experimental moment-rotation response. The aim was to achieve the closest possible correlation with the observed experimental frame behaviour. However, to comply with the findings reported in chapter 6, the connection stiffnesses used in the design process must be those derived from a cantilever type connection test, or those from a cruciform test which have been modified to take account of the column web flexibility effects.

It is evident from the calculations in Appendix C that the design process produces a reasonable approximation to the semi-rigid frame moments. Although the ultimate capacity is underestimated when using both the 'simplified' and the 'more exact' interaction equations, the  $P_{test}/P_{des}$  ratio is significantly smaller than those in section 8.3.7 where the simplified method of assessing the effective length has been used. It should be noted that the similarity in the predicted ultimate load using the 'simplified' approach (567kN) and the 'more exact' approach (570kN) is due to the increased conservatism of the 'more exact' approach when the disturbing moments are small - as in this instance.

Perhaps the most significant aspect of the calculation is that the effective length factor

for the column appears to be 0.56. This is significantly less than that which would be inferred from the basic guidance on standard effective length factors given in the code. Despite the fact that the column minor axis was restrained on one side only, and a 47% reduction in beam stiffness had been applied to take account of the connection stiffness, the  $K_2$  factor for the column top was relatively low with a value of 0.28. From the alignment charts it is evident that even if the base of the column had been pinned,  $K_1 = 1.0$ , then the effective length factor would have been 0.76. This compares with the suggested value of 0.7 in the code when both ends of the column are fully restrained in direction.

It is appreciated that the highly conservative 'standard' values of effective length factors stated in the code were chosen to reflect the difficulty of achieving a fully rigid, infinitely stiff, end condition in practice. However, as suggested from the alignment chart, and as observed in the parametric study performed to investigate column base stiffness (chapter 2), columns do not necessarily require large rotational restraint to achieve large increases in the critical load. Designers have not been able to utilise this phenomenon unless they have been performing a rigid frame design, in which case use of the alignment charts is permitted. Adopting the design procedure discussed above would, therefore, allow the calculation of realistic effective lengths for a much wider range of frame types. The application of this philosophy is discussed further in section 8.3.7 which compares simple interaction design predictions with experimental and analytical behaviour and proposes a modification to 'standard' effective length values.

### **8.3.6 The 'variable stiffness' method.**

The design techniques which have been discussed in the previous sections have concentrated on defining the appropriate terms for use in an interaction type equation. However,

the 'vanishing stiffness' method, developed by Wood [8.32] for rigid frame design, uses a different approach. It applies the concept of 'deteriorated critical load', defined as the load at which the overall stiffness of the remaining elastic parts of the structure become zero, to identify the ultimate capacity of members in a frame. The method therefore defines the vanishing of frame stiffness rather than the attainment of a limiting stress as the primary factor influencing member stability. The collapse load is defined as:-

$$P = C'.R'.P_E \quad (8.31)$$

where:

$P_E$  = The Euler load of the pinned-end column.

$C'$  = Ratio of the critical load to the Euler load,  
thereby representing the end conditions of the  
column - usually read from alignment charts.

$R'$  = The stiffness reduction factor.

The effects of major and minor axis disturbing moments are taken into account by modifying the stiffness reduction factor. For the case of a large major axis moment, the reduction in column stiffness is given approximately by:-

$$R'_x = 1 - \frac{M_{max}}{M_{ax}} (0.4 - 0.2m) (1 - F^2) \quad (8.32)$$

where:

$F$  = Collapse load/ squash load ratio.

$M_{ax}$  = Allowable major axis moment.

$M_{max}$  = Maximum applied column end moment.

$m$  = Correction factor to allow for the pattern of  
bending moments.

The inclusion of the collapse load factor,  $F$ , in the derivation of the reduced member stiffness means that the collapse load is determined using an iterative process.

Roberts [8.33] proposed a method by which the above procedure, specifically developed for fully rigid frames, was adapted for use in non-sway semi-rigid frame design. The method used a modified version of the technique in document PD 3343 which introduced the concept of standard semi-rigid connection stiffnesses, as discussed in section 8.3.6, for the design of the major axis beams. The secondary beams, connected to the minor column axis, were designed elastically assuming a fully rigid connection. Using the nomenclature adopted by Horne for plastic design, this corresponds to an  $S_x E_y$  configuration. From the beam design, the moments acting on the column can be determined and the variable stiffness method, described above, used to determine the critical load. Comparisons with existing structures showed that by using this design method, material weight savings of the order of 10% could be achieved.

Recently, Shea [8.34] used a modified version of the variable stiffness method to compare design predictions with the numerical models studied by the author in Chapter 7. The method included an equivalent beam stiffness, which incorporated a linear connection stiffness component, and proposed a modified version of the stiffness reduction factor. Whilst a relatively close correlation was observed between the design predictions and the numerical data, the 'variable stiffness' approach overestimated the capacity of the column in most cases - i.e. it was unsafe. This effect was most noticeable where large moments were applied to the minor column axis. It appeared that the proposed formulation for the deterioration of column stiffness was not sufficiently sensitive to large changes in the applied column moments. It is clear that further developments of this technique for use in semi-rigid frames should concentrate on refining this particular aspect of the method.

Whilst the 'variable stiffness' method represents a valid concept and is arguably 'more correct' than the interaction approach, it also represents a significant departure from the limiting stress principles which have been used by designers for many years. Conse-

quently, it is anticipated that designers would be resistant of its use in frame design.

### 8.3.7 Observations on the application of the BS 5950 simple design method.

In this section, the data obtained from the experimental studies of subassemblage response (Chapter 2), frame response (Chapter 5) and the analytical parametric study (Chapter 7) are compared with the predictions of the 'simple' design method in BS 5950. The aim of this study is not to validate, or otherwise, the 'simple' interaction formula, but merely to illustrate the potential increases in strength which can result from semi-rigid action.

The ultimate load capacities have been derived using the interaction equation 8.22 presented in section 8.3.3 using the appropriate 'standard' effective length factors recommended in the code. In each case, the design moments have been derived on the assumption that the beam reactions, at the end of the beam loading phase, act at an eccentricity of 100mm from the column face. Where possible, material properties corresponding to those observed in the experimental studies have been used in the design comparisons [8.35].

It is important to note that throughout this appraisal, the enhanced capacity of the experimental and analytical studies has been expressed in the non-dimensionalised form  $P_{test}/P_{des}$  - i.e. the increased axial load which can be sustained, over that predicted from the design, for a given pattern of disturbing moments. This is not necessarily the same as a universal load factor against collapse in which the effect of a 'pro-rata' increase in the loading from the beams would have to be taken into account.

A summary of the comparison between the design predictions and the experimental

subassemblage tests, part of the parametric study and the full scale frame test F1 is presented in tables 8.8, 8.9 and 8.10 respectively. The various columns in the tables show the moments at the column head,  $M_x$  and  $M_y$ , both design and actual; the effective length factors extracted from clause 4.7.2 of the code which are considered to closely reflect the degree of column restraint present; the design column capacity in the absence of disturbing moments,  $P_{cy}$ ; the design ultimate capacity,  $P_{des}$ ; the actual minor axis moments at the column head at the point of maximum load,  $M'_y$ ; and the actual maximum load carried,  $P_{test}$ .

There are a number of significant observations which can be made from the above tables regarding the assessment of effective length and the prediction, and subsequent effect, of the applied disturbing moments. For clarity, these two issues have been discussed separately in the following sections. In each case a refinement, or in the case of applied moments an alternative, to the present methods of simple frame design have been proposed which take greater account of the benefits of simple connection restraint. Due to the emphasis on experimental investigation in this particular research study, the available time in which to validate these design proposals has been limited. The proposals are therefore of a preliminary nature. However, it is hoped that these proposals will be of use to other researchers presented with the task of formulating simple methods of semi-rigid frame design.

### 8.3.8 The assessment of effective lengths in simple frame design.

It is evident from tables 8.8, 8.9 and 8.10 that in addition to the ultimate design capacities,  $P_{des}$ , the design values  $P_{cy}$ , i.e. ultimate capacity in the absence of disturbing moments, are significantly less than the actual ultimate capacities,  $P_{test}$ . This is quite surprising in view of the large disturbing column moments which were present in some of

the experimental tests. As discussed in section 8.3.7, this is primarily due to the inherent conservatism of the 'standard' effective length factors in clause 4.7.2 of the code, which are a means of taking into account the presence of column restraint, on which the design values  $P_{cy}$  were based. As an alternative, the author has shown how alignment charts can be used to predict a less conservative, more accurate, effective length for columns in semi-rigid frames. However, it is likely that practitioners would be unwilling to adopt this relatively arduous, refined technique in the 'everyday design' of compression members. It is important therefore that reliable 'benchmark' effective length factors are available for 'standard' cases which permit a quick assessment of the axial resistance of a member,  $P_c$ , using conventional means but which are more sensitive to the increased restraint effect of simple connections on moderate to slender columns.

Table 8.11 shows five standard cases for determining the effective lengths of columns in non-sway frames, together with the factors recommended in BS 5950:Part 1. Also shown are the theoretical values which have been derived assuming idealised end conditions. The higher, 'conservative', values in BS 5950:Part 1 have been purposely chosen to reflect the practical difficulties of constructing an infinitely stiff boundary condition. However, a recurring observation throughout this study has been that only a modest amount of restraint is necessary to achieve substantial increases in the critical load - this phenomenon becoming more pronounced with increasing column slenderness. It would therefore seem reasonable to consider the BS 5950 factors as an upper bound solution, the theoretical values as a lower bound, and permit interpolation between the two depending on the column slenderness. Considering the case of the column with fully fixed restraints at the top and bottom, a suitable interpolation for the effective length factor would be:-

$$k = 0.5 + 0.2 \left( \frac{P_{crit}}{P_{squash}} \right)^{\frac{1}{2}} \quad (8.33)$$

where the term in brackets is a convenient indicator of the column slenderness. The value of  $k$  would therefore tend towards the upper bound solution of 0.7 as  $P_{crit}$  tends to  $P_{squash}$  and tend towards the lower bound solution of 0.5 as  $P_{crit}$  tends to zero. Equation



8.33 can be rearranged such that:-

$$k = 0.5 + 0.2 \left( \frac{P_{crit}}{P_E} \right)^{\frac{1}{2}} \left( \frac{P_E}{P_{squash}} \right)^{\frac{1}{2}} \quad (8.34)$$

therefore:

$$k = 0.5 + 0.2 k \left( \frac{P_E}{P_{squash}} \right)^{\frac{1}{2}} \quad (8.35)$$

$$k = \frac{0.5}{1 - 0.2 \left( \frac{P_E}{P_{squash}} \right)^{\frac{1}{2}}} \quad k \neq 0.7 \quad (8.36)$$

Other forms of the equation, which may be applied to the other standard column support conditions (cases 1 and 3) are proposed in Table 8.11. A similar type of equation has also been proposed for those 'standard' end conditions for which there is a range of theoretical effective lengths, namely cases 2 and 4. In this instance, the precise form of the equation has been derived intuitively based on the nature of the equations for cases 1, 3 and 5. Therefore, rather than using a single effective length factor, the designer would have the option to expend slightly more design effort to enhance the effective length by taking into account the column slenderness. This 'enhanced' assessment of effective length would still rely on the intuitive selection of appropriate column end conditions by the designer. However, it is evident that significantly less design effort would be required than is necessary to accurately derive the effective length from alignment charts, as described in section 8.3.4., in which an assessment of the relative beam stiffnesses is required.

It is appreciated that the proposed simplified approach will only predict a significant improvement in the effective length of columns with a moderate to high slenderness, typically where the Euler buckling load,  $P_E$ , is less than 1.5 times the squash load,  $P_{squash}$ . In the case of UC type sections, this corresponds approximately to a slenderness in excess of 80 for grade 43 steel, decreasing to 65 for grade 50 steel.

Applying the approach to column C6/0-1 in the frame test, i.e. the lower segment, the effective length factor is given as 0.71 (case 4, Table 8.11). This compares with a value of 0.80 inferred from the current BS 5950 recommendations, and a value of 0.56

derived from the alignment chart in the refined semi-rigid design approach presented in Appendix C. Whilst the improvement in effective length using this approach falls short of that predicted using the alignment chart, it does equate to a 15% increase in the axial column resistance,  $P_{cy}$ , compared to that using the current 'standard' BS 5950 effective length guidelines.

Clearly, the proposed modifications to standard effective length guidelines need to be thoroughly validated with experimental and numerical data before they could ever appear as recommendations for design. However, it is believed that such an exercise would be justified as the proposals provide a theoretical basis for the simple assessment of effective lengths, and one in which the inherent sensitivity of relatively slender columns to end restraint is incorporated.

### **8.3.9 The treatment of column disturbing moments in simple frame design.**

It is evident from tables 8.8, 8.9 that the approach given in BS 5950:Part 1 for the design of simple frames overestimates the column minor axis disturbing moments at the end of beam loading in both the subassemblage tests and the numerical study. Due to the additive nature of the terms in the interaction equation, this results in quite a large underestimation of the ultimate load capacity, e.g. case 6 in table 8.9. In the frame test however (table 8.10), the observed minor axis moments at the centre column were significantly greater than that predicted using the 'simple' approach. This was primarily due to the large stiffness of the particular connection and the resulting high moment which was attracted from the beams. This disparity clearly demonstrates the inadequate and arbitrary nature of the simple method of assuming a 100mm beam eccentricity to derive the column disturbing moments in frames.

In all cases, the applied design disturbing moments bear no resemblance to those present on the column at the point of maximum load. This is demonstrated in figure 8.18 which shows the design distribution of bending moment and those at the ultimate condition for the minor column axis of one of the models investigated in the parametric study. The deformation, and hence increased end rotation, of the restrained column as failure approaches causes the applied moment to be shed back to the beams. In some cases, a full reversal of the moment is observed. This phenomenon adds weight to the inadequacy of present methods of appraising disturbing moments in simple frames.

Gent and Milner [8.36] investigated the effects of load shedding on the behaviour of restrained, biaxially loaded, small scale steel subassemblages. They concluded that in most cases, the specimens studied failed at loads quite close to their squash loads despite the presence of large disturbing moments and, in all cases, at loads greater than that predicted from the then current British steelwork design code, BS449 [8.29]. Due to the effects of moment shedding, about both axes, the column sections acted as 'plastic props'. Therefore, rather than concentrate on the precise magnitude of the applied moments, they proposed that disturbing moments could be treated in a similar fashion to initial imperfections. This led to the development of a permissible stress strut curve which was based on the tangent modulus,  $E_t$  concept. Rather than achieving significant economies in specified weight of columns, the proposed method significantly simplified the design process.

In the parametric study reported in chapter 7, a similar conclusion was made regarding the effect of disturbing moments from beams. It was observed that in nearly all the models studied, the value of  $\alpha_{pin}$  was greater than unity, i.e. the ultimate capacity of the restrained column with disturbing moments at one end only was larger than that of the axially loaded pinned-end column. This implied that the benefit of connection restraint was greater than the detrimental effect of the disturbing moments from the beams.

It would be convenient therefore to completely ignore the disturbing moments from the beams and design columns simply as struts with an appropriate effective length, possibly using a modified strut curve based on the tangent modulus concept. Clearly, this approach would result in a dramatic simplification of the design process. It is evident however that the limited parametric study reported in chapter 7 would need to be extended to investigate the  $\alpha_{pin}$  factor for a much wider range of structural arrangements and to determine the limits of application of this philosophy.

In developing the above approach using  $\alpha_{pin}$  factors, it must be remembered that the enhanced column loads in many cases, particularly for edge or corner columns, are due to a reversal of moment at the column head. This reversed moment is sustained by effectively lowering the free bending moment diagram for the interconnecting beam, thereby increasing the maximum span moment. Whether this increase would result in a beam span moment which is greater than the simple span moment (see figure 8.19) for all practical beam and column combinations needs to be investigated. Obviously, increasing the weight of beam steel for the sake of a lighter column is not desirable as it would probably result in an overall increase in the total weight of the structure. It should be noted that in the case of interior columns, the reversal of column head moment does not necessarily have a significant effect on the interconnecting beams. This was observed in the full scale frame tests reported in chapter 5 and its effect on the connection moment-rotation response were discussed at length in chapter 6.

On the assumption that future studies reveal that disregarding the column disturbing moments can significantly increase the cost of beams in the end bay of a structure, the author has proposed a relatively straight-forward method of column design which would limit the reliance on a full reversal of moment at the column head. The method uses a concept similar to that proposed by Gent and Milner but with one or two amendments. Rather than use a modified buckling curve to take account of the initial disturbing moments, the strength of the section at the column centre is assessed using minor axis moments derived from the deflected shape of the column at the point of moment reversal.

The design forces and deformed column shape are shown in figure 8.20. It is assumed that at the point of moment reversal the rotation at the column head,  $\phi_c$ , is the same as that at the end of a simply supported beam,  $\phi_b$ , and that the column deforms into the shape of a symmetrical half sine-wave. The deflection at the column centre,  $\delta_c$ , can therefore be easily determined and hence the design minor axis moment due to the design axial load acting through this eccentricity. The stability of the column is then checked by assessing the residual stiffness of the column, in a similar manner to that proposed by Gent and Milner. The method is best illustrated by considering the example in Appendix C (pages C8 and C9) in which the method is used to predict the capacity of the numerical model 6A with a one-way spanning floor system which was reported in chapter 7.

It is evident that the assumed deflection of 19.6mm at the column centre at the point of moment reversal is very close to that which was predicted from the finite element model (20.3mm). Consequently the design minor axis moment of 8.4 kN.m is close to that observed from the program (9.1 kN.m). The design axial load of 360 kN, which produces first yield at column centre, compares favourably with the load predicted from the finite element program of 400.5 kN at the point of moment reversal and a load of 420.0 kN at failure. Under this design condition, the stability of the column was checked by ensuring that the design axial load was less than the Euler load when the full minor axis inertia of the elastic section was taken into account. This implies that the member has residual stiffness and would not, therefore, rely on restraint from the beams.

It is appreciated that the approach presented in Appendix C considers only the simple uniaxial case. However, the approach can be modified to consider biaxial effects. The work by Gent and Milner had shown that complete reversal of the major axis moments at the column head occurred in nearly all the specimens they studied. This was principally due to the large major axis moments which were applied and the resulting major axis failure of the column. The design approach they proposed took into account the effect of major axis moments by assuming the compression flange of the section was fully plastic, the stability assessment being performed on the out-of-plane stiffness of the elastic tension

flange only. This is a principle which could be adopted in the approach proposed by the author presented in Appendix C.

However, when applied to frames with simple connections, it is expected that the applied major axis moments will be somewhat more modest than those considered by Gent and Milner. As a result, major axis failure of the column, and thus reversal of the major axis head moment, is unlikely to occur. Indeed, one observation which has been prevalent throughout this study, particularly in the subassemblage tests, is that major axis moments tend to remain relatively unchanged after application of the beam loads right up to the point of column collapse. It is proposed therefore that the actual applied major axis moment is considered in the design method proposed above. The strength criterion (local capacity check) at the column centre would then be of the form:-

$$\frac{P}{P_{squash}} + \frac{M_y}{M_{py}} + \frac{M_x}{M_{px}} \leq 1.0 \quad (8.37)$$

with the stability check being performed, as before, assuming the whole section remains elastic. Of course the applied major axis moment could be determined using the present approach by assuming a 100mm eccentricity of beam reaction. However, a more satisfactory alternative would be to consider the true semi-rigid moment by considering the  $\mu$  factors as described in section 8.3.5.

The above design approach is clearly geared towards the appraisal of columns with moderate to high slenderness. For stocky columns with small minor axis disturbing moments, it is evident that there may be insufficient capacity for column head rotation to occur thereby preventing a reversal of the column head moment to zero. Indeed this was observed in the case of column 'C3', the largest column considered in the parametric study described in chapter 7. However, due to the inclusion of a 'greater than actual' column deformation, it is anticipated that the above procedure would produce a conservative result by underestimating the ultimate capacity.

As discussed in the introduction, the proposed design procedure is of a preliminary nature and clearly warrants additional study. The principal areas requiring further attention

are:-

1. How the method could be applied to internal columns and take into account the effects of column continuity.
2. Defining the limits for which lateral torsional buckling can be ignored.
3. The degree of conservatism when applied to stocky columns with small disturbing moments.

Whilst it has been shown that the above design approach produces a reasonable prediction of the behaviour of one of the subassemblage columns, it is clear that a thorough verification is required to fully validate the technique. It is envisaged that this could take the form of a parametric study of column subassemblage behaviour, possibly using an analytical tool similar to that reported in Chapter 4. Typically, the study could investigate the accuracy of the approach for different beam/column combinations, connection types, applied disturbing moments, loading sequences, column slendernesses and base restraint conditions. It is hoped that the study, and subsequent comparisons with design predictions, would concentrate on investigating which are of practical proportions comparable to those encountered in 'real structures'.

## 8.4 Conclusions.

1. A method has been proposed for analysing semi-rigid non-sway frames under serviceability loading in which the members remain elastic. The predicted deflections compare favourably with those observed in the experimental full

scale frame test F1.

2. Comparisons of numerical and experimental data with the ultimate load design equations clearly illustrate the inadequacy of the present method of simple frame design in BS 5950:Part 1.
3. It has been demonstrated in the form of hand calculations how an ultimate load design technique proposed by the author can be applied to column C6 in frame test F1. The predicted column failure load was significantly closer to the actual when compared to that predicted from present BS 5950.
4. The author has proposed a 'simple' method of frame design in which the design minor axis moments are derived from consideration of the applied axial load acting through the deformed shape of the column. This method gave a close prediction of the ultimate capacity of one of the subassemblages in the parametric study (the only one studied).

## References.

- 8.1 Nethercot, D.A., '*Joint action and the design of steel frames.*', The Structural Engineer, Vol. 63A, No. 12, Dec. 1985, pp. 371-379.
- 8.2 Bjorhovde, R., '*Effect of end restraint on column strength - practical applications.*', A.I.S.C. Engineering Journal, Vol. 20, No. 1, First quarter, 1984, pp. 1-13.



- 8.3 Kleinlogel, A., *'Rigid frame formulas'*, Frederick Ungar Publishing Co., U.S.A., 1952.
- 8.4 Azizinamini, A., Bradburn, J.H. and Radzimirski, J.B., *'Initial stiffness of semi-rigid beam to column connections.'*, Journal Constructional Steel Research, No. 8, 1987, pp. 71-90.
- 8.5 Jones, S.W., Kirby, P.A. and Nethercot, D.A., *'Effect of semi-rigid connections on steel column strength.'*, Journal of Constructional Steel Research, No. 1, Sept. 1980, pp. 38-46.
- 8.6 Lothers, J.E., *'Elastic end restraint equations for semi-rigid connections.'*, Trans. Am. Soc. Civil Engrs., No. 116, 1951, pp. 480-502.
- 8.7 Barakat, M. and Chen, W.F., *'Practical analysis of semi-rigid frames.'*, A.I.S.C. Engineering Journal, Second quarter 1990, pp. 54-68.
- 8.8 Eurocode No. 3, *'Design of steel structures: Part 1: Genral rules for buildings'*, Draft version, Commission of the European Communities.
- 8.9 Poggi, C. and Zandonini, R., *'Behaviour and strength of steel frames with semi-rigid connections'*, in *'Flexibility and steel frames'*, Ed. W.F. Chen, Am. Soc. Civil Eng., 1985, pp. 57-76.
- 8.10 Davison, J.B., *'Strength of beam-columns in flexibly connected steel frames'*, Ph.D. Thesis, Department of Civil and Structural Engineering, University of Sheffield, U.K., June 1987.
- 8.11 British Standard BS 5950, *'The structural use of steelwork in buildings, Part 1: Code of practice for design in simple and continuous construction: Hot rolled sections.'*, London, British Standards Institution, 1985.
- 8.12 Davison, J.B., Lam, D. and Nethercot, D.A., *'Semi-rigid action of composite joints'*, The Structural Engineer (in press).
- 8.13 Wright, H.D. and Francis, R.W., *'Tests on composite beams with low levels of shear connection'*, The Structural Engineer, Vol. 68, No. 15, August 1990, pp. 293-298.
- 8.14 Chen, W.F., and Santathadaporn, S., *'Review of Column Behaviour under Biaxial Loading.'*, Am. Soc. Civil Engrs., Journal Struct. Div., Vol. 94, No. ST12, pp. 2999-3021, 1968.
- 8.15 Chen, W.F., and Atsuta, T., *'Theory of Beam-Columns.'*, Vols. 1 and 2, McGraw-Hill, New York, 1977.

- 8.16 Johnston, B.G., '*Guide to Stability Design Criteria for Metal Structures.*', (SSRC) 3rd ed., Wiley, New York, 1976.
- 8.17 Galambos, T.V., and Ketter, R.L., '*Columns under Combined Bending and Thrust.*', Trans. Am. Soc. Civil Engrs., Vol. 126, Part 1, 1961, pp. 1-25.
- 8.18 Massonnet, C., and Save, M., '*Plastic Analysis and Design.*', Vol. 1, Beams and Frames, Blaisdell Publishing Co., New York, 1965.
- 8.19 Lu, L.W., Shen, Z.Y., and Hu, X.R., '*Inelastic Instability Research at Lehigh University.*', '*Instability and Plastic Collapse of Steel Structures.*', (ed. L.J. Morris), Granada, London, 1983.
- 8.20 Austin, W.F., '*Strength and Design of Metal Beam-Columns.*', Am. Soc. Civil Engrs., Journal Struct. Div., Vol. 87, No. ST4, 1961, pp. 1-34.
- 8.21 Horne, M.R., '*The Flexural-Torsional Buckling of Members of Symmetrical I-Section under Combined Thrust and Unequal Terminal Moments.*', Q.J. Mech. Appl. Math., No. 4, 1956.
- 8.22 Hill, H.N., and Clark, J.W., '*Lateral Buckling of Eccentrically Loaded I-Section Columns.*', Trans. Am. Soc. Civil. Engrs., Vol. 116, 1951, p. 1179.
- 8.23 Vinnakota, S., '*Finite Difference Method for Plastic Beam-Columns.*', in '*Theory of Beam-Columns.*', (W.F. Chen and T. Atsuta), McGraw-Hill, New York, 1977, Chapter 10.
- 8.24 Tebedge, N., and Chen, W.F., '*Design Criteria for Steel H-Columns Under Biaxial Loading.*', Am. Soc. Civil Engrs., Journal Struct. Div., Vol. 100, No. ST3, March 1974, pp. 579-598.
- 8.25 Pillai, U.S., '*An Assessment of CSA Standard Equations for Beam-Column Design.*', Can. Journal Civil Engrs., Vol. 8, 1981.
- 8.26 Birnstiel, C., '*Experiments on H-Columns under Biaxial Bending.*', Am. Soc. Civil Engrs., Journal Struct. Div., Vol. 94, No. ST10, 1968, pp. 2429-2450.
- 8.27 Chubkin, G.M., '*Experimental Research on Stability of Thin Plate Steel Members with Biaxial Eccentricity.*', in '*Analysis of Spatial Structures*', Vol. 5, Moscow, Paper 6, 1959.
- 8.28 Kloppel, K. and Winkelmann, E., '*Experimentale und theoretische untersuchungen uber die traglast von zweiachsig assussermittigt gedruckten stahlstaben*', Stahlbau, 1962, Vol. 31, pp. 33.
- 8.29 British Standard BS 449: Part 1, '*The use of structural steel in buildings.*', British Standards Institution, London, 1971

- 8.30 Steel Structures Research Committee, Final report, H.M.S.O., London, 1936.
- 8.31 Lui, E.M. and Chen, W.F., '*Strength of columns with small end restraint.*', The Structural Engineer, Vol. 61B, No. 1, Part B, 1983, London, pp. 17-26.
- 8.32 Wood, R.H., '*A new approach to column design - with special reference to restrained steel stanchions.*', H.M.S.O, London, 1974.
- 8.33 Roberts, E.H., '*Semi-rigid design using the variable stiffness method of column design*', Joints in structural steelwork, ed. Howlett, J.H., Jenkins W.M. and Stainsby, R., London, Pentech Press, 1981, pp. 5.36-5.49
- 8.34 Shea, T.C., '*Variable stiffness design of steel columns.*', M.Sc.(Eng.) Thesis, University of Sheffield, September 1989.
- 8.35 Gibbons, C., '*The strength of biaxially loaded beam-columns in flexibly connected steel frames - Volume 2: A survey of the mechanical and geometric properties of structural steel sections*', Ph.D. thesis, Department of Civil and Structural Engineering, University of Sheffield, Dec. 1990.
- 8.36 Gent, A.R. and Milner, H.R., '*The ultimate load capacity of elastically restrained H-Columns under biaxial bending*', Proc. Inst. Civil Engrs., No. 41, 1968, pp. 685-704.

Beam connection moments			
Connection type	Joint reference	Rigid frame moment $M_{rigid}$ (kN.m)	Test frame moment $M_{test}$ (kN.m)
Minor axis INTERNAL column	d	29.5	27.2
	f	33.6	30.7
	i	33.8	30.6
	k	30.3	26.9
Minor axis EXTERNAL column	c	5.2	4.9
	e	10.9	7.2
	j	12.8	10.9
	l	4.8	3.4

Table 8.1: Summary of the rigid connection moments and actual the actual test frame moments.

Connection type	Joint reference	Connection stiffness kN.m/rad			
		$C_1$	$C_{10}$	$C_M$	$C_{ko}$
Minor axis INTERNAL column	d	90900	22700	54300	56000
	f	14800	7400	12400	10600
	i	18400	5000	10800	10700
	k	23500	13300	18100	18000
Minor axis EXTERNAL column	c	3800	2400	1400*	2000
	e	2500	1250	1400*	1300
	j	6800	2400	1400*	3500
	l	3800*	2400*	1400*	2000

Table 8.2: Linear stiffnesses determined from the actual experimental connection moment-rotation data.

Joint ref.	Beam rotn. $\theta_{pin}$ (rads)	Calculated connection moment - $M'_{sr}$ (kN.m)				Calculated $\mu$ factors			
		$C_1$	$C_{10}$	$C_M$	$C_{ko}$	$C_1$	$C_{10}$	$C_M$	$C_{ko}$
d	0.0066	28.1	24.7	27.3	27.3	0.95	0.84	0.93	0.93
f	0.0132	28.7	25.1	27.9	27.1	0.85	0.75	0.83	0.81
i	0.0132	29.7	22.3	27.4	27.1	0.88	0.66	0.81	0.81
k	0.0068	25.5	22.7	24.3	24.3	0.84	0.75	0.80	0.80
c	0.0066	4.3	3.9	3.4	3.7	0.83	0.75	0.65	0.72
e	0.0132	8.2	6.6	6.9	6.7	0.75	0.60	0.63	0.61
j	0.0133	11.2	9.2	7.7	10.1	0.88	0.72	0.60	0.79
l	0.0066	4.0	3.7	3.2	3.5	0.83	0.77	0.67	0.73

Table 8.3: Summary of the calculated semi-rigid moments and  $\mu$  factors for different linear connection stiffness.

Beam and Joint reference	Average $\mu$ factor $\mu_{ave}$			
	$C_1$	$C_{10}$	$C_M$	$C_{ko}$
B5 (c-d)	0.89	0.79	0.79	0.83
B6 (i-j)	0.88	0.69	0.72	0.80
B7 (f-e)	0.80	0.68	0.73	0.71
B8 (k-l)	0.84	0.76	0.74	0.77

Table 8.4: Average  $\mu$  factors for the four primary beams.

Beam and Joint reference	Simple span $\delta_{pin}$ (mm)	Rigid frame $\delta_{rigid}$ (mm)	Predicted semi-rigid deflection $\delta_{sr}$ (mm)				Measured test beam deflection $\delta_{test}$ (mm)
			$C_1$	$C_{10}$	$C_M$	$C_{ko}$	
B5 (c-d)	10.16	1.20	2.19	2.99	3.08	2.72	2.60
B6 (i-j)	20.45	8.50	9.93	12.20	11.85	10.89	10.48
B7 (f-e)	20.39	8.60	10.96	12.37	11.78	12.00	9.30
B8 (k-l)	10.33	1.40	2.83	3.54	3.72	3.45	2.40

Table 8.5: Comparison of the pinned, rigid, actual and predicted mid-beam deflections.

Beam and Joint reference	$\delta_{sr} - \delta_{test}$ (mm)				$\delta_{sr} / \delta_{test}$			
	$C_1$	$C_{10}$	$C_M$	$C_{ko}$	$C_1$	$C_{10}$	$C_M$	$C_{ko}$
B5 (c-d)	-0.41	0.39	0.48	0.12	0.84	1.15	1.18	1.05
B6 (i-j)	-0.55	1.72	1.37	0.41	0.95	1.16	1.13	1.04
B7 (f-e)	1.66	3.07	2.48	2.70	1.17	1.33	1.27	1.29
B8 (k-l)	0.43	1.14	1.32	1.05	1.18	1.47	1.55	1.43

Table 8.6: Comparison of predicted deflections with actual.

Beam and Joint reference	$\delta_{sr} / \delta_{pin}$			
	$C_1$	$C_{10}$	$C_M$	$C_{ko}$
B5 (c-d)	0.21	0.29	0.30	0.26
B6 (i-j)	0.48	0.59	0.58	0.53
B7 (f-e)	0.53	0.61	0.57	0.58
B8 (k-l)	0.27	0.34	0.36	0.33

Table 8.7: Comparison of predicted deflections with those of a simple beam span.

Comparison of design predictions with subassemblage test data											
Test Number	Design values					Actual values					$\frac{P_{test}}{P_{des}}$
	$M_x$ kN.m	$M_y$ kN.m	$\frac{L_e}{L}$	$P_{cy}$ kN	$P_{des}$ kN	$M_x$ kN.m	$M_y$ kN.m	$M_y'$ kN.m	$M_y'_{cen}$ kN.m	$P_{test}$ kN	
S1	8.8	4.5	0.8	286	213	5.0	0.8	-5.0	9.5	468	2.20
S2	8.8	0.0	0.8	279	244	8.9	-0.8	-8.9	8.9	503	2.06
S3	8.8	0.0	0.8	308	269	8.3	-0.1	-9.9	10.2	542	2.01
S4	8.8	5.0	0.8	294	216	9.8	2.6	-6.1	9.1	494	2.29
S5	5.3	3.0	0.8	295	248	1.9	0.6	-8.1	11.1	479	1.93
S6	5.3	3.0	0.8	295	248	3.4	2.3	-3.8	5.8	614	2.47
S7	7.9	4.5	0.8	300	229	4.9	2.0	-9.0	12.6	490	2.14
S8	14.9	0.0	0.8	300	234	9.7	-1.1	-8.9	11.0	482	2.05
S9	16.7	0.0	0.8	293	222	16.6	-2.1	-10.5	10.8	526	2.37
S10	23.2	0.0	0.8	289	191	23.9	-0.2	-10.0	11.8	520	2.72

Table 8.8: Predicted ultimate loads of the subassemblage tests using the 'simple' design method.

Comparison of design predictions with numerical models											
Model Number	Design values					Actual values					$\frac{P_{test}}{P_{des}}$
	$M_x$ kN.m	$M_y$ kN.m	$\frac{L_e}{L}$	$P_{cy}$ kN	$P_{des}$ kN	$M_x$ kN.m	$M_y$ kN.m	$M_y'$ kN.m	$M_y'_{cen}$ kN.m	$P_{test}$ kN	
1	0.0	0.0	0.9	397	397	0.61	-0.43	-4.52	6.05	524	1.32
2	0.0	12.9	0.9	397	188	0.28	2.28	-4.27	8.58	480	2.55
3	0.0	8.7	0.9	397	256	0.38	1.10	-4.50	7.73	497	1.94
4	0.0	6.4	0.9	397	293	0.14	1.43	-4.52	7.04	507	1.73
5	0.0	4.4	0.9	397	326	0.28	0.65	-4.64	6.68	514	1.57
6	0.0	12.9	0.95	384	182	0.27	5.27	-2.05	11.10	420	2.31
7	0.0	6.4	0.95	384	283	0.13	3.28	-3.28	8.62	465	1.64
8	0.0	8.5	0.95	384	250	0.18	4.09	-2.44	9.59	440	1.76
9	0.0	6.4	0.95	384	283	0.11	3.33	-3.42	9.24	459	1.62

Table 8.9: Predicted ultimate loads of subassemblages in the parametric study using the 'simple' design method.

Column Reference	Design values					Actual values					$\frac{P_{test}}{P_{des}}$
	$M_x$ kN.m	$M_y$ kN.m	$\frac{L_e}{L}$	$P_{cy}$ kN	$P_{des}$ kN	$M_x$ kN.m	$M_y$ kN.m	$M_y'$ kN.m	$P_{test}$ kN		
C5/1-2 Top	5.9	1.8				14.7	-1.7	-10.8			
C5/1-2 Bot	0.0	1.8	0.9	476	363	6.2	3.4	-0.9		660	1.82
C5/0-1 Top	0.0	1.8				2.1	5.2	3.2			
C5/0-1 Bot	0.0	0.0	0.8	548	512	0.3	-2.7	-14.0		779	1.52
C6/0-1 Top	5.9	1.8				8.8	1.8	-7.2			
C6/0-1 Bot	0.0	0.0	0.8	548	487	3.9	0.6	-15.9		756	1.55

Table 8.10: Predicted ultimate loads of column segments in frame test F1 using the 'simple' design method.








Effective length factors (K)			
Support condition	BS5950	Theory	Proposed
1 	1.0	1.0	1.0
2 	0.85	0.5-1.0	$\frac{0.7 \quad \text{not } > 0.85}{1 - 0.15 \left[ \frac{P_E}{P_{sq}} \right]^{\frac{1}{2}}}$
3 	0.85	0.7	$\frac{0.7 \quad \text{not } > 0.85}{1 - 0.15 \left[ \frac{P_E}{P_{sq}} \right]^{\frac{1}{2}}}$
4 	-	0.5-0.7	$\frac{0.6 \quad \text{not } > 0.8}{1 - 0.2 \left[ \frac{P_E}{P_{sq}} \right]^{\frac{1}{2}}}$
5 	0.7	0.5	$\frac{0.5 \quad \text{not } > 0.7}{1 - 0.2 \left[ \frac{P_E}{P_{sq}} \right]^{\frac{1}{2}}}$

Table 8.11: Proposed modification to the standard effective length factors in BS 5950.

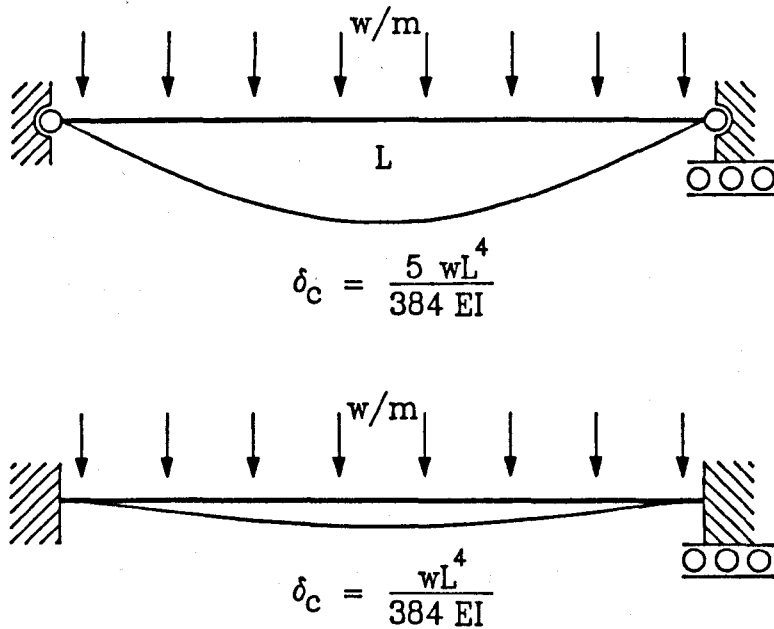


Figure 8.1: Comparison of the mid-span deflections for a beams with simple supports and fully rigid supports.

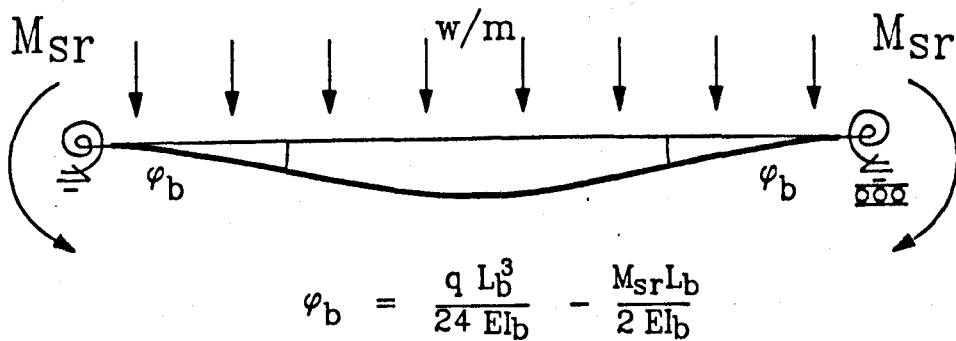


Figure 8.2: General equation for the rotation at the supports of beam flexibly connected beam.

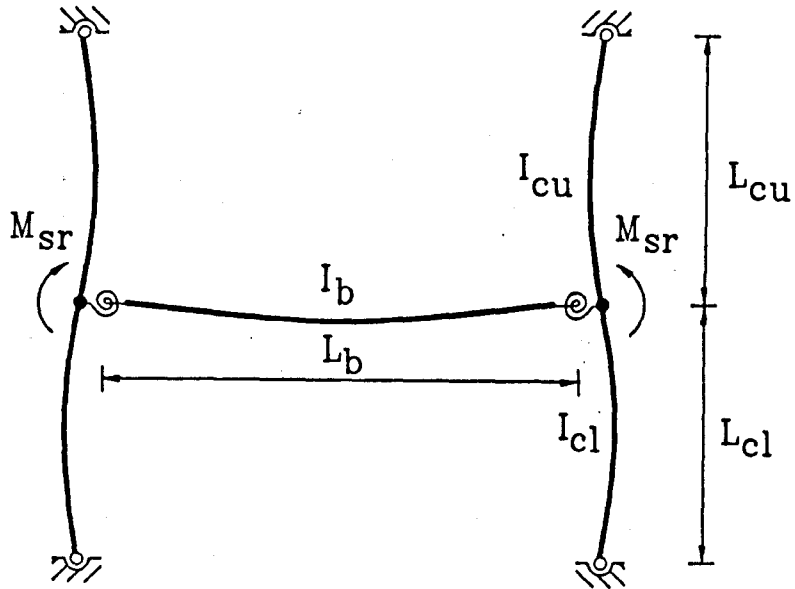


Figure 8.3: Beam and column subframe with semi-rigid beam to column connections.

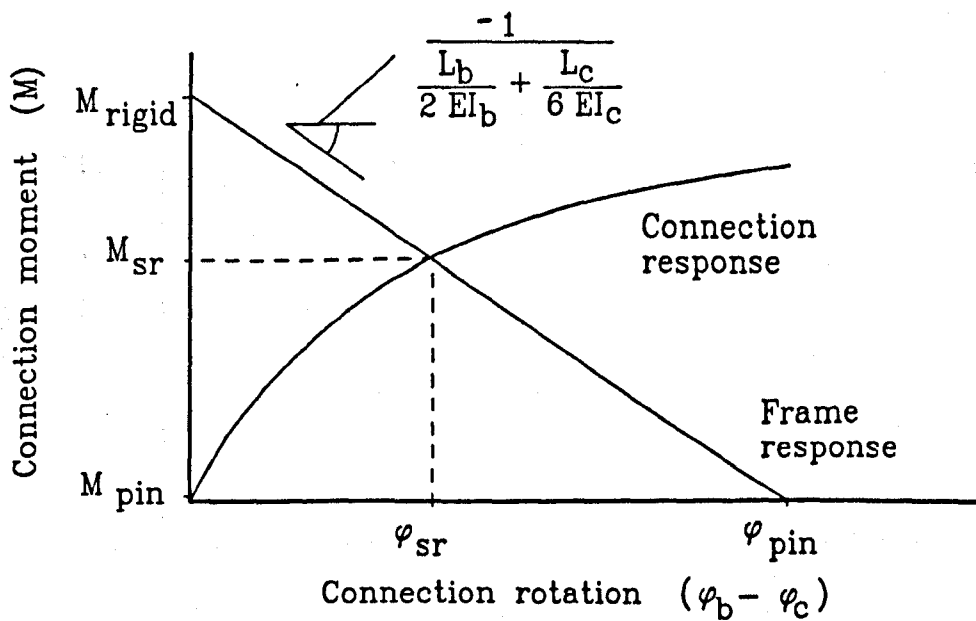


Figure 8.4: Plot of equation 8.4, the frame line, and a typical non-linear connection moment-rotation response.

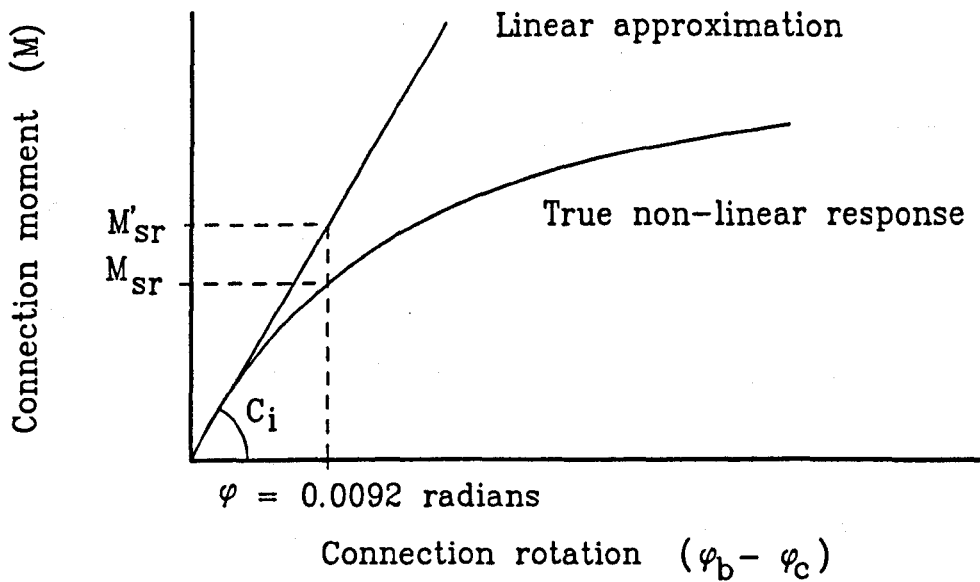


Figure 8.5: Plot illustrating the overestimation of the semi-rigid moment for a given rotation when using the linear initial tangent stiffness.

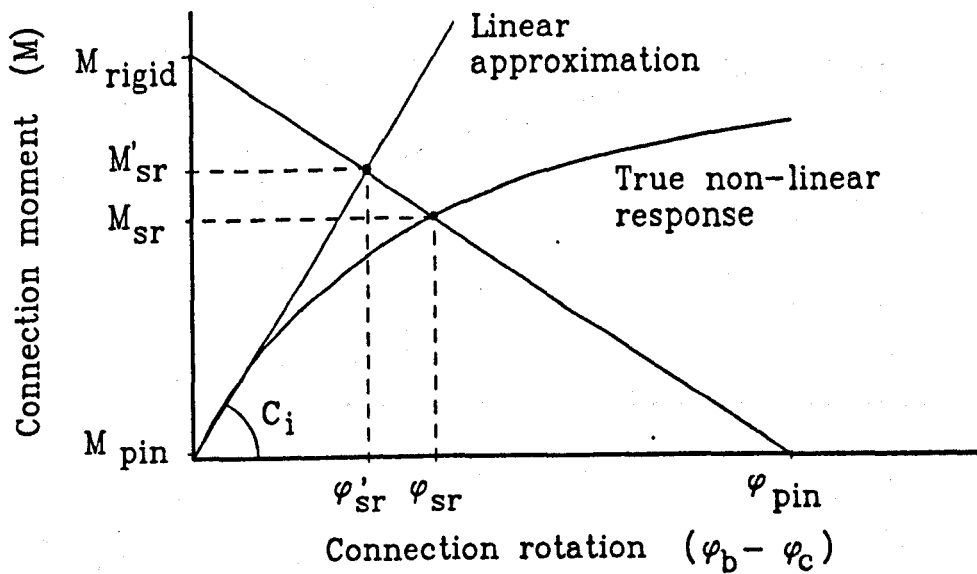


Figure 8.6: Plot showing the 'frame line', non-linear connection moment-rotation response and the initial tangent stiffness approximation.

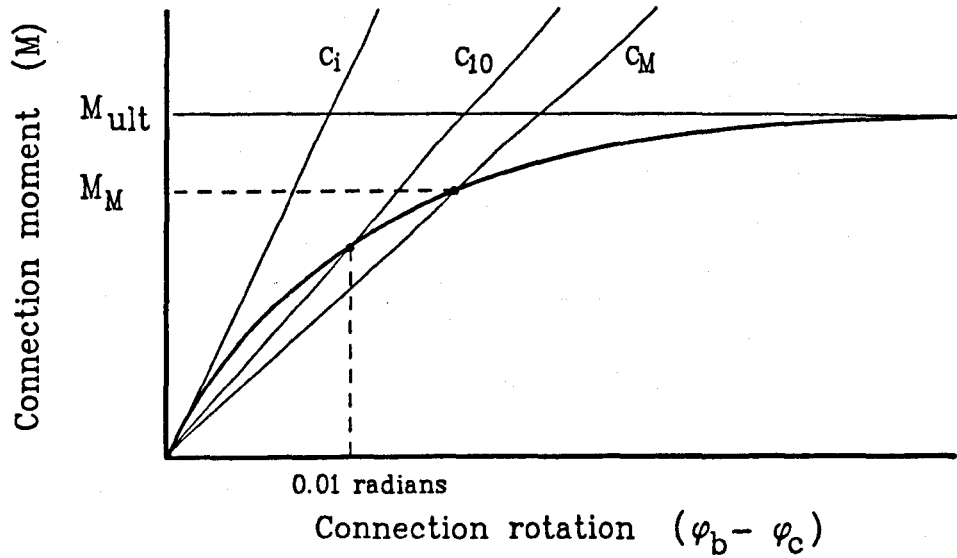


Figure 8.7: The different forms of linear secant stiffness considered in the study.

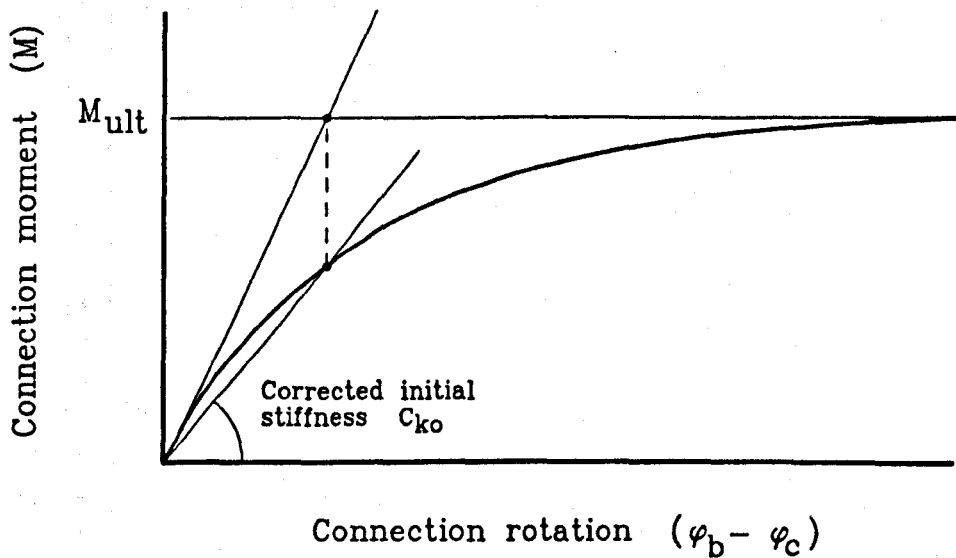


Figure 8.8 : Derivation of the modified initial tangent stiffness,  $C_{ko}$

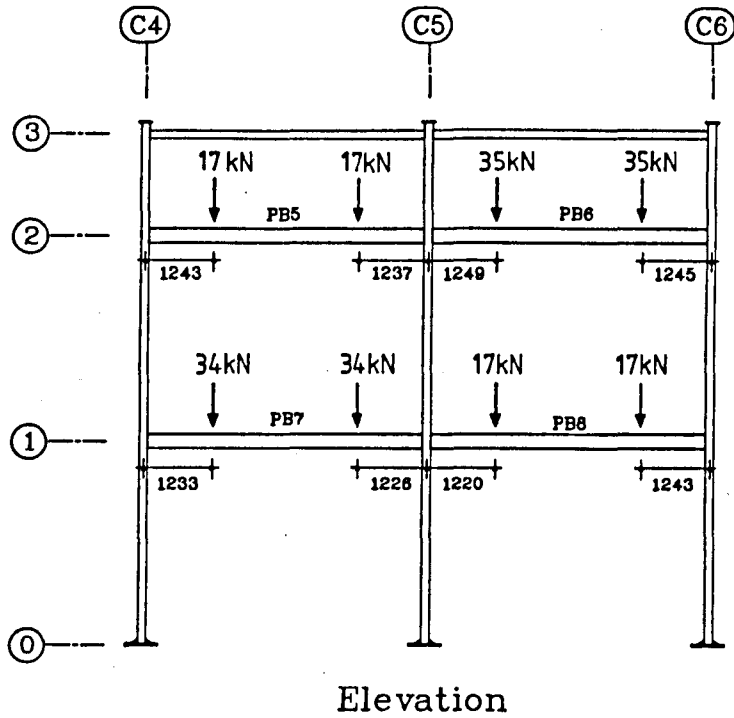


Figure 8.9 : Arrangement of test frame F1 illustrating the serviceability loadings.

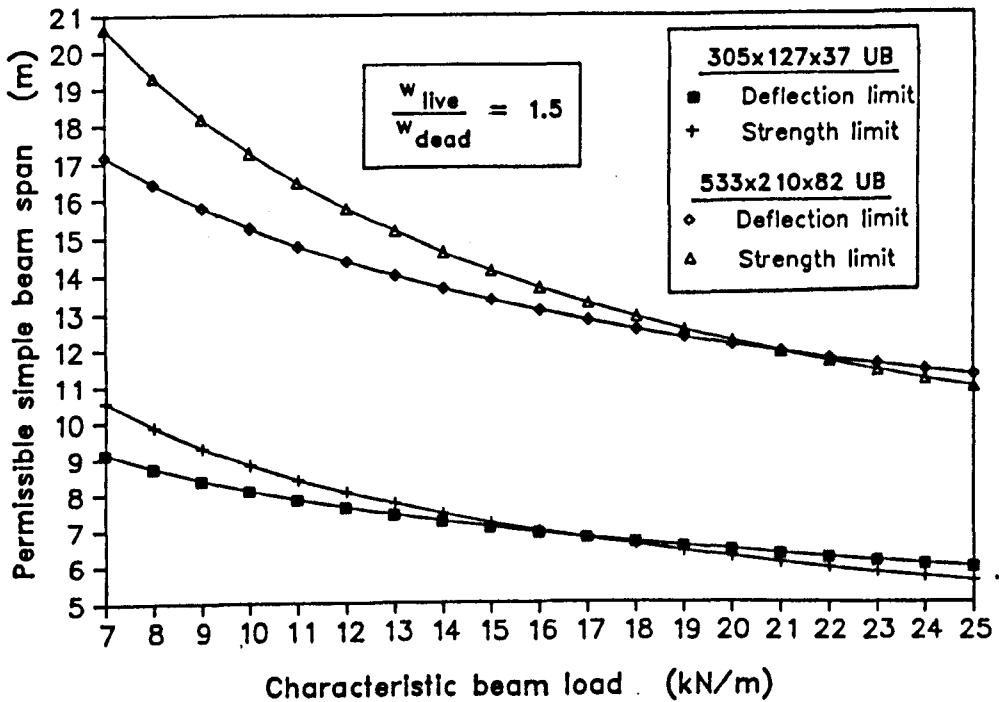


Figure 8.10: Plot of permissible beam spans against applied load illustrating the zones where deflection considerations dominate the design.

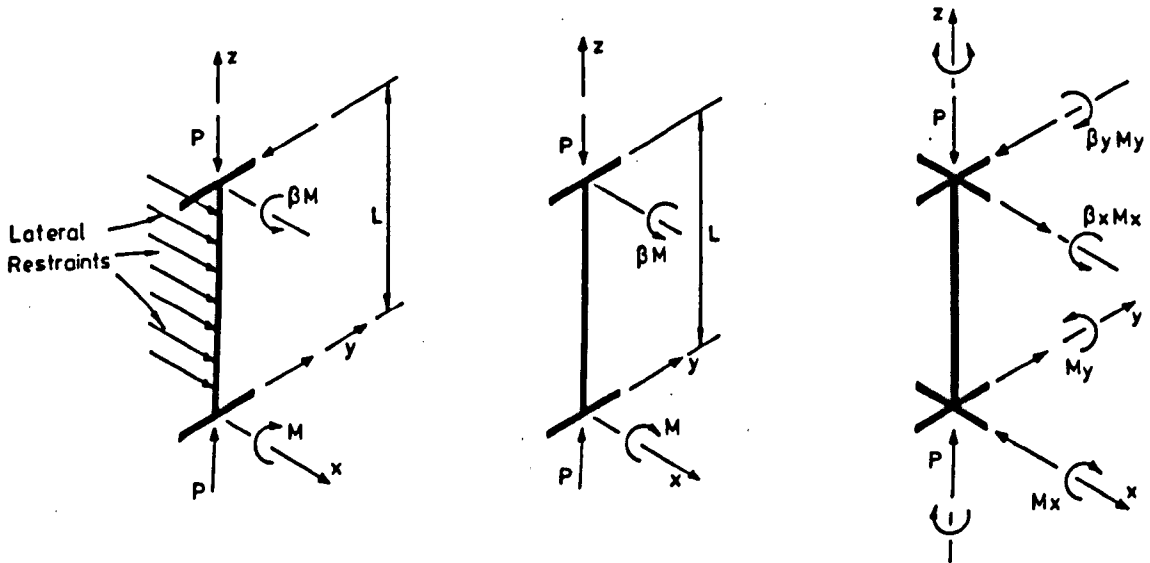


Figure 8.11: The three cases for the design of open section beam-columns.

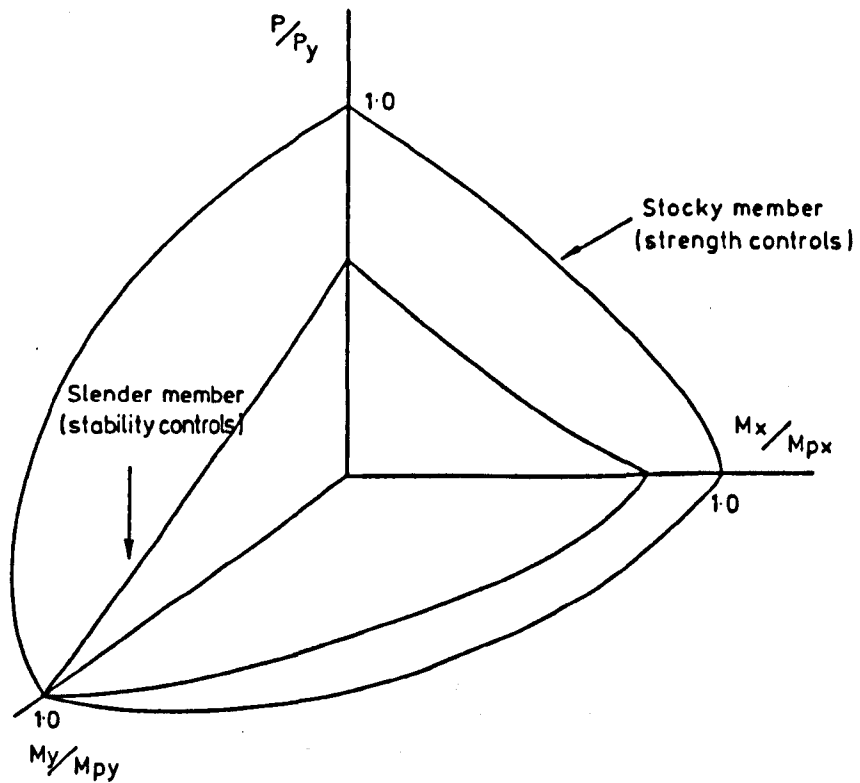


Figure 8.12: Three-dimensional interaction diagram.

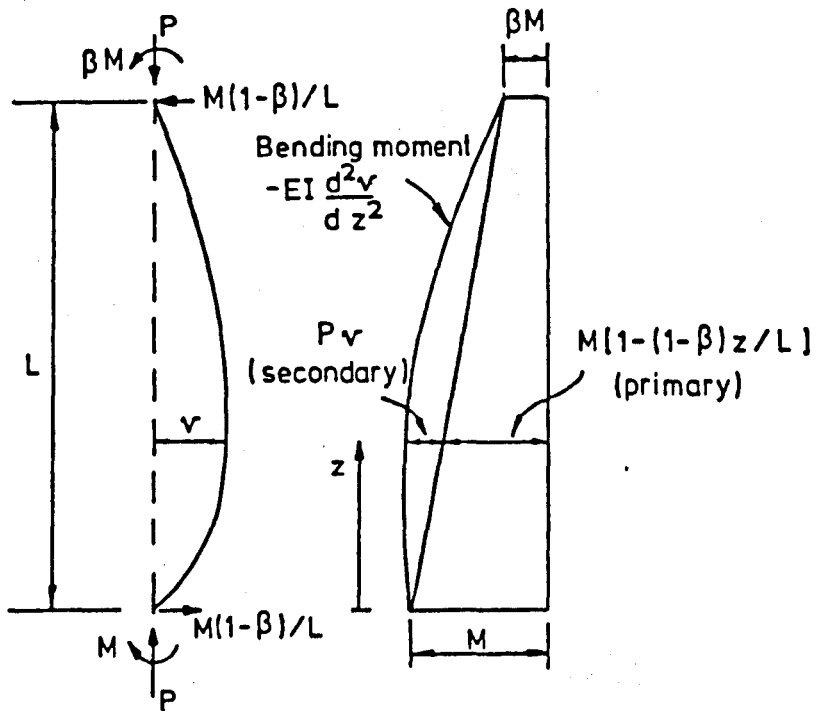


Figure 8.13: The amplification of the maximum moment due to the deformation of slender columns.

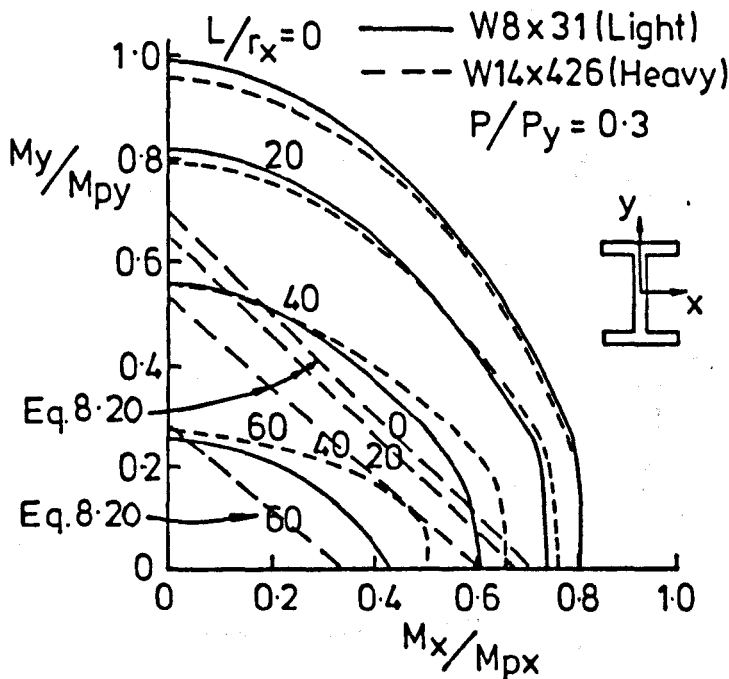


Figure 8.14: Comparison of equation 8.20 with numerical studies.



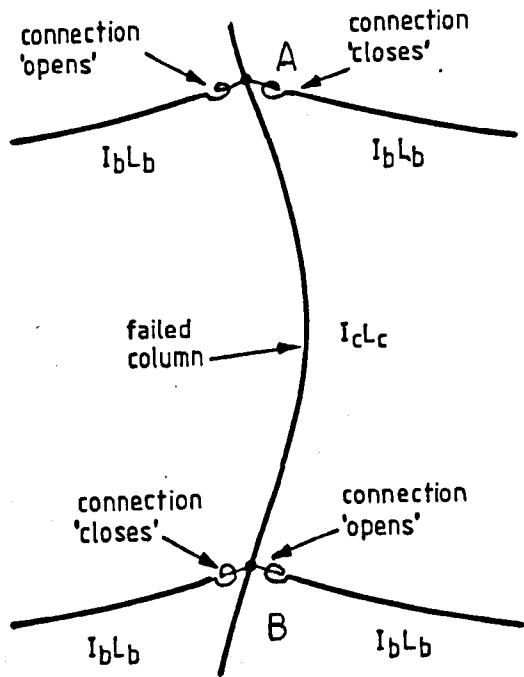


Figure 8.15: Buckled shape of an internal column showing the direction of connection rotation.

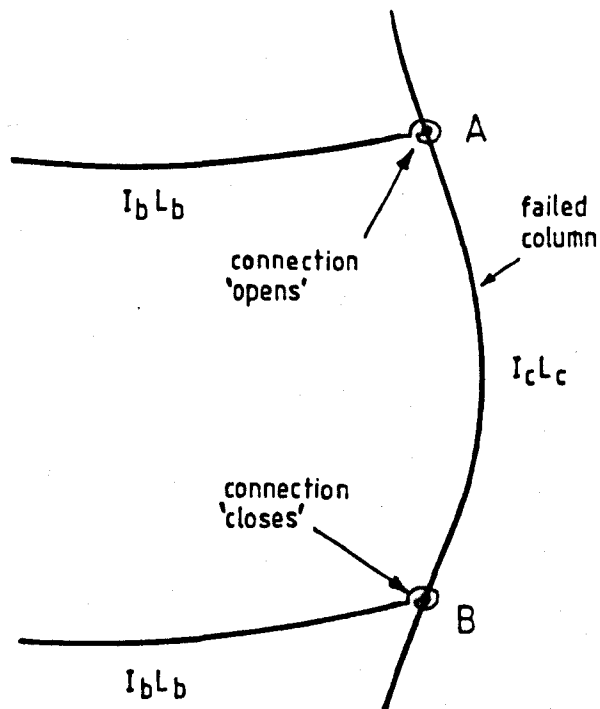


Figure 8.16: Buckled shape of an external column showing the direction of connection rotation.

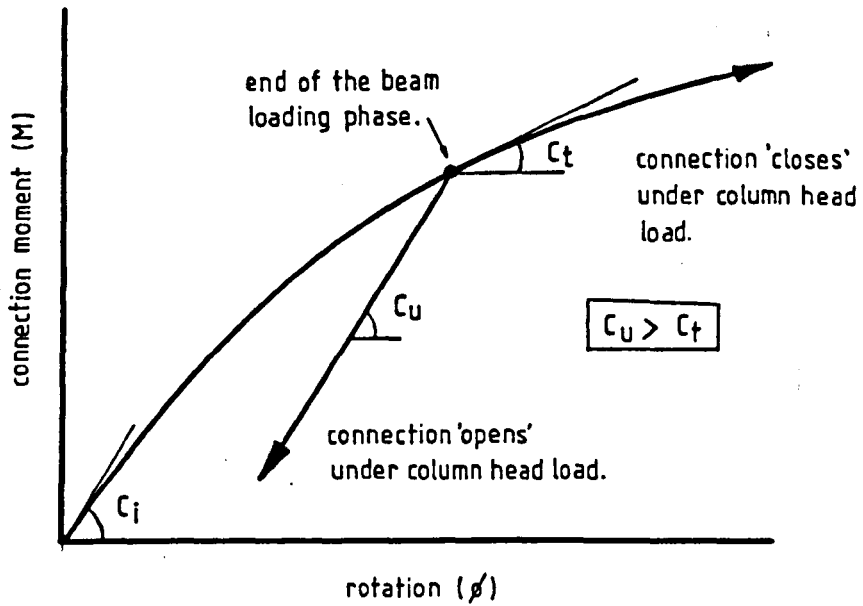


Figure 8.17: Moment-rotation response of the two connections at the same level but on either side of an internal column.

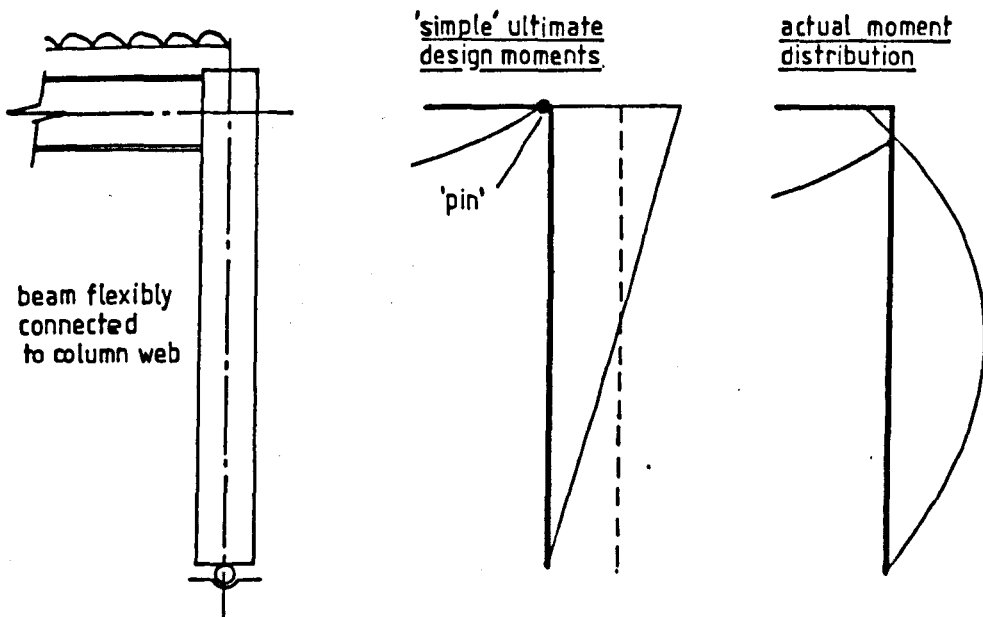


Figure 8.18: Comparison of column moments assumed in simple design and those at the point of collapse.

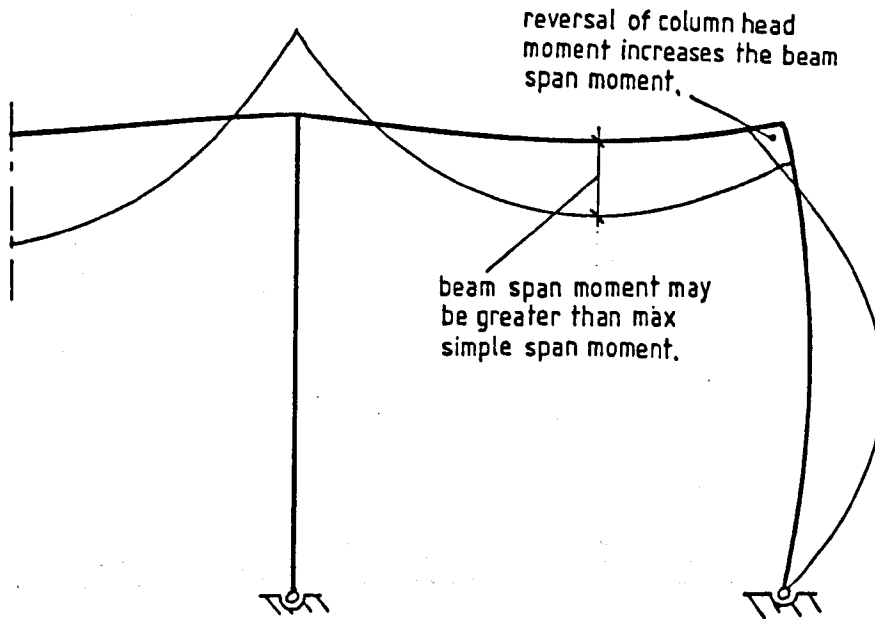


Figure 8.19: Effect of column head moment reversal on the maximum span moments of an end bay beam.

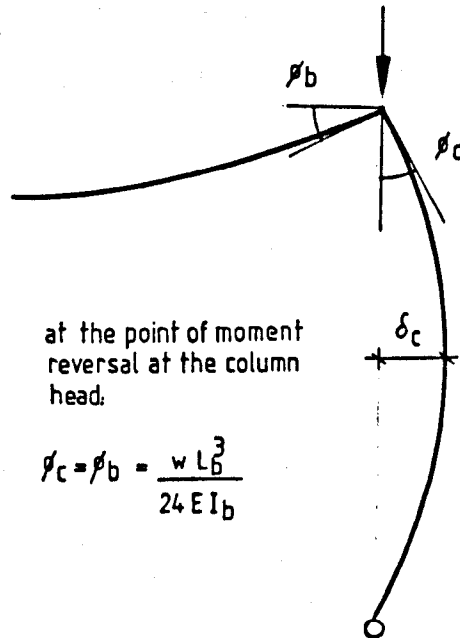


Figure 8.20: Deformed shape of an edge column when the column head moment reverses to zero.

## Chapter 9

# Proposals for Future Work.

### 9.1 Introduction

Throughout this thesis, the author has highlighted aspects of the work which would benefit most from further research. For clarity, and for the benefit of those who wish to pursue these studies, a brief summary of the most significant areas for future work have been collated in this section.

### 9.2 Connection moment-rotation.

One of the fundamental assumptions of semi-rigid behaviour has been that connections 'unload' with a stiffness,  $C_u$ , equal to that of the initial tangent stiffness,  $C_i$ . However, it was disclosed in chapter 6 that, under certain conditions, this assumption may not necessarily be valid. In the full scale frame tests, it was observed that the unloading stiffness of the primary beam connection to the minor axis of the internal column was

significantly less than  $C_1$ . This was a result of the combined effects of beam continuity, column web flexibility - accentuated by an imbalance of beam loads - and a connection reversal which was a result of column deformations rather than load removal. Clearly, not all of these parameters were present in the isolated connection tests on which the initial assessments of semi-rigid connection response were based.

The unloading stiffness of a connection is an important parameter which has been used in a number of semi-rigid design techniques. It is important therefore that its value can be proven for all conditions of loading and structural arrangement. The author has proposed a semi-empirical treatment of semi-rigid connection response which would enable the effect of the above parameters to be investigated without the need to develop complex experimental test procedures (section 8.5.5). It combines the experimentally determined connection moment-rotation response, e.g. from a cruciform test in which web flexibility effects are not present, with a finite element model of the column web panel. Combining these two stiffness components, possibly by adopting the mathematical expressions proposed by the author, it should be possible to determine the total effective column restraint for different combinations of beam load, beam size and column web panel size. In the first instance, the effectiveness of the technique could be assessed by trying to predict the moment-rotation response of a connection in an isolated cantilever test arrangement with the experimental data from a cruciform connection test [9.1].

### **9.3 The parametric study.**

The details of an in-depth parametric study which was conducted on both flexibly and rigidly connected subassemblages was reported in Chapter 7. The study investigated subassemblages which were of practical proportions and which were subjected to realistic load conditions. A number of significant conclusions were made regarding the effects of

column orientation, beam stiffness and the difficulty of producing a failure load which was less than that of a pinned end column (i.e.  $\alpha_{pin} \geq 1.0$ ).

Although a large number of different numerical models were analysed, the study was clearly limited when compared to the vast number of structural arrangements that might be encountered in practice. It is proposed therefore that the present study should be used as a base and extended to investigate the effects of long span beams, different sized beams on either side of the column, load history, different column lengths, the restraint effect from simple column bases and the effect of a wider range of different beam to column connection types.

#### **9.4 The full-scale frame tests.**

An in-depth report on the experimental testing of the two full-scale frames, F1 and F2, is presented in Chapter 5. It is evident that a large number of parameters were measured during the tests and, consequently, a large amount of data collected. In those sections which discuss and assess the results from the two tests, only a relatively limited amount of data has been presented. This typically comprises the most significant responses of load-moment and load-deflection for the beams and columns. Further studies are therefore necessary to investigate the measured connection bolt forces, moment-deflection responses, the spread of material yield, the interaction between primary and secondary bending moments and comparison with the results from other frame tests.

Chapter 4 reported the detailed comparison which had been performed between the observed experimental subassemblage behaviour and that predicted from a sophisticated finite element computer program. At the time of writing, there was no equivalent analytical tool capable of modelling the full-scale frame tests. However, it is envisaged

that in the near future such an analytical capability will become available. In such an event, other researchers will be able to use the frame test data to verify their analytical predictions and then use the validated program to investigate the applicability of sub-assembly behaviour in the context of frame response.

## 9.5 The design of semi-rigid frames.

Chapter 8 contains a review of past and present semi-rigid design methods and includes the author's proposals for the design of frames under ultimate and serviceability loading conditions. Although the predictions from the methods have been compared with the measured response of test frame F1, it is clear that a much more detailed and extensive comparison is required to fully verify and, if necessary, modify the proposed design techniques. Once verified, the design method could then be subjected to trials which would identify the limits of application, the possible economies in specified steel weight and the potential cost penalties resulting from increased design time.

One key parameter present in both the 'in-depth' and 'simplified' design methods proposed by the author was the rotation at the support of a simple beam,  $\phi_{pin}$ . Although Bjorhovde has suggested that the maximum value of  $\phi_{pin}$  is 0.0092 radians for most practical framing arrangements [9.2], it is the author's opinion that further work needs to be carried out to substantiate this assumption.

## **9.6 Future experimental studies of semi-rigid frame behaviour.**

Experimental research has already been conducted to investigate the behaviour of isolated connections in steel frames with composite concrete floor slabs [9.3]. The results of the study have shown that large increases were observed in both the connection stiffness and moment capacity when compared to the 'bare steel' condition. It is therefore postulated that there is a large potential for applying semi-rigid design principles to frames of this particular type of construction. It has already been proposed that experimental studies should be carried out on limited column subassemblages and full-scale three-dimensional frames with composite concrete floor construction. In the event of such tests being performed, the author hopes that the experimental researchers will consult, and where necessary employ, the experimental procedures and instrumentation techniques which have been developed for the equivalent 'bare steel' studies reported in this thesis.

## **9.7 The strengthening of existing steel stanchions.**

The recent popularity of building refurbishment has often resulted in loads being applied to existing steel columns which are larger than those originally intended. In some cases, steel columns have had to be strengthened by adding steel plates which effectively increases the area of the column flanges. This is quite a complex process as the existing steelwork has to be de-stressed, either by jacking or reducing the applied dead and live loads to a minimum, so that the most effective use is made of the new, additional steel area. It is proposed by the author that under certain conditions where the increase in applied load is moderate and the existing connections relatively flexible, i.e. additional



strength cannot be proven by conventional semi-rigid design techniques alone, then the connection can be modified to enhance the unloading stiffness and hence reduce the design effective length of the column. This would have the advantage of avoiding welding around the central region of the column and would alleviate the need to 'de-stress' the existing structural element.

Figure 9.1 shows a typical modification to the connection as envisaged by the author. The minor axis rotation at the column head would be resisted by a system of ties/struts via the torsional resistance of the major axis beam connections. The effect of increased disturbing moments associated with stiffer connections would not arise in this instance as the beam deformations and support rotations resulting from applied floor loads would be present at the time the ties/struts were installed. It is evident that whilst such a system would be relatively easy to install, the analysis of the force distributions would be complex and the method would have limited application. However, the author has included it here as a possible area warranting further study.

## **9.8 The use of tension control bolts.**

Tension control bolts (T.C.B.'s) are a new type of structural steelwork fastener which has recently arrived on the U.K. market. The bolts are made from high strength steel and are available in diameters ranging from 16mm up to 33mm. The bolt comprises a rounded head, conventional nut and a modified threaded shaft. The bolt, together with the fixing procedure, is illustrated in figure 9.2. The unique design of the bolt enables it to be tightened with relative ease up to a predefined torque with the aid of a special hand held power tool. As a result, the bolt exhibits a non-slip property similar to that of a High Strength Friction Grip (H.S.F.G.) bolt, but with the advantage of a much simplified fixing procedure.

It is clear that if such a bolt was used in a cleated beam to column connection, the detrimental effect of bolt slip on the moment-rotation response of the connection would be alleviated. The result would be a much more predictable, and in most cases stiffer, connection behaviour. It is expected that the present relatively high cost of these bolts would exclude their use in conventional 'simple' semi-rigid frames. However, with an increasing demand and increased distribution this situation may well change. In any event, it is proposed by the author that the influence of this particular bolt on the semi-rigid behaviour of steelwork connections should be investigated experimentally with subsequent analytical frame studies to investigate the potential economic benefits of this advanced bolt.

## References.

- 9.1 Celikag, M., '*Moment-rotation behaviour of steel beam-to-column connections.*', Ph.D. Thesis, Department of Civil and Structural Engineering, University of Sheffield, U.K., February 1990.
- 9.2 Bjorhovde, R., '*Effect of end restraint on column strength - practical applications.*', A.I.S.C. Engineering Journal, Vol. 20, No. 1, First quarter, 1984, pp. 1-13.
- 9.3 Davison, J.B., Lam, D. and Nethercot, D.A., '*Semi-rigid action of composite joints*', The Structural Engineer (in press).

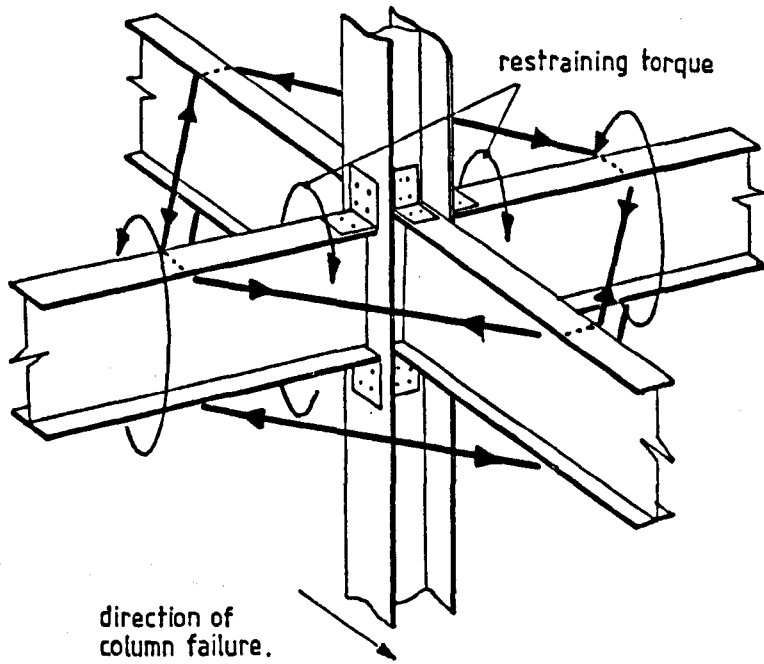


Figure 9.1: Possible method of increasing the restraint to the head of an existing column.

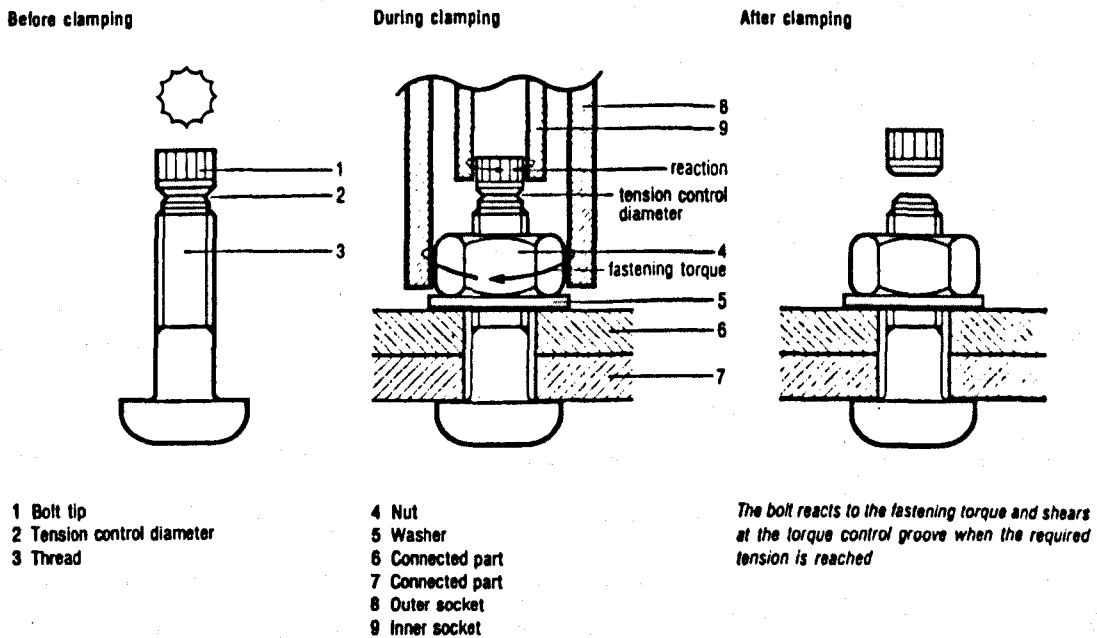


Figure 9.2: Installation of a tension control bolt (T.C.B.).

## Chapter 10

# Conclusions.

This thesis has reported the findings of an experimental study into the behaviour of a series of 10 full-scale column subassemblages and 2 full-scale multi-storey frames in which the general condition of non-sway, 3-dimensional response has been considered. The principal aim of the study was to examine the extent to which the inherent semi-rigid moment-rotation characteristics of 'simple' beam to column connections (i.e. those connections which are invariably assumed in steelwork design to act as 'pins' incapable of transferring moment) influence the behaviour of rectilinear steel structures.

Also reported is a comparison between the behaviour observed in the subassemblage tests with that predicted by a sophisticated finite element computer program developed by others at the University of Sheffield. The close correlation which was achieved validated the ability of this analytical tool to accurately predict the response of flexibly connected 3-dimensional subassemblages. The relatively limited observations on subassemblage response from the experimental tests were then extended by using this computer program to conduct a parametric study which examined the influence of semi-rigid connection characteristics on a wide range of subassemblage configurations.

Due to the emphasis on experimental testing in this research project, the time devoted

to formulating semi-rigid design methods has been limited. Although a number of design approaches which incorporate the inherent benefits of semi-rigid joint action have been proposed by the author, the principal objective of formulating a single concise thoroughly validated design approach, which can be used by practising designers, has not been achieved. It is evident that for such a target to be attained, extensive parametric studies are required using sophisticated computer software similar to that described above. In chapter 9, which summarises the proposals for future work, this topic has been addressed by highlighting possible extensions to the author's parametric study and semi-rigid design proposals.

This final chapter presents a concise itemised summary of the major conclusions that may be drawn from the execution of the research study and the interpretation of the results which have been obtained. For the convenience of the reader, the conclusions have been categorised under the headings experimentation techniques, connection behaviour, frame and subassemblage response and frame design techniques. Where appropriate, the source of the conclusions in the main body of the thesis has been cited for easy reference.

## **10.1 Experimentation techniques.**

1. A preliminary analytical study undertaken to optimise the experimental set-up had shown (section 2.2.2) that the effects of column behaviour due to the small amounts of friction at a column end intended to be 'pinned' can be significant. The problem can be alleviated by introducing a fixed, or near fixed, connection. It has been shown that the deviation in performance of such a support condition has a negligible effect on the performance of relatively slender columns and therefore provides a more consistent and easily defined experimental boundary condition.

2. A technique has been developed (section 2.3.3) by which the centroidal axis of relatively slender columns can be deformed in the weak direction into the shape of a smooth bow of prescribed amplitude under elastic conditions. By adopting this technique, an element of consistency was achieved between the different subassemblage tests and the subsequent analytical modelling of subassemblage behaviour was much simplified.
  
3. A technique has been developed (section 3.2) by which the readings from seven strategically placed L.V.D.T.'s can be used to monitor each of the six components of 3-dimensional deformation at a specific point on a member. The measurement system was designed to satisfy the requirements of ease of use, unrestricted access in and around the testing rig and a low cost achieved by utilising readily available proprietary measurement devices. Extensive studies of the performance of a prototype arrangement clearly validated the accuracy of the measurement technique.
  
4. An accurate measure of the internal actions, forces and moments occurring in a steel 'H' section can be computed by performing a linear least-square error approximation of the strains measured from a cluster containing 'redundant' strain gauges (section 3.3). The benefits of this approach are most pronounced for stress distributions in the elastic-plastic range where the often erratic measurements from individual gauges in yielded zones tend to be rationalised. The validity of the approach was proven by the close correlation which was achieved between the total load applied to the subassemblage specimens and the axial load measured from the cluster strain gauges well into the elastic-plastic range.

## 10.2 Connection behaviour.

1. It was reported in chapter 6 that, due to the effect of column web panel flexibility, the connection moment-rotation response measured from an isolated 'cantilever' connection test can be quite different from that measured from an isolated 'cruciform' test (chapter 6). However, the moment-rotation responses measured from these two types of test were, in general, similar to connection response observed in the subassemblage and frame test for the corresponding structural arrangement (i.e. connection response to an internal column was similar to that from a 'cruciform' test whilst that to an external column was similar to that observed in a 'cantilever' test). Surprisingly, there was little evidence of permanent deformation of any of the connection elements in either the subassemblage or frame tests, certainly less than that which has been observed in many tests on isolated connections. This was principally due to the relatively small connection rotations (typically less than 0.025 radians) which were observed at the point of maximum applied load.
2. For the particular arrangement in which a pair of beams frame into the column web, it has been shown (section 6.5) that due to the effects of beam continuity and web flexibility the unloading connection stiffness ( $C_u$ ) is not necessarily equal to the initial tangent stiffness ( $C_i$ ). The full 'loading-unloading' response for a connection in this particular arrangement does not, therefore, correspond to the measured response from either a conventional 'cantilever' or a 'cruciform' connection test. This discrepancy clearly illustrated a deficiency in the present experimental procedures for assessing isolated connection response. An improved experimental test method has therefore been proposed, together with an alternative semi-empirical approach, in which all the parameters influencing the performance of beam to column connections are included.

3. A  $\beta_{pin}$  factor, which is a measure of the increase in strength of a column restrained by semi-rigid connections compared to that achieved using fully rigid connections, has been used to illustrate the reduced 'efficiency' of a web cleat connection as the column slenderness is decreased (section 7.6).

### 10.3 Frame and subassemblage response.

1. A very close agreement has been achieved between the measured response of the subassemblage test specimens and the predictions of a sophisticated finite element computer program developed specifically for analysing three-dimensional column subassemblages (chapter 4). The degree of correlation which has been attained has validated the program and demonstrated its usefulness as an analytical research tool.
2. The parametric study reported in chapter 7 used the finite element program introduced above to investigate the performance of a range of different column subassemblage configurations employing a number of different member sizes for both web-cleat and fully rigid connection types. The predicted ultimate capacities were presented in the form of an  $\alpha_{pin}$  factor, defined as the ratio of the failure load of a semi-rigidly restrained column to that of the pinned-end column. This showed that for subassemblages comprising a 3.8m long column with web-cleat connections and subjected to a wide range of loading conditions, the beneficial effect of connection restraint on the ultimate column capacity out-weighed the detrimental effect of the transferred disturbing moment in nearly all cases. Only when subjected to the most onerous loading pattern with a single beam connection to the minor axis of a stocky column, in which strength criteria rather than buckling dictated the ultimate capacity, did the detrimental effect of the disturbing moment out-weigh the benefit of



connection restraint (section 7.6). However, the maximum reduction in the failure load compared to that of the pinned-end column was only of the order of a few percent. Under such loading conditions, it is interesting to note that the predicted ultimate capacities of the corresponding rigidly connected subassemblages were *less* than those for the subassemblages with web-cleat connections due to the more onerous effect of the increased column disturbing moment. The results from this aspect of the study clearly demonstrated that the enhancing effect of column restraint is more pronounced on columns of greater slenderness. In addition, it showed that significant improvements can be achieved in the axial capacity if, for a given floor loading, the column is orientated such that the load on the major axis beam is maximised, whilst the load on the minor axis beam, and hence the column minor axis disturbing moment, is minimised.

3. Despite inducing significant major axis disturbing moments, all the columns in both the experimental and numerical studies failed as a result of excessive minor axis deformation. In some of the frame test columns, this was accompanied by large twist rotations at the mid-height of the column - particularly as the ultimate load was approached (sections 2.5.1 and 5.10). It was also evident from the frame tests reported in chapter 5 that column segments in multi-storey steel frames do not behave as isolated elements, but that there is significant interaction between adjacent segments at all stages of loading. This is particularly apparent at the point of failure where a column, which may have initially been providing restraint, transfers a disturbing moment to an adjacent column as it deforms plastically. In one instance in frame test F1, this resulted in the progressive failure of a particular column segment initiating the failure of the adjacent lower segment.

4. A recurring observation throughout the study was that the capacity of the col-

umn sections in both the experimental and numerical studies was enhanced by the shedding of the minor axis disturbing moment. In instances where an initial disturbing moment was applied, this often resulted in a complete reversal of moment at the column head. Where there was no appreciable disturbing moment, the restraining column head moment simply increased in size without reversing. In both cases however, a pattern of minor axis moments were developed at the ultimate condition in which the head moment arising from the connection restraint was of the opposite sign to the moment at the column centre. The redistribution of major axis moments was, in most cases, negligible by comparison and only occurred when the column had little residual stiffness as the failure load was approached.

5. It is evident from both the experimental and numerical studies which have been conducted that the moment-rotation characteristics of 'simple' bolted steelwork connections have a significant influence on the ultimate capacity, distribution of bending moments and deflection of 'non-sway' steel subassemblies and frames.

## 10.4 Frame design.

1. Comparisons of the ultimate column capacities obtained from both the experimental and analytical studies with those predicted from 'simple' frame design techniques show that present methods of 'simple' non-sway frame design are very conservative (section 8.3.7). This was attributed to a number of factors.
  - (a) The pattern of column moments assumed in design is not representative of the actual distribution of moments at failure, particularly for the minor axis of columns with a moderate to high slenderness.

- (b) The actual disturbing moment from the beams does not correspond with that assumed in 'simple' design where the vertical beam reaction is considered to act at the centre of stiff bearing subject to a minimum distance of 100mm from the column face.
- (c) The combined effect of forces and moments acting on a column appear to be less onerous than that inferred from the additive nature of the terms in the interaction equation.
- (d) The guidance on the effective length, and hence the critical load, of columns with standard idealised end conditions is, in most cases, very conservative.

2. The author has proposed a number of ultimate limit state design approaches in which the inherent benefits of semi-rigid frame action are taken into account and consequently predict failure loads reasonably close to those observed in the experimental and analytical studies. Firstly, it was evident from the initial parametric study that small amounts of column restraint have a more pronounced effect on columns of greater slenderness. A method has been proposed in section 8.3.8 which utilises this phenomenon to provide a quick assessment of effective length in which the column slenderness is taken into account. This was developed as a modification to the present 'simple' method of column design. Using this approach, effective lengths were predicted which were closer to those observed in the experimental tests when compared to those predicted using current guidance. In addition a method of column design was proposed (section 8.3.9) in which the column was considered as part of a frame rather than as an isolated element. The forces were derived by considering the deformed shape of the member at the condition when the

transferred minor axis moment reduced to zero during the moment reversal stage. Comparisons with numerical data showed that this approach gave a close prediction of the column deformation, the actual mid-column moments and hence the ultimate capacity.

3. A method proposed by the author in section 8.2 for predicting the deflection of semi-rigid frames under serviceability loading conditions gave a good correlation with the measured deflections in frame test F1. In addition, it appeared that the proposed technique was relatively insensitive to the precise magnitude of the assumed linear connection stiffness. It was also shown how this method could be extended to generate the design moments and column effective lengths under ultimate loading conditions.